Northumbria Research Link

Citation: Suwanapingkarl, Pasist (2012) Power quality analysis of future power networks. Doctoral thesis, Northumbria University.

This version was downloaded from Northumbria Research Link: http://nrl.northumbria.ac.uk/id/eprint/12625/

Northumbria University has developed Northumbria Research Link (NRL) to enable users to access the University's research output. Copyright © and moral rights for items on NRL are retained by the individual author(s) and/or other copyright owners. Single copies of full items can be reproduced, displayed or performed, and given to third parties in any format or medium for personal research or study, educational, or not-for-profit purposes without prior permission or charge, provided the authors, title and full bibliographic details are given, as well as a hyperlink and/or URL to the original metadata page. The content must not be changed in any way. Full items must not be sold commercially in any format or medium without formal permission of the copyright holder. The full policy is available online: http://nrl.northumbria.ac.uk/policies.html

Northumbria University NEWCASTLE

University Library

POWER QUALITY ANALYSIS OF FUTURE POWER NETWORKS

PASIST SUWANAPINGKARL

PhD

2012

POWER QUALITY ANALYSIS OF FUTURE POWER NETWORKS

PASIST SUWANAPINGKARL

A thesis submitted in partial fulfilment
of the requirements of the
University of Northumbria at Newcastle
for the degree of Doctor of Philosophy
in Electrical Power Engineering

Research undertaken in the
Faculty of Engineering and Environment
Incorporating: Computing, Engineering and
Information Sciences

November 2012

Abstract

Green technologies are continually being deployed into Medium Voltage and Low Voltage distribution networks in order to reduce Carbon Dioxide emissions and combat climate change. These include Small-Scale Distributed Generators (mainly from renewable technologies such wind, hydro and photovoltaic) and green transport (battery powered and Plug-in Hybrid Electric Vehicles). The high penetration levels of Small-Scale Distributed Generators, Electric Vehicles and Plug-in Hybrid Electric Vehicles could have impacts on the quality of supply, particularly voltage and harmonic profiles. The output power of renewable energy resources is determined by the surrounding environment (which varies continually) whilst demand on the power network is determined by the behaviour of consumers (which also varies). In addition, power electronic converters are usually used to connect these resources to the power network, and these produce power quality problems e.g. harmonic distortion. These impacts could be minimised and/or prevented by employing appropriate power flow control under the “Smart Grids” concept using advanced Information and Communication Technology.

This thesis aims to analyse voltage variation and harmonic distortion in the distribution networks in the United Kingdom and Thailand, which may results from increased penetration levels of Small-Scale Distributed Generators and Electric Vehicles and Plug-in Hybrid Electric Vehicles. Accordingly, solutions to improve the performance of future power networks are proposed. These include the use of smart meters (involving two-way communication link between the local buses and central data bank or centralised control) in conjunction with Smart On-Load Tap Changing Transformer, Smart Electric Vehicles Grid Connections, Smart Electric Vehicles and Plug-in Hybrid Electric Vehicles Car Park, Smart Energy Storage and Smart Load Controller. To complete the analysis, computer models of typical distribution networks incorporating photovoltaic, small-scale Permanent Magnet Generator for wind and hydro turbines, and Electric Vehicles and Plug-in Hybrid Electric Vehicles are developed in MATLAB/Simulink environment. Furthermore, tools appropriate for analyses of future power networks are proposed, which includes Power Self-Monitoring, Analysis and Reporting for Distribution Networks.

CONTENTS

LIST OF FIGURES **PAGE**

LIST OF TABLES **PAGE**

Acknowledgements

The completion of this thesis has received generous supports from Prof. Ghanim Putrus and Prof. Nicola Pearsall who spent a large amount of time, provided consultation and advice to me throughout the research, for which I am deeply grateful. Beside I appreciated the knowledge and advise that Dr. David Johnston and Dr. Edward Bentley shared with me during this work. Because of, their patience and professional guidance, I am able to complete this research and achieve my objectives.

This thesis is supported by Rajamangala University of Technology Phra Nakhon (RMUTP), Bangkok, Thailand and Thailand government, for which I am deeply grateful. In addition, I am grateful to Mr. Sompong Pongsakulrangsee, Director of Samutprakarn Province (MEA), Mrs. Natenara Oonchai, Director of Electric Rate and Power Forecast Division (MEA), Mr. Lertchai Keawwichian, Director of System Development Division (MEA) and Mr. Payomsarit Sripattananon, Distributed Generation Division (MEA) for their guidance and support in providing the technical information for the Thailand network.

The success of this thesis is also due to all of my lecturers who taught, imparted knowledge and shared their experience with me, for which I would like to pay my gratitude. Last but not least, I wish to thank my lovely family and everyone who supported and encouraged me especially my father, Mr. Montri Suwanapingkarl and mother, Miss Tiwaporn Suwanapingkarl who spent their whole life to teach me. A special thanks to my lover; Miss Kwanchanok Srivallop, for her encouragement and patience during this journey.

Pasist Suwanapingkarl
November 2012

Declaration

I hereby declare that the work contained in this thesis has not been submitted for any other award and that it is all my work. I also confirm that this work fully acknowledge opinions, ideas and contributions from the work of others.

Name: Pasist Suwanapingkarl

Signature: _____

Date: _____

Nomenclature

A/D	=	Analogue to Digital devices
AC	=	Alternating Current
ADMD	=	After Diversity Maximum Demand
AL	=	Aluminium
AMR	=	Automatic Meter Reading
AVR	=	Automatic Voltage Regulator
CNE	=	Combine Neutral Earth
CO_2	=	Carbon Dioxide
CU	=	Copper
DAC	=	Data Acquisition Control
DC	=	Direct Current
DFL	=	Direct Feedback Linearization
DGs	=	Distributed generators
DMS	=	Distribution Management System
EMS	=	Energy Management System
EVs	=	Electric Vehicles
FACTS	=	Flexible AC Transmission System
FFT	=	Fast Fourier Transform
HAWT	=	Horizontal-Axis Wind Turbine
HMT	=	Harmonic Mitigating Transformer
HV	=	High Voltage
ICT	=	Information and Communications Technology
IGBT	=	Insulated Gate Bipolar Transistor
IP	=	Internet Protocol
IPCC	=	Intergovernmental Panel on Climate Change
KCL	=	Kirchhoff’s Current Law
LM	=	Load Management
LV	=	Low Voltage
MV	=	Medium Voltage
MOT	=	Ministry of Transport
MPP	=	Maximum Power Point
MPPT	=	Maximum Power Point Tracking
OLTC	=	On-Load Tap Changer Transformer
OPF	=	Optimal Power Flow

PD	=	Proportional Derivative
PDF	=	Probability Density Function
PFC	=	Power Factor Correction
PHEVs	=	Plug-in Hybrid Electric Vehicles
PID	=	Proportional Integral Derivative
PLL	=	Phase Lock Loop
PM	=	Permanent Magnet
PMG	=	Permanent Magnet Generator
PQ	=	Power Quality
PSmartDN	=	Power Self-Monitoring, Analysis and Reporting Tool for Distribution Networks
PST	=	Phase-Shifting Transformer
PV	=	Photovoltaic
PWM	=	Pulse-Width Modulation
RCB	=	Remote Circuit Breaker
RTDs	=	Real-Time Digital simulators
RTU	=	Remote Terminal Unit
SARFI	=	System Average RMS Frequency Index
SCADA	=	Supervisory Control and Data Acquisition
SCL	=	Short-Circuit Level
SCP	=	Smart EVs/PHEVs Car Park
SDSM	=	Smart Demand Side Management
SES	=	Smart Energy Storage
SEVGC	=	Smart EVs Grid Connection
SLC	=	Smart Load Controller
SOC	=	State of Charge
SOLTC	=	Smart On-Load Tap Changer Transformer
SSDGs	=	Small-Scale Distributed Generators
STATCOM	=	Static synchronous Compensator
TH	=	Thailand
THD	=	Total Harmonic Distortion
UK	=	United Kingdom
UKGDS	=	United Kingdom Generic Distribution System
UPS	=	Uninterruptible Power Supply
V2G	=	Vehicles to Grid
VAWT	=	Vertical-Axis Wind Turbine

VSAC = Variable Speed Air-Conditioner

XLPE = Cross-Linked Polyethylene

CHAPTER 1
INTRODUCTION

1.1 Background

Green technologies for power generation (mainly from renewable energy) and transportation (mainly Electric Vehicles and Plug-in Hybrid Electric Vehicles, EVs/PHEVs) are continually being deployed into distribution networks. These green technologies are usually connected to the grid via power electronic devices (having non-linear characteristics) in order to optimise the output/input power, hence they could produce harmonic distortion in the power networks. Moreover, the output power of Small-Scale Distributed Generators (SSDGs) is affected by the surrounding environment (e.g. solar radiation, wind speed, water velocity) and the consumers' behaviour, which causes variation in demand. Therefore, the quality of the electrical supply could be affected by high penetration levels of SSDGs and EVs/PHEVs. This thesis is particularly focused on the impacts of SSDGs (mainly PV, wind and hydro turbines) on the Medium Voltage (MV) and Low Voltage (LV) distribution networks in the United Kingdom (UK) and Thailand (TH). SSDGs have a small rating compared to other Distributed Generators (DGs with MW rating), and hence these are normally distributed in residential areas. That means the impacts of voltage variation and harmonic distortion will become more significant than frequency variation and Short-Circuit Level (SCL), especially for high penetration levels of SSDGs.

Therefore, it is necessary to investigate the voltage variation and harmonic distortion on the MV/LV distribution network, where penetration levels of SSDGs and EVs/PHEVs are continually increasing. Accordingly, solutions are proposed to improve both voltage variation and harmonic distortion in future distribution networks. The main structure of this thesis is shown in Figure 1.1.

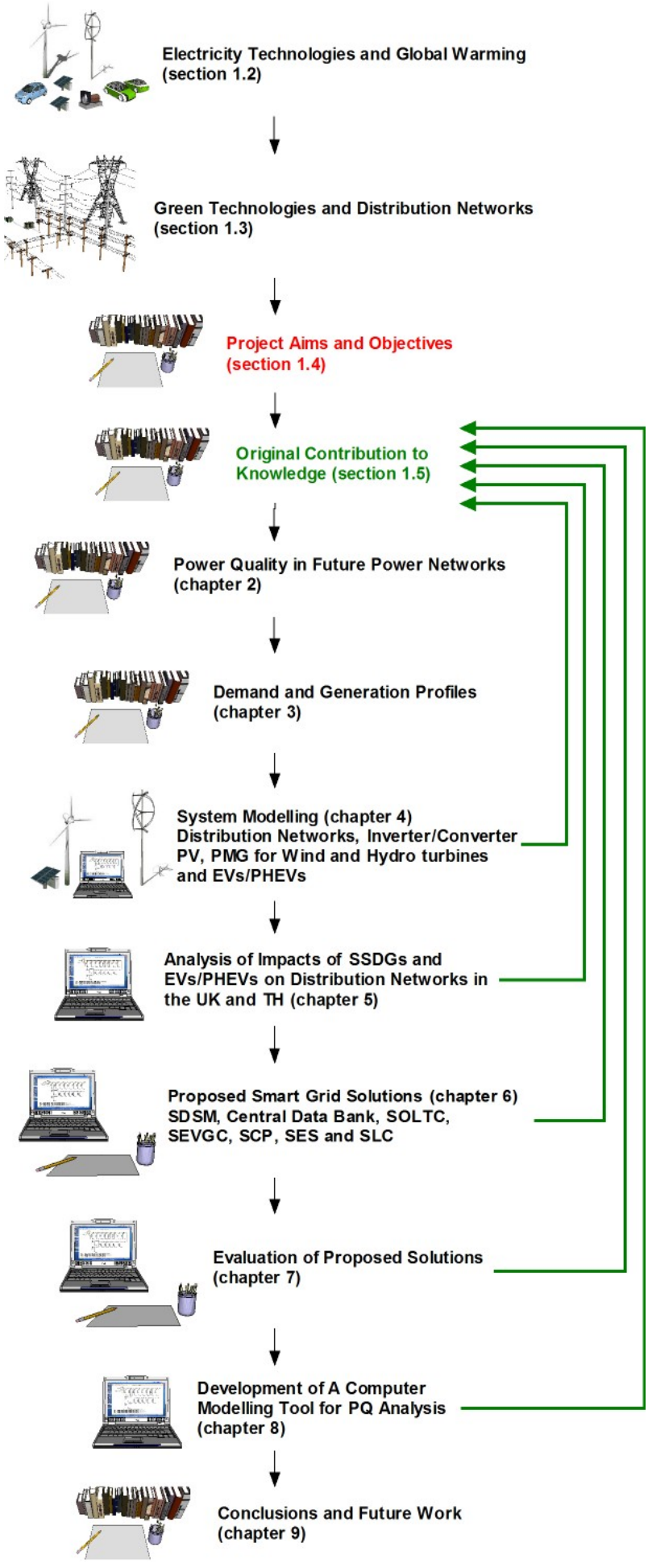

Figure 1.1 Main structure of thesis

1.2 Electricity Technologies and Global Warming

Scientists suggest that the CO_2 in the atmosphere increased by about 30 percent in the age of the industrial revolution, which occurred from the middle 1700s to the present [1]. This has led to the "Greenhouse Effect" in the earth. This effect happens when a large amount of CO_2 is trapped in the atmosphere preventing the heat of radiation emitted from the earth's surface escaping back into space. Therefore, the surface of the earth stores this heat and this result in the temperature of the earth gradually increasing. The greenhouse effect brings "Global Warming" at the worldwide scale with potential catastrophic effects for some coastal countries [2]. The International Energy Agency, [3] concluded that fuel combustion plays an important role in increasing the world emissions of greenhouse gases such as CO_2. Figure 1.2 shows that CO_2 emission are continuously increasing from close to zero Gt CO_2 in 1870 to about 29 Gt CO_2 in 2006.

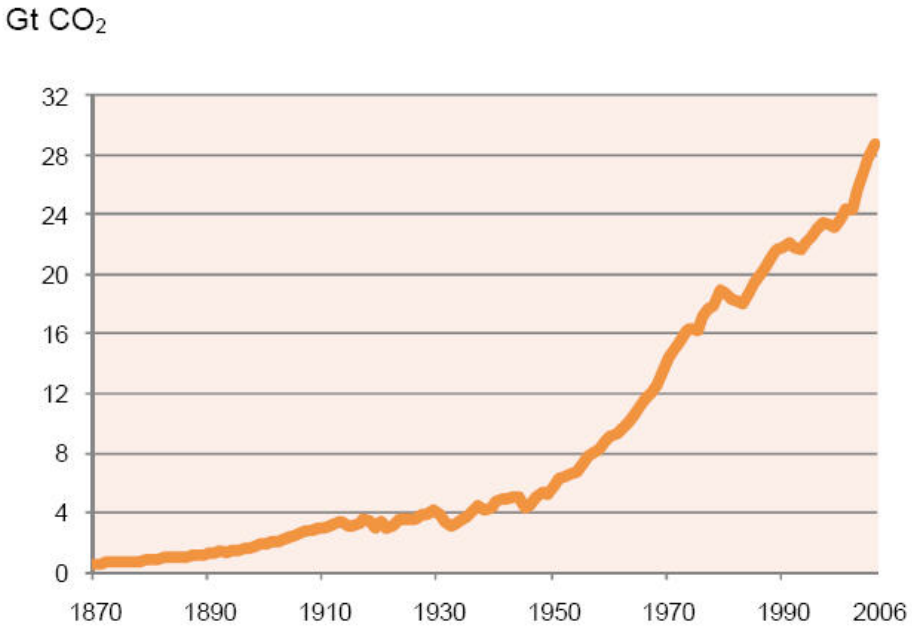

Figure 1.2 Trend in CO_2 emissions from fuel combustion [3]

Source: International Energy Agency, (2009)

It is important to note that the energy sector is largely responsible for CO_2 emissions (shown in Figure 1.3). As shown in Figure 1.4, in 2007, CO_2 emissions have increased 14 percent for the electricity sector and 3 percent for the transportation sector as compared to 1971 [3].

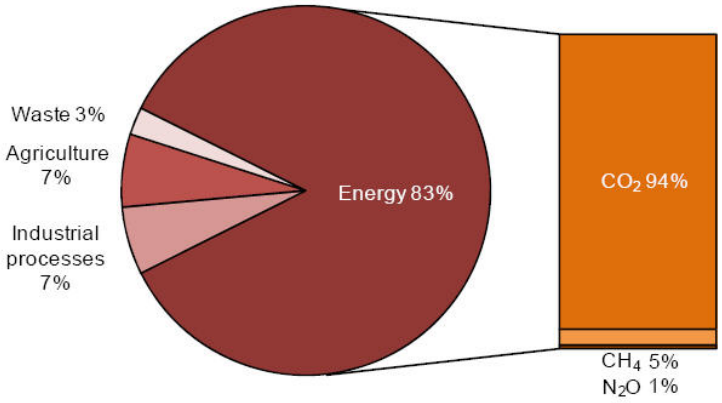

Figure 1.3 Proportion of emissions gases of the world in 2006 [3]

Source: International Energy Agency, (2009)

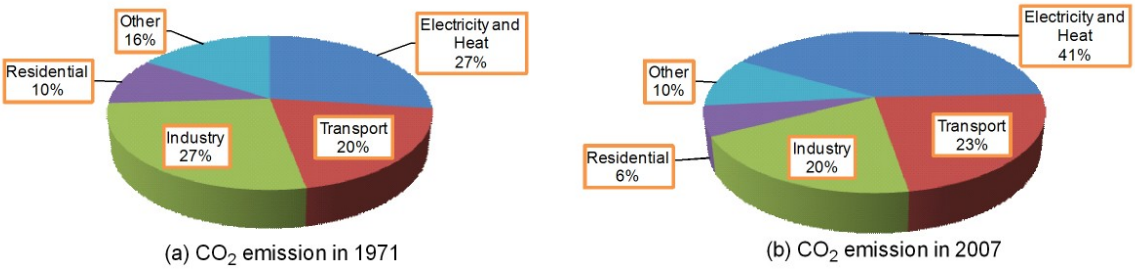

Figure 1.4 CO_2 emissions based on technologies in 1971 to 2007

Hassmann, [4] proposed that the traditional power generation is one of the main causes of increasing CO_2 emissions. This problem could be reduced by the use of advanced renewable energy technologies. References [5] and [6] analysed the market share of electricity generation and concluded that renewable energy sources such as hydropower and biomass, still have small shares in the market. Figure 1.5 demonstrates that oil has the largest shares at 33 percent in 1992 [5] and 33.2 percent in 2008 [6].

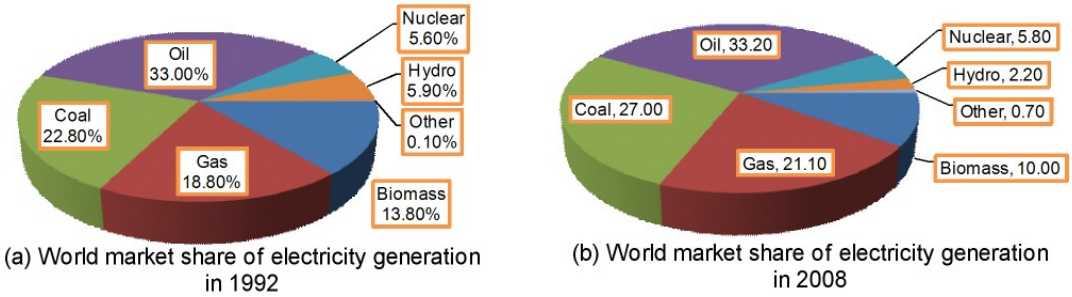

Figure 1.5 World market share of electricity generation in 1992 and 2008

The trend of power generation will need to be changed in the future in order to reduce CO_2 emissions by increasing the number of green technologies on the MV/LV distribution network. The Department of Energy and Climate Change, [7]

published the global emissions of greenhouse gases, especially CO_2 emissions in the UK, which represents a sample of developed countries. The report proposes three extreme future scenarios for CO_2 emissions based on the population, economic growth and energy usage. Figure 1.6 shows the three scenarios that affect the global CO_2 emissions and temperature.

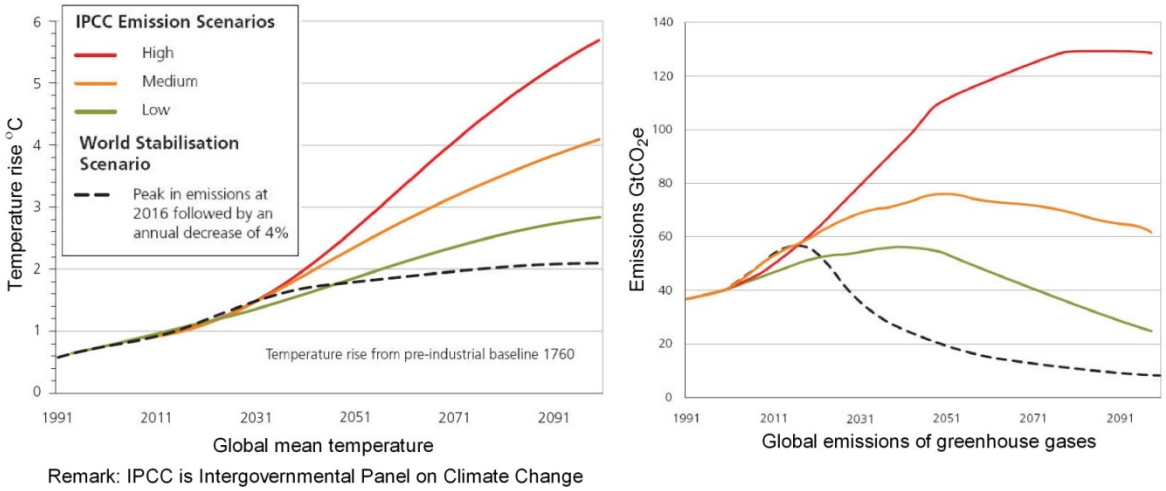

Figure 1.6 Effect of CO_2 emissions and the earth surface temperature

It can be noted that the high energy consumption from non-renewable energy (e.g., coal, gas, oil etc.), without considering any policies, causes high global emissions (red line; top line), whereas other scenarios (orange, green and dashed lines) move away from the use of fossil fuels. The main consumption of non-renewable energy is the traditional power generation (such as coal, gas and oil) and transportation systems (e.g. private vehicles, public transport, and industrial transport). The global warming effect will become greater in the future, if non-renewable energy continues to be used as the main source of energy.

In order to reduce emissions of greenhouse gases, the Framework Convention on Climate Change was presented at the Rio Earth Summit'92 in Brazil, which suggested the use of renewable energy as an option to reduce the emissions [8-9]. In addition, many conferences (e.g. Kyoto Conference'97 in Japan, Johannesburg Conference'02 in Africa, Montreal Conference'05 in Canada) were held to try to ensure the emissions of gases would be reduced [8-9]. In 2010, the Renewable Energy Policy Network for the 21st Century [8] reported that the renewable energy (such as PV, wind and hydro turbines, etc.) has increased to 19 percent of the total power generation in 2008 (shown in Figure 1.7) due to new technologies being developed.

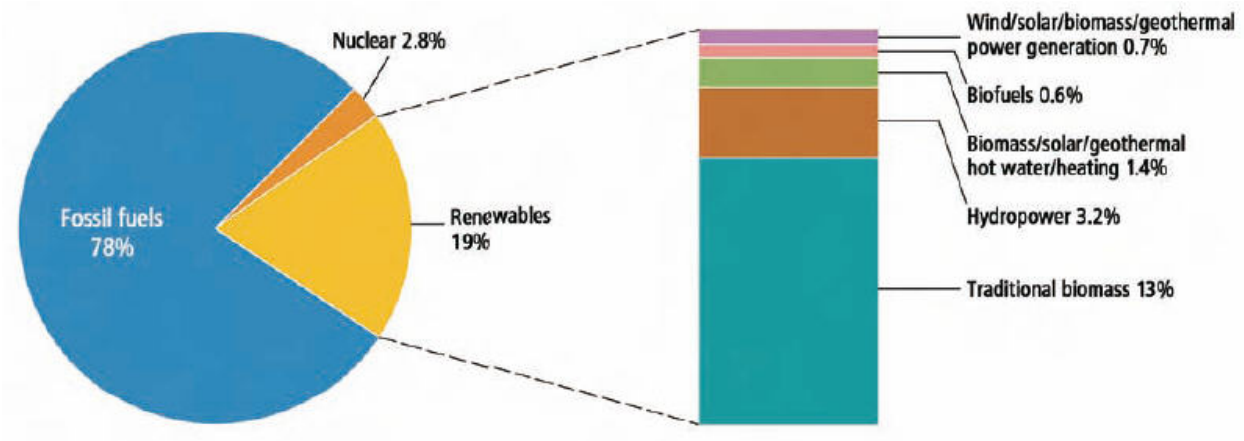

Figure 1.7 World energy consumption in 2008 [8]

Source: Renewable Energy Policy Network for the 21st Century, (2010)

In summary, green technologies are continually increasing on the distribution network, including SSDGs for power generation and EVs/PHEVs for transportation. Therefore, it is important to study the impacts of green technologies, including SSDGs (here mainly PV, wind and hydro turbines) and EVs/PHEVs on the distribution networks. This thesis is particularly focused on the impacts of these on Power Quality (PQ).

1.3 Green Technologies and Distribution Networks

The UK, TH and the world commitments to the reduction of CO_2 emissions and a cleaner atmosphere is leading to increased interest in green technologies, especially in renewable energy resources. The trend of energy use in the UK in 2020 is described in reference [10]. Figure 1.8 shows that in 2020 advanced technologies of renewable energy, will have large market shares in electricity generation and transportation at 30 percent and 31 percent, respectively.

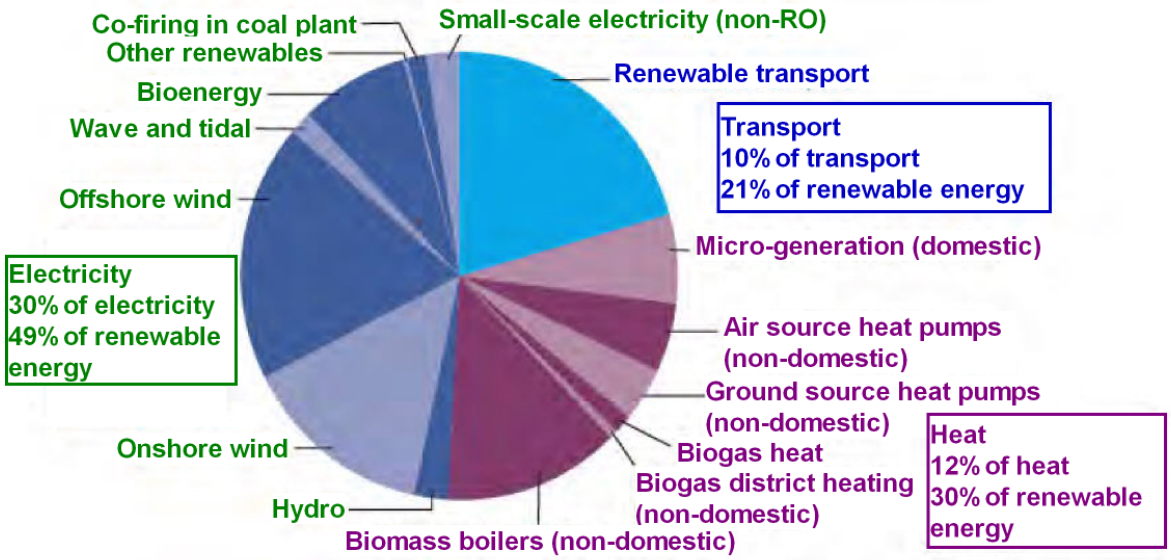

Figure 1.8 Trend of renewable technologies in 2020 [10]

Source: Department of Energy and Climate Change, (2009)

References [11-13] published extreme scenarios about the replacement of traditional power generation and transportation with renewable energy technologies in the UK. They claimed that renewable technologies in the distributed generation and transportation system would be important keys to reduce gas emissions in the future. Mott MacDonald, [13] suggested that the penetration levels of small-scale generations in the UK in 2020 for PV will reach 7.49 percent, wind turbine 1.78 percent and hydro turbine 2.54 percent. On the other hand, the penetration levels of SSDGs in TH in 2020 are not published yet, hence this thesis considered the penetration levels of SSDGs in TH in 2020 are similar to those for the UK.

In practice, many sources of SSDGs in the UK, such as PV, wind and hydro turbines, are usually in the small to medium power range (ranging from 1 kW to 50 kW) and connected to the MV/LV distribution networks [14-16]. Similarly, it is expected that SSDGs in TH (that represents developing countries) could provide generation up to 10 MW [17]. Hence, it is necessary to understand the performance of existing power networks before/after connection of SSDGs and EVs/PHEVs.

1.3.1 Existing power networks

Existing power networks are designed such that the power flows from centralised generating units to consumers. This power is distributed by passive networks, which supply electricity through integrated transmission and distribution systems to the consumer, as shown in Figure 1.9. Therefore, voltage and frequency control is ensured by centralised control. In practice, central control is provided by Supervisory Control and Data Acquisition (SCADA) systems.

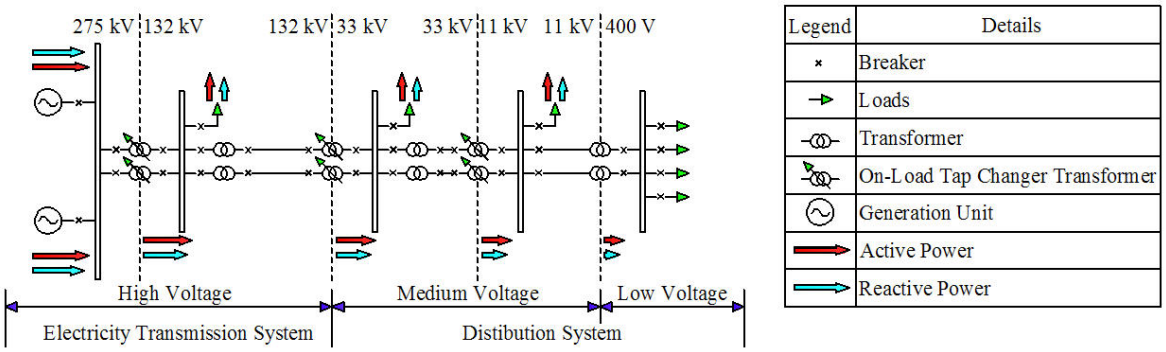

Figure 1.9 Typical existing (passive) power networks

The existing SCADA system incorporates a central computer that allows the network operator to monitor and control devices, used at high voltage (HV) and MV substations and large power plants. It should be noted that data is gathered and processed at the central control before sending signals to take actions, which are usually done via the automatic system and flexible management. The SCADA system has been in use in the transmission system since 1980 [18]. Therefore, its functions are continually being developed because of the improvement in protective and control devices. The three main keys of SCADA systems are the central coordination function, the regional function at each member system and the device control and Data Acquisition Control (DAC) functions.

In practice, central coordination functions of existing power networks are basically divided into four major areas; data acquisition (which receives data from local devices), load prediction (that is used to predict the possible situation in the near future), load control operating strategies and load control location among member systems. The revenue metering is typically used to monitor the demand and this is part of a load management in the SCADA system. The communication between the substation and the member could be part of the DAC functions. Figure 1.10 shows a typical communication system of an existing power network.

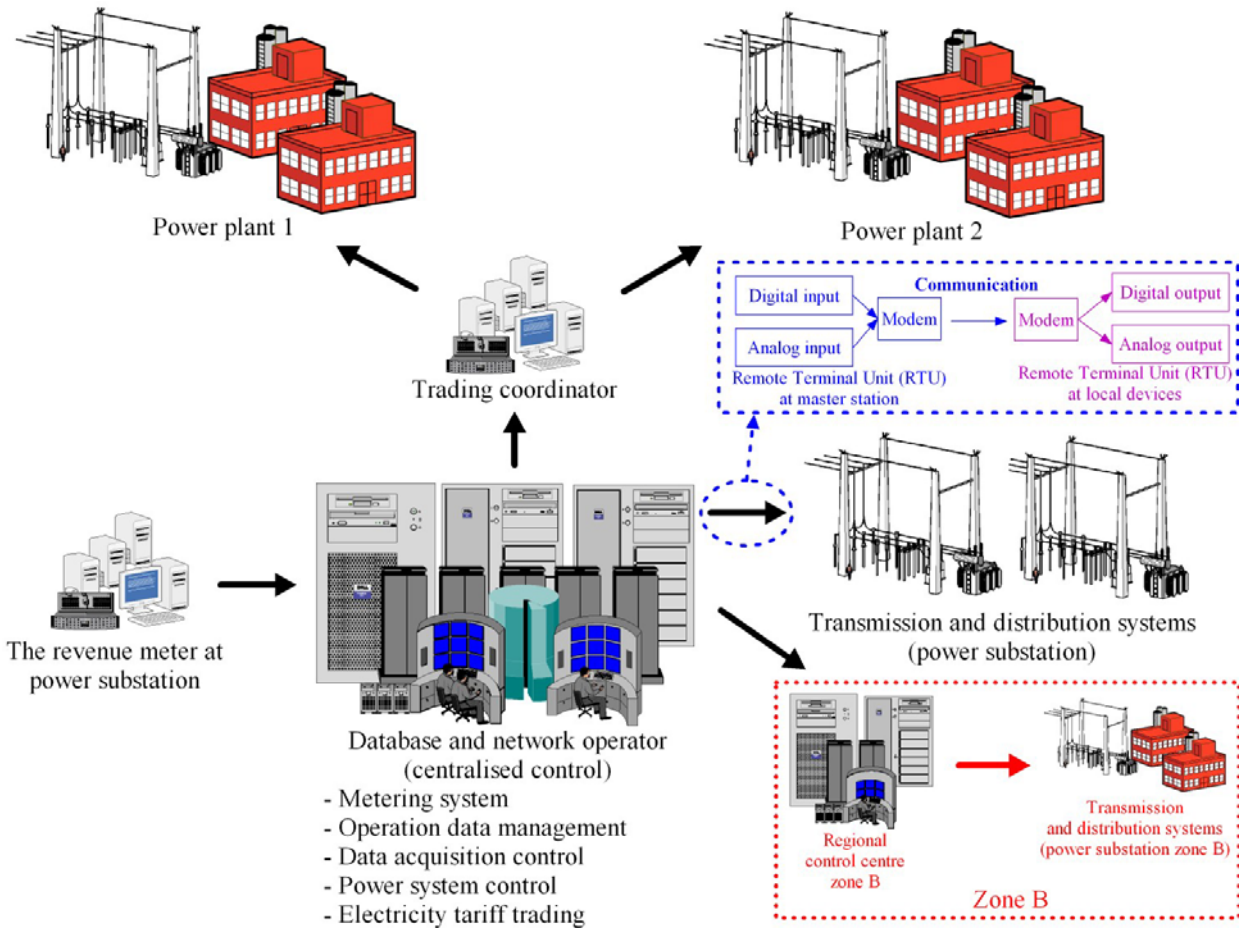

Figure 1.10 Typical communication system of existing power network

It can be seen that the communication between the centralised and the individual substation is usually one-way communication. Hauser, Bakken and Bose, [19] studied the electric power networks in Western Europe and North America where both networks have highly complex infrastructure. Their results show that the networks require fast and safety control technologies, in order to keep the generation and demands in balance. Ackerman and Block, [20] investigated the operation of the SCADA system, which is based on the IEEE tutorial fundamental of supervisory systems. They concluded that a successful operating SCADA system should use the Remote Terminal Unit (RTU). This device is used to gather data and control signals for automated control systems. Figure 1.10 also shows that the RTU is used as a communication link between the number station and the local equipment such as the main electricity supply and protection systems (e.g. relay switch, switchgear, etc.). That means the capacity of the monitoring and controlling network is usually restricted by the number of RTUs. Therefore, a large size power network will include multiple master stations or sub-master stations to monitor and control.

Basically, the SCADA system can be divided into six types. Firstly, a traditional simple SCADA system receives the local data, which allows network operator to directly monitor and control. Secondly, the simple SCADA incorporates automated generation control. This system can automatically calculate the error of control area, monitoring frequency and the economic dispatch of generating units. Thirdly, the Energy Management System (EMS) is used to express the system that includes gathering data, control and online data storage. Next, the Distribution Management System (DMS) is the low cost technology when compared to the other types as it is used to monitor distribution feeders and control the distribution portion of substations. In practice, the DMS is normally implemented with the EMS. Fifth, the intent of a Load Management (LM), SCADA system is used to control peak demand and provide convenient update in economy tariff. It works either as a stand-alone system or as an integrated system (as part of the EMS and DMS). This requires a one-way communication system at the consumers' level. Lastly, the Automatic Meter Reading (AMR) is similar to the LM but uses two-way communication systems.

Although existing (passive) power networks have successfully implemented automated schemes of supply restoration (or SCADA) at HV and MV levels, this automation is still not enough to control power distribution networks in future, especially at the LV level because the existing SCADA system does not operate in real-time [21]. In practice, the SCADA system updates the signals with 5-15 sec time intervals, and hence this results in the delay of monitoring and controlling signals. It can be noted that this system was originally designed for low bandwidth communication channels, which were in place at that time (in the past) where this system is currently not supported at the consumers' level. These barriers of existing control could be improved by using the logical controller embedded in all local RTUs, which allows dynamic operation, but it still requires real-time monitoring at the consumers' level. Sciacca and Block, [22] suggested that the network operator must consider operating costs in order to match supply/demand with low budget.

1.3.2 Future power networks

Distributed generation increases the power generation capacity (supports high demand for electricity), and may improve power generation efficiency (optimises power flow) and network reliability. However, large numbers of DGs may also lead to problems, such as reverse power flow, potential voltage unbalance, increased SCL and change in existing protection systems, particularly in weak distribution networks [23-24]. Distribution networks in the future are expected to include various types of green technologies (e.g. PV, wind and hydro turbines and EVs/PHEVs) and this may lead to a bi-directional power flow in the network, as shown in Figure 1.11.

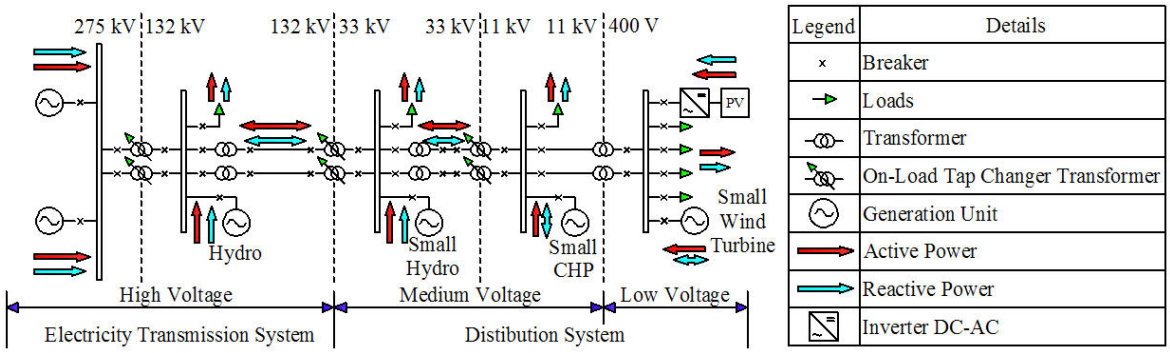

Figure 1.11 Typical future power networks

This means that operating future power networks without appropriate management of power flow could lead to PQ problems. The power network may experience potential violation of statutory voltage limits [23-28]. This is because the output power of DGs/SSDGs (mainly from renewable energy resources) is determined by the surrounding environment in that area. In addition, the daily consumers' electricity demand is usually dynamic and varies all the time depending on the season and consumers' behaviour. In addition, harmonic distortion in the power network may result from the use of power electronic devices with DGs/SSDGs and EVs/PHEVs (used to optimise their output/input power).

In order to achieve reliable performance, future power networks will need to be changed from existing (passive) networks to smart (active) networks, which incorporate significant non-centralised control [29]. This is based on the concept of the "Smart Grid", which uses advanced Information and Communications Technology (ICT) and smart local controllers. Much research has been conducted to develop algorithms to locate the problematic areas [30-32] and/or develop new

approaches for communication systems, which identify sub-devices in the network via Internet Protocol (IP) addresses [33-34]. Therefore, this thesis investigates the requirements of smart grids (smart networks) by using smart meters to acquire local data at the consumers' level and smart control devices in order to ensure the reliability and safety of the network.

In practice, existing control of power networks (SCADA system) is based on the star topology, which requires information and control signals to be sent back and forth within a period of several seconds. Hence, this technique has a barrier in real-time monitoring at the consumers' level due to low speed of operation. For instance, weak power networks and rural areas with high complexity require excessive monitoring and high-speed communication systems in order to secure the safety of operation. This includes identifying significant issues in the power network before taking any actions (e.g. constrain load and fault levels management). These operations require high-speed time response in order to ensure that the infrastructure of the power network could support the supply/demand balance. To ensure high quality of supply, some extra controls (such as RTUs, disturbance voltage correction, etc.) may be considered in order to provide fast response and support supply/demand management and protection systems.

From a technical point of view, the two crucial keys that would be necessary in future power networks are smart control and advanced ICT. This includes the communication system between the centralised control, consumers and local devices. However, this improvement requires large amounts of investment and a number of years to develop the existing systems as the green technologies are continually expanding. One of the key aspects to reduce the effects of accommodating DGs and EVs/PHEVs is the use of the Smart Demand Side Management (SDSM) technique with smart controllers that are based on the smart grid concept. These smart devices may independently communicate to each other via either local smart meters or a central data bank instead of a centralised network control. This could monitor supply/demand and maintain PQ within acceptable limits in the presence of a large number of DGs/SSDGs and EVs/PHEVs (explained in chapter 6).

The thesis is focused on investigating the requirements of SDSM and smart controllers as they will play an important role (together with smart meters) in future power networks. To achieve this, the thesis presents the development of computer models of PV, small-scale wind and hydro turbines, EVs/PHEVs, Smart On-Load Tap Changer Transformer (SOLTC), Smart EVs Grid Connections (SEVGC), Smart EVs/PHEVs Car Park (SCP), Smart Energy Storage (SES) and Smart Load Controller (SLC) to optimise power flow in the distributed generation local area. These smart controllers would be connected at key points in the distribution network in order to increase the reliability and quality of supply. These solutions will allow high penetration levels of green technologies to be integrated in existing MV/LV distribution networks with minimum change to the infrastructure and investment. This thesis also proposes a Power Self-Monitoring, Analysis and Reporting for Distribution Networks Tool (PSmartDN Tool) to investigate the voltage profiles, active and reactive power flow in distribution networks.

1.4 Project Aims and Objectives

The aim of this thesis is to investigate the impacts of high penetration levels of SSDGs (mainly focused on PV, wind and hydro turbines) and EVs/PHEVs on the MV/LV distribution networks in the UK and TH. The impacts on voltage variation and harmonic distortion are of particular interest, as the impacts of SSDGs and EVs/PHEVs on the voltage unbalance and SCL (or fault level) are not significant [24]. Accordingly, the thesis identifies the anticipated problems in future networks and proposes innovative solutions to improve voltage and harmonic profiles. A MATLAB/Simulink programme has been used to simulate typical distribution networks in an urban area of the UK, which represents developed countries, and a rural area in TH, which represents developing countries. The following are the main objectives of this research:

1) Investigate voltage variation and harmonic distortion, in existing and future power networks (with significant levels of SSDGs of renewable energy resources and EVs/PHEVs). Accordingly, propose solutions to improve voltage and harmonic profiles, in future power networks.

2) Analyse the improvement of network performance by the use of smart meters implemented together with SOLTC, SEVGC, SCP, SES and SLC under SDSM technique. In addition, develop a computer modelling tool (PSmartDN Tool) to investigate voltage profiles, active and reactive power flow in future power networks.

3) Investigate voltage and harmonic profiles in islanded distribution networks, including potential advantages, problems and possible solutions to allow islanding operation.

4) Demonstrate the effectiveness of the proposed solutions.

1.5 Original Contribution to Knowledge

1) Develop generic computer models of SSDGs (mainly PV, wind and hydro turbines) that allow investigating daily voltage profiles and harmonic distortion in distribution networks.

2) Analyse the combined impacts of SSDGs and EVs on voltage variation and harmonic distortion in MV/LV distribution networks, in the UK and TH.

3) Propose solutions for future power networks and demonstrate their effectiveness, including the SDSM technique incorporated with smart meters, SOLTC, SEVGC, SCP, SES, SLC and active filter. Results show that these solutions would allow increased penetration levels of green technologies whilst maintaining voltage and harmonic profiles within acceptable limits. The SLC is considered as an important key for islanding operation, as it can manage loads when operating in an islanded network.

4) Develop a modelling tool based on a combination of Microsoft Excel (MS Excel) and MATLAB/Simulink programmes that allows investigating the daily voltage profiles, active and reactive power flow in MV/LV distribution networks. This tool also allows modelling of small-scale PV, wind and hydro turbines, EVs/PHEVs and smart controllers, which allow investigating their impacts on future power networks.

1.6 Thesis Outline

Chapter 2 investigates the impacts of SSDGs and EVs/PHEVs on voltage and harmonic profiles in existing MV/LV distribution networks in urban and rural areas. It is shown that the voltage variation will be unavoidable because the output power of SSDGs depends on the surrounding environment in that local area and the connection/disconnection of EVs/PHEVs depends on the consumer's behaviour. As both SSDGs and EVs/PHEVs are mostly connected to the grid via power electronics converters, harmonic profiles in the power network need to be considered and are analysed in this chapter. Another issue that is considered in this chapter is the performance of SSDGs and EVs/PHEVs when operated in an islanded network.

Chapter 3 presents the realistic (practical) parameters of selected networks in the UK and TH and define extreme scenarios used to analyse the impacts of SSDGs and EVs/PHEVs on the distribution networks. Scenarios considered include a typical urban area from the UK network and rural area from the TH network, including extreme consumers' behaviour, which is obtained from winter and summer demand profiles. Penetration levels of SSDGs and EVs/PHEVs as forecasted for 2020 and the connection time allowance of EVs/PHEVs at public car park are taken into account to allow investigation of more realistic scenarios.

Chapter 4 gives details of the computer modelling and simulation parameters for the networks considered. Simplified computer models for both UK and TH distribution networks, inverter/converter, PV, wind and hydro turbines, EVs are described in this chapter. The computer models were developed and simulated in the MATLAB/Simulink programme. In order to ensure the accuracy of the models, they were validated against experimental results, computer software (e.g. Fronius Solar Configurator, Wind Power Program) and commercial datasheets.

Chapter 5 discusses the simulation results of the impacts of SSDGs and EVs in both the UK network (urban area) and TH network (rural area). The power flow equation is used as guidance to analyse the voltage profiles at different buses in the distribution network. The Fast Fourier Transform (FFT) is used to analyse the harmonic spectrum.

Chapter 6 proposes the smart grid solutions and computer models developed in this thesis for SDSM, SOLTC, SEVGC, SCP, SES and SLC. These are described using control diagrams and flow charts and modelled using Boolean logic equations. The key to successful implementation of the proposed solutions is the use of smart meters to obtain the necessary information at the consumers' level and the central data bank, which allows the other smart controllers to retrieve necessary data. Proposals to deal with harmonics in future power network are also suggested.

Chapter 7 presents evaluation of the proposed solutions and demonstrate their effectiveness, The SDSM technique with smart meters, SOLTC, SEVGC, SCP, SES, SLC and harmonic solutions are implemented in typical MV/LV distribution networks of the UK and TH. Extreme scenarios (described in chapter 3) were chosen for this analysis.

Chapter 8 gives details of the computer modelling tool developed for PQ analysis of future power networks. This tool is used to investigate voltage profiles, active and reactive power flow in the distribution network by using MS Excel and MATLAB/Simulink programmes. This tool is useful for network operators and stakeholders to analyse the impacts of SSDGs, EVs/PHEVs and the effectiveness of smart controllers in future power networks.

Chapter 9 concludes the study of impacts of SSDGs and EVs/PHEVs and summaries the requirements and solutions to maintain voltage and harmonic profiles in existing and future power networks within acceptable limits. It should be noted that these solutions are developed based on existing guidelines and practices in order to ensure that they can be applied for existing distribution networks.

Appendix A presents the parameters of typical data of the UK and TH networks. MATLAB/Simulink schematic diagrams of the computer models and simulation networks are shown in appendix B. Appendix C gives the typical command (m-files) of the computer modelling tool (PSmartDN Tool). Appendix D presents a list of the author's publications.

CHAPTER 2
POWER QUALITY AND FUTURE POWER NETWORKS

2.1 Impacts of SSDGs and EVs/PHEVs on Power Networks

Future power networks, especially MV/LV distribution networks will face new challenges with regard to the reliability of supply and PQ due to large penetration of DGs/SSDGs and EVs/PHEVs. Mott MacDonald, [13] studied the impacts of large numbers of DGs on power networks and found that these will have significant effect on the quality of supply. The increased number of DGs can affect the voltage/frequency profiles, harmonic distortion, fault level (short circuit level) [24, 35]. This thesis is particularly focused on the impacts of SSDGs (mainly PV, wind and hydro turbines) on the MV/LV distribution networks in the UK and TH with ratings less than 5 kW for each unit. In practice, SSDGs usually employ grid interface power electronic devices with frequency and fault current limiting control [15-16, 24, 36]. Hence, the effect on frequency variation and fault level are not significant and these are not considered in this thesis. SSDGs are normally distributed in residential areas, therefore their impact is considered to be small compared to DGs with MW rating. That means the significant PQ problems in the distribution network due to SSDGs are voltage variation, transient voltage and harmonic distortion, which is similar to the EVs/PHEVs. The output power of SSDGs is mainly affected by the surrounding environment (e.g., solar radiation, wind speed and water velocity) and consumers' behaviour, which causes variation in demands.

As a result, there will be unavoidable variation in the bi-directional power flow and hence in the network voltage. Furthermore, transient voltage can happen due to connection/disconnection of large numbers of SSDGs and EVs/PHEVs at the same time. Consequently, the loss of central control can lead to difficulties in managing the quality of supply. In addition, grid interface devices of SSDGs and EVs/PHEVs could affect the harmonic profiles of the network, particularly when they operate at less than 10 percent of full rating [37-38].

A power quality problem is defined as any deviation of the voltage and current from nominal, which is capable of causing appliances to malfunction or preventing their use [35], [39-45]. The main voltage variation events are voltage sags and swells where the line voltage deviates from nominal values for a short duration, usually caused by connection of variable amounts of generation and/or starting/switching large loads (more details are given in appendix A). The other PQ problem that is investigated in this thesis is harmonic profiles in existing (passive) power networks, which were originally designed to deal with linear loads. However, as technologies are continually developed, non-linear loads have become the biggest share in the current loading of the network. Hence, the distortion in voltage and current waveforms arise from a perfect sinusoidal shape "Harmonic Distortion". It is important to note that the grid interface devices of SSDGs and EVs/PHEVs use power electronics converters to optimise their input/output power, and hence these can cause harmonic distortion in the network [37-38, 40, 46-47].

2.2 Voltage Variation Due to SSDGs

DGs/SSDGs can be beneficial in order to increase network reliability and provide backup power to the local area where they are installed. The DGs/SSDGs are connected close to the consumers and therefore they can reduce transmission losses [48-49]. However, DGs/SSDGs fundamentally change the nature of existing distribution networks because the surrounding environment directly affects their output power. For instance, the output of wind turbines is unpredictable due to variations in wind speed and direction and this can results in cyclic variation of electrical output power. A similar scenario can be applied to the PV regarding the solar radiation, which is also variable. However, this issue is not too problematic in hydropower system because the water velocity is more stable. Therefore, careful consideration is needed to investigate the impacts of DGs/SSDGs on the distribution network. Conti, Raiti and Tina, [50] described how typical traditional distribution networks are designed and operated based on centralised generation. Normally, the power flows in one direction from the generation units via the MV network to consumers on the LV network. That means the widespread implementation of DGs will affect the power flow, and hence the voltage profiles in the network. In addition, consumers' behaviour switching large loads can also cause large voltage variations in distribution networks (even without any DGs

connected into the network). References [51-59] showed that DGs could raise the local voltage levels outside acceptable levels. Consequently, to prevent this situation, network operator usually put a conservative limit on the rated power of DGs, particularly when the network voltage is close to the voltage statutory limits. Persaud, Fox and Flynn, [60] investigated the consumer demand in radial distribution feeders with remotely connected wind turbines by using a recursive, load flow based simulation algorithm and time series data. They found that the wind turbine and feeder characteristics determine the maximum capacity that can be allowed to operate in that area.

Jayaweera, Burt and Mcdonald, [61] showed that consumer damage cost can be caused by operating DGs without standing reserve. This is because operating DGs (e.g. wind turbine, etc.) can cause poor quality of supply, as it cannot meet the consumers' demand. In order to study the reserve to mitigate intermittency of wind turbine, they used Monte Carlo simulation, which incorporates linear programming-based re-dispatching of generation and load shedding to eliminate constraint violations. The scenarios considered are based on steady-state conditions incorporating intermittency of wind power and demand variations. The results show that increasing penetration levels of new and renewable energy in distribution networks can cause variations in system losses, voltage profiles, direction of power flow, fault levels, stability levels, and problems in coordinating protective relays (with possible combinations of overload and undervoltage, cascaded tripping, which may lead to a total or partial system collapse).

Quezada, Abbad and Roman, [62] show that penetration levels of DGs can be a new challenge for traditional electric power systems. They used the IEEE 34-node, test feeder computer model, which is based on the radial distribution networks, where the penetration level of DGs in each node was assumed to be proportional to the load demand at that node. As a result, the higher the penetration of DGs dispersed along the network feeders, the higher reduction in losses can be expected. However, it can be noted that localised large wind turbines have the worst behaviour in loss reduction [61].

The other interesting phenomenon to considers is the voltage variation when DGs are suddenly connected or disconnected, which can cause "Transient Voltage". This phenomenon can be clearly seen when a DG (operating at full load)

is suddenly connected or disconnected DGs [43, 63]. Dent, Ochoa and Harrison, [63] demonstrated the numbers and rating of DGs that can influence the step voltage change in power networks leading to the voltage or frequency exceeding the acceptable limits.

Therefore, the Optimal Power Flow (OPF) method has been used to determine the capacity of the network to accommodate distributed generation [63-67]. The analytical procedure is based on power flow study, which uses mathematical and linear formulation during steady state. It was found that the greater change in voltage levels happens when the DG has lagging power factor and either suddenly disconnect, connect or feed power back into the network. In this case, the active and reactive power flow contributions reinforce each other, whereas operation at leading power factor tends to alleviate both voltage and voltage step constraints. That means the point of connection of DGs has significant influence on the impacts on power networks. Therefore, network operators need to determine the point of connection for DGs, especially the DGs with high power rating.

It can be noted that SSDGs (from renewable energy resources) can improve the network capacity, but they can also cause voltage variation, as the output power of renewable is unpredictable. Then, developments in advanced renewable technologies require the advanced management to integrate into the power networks. Accordingly, distribution utilities are responsible for ensuring that the supply voltage must not change beyond acceptable levels, which are defined by national and international standards (e.g. IEEE-1159, IEE-1547, IEEE-519, IEEE-929, EN50160).

Jayaweera, Burt and McDonald, [61] suggested that adequate mean to accommodate DGs could be achieved by increasing investment in local controllers and network automation. This investment could have benefits in using DGs to improve reliability of the network and lower the operating cost through peak savings. Jovanovic, Hogg and Fox, [68] proposed an intelligent adaptive turbine controller where implemented a supplementary control signal on the speed control of turbo generator, which improved the quality of control of generator speed and power system frequency. Quezada, Abbad and Roman, [62] recommended that local controllers that manage power flow in a distribution network with DGs must implement real-time monitoring and control. Hence, the operation of DGs can

result in low losses and voltage variation if incorporated with reactive power controllers. Brooks, Dugan, Waclawiak, et al., [69] suggested the use of power quality index to measure the average variation (in RMS value) of voltage sags and swells on the LV network. Their results show that the number and duration of power interruptions can be reduced by using fast response controller for distributed generation.

Kiprakis and Wallace, [70] investigated the implications of increasing capacity of synchronous generators at the ends-user in rural areas. They examined the voltage variation due to realistic demands by using computer simulations and suggested two methods of compensation. Firstly, a set of rules for the DGs grid interface devices to constrain the voltage and power factor of DGs within the acceptable levels. However, this method can conflict with the operation of DGs during steady-state periods (constant voltage), if the setting is not correlated with the network equipment, which requires an experienced network operator. Secondly, the use of a Fuzzy inference system to adjust the reference setting of the automatic power factor controller in response to changes in the terminal voltage. The other suggestion is to use advanced controllers to preserve the voltage within limits, such as Flexible AC Transmission Systems (FACTS) devices. These are normally used to the regulate voltage and improve the system dynamic stability.

Cong and Wang, [71] studied a coordinated control of generator excitation and Static synchronous Compensator (STATCOM) controllers. They showed that generator excitation controllers are very helpful to stabilise the rotor angle/voltage regulation of a generator more than improve voltage variation in the network. Conversely, FACTS controllers' such as the STATCOM, can provide smooth reactive power and fast response. The scenarios are set up in dynamic models based on Real-Time Digital simulators (RTDs). Results presented show that the coordination of the generator excitation and STATCOM controllers can solve the dynamic voltage variation problems. However, these controllers cannot adequately compensate for high variation, e.g. sudden disconnection of a DG because existing generator excitation and STATCOM controllers have been designed to work separately. Indeed, many researchers have proposed solutions to compensate voltage variation, such as developing high-speed response

algorithms [72-78], advanced communication system [33-34], the use of FACTS technology and advanced power electronic devices [79-82].

This thesis proposes smart controllers (mainly SOLTC, SEVGC, SCP, SES and SLC) in order to monitor and control power flow in the network in, which DGs are connected. These controllers can coexist with the existing distribution networks controllers, support large deployment of SSDGs and EVs/PHEVs on the MV/LV distribution network, as demonstrated in chapter 7.

2.3 Voltage Variation Due to EVs/PHEVs

The use of electricity for transport appears to be the most appropriate strategy for clean energy and future demand [83-84]. Therefore, technologies for electricity transportation are being developed to meet the user requirements such as EV charging instrument, improved battery capacity, low-cost material, etc. [85-86]. Furthermore, EVs/PHEVs can reduce the emissions of gases in transportation system if they are powered from renewable energy sources. Cook, [87] reported that private (passenger) car is largest part in the transportation sector. Hence, the Department of Energy and Climate Change, [11] defined the trend of transport development in 2050 in the UK into three different categories; travel activities, change in technologies and change in efficiency. It showed that government policies, development in green technologies and education would influence the development of transportation and penetration levels of EVs/PHEVs in 2050. It anticipated that about 31 percent of the passenger cars (which is fully petrol driven vehicles) would be replaced by EVs/PHEVs in 2020 [10] and about 80 percent by 2050 [11].

Therefore, this thesis focuses on the private EVs/PHEVs and their significant deployment in the future, as it is considered as the biggest share in the transportation system and causes unpredictable bi-directional power flow in the power networks. This can in addition result in violation of the voltage statutory limits [88]. EVs/PHEVs can operate as mobile active loads that increase the demand on the network during charging, and as generators when operating in Vehicle-to-Grid (V2G) mode whenever they plug in into the network. Koyanagi, Inuzuka, Uriu, et al., [89] studied the impact of demand of fast chargers of EVs/PHEVs by using Monte Carlo simulations. It is claimed that the charging of

EVs/PHEVs batteries has the potential to cause problems to the distribution network. Hence, it is necessary to investigate the impacts of penetration levels of EVs/PHEVs on the distribution network.

Salihi, [90] investigated the requirements for EVs/PHEVs charging and their impact on the distribution networks. The case studies conducted focused on the EVs/PHEVs plugged in residential areas where different the penetration levels of EVs/PHEVs and charging durations were considered. Results show that EVs/PHEVs can be accommodated with careful power management by employing advanced control devices. In fact, with appropriate control and communication to the grid, EVs/PHEVs could be used to reduce the difference between demand in peak and off-peak periods. For instances, charging of EVs/PHEVs at night can act as a reservoir for surplus network energy without extra investment [91]. That means interface devices of EVs/PHEVs may be designed to minimise or even eliminate some of the effects of EVs/PHEVs on the network. This means that EVs/PHEVs may be operated as part of a smart grid to provide ancillary services such as supply/demand matching and voltage/frequency control. This is one of the proposed solutions in the thesis regarding SDSM technique using smart meters incorporated with smart controllers to match supply/demand, as described in chapter 6.

It can be summarised that significant number of SSDGs and EVs/PHEVs can affect the voltage variation in the power network, especially in the MV/LV distribution network. The output power of SSDGs depends on the surrounding environment in each area including the connection of EVs/PHEVs based on the consumers' behaviour. Furthermore, the connection/disconnection of large numbers of EVs/PHEVs at the same time is considered similar to connecting/disconnecting a large load, which will of course cause the high values of step voltage. In addition, the daily demand of consumers' can cause the voltage variation as can be clearly seen in winter and summer. Lastly, the weakest buses in the existing distribution network need to be investigated as they can cause significant PQ problems.

As the thesis is concerned with the distribution network of the UK in urban areas and TH in rural areas, the impacts of SSDGs and EVs/PHEVs are investigated. Hence, the small-scale PV, PMG for wind and hydro turbines, which support reactive power in the power networks, were chosen. It is important to note that these green technologies are normally connected directly on either MV or LV distribution networks, as shown in Figure 2.1. Therefore, the power quality problems are often encountered since significant penetration levels of SSDGs and EVs/PHEVs are continually deployed into the distribution network without an appropriate management of power flow, causing voltage variation and harmonic distortion.

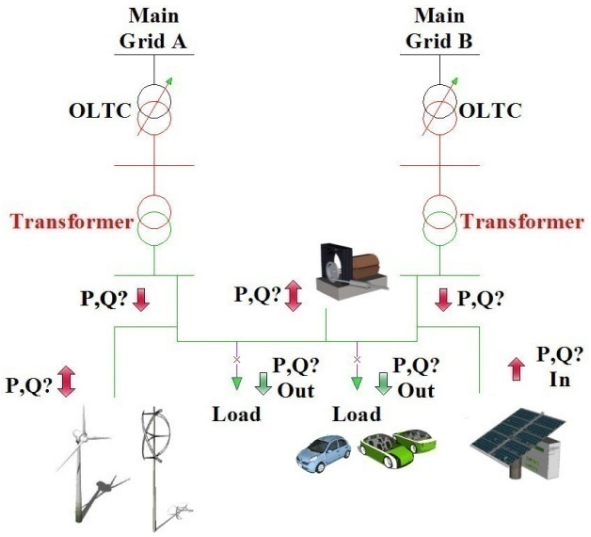

Figure 2.1 Green technologies deploy in typical distribution networks

Therefore, in order to understand the voltage profiles between buses, power flow equations are considered. The simple explanation of power flow of SSDG, which is connected at the far end of the LV feeder of a basic radial distribution network, is described in Figure 2.2.

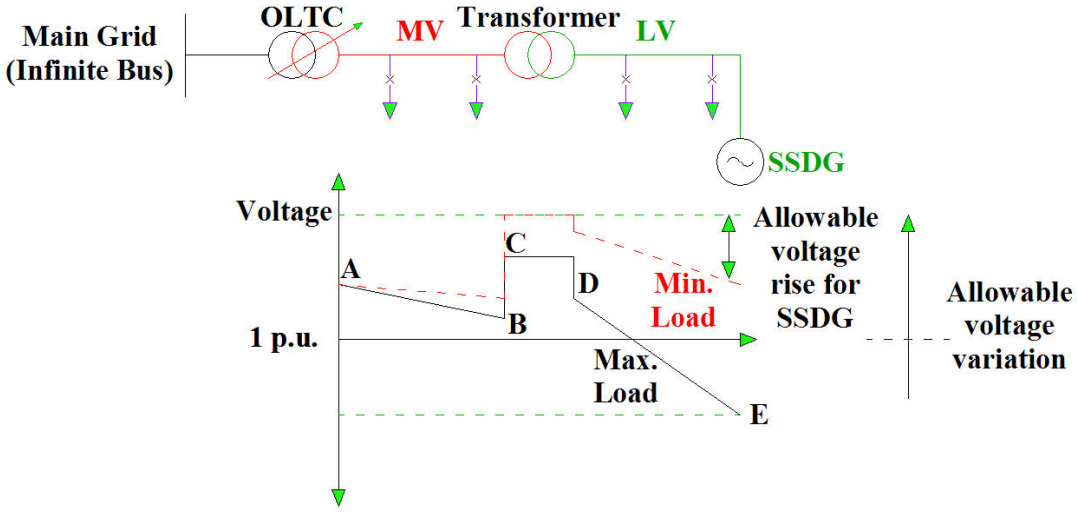

Figure 2.2 Voltage variations due to SSDG in the basis radial distribution network

The voltage at SSDG bus (shown in Figure 2.2) may exceed the statutory limits if the transmission capacity and LV transformer ratio (off-load taps changer) are unsuitable. Then, the most remote consumer would receive the acceptable voltage during minimum load demands. On the other hand, the sending voltage is sometimes below the minimum voltage statutory limit when the network experiences maximum demands. Then, the On-Load Tap Changer Transformer (OLTC) attempts to maintain the voltage at point A at the reference value. However, the voltage between points A and B is gradually decreasing due to the loads connected to the MV transmission. The voltage is raised up again due to the transformer ratio of the off-load tap changer transformer (continuous black line) and it is affected by the SSDG (dash red line) and consumers' behaviour, which can be seen in the regions B to C. From points C to D, the voltage drops slightly because of the MV/LV transformer impedance. The voltage region between points D to E (in LV transmission) decreases dramatically because the residential consumers are connected. These can be explained by the approximate voltage change (ΔV) equation as follows:

$$\Delta V = \frac{(PR+XQ)}{V} \tag{2.1}$$

Where,

P = Active power flow (W)

Q = Reactive power flow (VAR)

R = Resistance of the network (Ω)

X = Inductive reactance of the network (Ω)

V = Nominal voltage of the network (V)

The approximate voltage change equation (ΔV) can be derived with reactance to the network shown in Figure 2.3

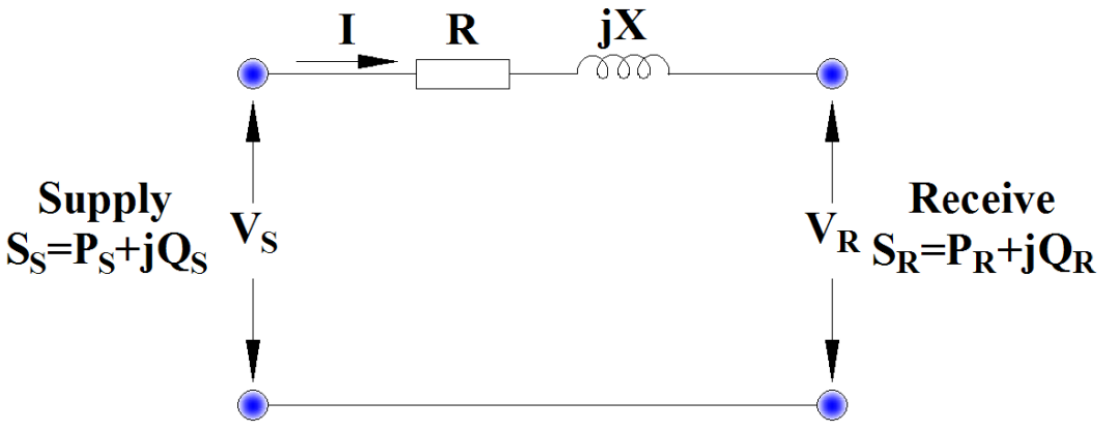

Figure 2.3 Equivalent circuit of power flow in basis power networks

Where, S_S is the apparent power at the supply, S_R is the apparent power at the receiving end, P_S describes the active power at the supply, P_R is the active power at the receiving end, Q_S represents the reactive power at the supply, Q_R is the reactive power at the receiving end, V_S is the voltage at the supply and also V_R is the voltage at the receiving end. The apparent power at the receiving end is:

$$\boldsymbol{S} = \boldsymbol{V_R I^*} = P + jQ \tag{2.2}$$

Where, V_R is the reference $(V_R \angle 0^{\circ})$. Then,

$$I = \frac{P - jQ}{V_R} \tag{2.3}$$

So, the V_S is:

$$V_S = V_R + (R + jX)\left(\frac{P - jQ}{V_R}\right) \Rightarrow V_S = V_R + \left(\frac{RP + XQ}{V_R}\right) + j\left(\frac{XP - RQ}{V_R}\right) \tag{2.4}$$

Thus,

$$\Delta V = V_S - V_R \Rightarrow \Delta V = \left(\frac{RP + XQ}{V_R}\right) + j\left(\frac{XP - RQ}{V_R}\right) \tag{2.5}$$

Therefore, the approximate voltage change (ΔV) and the angular shift (δV) equations are:

$$\Delta V \approx \left(\frac{RP + XQ}{V_R}\right) \text{ And, } \delta V \approx \left(\frac{XP - RQ}{V_R}\right) \tag{2.6}$$

In distribution networks, the impact of the line resistance is significant. However, in transmission systems, $\frac{X}{R}$ ratio of transmission line is normally high, and therefore the impact of the line resistance is very small and may be neglected (in transmission network). This allows RP term in equation (2.6) equal to zero. Hence, in order to investigate an approximate power transfer in the transmission line, the relationship of ΔV due to the impedance of the transmission line that affects the power transfer in the distribution network can be summarised as follows:

$$\Delta V = \left(\frac{XQ}{V_R}\right) \text{ Hence, } \Delta V \propto Q \tag{2.7}$$

Therefore, the relative change in reactive power due to the voltage variation $\left(\frac{\partial Q}{\partial V_R}\right)$ is:

$$Q = \frac{V_S V_R - {V_R}^2}{X} \Rightarrow \frac{\partial Q}{\partial V_R} = \frac{V_S - 2V_R}{X} \tag{2.8}$$

From the equation (2.8), it can be noted that a slight change of inductive reactance (X) in the network is affecting the change of reactive power. That means the network also requires a monitoring and controlling systems for reactive power in order to balance active and reactive power. This can be done by reactive power compensation such as provided by capacitor banks, FACTS devices, etc. This compensator could be connected in parallel with the supply. In the mean time, the

reactance in the network is a function of network infrastructure and the number of transmission lines that meet at the node. The power transfer in a transmission line equation can be expressed by the use of angular shift as follows:

$$\delta V = \left(\frac{XP}{V_R}\right) \text{ Therefore, } \delta V \propto P \tag{2.9}$$

It can be noted that the angle of transmission (δ) is:

$$\delta = sin^{-1}\left(\frac{XP}{V_R}\right) \tag{2.10}$$

Also, the δ between V_S and V_R is:

$$\delta = sin^{-1}\left(\frac{\delta V}{V_S}\right) \tag{2.11}$$

Where,

$$sin\delta = \left(\frac{\delta V}{V_S}\right) \Rightarrow sin\delta = \left(\frac{1}{V_S}\right)\left(\frac{XP}{V_R}\right) \tag{2.12}$$

Therefore, the power transfer through a network (P) is:

$$P = \left(\frac{V_S V_R}{X}\right) sin\delta \tag{2.13}$$

2.4 Islanded Networks

The other event that is worth considering when analysing the impacts of DGs is islanding operation or an intentionally islanded network. Islanding operation is the term used to describe the operation of a distribution network section with one or more DGs isolated from the main network and still supplying power to local consumers at voltage and frequency within acceptable limits whilst ensuring personnel safety [49]. This operation can increase the reliability of power supply, if it would be allowed in the future, as appropriate technologies are developed. However, islanding operation is currently not allowed due to safety and difficulties to maintain the voltage, frequency and fault levels within acceptable limits [92]. Figure 2.4 shows a typical network where a fault occurs at the 11 kV feeder and the main circuit breakers on the 11kV feeder trip to protect the low level network and allow it to operate in islanding mode with the local DGs [93-95].

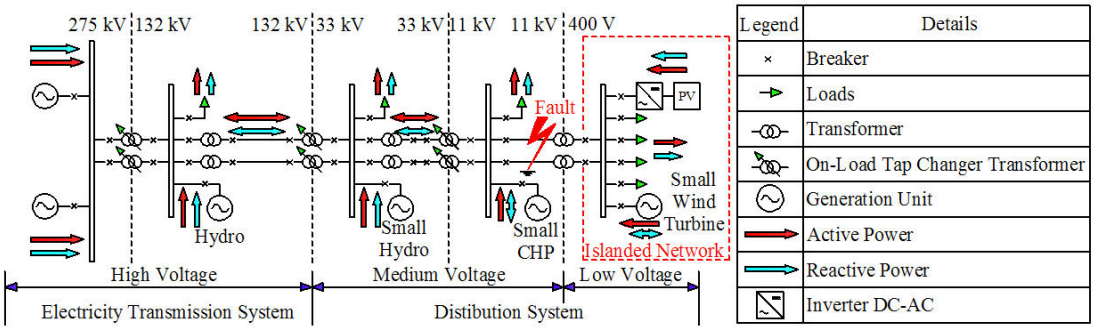

Figure 2.4 Islanded network in a typical distribution network

It is known that connecting SSDGs in existing distribution networks usually increase the SCL in the network. However, the SCL in an islanded network decrease significantly due to the loss of the main supply. Hence, it is important to understand the relationship between the SCL and power flow in order to describe the operation of DGs in an islanded network.

The short-circuit current (I_{SC}) in a power network with ignoring the effect of network resistance can be reduced in form from Figure 2.3 and described as:

$$SCL = \frac{{V_S}^2}{X} \tag{2.14}$$

It can be noted that for HV system X of transmission is much higher than R. Then, under normal loading conditions, V_S is approximately equal to V_R. Hence,

$$SCL = \frac{{V_R}^2}{X} \tag{2.15}$$

The relative ΔV across the line in Figure 2.3 may be expressed as:

$$\frac{\Delta V}{V_R} = \left(\frac{RP+XQ}{V_R}\right)\left(\frac{1}{V_R}\right) \tag{2.16}$$

Therefore, the relationship between SCL and the relative ΔV across the line may be given as:

$$\frac{\Delta V}{V_R} = \left[\left(\frac{RP}{V_R}\right) + \left(\frac{XQ}{V_R}\right)\right]\left(\frac{1}{V_R}\right)\left(\frac{X}{X}\right) \Rightarrow \frac{\Delta V}{V_R} = \left[\left(\frac{RP}{V_R}\right)\left(\frac{1}{V_R}\right)\left(\frac{X}{X}\right) + \left(\frac{XQ}{V_R}\right)\left(\frac{1}{V_R}\right)\left(\frac{X}{X}\right)\right] \tag{2.17}$$

The relative ΔV across the line in term of the SCL can be explained as:

$$\frac{\Delta V}{V_R} = \left(\frac{X}{{V_R}^2}\right)\left(\frac{RP}{X} + Q\right) \Rightarrow \frac{\Delta V}{V_R} = \left(\frac{1}{SCL}\right)\left(\frac{RP}{X} + Q\right) \tag{2.18}$$

Let R in equation (2.18) is equal to zero, then $\frac{\Delta V}{V_R}$ is:

$$\frac{\Delta V}{V_R} = \frac{Q}{SCL} \Rightarrow \frac{V_S - V_R}{V_R} = \frac{Q}{SCL} \tag{2.19}$$

Hence,

$$Q = \left(\frac{V_S - V_R}{V_R}\right)(SCL) \Rightarrow Q = \left[\left(\frac{V_S}{V_R}\right) - \left(\frac{V_R}{V_R}\right)\right](SCL) \tag{2.20}$$

Therefore, the reactive power with SCL term in the power network is:

$$Q = \left(\frac{V_S}{V_R}\right)(SCL) - (SCL) \tag{2.21}$$

In practice, the feedback of reactive power into the existing distribution networks is a proportional function of $\frac{\partial Q}{\partial V_R}$ as explained in equation (2.8). That means the greater value of $\frac{\partial Q}{\partial V_R}$, the more reactive power feedback is reversed to be injected into the network in order to maintain the voltage levels. However, the relative change in the voltage due to variation in reactive power with SCL term is:

$$\frac{\partial Q}{\partial V_R} = -\left(\frac{V_S SCL}{{V_R}^2}\right) \tag{2.22}$$

Again, under on-load condition, V_S is equal to V_R, hence

$$\frac{\partial Q}{\partial V_R} = -\left(\frac{SCL}{V_R}\right) \tag{2.23}$$

It can be clearly seen that the SCL is a function of $\frac{\partial Q}{\partial V_R}$ where the significant change of V_R is an inversely proportional function of $\frac{\partial Q}{\partial V_R}$. Then, the greater the value of $\frac{\partial Q}{\partial V_R}$ the less received voltage in the islanded network.

Therefore, in an islanded network, the voltage and frequency may fluctuate, which is caused by the reduce SCL and excursion of active and reactive power flow when the generator is disconnected from the grid. The DGs need to be adequately controlled in order to maintain the system voltage and frequency within acceptable limits by using an Automatic Voltage Regulator (AVR) and governor, as shown in Figure 2.5 [93-95]. Northern Ireland Environment Link, [96] reported that the response of DG controllers is a crucial key to manage power flow in the network. The report also suggested that a fault must be cleared by the system protection within 200 ms in order to maintain network control and ensure personnel safety.

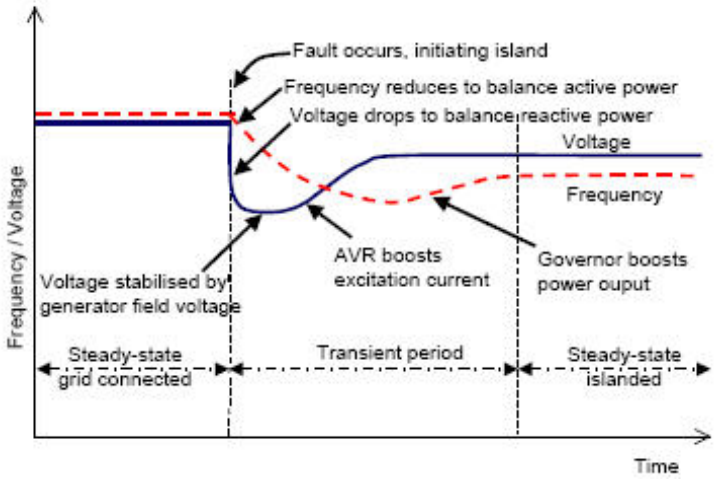

Figure 2.5 Response of voltage/frequency of DG in an islanded network [95]
Source: Econnect Ltd. (2005)

The problems of islanded operation of a network are voltage/frequency control and safety hazard in addition to transient during disconnection and reconnection to the main grid [49]. Because of the loss of main network, DG units may not be grounded properly and therefore the grounding connection for an isolated system using DGs will of course mostly be defined by the loads (consumers'). This can result in voltage imbalance, which may also affect the distribution transformer as no zero-sequence currents flow in the system.

Therefore, it is essential to ensure that the grounding connection for isolated units is maintained [97]. When the network supply is restored, the DGs need to be resynchronised to the network, then it needs to ensure that the isolated units have the same grounding connection as the main network. Another significant safety hazard of islanded network is the need for changing protection relays setting (due to change of SCL) [98-99]. The existing protection system setting may malfunction because the fault current in an islanded network is not as high as when connected to the main network.

In order to allow islanding operation, the control system must handle the power variation of DGs. That means the controller system must have fast response to detect islanding or abnormal situation. References [100] and [101] suggested that DGs must include advanced power electronics controllers to provide the fast power exchange with the power network. This control should be dynamic and may be used to control output power; frequency voltage and provide harmonic damping [15-16, 36, 48]. Sontidpanya, Radman and Craven, [48] used a Laboratory sized power Grid (LabGrid) as a practical model for investigating islanding phenomenon in the power network. Results show that then DGs need appropriate control to balance the voltage/active power and maintain the voltage within statutory limits.

Vandoorn, Renders, Degroote, et al., [102] suggested that a well designed droop control of DGs and demand dispatch technique can allow large numbers of DGs to operate in an islanded micro grid. In addition, the rate-limit for real power set-points can be done by the Proportional Derivative (PD) phase difference controller and Proportional Integral Derivative (PID) governor [103]. These allow changing the real power set-points of DGs without introducing a frequency disturbance thus, the phase deviation is decreased. Saha, Chowdhury, Chowdhury, et al., [104] suggested that the fast response control could be achieved by using the communication in the island to control the dynamic setting of DGs.

Best, Morrow, Laverty, et al., [103] recommended that a control strategy that provides load sharing via communications is required to allow DGs to operate in islanded network, particularly those at remote nodes, with the smart control [105]. It is important to note that the only smart controllers of DGs alone cannot achieve the supply/demand matching in islanded networks. Hence, other smart controllers become necessary in islanded networks, such as the SOLTC, SEVGC, SCP, SES

and SLC proposed in this thesis. These devices use fast estimation algorithms to match the dynamic responses of compensation systems in order to avoid severe unbalances in the power network. Network control can also be supported by using demand side management and power storage systems, which are part of the concept of smart grids.

Invernizzi, [106] analysed the technical impacts of widespread adoption of DG and the improvement of rural electricity supply by using small-scale low cost technologies with low environmental impact (e.g. renewable and distributed generation). Results showed that the demand side management can be used to manage power flow in the network. Costabeber, Tenti and Mattavelli, [100] proposed a control approach in which narrowband communication between neighbour units only (in an islanded network) is used, which holds even in the presence of multiple feeding points from the utility. As a result, the units that operate in an islanded network receive multiple signals, thus complicating data management. This problem can be alleviated by using the SDSM techniques incorporated with smart meters and control devices to update the necessary signal via a central data bank, which is proposed in this thesis.

Paredes, Costabeber and Tenti, [107] proposed a fast control algorithm based on Conservative Power Theory to control an islanded network. This technique used to detect the presence of non-sinusoidal waveforms in an islanded network, and hence is allowing the compensator to operate. Shang and Redfern, [97] suggested that the main key to successful operation of smart grids to operate as an islanded network is the management of the output power of DGs in the islanded network by minimising the delivery loss in real power and ensuring that the supply voltage is within the limits. Moreover, DGs must have smart controllers to operate during normal and islanded modes. For instance, the controller is set as slave control during normal mode and independent voltage and frequency control during islanding mode. It is important to note that the location of DGs and capacitor banks, which are located in the islanded network, need to be considered in order to define the proper location to connect smart controllers [108].

Best, Morrow, Laverty, et al., [109] studied the detection and state of an islanded network, which develops from an unintentional islanding. They proposed a management technique for synchronous islands by using the supervisory controller to optimise loads in the islanded network. This supervisory controller identified the islanded DGs by monitoring variation in voltage and phase angle. Once the island is identified, control functions can begin by considering the following factors [49, 92, 110-111].

1) Remote Circuit Breaker (RCB) are needed into all MV/LV buses to ensure personnel safety in the power network (e.g. loss of main or cable fault at any load feeder) where they also provide data to a central data bank. Either active detection (e.g. pulse/echo), passive detection (e.g. impedance measuring, vector surge, frequency gradient) detection-method or the coordination of a series of measures can be used to specify the islanded network, which depends on the tripping signal from RCB or the measurement from passive/active detections.

2) The isolated DGs in the islanded network must include controllers that allow an islanding operation in order to maintain voltage and frequency control.

3) Allow load shedding management in the islanded network in order to match supplies/demands in the islanded network. Hence, high speed detection and fast response of load shedding management that handle the over frequency and low voltage of the isolated DGs and loads are required.

4) Consider the voltage, phase angle, frequency and neutral/earth grounding connection while reconnecting the islanded network back to the main network. This can be done by using synchronised-phasor measurements and Phase Lock Loop (PLL) control, which are used to perform reconnection. The main network provides the reference signal.

5) Appropriate standards and regulations will be required in case of parallel operation of the isolated DGs.

It can be concluded that the main problems of islanding operation are voltage/frequency control and protection. Recently, most modern DGs are integrated with smart controllers in order to maintain their terminal

voltage/frequency within the limits. Hence, this thesis proposes the use of SDSM technique to support both DGs and EVs, which can handle the power imbalance in islanded networks by managing the demand and voltage profiles of the islanded network.

2.5 Harmonic Distortion

Over the years, power electronics devices are increasingly used in residential, commercial and industrial appliances. Most of these equipments behave as non-linear loads and often have low power factor e.g. television, air conditioning unit, etc. [40, 112-114]. These devices (called "Distorting Loads") draw a non-sinusoidal current and change the waveform of the supply voltage from an ideal sinusoidal waveform. High frequency components are multiples of the supply frequency and the ratio of the harmonic frequency to the supply frequency is called the "Harmonic Order" (more details in appendix A). In power networks, generation and demand always change and consequently the frequency of harmonic disturbances change [53, 93-94, 115].

A significant factor that affects the harmonic distortion in a power network is the interaction between consumers' devices and the impedance of the supply network. An important problem that results from harmonic distortion in distribution networks is system resonance between the inductive and capacitive impedances in the network at the harmonic frequency. In fact, power networks have source impedances, which are highly inductive, in order to constrain the flow of current. Then, the increasing of high frequency harmonic currents results in a proportional increase of the inductive reactance and reduction of capacitive reactance (e.g. Power Factor Correction capacitors; PFC). A small harmonic current with a frequency around the resonance value can cause the high voltage/current in the power network. For instance, if the supply bus has a fault level 500 MVA and a capacitor bank has a rating 4 MVA, then harmonic order 11^{th} has the highest chance to produce resonance and threaten any nearby non-linear devices on the network, which produce the same harmonic order (here is order 11^{th}). The harmonic order at resonance can be expressed by:

$$Harmonic\ Order = \sqrt{\frac{\text{Fault Level}}{\text{Rating of Capacitor Bank}}} \tag{2.24}$$

Then,

$$Harmonic\ Order = \sqrt{\frac{500}{4}} \Longrightarrow Harmonic\ Order \approx 11 \quad (2.25)$$

Harmonic distortion in power networks can cause extra heating losses (I^2R) in devices (e.g. feeder, transformers, motors, etc.) and could interfere with the communication and measurement systems because most meters and sensors are traditionally designed to operate with an ideal sinusoidal waveform. The presence of harmonics can also affect control and protection systems (particularly when resonance conditions occur) e.g. false tripping of protective relays. Furthermore, it can cause the mechanical vibration in machines, when the natural frequency of the mechanical system excites the shaft vibration and results in either noise pollution or a damaged machine.

Currently, grid interface devices of DGs include power electronic devices in order to optimise their output power and synchronise to the grid [116]. In the same way, those battery charger controllers of EVs usually use switching control devices to manage power flow during charging/regenerating modes. In the current market, EV chargers usually employ bridge rectifiers or advanced power electronic systems with Pulse-Width Modulation (PWM) [36]. These are non-linear devices and may cause high frequency harmonics and transients, which feed into the network and degrade PQ of the network [37-38, 117-119]. Wang, O'Connell and Brownfield, [120] analysed the voltage distortion caused by two types of non-linear loads; EVs chargers and Variable Speed Air-Conditioners (VSAC). They found that the limit of Total Harmonic Distortion (THD) of voltage could easily to be exceeded when the highly non-linear loads are connected to the distribution feeder.

Much research has been conducted on the characteristics of different types of EV chargers (individual and/or group connection), the location of connection point, penetration levels of EVs and the capacity of the network and transformers [121-131]. Results obtained show that the widespread of EVs charging may affect the power system components such as transformers and feeders.

CHAPTER 3
DEMAND AND GENERATION PROFILES

The demand for electricity depends on consumers' behaviour and the type of loads connected, such as air conditioning, EVs and SSDGs. Future power networks will incorporate renewable energy resources together with EVs/PHEVs, and hence variations in demand and generation profiles will be more difficult to predict. The EVs/PHEVs may be considered as active mobile loads, as they can be plugged anywhere in the network, and may be operated in charging or V2G mode. This will result in bi-directional power flow in the power network. Hence, it is important to investigate the requirements to optimise power flow in future distribution networks. To achieve this, realistic parameters of existing distribution networks were chosen. Typical distribution networks in the UK and TH have been selected together with realistic case study that reflects the network structure, daily load and generation profiles of extreme seasons (winter and summer).

3.1 Demand and Generation Profiles for the UK Distribution Networks

The daily load profiles for the UK distribution networks are shown in Figure 3.1, based on After Diversity Maximum Demand (ADMD) referenced to a nominal 100 consumers and measured at a distribution substation level of the outgoing feeder [13]. This daily profiles vary throughout the year, due to seasonal variations in particular demands, e.g., space heating results in a higher demand in winter.

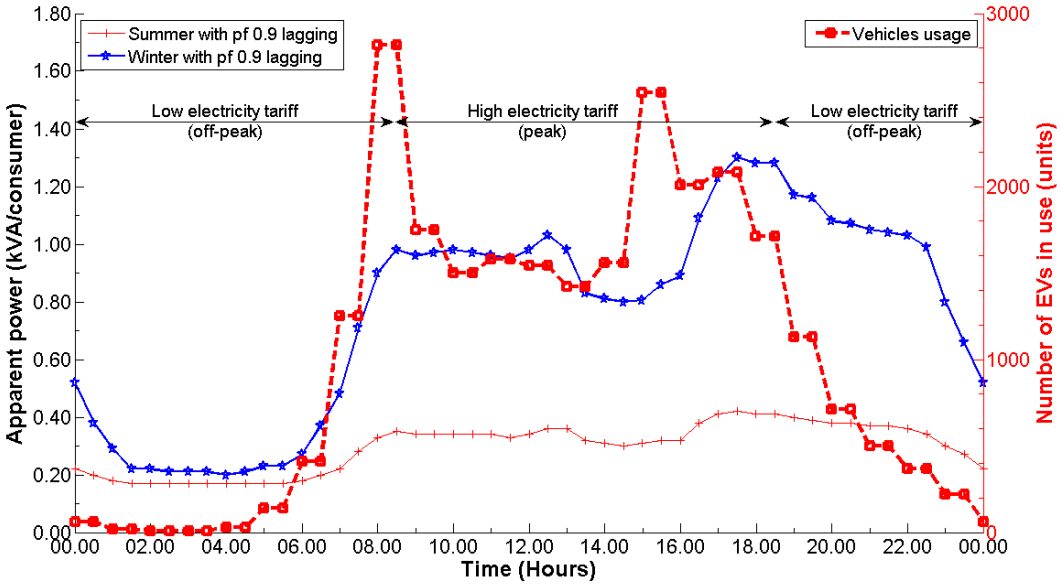

Figure 3.1 Average daily ADMD in the UK distribution networks

Figure 3.1 also shows that the electricity demands in the UK have a saw tooth pattern where most electricity usage is in the daytime (approximate 08.00-22.00) and the lowest usage of electricity is in the late night (approximate 22.00-07.00). About 3000 samples of EVs/PHEVs were used to estimate the hour usage of private vehicles in the UK, which results in the M pattern of daily usage, as shown in Figure 3.2 [132]. Accordingly, the daily availability of EVs/PHEVs for possible connection to grid is shown in Figure 3.2.

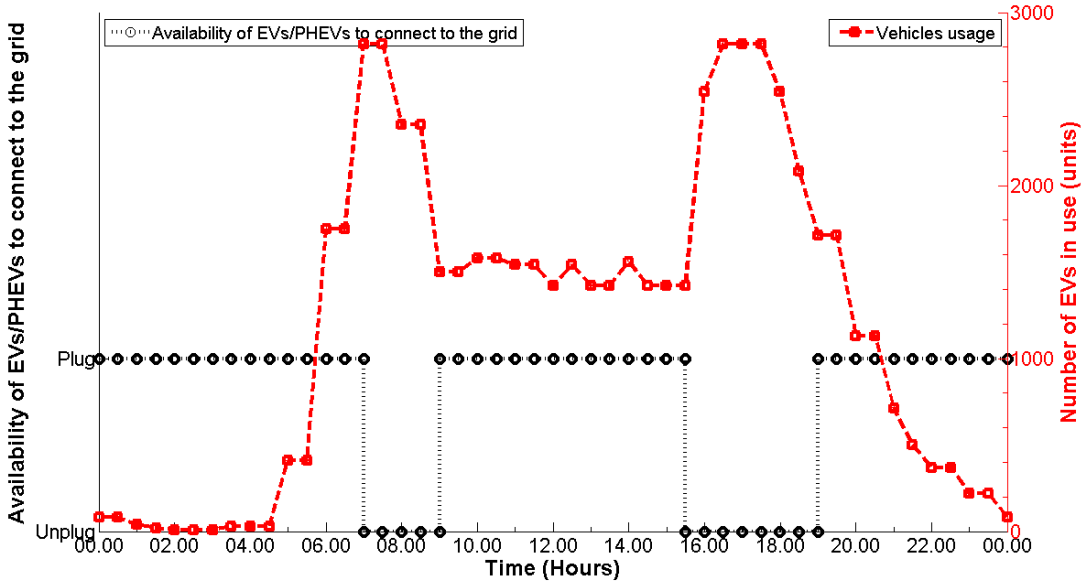

Figure 3.2 Average daily usages of private vehicles in the UK

The available connection time and connection time allowances of EVs/PHEVs need to be considered in order to define their demand profile. In weekdays, private EVs/PHEVs are not available for either absorbing or supplying electrical energy at the morning and evening rush hours (approximate 07:00-09:00 and 17:00-19:00). Currently, public parking of EVs/PHEVs allows charging only 4 hours during 08.30-18.30, whereas “Anytime Charging” is allowed in car parks, as shown in Figure 3.3. Standard 3 kW domestic chargers that use 6 to 8 hours (here considers 6 hours) for recharging is also considered [13]. Therefore, the extreme scenarios selected for EVs/PHEVs connection into the UK networks are identified by using daily electricity demand and generation profiles, EVs/PHEVs charging time, connection time allowance in public/private areas, electricity tariffs and consumer behaviour, as presented in Table 3.1. It is important to note that the EVs/PHEVs owners’ are willing to connect their vehicles in V2G mode where the connection tariff is high (during the peak demand).

Figure 3.3 Connection time allowances of EVs/PHEVs in public parking and car park

Table 3.1: Connection time of EVs/PHEVs in the UK distribution network

	Worse scenario
EVs/PHEVs operate in	Charging mode 19.00–01.00
	Regenerating mode 13.30–15.30

The generation profiles of PV, small-scale wind and hydro turbines in the UK are shown in Figure 3.4 [133-134]. It should be noted that United Kingdom Generic Distribution System (UKGDS), [133] proposed these generation profiles in per unit, hence base power is given here for a typical generation rating of 4 kW, [135]. In addition, the generation profiles of wind turbine are supported by Narec Company, which is given in the terms of wind speed [134]. It is important to note that all generation profiles are considered to be average annual data.

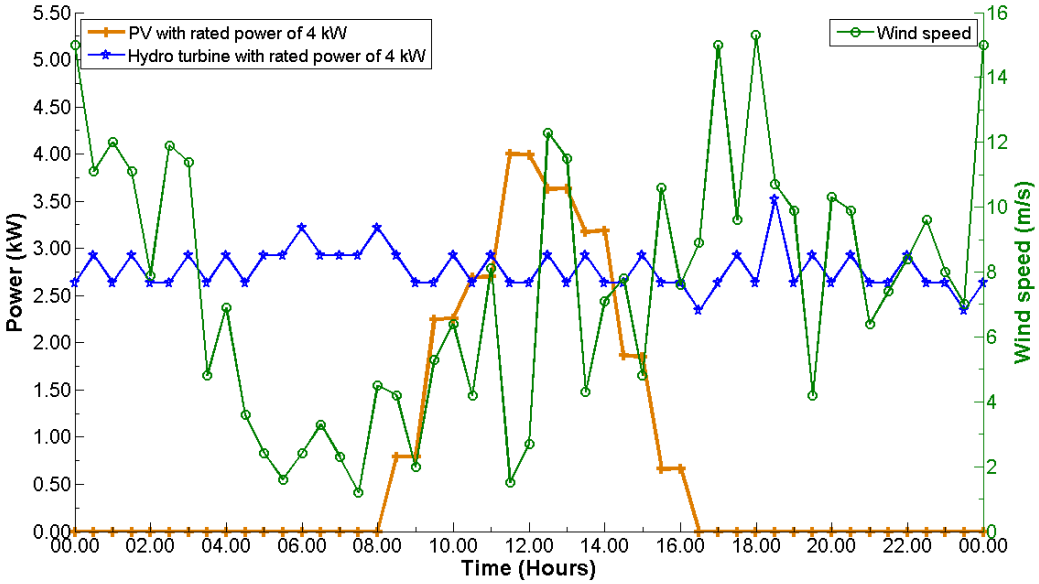

Figure 3.4 Average generation profiles of PV, small-scale hydro and wind turbines in the UK

From the generation profiles in the UK, it can be seen that the PV has the highest potential generation during the daytime, whereas the generation profile of wind turbines is intermittent. The generation profile of hydropower system generally steady as compared to PV and wind systems.

3.2 Demand and Generation Profiles for the TH Distribution Networks

This section presents the demand and generation profiles in the distribution networks in TH. The highest electricity demand in TH mostly occurs in summer due to the use of air conditioning. The daily profiles of community area in rural area of TH are based on ADMD referenced to a nominal 297 consumers in summer and 205 consumers in winter whilst the daily profiles of countryside (out skirt) area in rural area of are based on ADMD referenced to a nominal 191 consumers in summer and 154 consumers in winter [17]. Both community and countryside areas profiles measured at a distribution substation on an outgoing feeder, as shown in Figure 3.5. It is interesting to note that these daily electricity demands for community area have the M pattern because the TH government proposed energy saving policies during lunch break (approximate 12.00-13.00). Moreover, the highest electricity usage is most likely during morning until evening (approximate 08.00-00.00) and the lowest usage is in the early morning (approximate 00.00-07.00).

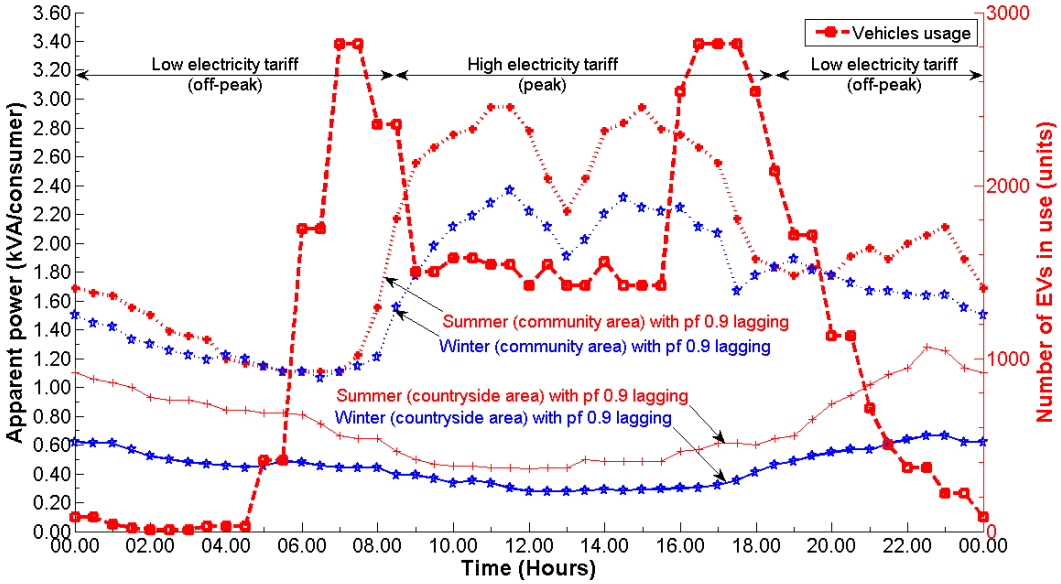

Figure 3.5 Average daily ADMD of small consumers' in the TH distribution network

The infrastructure power network of TH here includes large domestic loads, such as public buildings (which include many government institutes and universities) thus, the daily demands are also presented. Figure 3.6 presents the service hours of government institute and university in TH and it shows that the service hours usually start from 08.00 in the morning until 15.30 in the afternoon where the energy saving policies are used during lunch break. Hence, the demand pattern is similar to the small consumers, which has the M pattern. The average demand in the winter is defined by a nominal 50 consumers while, the summer is referenced to a nominal 68 consumers [17].

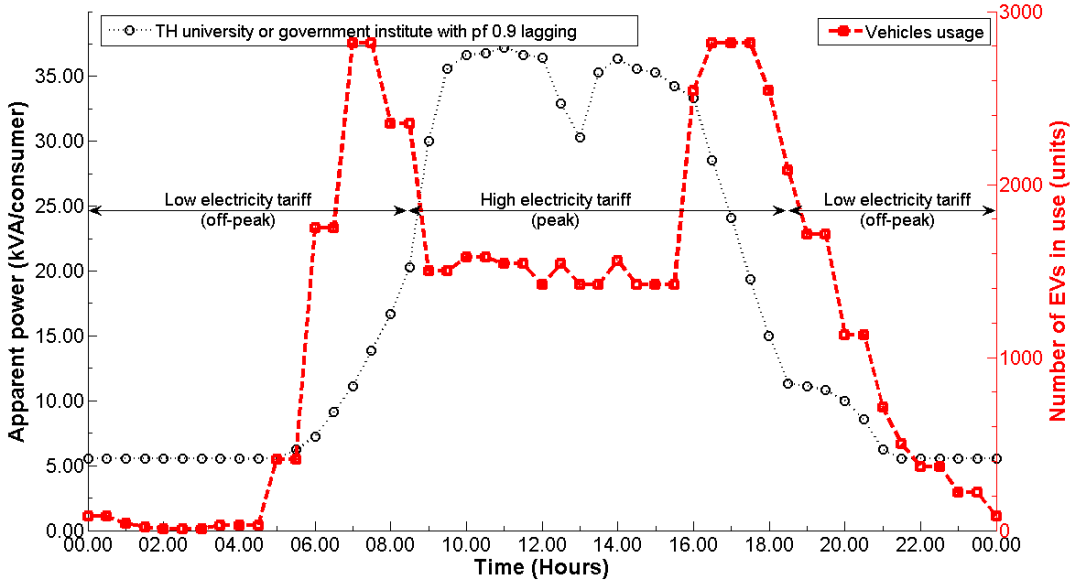

Figure 3.6 Average daily ADMD of large consumers' in the TH distribution network

In order to investigate the impacts of EVs/PHEVs in TH, the available connection time and the connection time allowances of EVs/PHEVs need to be taken into account. It is important to note that the connection time allowance in TH is assumed similar to the UK due to insufficient information of EVs/PHEVs in TH. The Ministry of Transport (MOT) in TH, [136] studied the hour usage of private vehicle during the weekday in TH based on 3000 samples. Results show that private vehicles are most likely to be used during the rush hours period, which is usually between 05:30-08:00 and 15:30-19:00, as shown in Figure 3.7.

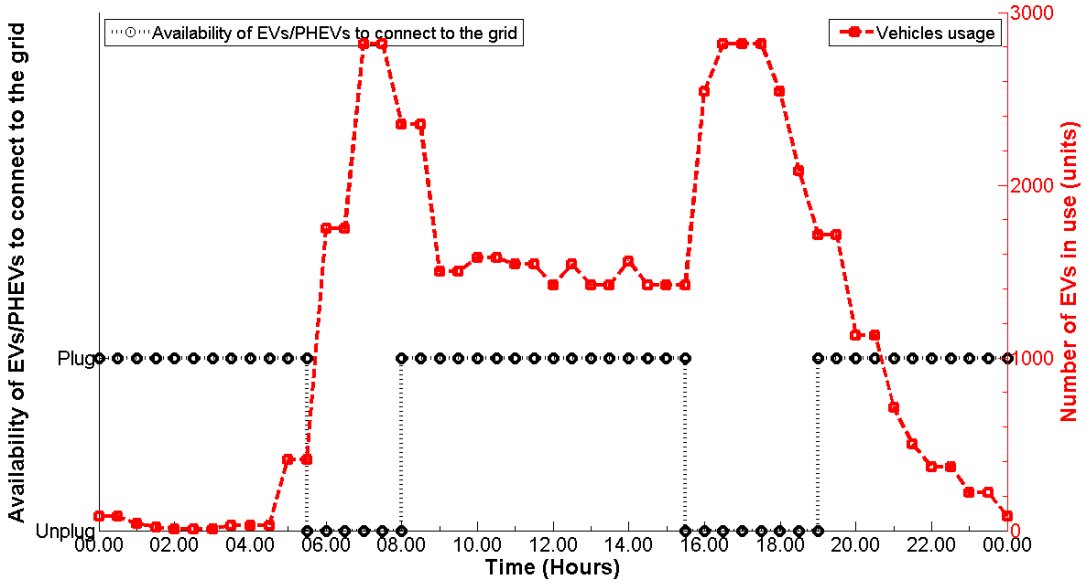

Figure 3.7 Average daily usages of private vehicles in TH

Based on the above, similar to those used for scenarios in the UK are selected for the TH network, as presented in Table 3.2.

Table 3.2: Connection time of EVs/PHEVs in the TH distribution network

	Worse scenario
EVs/PHEVs operate in	Charging mode 20.00–02.00
	Regenerating mode 11.30–13.30

Figures 3.8 and 3.9 show average generation profiles of PV, small-scale wind and hydro turbines in TH [137]. It can be clearly seen that these generation profiles are similar to the generation profiles in the UK. It can be noted that the generation profile of hydropower system is steady, whilst PV has the highest potential generation during the daytime and wind turbine has more fluctuation.

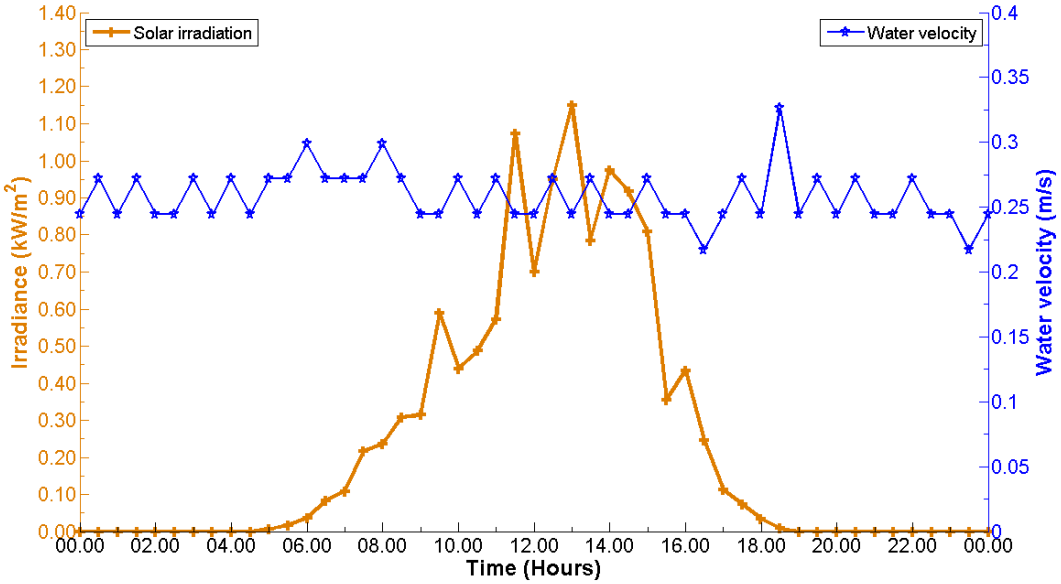

Figure 3.8 Average generation profiles of PV and small-scale hydro turbine in TH

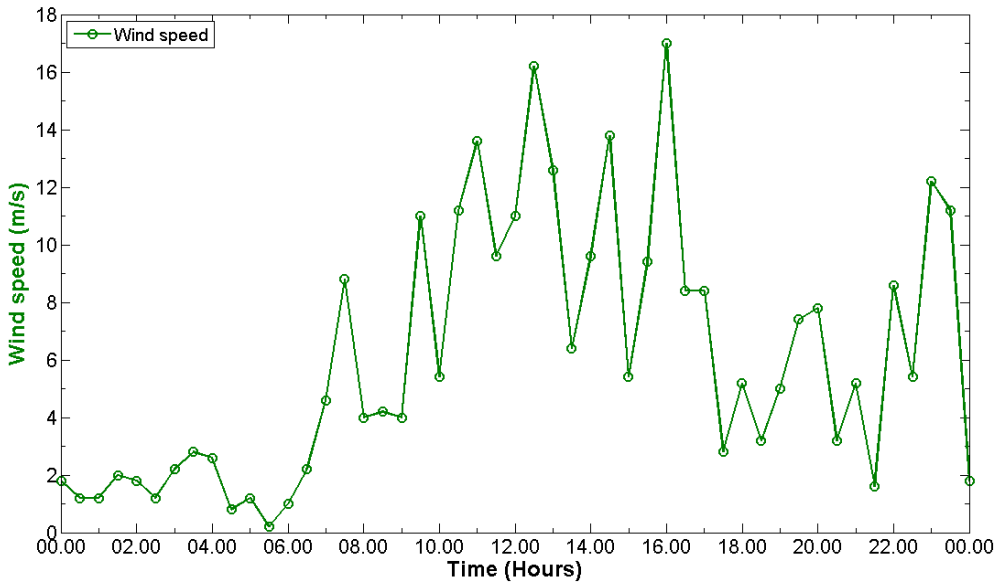

Figure 3.9 Average generation profiles of small-scale wind turbine in TH

3.3 Scenarios Considered for the UK and TH Distribution Networks

Extreme demand and generation profiles for the UK and TH were used for the analysis and the scenarios selected based on types of network (urban area based on the UK network and rural area based on the TH network). A single line diagram of a typical distribution network in the UK is shown in Figure 3.10, where a 33 kV grid supply (has a three-phase short-circuit level 500 MVA) is connected to a 33/11.5 kV substation (shown in Figure 3.10). The 33/11.5 kV substation

contains two 33/11.5 kV OLTCs, each rated at 15 MVA. This substation supplies six 11 kV outgoing feeders and each 11 kV feeder supplies eight low voltage distribution substations. All low voltage substations contain an 11/0.433 kV off-load tap changer transformer, rated at 500 kVA. Details of the network feeders are given in Table 3.3.

Table 3.3: Details of the UK distribution network feeders

Type	Conductor	Ohm (Ω)/km	Henry (H)/km	Remark
185mm XLPE	CU	0.1280	0.000289662	3-core
95mm XLPE	CU	0.2470	0.000318310	
240 CNE	AL	0.1258	0.000218042	Combine neutral and earth
120 CNE	AL	0.2533	0.000218042	
70 CONSAC	AL	0.4430	0.000224408	Changed to Wavecon, CNE or SNE

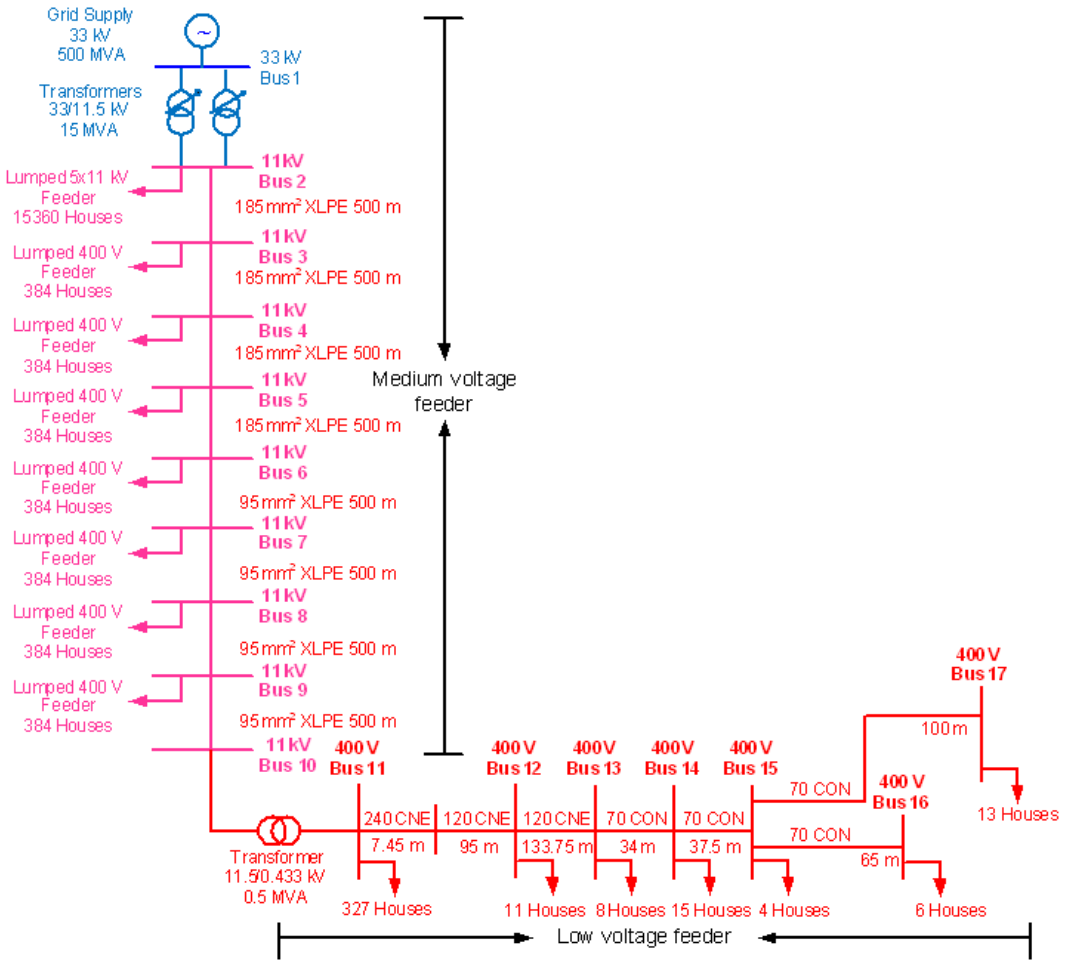

Figure 3.10 Typical distribution networks in urban area in the UK

The single line diagram of a distribution network in rural area in TH is shown in Figure 3.11. The TH network is supplied from the grid at 69 kV and has a three-phase short-circuit level of 484 MVA. It directly supplies power into a 69/22 kV substation with OLTC, rated at 30 MVA. A grounding transformer is also provided (at bus 1) to reduce fault level and harmonics. The outgoing feeders of the substation supply two low voltage substations (22/0.4 kV). The low voltage substations each contain a 22/0.4 kV off-load tap changer transformer, rated at 5 MVA. Details of the TH network feeders are given in Table 3.4.

Table 3.4: Details of the TH distribution network feeders

Type	Conductor	Ohm (Ω)/km	Henry (H)/km	Remark
185mm XLPE	CU	0.1280	0.000289662	3-core
240 CNE	AL	0.1258	0.000218042	Combine neutral and earth
120 CNE	AL	0.2533	0.000218042	

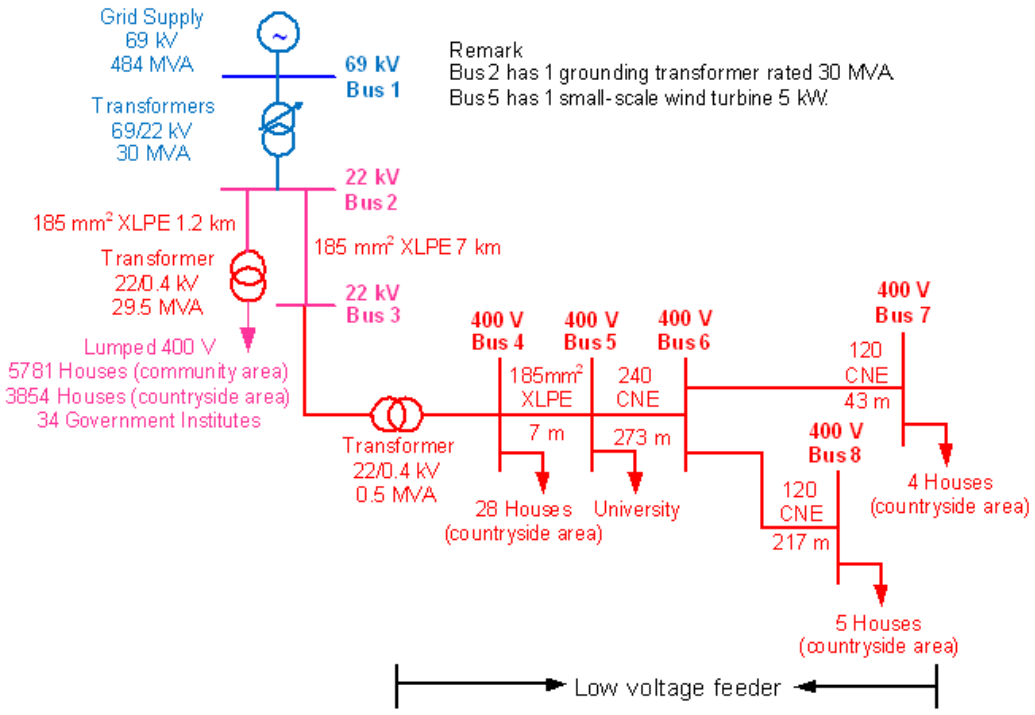

Figure 3.11 Typical distribution networks in rural area in TH

Scenarios considered in this thesis are selected based on existing standards and regulations (e.g. IEEE standard, EN standard, G83/1, G59/2) to ensure that the analysis is realistic. Table 3.5 presents the extreme scenarios that allow analysing the impacts of SSDGs (mainly PV, wind and hydro turbines) and EVs/PHEVs, including identifying the potential requirements to successfully manage power flow in future power networks. The EVs in both the UK and TH networks operate in charging and V2G mode from either Tables 3.1 or 3.2, which base on the network. The penetration levels of SSDGs and EVs/PHEVs as forecasted for 2020, which includes 7.49 percent for PV, 2.54 percent for hydro turbine, 1.78 percent for wind turbine and 31 percent for EVs/PHEVs are considered in order to ensure the scenarios are close to those in a realistic power network [10, 13]. It must be noted that the percent penetration level in this thesis depends on the consumers' at each bus, not the total number of consumer in the network. To ensure that the number of SSDGs and EVs at each bus is a positive integer, the decimal number of SSDGs and EVs is rounded off. For instance, if bus 4 in the TH network (shown in Figure 3.11) has PV 7.49 percent of 28 consumers then only 2 consumers will install small-scale PV system.

Table 3.5: Scenarios for the UK and TH distribution network analysis

Scenario		Description	Aims
1	1.1	Uniformly distributed EVs (operating in charging and V2G modes, as given in Tables 3.1 or 3.2), PV or small-scale of wind/hydro turbines. Each is applied with increased penetration levels in 5 percent per step until the voltage profiles reaches the voltage statutory limits (excluding bus 5 in the TH network, which has a single EVs car park with 10 parking slots).	Define the limits for penetration levels for each scenario and the combination of green technologies that may be connected into existing distribution networks (assuming uniform distribution).
	1.2	Same as scenario 1.1, but a combination of the four types of green technologies are considered instead of individual type.	
2	2.1	Same as scenario 1.2, except that the voltage control signal of the OLTC is changed from the local OLTC bus to the bus at the far end of the MV feeder.	Investigate the effects of changing the OLTC reference voltage control signal (active power control).
	2.2	Same as scenario 1.2, except that the voltage control signal of the OLTC is changed from the local OLTC bus to the bus at the far end of the LV feeder.	
3		Same as scenario 1.2, but with penetration levels of SSDGs and EVs as forecasted for 2020.	Investigate likely voltage profiles of future power networks in 2020 (assuming uniform distribution).
4	4.1	UK and TH networks localised SSDGs and EVs close to the OLTC (at bus 2 for the UK and TH networks) with penetration levels as forecasted for 2020. For the TH network, a single EVs car park with 10 parking slots is also connected at bus 5.	Investigate the combined impacts of non-uniform distribution of SSDGs and EVs.
	4.2	Same as scenario 4.1, except SSDGs and EVs are moved to the LV bus, close to the LV transformer substation (at bus 11 for the UK network and bus 4 for the TH network).	
	4.3	Same as scenario 4.1, except the SSDGs and EVs moved to the far end of the LV feeder.	
5	5.1	EVs car parks with 200 units each are connected at buses 7, 8 and 9 of the UK network. The TH network has a single EVs car park with 96 parking at bus 2 and 10 parking at bus 5. Both the UK and TH networks have distributed SSDGs and EVs with penetration levels as forecasted for 2020 (excluding the buses with EVs car park).	Investigate the effects of EVs car parks on the weakest buses (assuming connect at the far end of either the MV feeder or LV feeder).
	5.2	Same as scenario 5.1, except a single EVs car park with 30 parking is connected at the far end of the LV feeder in the UK and TH networks instead of EVs car park with 200 and 96 parking slots.	
6		EVs car parks with 200 parking each are connected at buses 7, 8 and 9 of the UK network. The UK network also has a single EVs car park with 30 parking and a small wind turbine farm with 50 kW at the far end of the LV feeder. The TH network has three EVs car parks with 96 parking, 10 parking and 30 parking at buses 2, 5 and 8, respectively. The TH network also has a small PV farm with 48 kW at the far end of the LV feeder. Both the UK and TH networks have distributed SSDGs with penetration levels as forecasted for 2020 (excluding the bus at the far end of the LV feeder).	Investigate voltage profiles of future power networks in 2020 (assuming non-uniform distribution). Identify the weakest buses in existing distribution network where the voltage or thermal capacity limits could be exceeded.

In order to analyse the effectiveness of the proposed smart controllers on network operation in islanding mode, scenario 6 from Table 3.5 was selected, as it has a small farm of SSDGs (with total generation of 48 to 50 kW at the far end of the LV feeder), which increases the chances of operating in islanding mode. In scenario 6, a three-phase fault that has the highest SCL is chosen and applied at the far end of the MV feeder (at bus 10 for the UK network and bus 3 for the TH network) during the highest demand and generation profiles in the winter for the UK network and in the summer for the TH network. In addition, the highest demand and lowest generation profiles are also considered in this scenario. The line service is interrupted for 15 minutes (out of 30 minutes investigation period) and this has significant effects on the residential area. Table 3.6 presents details of a scenario to investigate the voltage profiles without the smart controllers in the islanded network (results shown in section 5.2). The impacts of smart controllers in islanded network analysis scenario 1 from Table 3.6 are given in section 7.2. In order to investigate the effectiveness of the smart controllers in the islanded networks (scenario 2 from Table 3.6), the existing OLTC is replaced by the proposed SOLTC. Moreover, a single SES rated at 1.6 MW is included at the far end of the LV feeder of the UK network and 0.8 MW for the TH network. Lastly, each load in the detailed LV feeder is assigned a priority number so that the SLC can appropriately manage the loads in the islanded network.

Table 3.6: Scenarios for islanded network analysis

Scenario		Description	Aims
1	1.1	Same as scenario 6 from Table 3.5, except a three-phase fault is applied at bus 10 in the UK network and bus 3 in the TH network, and line service is interrupted for 15 minutes during the highest demand and generation profiles.	Investigate the voltage profiles in islanded network without smart controllers.
	1.2	Same as scenario 1.1 from Table 3.6, but for highest demand and lowest generation profiles.	
2		Same as scenario 1.1 from Table 3.6, except a single SCP with 200 parking is connected at buses 7, 8, 9 and a single EVs car park with 30 units is connected at the far end of the LV feeder in the UK network. For the TH network a single SCP with 96 parking, a single EVs car park with 10 parking and 30 parking at bus 2, 5 and at the far end of the LV feeder, respectively (results showed in section 7.2). All smart controllers operate in independent mode.	Demonstrate the effectiveness of SDSM and smart controllers to manage the voltage profiles in order to allow islanding operation.

To investigate the harmonic profiles in distribution networks, grid interface devices of SSDGs and EVs based on PWM and IGBT technologies are considered. In practice, the switching frequency of PWM applications for SSDGs (e.g. inverter, converter) varies between 10 kHz (for SSDGs) and 1 kHz (for large DGs) [138] and for EVs/PHEVs chargers is less than 2 kHz [37]. A computer model of PWM applications is developed under the EN50160 standard in order to ensure that the individual harmonics are within acceptable limits. In order to examine the effects of applying diversity of inverters and chargers to the system, it was evident that the most pronounced effects would be measured where the system is weakest (here at the far end of the LV feeder). Initially, inverter and charger models were connected to the weakest buses in the system models, and the current harmonic distortion was measured via FFT analysis at the input to the relevant substation. Then, other inverter and charger models were applied in parallel. The performance of SSDGs operating with PWM converters between 0 to 10 percent of full rating and the State of Charge (SOC) of EVs batteries were taken into account. Table 3.7 describes the scenario used for harmonic analysis.

Table 3.7: Scenario for analysis harmonic distortion

Scenario	Description	Aims
1	Distributed SSDGs and EVs with penetration levels as forecasted for 2020 during maximum demand. A details model of single-phase inverters with PWM is connected to each section of the LV network. The scenario is carried out during low solar irradiation and low wind speed where EVs/PHEVs operate in charging mode.	Analyse the THD of combined effects of SSDGs and EVs distortion.

CHAPTER 4
SYSTEM MODELLING

This chapter presents details of the computer modelling, which includes distribution networks of the UK and TH, inverter/converter, PV, PMG for wind and hydro turbines and EVs. MATLAB/Simulink programme was chosen, as it includes several tool blocks, which allow flexible modelling in both steady and dynamic states. The computer models are developed by a combination of Simulink block sets (e.g. logic and bit operation block, lookup table, signal routing, etc.) and SimPowerSystem block sets (such as transformers, electrical sources, etc.) and MATLAB command (m-file). The iterative technique based on the Newton Raphson method allows analysis of power flow in the network and the FFT technique is used to study the harmonic profiles. It is important to note that this programme also provides the continuous and fixed step calculations accordingly; the speed of computation simulation is increasing. The MS Excel and MATLAB/Simulink programmes are used together to develop the computer modelling tool (PSmartDN Tool), as explained in chapter 8.

4.1 Modelling of Distribution Networks for the UK and TH

The computer simulation of the UK network, the supply nominal voltage is set to 33 kV (ph-ph V_{RMS}) and the three-phase short circuit level is 500 MVA whilst those for the TH network are set to 69 kV and 484 MVA, respectively. Both the UK and TH networks have distribution transformer with OLTC type DY1 feeding from the 33 kV or 69 kV networks. Both countries have frequency at 50 Hz. The nominal transformer ratio of the OLTC in the UK network is 33/11.5 kV and 69/22 kV for the TH network. The OLTC is performed by eight series regulation winding (tapped winding) for each phase. A reversing switch inside the OLTC allows reversing connections of the regulation winding. Therefore, the OLTC operates with 17 taps; eight positive (eight additive positions), eight negative (eight subtractive positions) and zero positions, which provides the nominal transformer ratio. The response time of tap changer is 8 sec per tap and this is defined by the OLTC controller. The voltage regulation of the OLTC is a function of the transformer ratio and has specified dead zone.

Typically, the dead zone of the OLTC (DZ_{OLTC}) can be expressed as:

$$DZ_{OLTC} = (2)(\text{StepVoltage}) \quad (4.1)$$

Where,

StepVoltage = Step voltage per tap (per unit)

Therefore, the voltage regulator of the OLTC orders further voltage boosting and stabilises the voltage within a maximum voltage error (which is equal to StepVoltage), and hence the maximum and minimum permitted voltage of the OLTC is given as:

$$V_{ref} - \left(\frac{DZ_{OLTC}}{2}\right) < V < V_{initialtapposition} + \left(\frac{DZ_{OLTC}}{2}\right) \quad (4.2)$$

Where,

V_{ref} = Reference voltage for the OLTC (per unit)

$V_{initialtapposition}$ = Voltage at initial tap position (per unit)

The UK network includes two parallel OLTCs rated at 15 MVA. The voltage step of the OLTCs is ±0.0167 per unit where it is determined by the percent voltage deviation and the number of steps of the OLTCs. The step voltage is linked to the upper and lower limits of the system medium voltage 11 kV, which is ±6 percent. That means the OLTCs operates between 0.8664 per unit (28.5912 kV) and 1.1336 per unit (37.4088 kV) for 33 kV. Moreover, DZ_{OLTC} of the OLTCs is set at 0.025 per unit (due to the infrastructure of the UK network) and the voltage reference at the voltage regulator is set at 1 per unit, which results in maximum and minimum voltage errors per tap changing of 0.9875 per unit < V< 1.0125 per unit. Conversely, the TH network has a single OLTC with 30 MVA rating and a step voltage of the OLTC of ±0.0263 per unit (due to the infrastructure of the TH network). This step voltage is linked to the upper and lower limits ±6 percent at 22 kV. This is in addition to operate the OLTC in the TH network between 0.7895 per unit (54.4755 kV) and 1.2105 per unit (83.145 kV) for the 69kV. Furthermore, DZ_{OLTC} of the OLTC in the TH network is set at two times step voltage (which is 0.0526 per unit) and the voltage reference at the voltage regulator is set at 1 per unit, and hence the voltage error of tap changing is kept between 0.9736 per unit < V< 1.0263 per unit.

4.2 Modelling of Inverter/Converter System

Nowadays, many types of inverter/converter are connected into power networks in order to optimise input/output power of AC/DC devices (e.g. DGs, EVs/PHEVs, AC/DC load, etc.). For this reason, an optimised design of advanced power electronics is required. This thesis investigates power flow in power networks, which is influenced by the inverter/converter performance (e.g. the Maximum Power Point Tracking control, MPPT), as shown in Figure 4.1.

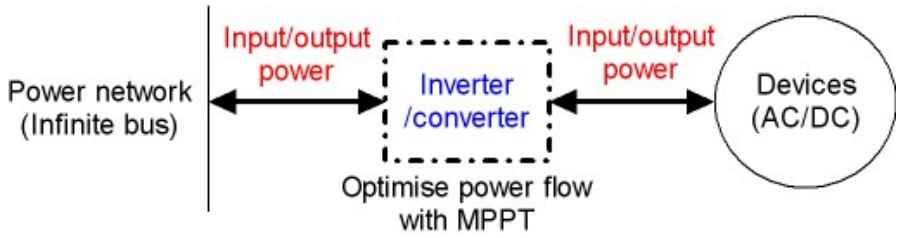

Figure 4.1 Inverter/converter optimise power for connection devices

The use of MPPT control of inverter/converter systems may reduce the energy consumption because the inverter/converter is usually designed to achieve high efficiency [139]. In this thesis, to simplify the inverter/converter model, the Interpolation-Extrapolation technique is considered to duplicate the actual efficiency curve of conversion performance of the inverter/converter. This is a main key to successfully developing a simplified computer model, which is needed in this research. Häberlin and Borgna, [140] claimed that modelling of the actual performance of MPPT requires complicated system thus most of simulation programme usually assume that the inverter/converter operates at the Maximum Power Points (MPP). As, the input/output power of an inverter/converter impact could be expressed with a conversion efficiency function [139, 141-143], this leads to a simpler model of a complex inverter/converter, which supports various types of inverter/converter and provide relatively fast and computationally less demanding simulation.

In practice, the efficiency of an inverter/converter is usually defined at 10, 20, 30 50, 75 and 100 percent of rated output power. Therefore, an Interpolation technique can be used to define the values between efficiency points (e.g. between 0 to 10 percent, 10 to 20 percent, etc), which is a function of the array input and within the array limits. It should be noted that the Extrapolation technique is normally used to define the values that are out of the array boundaries for the input. Consequently, it commonly uses a nearby function to define an

approximation of the linear and quadratic functions of polynomial that apply in the small region. This section aim to achieve the simplified inverter/converter model for power flows study thus a linear interpolation/extrapolation was chosen accordingly, it is sufficient to duplicate the curve of inverter efficiency, which is usually close to linear.

The efficiency data can be considered as an array function in a Simulink programme [144]. In addition, the programme also provides the 1-D look-up table block, which has the capabilities of linear interpolation/extrapolation techniques, and then the significant points of actual measurement of inverter/converter efficiency can be assigned in the look-up table block. The proposed inverter/converter model was validated against practical results as given in references [145] and [146]. In references [145] and [146], the inverter performance was measured by decreasing the load resistance in order to match the 10, 20, 30 50, 75 and 100 percent of rated output of inverter. Figure 4.2 demonstrates the efficiency data at 10, 20, 30 50, 75 and 100 percent of inverter models for SSDGs, which include Fronius IG Plus 50 V-1 for PV 4 kW, WINDYBOY 5000-US for wind turbine 5 kW and typical inverter for hydro turbine 5 kW. The efficiency data of Fornius and WINDYBOY were taken from practical experiment [145-146]. In addition, the efficiency data of a typical 5 kW inverter was collected by experiment, which is connected to power resistors 6 kW (12 paralleled metal blade resistor, each with a rating of 0.5 kW), and hence the DC input power and AC output power were measured. The experiment was carried out 5 times with the same setting in order to ensure the error is minimised. Table 4.1 presents the equipment details of a set inverter experimenter in laboratory.

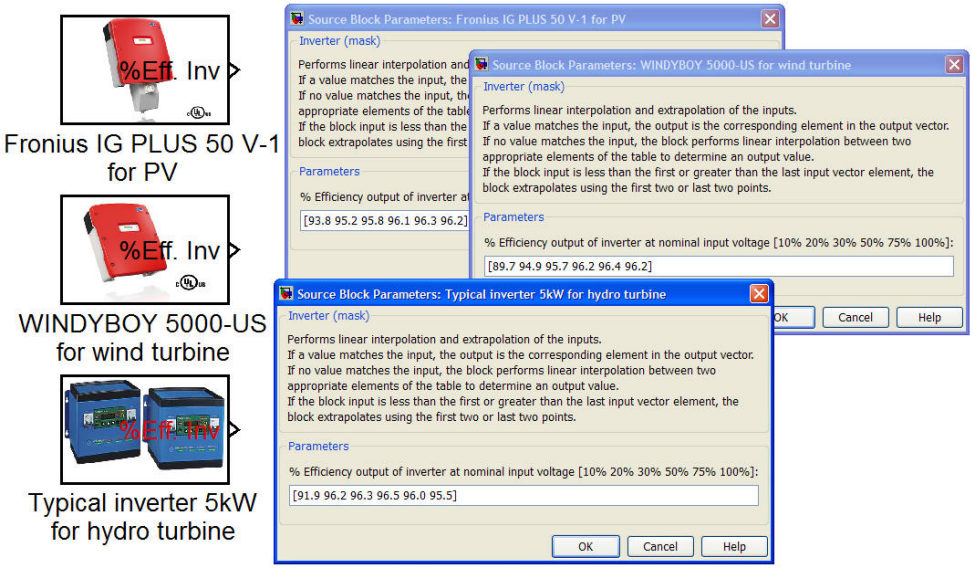

Figure 4.2 Input functions of the proposed inverter/converter computer model

Table 4.1: Equipment details of inverter experimenter

Equipment	Model	Units	Remark
Inverter 5 kW	Typical inverter	1	n/a
Multi meter	Fluke 115	2	AC accuracy ±1% and DC accuracy ±0.5% of reading range with 3 digits[147]
Power resistor	22 Ω	12	Pulse power rating 0.5 kW[148]

Source: [147-148]

Figures 4.3 to 4.5 demonstrate that the percentage efficiency of the inverter (η_{Inv}) for SSDGs as a function of rated output power of proposed models is similar to that of the practical inverter.

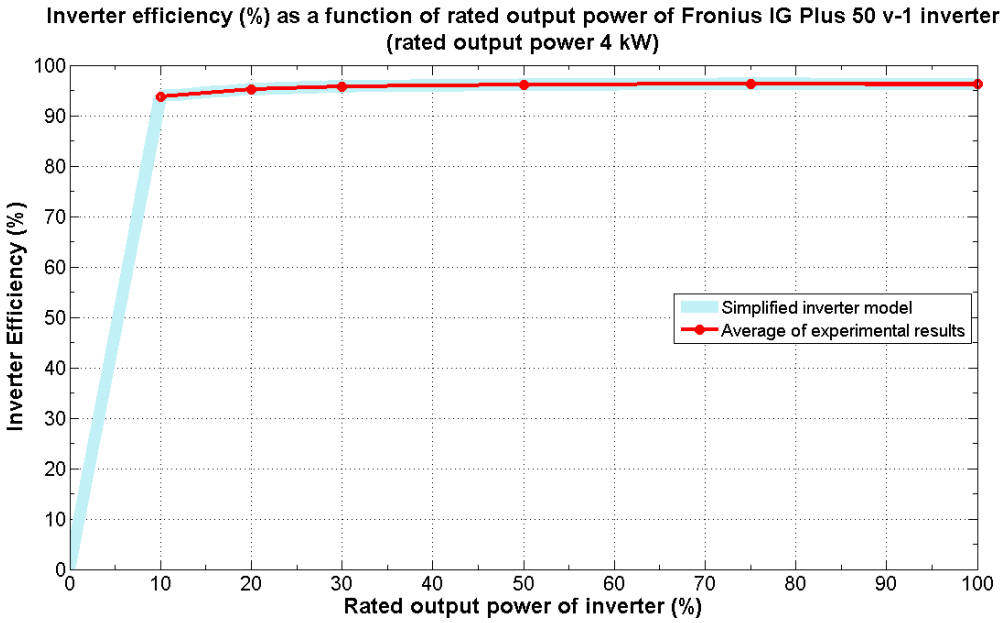

Figure 4.3 Comparison percent efficiency of output power of PV Inverter

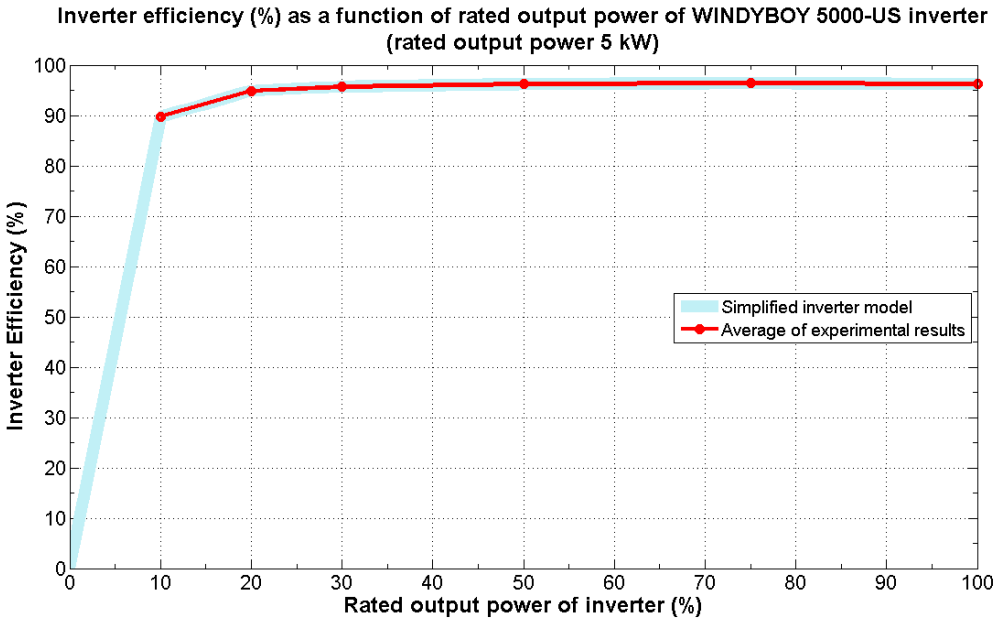

Figure 4.4 Comparison percent efficiency of output power of wind turbine Inverter

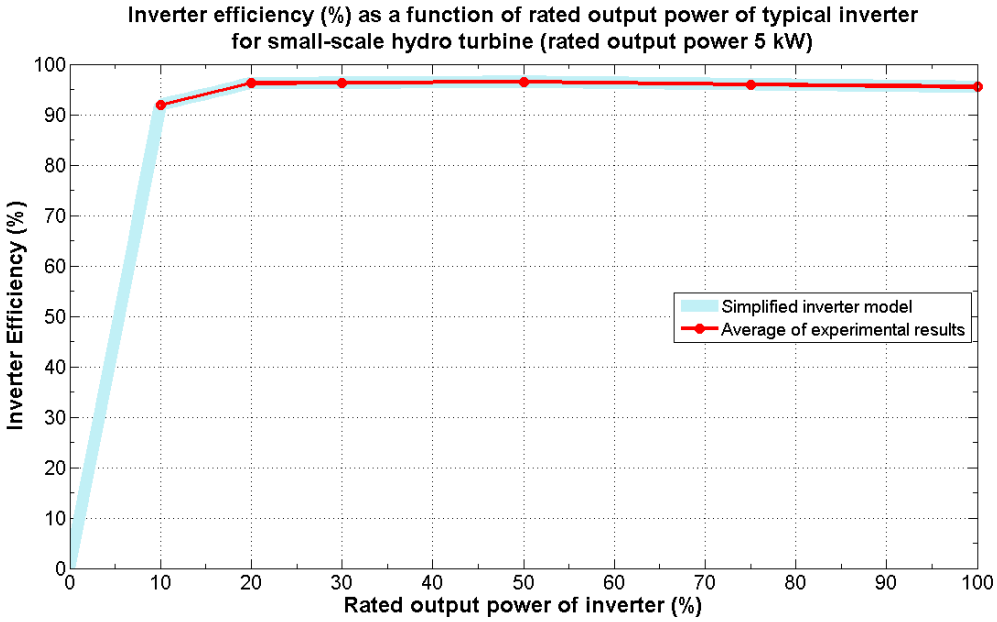

Figure 4.5 Comparison percent efficiency of output power of hydro turbine Inverter

It can be seen that if an array function matches the array input, then the output responds in the output vector. On the other hand, if there is any difference in array input and array function, which is still within the boundaries of array function, then the block performs linear interpolation between two appropriate elements of the table to determine an output value. If the array input is below/exceeds the boundaries, the block uses linear extrapolation instead of interpolation. An approximation for linear interpolation function can be obtained with two data points (which usually use a two-point formula for a line) by:

$$y = y_1 + \left[\frac{(y_2 - y_1)}{(x_2 - x_1)}(x - x_1)\right] \quad (4.3)$$

Regarding, x and y in this formula represent the point on x-axis and y axis between two reference points and therefore, the middle point of two reference points on x-axis and y-axis vector can be estimated by:

$$x = \frac{(x_1 + x_2)}{2} \text{ And } y = \frac{(y_1 + y_2)}{2} \quad (4.4)$$

If the last two values in the array function are given by f_{N-1} and f_N respectively, the linear extrapolation is given as:

$$f_{N+1} = 2f_N - f_{N-1} \quad (4.5)$$

As this thesis also aims to study the harmonic profiles in future power network, a typical single-phase application with PWM was developed under EN50160 standard. The switching frequency of the PWM application for SSDGs (e.g. inverter, converter) varies between 10 kHz (for SSDGs) and 1 kHz (for large

DGs) [138]. The average THD of grid interface devices (e.g. grid inverter, EVs/PHEVs grid connection, etc.) is 3 percent and the maximum THD is 8 percent [47]. This technology has the biggest share in the current market because a well designed PWM inverter produces a low level harmonic. The schematic of the typical inverter/converter is shown in Figure 4.6.

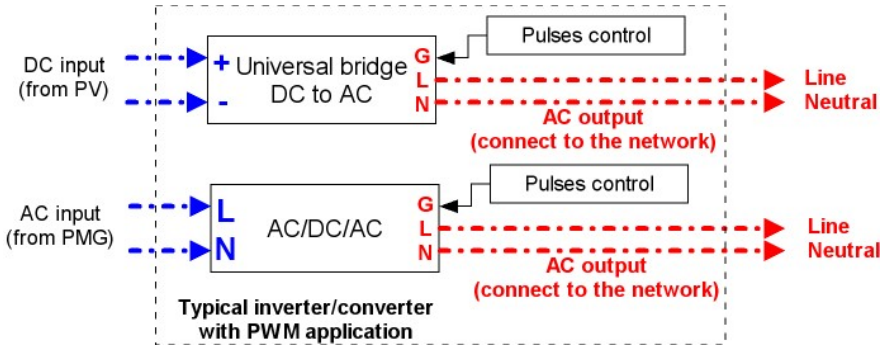

Figure 4.6 Schematic of the typical inverter/converter with PWM application

4.3 Modelling of PV Systems

A single-diode model for PV equivalent circuit (Shockley diode equation) and methodology to evaluate both the IV characteristic and MPP with various environmental conditions (such as installation, effects of temperature, solar irradiation and wind speed) are presented in this section. The proposed PV model also allows investigating dynamic input data such as temperature, irradiation and wind speed. The output of the PV model feeds into the inverter model (described in section 4.2). Accordingly, investigation of the power flow of various operating condition for the PV and the inverter is offered. A user friendly interface that supports the commercial datasheets is also considered. That means this model would be useful for the remote-users who cannot carry out the experiment at the practical site but could obtain the realistic data of surrounding environment (such as temperature, solar irradiation and wind speed). To ensure the accuracy of the model, simulation results have been validated against commercial datasheets and experimental results in the laboratory.

In practice, the typical PV cell absorbs energy (the photons, light particle) from the sunlight, as shown in Figure 4.7a. The energy from the photon is transferred to the mobile electron-hole pairs on both sides of the p–n junction where, the n-type emitter is the upper layer and the p-type base is the lower layer (shown in Figure 4.7b). Then, the electric field loosens the bond between the generated electrons and holes within the cell, and hence the numbers of electrons

and holes are dramatically increased until they can disperse near the electric field of the depletion area. The electric charges are divided where the electrons go to the n area and the holes go to the p area since these particles carry the opposite charges (shown in Figures 4.7c and 4.7d). Hence, the current flows through the load because the freed electrons attempt to return to the positively charged holes, as demonstrated in Figure 4.7e. That means the electricity can be generated by separating the electrons and holes from each other.

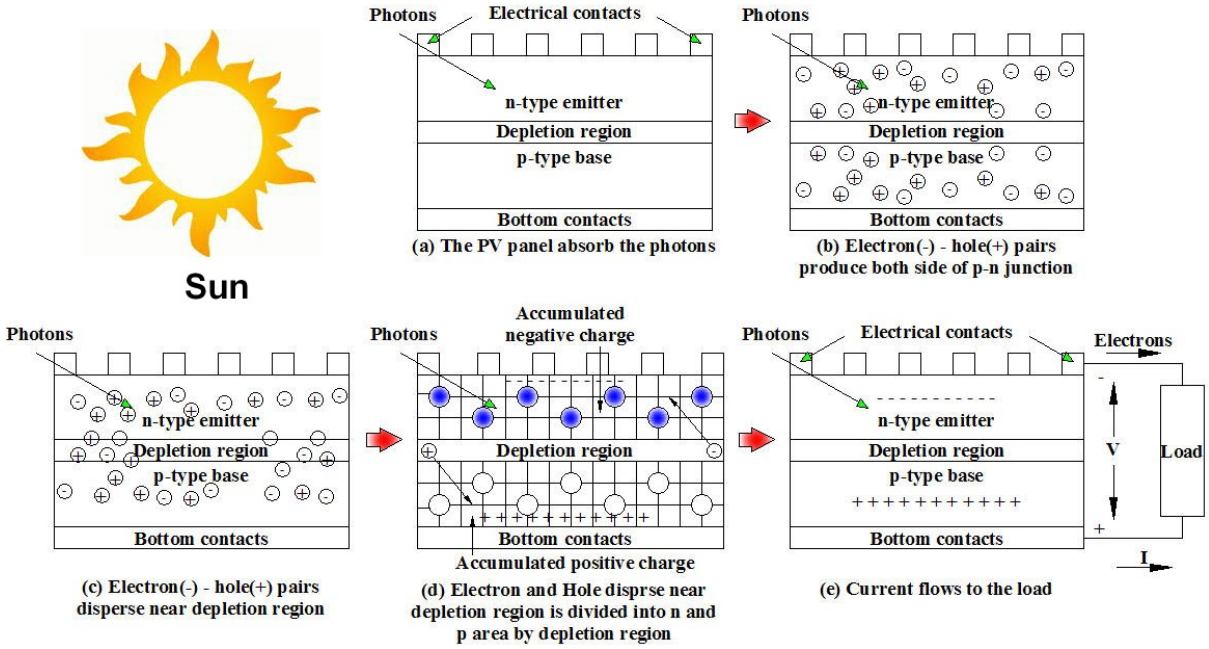

Figure 4.7 Characteristic of ideal PV cell

Many PV computer models have been developed, which are based on the modelling of semiconductor junction. For instance, reference [149-152] used parasitic resistance with constant value where [151-156] considered either the temperature effect in output voltage or the irradiation effect in output current. However, the output power of these models may not give accurate representation of the PV characteristics under realistic conditions (such as output voltage/current and parasitic resistance), which are functions of the ambient temperature (T_{opt}), irradiation (G_{opt}) and wind speed (W_s) [157-164].

The computer modelling in this thesis considered the influences of T_{opt} and G_{opt} on the parasitic resistance including type of installation and W_s to minimise inaccuracy results of MPP output power of PV. The exponential equation of the ideal diode (Shockley diode equation for p-n junction) was used to determine the IV characteristic [165]. This PV model was simplified from a typical crystalline Silicon (c-Si) PV cells because its characteristic is close to the ideal cells and is

commonly used in the current market. The traditional equivalent circuit of a PV cell with a single-diode is shown in Figure 4.8.

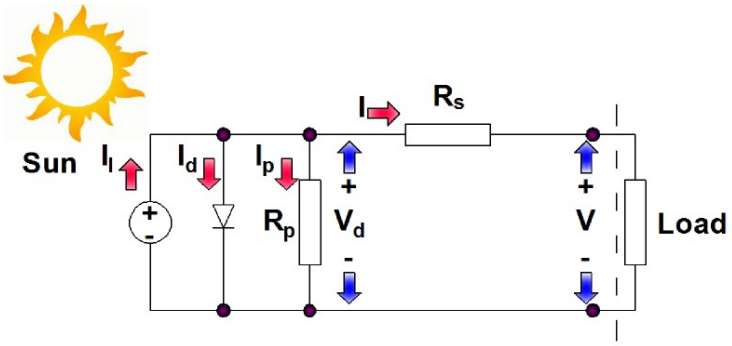

Figure 4.8 Equivalent circuit of PV cell (simplify by a single-diode) connected with resistive load

Where,

I_l = Photon generated current (A)

I_d = Diode current or dark current (A)

I_p = Parallel resistance current (A)

I = Current generated by PV (A)

R_p = The parallel resistance (Ω)

R_s = The series resistance (Ω)

V_d = Voltage across the diode (V)

V = Terminal voltage of PV (V)

Accordingly, I_d presents as the dark current during the PV cell in the absence of the sun light, which is similar to p-n semiconductor [165-167]. Hence, I_d can be described by the Shockley ideal diode equation as follows:

$$I_d = I_o \left[e^{\left(\frac{qV_d}{mkT}\right)} - 1 \right] \quad (4.6)$$

Where,

I_o = Diode saturation current (A)

q = Electrical charge on the electron is 1.602×10^{-19} (C)

m = Diode quality factor or ideal factor or ideal factor of p-n junction

k = Boltzmann's constant is 1.381×10^{-23} (J/K)

T = Temperature in Kelvin or 273.15 + temperature (°C)

In addition, R_s is the sum of PV cell structure resistance due to PV materials, the contact resistance between the contacts and the materials and the resistance between contacts and interconnections where the resistance value depends on cell manufacturing [168]. This resistance can cause a significant effect on a PV module performance where many PV cells are connected in series [159-160, 169-178]. Hence, this resistance was taken into account in order to improve the modelling accuracy of MPPT of output power. In practice, the smaller R_s is the better the quality of PV, as shown in Figure 4.9a.

Conversely, R_p is the current leakage proportional to the voltage (the current flows through the PV junction and reduces the voltage). Mitroi, Iancu, Fara, L., et al., [168] explained that this loss depends on the composite material of the active layer during recombination processes in the space charge region and leakage current at the surface of PV. Thus, the larger R_p is the better the quality of PV, as shown in Figure 4.9b.

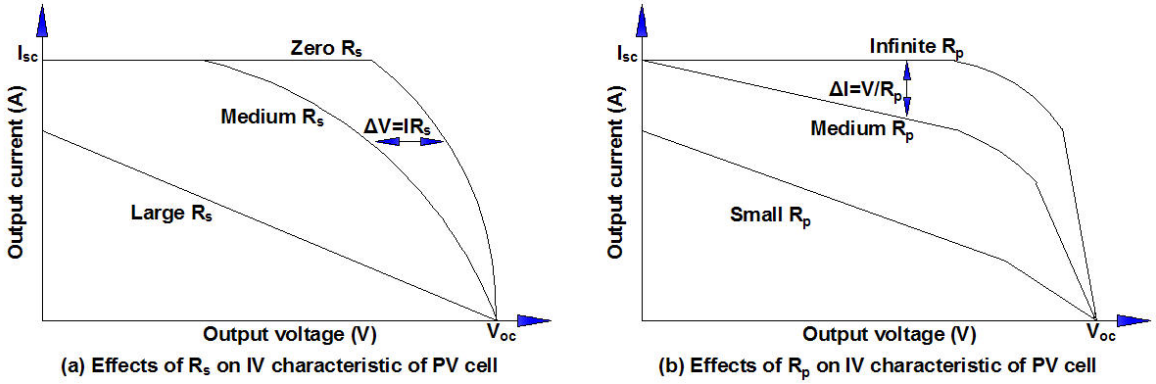

Figure 4.9 Effects of parasitic resistance (R_s and R_p) on the IV characteristic of PV cell

The ideal factor (m) in the PV equation (4.6) is described by the recombination of a PV layer, which is directly measured from the PV cell [175]. In practice, typically values of m varies between $1 < m < 2$ [165, 168, 170, 176-177, 179]. Table 4.2 shows that the ideality factor depends on PV recombination technologies.

Table 4.2: The ideal factor depends on PV recombination technologies

PV technology	m	Remark
Augar[180]	2/3	Two majority and one minority carries required for recombination.
SRH, band to band (low level injection)[180]	1.0	Recombination limited by minority carrier.
Si-mono[165]	1.2	n/a
Si-poly[181] and [182]	1.3	n/a
AsGa[181] and [182]	1.3	n/a
CdTe[181] and [182]	1.5	n/a
CIS[181] and [182]	1.5	n/a
a-Si:H[181] and [182]	1.8	n/a
SRH, band to band (high level injection)[180]	2.0	Recombination limited by both carrier types.
Depletion region (junction)[180]	2.0	Two carriers limit recombination.
a-Si:H tandem[181] and [182]	3.3	n/a
a-Si:H triple[181] and [182]	5.0	n/a

Source: [165, 180-182]

In practice, some parameters cannot be easily obtained from commercial datasheets e.g. the diode saturation current (I_o), ideality factor (m), etc. Hence, in order to obtain the IV characteristic of a PV cell, the short-circuit test (shown in Figure 4.10) and open-circuit test (shown in Figure 4.11) are used together with the following assumptions to overcome insufficient information about PV cell:

1) The PV cells in the module are identical in all manners.

2) The PV panel is fully illuminated without shading $(Q = 1)$ [183].

3) The estimation technique of R_s already includes the compensation of R_p in order to ensures that the MPP of the computer model curve closely corresponds to the practice module [159-160, 173, 177].

4) The term of $e^{\left[\frac{q(V+IR_S)}{mkT}\right]} \gg 1$ under all working conditions (not considered in low intensity light) [171, 174].

5) The effects of temperature (e.g. the voltage coefficient due to temperature; $T_{coeffVoc}$ and the current coefficient due to temperature; $T_{coeffIsc}$) and solar irradiation effects on voltage and current at the operating condition are considered.

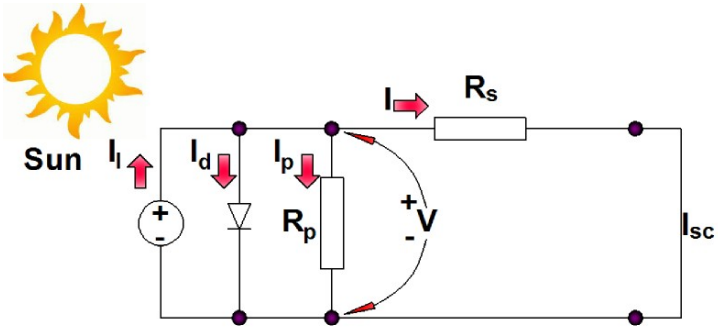

Figure 4.10 Equivalent circuit of PV cell during short-circuit test

Figure 4.10 shows that I could be obtained by using Kirchhoff's Current Law (KCL), which describes the summation of current flowing into the node is equal to the summation of current flowing out of that node. Then, the equation of current generated by PV (I) during short-circuit test is:

$$I = I_l - I_d - I_p \tag{4.7}$$

Substituting equation (4.6) into equation (4.7):

$$I = I_l - I_o \left[e^{\left(\frac{qV_d}{mkT}\right)} - 1 \right] - I_p \tag{4.8}$$

Where,

$$I_p = \frac{V_d}{R_p} \text{ And } V_d = V + IR_s \tag{4.9}$$

Substituting equation (4.9) into equation (4.8), gives:

$$I = I_l - I_o \left\{ e^{\left[\frac{q(V+IR_s)}{mkT}\right]} - 1 \right\} - \left(\frac{V+IR_s}{R_p}\right) \tag{4.10}$$

From the above assumptions, the photon generated current (I_l) during short-circuit test flows similar to the short-circuit current (I_{sc}). That means $I_l \approx I_{sc}$ [159-160, 164, 173]. In practice, the PV module is usually designed with small R_s and high R_p, therefore:

$$I = I_{sc} - I_o \left\{ e^{\left[\frac{q(V+IR_s)}{mkT}\right]} \right\} \tag{4.11}$$

Figure 4.11 shows the open-circuit at the terminal of the PV cell, which leads I equal to zero. Thus, the open-circuit voltage (V_{oc}) is equal to V_d.

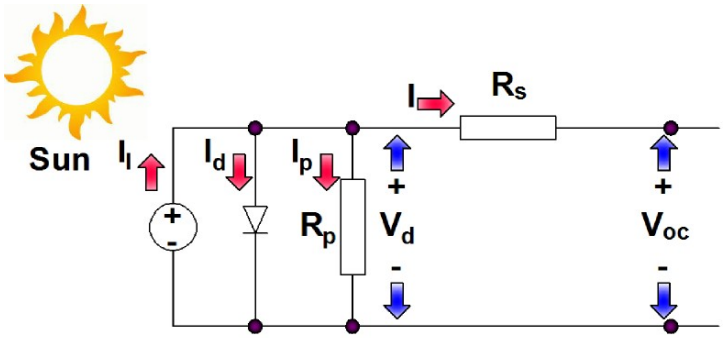

Figure 4.11 Equivalent circuit of PV cell during open-circuit test

Therefore, V_{oc} can be determined by:

$$V_{oc} = \left(\frac{mkT}{q}\right) \ln\left(\frac{I_{sc}}{I_o}\right) \quad (4.12)$$

Where, the thermal voltage of cell (V_t) is the flow characteristic of voltage across p-n junction in the semiconductor.

Therefore:

$$V_t = \frac{mkT}{q} \quad (4.13)$$

Substituting the thermal voltage term (equation 4.13) into equation (4.12):

$$V_{oc} = V_t \ln\left(\frac{I_{sc}}{I_o}\right) \quad (4.14)$$

Hence, I_o could be determined as:

$$I_o = I_{sc} e^{\left(-\frac{V_{oc}}{V_t}\right)} \quad (4.15)$$

Substituting equation (4.15) into equation (4.11), the current produced by the PV cell is:

$$I = I_{sc} - \left[I_{sc} e^{\left(-\frac{V_{oc}}{V_t}\right)}\right]\left[e^{\left(\frac{(V+IR_S)}{V_t}\right)}\right] \quad (4.16)$$

Or,

$$I = I_{sc}\left\{1 - e^{\left[\frac{(V-V_{oc}+IR_S)}{V_t}\right]}\right\} \quad (4.17)$$

It should be noted that equation (4.17) is usually used together with an iteration technique (normally Newton Raphson method) in order to determine the IV characteristic of the PV, which is the generated current corresponding to the generated voltage. The first iterative value of the generated voltage is usually set at $\mathrm{V} \leq 0.8V_{oc}$ where all iterative values must be within $0 \leq V \leq V_{oc}$ [160]. That means this equation is the implicit function of the generated current of the PV. The equation can be solved by the algebraic constraint block in the Simulink block set (more details in appendix B). This thesis proposes a simplified PV model (which considers the effects of R_p and R_s and the surrounding environment), and hence the MPP equation of PV during operating in realistic conditions by using $\frac{\mathrm{I_m}}{\mathrm{I_{sc}}}$ and $\frac{\mathrm{V_m}}{\mathrm{V_{oc}}}$ ratios and the fill factor are considered [159-160, 173]. Furthermore, in order to determine the parasitic resistance of a PV cell that operates in realistic condition, the parasitic resistance of the PV cell at standard conditions (the ambient temperature at 25°C and solar irradiation at 1 kW/m^2) is used as the initial value. The input parameters of the proposed PV model are shown in Figure 4.12.

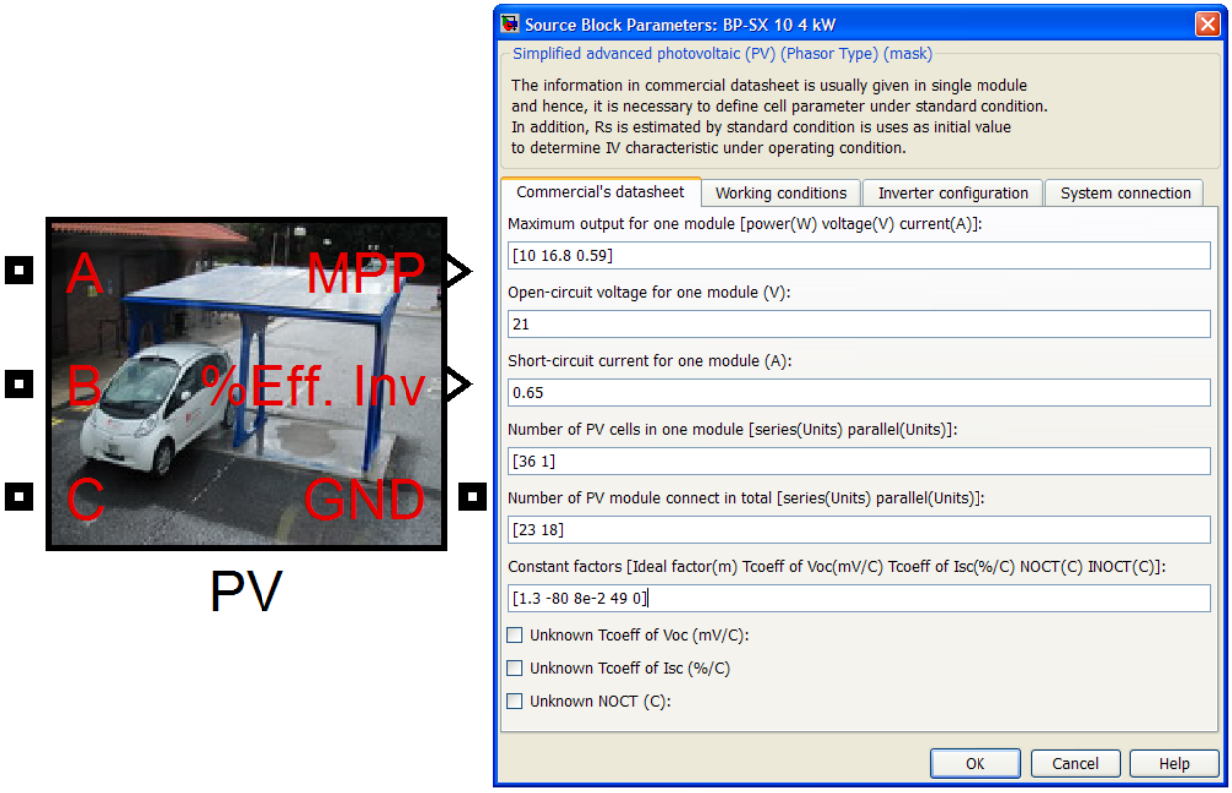

Figure 4.12 Input parameters of the proposed PV model for BP-SX10 of 4 kW

These input data are used to determine the parasitic resistance of the PV cell at standard condition with ambient temperature at 25°C (T_{std}) and solar irradiation at 1 kW/m^2 (G_{std}). According to the third assumption, the open-circuit voltage of the single cell (V_{occ}) can be determined by the open-circuit voltage of a single module (V_{ocm}) and the number of PV cells in series in a single module (N_{sc}), that is:

$$V_{occ} = \frac{V_{ocm}}{N_{sc}} \tag{4.18}$$

Similarly, the short-circuit current of single cell (I_{scc}) is:

$$I_{scc} = \frac{I_{scm}}{N_{pc}} \tag{4.19}$$

Where, I_{scm} is the short-circuit current for a single module and N_{pc} is the number of PV cells in parallel.

Therefore, the maximum output power of a single cell (P_{mc}) is:

$$P_{mc} = \frac{P_{mm}}{N_{sc}N_{pc}} \tag{4.20}$$

Where, P_{mm} is the maximum output power of a single module.

The thermal voltage of the cell at standard conditions (V_{tstd}) can be estimated as:

$$V_{tstd} = \frac{mk(273.15+T_{std})}{q} \tag{4.21}$$

Normalised voltage at standard conditions (v_{oc}) is: [171]

$$v_{oc} = \frac{V_{occ}}{V_{tstd}} \tag{4.22}$$

In addition, the fill factor is considered from the output power (FF) is: [172]

$$FF = \frac{P_{mc}}{V_{occ} I_{scc}} \tag{4.23}$$

Where, the fill factor with negligible series and parallel resistances effects (FF_o) is: [172]

$$FF_o = \frac{v_{oc} - \ln(v_{oc}+0.72)}{(v_{oc}+1)} \tag{4.24}$$

Thus, fill factor due to R_s (FF_s) is: [173, 177]

$$FF_s = FF_o(1 - 1.1r_s) + \frac{{r_s}^2}{5.4} \tag{4.25}$$

Therefore, normalised series resistance at standard conditions (r_s) is:

$$r_s = \frac{-(-1.1) - \sqrt{(-1.1)^2 - (4)\left(\frac{1}{5.4}\right)\left(1 - \frac{FF}{FF_o}\right)}}{(2)\left(\frac{1}{5.4}\right)} \tag{4.26}$$

Hence, R_s can be defined by: [169, 176, 177]

$$R_s = (r_s)\left(\frac{V_{occ}}{I_{scc}}\right) \tag{4.27}$$

Where, fill factor due to R_p $\left(FF_p\right)$ is: [172]

$$FF_p = FF_o\left[1 - \left(\frac{v_{oc}+0.7}{v_{oc}}\right)\left(\frac{FF_o}{r_p}\right)\right] \tag{4.28}$$

Then, normalised parallel resistance at standard conditions $\left(r_p\right)$ is:

$$r_p = \frac{(FF_o)\left(\frac{-v_{oc}-0.7}{v_{oc}}\right)}{\left(\frac{FF}{FF_o}\right)-1} \tag{4.29}$$

Where, R_p is: [176-177]

$$R_p = (r_p)\left(\frac{V_{occ}}{I_{scc}}\right) \tag{4.30}$$

To ensure the estimation technique of R_s (which includes the compensation of R_p) become more effective and allows the relative error to be less than 1 percent (compared with commercial datasheet) and the MPP of output power close to the realistic module, v_{oc} > 10, r_s < 0.4, r_p > 2.5 and the empirical expression of fill factor must have significant number with four digits [176-177]. It is known that the surrounding environment directly affects the output power of PV, which operates in realistic condition, here called “Operating Condition”. The PV module and its configuration are functional to the surrounding environment e.g. the increasing of cell temperature affects both generated voltage $\left(T_{coeffVoc}\text{ or }\frac{dV_{oc}}{dT_c}\right)$ and current $\left(T_{coeffIsc}\text{ or }\frac{dI_{sc}}{dT_c}\right)$. The typical values of $T_{coeffVoc}$ is -2.3x10^{-3}mV/°C/cell and

$T_{coeffIsc}$ is 3.1x10^{-4}A/°C/cell [160]. It should be noted that the temperature coefficient in the commercial datasheets is usually given in Celsius per module.

Therefore, the proposed model was designed to estimate operating cell temperature (T_c) in three different conditions in order to support various input data. Firstly, lump overall heat coefficients from module and mounting configuration by using a combination of Nominal Operating Cell Temperature ($NOCT$) and Installed Nominal Operating Cell Temperature ($INOCT$) in order to increase the accuracy in the linear relationship between module temperature and solar irradiation [184-191]. The typical value of $NOCT$ is 44°C [176] and those for $INOCT$ are shown in Table 4.3. Therefore, T_c equation corresponds to heat-losses due to module and mounting [190]:

$$T_c = T_{opt} + \left[\frac{(NOCT+INOCT)-20}{0.8}\right]\left(\frac{G_{opt}}{G_{std}}\right) \quad (4.31)$$

Table 4.3: Typical $INOCT$ for PV module

PV module mount type	$INOCT$ (°C)
Rack mount	-3
Direct mount	18
Typical standoff/integral	4
Standoff/integral, entrance or exit height/width, whichever is minimum 2.5 cm	11
Standoff/integral, entrance or exit height/width, whichever is minimum 7.5 cm	2
Standoff/integral, entrance or exit height/width, whichever is minimum 15 cm	-1

Source: [190]

Secondly, the other simplest way to determine T_c from type of PV module is by using the Ross coefficient [184]. The parameters of the Ross coefficient (k_r) are given in Table 4.4.

$$T_c = T_{opt} + k_r\left(\frac{G_{opt}}{G_{std}}\right) \quad (4.32)$$

Table 4.4: Ross coefficient (k_r) for various types and mounting of PV module

PV module type	k_r (km^2/W)
Well cooled	0.0200
Free standing	0.0208
Flat on roof	0.0260
Not so well cooled	0.0342
Transparent PV	0.0455
Facade integrated	0.0538
On sloped roof	0.0563

Source: [184, 191-192]

Lastly, the proposed computer model also offers the extra function by considering the impacts of wind speed in T_c [193]. The parameters are given in Table 4.5.

$$T_c = T_{opt} + \{[T_{up} e^{(bw_s)}] + T_{lo}\}\left(\frac{G_{opt}}{G_{std}}\right) + \left[(\Delta T)\left(\frac{G_{opt}}{G_{std}}\right)\right] \quad (4.33)$$

Where,

T_{up} = The coefficient of the upper temperature limit at low wind speed

T_{lo} = The coefficient of the lower temperature limit at high wind speed

b = The coefficient of the module temperature drops as wind speed increases

w_s = The wind speed measured at standard height 10m (m/s)

ΔT = The coefficient of the temperature gap and the back encapsulation material

Table 4.5: The impacts of W_s on PV cell temperature based on thermal model form

Type	T_{up} (°C)	T_{lo} (°C)	b	ΔT (°C)
Glass/Cell/Glass	25.0	8.2	-0.112	2
Glass/Cell/Tedlar(Film)	19.6	11.6	-0.223	3

Source: [189, 191, 193-195]

Substitute T_c equation (4.31, 4.32 or 4.33) into equation (4.34) in order to determine the thermal voltage of the cell at operating conditions (V_{topt}), gives:

$$V_{topt} = \frac{mk(273.15+T_c)}{q} \quad (4.34)$$

Therefore, the open-circuit voltage of a single cell at operating conditions (V_{occopt}) is:

$$V_{occopt} = \mathrm{V}_{occ} + \left[\left(\frac{T_{coeffVoc}}{N_{sc}}\right)(T_c + T_{std})\right] + V_{topt} \ln\left(\frac{G_{opt}}{G_{std}}\right) \quad (4.35)$$

Normalised voltage at operating conditions (v_{ocopt}) is:

$$v_{ocopt} = \frac{V_{occopt}}{V_{topt}} \quad (4.36)$$

Then, normalised fill factor at operating conditions (FF_{oopt}) is:

$$FF_{oopt} = \frac{v_{ocopt} - \ln(v_{ocopt}+0.72)}{(v_{ocopt}+1)} \quad (4.37)$$

The short-circuit current of single cell at operating conditions (I_{sccopt}) is:

$$I_{sccopt} = I_{scc}\left(\frac{G_{opt}}{G_{std}}\right)\left[1 + \left(\frac{T_{coeffIsc}}{N_{pc}}\right)(T_c + T_{std})\right] \quad (4.38)$$

The normalised series resistance at operating conditions (r_{sopt}) is:

$$r_{sopt} = \frac{R_s}{\left(\frac{V_{occopt}}{I_{sccopt}}\right)} \quad (4.39)$$

Therefore, fill factor at operating conditions (FF_{opt}) is:

$$FF_{opt} = FF_{oopt}(1 - 1.1r_{sopt}) + \frac{{r_{sopt}}^2}{5.4} \quad (4.40)$$

The open-circuit voltage for a single module at operating conditions (V_{ocmopt}) is:

$$V_{ocmopt} = V_{occopt}N_{sc} \quad (4.41)$$

The short-circuit current for a single module at operating conditions (I_{scmopt}) is:

$$I_{scmopt} = I_{sccopt}N_{pc} \quad (4.42)$$

Therefore, the approximate analytical equations for calculating the maximum voltage and current at MPP by using $\frac{I_m}{I_{sc}}$ and $\frac{V_m}{V_{oc}}$ ratios and the fill factor are: [159-160, 173]

$$a_{opt} = v_{ocopt} + 1 - 2v_{ocopt}r_{sopt} \quad (4.43)$$

$$b_{opt} = \frac{a_{opt}}{1+a_{opt}} \quad (4.44)$$

$$\frac{V_{mcopt}}{V_{occopt}} = 1 - \left(\frac{b_{opt}}{v_{ocopt}}\right)\ln\{a_{opt} - r_{sopt}[1 - {a_{opt}}^{-(b_{opt})}]\} \quad (4.45)$$

$$\frac{I_{mcopt}}{I_{sccopt}} = 1 - {a_{opt}}^{-(b_{opt})} \quad (4.46)$$

Where, N_{sm} is the total number of PV modules connected in series and N_{pm} is the total number of PV modules connected in parallel (Units).

Hence, the maximum voltage at MPP of the total modules that connects in series and parallel at operating conditions $(V_{mtmMPPopt})$ is:

$$V_{mtmMPPopt} = V_{occopt}\langle 1 - \left(\frac{b_{opt}}{v_{ocstd}}\right)\ln\{a_{opt} - r_{sopt}[1 - {a_{opt}}^{-(b_{opt})}]\}\rangle (N_{sc}N_{sm}) \quad (4.47)$$

It follows that the maximum current at MPP of the total modules that connects in series and parallel at operating conditions $(I_{mtmMPPopt})$ is:

$$I_{mtmMPPopt} = I_{sccopt}[1 - {a_{opt}}^{-(b_{opt})}](N_{pc}N_{pm}) \quad (4.48)$$

Therefore, the maximum power at MPP output power of the total modules that connects in series and parallel at operating conditions $(P_{mtmMPPopt})$ is:

$$P_{mtmMPPopt} = V_{mtmMPPopt}I_{mtmMPPopt} \quad (4.49)$$

In summary, the computer modelling is divided into two main steps, firstly the calculation of PV parameters at standard conditions and then determination of PV characteristic at operating conditions, as demonstrated in Figure 4.13. The characteristics of a proposed PV model were validated against commercial datasheets and experimental tests in the laboratory of a single solar module 10 W (BPsolar, BP-SX10). Table 4.6 gives the data of a BP-SX10 module, which includes 36 polycrystalline cells connected in series [196].

Table 4.7 presents the equipment details and Figure 4.14 shows the PV experimental set up in the laboratory.

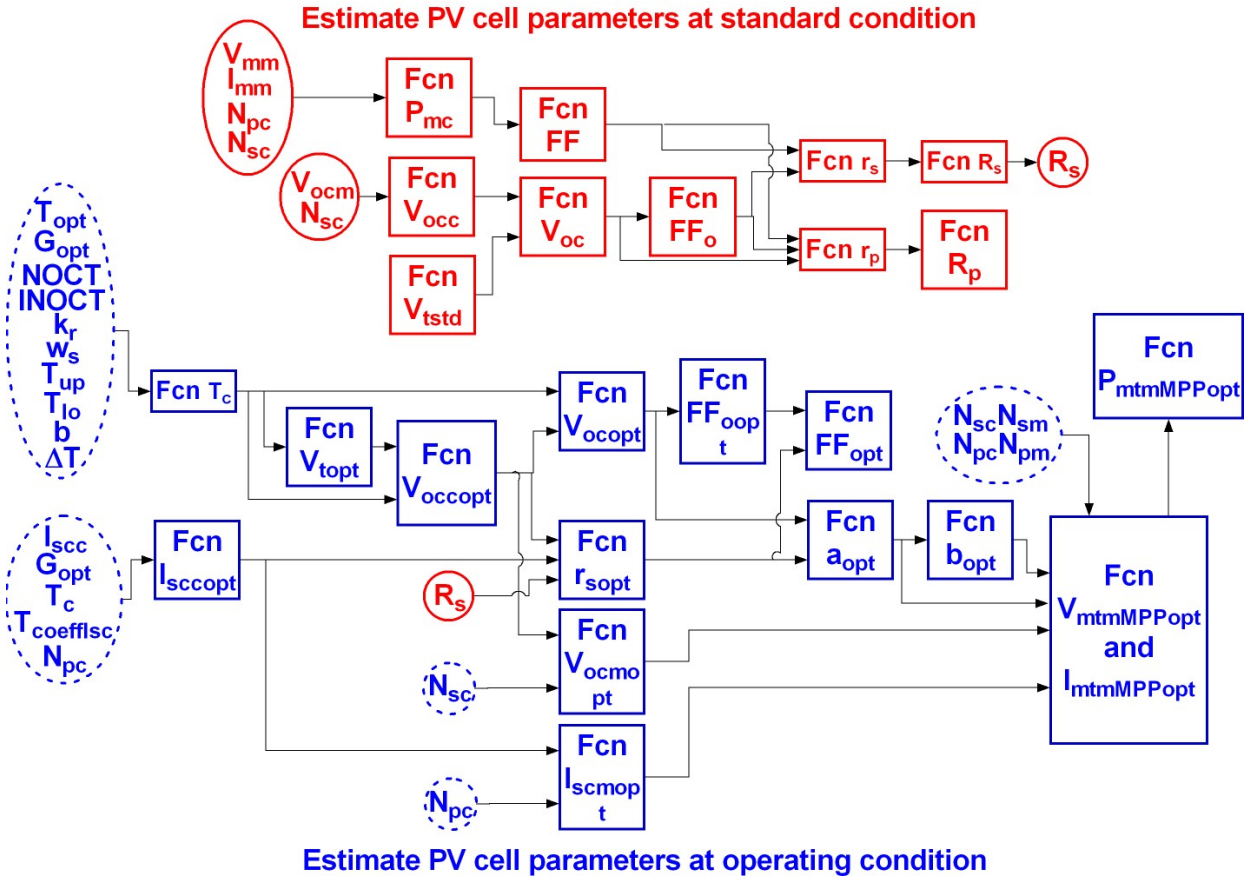

Figure 4.13 Schematic of the proposed PV model

Table 4.6: Characteristic of PV module (BPsolar, BP-SX10)

Characteristic of PV module	Model BP-SX10
Maximum power	10 W
Voltage at maximum power	16.8 V
Current at maximum power	0.59 A
Warranted minimum	9 W
Short-circuit current	0.65 A
Open-circuit voltage	21.0 V
Temperature coefficient of I_{sc}	(0.065 ±0.015) %/°C
Temperature coefficient of V_{oc}	-(80 ±10) mV/°C
Temperature coefficient of power	-(0.5 ±0.05) %/°C
NOCT	47 ±2°C

Source: [196]

Table 4.7: Equipment details of PV experimenter

Equipment	Model	Units	Remark
PV module	BP Solar: BP-SX10	1	Details in Table 4.6[196]
Bulb	Osram: HQI-T 400W/D	3	Colour temperature 5200 Kelvin[197]
Irradiance meter	Solar light: PMA 2200	1	Accuracy ±0.5% of full scale reading[198]
Thermometer	Testo: Pen style surface thermometer	1	Accuracy ±1°C of (-30°C to 250°C)[199]
Power meter	Voltech: PM1000	1	Accuracy ±0.1% of reading range[200]
Rheostat	212 Ω	1	n/a

Source: [196-200]

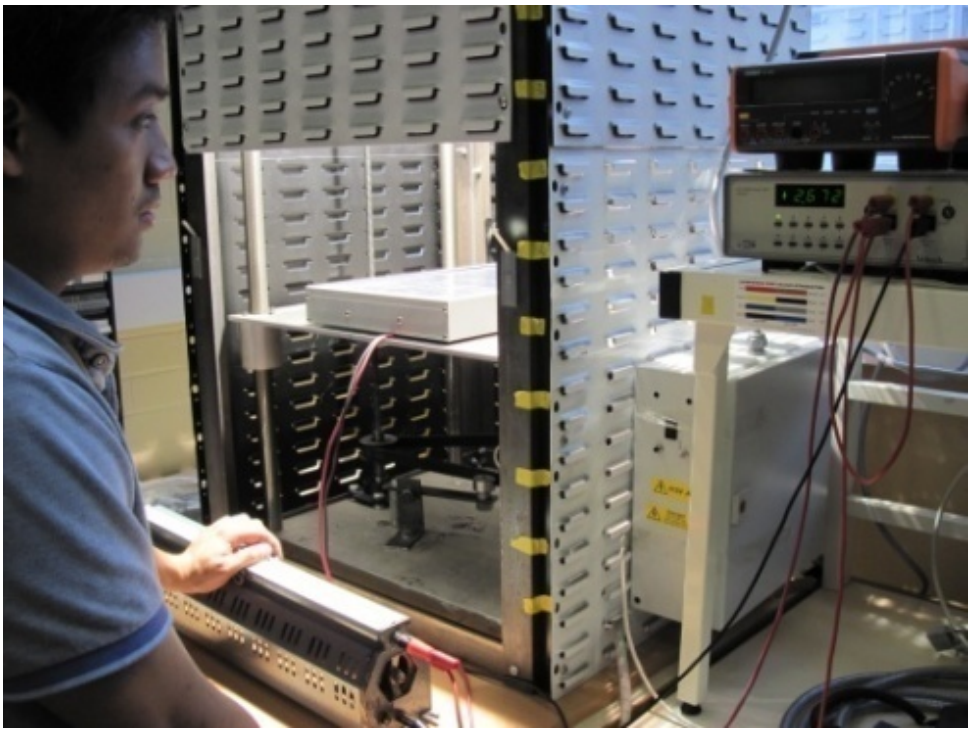

Figure 4.14 PV experimenter in laboratory

It can be clearly seen that the validation of the computer model uses a simple practice measurement (voltmeter and amp-meter) to collect the experimental data. The IV characteristics of the computer model are plotted against those from commercial datasheets of BP-SX10 with constant irradiance 1 kW/m^2 and varying temperatures (from 0°C to 75°C) and the excellent results are shown in Figure 4.15. The computer model was also validated against experimental results in the laboratory, which are shown in Figure 4.16. During the experiment, the approximate ambient temperature of 21.4°C and irradiance of 300 W/m^2 were measured. After that, the experimental results were recorded by varying the resistive load that connects to a single PV module into 25 steps from open-circuit until short-circuit. To ensure the error is minimised, and hence the experiment was carried out for 5 times with the same setting and conditions.

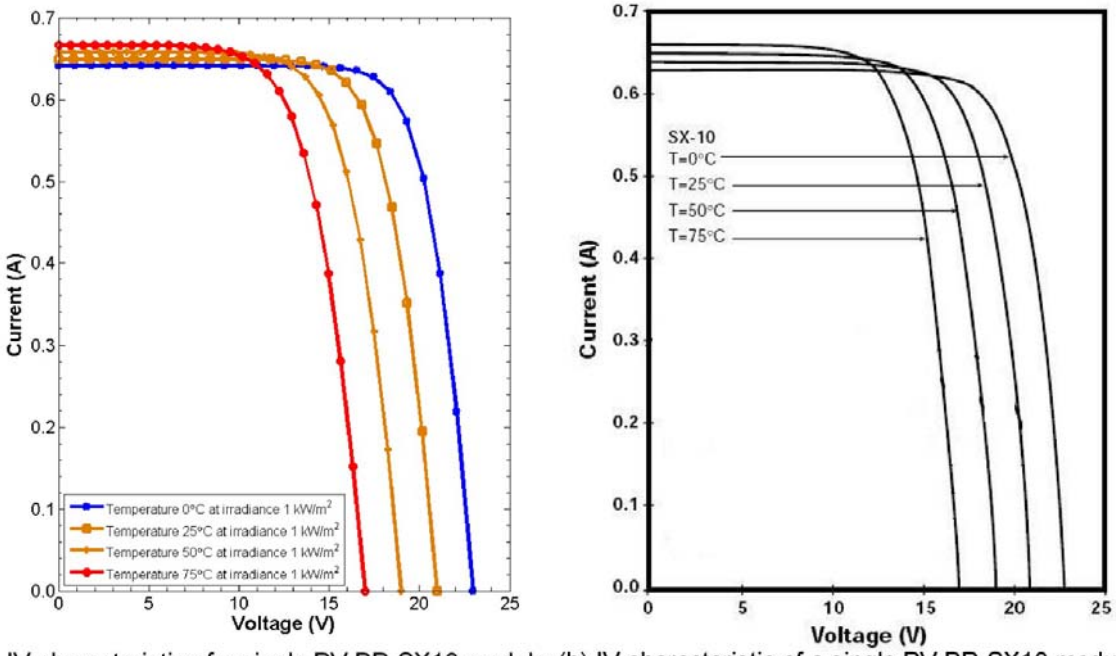

(a) IV characteristic of a single PV BP-SX10 module from MATLAB/Simulink computer model

(b) IV characteristic of a single PV BP-SX10 module from commercial manufacture's datasheet

Figure 4.15 Comparison IV characteristic of PV module between simplified model and commercial datasheet at standard condition

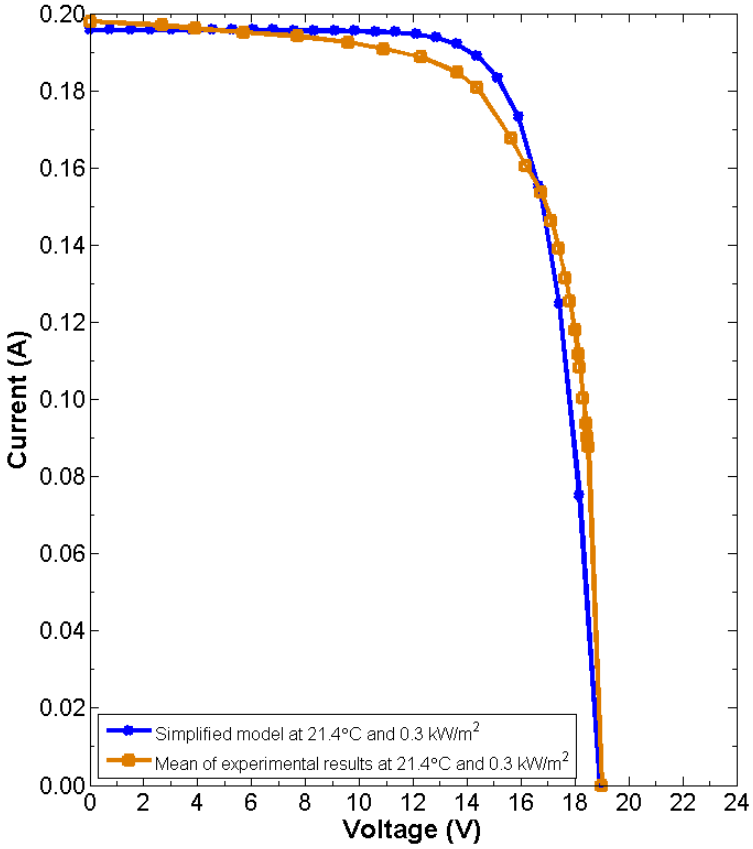

Figure 4.16 Comparison IV characteristic of PV module between simplified model and experimental results (in laboratory)

In order to investigate the impacts of variable surrounding environment, the interval data of T_{opt}, G_{opt} and W_s at every 30 minutes on 18th January 2011 at Ratchaburi (countryside area in TH) were considered and shown in Figure 4.17 [137].

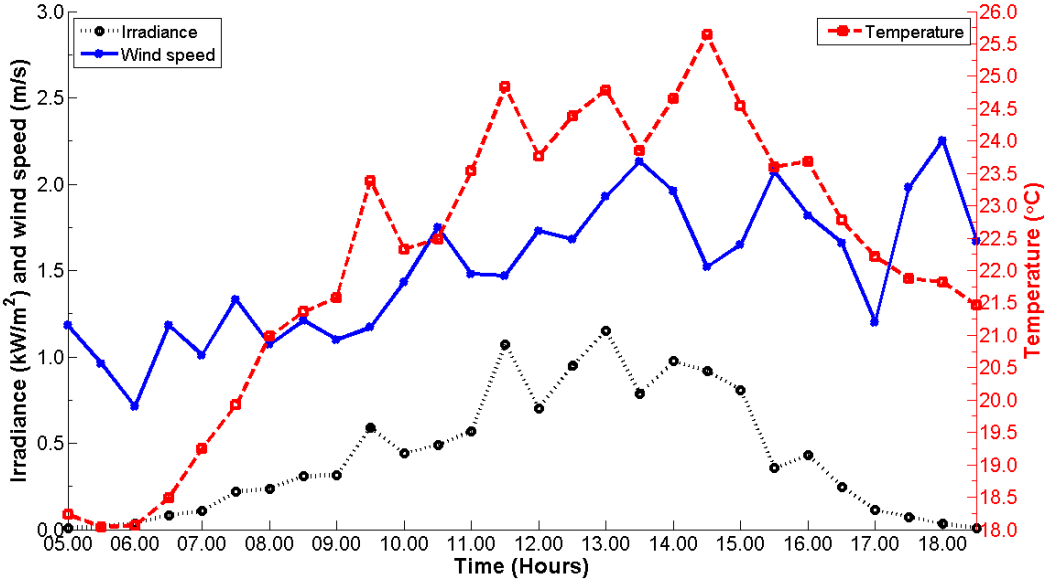

Figure 4.17 Typical environmental profiles at PV area in TH

The TH system includes 18 sets of BP-SX10 PV module connected in parallel where each set have 23 modules connected in series and a single inverter of Fronius-IG PLUS 50 V-1 [201]. It should be mentioned that the MPPT of the inverter uses at least 3 sec to optimise the AC output power. In addition, it is well known that the MPP output power of PV that connect with inverter under operating condition $(P_{mtmMPPopt})$ is a proportional function of the maximum nominal input power of the inverter $(P_{mnomInv})$ [139, 141-142]. Therefore, the MMP output power at the AC side can be defined as:

$$P_{mtmMPPoptAC} = P_{mtmMPPopt}(\eta_{Inv})(P_{normInInv}) \quad (4.50)$$

Where, the inverter efficient (η_{Inv}) is a function of the rated output power of the inverter, which described in section (4.2). Consequently, the normalised power is the ratio between the actual power of and nominal power, hence the normalised power of inverter $(P_{normInInv})$ is:

$$P_{normInInv} = \frac{P_{mtmMPPopt}}{P_{mnomInv}} \quad (4.51)$$

Figure 4.18 shows the impacts of dynamic input data in TH (Figure 4.17) and MPPT of the inverter of a small-scale PV of 4 kW at Ratchaburi, TH.

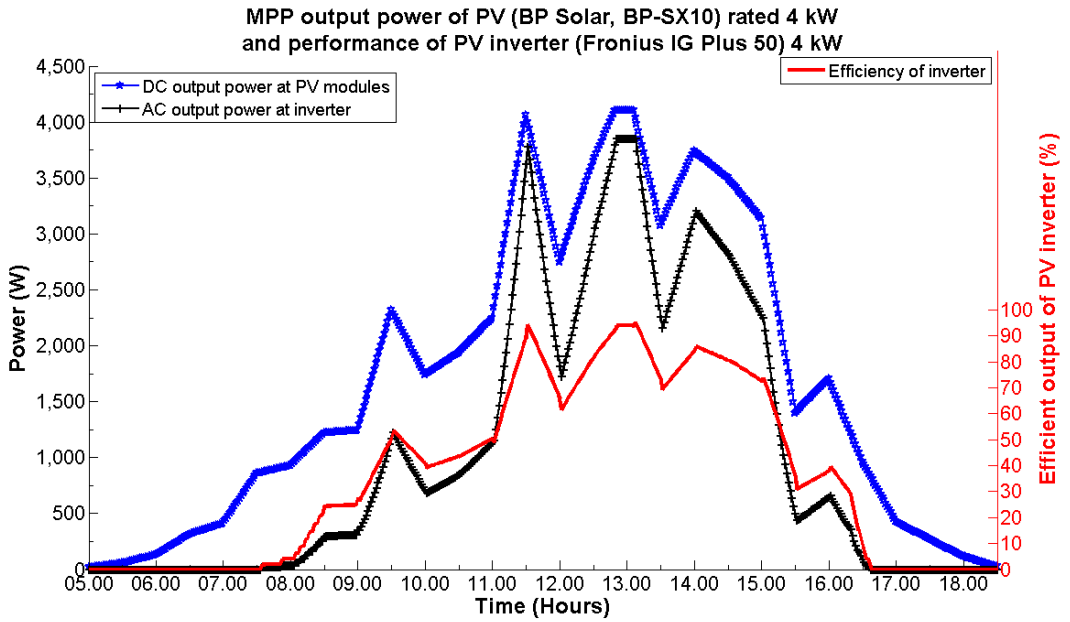

Figure 4.18 MPP output power and inverter performance of PV modules under variable environment (T_{opt}, G_{opt} and W_s) in TH

It can be clearly seen that the solar irradiation, temperature and wind speed affect the output power of the PV. The efficiency of conversion form DC to AC of the inverter greatly reduces the PV output power when the generated power of PV module is less than 10 percent of rated output power. However, the performance of the inverter improves when the generated power of PV module is more than 10 percent because the inverter is normally designed to optimise the output power. It can be noted that the power generation profile of PV systems in the UK has been obtained from the UKGDS [133], and hence the computer simulation is not necessary.

The simplified PV model has the feasibility functions for the engineer who would like to investigate output power for both steady and dynamic states with various and variable environment. These functions support unknown NOCT, $\mathrm{T_{coeffVoc}}$, $\mathrm{T_{coeffIsc}}$, know only type of PV module and impacts of wind speed. In order to increase the potential of power flow study, the combination of simplified PV and inverter models are allowed to mix and match the various types of PV and inverter where the commercial datasheets in the current market is supported.

4.4 Modelling of Small-Scale Wind and Hydro Energy Conversion Systems

Even though Simulink programme provides the PMG wind turbine model but still, it cannot simulate together with the OLTC model because the PMG wind turbine block includes an ideal switch, which does not respond in the phasor mode. Moreover, the generated power of small-scale wind turbines in the UK is not available in reference [133]. In addition, the available information for small-scale wind and hydro turbines in the TH network are wind speed, water velocity, site location and some technical parameters for hydropower system (e.g. diameter of nozzle). Therefore, in order to investigate the power flow in existing and future distribution network with the OLTC, the simplified wind and hydro turbines models are required.

This section describes the proposed simplified a small-scale wind turbine model with variable wind speed and a small-scale hydro turbine with constant water velocity in a closed pipe system and variable water velocity in an open channel system. These proposed models are developed to work with PMG. As their size is small and they produce low noise. Hence, they are usually used in residential areas [202]. The PMG is suitable for direct drive, which does not require a gearbox system, as a multi pole PMG supports low wind speed opreration. Another advantage of the PMG is that it is capable of active/reactive power control because a voltage source converter is self-commutated. Hence, the grid side of inverter/converter can feed either leading or lagging current into the network, which allows it to supply/consume reactive power where the details are explained in second part of this section. From these advantages, the simplified PMG for small-scale wind and hydro turbines is essential.

In this thesis, proposed wind and hydro turbines models were developed to work with the simplified inverter model (described in section 4.2). This offered an investigation of the various combinations of wind and hydro turbines with different types of inverter where they allow investigating various types of impacts (e.g. voltage variation, harmonic distortion, impacts of inverter sizing). These models were developed by implementing a user friendly interface that uses typical values from commercial datasheet, if parameters are not available. Therefore, the user can investigate the behaviour of these turbines by obtaining the commercial datasheets and environment data from the actual site (e.g. wind speed, water

velocity). The simulation results of the proposed models have been validated against commercial datasheets, experimental results and other software in the current market in order to ensure its accuracy. The proposed models are divided into two main parts, which are modelling of the turbine (converting energy from wind speed and water velocity to mechanical power), and modelling the Permanent Magnet Generator (PMG).

4.4.1 Modelling of the turbines

4.4.1a) Wind turbine

In practice, the axis of the wind turbine is used to divide the types of wind turbine; Horizontal Axis Wind Turbine (HAWT) and Vertical Axis Wind Turbine (VAWT), as shown in Figure 4.19 [203-204]. These turbines are considered as a prime mover that drives the generator by converting the wind power into mechanical power. This output power depends on the size of the wind turbine. The wind energy conversion could be explained by the interaction between the wind and the turbine rotor. The blades of a wind turbine extract the wind energy, within the action region (cut-in and cut-off).

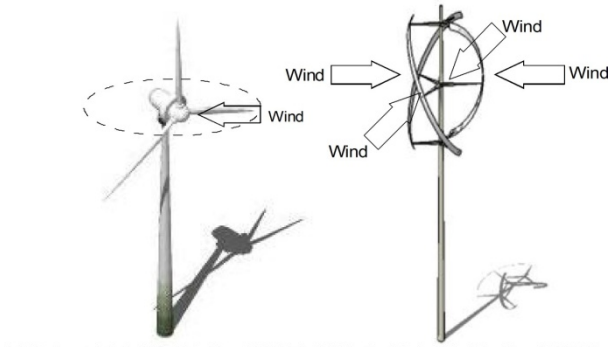

Figure 4.19 HAWT and VAWT

As can be seen in Figure 4.19, the rotor absorbs the energy from the air stream and can therefore influence its velocity. In this situation, the rotational energy is converted via a mechanical drive and fed into the generator. However, the high wind speed may result in unbalance between the mechanical power extracted from the wind turbine and generated electrical power because it is increasing the rotor speed. This problem can be reduced by blade design, pitch controller or inverter/converter. The efficiency of the wind turbine that converts wind power into useable electrical power is called “Power Coefficient (C_P)”. It is a function of the

ratio of the actual power delivered by the turbine and the theoretical power available in the wind. That means C_P can be defined by, the non-dimensional factors, known as the Tip Speed Ratio (λ or TSR) where λ is the relationship between the wind speed (V_W) and blade tip speed (BTS), it can be called rate of rotation of the rotor as well. In theory, C_p is typically less than $\frac{16}{27}$, Betz's limit [205]. In order to describe the characteristics of a wind turbine, many models and advanced methods were proposed [204, 206-216]. Most studies show that additional wind turbine data such as blade and gearbox profiles, which are not usually provided in commercial datasheets. Therefore, the following assumptions are made in order to develop a simplified small-scale wind turbine models:

1) Use the non-linear blade dynamics equation to simulate the dynamic performance of the wind turbine [204, 207]. This equation is used to investigate the variable speed wind turbine by using the constant speed rotor and variable wind speed [203-204, 211-214]. The tip speed ratio is considered identical at all blades.

2) The wind speed changes very quickly in urban environment, and hence its impacts on the rotor speed depend on the inertia of the rotor. The proposed model is based on a small-scale wind turbine, and hence this impact could be neglected as the thesis is more focused on the power flow in the distribution network (the grid interaction). Therefore, in order to neglect the inertia rotor, the change in wind speed is considered as the instantaneous change to the rotor speed, a similar suggestion is found in references [216] and [217].

3) In order that the wind turbine model can support various types of turbines, the significant effects of mechanical losses in the turbine (e.g. gearbox system) are lumped together in percent efficiency term. Consequently, the other mechanical losses due to wind turbine structure, e.g. tower and flag bending modes are neglected because they are considered as minor loss in small-scale wind turbines.

4) The pitch controller by advanced power electronics is neglected because the current size of active pitch controller (e.g. by hydraulic and advanced power electronics) cannot mount into small blades. However, the blades with a stall design (normally used to stall rotor speed during high wind speed) and tail vanes (passive yaw) are used in the small-scale wind turbine instead of active pitch controller. It should be noted that the tail vane is usually used in HAWT in order to maintain the rotor facing into wind direction as it is not Omni-directional like the VAWT.

Therefore, BTS can be defined by:

$$BTS = (\omega_r)(r) \tag{4.52}$$

Where, ω_r is the angular velocity of wind turbine rotor in rad/sec and r is the radius of the rotor in metres.

Hence,

$$BTS = \left(\frac{2\pi NomRs}{60}\right)\left(\frac{RotorDia}{2}\right) \tag{4.53}$$

Where, $NomRs$ is the nominal rotor speed in revolution per minute (rpm) and $RotorDia$ is the diameter of wind rotor in metres. Both $NomRs$ and $RotorDia$ can be easily obtained from commercial datasheets.

In practice, BTS is a function of λ, which plays an important role in wind turbine design where it can be measured by the tachometer at the blades' speed. A high λ can cause turbulences between the blades where therefore the blades will blur and act like a solid wall to the wind. This turbulence can affect the blade that arrives too quickly, and hence reduces the power extraction. Conversely, the rotor with slow speeds could result in less power extraction because most of wind passes straight through the gaps between the blades. That means λ depends on the blade airfoil profile, the number of blades and the type of wind turbine. Then,

$$\lambda = \frac{BTS}{V_W} \Longrightarrow \lambda = \frac{\omega_m r}{V_W} \tag{4.54}$$

Consequently, in order to understand the performance of a wind turbine, C_P and power curves are analysed. From commercial datasheets, it can be seen that the pattern of C_P is usually similar for the same type of wind turbines but its characteristic is not similar. In order to achieve the simplified model (which supports various types of wind turbine), the non-linear blade dynamics equation is used to simulate the dynamic performance of C_P.

Here, the equation of C_P of a simplified HAWT is determined by taking both λ and pitch angle (β) into account [203, 211]:

$$C_P(\lambda,\beta) = \left\{c_1\left[\left(\frac{c_2}{\lambda_i}\right) - (c_3\beta) - (c_4\beta^{c_5}) - c_6\right]\right\} e^{\left(\frac{-c_7}{\lambda_i}\right)} \quad (4.55)$$

$$\lambda_i = \frac{1}{\left(\frac{1}{\lambda+c_8\beta}\right)+\left(\frac{c_9}{\beta^3+1}\right)} \quad (4.56)$$

Where, C_P of simplified VAWT is given by [204]:

$$C_P(\lambda) = \left\{c_1\left[\left(\frac{c_2}{\lambda_i}\right) - c_6\right]\right\} e^{\left(\frac{-c_7}{\lambda_i}\right)} \quad (4.57)$$

$$\lambda_i = \frac{\lambda}{1-c_9\lambda} \quad (4.58)$$

The constant parameters c_1 to c_9 of the non-linear dynamic equation are important factors and they could be varied to match the wind turbine profiles [203-204, 211-214, 218-220]. This set of equations (4.55 to 4.58) was adopted in order to optimise the multidimensional equation for wind turbine performance, and hence the effects of drag forces and tip losses that reduces C_p of the turbine are considered [206-207]. The thesis proposed parameters c_1 to c_9 of the simplified wind turbine model for the Evance R9000 of 5 kW with β at 15 degree (HAWT) and the Quiet Revolution qr5 of 6 kW (VAWT). The Probability Density Function (PDF) of a Weibull distribution equation that applies with variable wind speed (used to identify the range of these parameters) was used to obtain these parameters because it supports the continuous probability distribution [221]. The MATLAB/Simulink routine can be used to define these parameters, and hence both other constant values and study parameters are presented together with other types of wind turbine in Table 4.8.

Table 4.8: Constant parameters c_1 to c_9 of C_p for HAWT and VAWT

	c_1	c_2	c_3	c_4	c_5	c_6	c_7	c_8	c_9
This thesis proposed Evance R9000 HAWT model	**0.287**	**117**	**-0.04**	**0.5**	**-1.2**	**6.94**	**15**	**-0.02**	**-0.003**
Constant–speed model HAWT model[203]	0.44	125	0	0	0	6.94	16.5	0	-0.002
Variable–speed model HAWT model[203]	0.73	151	0.58	0.002	2.14	13.2	18.4	-0.02	-0.003
HAWT model[211]	0.5	116	9.4	0	0	5	21	0.08	0.035
HAWT model[219]	0.5	116	0.4	0	0	5	16.5	0.089	0.035
HAWT model[220]	0.02	116	0.4	0	0	5	12.5	0.08	0.035
This thesis proposed Quiet Revolution qr5 VAWT model	**0.3**	**86**	**0**	**0**	**0**	**16**	**8.7**	**0**	**-0.032**
VAWT model[204]	1.06	112	0	0	0	13.2	16.5	0	-0.001

Source: [203-204, 211, 219-220]

Therefore, the available mechanical power in watts and mechanical torque in N.m from the wind turbine are given as:

$$P_W = \frac{1}{2}\rho A_W C_P(\lambda,\beta){V_W}^3 \tag{4.59}$$

$$T_W = \frac{1}{2\lambda}\rho A_W r C_P(\lambda,\beta){V_W}^2 \Longrightarrow T_W = \frac{1}{2}\rho A_W r C_T(\lambda,\beta){V_W}^2 \tag{4.60}$$

Where, A_W is considered as the wind extraction area (swept area) of the turbine. Consequently, C_T is the torque coefficient of the wind turbine and it is a function of $C_P(\lambda,\beta)$ and λ, given as.

$$C_T = \frac{C_P(\lambda,\beta)}{\lambda} \tag{4.61}$$

If a gearbox is used to regulate the rotor speed, the percent efficiency of the gearbox system (η_{TG}) need to be used to estimate the available mechanical power that is transferred through the gearbox (P_{WTG}):

$$P_{WTG} = \eta_{TG} P_W \tag{4.62}$$

Figure 4.20 shows the input parameters of the proposed wind turbine model for the Evance R9000 and the Quiet Revolution qr5. A schematic of the computer non-linear dynamic model of a wind energy conversion system is given in Figure 4.21 (more details in appendix B).

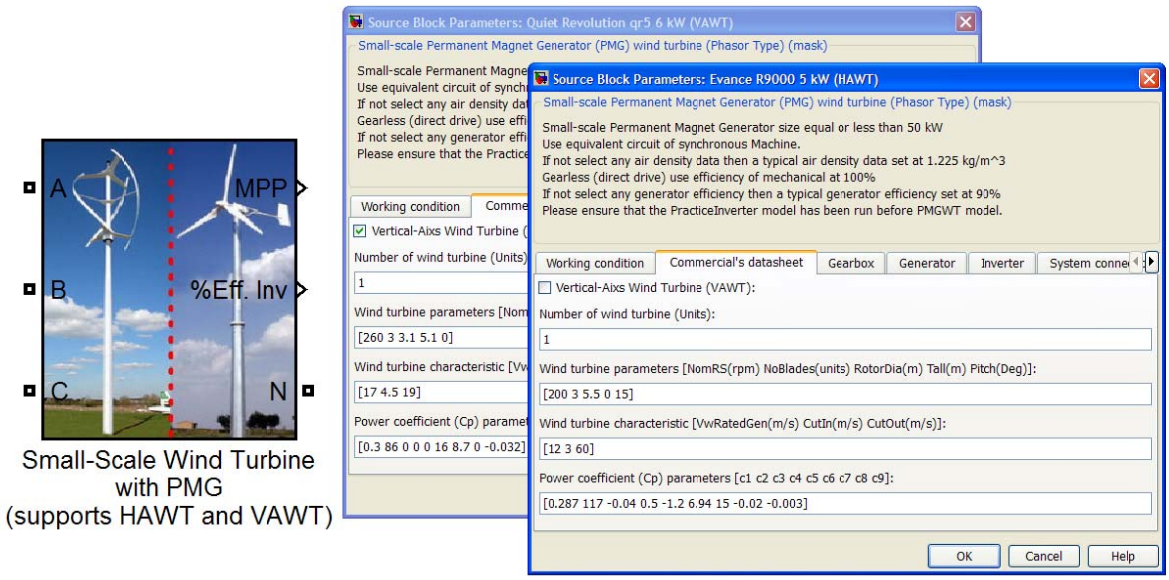

Figure 4.20 Input parameters of the proposed wind turbine model for the Evance R9000 of 5 kW (HAWT) and the Quiet Revolution qr5 of 6 kW (VAWT)

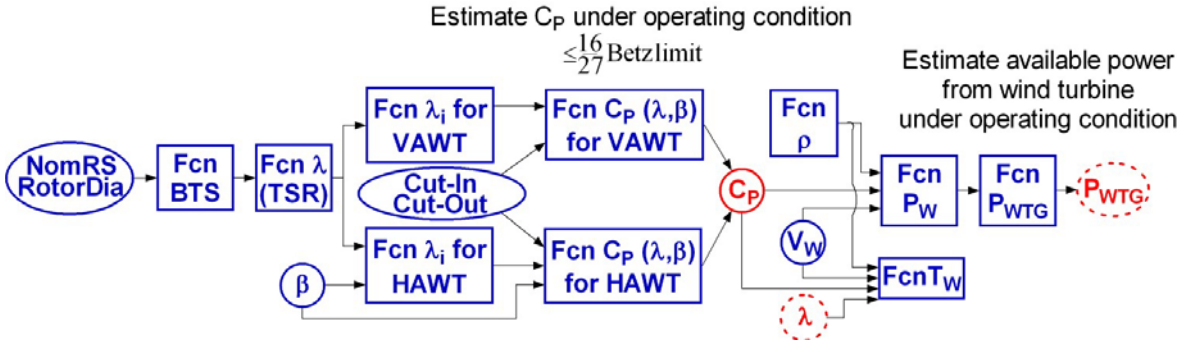

Figure 4.21 Schematic of the proposed small-scale wind turbine model

It can be noted that the feasibility function of the proposed model supports the single/dynamic input data of air density (ρ) in various conditions. Hence, the estimation function of ρ in the proposed model is divided into three conditions [222]. Firstly, ρ is determine by the elevation above sea level of location (S_{lw}) where the atmospheric pressure at standard sea level is equal to 101.325 kPa (P_{std}). Then,

$$\rho = 1.225 - (1.194 \times 10^{-4})(S_{lw}) \tag{4.63}$$

Consequently, the use of S_{lw} and ambient temperature (T_{aw}) improves the accuracy of the approximation of ρ. Therefore,

$$\rho = \left[\frac{P_{std}}{R(273.15+T_{aw})}\right] e^{\left[\frac{gS_{lw}}{R(273.15+T_{aw})}\right]} \tag{4.64}$$

Where, the specific gas constant (R) in dry air is 287 J/kg.K and the gravitation acceleration (g) is 9.81 m/s^2.

On the other hand, without information of the elevation of installation location, ρ can be determined by the relationship between gauge pressure (P_{aw}) and T_{aw}:

$$\rho = \frac{P_{aw}}{(287)(273.15+T_{aw})} \tag{4.65}$$

To evaluate the accuracy of the proposed model, both the Evance R9000 and the Quiet Revolution qr5 models were validated against experimental data (certificate commercial datasheets) and the Wind Power Program (using PDF with variable wind speed for Weibull distribution equation). The results are shown in Figures 4.22 and 4.23 [223-225]. It can be clearly seen that both HAWT and VAWT models have a very small relative error, which is less than 1 percent.

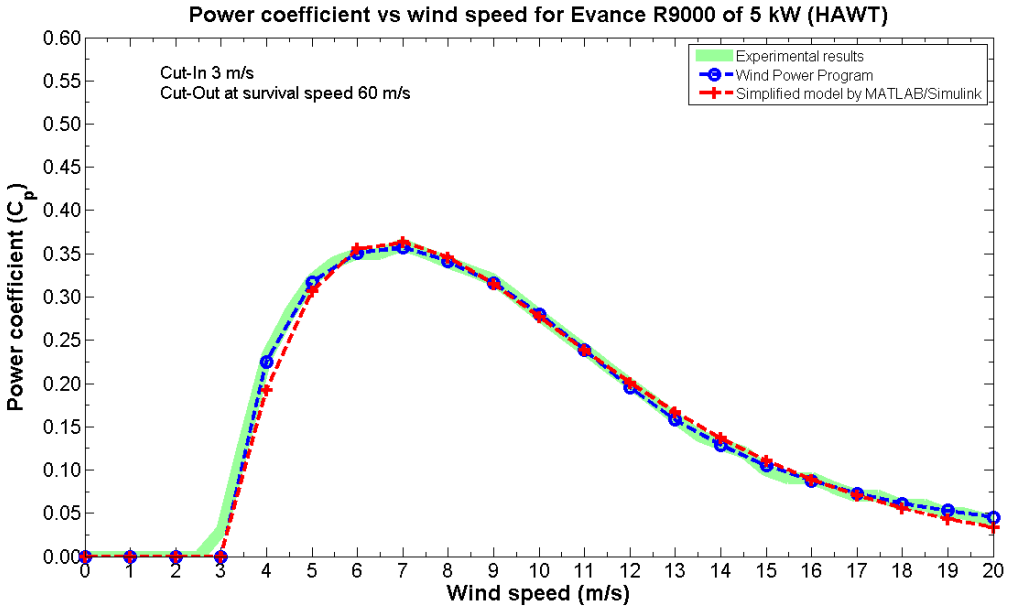

Figure 4.22 Comparison of C_P-V_W of the Evance R9000 (HAWT) between computer simulation, experimental results and Wind Power Program

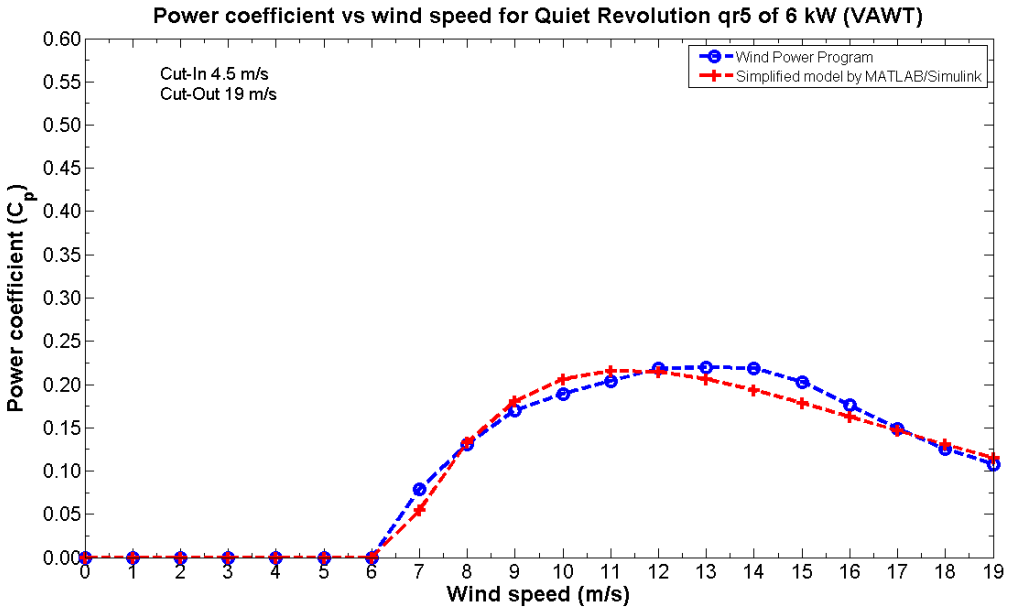

Figure 4.23 Comparison of C_P-V_W of the Quiet Revolution qr5 (VAWT) between computer simulation and Wind Power Program

4.4.1b) Hydro turbine

The other renewable energy resource that is considered in this thesis is the small-scale hydro turbine, where two types are modelled; closed pipe system and open channel (e.g. run-of-the-river systems, etc.), as shown in Figure 4.24.

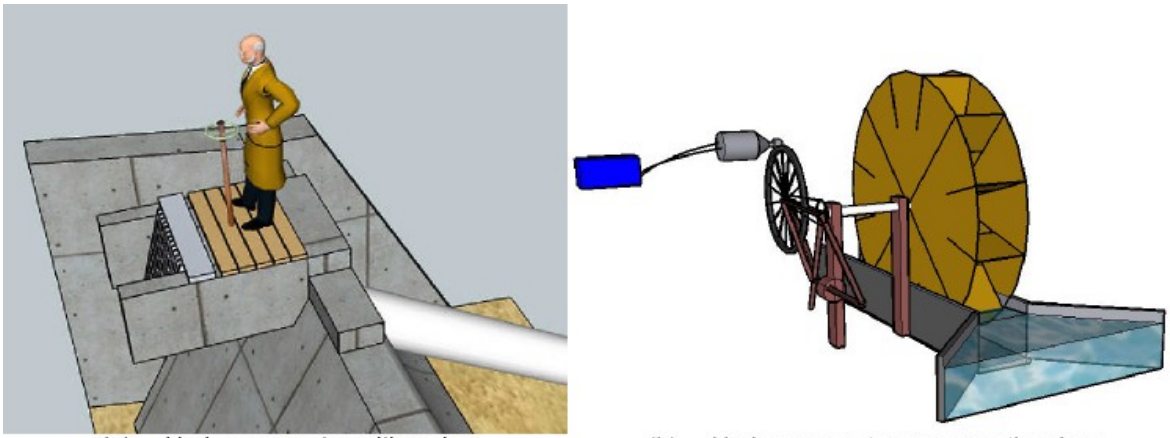

(a) μ-Hydro generator with weir (closed pipe system)

(b) μ-Hydro generator run over the river (open channel system)

Figure 4.24 Typical installation of small-scale hydropower system

It is obvious that the water flowing in the pipeline and open channel is different, and hence both systems were studied and applied in the simplified model. However, in the simplified hydro turbine model in references [149] and [150], the main (friction) losses due to pipe and nozzle in the closed system are not considered and are not supported in the open channel system as well. Therefore, this thesis proposed the simplified small-scale hydro turbine model (for closed or open channel systems), which supports single/dynamic input data. The following assumptions are used:

1) In the closed pipe system, the water fully flows uniformly and steadily through the pipe where all pipes are considered identical to each other.

2) The water flow in the close pipes only considers the loss of head due to friction (h_f), which is usually considered as a main loss in the pipe system. This friction has a proportional linear relationship to its length. The other minor losses such as loss due to turbulence, trash rack, bends in pipe, valves, etc. are neglected. Here, loss due to cavitations is also neglected because this phenomenon happens when the turbine is rotating at high speed, which quite difficult for small hydropower system to experience. Penche and Minas, [226] suggested that h_f is considered as the main loss and other losses are minor. Here, the pipe with neither completely smooth nor completely rough is considered in order to investigate realistic conditions.

3) In an open channel system, the water flows uniformly through the channel with the free surface, which means the absolute pressure is equal to the atmospheric pressure. Therefore, gauge pressure is equal to zero. This assumption is commonly set as reference along the length of the open channel (e.g. river, canal, etc.).

4) The water depth, area, water velocity and energy at the free surface in every cross section of the open channel system are considered to be uniform (constant). Moreover, gradient (sides slope) and the bottom lines are parallel to each other.

5) The mechanical loss due to the gearbox is lumped in a percent efficiency term and it is used in open channel system. Because the small hydro turbine in the open channel is usually using the gearbox to regulate the rotation speed of the turbine where the closed pipe systems are normally designed without gearbox.

From assumptions (1) and (2), the water flow in the pipe line can use Bernoulli's equation for steady frictionless incompressible flow along a streamline to estimate the total energy (H), and hence it is normally given in the term:

$$H = h_n + \left(\frac{P}{\gamma}\right) + \left(\frac{{V_W}^2}{2g}\right) \quad (4.66)$$

Where, h_n is the summation of the potential energy, the term of $\frac{P}{\gamma}$ is the pressure energy and the term of $\frac{{V_W}^2}{2g}$ is kinetic energy, P is the pressure in kPa. The specific weight of water per unit volume (γ) is 9790 N/m^3, V_W is the average velocity of water in m/s and the gravitation acceleration (g) is 9.81 m/s^2 [227]. In practice, the water flow in the pipeline is needed to consider the ratio of the inertia force to the viscous force because the water flow depends, not only on the velocity but also on the diameter of the pipe and the viscosity of the fluid.

Therefore, the proposed model of a closed pipe system is here considered as a circular pipe where, the diameter of the pipe (D_p) is in metres and the kinematic viscosity of the water (v) at 20°C is 1.005x10^{-6} m^2/s. These parameters are applied in order to define the Reynolds number, N_R: [227]

$$N_R = \frac{D_p V_W}{v} \quad (4.67)$$

The principle of conservation of mass to control volume is applied to estimate a certain amount of energy lost due to the friction in the pipe line in the steady-state, hence h_f: [227]

$$h_f = f\left(\frac{L_p}{D_p}\right)\left(\frac{{V_W}^2}{2g}\right) \tag{4.68}$$

In equation (4.68), the friction loss in the pipe is a function of D_p and length of pipe (L_p) in metres. Hence, the friction factor of the pipe (f) with the laminar flow can be directly estimated by: [227]

$$f = \frac{64\mu}{\rho V_W D_p} \Longrightarrow f = \frac{64}{N_R} \tag{4.69}$$

The friction factor term (equation 4.69) is substituted into equation (4.68), and hence h_f is proportional to V_W and inversely proportional to D_p because:

$$h_f = \left(\frac{64\mu}{\rho V_W D_p}\right)\left(\frac{L_p}{D_p}\right)\left(\frac{{V_W}^2}{2g}\right) \Longrightarrow h_f = \left(\frac{64}{N_R}\right)\left(\frac{L_p}{D_p}\right)\left(\frac{{V_W}^2}{2g}\right) \Longrightarrow h_f = \frac{32 L_p {V_W}^2}{N_R g D_p} \tag{4.70}$$

Equation (4.70) is normally used to estimate f in the laminar flow where, N_R is equal or less than 2300 [227]. However, the equation of f of a pipe neither completely smooth nor completely rough at turbulent flow $(N_R > 2300)$ is: [226-227]

$$\frac{1}{\sqrt{f}} = -2\log\left[\left(\frac{\frac{e}{D_p}}{3.7}\right) + \left(\frac{2.51}{N_R\sqrt{f}}\right)\right] \tag{4.71}$$

Hence, f is determined by the relationship between the proportion function of roughness factor of pipes (e) and D_p together with N_R (normally available in the Moody chart). Table 4.9 shows the typical roughness factor of pipes.

Table 4.9: The roughness factor (e) of various commercial pipes

Pipe material	e (mm)
Polyethylene[226]	0.003
Fiberglas with epoxy[226]	0.003
Seamless commercial steel (new)[226]	0.025
Seamless commercial steel (light rust)[226]	0.250
Seamless commercial steel (galvanised)[226]	0.150
Commercial steel (new)[227]	0.046
Metal sheet steel (new)[227]	0.050
Riveted steel[227]	3.000
Welded steel[226]	0.600
Stainless steel (new)[227]	0.002
Wrought iron[227]	0.046
Cast iron (enamel coated)[226]	0.120
Asphalt cast iron[227]	0.120
Iron (galvanised)[227]	0.150
Asbestos cement[226]	0.025
Concrete (steel forms, with smooth joints)[226]	0.180
Wood stave[226]	0.600
Smoothed rubber[227]	0.010

Source: [226-227]

However, some materials are not available in the Moody chart, and hence an iterative technique is required to determine f. References [226] and [227] suggested a set of friction equations, which supports various types of pipe, and hence it was chosen to simplify the hydro turbine model in this section. Therefore, f for various types of pipe is:

$$\alpha = -2\log\left[\left(\frac{\frac{e}{D_p}}{3.7}\right) + \alpha\left(\frac{2.51}{N_R}\right)\right] \tag{4.72}$$

Moreover, $\alpha = \sqrt{\frac{1}{f}}$ that means the friction factor of pipes for various materials is:

$$f = \frac{1}{\alpha^2} \tag{4.73}$$

The head losses due to the pipe friction can be obtained by substituting the friction factor term (equation 4.73) into equation (4.68):

$$h_f = \left(\frac{1}{\alpha^2}\right)\left(\frac{L_p}{D_p}\right)\left(\frac{{V_W}^2}{2g}\right) \tag{4.74}$$

Conversely, the Hazen-Williams coefficient (C) is used for pipe diameter more than 0.05 m and water velocity under 3 m/s (equation 4.75), and hence it is also applied into the proposed model as well. Table 4.10 presents the Hazen-William coefficient for various pipes.

$$h_f = \left(\frac{6.87L_p}{{D_p}^{1.165}}\right)\left(\frac{V_W}{C}\right)^{1.85} \tag{4.75}$$

Table 4.10: Hazen-William coefficient (C) for various pipes

Pipe material	**Hazen-William coefficient (C)**
Steel (brush tar and asphalt)	150
Steel (new uncoated)	150
Steel (Riveted)	110
Cast iron (new)	130
Cast iron (10 years)	107-113
Cast iron (20 years)	89-100
Cast iron (30 years)	75-90
Concrete (cast on site-steel forms)	140
Concrete (cast on site-wood forms)	120
Concrete (Centrifugal cast)	135
Asbestos cement	140
Wood stave	120
Plastic	135-140

Source: [226]

Therefore, the principle of conservation of mass to control volume and assumption (1) can define the water flow rate (or water discharge, Q). The fluid in the proposed model is considered nearly incompressible flow, and hence the variation of density can be considered negligible, if the mass-conservation equation is used. Then,

$$Q = AV_W \tag{4.76}$$

Where, A is the cross section of flow area in m^2.

Then the available mechanical power from the hydro turbine (P_W) is:

$$P_W = \gamma h_n Q \tag{4.77}$$

Where, h_n is the summation between potential head (h). Penche and Minas, [226] reported that the site installation can be divided into three categories, low head (less than 30 m), medium head (30 m-100 m) and high head (100 m and above).

It must be noted that Q in the proposed model is a function of the relative velocity between the water velocity available at the runner (either the water velocity at output nozzle; v_{jet} or the water velocity that immerse the blades; v_f) and the velocity of the runner (v_{rs}) where the cross section of flow area that project into the blades (A_{pb}) is affected. That means the turbine profile and site installation data are known.

In practice, the hydro turbine is divided into impulse and reaction turbines. The impulse turbine uses kinetic energy of a jet of water striking the blades in the air in order to rotate the blades (which normally use the nozzle), then v_{jet} is:

$$v_{jet} = \eta_{jet}\sqrt{2gh_n} \tag{4.78}$$

Where, η_{jet} is efficiency of nozzle.

On the other hand, the reaction turbine is usually immersed with the blades in the flow of water to convert kinetic energy of water into shaft power (based on linear momentum). Hence, v_f is:

$$v_f = \frac{Q}{b_k b_w 2\pi r_r} \tag{4.79}$$

In equation (4.79), b_k is the blades factor that is estimated from the number of blades, b_w is the width of the blade of the runner and r_r is the radius of the runner in metres. Penche and Minas, [226] reported that v_{rs} is typically equal to or less than 47 percent of available water velocity that strikes the blades:

$$v_{rs} = 0.47(v_{jet}, v_f) \tag{4.80}$$

Furthermore, A_{pb} depends on the site installation system, either closed pipe or open channel systems. Here, the circular pipe is considered in the closed pipe system, and hence A_{pb} (cross section) at exit nozzle is:

$$A_{pb} = \pi {r_j}^2 \tag{4.81}$$

Where, r_j is the radius at the exit of the nozzle in metres.

Substitute h_f term (equation 4.70, 4.74 or 4.75), A_{pb} term (equation 4.81), v_{jet} or v_f term (equation 4.78 or 4.79), and then v_{rs} term (equation 4.80) into equation (4.82) gives the available mechanical power of water turbine in a closed pipe system (P_{WC}) as:

$$P_{WC} = \gamma(h - h_f)A_{pb}[(v_{jet}, v_f) - v_{rs}] \tag{4.82}$$

Indeed, equations (4.67) to (4.82) explain the water flow in closed pipe system, which takes into account the head losses due to friction of pipe.

However, this proposed small hydropower system model also considers the water flow in an open channel where the assumptions (3), (4) and (5) are used to estimate the specific energy due to water area, Q and V_W. The V_W in an open channel system is given by: [226]

$$V_W = C\sqrt{R_h S_e} \tag{4.83}$$

Where, C is the Chezy's resistance factor, R_h is hydraulic radius of the channel and S_e is the hydraulic gradient of channel (head loss due to slope per 100 m e.g. if the channel falls 0.5 m every 100 m, then S_e is equal to 0.5).

In order to estimate C, the Manning roughness coefficient (n) for an open channel system in Table 4.11 is considered: [226]

$$C = \left(\frac{1}{n}\right) {R_h}^{\left(\frac{1}{6}\right)} \tag{4.84}$$

Table 4.11: Manning roughness coefficient (n) for open channel system

Channel	Type of channel	Manning coefficient (n)
Natural	Clean	0.022
	Gravelly	0.025
	Weedy	0.030
	Stony, cobbles (or natural streams)	0.035
Artificial	Brass	0.011
	Steel (smooth)	0.012
	Steel (painted)	0.014
	Cast iron	0.013
	Concrete (well finished)	0.012
	Concrete (unfinished)	0.014
	Planed wood	0.012
	Clay tile	0.014
	Brickwork	0.015
	Asphalt	0.016
	Corrugated metal	0.022
	Rubble masonry	0.025

Source: [226]

Substituting equation (4.84) into equation (4.83), gives R_h as:

$$R_h = 10^{\left[\frac{\log\left(\frac{V_W n}{\sqrt{S_e}}\right)}{\left(\frac{2}{3}\right)}\right]} \tag{4.85}$$

It is well known that the average water velocity (V_W) in an open channel system is usually kept within acceptable limits, which depends on the type of channel in order to avoid the erosion and plant growth at the gradient area. For a typical natural channel is below 0.7 m/s, except the sandy soil channel is 0.4-0.6 m/s. Furthermore, the artificial channel (concrete), V_W can increase up to 10 m/s without any danger however, to avoid silt flow in the channel, V_W should be at least 0.3-0.5 m/s [226]. From the Manning equation, Q in open channel system is:

$$Q = \left(\frac{1}{n}\right) A R_h^{\left(\frac{2}{3}\right)} \sqrt{S_e} \Longrightarrow Q = \frac{A^{\left(\frac{5}{3}\right)} \sqrt{S_e}}{n P^{\left(\frac{2}{3}\right)}} \tag{4.86}$$

From equation (4.86), both V_W and Q are required properties of the open channel system, as shown in Table 4.12. It should be noted that the trapezoid channel model is needed, if the side slope (m) with inclination between depth of channel (vertical) and bottom width of channel (horizontal) is to be considered.

Table 4.12: Geometrical properties of typical open channels

Properties	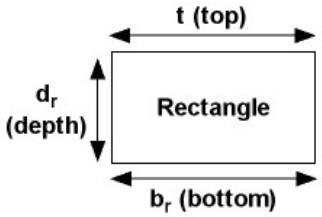	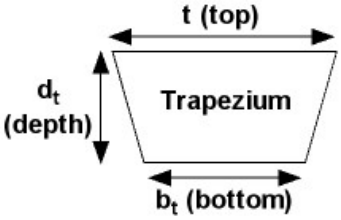
Cross section of flow area (A)	$b_r d_r$	$(b_t + md_t)d_t$
Wetted perimeter (P)	$b_r + 2d_r$	$b_t + 2d_t\sqrt{1+m^2}$
Hydraulic radius (R_h)	$\frac{b_r d_r}{(b_r + 2d_r)}$	$\frac{(b_t + md_t)d_t}{(b_t + 2d_t\sqrt{1+m^2})}$
Top width of section (T)	b_r	$b_t + 2md_t$
Hydraulic depth (D)	d_r	$\frac{d_t(b_t + md_t)}{b_t + 2md_t}$
Section factor	$b_r {d_r}^{1.5}$	$\frac{[(b_t + md_t)d_t]^{1.5}}{\sqrt{b_t + 2md_t}}$

Source: [226-227]

Therefore, the available mechanical power of water turbine in an open channel system (P_{WO}) is:

$$P_{WO} = \gamma h_n A_{pb}[v_f - v_{rs}] \quad (4.87)$$

Where, h_n describes the depth of flow and A_{pb} is the cross section area of blades (bucket) that are immersed in the water.

In an open channel system, a gearbox system may be used and this is defined by the percent efficiency of the gearbox system (η_{TG}). The available mechanical power transfer through the gearbox system (P_{WOTG}) is:

$$P_{WOTG} = \eta_{TG} P_{WO} \quad (4.88)$$

It can be concluded that the computer modelling of a small-scale hydro turbine is divided into two main types; closed pipe and open channel systems. The schematic of the proposed small hydropower system for closed pipe and open channel systems is summarised in Figure 4.25.

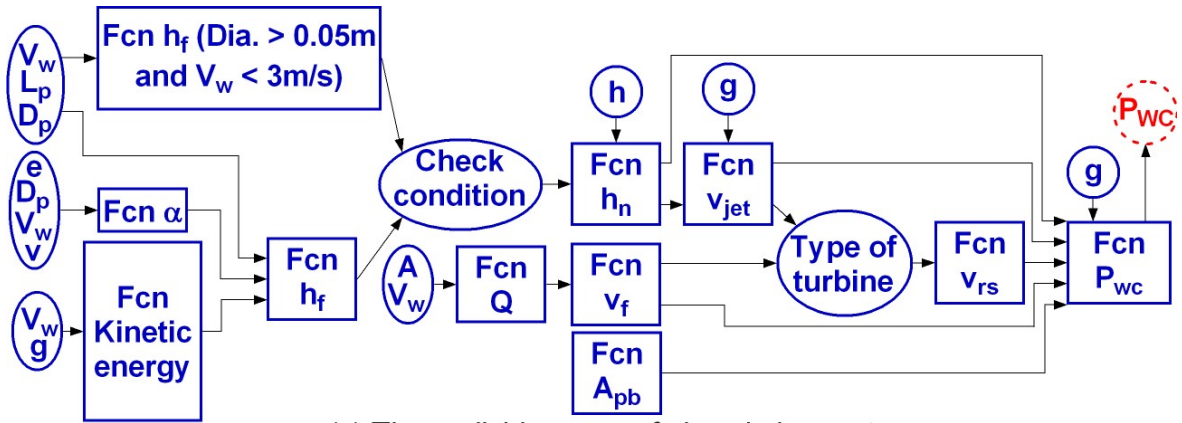

(a) The available power of closed pipe system

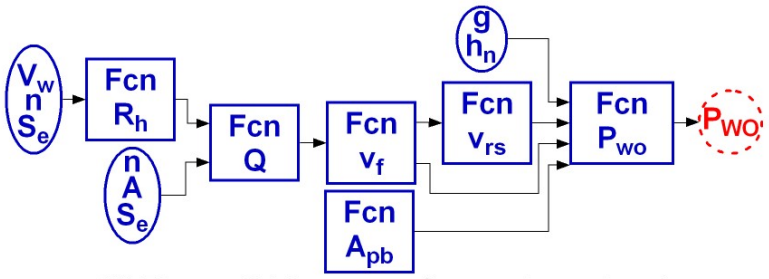

(b) The available power of open channel system

Figure 4.25 Schematic of the proposed small-scale hydro turbine model

In order to define a suitable type of hydro turbine for an installation, the specific speed (n_s), Q, and h_n are required [226]. The optimum rotational speed of a hydro turbine (n) in rpm is: [226]

$$n = n_s \left(\frac{h_n^{\frac{3}{4}}}{\sqrt{Q}} \right) \tag{4.89}$$

It can be mentioned that the different sizes of hydro turbine can have the same specific speed, this phenomenon is shown by applying equation (4.89): [226]

$$n_s = n \left(\frac{\sqrt{Q}}{h_n^{\frac{3}{4}}} \right) \text{ or } n_s = n \left(\frac{\sqrt{P}}{h_n^{\frac{5}{4}}} \right) \tag{4.90}$$

Table 4.13 shows the typical n_s based on characteristics of hydro turbines and Figure 4.26 explains the relationship between the rated flow and net head of various hydro turbines. It can be seen that the small hydro turbine usually has low water discharge less than 1.5 m^3/s and net head less than 30 m, hence either Propeller, Kaplan, Francis or Cross-flow is suggested.

The generated power data of small-scale hydro turbines are available in the UK, and hence the simulation of small hydropower for TH is conducted where the input parameters of the proposed small hydropower of 5 kW are shown in Figure 4.27 (more details in appendix B).

Table 4.13: Typical specific speed (n_s) of various types of hydro turbines

Characteristic	Type	n_s
Impulse	Pelton (1 jet)	$\frac{85.49}{h_n^{0.243}}$
	Pelton (n jets)	$\left(\frac{85.49}{h_n^{0.243}}\right)\sqrt{n}$
	Kaplan	$\frac{2283}{h_n^{0.486}}$
	Cross-flow (or Mitchell-Banki)	$\frac{513.25}{h_n^{0.505}}$
Reaction	Francis	$\frac{3763}{h_n^{0.854}}$
	Propeller	$\frac{2702}{h_n^{0.5}}$

Source: [226, 228]

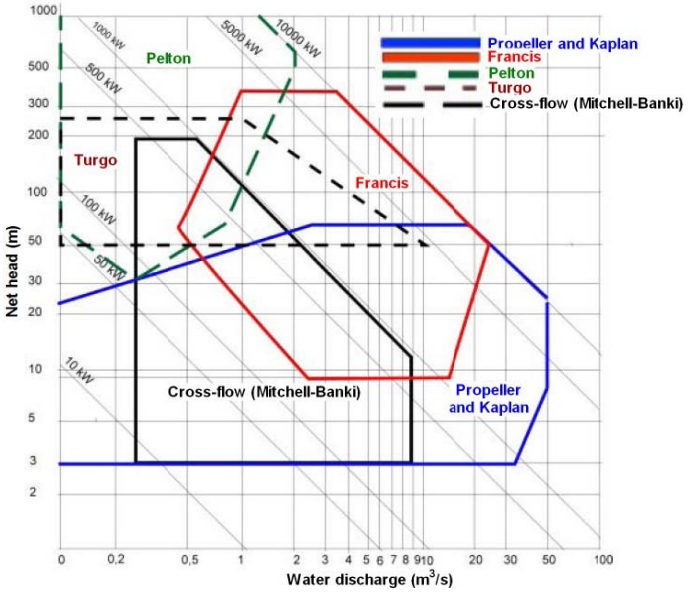

Figure 4.26 Relationship between rate flow and net head of turbine

Small-Scale Hydro Turbine
with PMG
Incorporate with either
Impulse or Reaction Turbine
for Closed Pipe or Open Channel

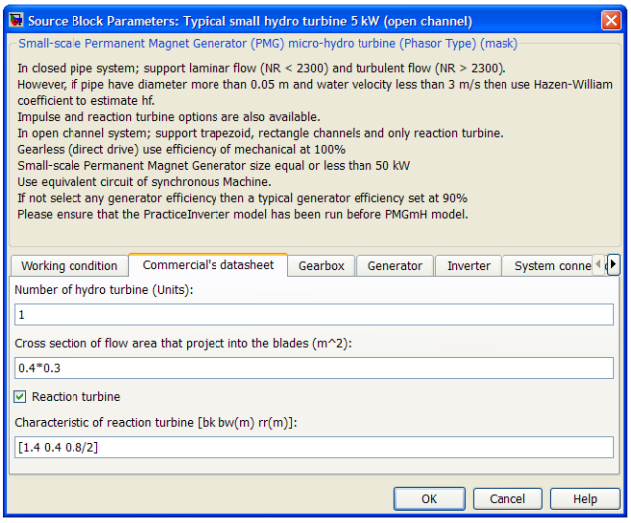

Figure 4.27 Input parameters of the proposed small hydropower of 5 kW in open channel system in TH

4.4.2 Modelling of Permanent Magnet Generators (PMG)

Small-scale generators for wind and hydro turbines usually employ synchronous generators with Permanent Magnet. This is because they are robust (no brush and slip ring), no excitation winding, and hence small size and lightweight. They can also offer direct drive (multi pole, hence supports low rotating speed). The proposed PMG model was developed by using Two-axis theory to estimate the armature current and evaluate the winding and armature core losses. The following assumptions were considered in order to simplify the PMG model:

1) The performance of wind and hydro turbines is carefully selected to match the size of the turbine and the rated power of generator. Thus, the simplified models of wind and hydro turbines provide the optimum mechanical output power.

2) The terminal voltage (V_t) is considered to be constant because the generator connects into the network (which is considered as an infinite bus) [137, 229-230].

3) In small PMGs, the armature winding resistance (R_a) is higher than the synchronous inductive reactance (X_s) [231].

4) In practice, the structure of PMG is usually based on salient pole, and hence its physical size is large when multi poles are required. However, small size of PMGs will behave as cylindrical (wound or round) rotor instead of salient pole regarding the large numbers of magnetic pole pairs, which will be mounted into that small rotor. Therefore, the air-gap between north/south magnetic poles becomes less as the proportion of magnetic pole pairs. That means the armature reaction reactance almost take place on the centre axis of the magnetic pole. Hence, the inductive reactance of the direct axis armature reaction reactance (X_{md}; d-axis mutual reactance) is equal to the inductive reactance of the quadrature axis armature reaction reactance (X_{mq}; q-axis mutual reactance) [229-230].

5) The distribution of magnetic flux is sinusoidal. In practice, this depends on the number of pole pairs (P). Therefore, the small PMG has high magnetic flux, hence the distribution of magnetic flux become more sinusoidal, for the reason explained in assumption (4) and [138].

6) The stator commencing by non-magnetic materials is considered in order to prevent interlock between stator and rotor, which supports low wind speed and torque. Since magnetic materials are used for Permanent Magnet (PM), the high and strong magnetic field is produced. If the stator uses magnetic materials, then the high torque and wind speed are required. Accordingly, the field winding of the rotor is changed into PM that means the loss from magnetic field winding become less. This magnetic field is considered a constant.

7) Negligible damper winding effect in the generator, as the generator is usually connected to the network via an inverter. That means the feasibility functions of the inverter can maintain the output power at acceptable limits.

8) Negligible rotor inertia, friction and windage losses, as the physical size is too small.

In this thesis, the armature winding is referred to as Alternating Current (AC) winding. Based on these assumptions, the phasor diagram of a PMG with R_a and X_s can be derived and is shown in Figure 4.28.

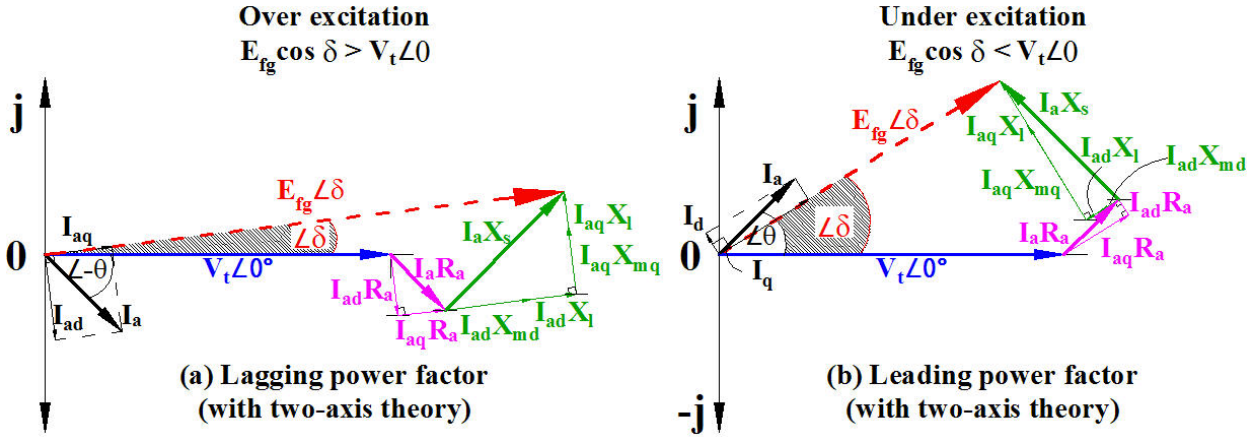

Figure 4.28 Phasor diagrams with Two-axis theory of a synchronous machine

Figure 4.28 shows the phasor diagrams of lagging and leading power factor of PMG by using Two-axis theory and considering constant power and angle. It can be noted that the synchronous generator (connected to the network) can support

the active/reactive power controls because the grid side of the inverter/converter can feed either leading or lagging current into the network. This control allows it to supply/consume reactive power where it is affected by the power angle (δ) between V_t and the induced voltage (E_{fg}). The higher the power angle, the more reactive power it can supply/consume.

In order to use Two-axis theory to analyse the armature current (I_a), the armature current on the q-axis (I_{aq}) is always projected on the E_{fg} axis, whereas the armature current on the d-axis (I_{ad}) is orthogonal 90 degree electrical to the I_{aq}. Then, I_a can be found from vectors I_{ad} and I_{aq} as:

$$I_a = \sqrt{{I_{ad}}^2 + {I_{aq}}^2} \tag{4.91}$$

It can be seen that two interesting conditions are obtained from Figures 4.28a and 4.28b,

$$E_{fg} = V_t \cos\delta + I_{aq}R_a + I_{ad}X_{sd} \tag{4.92}$$

$$0 = V_t \sin\delta + I_{ad}R_a - I_{aq}X_{sq} \tag{4.93}$$

Moreover, both the synchronous inductive reactance of the d-axis (X_{sd}) and the q-axis (X_{sq}) are functions of the leakage reactance (X_l) and armature reaction reactance on the d-axis and the q-axis respectively; that is:

$$X_{sd} = X_l + X_{md} \tag{4.94}$$

$$X_{sq} = X_l + X_{mq} \tag{4.95}$$

Where, X_l in Ω/phase is:

$$X_l = 2\pi f l \tag{4.96}$$

Where, f is the generated frequency at generator in Hz and l is the armature winding leakage inductance in Henrys.

As mentioned before, a small-scale PMG based on cylindrical rotor is considered in this thesis, hence $X_{md} = X_{mq}$. These conditions allow $X_{sd} = X_{sq}$ where it is equal to X_s of the cylindrical rotor. Because the presence of un-slotted portions that act as the poles are not projecting out. For these reasons, the surface of the cylindrical rotor is almost smooth then its presence can maintain as a uniform air-gap between the stator and the rotor. Consequently, X_{md} in Ω/phase may be expressed as: [229]

$$X_{md} = 2mf\left(\frac{\mu_0 DL}{k_\delta k_\mu \delta}\right)\left(\frac{Nk_w}{P}\right)^2 \tag{4.97}$$

Where, m is the relative function of number of phase, the magnetic permeability of free space (μ_0) is 4πx10^{-7} H/m, D is the diameter of the stator bore in metres , L is the effective length of the stator in metres, k_δ is the coefficient factor of the air-gap between stator and rotor, k_μ is the coefficient factor of magnetising at saturation, δ is the air-gap between stator and rotor in metres, N is the number of armature (coil) turns per phase, k_w is the coefficient factor of armature winding and P is number of pole pairs.

Both equation (4.96) and (4.97) require excessive details of the generator, which are hard to obtain from commercial datasheets. Therefore, an alternative way is to use open and short circuit tests at the generator in order to define the open-circuit voltage (V_{oc}), short-circuit current (I_{sc}) and obtain synchronous impedance (Z_s). Then,

$$Z_s = \frac{V_{oc}}{I_{sc}} \tag{4.98}$$

Moreover, R_a can be directly measured at the generator terminals. Hence,

$$X_s = \sqrt{{Z_s}^2 - {R_a}^2} \tag{4.99}$$

Then, I_{ad} and I_{aq} of small-scale PMG can be defined as:

$$I_{ad} = \frac{(E_{fg}+V_t\cos\delta)X_s - V_t R_a \sin\delta}{({X_s}^2+{R_a}^2)} \tag{4.100}$$

$$I_{aq} = \frac{(E_{fg}+V_t\cos\delta)R_a - V_t X_s \sin\delta}{({X_s}^2+{R_a}^2)} \tag{4.101}$$

It can be noted that E_{fg} in equations (4.100) and (4.101) is determined by the component of magnetic flux: [232]

$$E_{fg} = \pi\sqrt{2}k_p k_b N\phi f \tag{4.102}$$

This E_{fg} is a function of pitch factor or coil span factor of the armature winding (k_p), breadth or distributed factor of armature winding (k_b) and magnetic flux (ϕ). In addition, the approximate equivalent circuit of a typical synchronous machine (shown in Figure 4.29) can be used to define E_{fg} as well, and hence the equation is:

$$E_{fg}\angle\delta = V_t\angle 0° + (I_a\angle\theta)(R_a + jX_s) \tag{4.103}$$

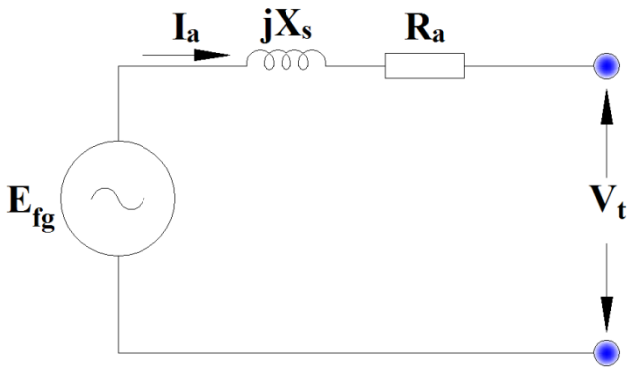

Figure 4.29 Approximate equivalent circuit of a typical synchronous machine

In a typical synchronous machine operated in standalone mode, E_{fg} depends on ϕ, which is determined by the field current. Conversely, V_t of a synchronous machine is constant when it synchronises to the network (considered as infinite bus), and hence E_{fg} and f are constant. Then adjusting the field current changes the power factor (shown in Figure 4.28). However, E_{fg} of a PMG (usually used in small-scale renewable energy) is induced by the magnetic flux of the PM, hence ϕ is constant. That means PMG incorporated with renewable energy, E_{fg} is a function of rotational speed (N_s) instead of ϕ. Therefore, the approximate electrical output power of a PMG (P_{Gen}), used with wind (equation 4.62) or hydro turbines (equation 4.82 or 4.88) and considering the percentage efficiency of the generator (η_{Gen}) is:

$$P_{Gen} = \eta_{Gen}(P_{WTG}, P_{WC}, P_{WOTG}) \tag{4.104}$$

On the other hand, the accuracy of the model is improved by considering the armature winding loss (P_{aw}) and/or armature core loss (P_{ac}). Thus,

$$P_{Gen} = (P_{WTG}, P_{WC}, P_{WOTG}) - P_{aw} - P_{ac} \tag{4.105}$$

Then, P_{aw} is defined by: [229]

$$P_{aw} = mR_a{I_a}^2 \tag{4.106}$$

Where, m is number of phases and I_a is defined from equation (4.100).

Consequently, P_{ac} is determined by: [229-231]

$$P_{ac} = \Delta p_{\frac{1}{50}} \left(\frac{f}{50}\right)^{\frac{4}{3}} \left(k_{adt}{B_t}^2 m_t + k_{ady}{B_y}^2 m_y\right) \tag{4.107}$$

Where, P_{ac} is a relative function of the specific core loss $\left(\Delta p_{\frac{1}{50}}\right)$ at 1Tesla or 1 Wb/m^2 with 50 Hz in W/kg, k_{adt} is the coefficient factor of magnetic flux density in the armature teeth, k_{ady} is the coefficient factor of magnetic flux density in the armature yoke, B_t is the magnetic flux density in the armature tooth, B_y is the magnetic flux density in the armature yoke, m_t is mass of armature teeth in kg and m_y is the mass of armature yoke in kg.

It can be noted that P_{ac} can be neglected in the simplified model of PMG because P_{aw} is much higher than P_{ac} [202, 229-230, 233-239]. However, the proposed PMG model in this thesis includes P_{ac} as an extra function, which improves the model accuracy. The schematic of the proposed PMG model is shown in Figure 4.30.

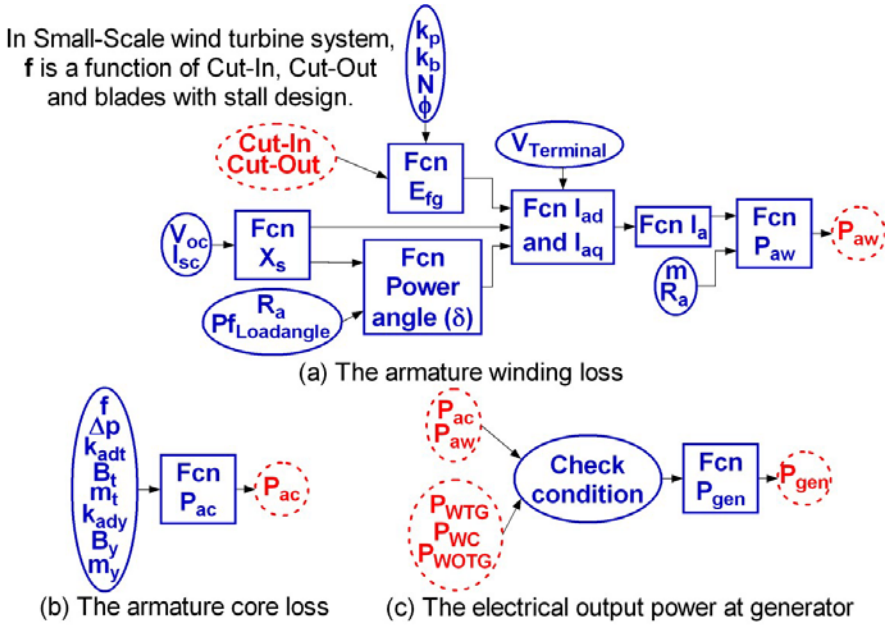

Figure 4.30 Schematic of the proposed PMG model

Therefore, the proposed turbine models (explained in section 4.4.1) and PMG model (described in section 4.4.2) are combined together in order to investigate the overall performance of small-scale wind and hydro turbines. Both simplified Evance R9000 (HAWT) and Quiet Revolution qr5 (VAWT) models were validated against experimental results (in certificate commercial datasheets) and Wind Power Program to ensure the accuracy of the model, as shown in Figures 4.31 and 4.32 (more details in appendix B).

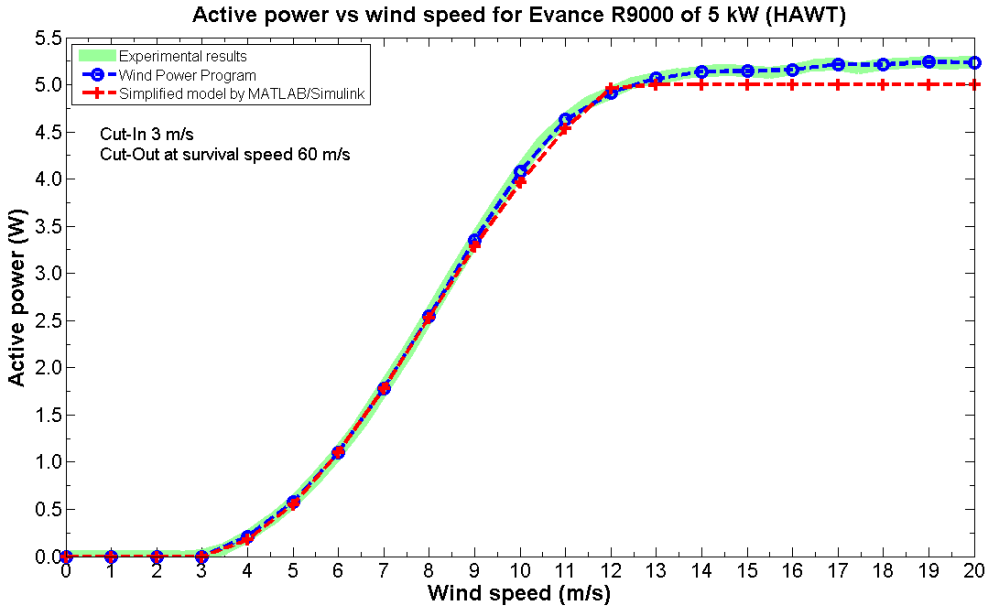

Figure 4.31 Comparison of P-V_W of the Evance R9000 (HAWT) between computer simulation, experimental results and Wind Power Program

Figure 4.31 shows that the simulation results of the computer model of the HAWT are slightly less than the experimental results at the stall region (where the wind speed is 11 to 20m/s). Because the model is more relevant at the starting point and maximum output power where the stall region at high wind speed is designed with the constant output power, as mention in the assumption (4) in section 4.4.1a. However, the VAWT model has a slightly larger error than the HAWT model because it was developed for the generic VAWT (shown in Figure 4.32).

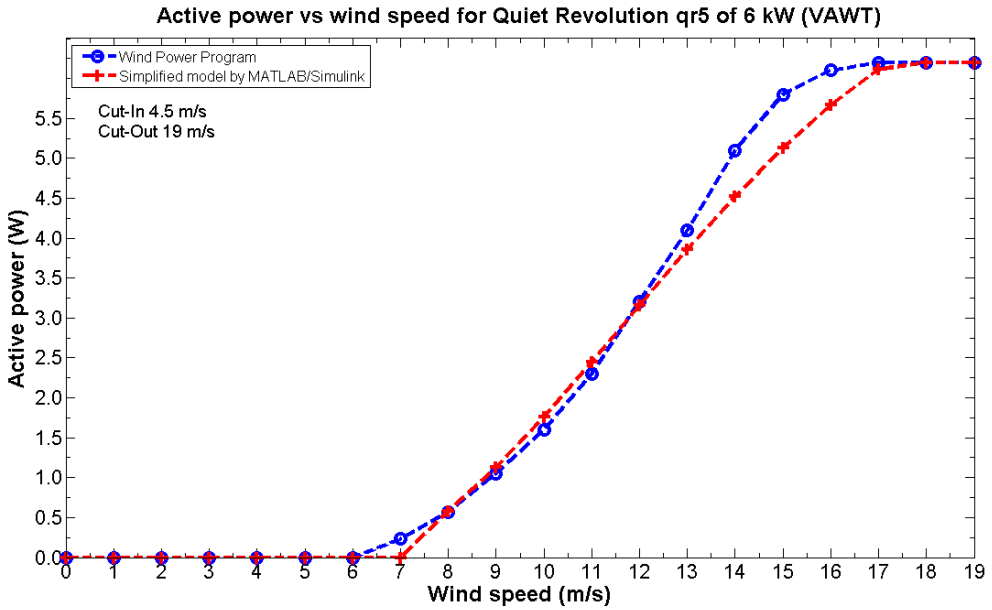

Figure 4.32 Comparison of P-V_W of the Quiet Revolution qr5 (VAWT) between computer simulation and Wind Power Program

As the aim of this thesis is to investigate the impacts of SSDGs on the distribution network, the Evance R9000 (HAWT rated at 5 kW) and the WINDYBOY 5000-US (inverter rated at 5 kW) were chosen and connected on the UK and TH networks models (technical data provided by the manufacturers) [146, 223]. The conversion energy system of wind or hydro turbines model is combined with the inverter model (described section 4.2). The variable wind speed and air density data in the UK are shown in Figure 4.33 [134].

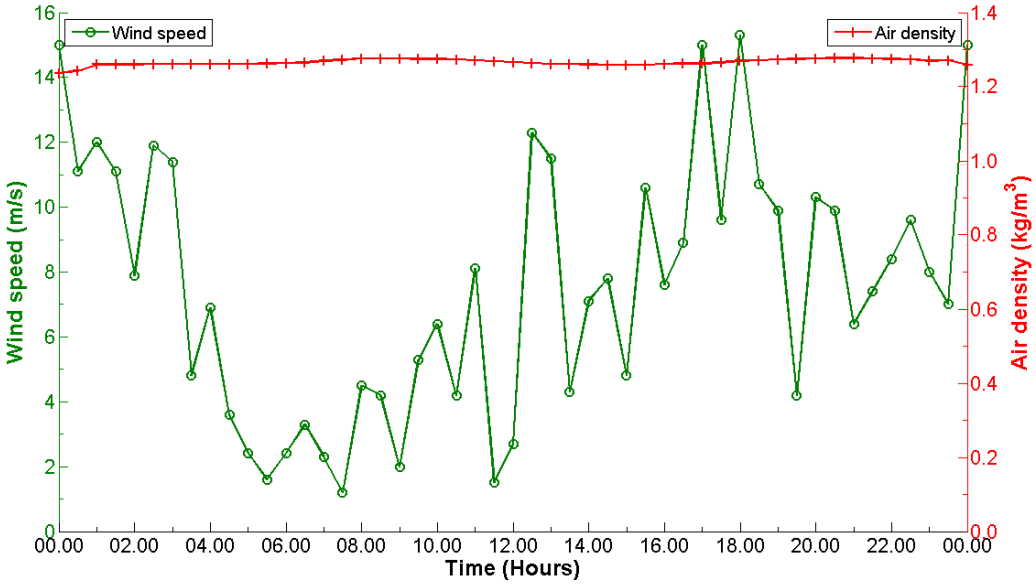

Figure 4.33 Average wind speed and air density in the UK

The MPP output power of the Evance R9000 in the UK is shown in Figure 4.34. As can be seen, the inverter may be insufficient during 04.00-10.00 because the wind turbine generated power is less than 10 percent of the rated output power of the inverter.

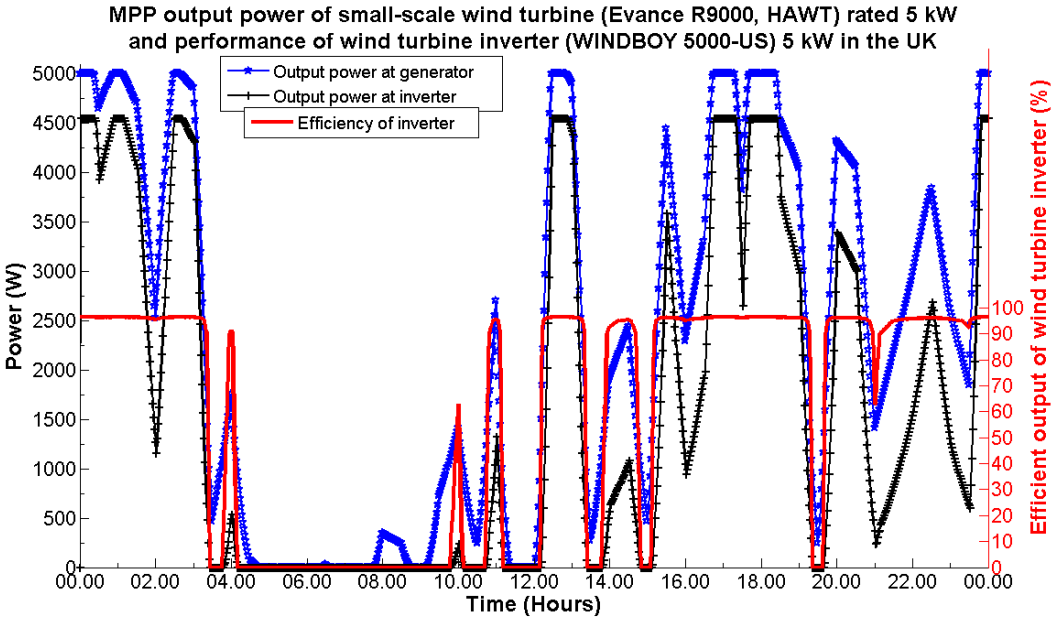

Figure 4.34 MPP output power and inverter performance of the Evance R9000 (small-scale HAWT) under variable wind speed in the UK

Figure 4.35 shows the variable wind speed and air density data in TH [137]. The MPP output power of the Evance R9000 in TH is shown in Figure 4.36. In TH, the output power of the inverter is insufficient at 00.00-07.00, 17.00-19.00 and again 20.00-22.00 because of low wind speed (lower than 3 m/s, cut-in of wind turbine), hence the wind turbine cannot extract the wind energy. This is also affected by the slow response of the MPPT of the inverter, where it needs some time to match the sudden change of wind speed (here delayed up to 3 sec).

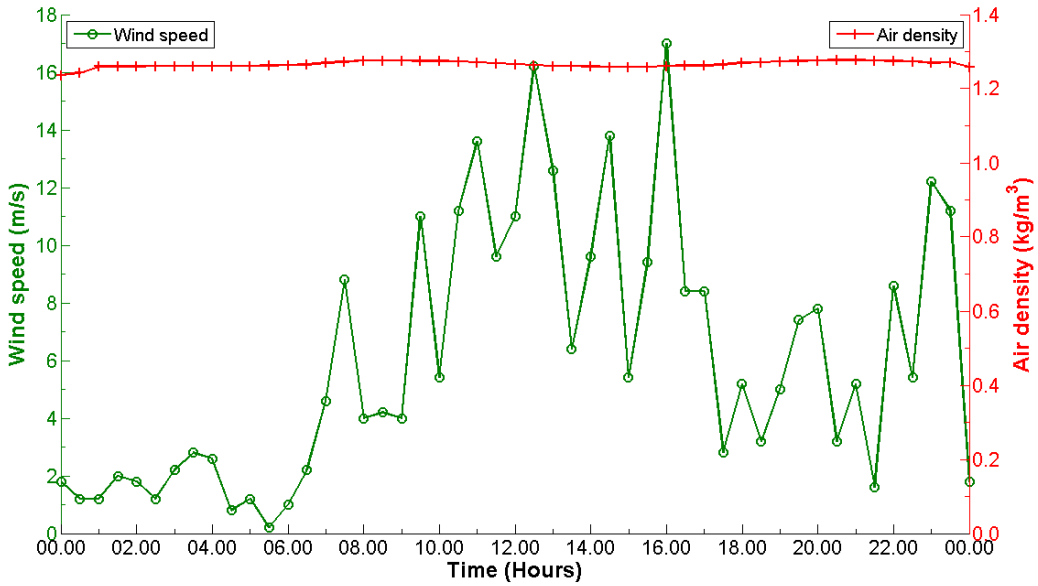

Figure 4.35 Average wind speed and air density in TH

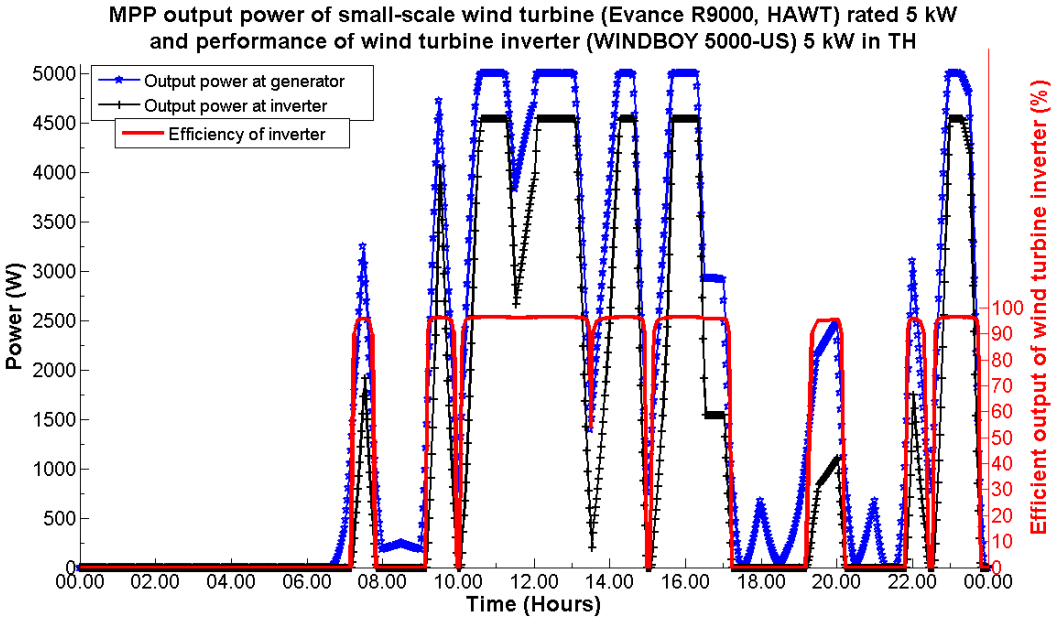

Figure 4.36 MPP output power and inverter performance of the Evance R9000 (small-scale HAWT) under variable wind speed in TH

Moreover, here the proposed computer models of a small hydro turbine and inverter rated at 5 kW were combined with the reaction turbine with 8 blades (diameter 0.80 m and blades size 0.4 m x 0.3 m x 0.06 m) and connected the gear box system with efficiency 90 percent. The turbine installed in an open trapezoid channel (depth 2 m, width 5 m and slide slope at 1:2). Figure 4.37 shows the interval data of water velocity at every 30 minutes on 18th January 2011 at Ratchaburi (countryside area in TH) where it is similar to the average water velocity data in TH (shown in Figure 3.8).

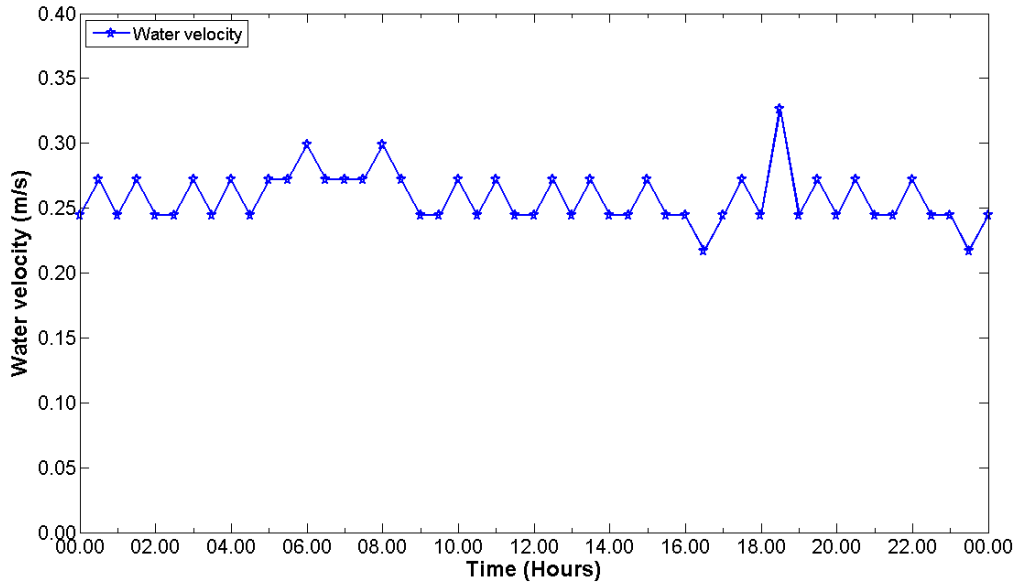

Figure 4.37 Typical water velocity of canal (open trapezoid channel) in TH

This set of water velocity data was recorded by digital water velocity meter (Xylem-FP211, shown in Table 4.15). Tables 4.14 and 4.15 present the characteristic of small hydropower (PMG rated at 5 kW) and equipment details of the small hydropower experiment.

Table 4.14: Characteristic of small-scale PMG of hydro turbine rated at 5 kW

Characteristic of small-scale PMG of 5 kW	Details
Specific speed of hydro turbine (N_s)	200 rpm
Number of slots	36 slots
Number of pole pairs (P)	6 poles
Pitch factor of armature winding (k_p)	1
Breadth factor of armature winding (k_b)	0.644
Magnetic flux (ϕ) from Neodymium magnet	0.0398 Wb
Total number of armature turns per phase (N)	360 turns
Armature winding resistance (R_a)	1.2 Ω
Synchronous inductive reactance (X_s)	9.9632 Ω

Table 4.15: Equipment details of small hydropower experimenter

Equipment	Model	Units	Remark
Digital water velocity meter	Xylem-FP211	1	Velocity accuracy 0.1 FPS[240]
Multi meter	Fluke 434	2	AC accuracy ±0.5% and DC accuracy ±0.1% of reading range[241]
Gauss (Tesla) meter	Magna MG-701	1	Accuracy ± 5% of reading with 10 digits[242]
Oscilloscope	Trktronix-1001B	1	40MHz, 500 MS/s, vertical sensitivity 2mV to 5V/div on all models, 2mV to 200mV/div+2V and >200mV to 5V/div + 50V[243]

Source: [240-243]

Figure 4.38 shows the MPP output power of a small-scale hydro turbine system. As can be noted, the output power of a small hydropower system is much steadier than PV and wind turbine systems because the water velocity (in the river, the canal or closed pipe) does not change very quickly like solar irradiation and wind speed. However, the generation profile of small-scale hydropower in the UK had been provided by UKGDS [133], and therefore is not simulated in this thesis.

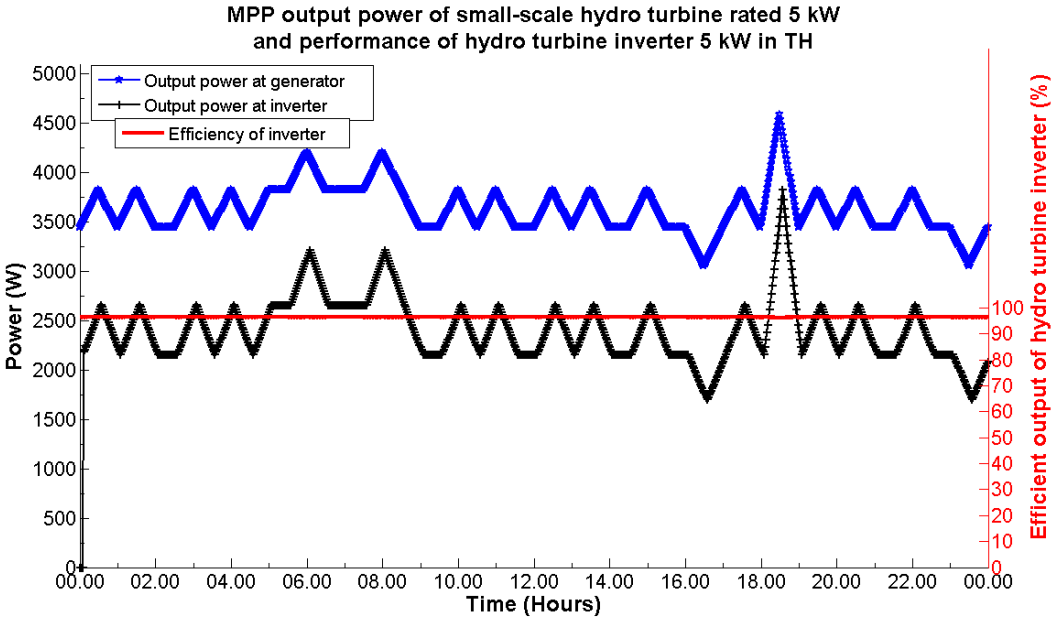

Figure 4.38 MPP output power and inverter performance of small hydro turbine under variable water velocity in TH

4.5 Modelling of EVs/PHEVs

From the network perspective, EVs/PHEVs that are connect to the network is considered as an active mobile load. As EVs/PHEVs can plug in anywhere in the network, and can increase the network demand (operated in charging mode) or supply power back into the network (operated in V2G mode). It is anticipated that V2G mode will be allowed in the future as grid interface devices of EVs/PHEVs are continually developing. Accordingly, these vehicles may be considered as an active load connected to the network (an infinite bus), hence they supply/consume constant power at constant voltage. Therefore, in this thesis, the fixed charging/regenerating current of EVs/PHEVs and the SOC of batteries were assumed.

This section presents the two proposed models of EVs/PHEVs, which are used to investigate their impacts on power networks (particularly voltage variation and harmonic distortion). Firstly, in order to study voltage variation in the power network, the controlled current source in the SimPowerSystem block set of Simulink programme was used for the EVs/PHEVs either charging or V2G modes. Both charging and V2G models are modelled by changing the direction of controlled current source with respect to the grid (more details in appendix B). Figure 4.39 shows the input parameters of the proposed EVs/PHEVs model for

voltage study. The feasibility function of the model includes number of EVs/PHEVs, rating of EVs/PHEVs (based on charging current) and phase angle (to ensure the same phase angle of EVs/PHEVs with respect to the local bus).

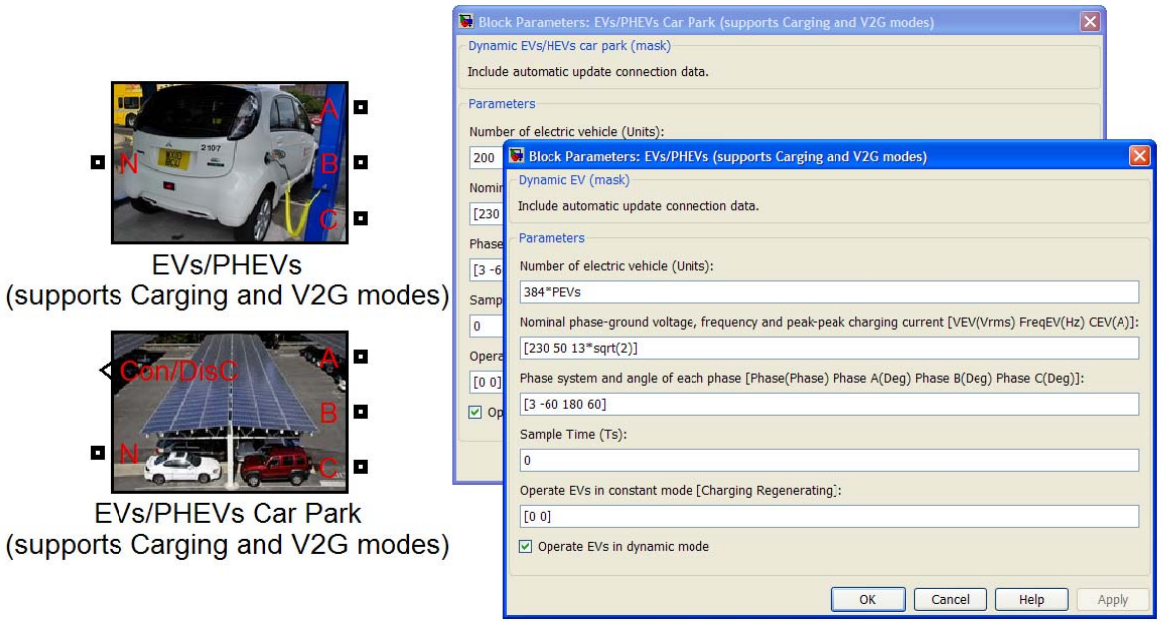

Figure 4.39 Input parameters of the proposed EVs/PHEVs model for voltage variation scenarios

The second model of EVs/PHEVs developed is based on the single-phase PWM controller, as shown in Figure 4.40. In practice, the PWM controller for EVs/PHEVs normally uses a switching frequency less than 2 kHz in order to generate the switching control signal for the rectifier circuit [37]. The average THD of the grid interface devices (e.g. grid inverter, EVs/PHEVs grid connection, etc.) is usually around 3 percent and the maximum THD is 8 percent [47].

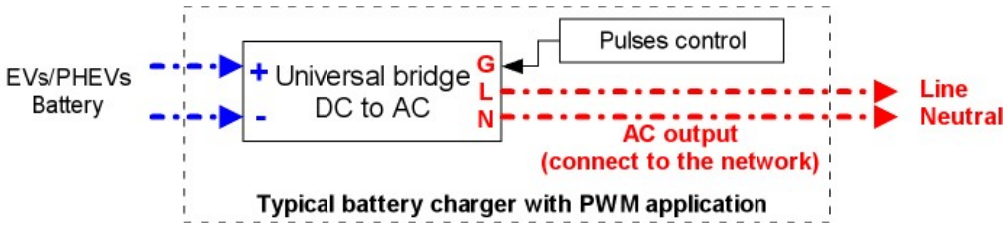

Figure 4.40 Modelling of EVs/PHEVs with single-phase PWM controller for harmonic distortion scenarios

CHAPTER 5
ANLYSIS OF IMPACTS OF SSDGs AND EVs/PHEVs ON DISTRIBUTION NETWORKS IN THE UK AND TH

In practice, distribution network operators are oblige to supply power to their consumers at acceptable levels. Each country has its own standard but still these standards must be based on the international standards as well. Thus, the worldwide standards about voltage levels in the distribution network that mostly apply to every country are the IEEE standards [36, 40, 45, 244]. This thesis investigates the voltage profile in the UK and TH and hence their standards need to be considered (more details in appendix A). The typical UK and TH networks described in chapter 3 were used for all scenarios considered in order to analyse and compare the impacts of SSDGs and EVs on different types of network. Details of the UK and TH networks are shown in table 5.1 (more details described in chapter 3).

Table 5.1: Details of the UK and TH networks

Details		UK network (urban area)	TH network (rural area)
Total length of feeder from MV to LV (m)		2407.7	7497
Total number of consumer (units)		18432	9673
General consumer (typical residence)	Maximum demand per consumer in community area (kVA)	1.30 (in winter)	2.94 (in summer)
	Minimum demand per consumer in community area (kVA)	0.17 (in summer)	1.07 (in winter)
	Maximum demand per consumer in countryside area (kVA)	Not available	1.28 (in summer)
	Minimum demand per consumer in countryside area (kVA)	Not available	0.28 (in winter)
Large consumer (such as university, etc.)	Maximum demand per consumer (kVA)	Not available	37.22
	Minimum demand per consumer (kVA)	Not available	5.53
The percentage of total maximum demand bases on the network capacity		~100	~73

The 30 minutes data intervals was used for the demand and generation profiles of the UK and TH because the energy spectrum of the wind profiles permits operation without lost of accuracy [245]. For both the UK and TH networks simulation time was set at 960 (equal to 86400 second or 24 hours) in order to prevent data over flow in MATLAB/Simulink programme and run out of memory of computer. MATLAB/Simulink solver ode23tb (which computes the time of the next step by adding a step size that varies depending on the rate of change of the model states) is set together with Interpolation-Extrapolation technique. The

relative tolerance and absolute tolerance for the solver ode23tb are set at 0.000001 and 0.0001. Hence, the number of sample data between each point of input data can be defined around 50 and up to 60 sample data for 1 simulation period. The solver ode23tb implements a multistep of implicit Runge-Kutta formula with a trapezoidal rule (TR-BDF2), which is at first stage, and second stage consisting of a backward differentiation formula of order two, and hence the same iteration matrix is used in evaluating both stages by their construction [144]. These techniques provide fast simulation and more efficiency.

It must be noted that the simulation results in this thesis may include unrealistic transient voltages, which are caused by the sudden connection/disconnection of large numbers of EVs/PHEVs in the simulation network at the same time (similar to connection/disconnection of a large load). It is known that the connection/disconnection of EVs/PHEVs in a real network would normally take a finite length of time and therefore it is not similar to this computer simulation. Moreover, the model of the OLTC is slightly different the realistic network as the size of step voltage of the OLTC model is larger than the real OLTC in order to match the step voltage with less tap changer. This is to prevent overflow data and run out of computer memory, similar results are shown in references [246-248]. This explains the transient voltages for all scenarios in this thesis.

5.1 Analysis of Voltage Profiles for the UK and TH Distribution Networks

Accordingly, this thesis is to simplify the distribution network in order to investigate the impacts of the SSDGs and EVs. Therefore, scenarios 1 to 6 from Table 3.5 were conducted in order to analyse the impacts of SSDGs (up to 5 kW) and EVs/PHEVs (domestic charging/regenerating at 3 kW) on the voltage variation in distribution networks. Figure 5.1 shows the single line diagram of the UK network for scenarios 1 to 3 (from Table 3.5).

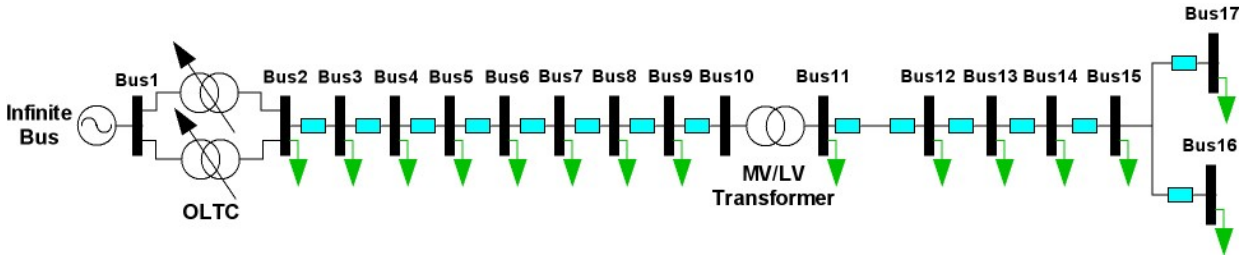

Figure 5.1 Single line diagram of the UK network for scenarios 1 to 3 (from Table 3.5)

The voltage profiles at the far of the feeder of the UK network in the winter and the summer, without SSDGs and EVs/PHEVs are shown in Figure 5.2. It is seen that the OLTCs that use the reference voltage (control) signal from local bus (bus 2) kept the voltage at all buses within the limits.

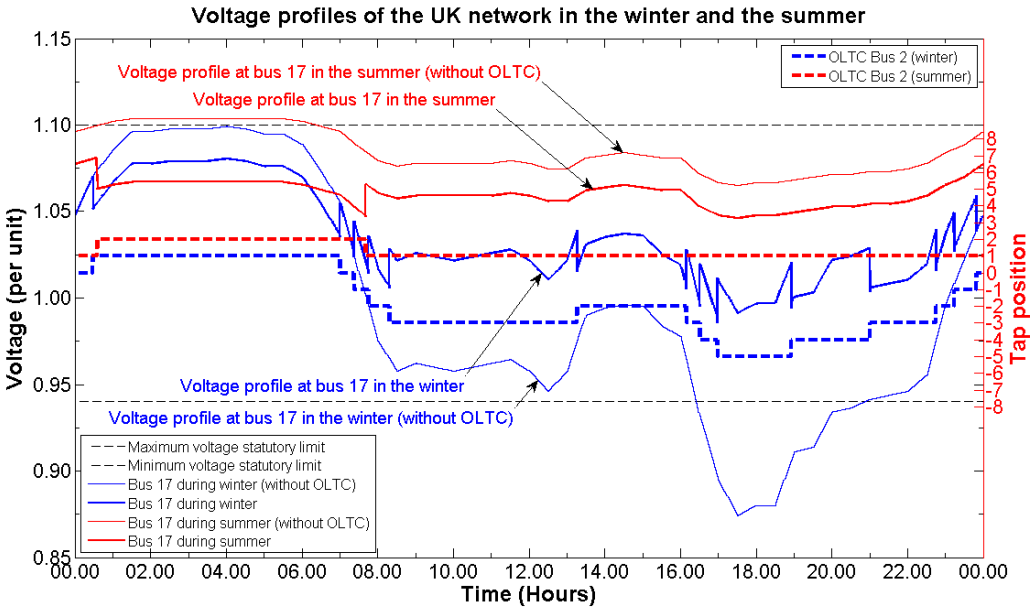

Figure 5.2 Voltage profiles of the UK network in the winter and the summer without SSDGs and EVs

The infrastructure of the TH network (shown in Figure 5.3) is different from the UK network as it is a rural area.

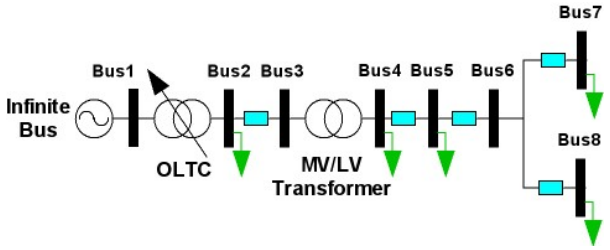

Figure 5.3 Single line diagram of the TH network for scenarios 1 to 3 (from Table 3.5)

The voltage profiles at the far of the feeder of the TH network in the winter and the summer, without SSDGs and EVs/PHEVs are shown in Figure 5.4. As can be seen, the OLTC that uses the reference voltage (control) signal from local bus (bus 2) kept the voltage at all buses within the limits.

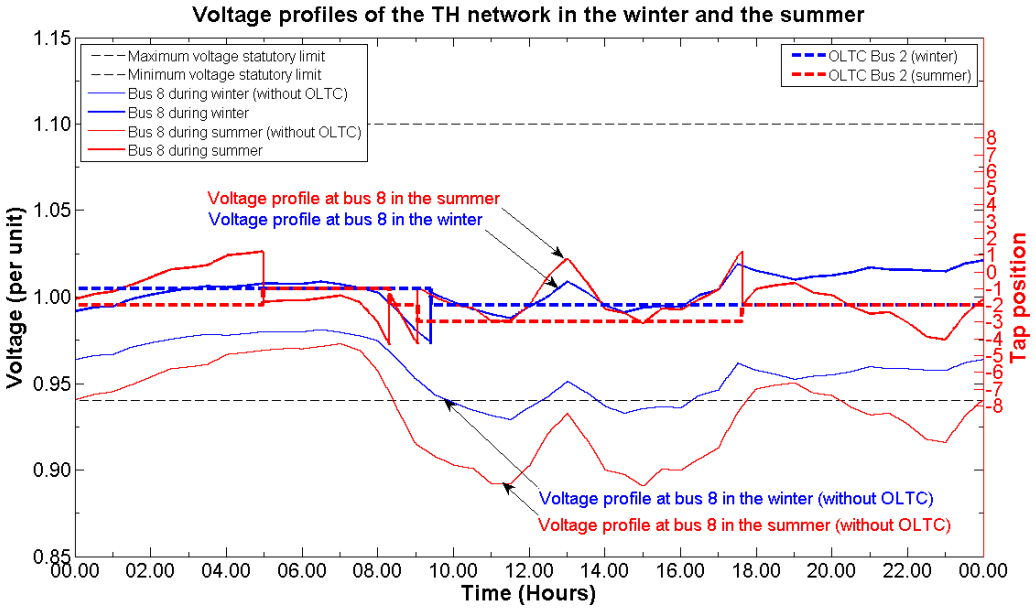

Figure 5.4 Voltage profiles of the TH network in the winter and the summer without connecting SSDGs and EVs on the network

Hence, it is expected that the difference of penetration levels of green technologies between the UK and TH networks is caused by the characteristics of the networks. The TH network is designed with long feeders (normally used in rural areas), and the UK network has short feeders (distributes power in urban areas). It is important to note that a long feeder is defined as that which extends beyond 15 km radius from a main substation (bulk supply point) and therefore the voltage is not below the minimum voltage statutory limit of 6 percent for 400 V. Accordingly, the number of consumers' on distribution networks with long feeders is normally less than that for short feeders, if both networks have the same supply capacity. Indeed, the number of consumers' in the urban network is usually close to the network capacity. Therefore, it can be seen that the total demand in the UK network is close to its network capacity, whereas the total demand in the TH network is about 73 percent of network capacity. In addition, the voltage profiles for the MV network in the UK and TH decrease from the main supply substation to the substation at the far end of the MV feeder. Then, the voltage level at the LV side of the secondary distribution transformer level is stepped up by transformer ratio of the off-load tap changer transformer. This phenomenon can be explained by the power flow equations (2.1) to (2.13) in chapter 2.

5.1.1 Scenario 1: Uniformly distributed SSDGs and EVs

Table 5.2: Details of scenario 1 for the UK and TH distribution network analysis

Scenario		Description	Aims
1	1.1	Uniformly distributed EVs (operating in charging and V2G modes, as given in Tables 3.1 or 3.2), PV or small-scale of wind/hydro turbines. Each is applied with increased penetration levels in 5 percent per step until the voltage profiles reaches the voltage statutory limits (excluding bus 5 in the TH network, which has a single EVs car park with 10 parking slots).	Define the limits for penetration levels for each scenario and the combination of green technologies that may be connected into existing distribution networks (assuming uniform distribution).
	1.2	Same as scenario 1.1, but a combination of the four types of green technologies are considered instead of individual type.	

Generation profiles of SSDGs in the UK are given in Figure 5.5. The profiles show that the potential generation in the early morning comes from wind and hydro turbines whereas the highest total generation is in the afternoon during 11.30-13.00.

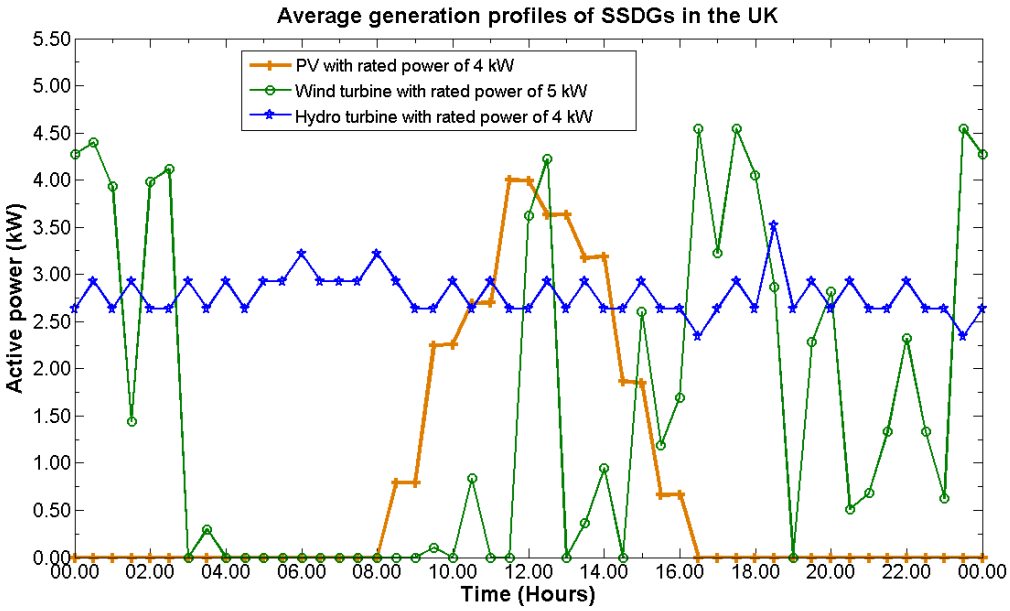

Figure 5.5 Average generation profiles of SSDGs in the UK

Figure 5.6 shows generation profiles of SSDGs in TH. The potential generation in the early morning comes from hydro turbine whereas the highest total generation is in the afternoon during 11.30-13.00.

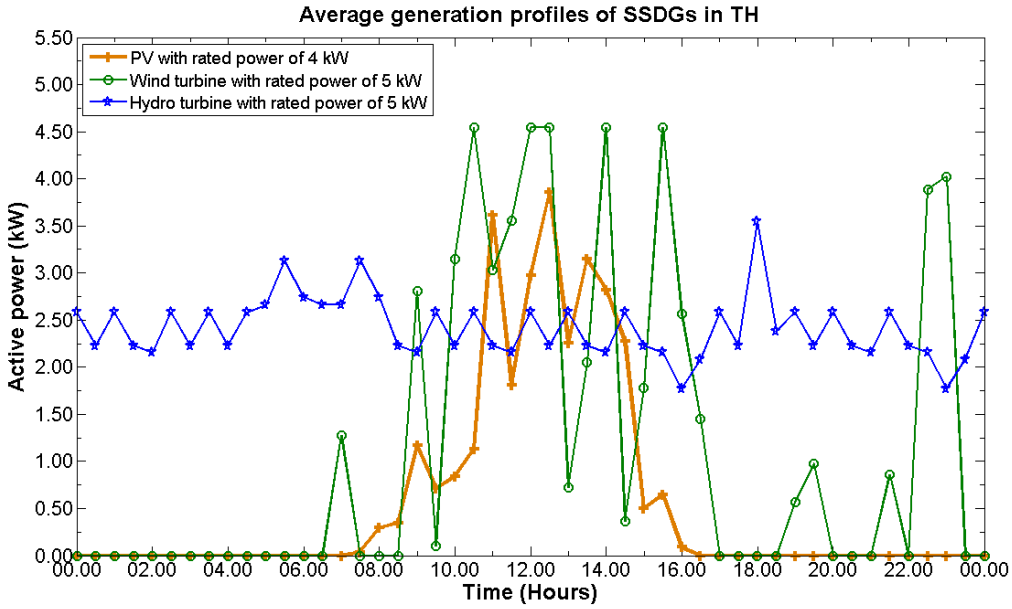

Figure 5.6 Average generation profiles of SSDGs in TH

5.1.1a) Scenario 1.1

Scenario 1.1 is used to identify the effects of different penetration levels and types of green technologies (mainly small-scale PV, wind, hydro turbines and EVs/PHEVs), hence extreme scenarios, based on the uniformly distributed EVs/PHEVs in the winter and the summer were considered. In these scenarios, the local OLTC bus sets the control signal for the OLTC. Figure 5.7 shows the voltage profiles in the UK network with 40 percent EVs uniformly distributed in the winter. As can be seen, the OLTCs at bus 2 keep the voltage at all buses within the limits except at the far end of the MV and LV feeders (at buses 10 and 17). The voltage at buses 10 and 17 are below the minimum voltage statutory limit of 6 percent for 400 V level (about 1 and 0.3 percent lower than the limit, respectively) during 19.00-19.30. The voltage at the far end of the LV feeder in the UK network reaches the maximum voltage statutory limit of 10 percent for 400 V level in the summer during 13.30-15.30 with 25 percent EVs uniformly distributed in the network, as shown in Figure 5.8. The reason is due to low demand and high generation from SSDGs and EVs operate in V2G mode.

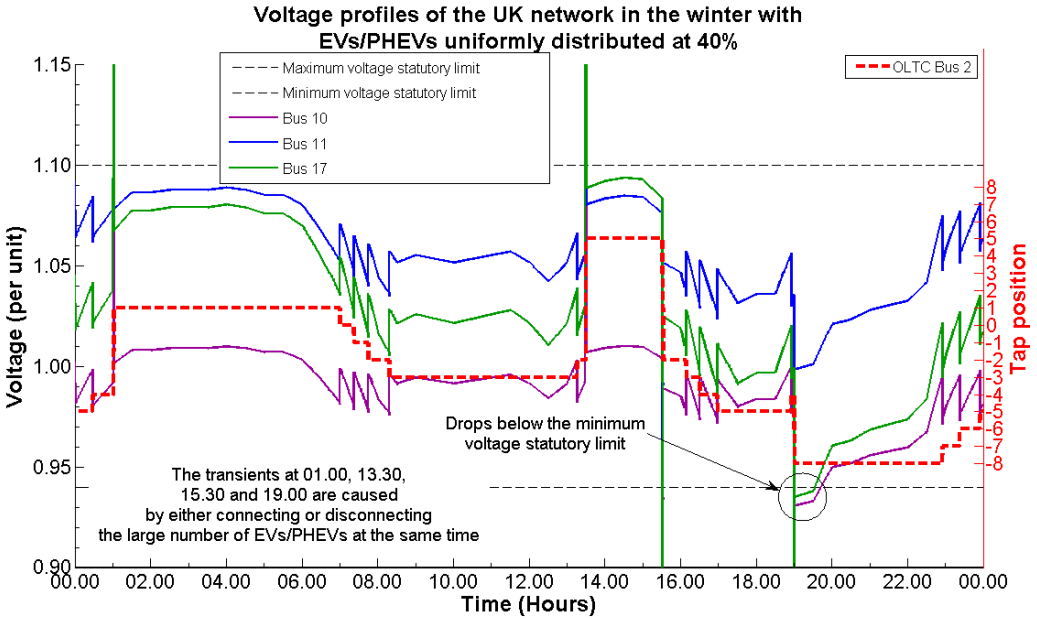

Figure 5.7 Voltage profiles of the UK network in the winter for scenario 1.1 (from Table 3.5)

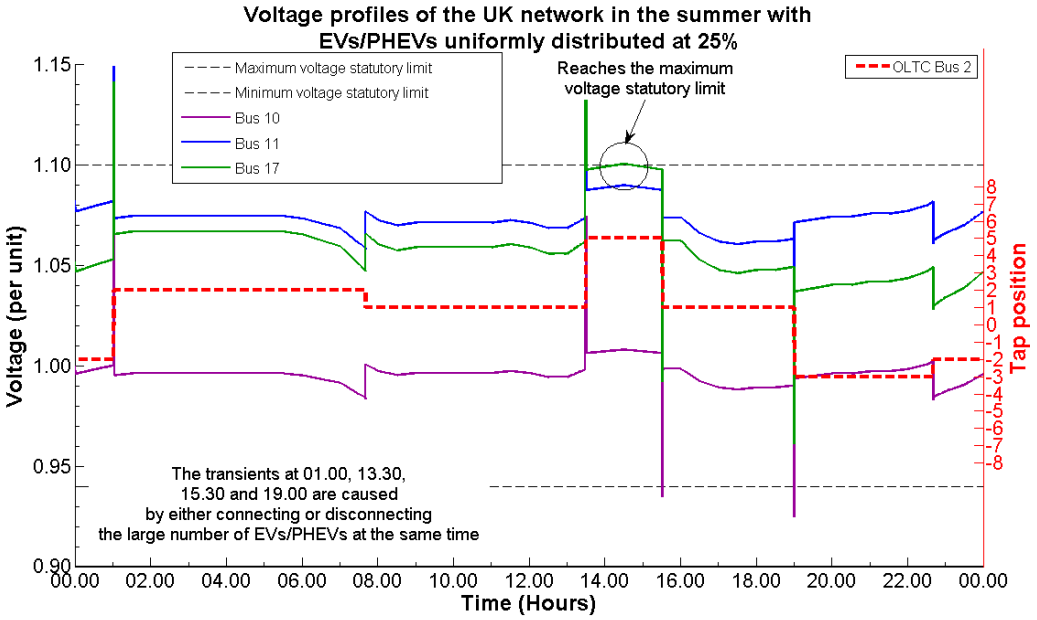

Figure 5.8 Voltage profiles of the UK network in the summer for scenario 1.1 (from Table 3.5)

From this scenario, it is found that the maximum penetration level of uniformly distributed PV (rated at 4 kW) is 15 percent whilst 10 percent for wind turbine (rated at 5 kW) and 15 percent for hydro turbine (rated at 4 kW). These penetration levels are defined by the minimum loading condition, which is summer in the UK.

On the other hand, in the winter and the summer in TH, the OLTC at bus 2 keeps the voltage at all buses within the limits with 100 percent uniformly distributed EVs, as shown in Figures 5.9 and 5.10. Furthermore, the maximum penetration levels for each type of SSDGs (uniformly distributed) in the TH network are 100 percent for PV (rated at 4 kW) and 100 percent for wind and hydro turbines (rated at 5 kW). The maximum penetration levels of SSDGs are defined by the minimum loading condition in the winter for the TH network.

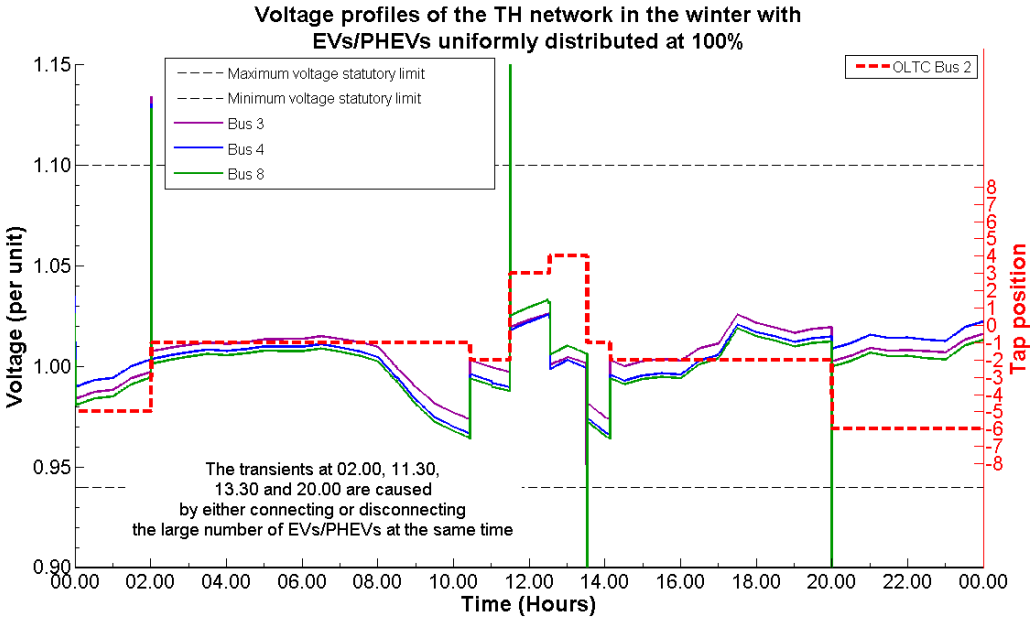

Figure 5.9 Voltage profiles of the TH network in the winter for scenario 1.1 (from Table 3.5)

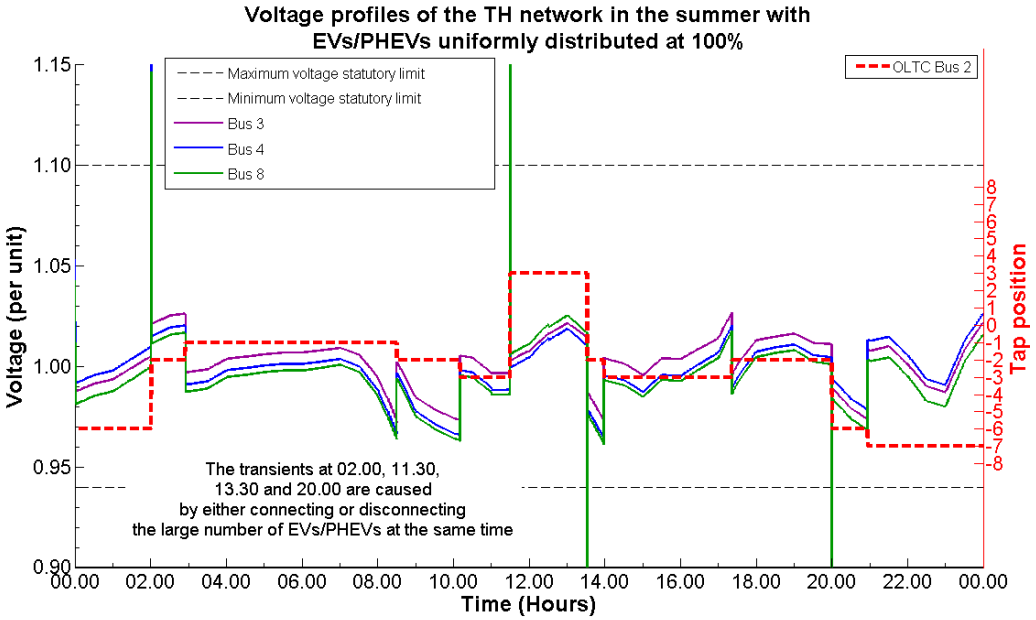

Figure 5.10 Voltage profiles of the TH network in the summer for scenario 1.1 (from Table 3.5)

5.1.1b) Scenario 1.2

Scenario 1.2 is used to identify the effects of different penetration levels of a combination of SSDGs (mainly small-scale PV, wind and hydro turbines) and EVs/PHEVs, and hence extreme scenarios (in the winter and the summer) are presented. The local OLTC bus sets the control signal for the OLTC. Figure 5.11 shows the voltage profiles of the combination of SSDGs and EVs/PHEVs scenario in the UK (in the winter) with 10 percent uniformly distributed SSDGs and EVs/PHEVs. As can be seen, the OLTCs at bus 2 kept the voltage at all buses within the limits except at the far end of the LV feeder (at bus 17). The voltage at the far end of the LV feeder exceeds the maximum voltage statutory limit of 10 percent for 400 V level (about 1 percent higher than the limit) during the early morning. The voltage at the far end of the LV feeder is also near to its limit again in the afternoon.

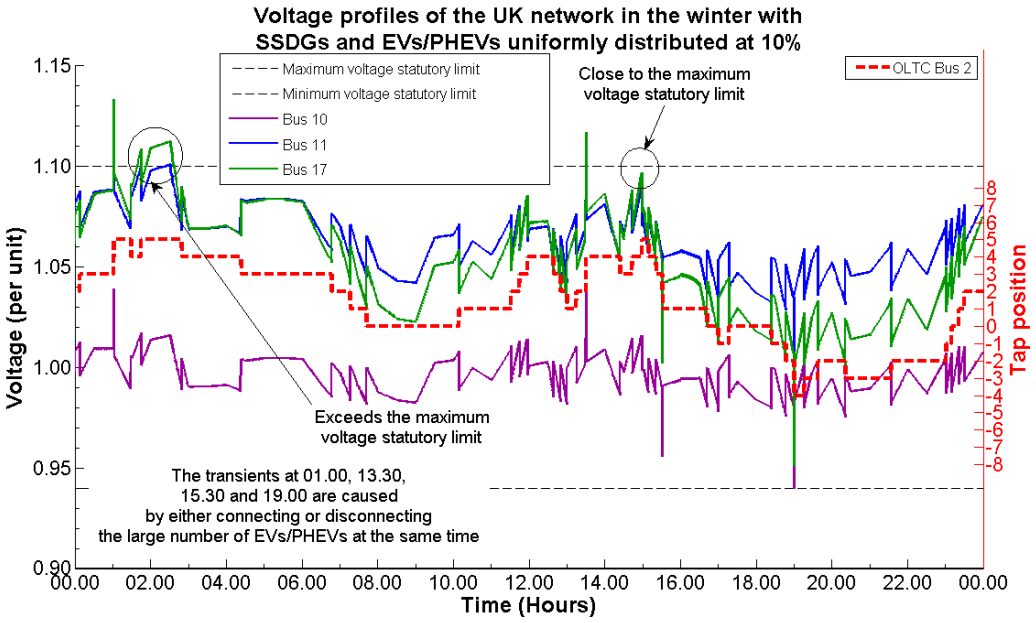

Figure 5.11 Voltage profiles of the UK network in the winter for scenario 1.2 (from Table 3.5)

Figure 5.12 shows the results of the UK network in the summer with only 5 percent penetration levels of the combination of SSDGs and EVs/PHEVs. The results show that the OLTCs at bus 2 can keep the voltage at all buses within the limits, the voltage profile at the far end of the LV feeder in the early morning and early afternoon is close the limits. In Figures 5.11 and 5.12, the voltage profiles exceed the limits at certain times when the SSDGs supply more power than the consumers' demand.

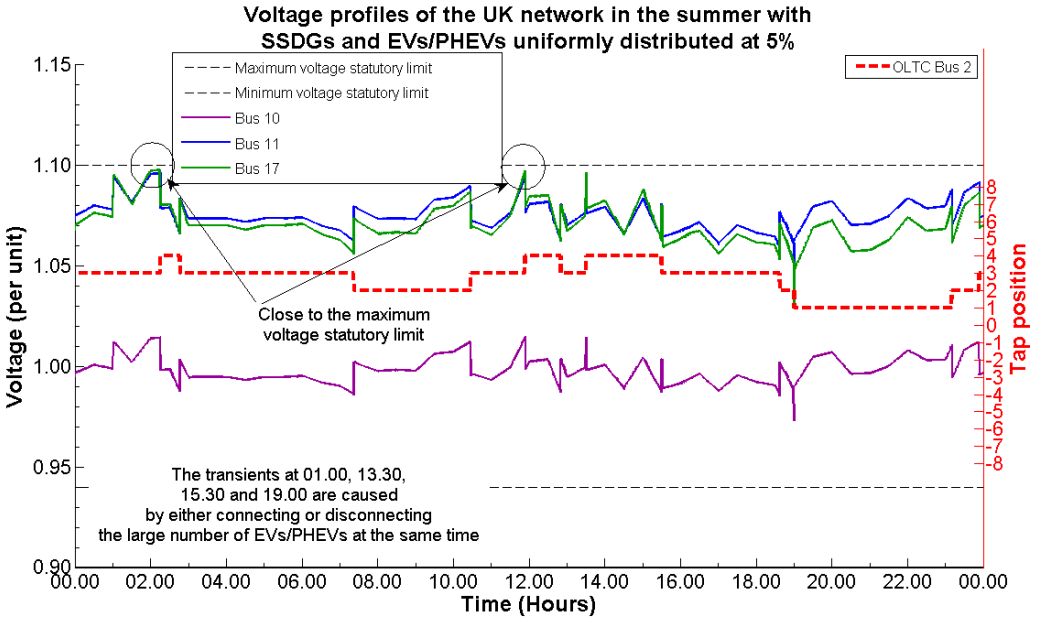

Figure 5.12 Voltage profiles of the UK network in the summer for scenario 1.2 (from Table 3.5)

A penetration level of SSDGs and EVs/PHEVs that potentially violates the voltage statutory limits in the winter in TH is 45 percent, as shown in Figure 5.13. The voltage at the far end of the MV and LV feeders exceeds the maximum statutory limit of 10 percent for 400 V (about 0.2 and 2 percent higher than the limit, respectively) in the afternoon. This is due to the high generation of SSDGs (shown in Figure 5.6), the EVs/PHEVs that operates in V2G mode and low demand (due to the energy saving policies as shown in Figures 3.5 and 3.6).

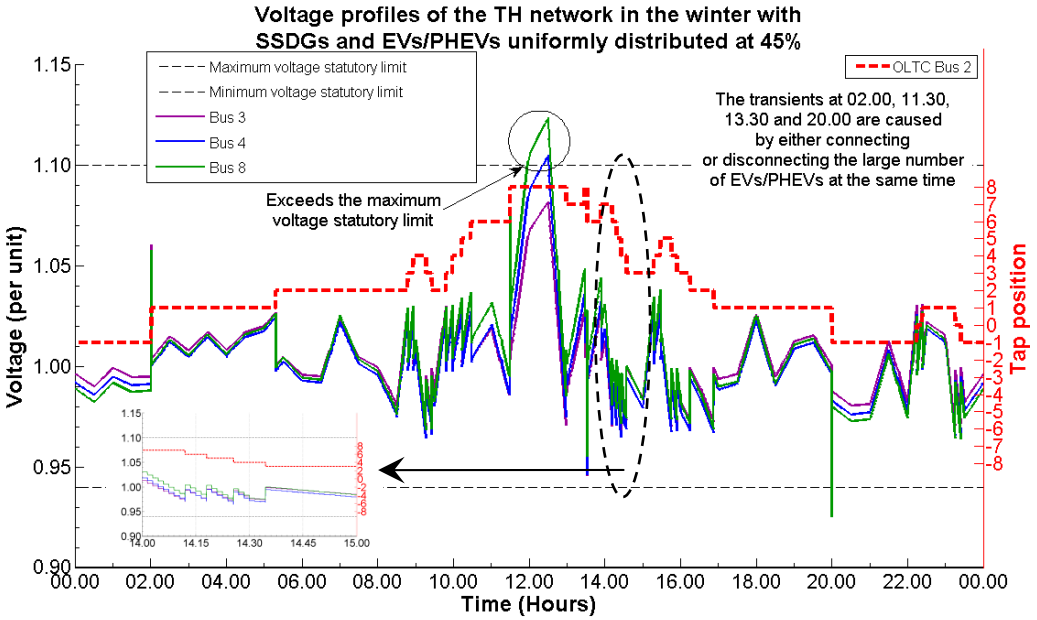

Figure 5.13 Voltage profiles of the TH network in the winter for scenario 1.2 (from Table 3.5)

Figure 5.14 shows that with 45 percent uniformly distributed SSDGs and EVs/PHEVs in TH network in the summer, the voltage at the far end of the LV feeder exceeds the maximum voltage statutory limit (about 1.5 percent higher than the limit) due to the operation of the OLTC and high generation of SSDGs.

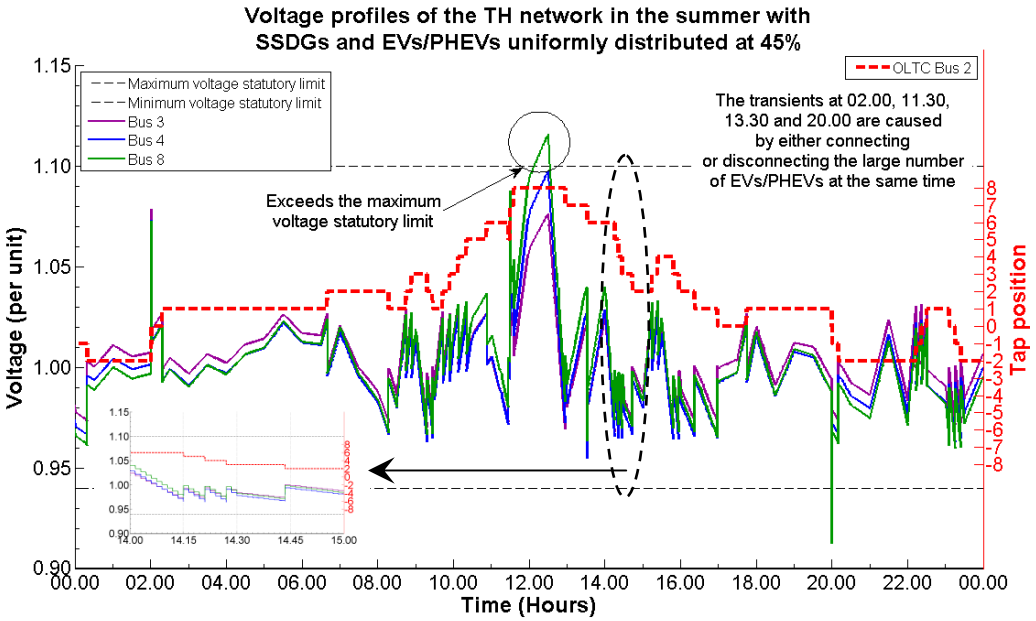

Figure 5.14 Voltage profiles of the TH network in the summer for scenario 1.2 (from Table 3.5)

From the voltage variation for scenario 1, it can be seen that the profiles of electricity demand and the generation determine the voltage variation in the distribution network. The peak demand is supported by the high penetration level of SSDGs and EVs/PHEVs (operating in V2G mode). In the UK network, a large demand in the winter is due to the heating loads, which are usually turned off during the night. Hence, 10 percent penetration level of the combination of SSDGs and EVs/PHEVs resulted in voltage rise in the early hours of the morning (shown in Figure 5.11). However, the TH network has the highest demand in the summer due to the use of air conditioning systems, and hence 45 percent penetration level is presented (shown in Figure 5.14) where it is higher than 35 percent in the UK network (in the winter) because of the long feeders for the TH network. In addition, it is interesting to note that the lower demand supports the high penetration level of EVs/PHEVs (operating in charging mode) as the available power in the network is sufficient to supply EVs/PHEVs. This observation applies to both the UK and TH networks.

Thus, it can be summarised that the maximum penetration level of green technologies that supply power back into the power should be determined by using the minimum demand, hence it is a function of the demand. This is opposite to the maximum penetration level that draws the power from the network, which is evaluated by the maximum demand. The large difference of penetration level of green technologies between the UK and TH networks is caused by the characteristic of the network which in the TH network is designed with the long feeder (distributes power in rural area), and the UK network is the short feeder (distributes power in urban area). The results shown in Figures 5.7 to 5.14 show that the typical OLTC on the MV/LV distribution networks still cannot support the high penetration levels of SSDGs and EVs/PHEVs in future power networks.

5.1.2 Scenario 2: Uniformly distributed SSDGs and EVs with active network control

Table 5.3: Details of scenario 2 for the UK and TH distribution network analysis

Scenario		Description	Aims
2	2.1	Same as scenario 1.2, except that the voltage control signal of the OLTC is changed from the local OLTC bus to the bus at the far end of the MV feeder.	Investigate the effects of changing the OLTC reference voltage control signal (active power control).
	2.2	Same as scenario 1.2, except that the voltage control signal of the OLTC is changed from the local OLTC bus to the bus at the far end of the LV feeder.	

5.1.2a) Scenario 2.1

Figures 5.15 to 5.18 show the voltage profiles in the winter and the summer for the UK and TH with network the highest penetration levels of SSDGs and EVs/PHEVs that are uniformly distributed (same as in scenario 1.2). However, the control signal for the OLTC is changed from the OLTC substation (at bus 2) to the far end of the MV feeder (at bus 10 for the UK network and bus 3 for the TH network). This is to allow investigation of active network control. Figure 5.15 shows that the voltage profile at the far end of the LV feeder in the UK network (at bus 17) exceeds the maximum voltage statutory limit of voltage for 400 V in the early morning during the winter, with 10 percent of SSDGs and EVs/PHEVs uniformly distributed in the UK network.

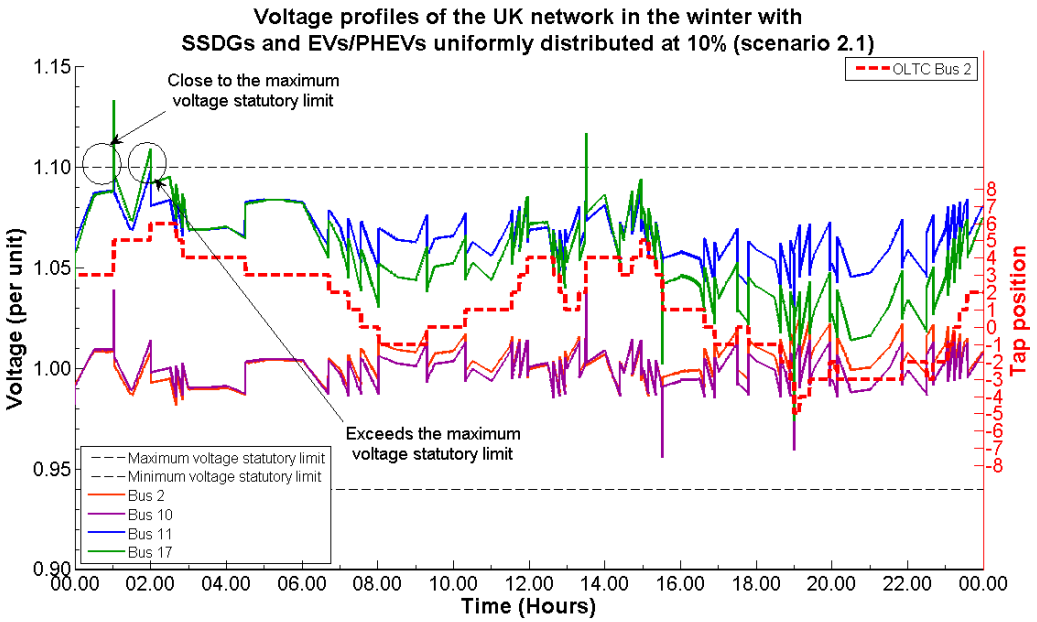

Figure 5.15 Voltage profiles of the UK network in the winter for scenario 2.1 (from Table 3.5)

Figure 5.16 shows that with 5 percent of SSDGs and EVs/PHEVs uniformly distributed along the distribution network in the UK in the summer, the OLTCs at bus 2 kept the voltage at all buses within the limits. The voltage at the far end of the LV feeder is close to the maximum voltage statutory limit of 400 V in the early morning during 01.30-02.00 due to the low demand and high generation in the power network.

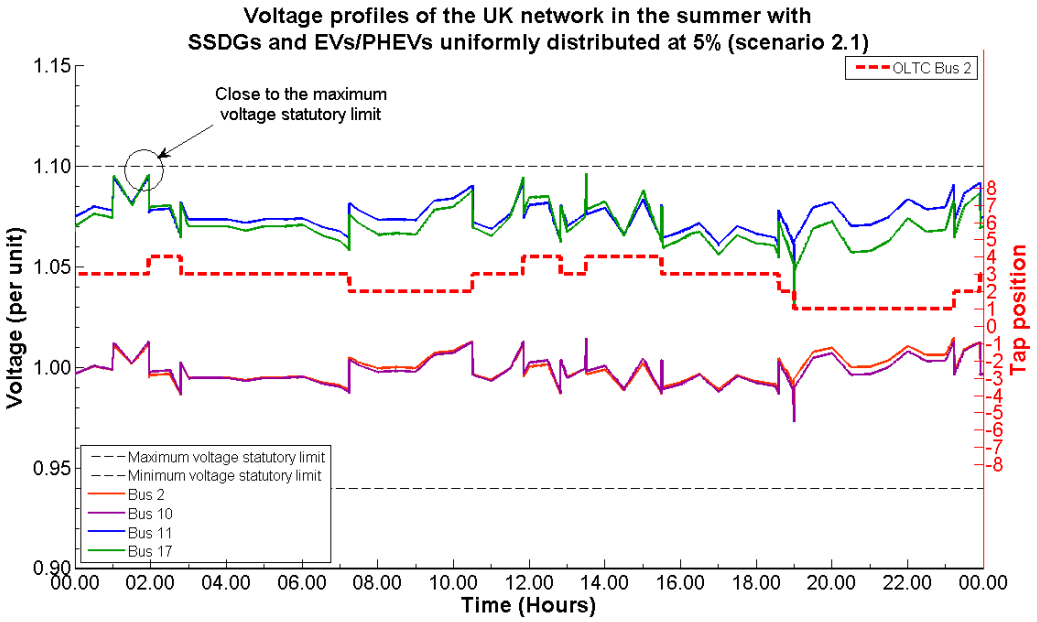

Figure 5.16 Voltage profiles of the UK network in the summer for scenario 2.1 (from Table 3.5)

However, a possible penetration level of SSDGs and EVs/PHEVs that violates the voltage statutory limits in the winter and the summer in TH is still 45 percent, as shown in Figures 5.17 and 5.18. The pattern of voltage and tap changer profiles for both winter and summer in this scenario is not similar to that in scenario 1.2 (shown in Figures 5.13 and 5.14) particularly the voltage rise at the far end of the MV and LV feeders.

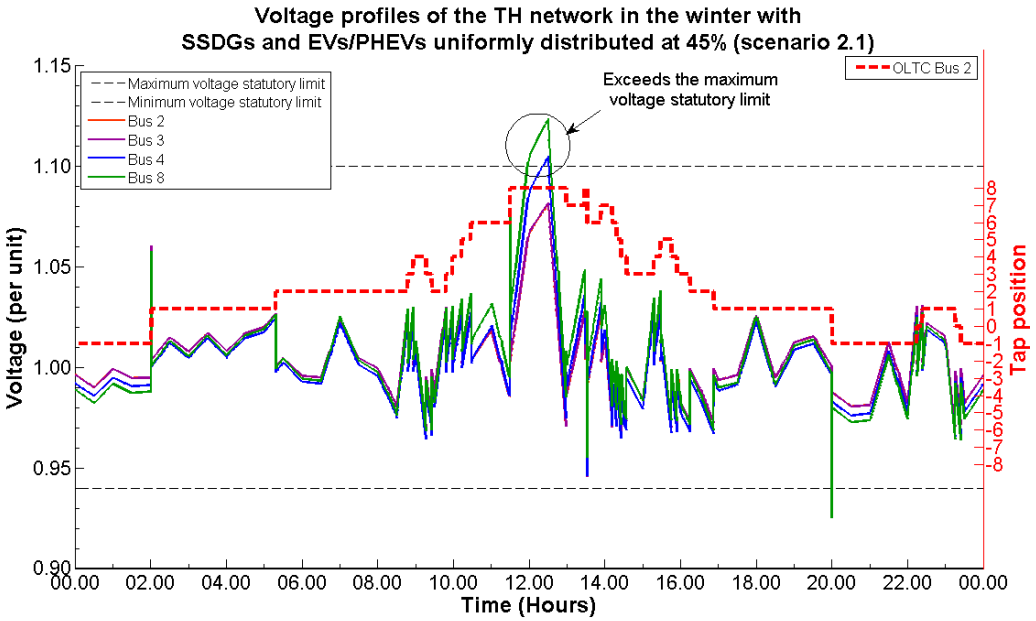

Figure 5.17 Voltage profiles of the TH network in the winter for scenario 2.1 (from Table 3.5)

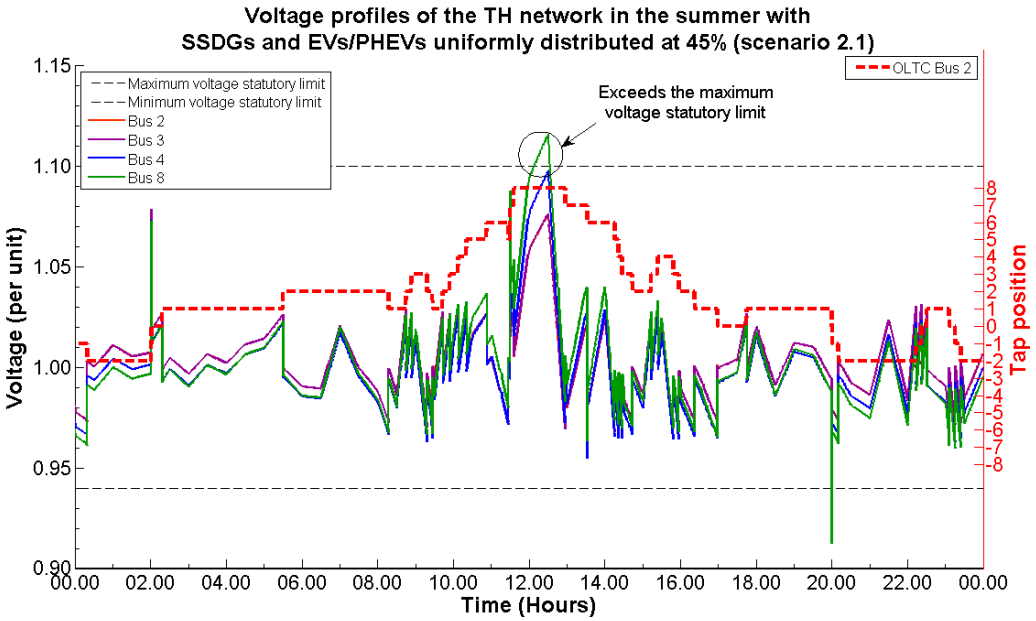

Figure 5.18 Voltage profiles of the TH network in the summer for scenario 2.1 (from Table 3.5)

5.1.2b) Scenario 2.2

In scenario 2.2, the control signal for the OLTC is changed from the local substation (at bus 2) to the far end of the LV feeder (at bus 17 for the UK network and bus 8 for the TH network), which allows investigation of active network control. Figure 5.19 shows the voltage profiles in the winter for the UK network with 10 percent uniformly distributed of SSDGs and EVs/PHEVs. The voltage profile at the OLTC bus (at bus 2) and the far end of the MV feeder (at bus 10) is below the minimum statutory limit for 11 kV in the early morning and in the afternoon. This is due to the OLTCs are attempting to maintain the voltage profile at the far end of the LV feeder within acceptable levels.

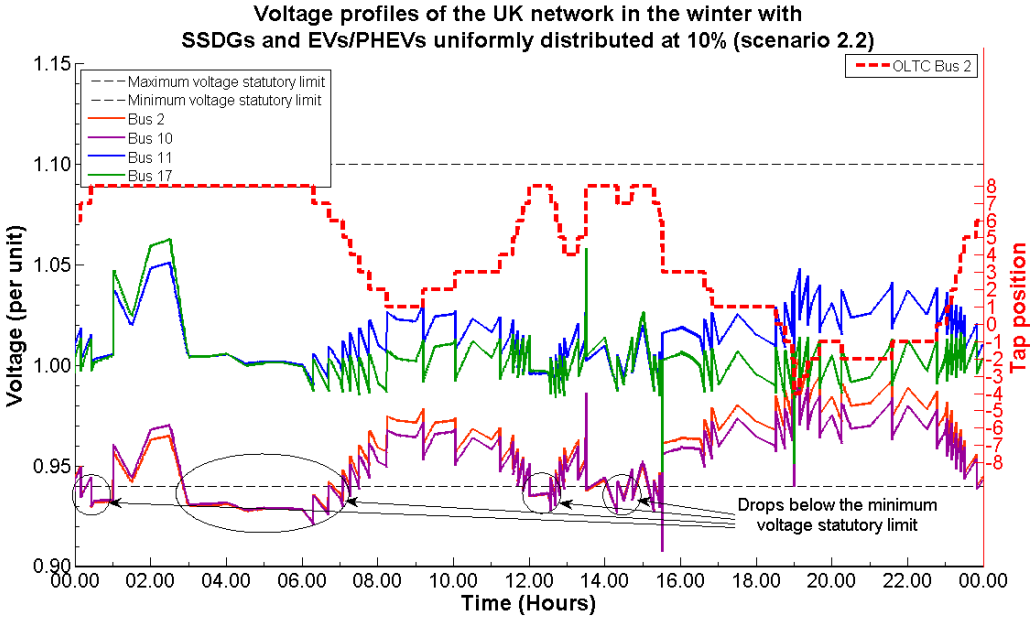

Figure 5.19 Voltage profiles of the UK network in the winter for scenario 2.2 (from Table 3.5)

Figure 5.20 shows that with 5 percent of SSDGs and EVs/PHEVs uniformly distributed along the distribution network in the UK in the summer, the voltage at the OLTC bus (at bus 2) and the far end of the MV feeder (at bus 10) is below the minimum statutory limit of 11 kV (about 2.5 percent lower than the limit), which is because the tap changer reaches its limit.

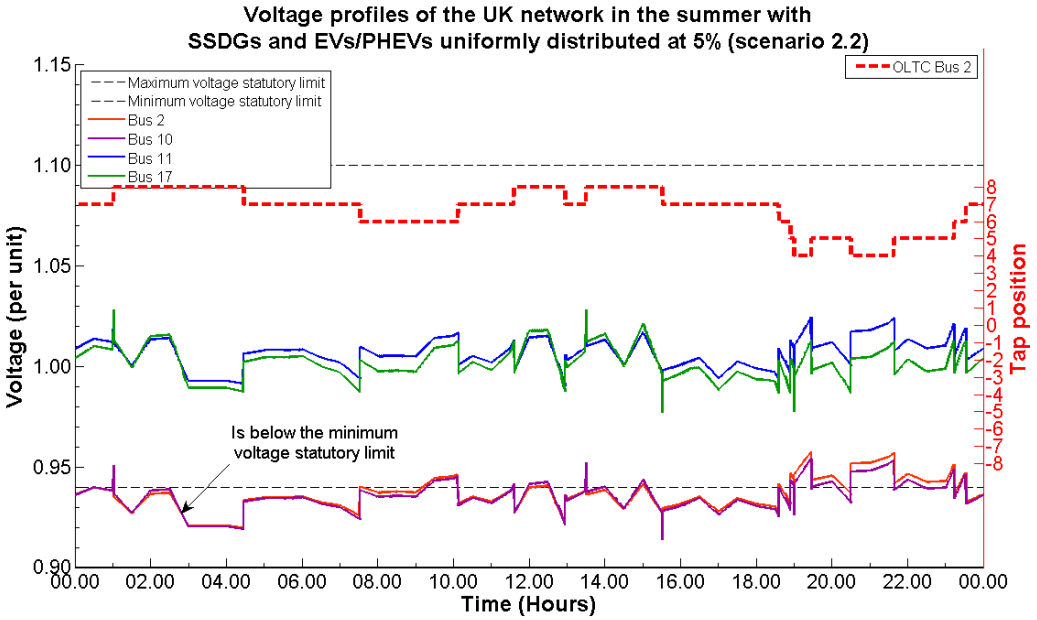

Figure 5.20 Voltage profiles of the UK network in the summer for scenario 2.2 (from Table 3.5)

Penetration level of SSDGs and EVs/PHEVs that violates the voltage statutory limits in the winter in TH is around 45 percent, as shown in Figure 5.21. The voltage profile at the far end of the MV and LV feeders exceeds the maximum limit of 10 percent for 400 V during 12.00-12.30 due to the high generation of SSDGs and the EVs/PHEVs (operating in V2G mode) and the effects of energy saving policies as it leads to low demand at that time.

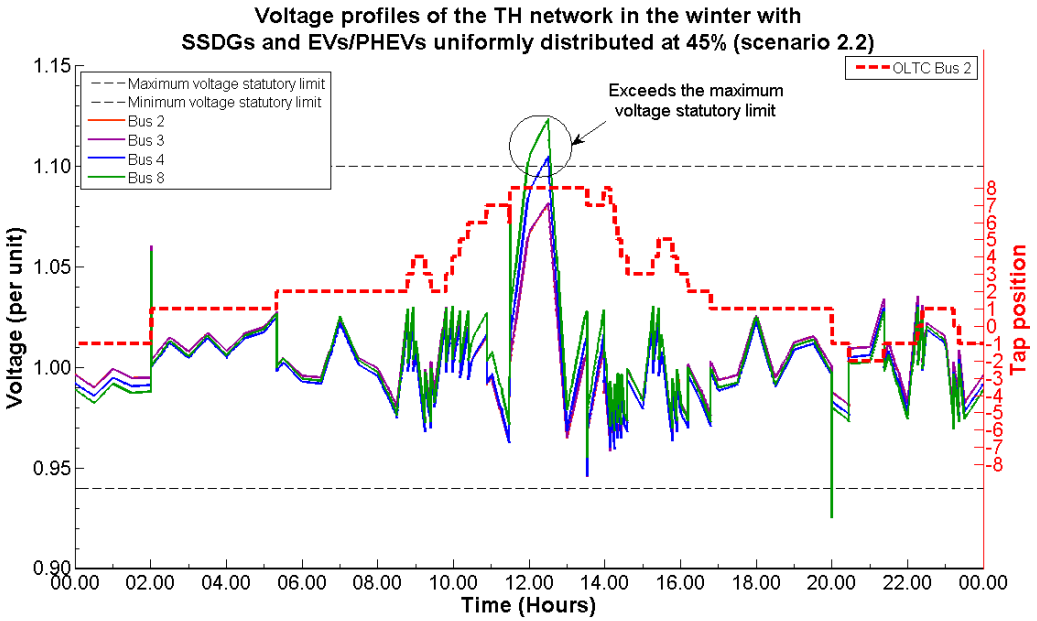

Figure 5.21 Voltage profiles of the TH network in the winter for scenario 2.2 (from Table 3.5)

Figure 5.22 demonstrates that with 45 percent penetration level of SSDGs and EVs/PHEVs in the TH network in the summer, the voltage at all buses remained within the statutory limits except the voltage profile at the far end of the LV feeder exceeds the maximum voltage stator limit (about 2 percent higher than the limit) in the afternoon. This is due to the generation is higher than demand.

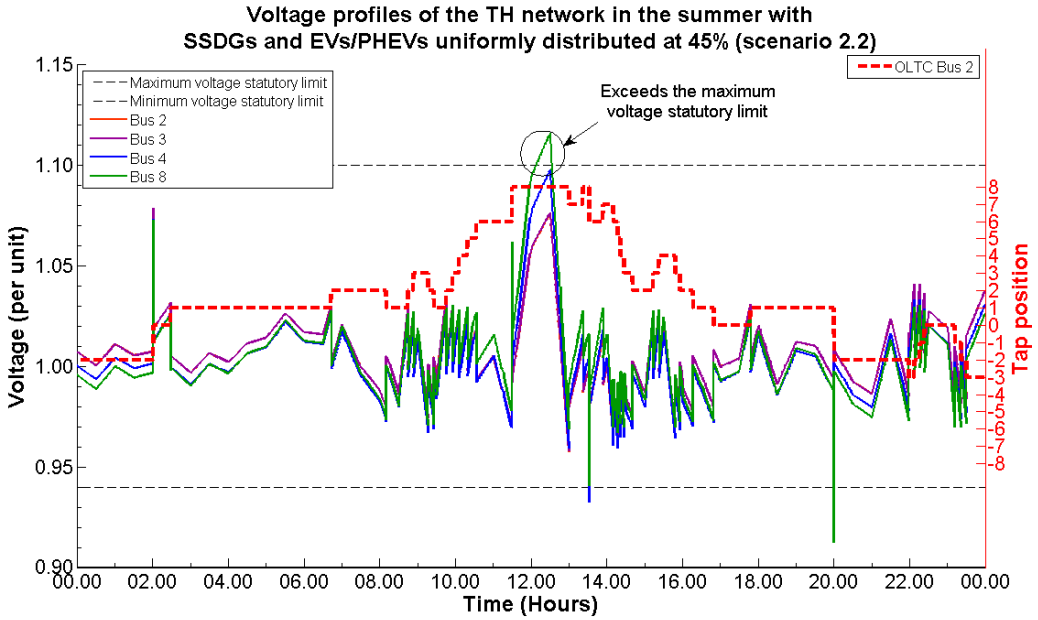

Figure 5.22 Voltage profiles of the TH network in the summer for scenario 2.2 (from Table 3.5)

From both scenarios 1 and 2 considered so far show that the change of OLTC control signal does affect the penetration levels of green technologies in that network. In scenario 1, the OLTC in the UK and TH networks reach their limits and are not able to maintain the voltage at the far end of the LV feeder within acceptable levels at all the times (shown in Figures 5.7 to 5.14). This is due to the radial distribution network design, which supplies the power downward to the consumers, and hence the voltage at the far end of the LV feeder may exceed the voltage statutory limits. Figures 5.15 to 5.22 show the performance of the UK and TH networks with active network control (use the voltage at the far end of MV or LV feeder to control the OLTC). These results show that appropriate control signal of the OLTC can increase the penetration levels of SSDGs and EVs/PHEVs. The results of voltage profiles demonstrate the need to develop the proposed SOLTC (described in section 6.2). The SOLTC for the future power network must allow an increase the penetration levels of green technologies where the signal must be available at all times by either local OLTC bus or the furthest bus that is available at that time.

5.1.3 Scenario 3: Uniformly distributed SSDGs and EVs with 2020 forecast

Table 5.4: Details of scenario 3 for the UK and TH distribution network analysis

Scenario	Description	Aims
3	Same as scenario 1.2, but with penetration levels of SSDGs and EVs as forecasted for 2020.	Investigate likely voltage profiles of future power networks in 2020 (assuming uniform distribution).

Scenario 3 is used to analyse more realistic penetration levels of SSDGs and EVs/PHEVs as forecasted for 2020 (7.49 percent of PV, 1.78 percent of wind turbine, 2.54 percent of hydro turbine and 31 percent of EVs/PHEVs). In this scenario, it is assumed that SSDGs and EVs are uniformly distributed along the network and that the OLTC control signal is delivered from the OLTC bus. The results of the UK network performance for these penetration levels and winter demand profile are shown in Figure 5.23. It can be seen that operation of the OLTCs at bus 2 keep the voltage at all buses within the voltage statutory limits.

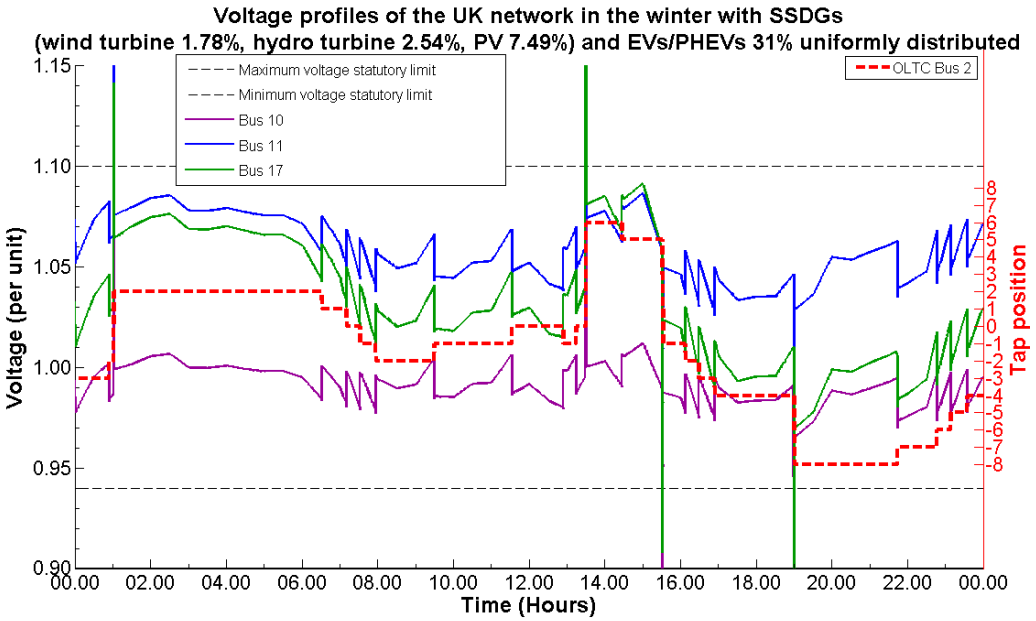

Figure 5.23 Voltage profiles of the UK network in the winter for scenario 3 (from Table 3.5)

Figure 5.24 shows the results for the summer demand profile. As can be seen, the voltage profiles at the LV feeder (at buses 11 and 17) exceed the maximum voltage statutory limit of 400 V in the afternoon (during 13.30-15.30) due to the high generation from SSDGs and EVs/PHEVs operating in V2G mode.

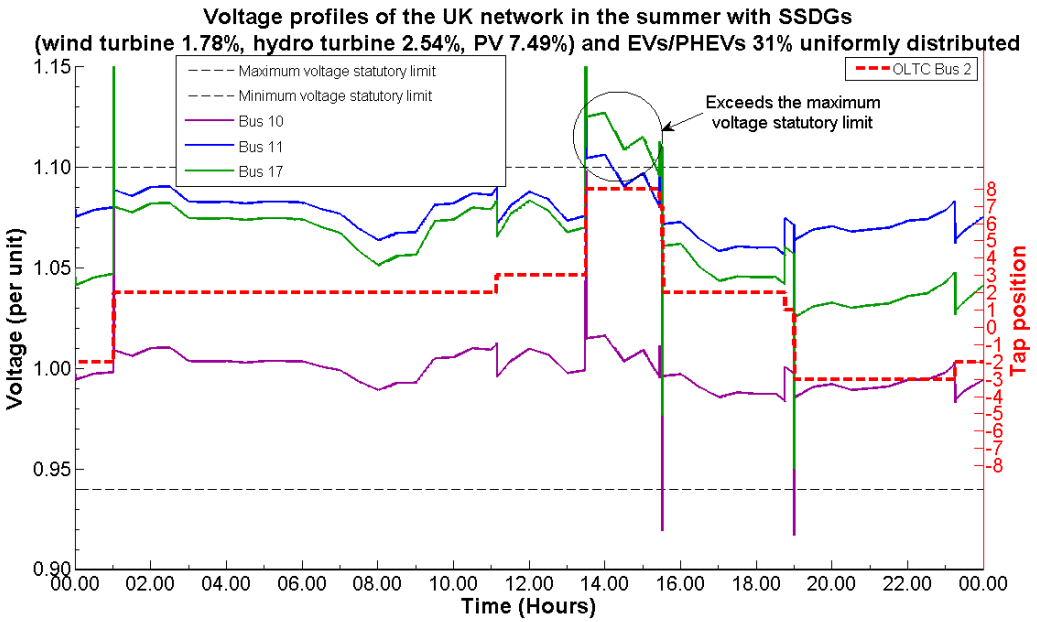

Figure 5.24 Voltage profiles of the UK network in the summer for scenario 3 (from Table 3.5)

Simulation of the TH network in the winter and the summer shows that the voltage at all buses is kept within the voltage statutory limits by the operation of the OLTC at bus 2, see Figures 5.25 and 5.26.

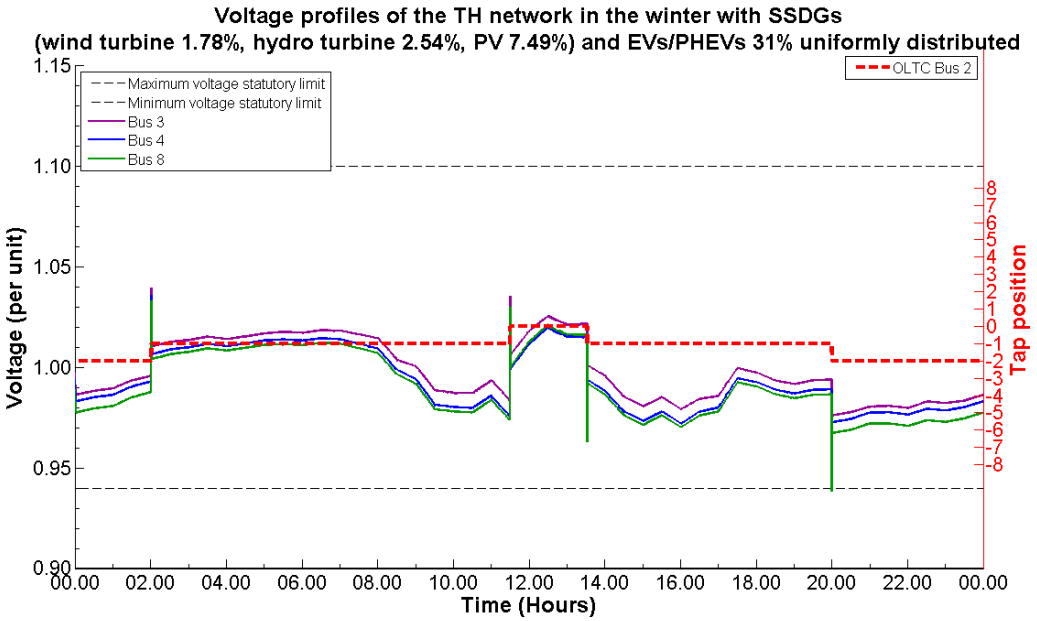

Figure 5.25 Voltage profiles of the TH network in the winter for scenario 3 (from Table 3.5)

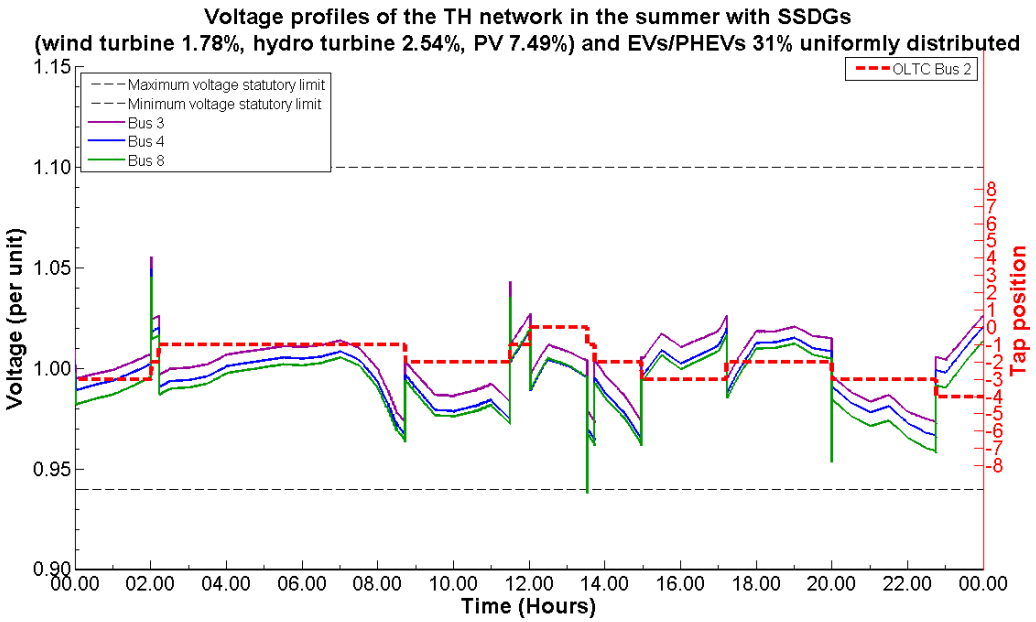

Figure 5.26 Voltage profiles of the TH network in the summer for scenario 3 (from Table 3.5)

5.1.4 Scenario 4: Non-uniformly distributed (localised) SSDGs and EVs

Table 5.5: Details of scenario 4 for the UK and TH distribution network analysis

Scenario		Description	Aims
4	4.1	UK and TH networks localised SSDGs and EVs close to the OLTC (at bus 2 for the UK and TH networks) with penetration levels as forecasted for 2020. For the TH network, a single EVs car park with 10 parking slots is also connected at bus 5.	Investigate the combined impacts of non-uniform distribution of SSDGs and EVs.
	4.2	Same as scenario 4.1, except SSDGs and EVs are moved to the LV bus, close to the LV transformer substation (at bus 11 for the UK network and bus 4 for the TH network).	
	4.3	Same as scenario 4.1, except the SSDGs and EVs moved to the far end of the LV feeder.	

According to the results of scenarios 1 to 3, it can be summarised that the voltage profiles in the distribution networks are directly affected by the penetration level of SSDGs and EVs/PHEVs. Results also show that the weakest buses depends on the demand profiles and network infrastructure. Three potentially weak buses in the distribution network were found to be the OLTC bus and the two buses, at the far end of the MV and LV feeders. These buses were further analysed in this scenario. The OLTC control signal was derived from the local OLTC bus and penetration levels of SSDGs and EVs/PHEVs as forecasted

for 2020 were assumed. The extreme demand profiles (winter for the UK network and summer for the TH network) are used in this analysis.

5.1.4a) Scenario 4.1 to 4.3 for the UK network

Figure 5.27 shows the single line diagram of the UK network, which is used in this investigation.

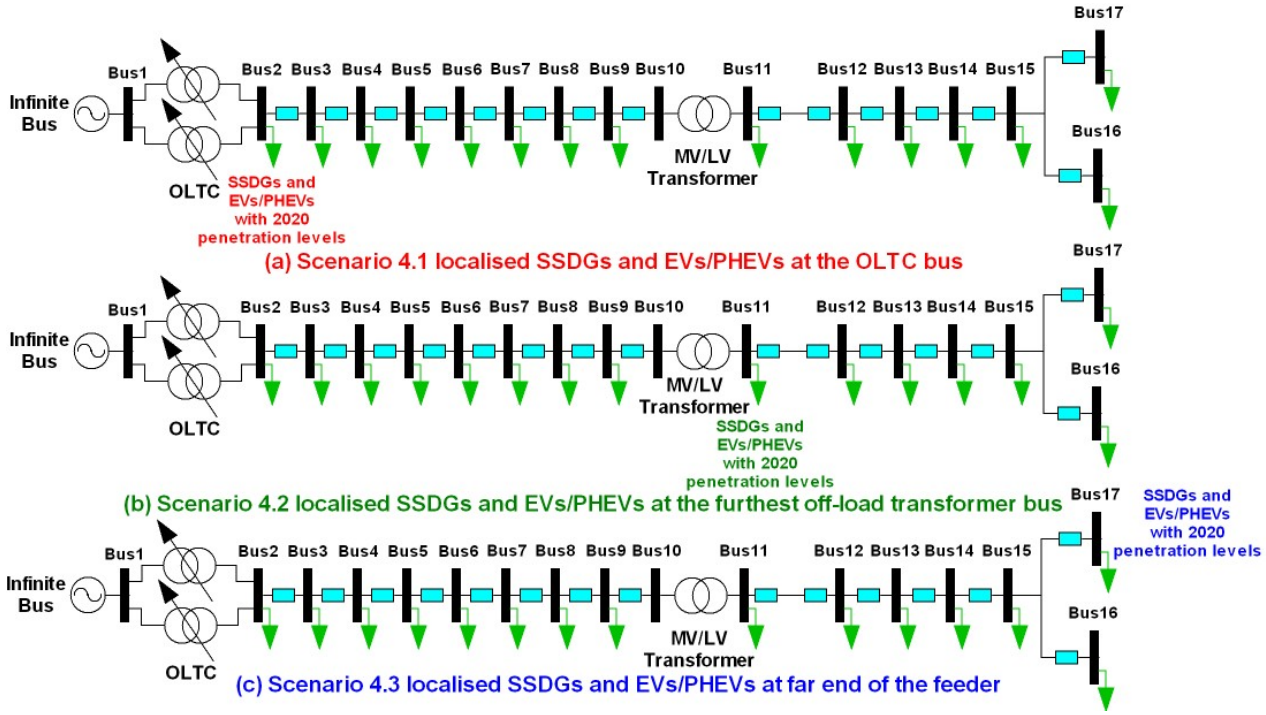

Figure 5.27 Single line diagram of the UK network for scenario 4 (from Table 3.5)

Figure 5.28 demonstrates the effects of SSDGs and EVs/PHEVs that are localised at bus 2 (shown in Figure 5.27a), where the OLTCs at bus 2 maintain the voltage at all buses within the statutory limits, when the tap changer operate at its limit. Figure 5.29 shows the voltage profiles when the localised SSDGs and EVs/PHEVs are connected at bus 11 (shown in Figure 5.27b). As can be seen, the voltage levels at all buses are kept within the voltage statutory limits by the operation of the OLTCs at bus 2. Moreover, it is interesting to note that the voltage levels at all buses are still kept within the voltage statutory limits even when SSDGs and EVs/PHEVs are localised at the far end of the LV feeder (at bus 17, Figure 5.27c), as shown in Figure 5.30. As can be seen in Figure 5.30, the voltage at the far end of the LV feeder drops significantly as compared to scenarios 4.1 and 4.2.

Although, the three different localised sets of SSDGs and EVs/PHEVs in the UK network (representing the urban area) have considerable effects on the voltage profiles in the winter (with high demand), these effects do not results in the voltages exceeding the statutory levels.

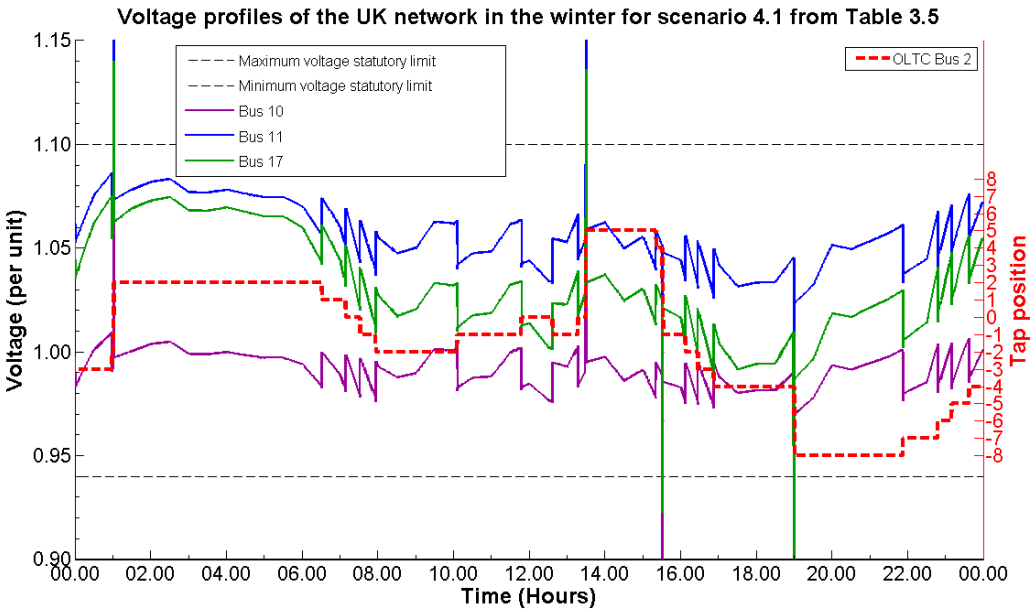

Figure 5.28 Voltage profiles of the UK network in the winter for scenario 4.1 (from Table 3.5)

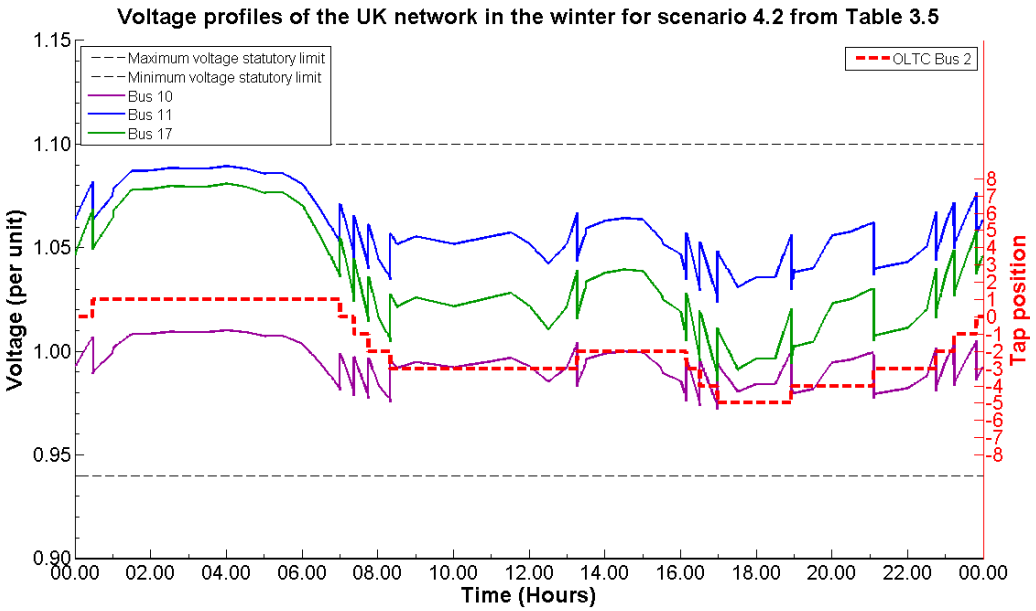

Figure 5.29 Voltage profiles of the UK network in the winter for scenario 4.2 (from Table 3.5)

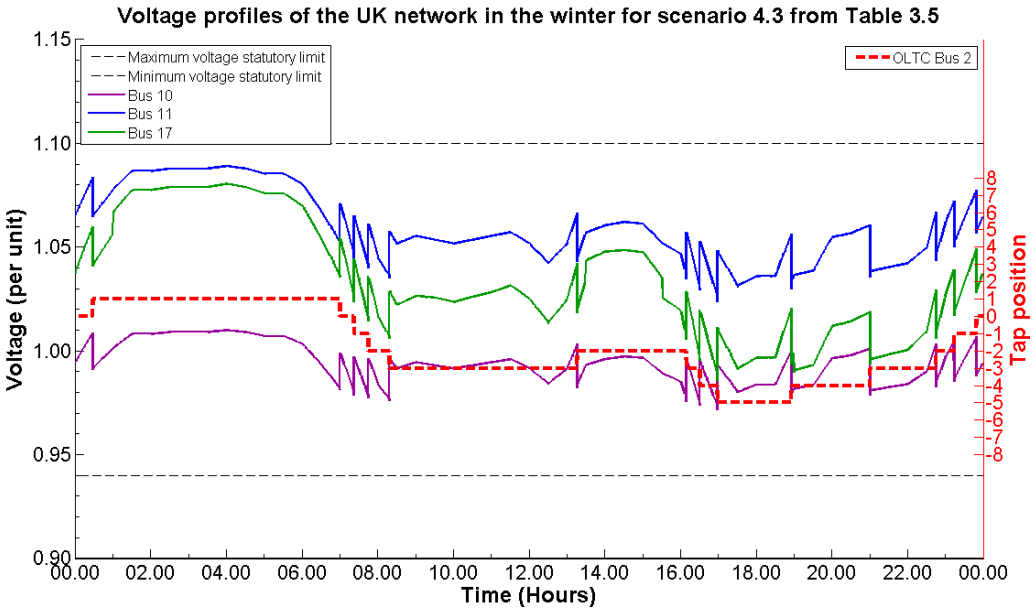

Figure 5.30 Voltage profiles of the UK network in the winter for scenario 4.3 (from Table 3.5)

5.1.4b) Scenario 4.1 to 4.3 for the TH network

The single line diagram of the TH network used to analyse the weak buses is shown in Figure 5.31.

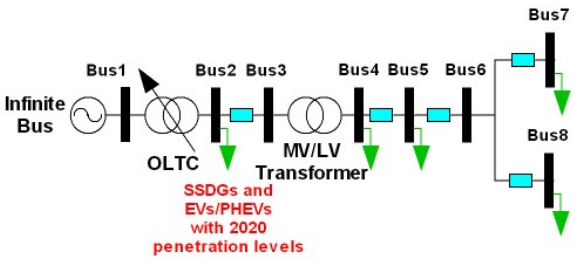

(a) Scenario 4.1 localised SSDGs and EVs/PHEVs at the OLTC bus

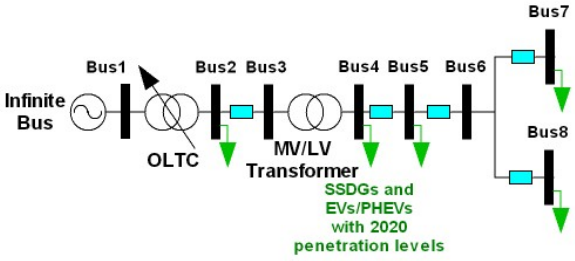

(b) Scenario 4.2 localised SSDGs and EVs/PHEVs at the furthest off-load transformer bus

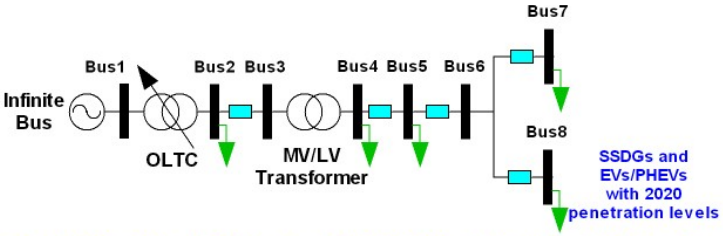

(c) Scenario 4.3 localised SSDGs and EVs/PHEVs at far end of the feeder

Figure 5.31 Single line diagram of the TH network for scenario 4 (from Table 3.5)

Figure 5.32 shows the voltage profiles in the summer with localised SSDGs and EVs/PHEVs at bus 2 (shown in Figure 5.31a) in the TH network. The results show that the voltage levels at all buses are kept within the limits by the operation of the OLTC.

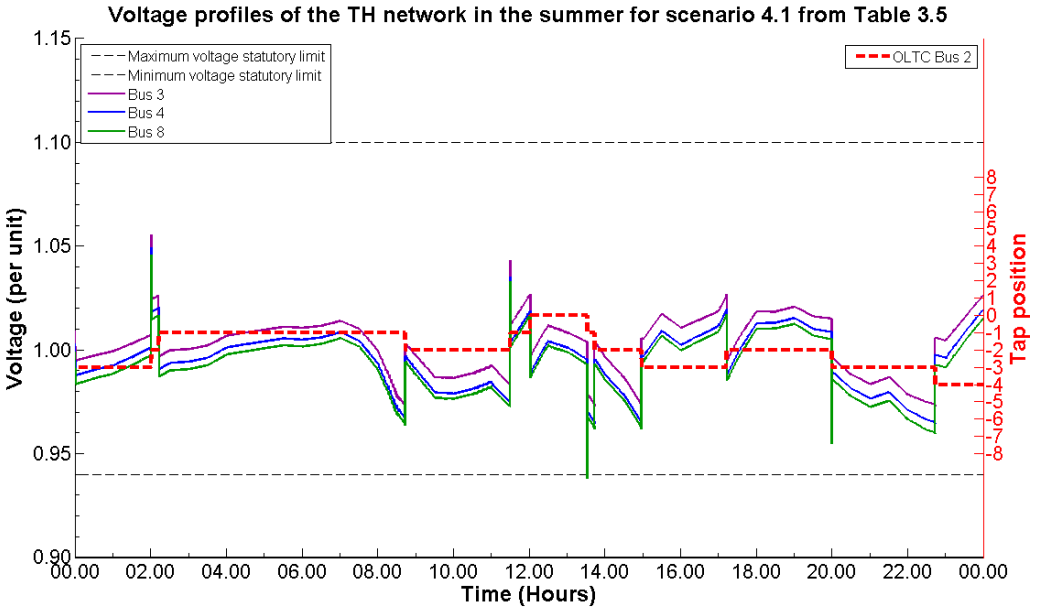

Figure 5.32 Voltage profiles of the TH network in the summer for scenario 4.1 (from Table 3.5)

The voltage profiles when SSDGs and EVs/PHEVs are localised at bus 4 (shown in Figure 5.31b) in the winter are shown in Figure 5.33. As can be seen, the voltage at all buses is still within the voltage statutory limits (by the OLTC).

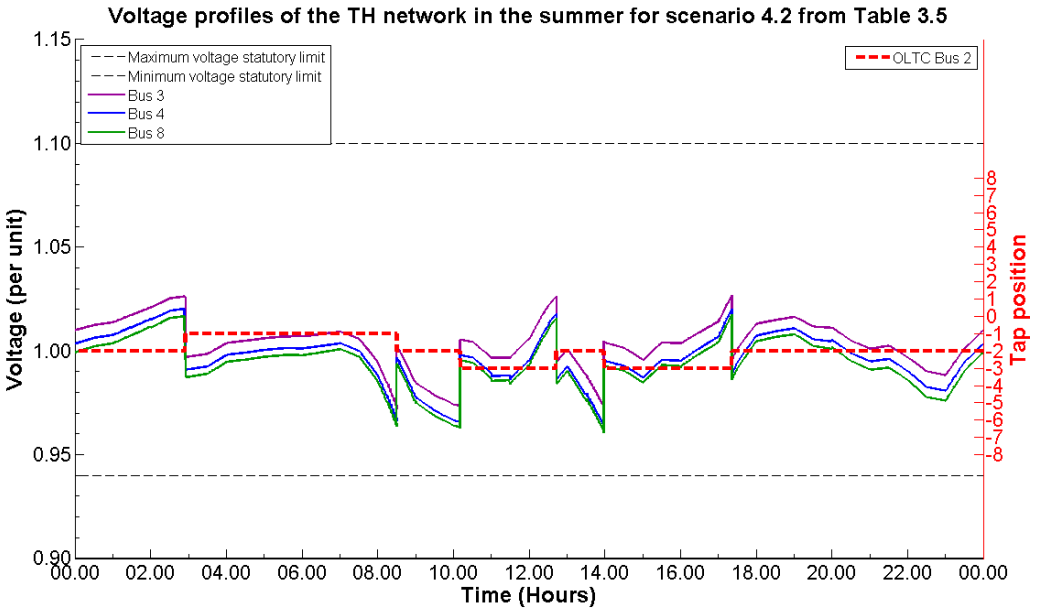

Figure 5.33 Voltage profiles of the TH network in the summer for scenario 4.2 (from Table 3.5)

Figure 5.34 shows that the voltage at the far end of the LV feeder drops because of low generation of SSDGs, high consumers' demand and EVs/PHEVs that operate in charging mode (the SSDGs and EVs/PHEVs located at bus 8, Figure 5.31c). The voltage at all buses is kept within the limits by the operation of the OLTC.

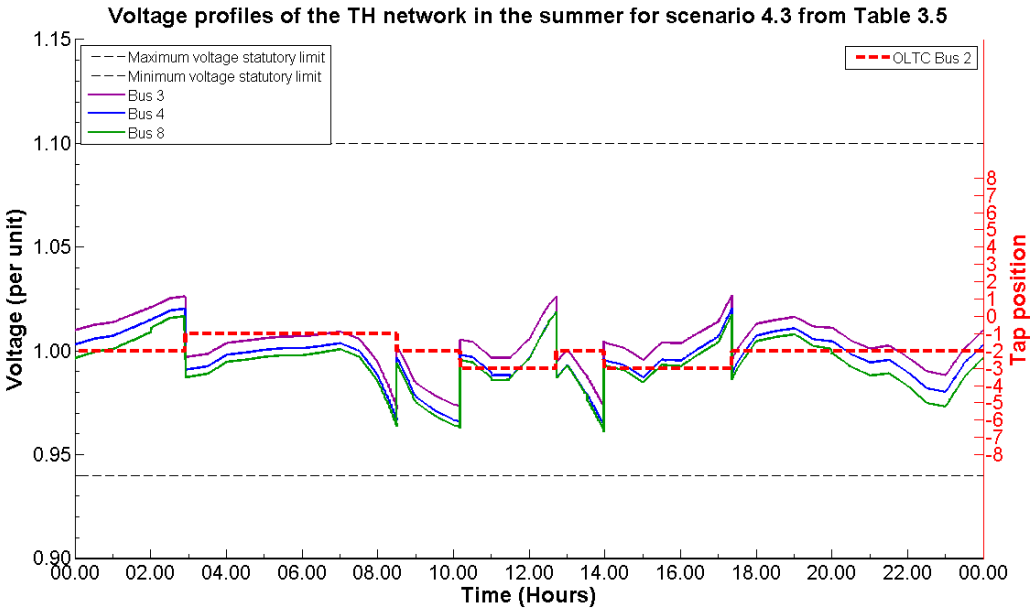

Figure 5.34 Voltage profiles of the TH network in the summer for scenario 4.3 (from Table 3.5)

The results obtained in scenario 4 demonstrate that the potential weak buses in the distribution network are at the far end of the LV feeder, the far end of the MV feeder and the OLTC bus, respectively. Because the distribution network is originally designed for a power flow from central generation downward to the consumers, the voltage profiles are determined by the impedance of the feeders as well as tap changer settings of the transformers (both MV and LV). The voltage profile is also a function of the consumers' demand in the power network as seen in the winter (for the UK network) and the summer (for the TH network) seasons.

5.1.5 Scenario 5: Non-uniformly distributed (localised) EVs car parks

Table 5.6: Details of scenario 5 for the UK and TH distribution network analysis

Scenario		Description	Aims
5	5.1	EVs car parks with 200 units each are connected at buses 7, 8 and 9 of the UK network. The TH network has a single EVs car park with 96 parking at bus 2 and 10 parking at bus 5. Both the UK and TH networks have distributed SSDGs and EVs with penetration levels as forecasted for 2020 (excluding the buses with EVs car park).	Investigate the effects of EVs car parks on the weakest buses (assuming connect at the far end of either the MV feeder or LV feeder).
	5.2	Same as scenario 5.1, except a single EVs car park with 30 parking is connected at the far end of the LV feeder in the UK and TH networks instead of EVs car park with 200 and 96 parking slots.	

The use of EVs/PHEVs is expected to continually increase and this may be lead to unavoidable increase in localised loading of the distribution network such as car parks in community, attraction and/or sightseeing areas (amusement park, beach, etc.). Hence, EVs/PHEVs public parking on the street and in car parks was considered and extreme cases as in scenarios 5 are presented.

5.1.5a) Scenario 5.1 to 5.2 for the UK network

Figure 5.35 shows the single line diagram of the UK network used in this investigation.

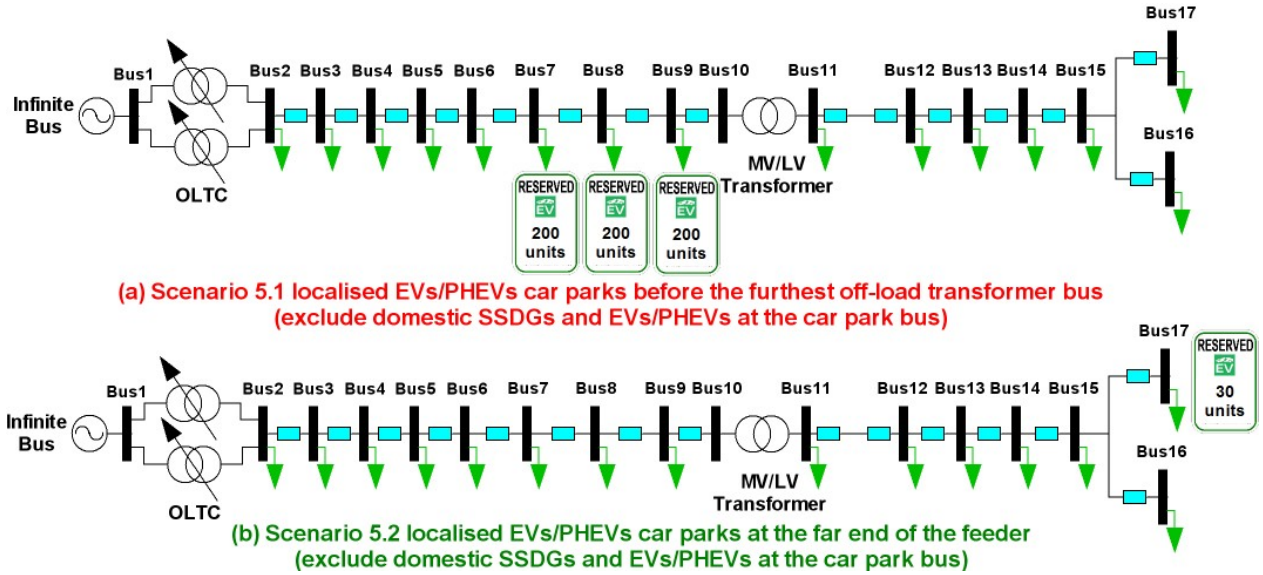

Figure 5.35 Single line diagram of the UK network for scenario 5 (from Table 3.5)

As shown in Figure 5.35a, three EVs/PHEVs car parks are located before the far end of the MV feeder at buses 7, 8 and 9, which results in an unavoidable voltage drop at bus 10 and the LV feeder. This is clearly seen in the winter demand profile shown in Figure 5.36. The voltage at the far end of the LV feeder is still within the statutory limits of 400 V but close to the maximum statutory limit during 14.30-15.30 due to the high generation of SSDGs and EVs/PHEVs that operate in V2G mode as well as low consumers' demand at that time. The voltage at the far end of the LV feeder drops to the minimum statutory limit of 400 V during 19.00-01.00 due to the high consumers' demand and low generation (no PV generation).

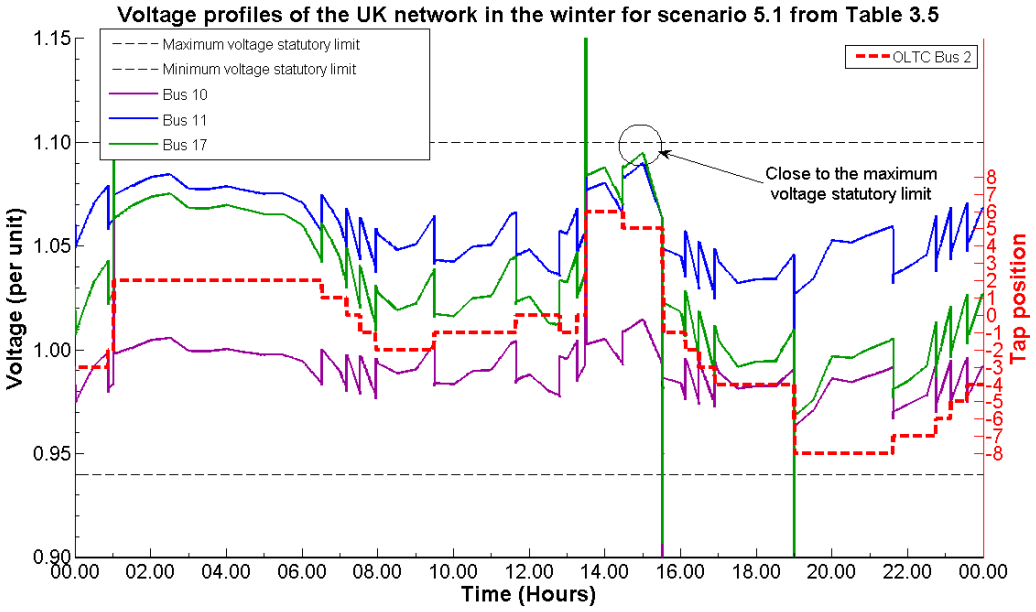

Figure 5.36 Voltage profiles of the UK network in the winter for scenario 5.1 (from Table 3.5)

Figure 5.37 demonstrates the voltage profiles in the UK network in the summer for scenario 5.1. The voltage profiles at the LV side of the transformer (at bus 11) and the far end of the LV feeder exceed the maximum statutory limit of 400 V during 13.30-15.30 (about 1 and 3 percent higher than the limit, respectively). The voltage rise is caused by the high generation from SSDGs and EVs/PHEVs operating in V2G mode. However, the voltages at the other buses are still within the statutory limits because of the operation of the OLTCs.

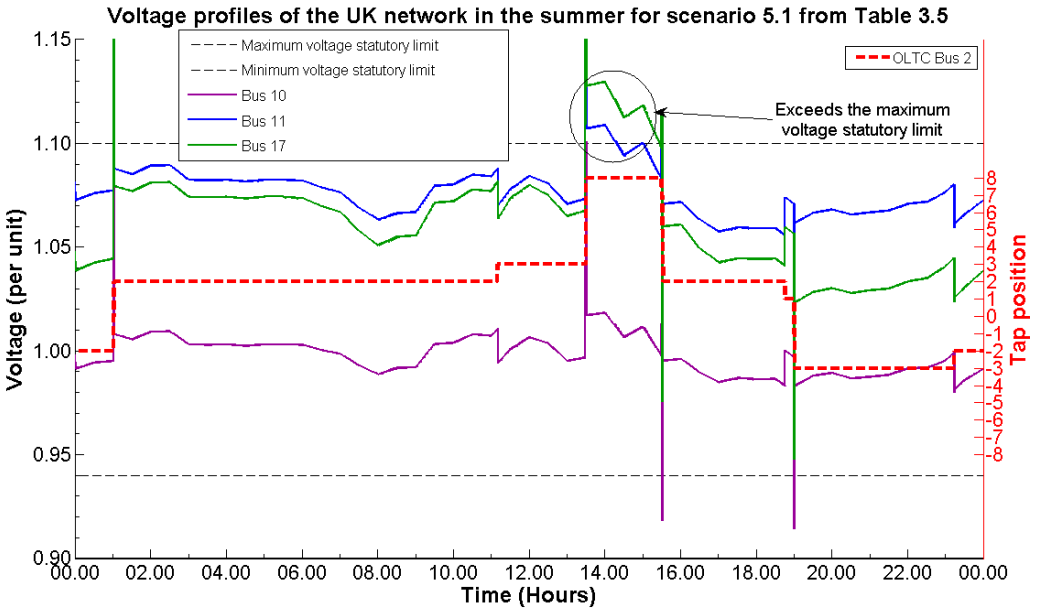

Figure 5.37 Voltage profiles of the UK network in the summer for scenario 5.1 (from Table 3.5)

In scenario 5.2, the three EVs/PHEVs car parks in the UK network (from scenario 5.1) were reduced to a single car park (with 30 parking spaces) and located at the far end of the LV feeder (weakest bus in the distribution network), as shown in Figure 5.35b. Because of the high generation of SSDGs and EVs/PHEVs that operate in V2G mode during 13.30-15.30 in the winter, the voltage at the far end of the LV feeder exceeded the maximum statutory limit of 400 V (about 5.25 percent higher than the limit), as shown in Figure 5.38. The voltages at the other buses were kept within the limits by the OLTCs. Conversely, the voltage at the far end of the LV feeder drops below the minimum statutory limit of 400 V during 19.00-20.00 and 21.30-22.30 (about 2 and 1 percent lower than the limit, respectively) due to loss of PV generation and the high consumers' demand (many household utilities and EVs/PHEVs).

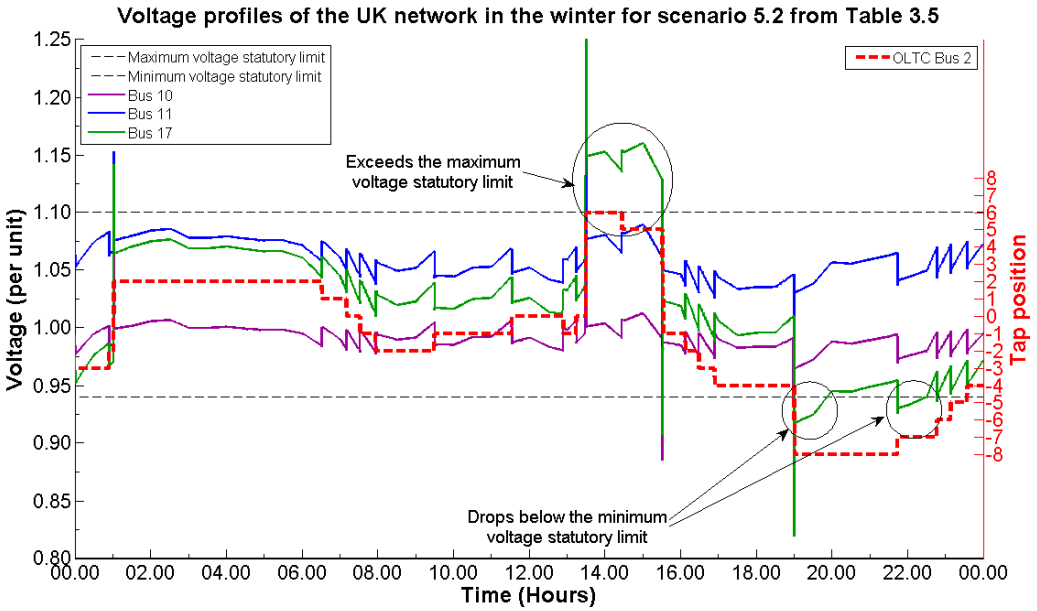

Figure 5.38 Voltage profiles of the UK network in the winter for scenario 5.2 (from Table 3.5)

Figure 5.39 shows the voltage profiles in the summer for the same SSDGs and EVs/PHEVs as in Figure 5.38. Again, the voltage at bus 11 and at the far end of the LV feeder exceeds the maximum statutory limit of 400 V by about 1 and 10 percent, respectively. This is due to high generation of SSDGs and EVs/PHEVs that operate in V2G mode.

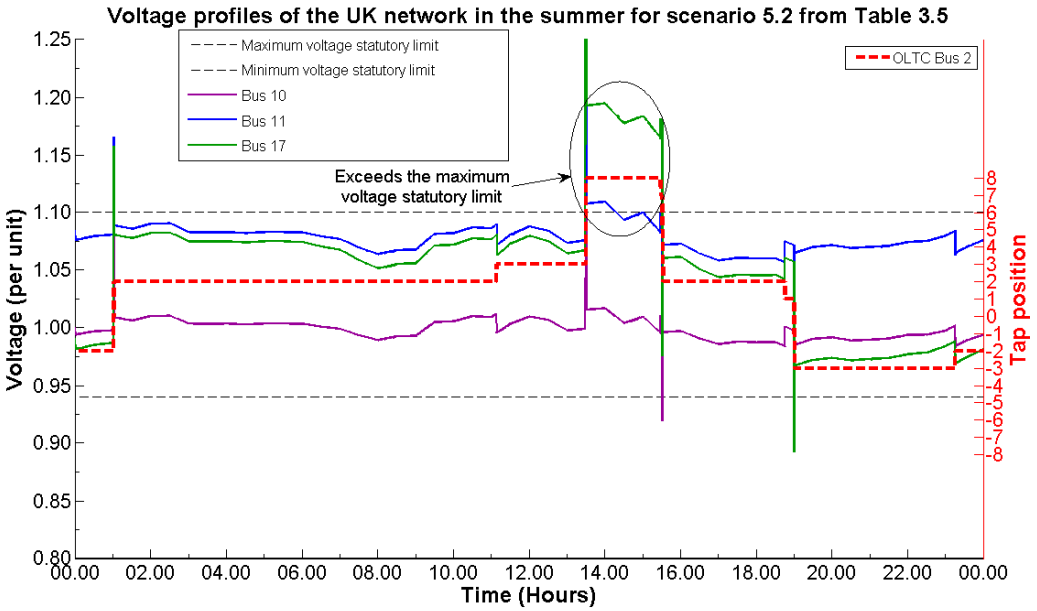

Figure 5.39 Voltage profiles of the UK network in the summer for scenario 5.2 (from Table 3.5)

5.1.5b) Scenario 5.1 to 5.2 for the TH network

A single EVs/PHEVs car park that supports 96 EVs/PHEVs units and locates at the OLTC substation (at bus 2) was considered for the TH network, as shown in Figure 5.40a.

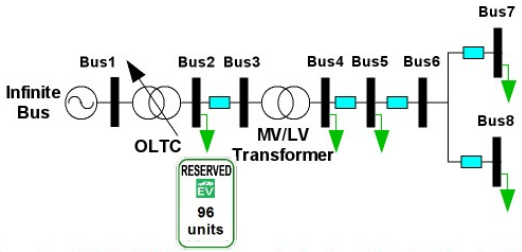

(a) Scenario 5.1 localised EVs/PHEVs car parks before the furthest off-load transformer bus (exclude domestic SSDGs and EVs/PHEVs at the car park bus)

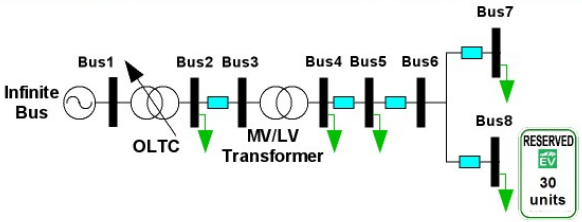

(b) Scenario 5.2 localised EVs/PHEVs car parks at the far end of the feeder (exclude domestic SSDGs and EVs/PHEVs at the car park bus)

Figure 5.40 Single line diagram of the TH network for scenario 5 (from Table 3.5)

Figures 5.41 and 5.42 show the voltage profiles of the TH network for scenario 5.1. As can be seen in the winter (shown in Figure 5.41) and the summer (shown in Figure 5.42), the OLTC at bus 2 kept the voltages at all buses within the limits. Moreover, the voltage at the far end of the LV feeder in the summer drops more than in the winter. This is due to high electricity demand.

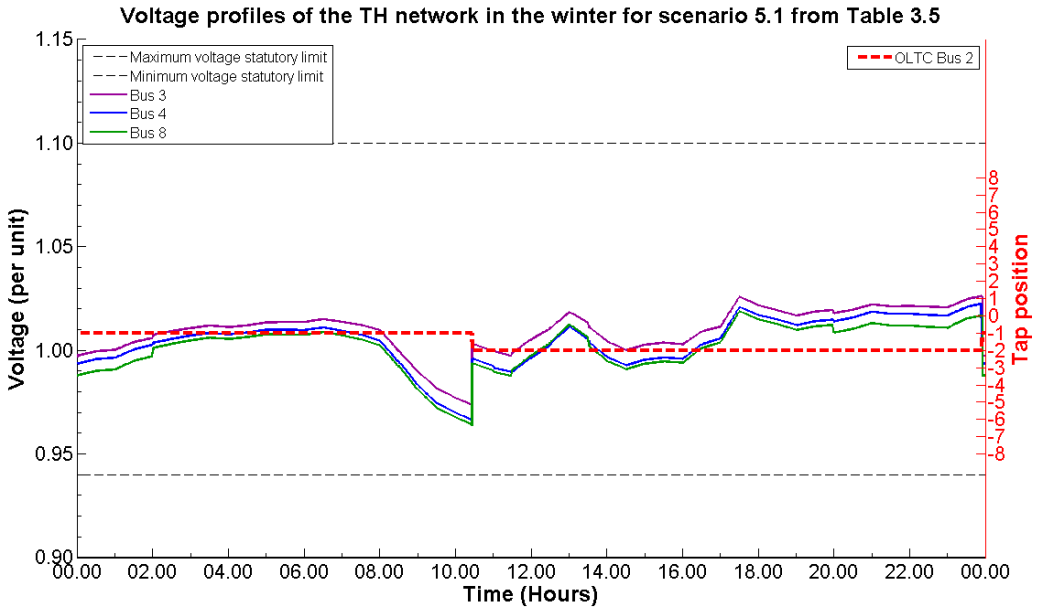

Figure 5.41 Voltage profiles of the TH network in the winter for scenario 5.1 (from Table 3.5)

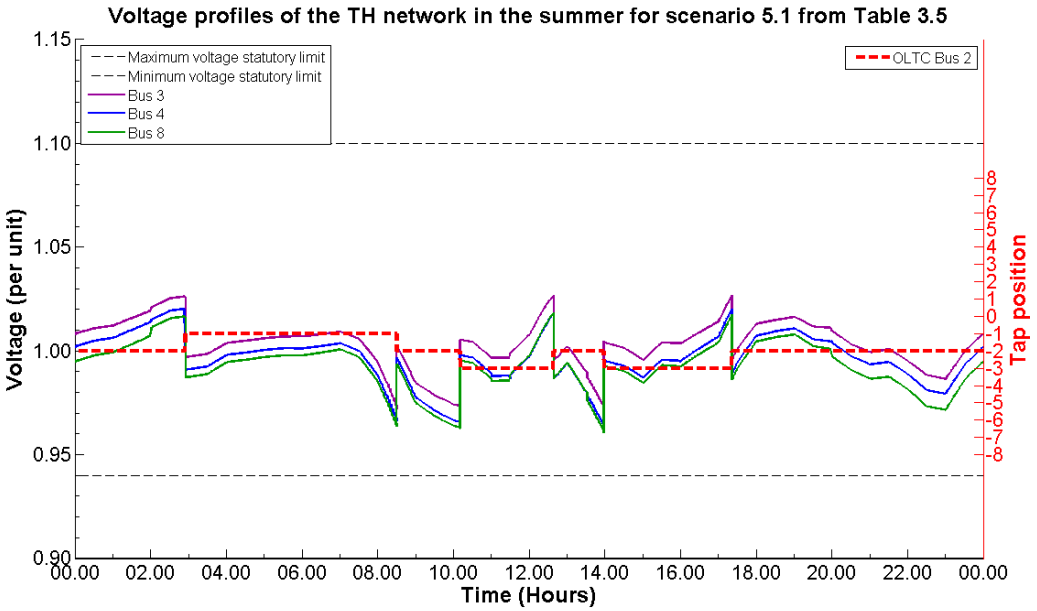

Figure 5.42 Voltage profiles of the TH network in the summer for scenario 5.1 (from Table 3.5)

Figure 5.40b shows the TH network with the EVs/PHEVs car park re-located to the far end of the LV feeder and the size of the car park was reduced to 30 units. The voltages at the all buses were kept within the limits by the OLTC, as shown in Figure 5.43. During 20.00-02.00 the voltage drop at the far end of the LV feeder is due to the demand is more than the supply. This is due to the low generation (no PV generation) and EVs/PHEVs (operating in charging mode).

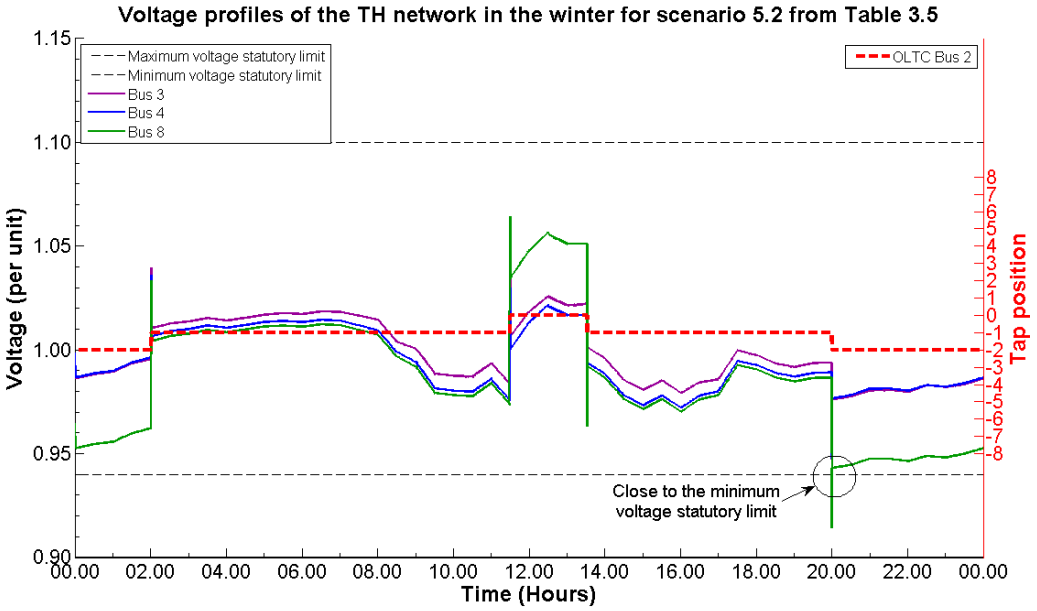

Figure 5.43 Voltage profiles of the TH network in the winter for scenario 5.2 (from Table 3.5)

Figure 5.44 shows the voltage profile for the summer loading. The voltage profile at the far end of the LV feeder drops below the minimum statutory limit of 400 V due to the high consumers' demand in the summer.

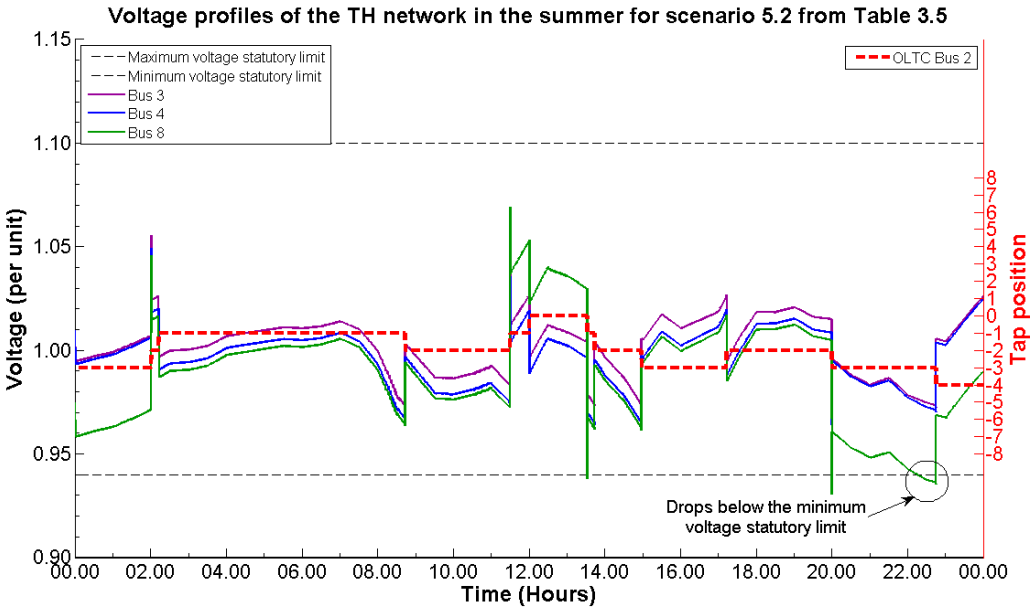

Figure 5.44 Voltage profiles of the TH network in the summer for scenario 5.2 (from Table 3.5)

The impacts of EVs/PHEVs car parks investigated in scenarios 5 show that the EVs/PHEVs car parks mostly affect the voltage at the far end of the LV feeder where the voltage profile is a function of the number of EVs/PHEVs in the car park as well as the infrastructure of the network. As a result, the EVs/PHEVs car park could become a challenge for future power network, which may be resolved by implementing the smart controllers proposed in chapter 6. In order to encourage the consumer to use the EVs/PHEVs public parking and car park, the Smart EVs Grid Connection (SEVGC) was proposed (explained in section 6.4) in which most of the vehicle owners are willing to plug in their vehicles with favourable charging/regenerating tariffs. The smart controllers will communicate with the Smart EVs/PHEVs Car Park (SCP) and the vehicles are charged/regenerating automatically. This concept also supports the use of energy storage systems to supply/consume energy instead of using an Uninterruptible Power System (UPS) during the power outage, here called "Smart Energy Storage system (SES)". Both SCP and SES are described in section 6.5.

5.1.6 Scenario 6: Non-uniformly distributed (localised) SSDGs and EVs with 2020 forecast

Table 5.7: Details of scenario 6 for the UK and TH distribution network analysis

Scenario	Description	Aims
6	EVs car parks with 200 parking each are connected at buses 7, 8 and 9 of the UK network. The UK network also has a single EVs car park with 30 parking and a small wind turbine farm with 50 kW at the far end of the LV feeder. The TH network has three EVs car parks with 96 parking, 10 parking and 30 parking at buses 2, 5 and 8, respectively. The TH network also has a small PV farm with 48 kW at the far end of the LV feeder. Both the UK and TH networks have distributed SSDGs with penetration levels as forecasted for 2020 (excluding the bus at the far end of the LV feeder).	Investigate voltage profiles of future power networks in 2020 (assuming non-uniform distribution). Identify the weakest buses in existing distribution network where the voltage or thermal capacity limits could be exceeded.

Another extreme scenario that might affect the voltage profiles in the distribution network is a large DG (or a number of localised SSDGs) installed at the far end of the LV feeder (voltage variation scenario 6 from Table 3.5). This scenario (together with scenario 5) is also relevant in the community and/or attraction areas. The OLTC bus sets the control signal of the OLTC where the SSDGs and EVs/PHEVs with 2020 penetration levels are distributed in the network (except at the far end of the LV feeder).

5.1.6a) Scenario 6 for the UK network

In the UK network, the EVs/PHEVs car parks that support 200 units each are located at buses 7, 8, 9 where the EVs/PHEVs car park with 30 parking is located at bus 17, as shown in Figure 5.45.

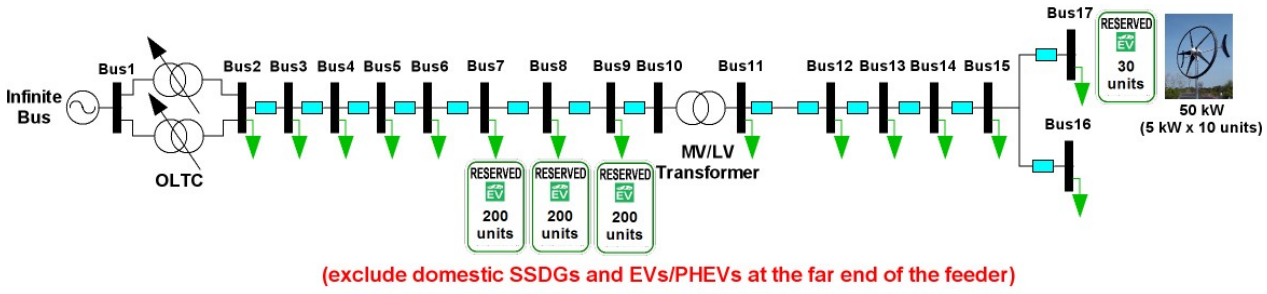

Figure 5.45 Single line diagram of the UK network for scenario 6 (from Table 3.5)

Both results for the winter (shown in Figure 5.46) and for the summer (shown in Figure 5.47) have similar patterns to scenario 5.2. However, the voltage profiles in scenario 6 are higher than scenario 5.2, and hence the OLTCs operate at their limits, because a small-scale wind turbine farm of 50 kW was installed at the far end of the LV feeder.

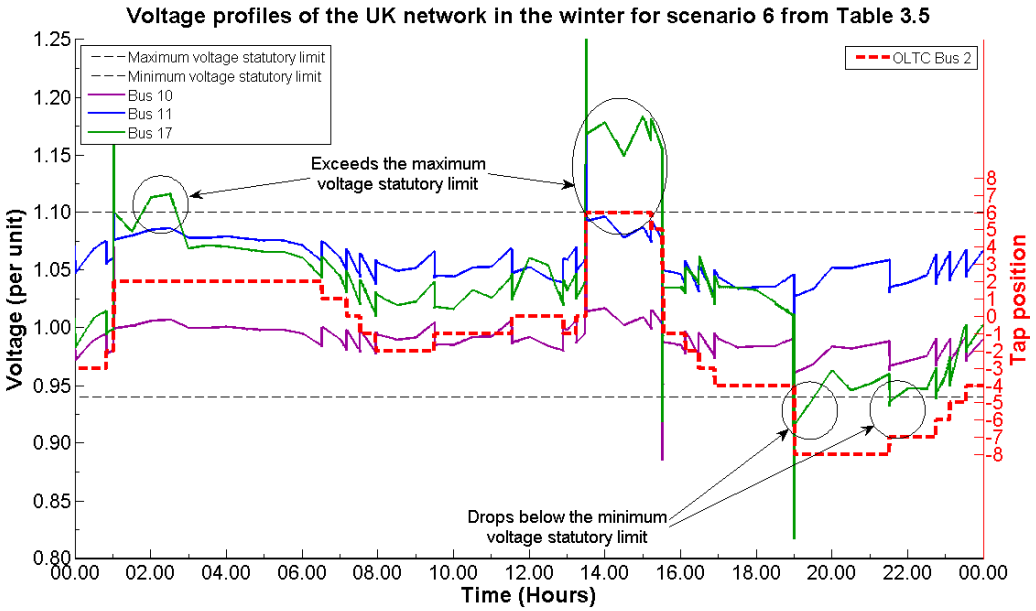

Figure 5.46 Voltage profiles of the UK network in the winter for scenario 6 (from Table 3.5)

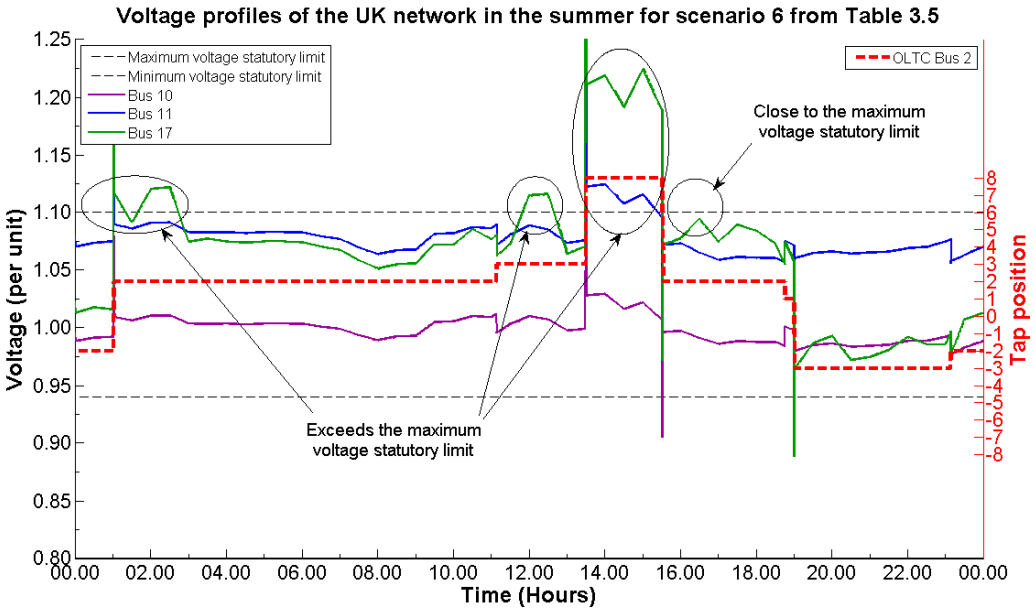

Figure 5.47 Voltage profiles of the UK network in the summer for scenario 6 (from Table 3.5)

5.1.6b) Scenario 6 for the TH network

The single line diagram of the TH network for scenario 6 is shown in Figure 5.48. The EVs/PHEVs car parks that support 96 and 30 units are also located at buses 2 and 8, respectively. Here, a small PV farm of 48 kW is installed at the far end of the LV feeder. It should be noted that a different type of SSDG farm selected for each country is based on the geography of the country where the wind turbine is suitable for the UK and PV system is an appropriate system for TH.

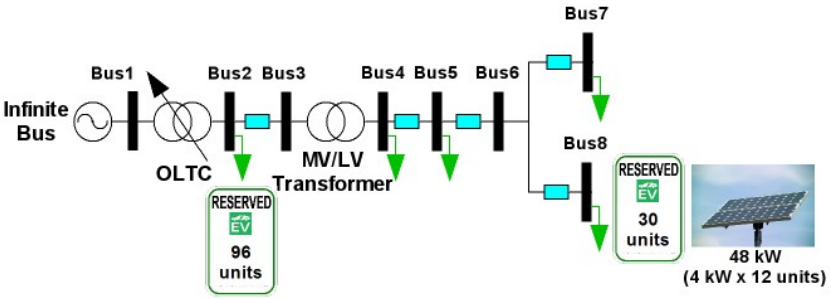

Figure 5.48 Single line diagram of the TH network for scenario 6 (from Table 3.5)

Figure 5.49 shows the voltage profiles for the TH network in the winter. With a long feeder, the voltage at the far end of the LV feeder is close to the minimum statutory limit of 400 V in the evening during 20.00-02.00 because of the low generation of SSDGs (due to no PV generation in evening), high consumers' demand and EVs/PHEVs operating in charging mode at that time.

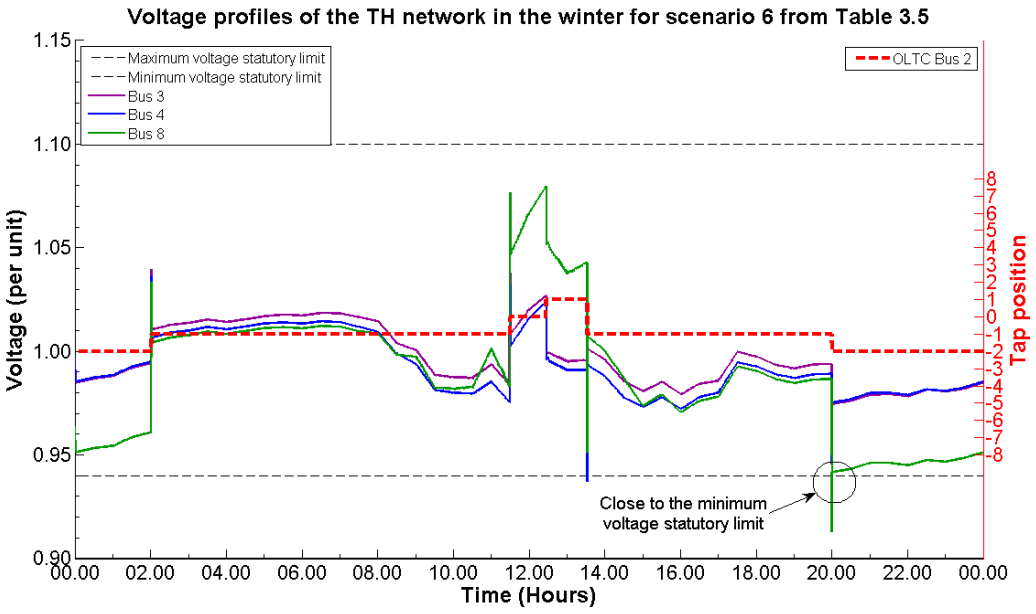

Figure 5.49 Voltage profiles of the TH network in the winter for scenario 6 (from Table 3.5)

Figure 5.50 shows that the voltages at all buses were kept within the limits by the operation of the OLTC except at the far end of the LV feeder (at bus 8). The voltage at bus 8 is below the minimum statutory limit of 6 percent for 400 V in the evening during 22.00-23.00 (about 0.2 lower than the limit) due to the high consumers' demand and low generation of SSDGs.

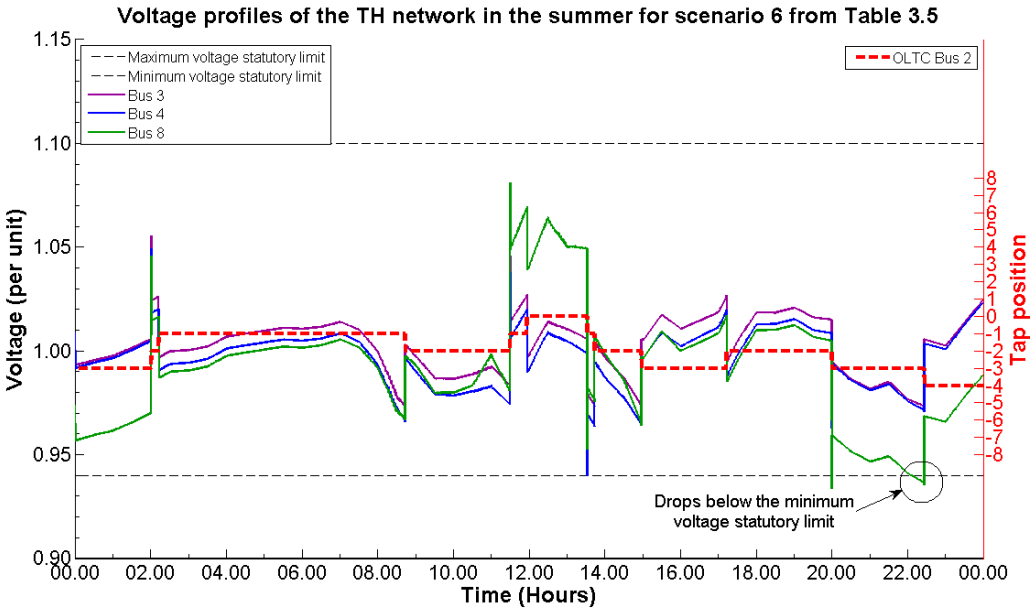

Figure 5.50 Voltage profiles of the TH network in the summer for scenario 6 (from Table 3.3)

The results obtained from scenarios 4 to 6 demonstrate that the weakest buses in the distribution network are the far end of the LV feeder where the significant penetration level of green technologies are also considered. The considerable voltage variation in the power network is a function of the supply and demand at that time. The voltage rise above maximum statutory limit is caused by the high generation of SSDGs, low consumers' demand and EVs/PHEVs operating in V2G mode. On the other hand, the voltage profiles in the network that drop below the statutory level are caused by low supply and high demand. This performance is clearly seen in the winter for UK network and the summer for the TH network. It can be noted that EVs/PHEVs must be considered as mobile active loads because they can plug in anywhere in the network, creating extra loading on the feeders (operating in charging mode) or feeding power back into the network (under V2G mode).

5.2 Islanding Operation without Smart Controllers

5.2.1 Scenario 1: Islanding operation without smart controllers

Table 5.8: Details of scenario 1 for islanded network analysis

Scenario		Description	Aims
1	1.1	Same as scenario 6 from Table 3.5, except a three-phase fault is applied at bus 10 in the UK network and bus 3 in the TH network, and line service is interrupted for 15 minutes during the highest demand and generation profiles.	Investigate the voltage profiles in islanded network without smart controllers.
	1.2	Same as scenario 1.1 from Table 3.6, but for highest demand and lowest generation profiles.	

In order to allow islanding operation in future power network, the impacts of SSDGs and EVs/PHEVs on the voltage profiles in the islanded network need to be investigated. These impacts may be analysed by using the relationship between SCL and power flow equations (described in section 2.4). The islanded network scenario 1 from Table 3.6 was chosen as an extreme example (without smart controllers). The scenario is based on either community or attraction areas, which include areas for EVs/PHEVs car parks and a small farm of SSDGs. Therefore, this scenario allows islanding operation of the LV network, thus increasing the reliability of supply to consumers connected to this network. The SSDGs and EVs/PHEVs with 2020 penetration levels are assumed to be distributed along the network except at the far end of the LV feeder. It is also assumed that both the UK and TH networks experience a three-phase fault at the far end of the MV feeder for 15 minutes out of 30 minutes.

5.2.1a) Scenario 1 for the UK network

Figure 5.51 shows a single line diagram of the UK network, which experience a fault at bus 10, and hence buses 11 to 17 are isolated from the main network.

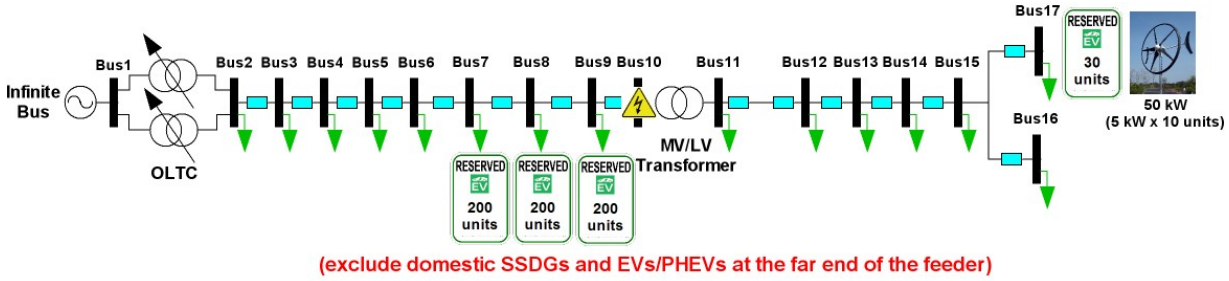

Figure 5.51 Single line diagram of the UK network for scenario 1 (from Table 3.6)

Figure 5.52 presents the voltage profiles of the UK network while experiencing a fault with highest demand and generation profiles. During 0 to 10 minutes and 25 to 30 minutes, the OLTCs at bus 2 operate at their limit (with tap -8), and hence the voltage at all buses keeps within the voltage statutory limits. The three-phase fault at bus 10 was detected (during 10 to 25 minutes), and hence the breaker at the MV side of the transformer operated and isolated the LV network (buses 11 to 17) from the main network until the fault is cleared. It is assumed that the MV service line is interrupted for 15 minutes when the voltage at bus 10 drops to zero. The voltage profiles in the islanded network are below the minimum voltage statutory limit because high demand and all EVs parked in four EVs car parks operate in charging mode. The total generation of SSDGs in the islanded network (about ~212 kVA) is lower than the demand (about ~893 kVA), and hence the controllers of SSDGs are attempting to maintain the output voltage and frequency within acceptable levels.

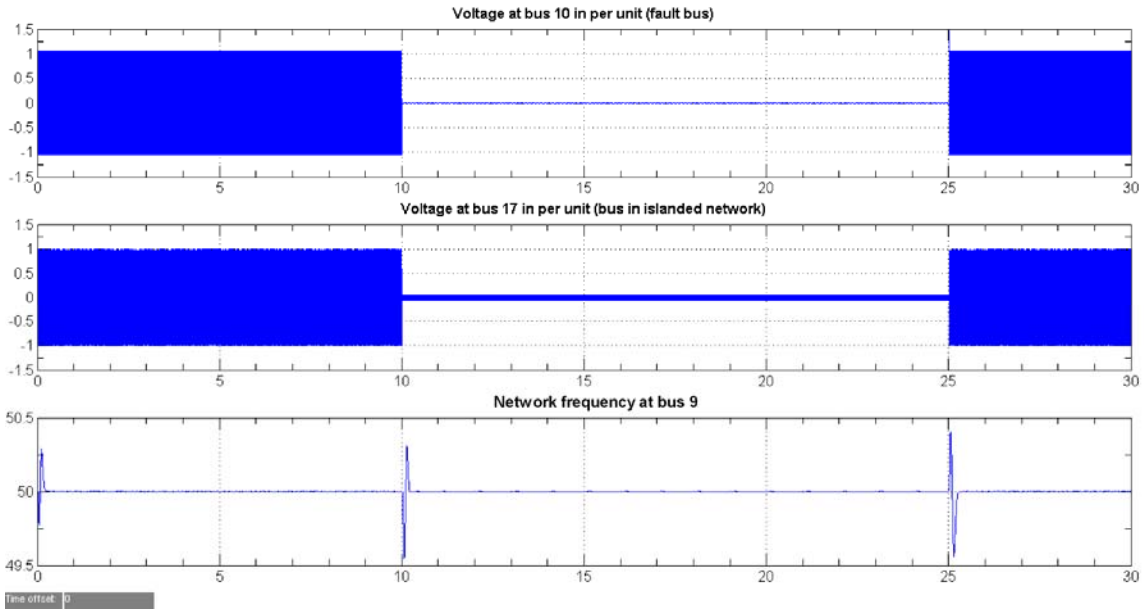

Figure 5.52 Voltage profiles of the UK network with highest demand and generation profiles for scenario 1.1 (from Table 3.6)

Figure 5.53 shows the results of islanding operation of the UK network, as before but with highest demand and lowest generation profiles. It can be noted that the frequency in the network oscillates and takes shorter time (~20 sec) before reaching steady state. Moreover, the voltage profiles are similar to Figure 5.52 because the OLTCs at bus 2 operate at tap -8.

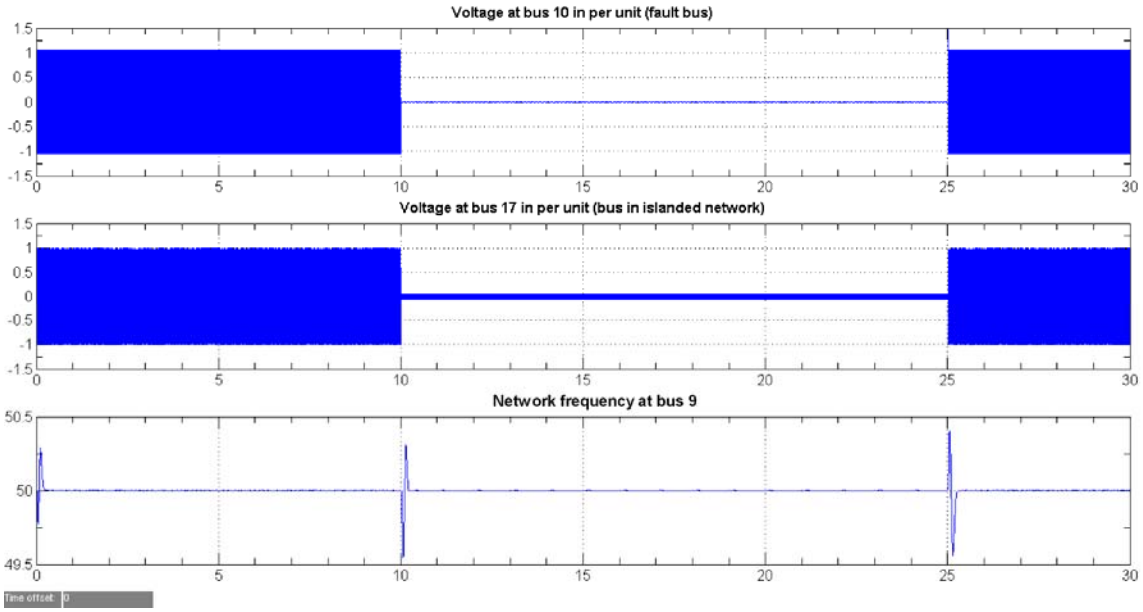

Figure 5.53 Voltage profiles of the UK network with highest demand and lowest generation profiles for scenario 1.2 (from Table 3.6)

5.2.1b) Scenario 1 for the TH network

Figure 5.54 shows the single line diagram of the TH network, which experience a fault at bus 3, and hence the LV network (buses 4 to 8) is isolated from the main MV network.

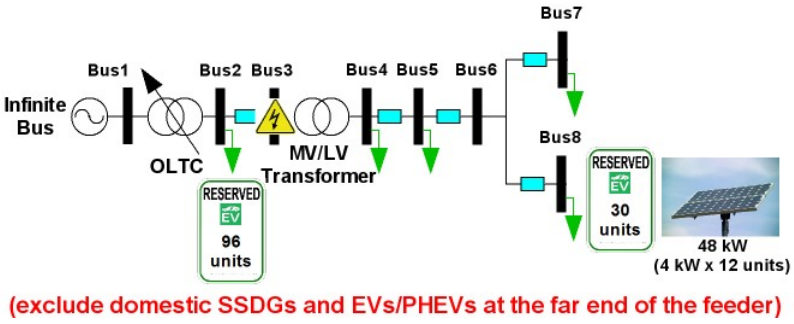

Figure 5.54 Single line diagram of the TH network for scenario 1 (from Table 3.6)

The results of the TH network while experiencing a fault during highest demand and generation profiles is shown in Figure 5.55. The voltage at all buses is within the voltage statutory limits by operation of the OLTC at bus 2 (during 0 to 10 minutes and 25 to 30 minutes). The three-phase fault at bus 3 was detected during 10 to 25 minutes, and hence the breaker at the MV side of the transformer operated and isolated the LV network (buses 4 to 8) from the main network until the fault is cleared. The voltage profiles in the islanded network are below the limits because high demand and all EVs parked in four EVs car parks operate in charging mode. The frequency voltage suddenly drops below the minimum

frequency voltage limit of 49.5 Hz (about 0.5 Hz lower than the limit) and slightly exceeds the maximum frequency limit of 50.5 Hz (about 0.0625 Hz higher than the limit) before settling again at 50 Hz within 50 sec. In addition, the total generation of SSDGs in the islanded network (about ~62 kVA) is lower than the demand (about ~262 kVA). However, the fluctuation of the frequency voltage violation becomes lower and takes shorter time (about ~40 sec) before reaching steady state during lowest generation profiles, as shown in Figure 5.56.

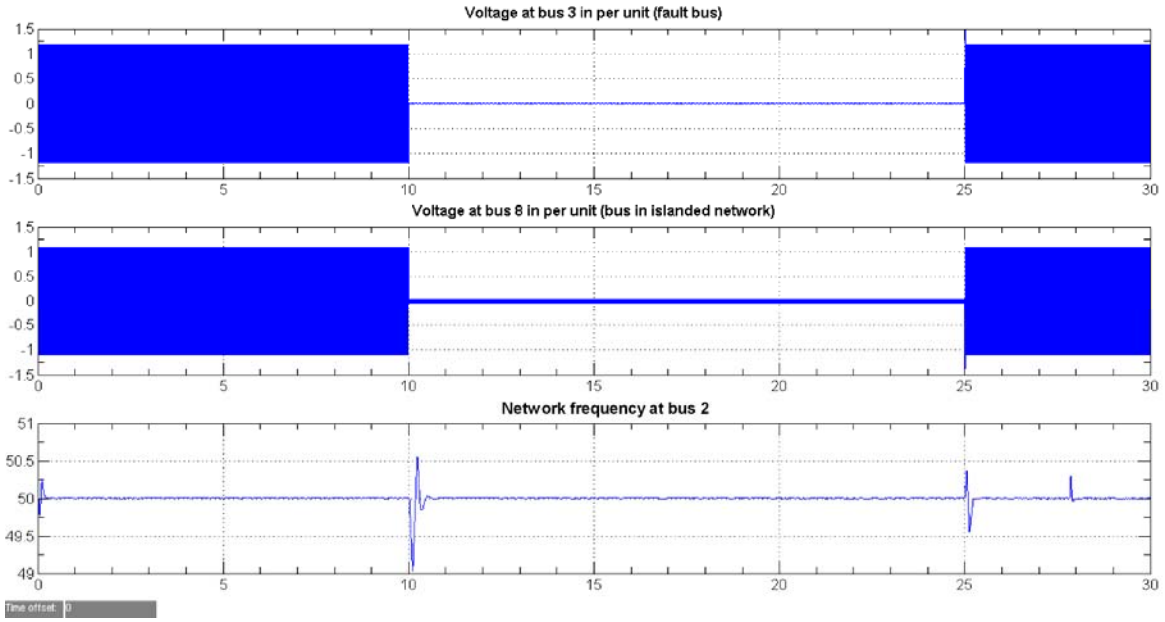

Figure 5.55 Voltage profiles of the TH network with highest demand and generation profiles for scenario 1.1 (from Table 3.6)

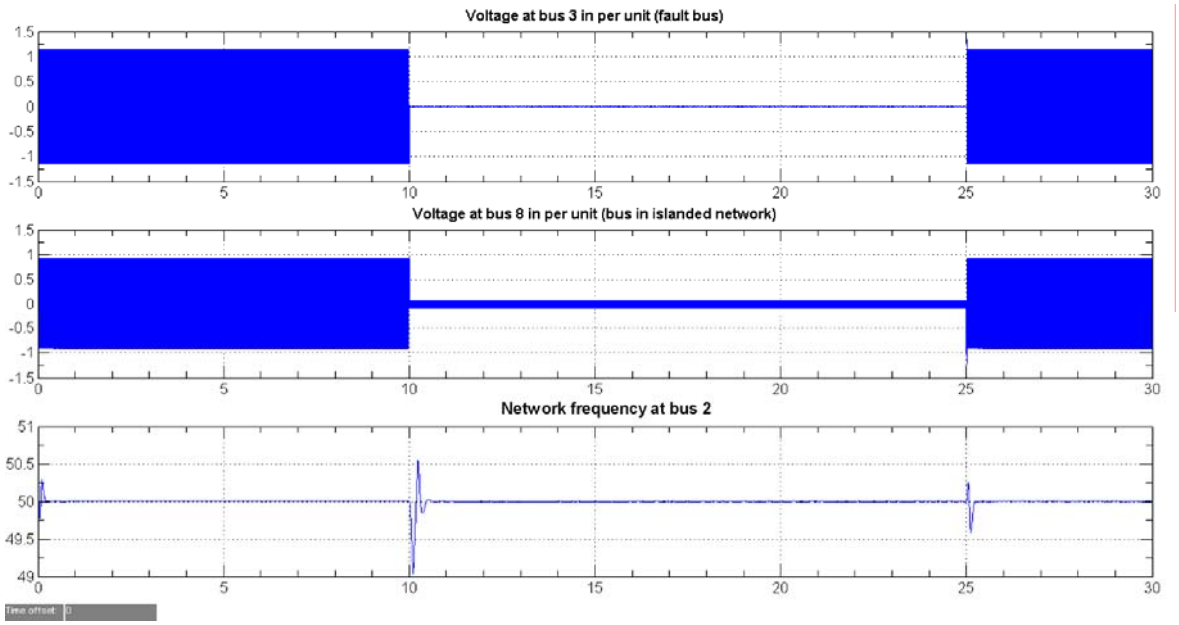

Figure 5.56 Voltage profiles of the TH network with highest demand and lowest generation profiles for scenario 1.2 (from Table 3.6)

In summary, the results shown in section 5.2 shows that the islanding operation still needs controllers to support supply/demand in the islanded network. These controllers must consider the voltage, frequency voltage and load priority in order to allow load shedding in the islanded network.

5.3 Harmonic Distortion

Table 5.9: Details of scenario 1 for harmonic distortion analysis

Scenario	Description	Aims
1	Distributed SSDGs and EVs with penetration levels as forecasted for 2020 during maximum demand. A details model of single-phase inverters with PWM is connected to each section of the LV network. The scenario is carried out during low solar irradiation and low wind speed where EVs/PHEVs operate in charging mode.	Analyse the THD of combined effects of SSDGs and EVs distortion.

It is known that harmonic distortion in power networks is one of the many PQ issues, and hence it is investigated in this thesis. In practice, current harmonics results in the distortion of the normal sine wave voltage provided by utilities. When non-linear devices (e.g. IGBT, PWM, etc.) are connected to the grid, two significant consequences arise because of harmonic generation. First, because of finite impedances of power lines, voltage distortion is generated that other equipment on the line experience. Second, harmonics may cause several problems, including overheating of transformers and neutral lines when generated in a three-phase system.

Many SSDGs and automotive manufacturers claim that their devices (inverters/converters) produce a good PQ (mainly with regard to harmonics and power factor), and hence no significant PQ issues should arise during normal operation of the system. This may be true when these devices operate over 10 percent of full rating (at steady-state condition). Therefore, the impacts of EV chargers, particularly single-phase converter with typical bridge rectifier and PWM, which are in common use are compared and analysed.

The effects of diversity in varying the converters harmonic contribution is examined in the UK and TH networks and presented in this thesis. To simplify the analysis, only one 400 V feeder together with its connected loads and EV was modelled in detail. The loading of individual consumers is assumed to be at full load. A single instance of each charger model was applied to the appropriate point in the system model, and the current harmonic distortion measured via FFT analysis at the input to the relevant bus in each case. Then a second, third and fourth samples of the same charger was applied in parallel to the first, and in each case the THD was measured. This work examines the PQ effects of a number of types of EV charging systems, and measures the effects of diversity (multiple instances of such chargers) on a simulated network. It is assumed that the rating of parallel inverters is the same, as the number of charger increases. The effects of diversity were investigated in each case and the THD was found to decrease in a function of the number of chargers applied at the bus, as shown in Figure 5.57. As can be seen, the appropriate PWM charger can cancel certain harmonics produced by others due to the effects of diversity (more discussed in reference [121]).

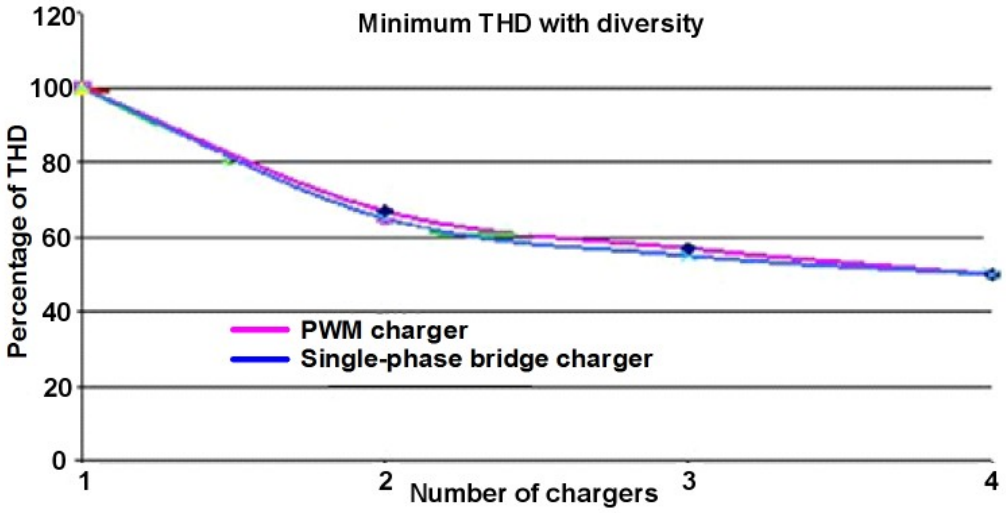

Figure 5.57 harmonic distortion measured via FFT analysis at the input to the relevant bus for the UK networks

As can be seen in Figure 5.57, PWM will be the application of choice for SSDGs and EVs/PHEVs grid interface in view of its flexibility and operation. PWM converters may be designed to cancel harmonics as well as support EVs/PHEVs in V2G mode to support power networks. The PWM operating regime has the capability to produce any given harmonic at pre-determined amplitude and phase angle (described in equation 5.1). Hence, PWM can reduce or remove certain

harmonics produced by others devices, and the others devices may magnify the levels of particular harmonics.

The Fourier series of a leading-edge PWM signal $(F_{L(t)})$ can be obtained from the following equation [121]:

$$F_{L(t)} = k + \frac{M}{2}\cos(\omega_s t) - \sum_{m=1}^{\infty}\left\{\frac{1}{m\pi}\sin(m\omega_c t) + \frac{J_0(m\pi M)}{m\pi}\sin(m\omega_c t + 2m\pi k)\right\} \quad (5.1)$$

$$+ \sum_{m-1}^{\infty}\sum_{n=\pm 1}^{\pm\infty}\frac{J_n(m\pi M)}{m\pi}\sin\left(m\omega_c t + n\omega_s t + 2m\pi k + \frac{n\pi}{2}\right)$$

Where,

J_n = Bessel function of the first kind with integer order n

k = Zero-input duty-cycle of PWM signal

m = Carrier harmonic index

M = Modulation index ($0 \leq M \leq 1$) or equivalently,
the value of the signal level normalised to the maximum signal level

n = Signal harmonic index

ω_s = Angular frequency of the modulating signal (rad/s)

ω_c = Angular frequency of the carrier in (rad/s)

However, the most pronounced effects of harmonic profiles in the distribution network are caused by the performance of SSDG inverters that operate at less than 10 percent of full rating (mostly PV and wind turbine inverters as solar irradiation and wind speed fluctuate more than the water velocity) and the EVs/PHEVs converters operating in charging mode. This is due to these devices are mostly power electronic and highly non-linear hence they generate high levels of current harmonic. It is also evident that the most pronounced effects would be measured at weakest bus, which is at the far end of the LV feeder (explained in section 2.5). Due to this reason, the computer models were developed (described in sections 4.2 for SSDGs inverter and 4.5 for EVs/PHEVs).

In order to investigate the impacts of SSDGs and EVs/PHEVs on harmonic distortion in the distribution network, the computer models for grid interface devices must comply with standards and regulations. The average THD of grid interface devices (e.g. grid inverter, EVs/PHEVs grid connection, etc.) is 3 percent and the maximum THD is 8 percent [47]. References [37] and [138] suggested that the switching frequency of PWM application for SSDGs (e.g. inverter, converter) varies between 10 kHz (for SSDGs) and 1 kHz (for large DGs) and for EVs/PHEVs

(normally as battery charger) it is less than 2 kHz. Therefore, a switching frequency of 10 kHz was applied to the simplified PWM application of SSDGs and 2 kHz was set in the simplified EVs/PHEVs PWM charger model in this thesis.

It can be noted that FFT Analysis Tool dialog box of MATLAB/Simulink analyses the harmonic order that bases on the portion of a signal at the specified time for a specified number of cycles (here 1 cycle). Bar (relative to fundamental) and Harmonic order taps are selected to display the relation of the spectrum and the harmonic order to the fundamental frequency. Thus, the harmonic order was identified by the ratio of frequency of the harmonic to the fundamental frequency, and hence the THD is the ratio of the sum of all harmonic components to the fundamental frequency. The reference fundamental frequency is set at 50 Hz. Figure 5.58 shows the harmonics profile of a typical PV inverter rated 4 kW (simulated from model in section 4.2) when operating at less than 10 percent of full rating.

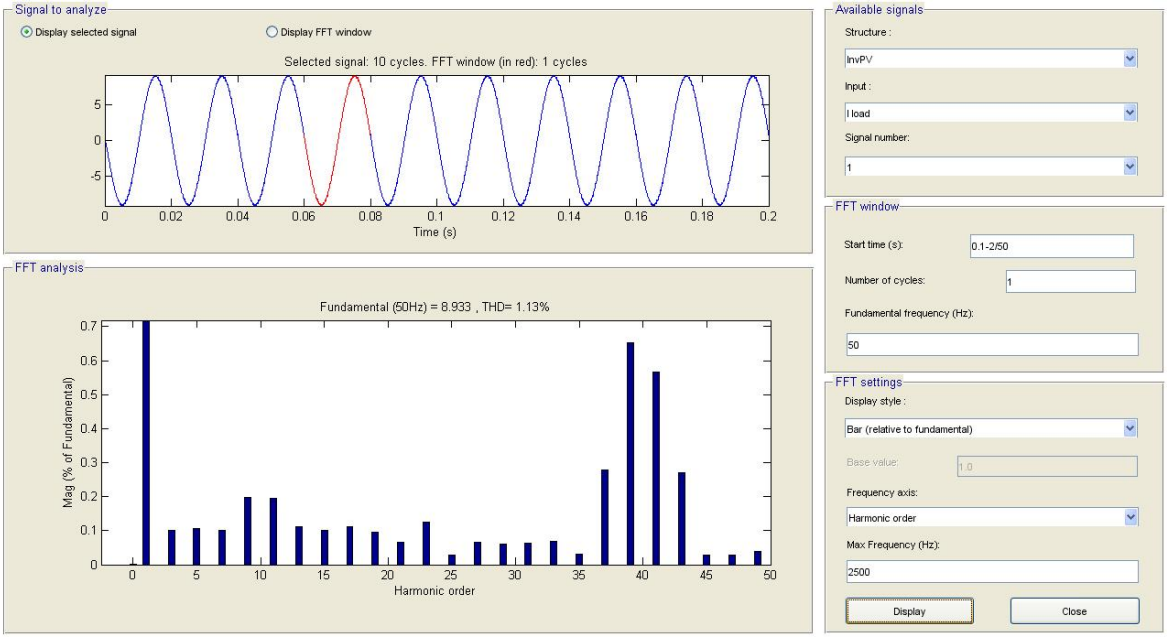

Figure 5.58 Harmonic profiles of typical PV inverter
with switching frequency of 10 kHz and duty cycle at 0.1 (with ~9A)

As can be seen in Figure 5.58, with switching frequency 10 kHz and the fundamental 50 Hz, the typical PV inverter with 0.1 duty cycle has a total THD of 1.13 percent. This similar explanation is applied to a typical wind turbine inverter rated 5 kW, as shown in Figure 5.59 (simulated from model in section 4.2).

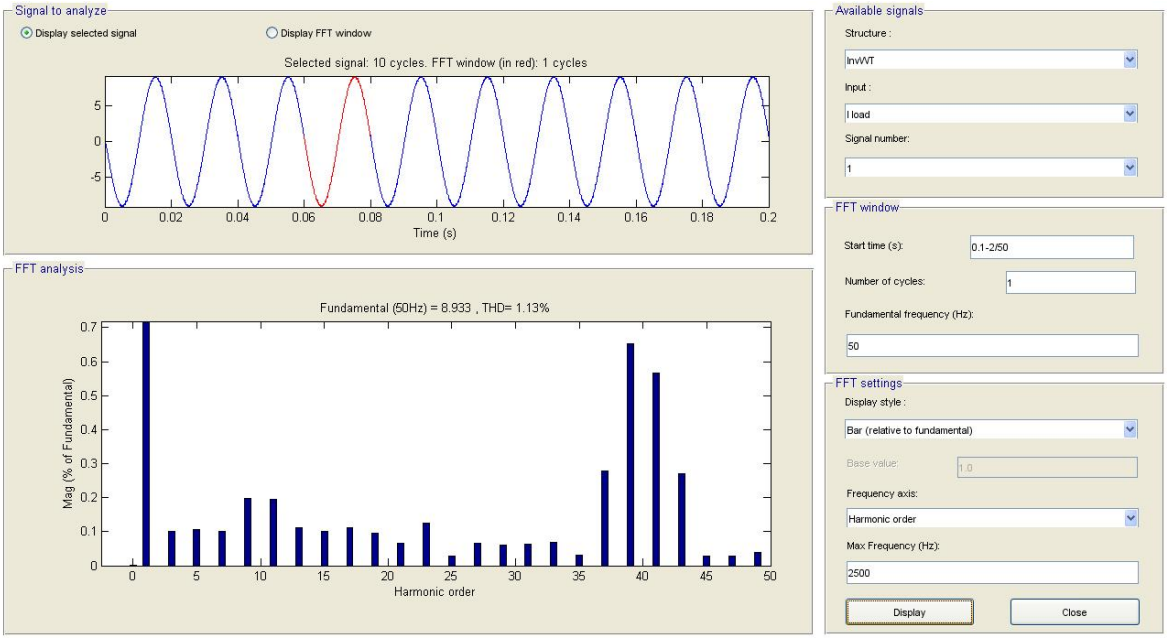

Figure 5.59 Harmonic profiles of typical wind turbine inverter with switching frequency of 10 kHz and duty cycle at 0.1 (with ~9A)

It is often known that the water in the canal or small-river flow is steadier than solar irradiation and wind speed and therefore the performance of a typical small hydropower inverter is in the appropriate range (between 95 to 100 percent). Accordingly, the size of inverter must be chosen to match the rated output power of the SSDG in order to optimise its output power. Figure 5.60 shows a typical small hydropower inverter rated 5 kW has THD 0.98 percent with switching frequency of 10 kHz and 0.8 duty cycle (simulated from model in section 4.2).

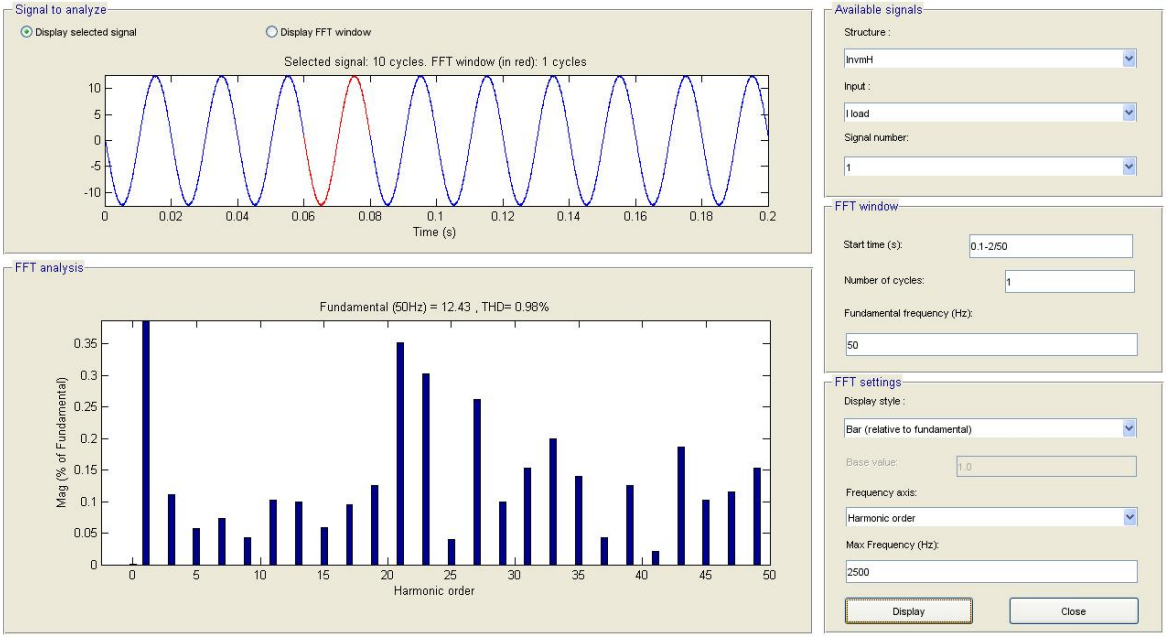

Figure 5.60 Harmonic profiles of typical small hydropower inverter with switching frequency 10 kHz and duty cycle at 0.8 (with ~13A)

Figure 5.61 demonstrates the harmonic profiles of a typical EVs/PHEVs domestic charger with PWM application during fully charging (~13A, single-phase). It can be seen that at a switching frequency of 2 kHz and duty cycle 0.8, the THD is 2.88 percent.

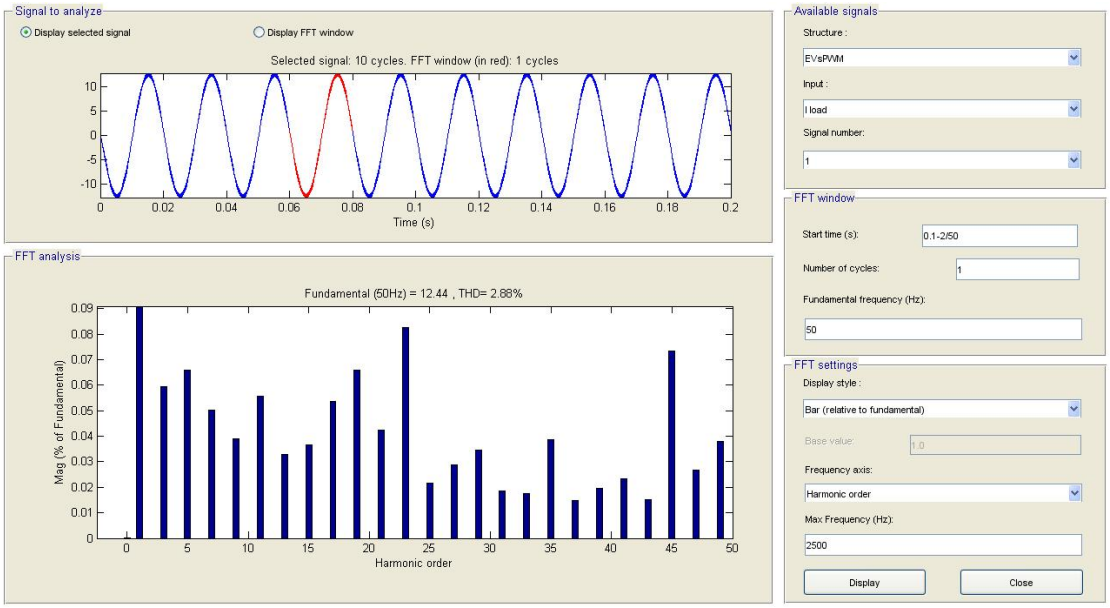

Figure 5.61 Harmonic profiles of typical EVs/PHEVs battery charger with switching frequency of 2 kHz and duty cycle at 0.8 (with ~13A)

Hence, the proposed inverter and charger models (given in Figures 5.58 to 5.61) were applied in parallel from the start to the far end of the LV feeder as shown in Figures 5.62 for the UK network and 5.63 for the TH network in order to examine the effects of applying a multiplicity of SSDG inverters and EVs/PHEVs chargers on power network. It is important to note that here the SOC of all EVs/PHEVs batteries were considered to be at the same level. The current harmonic distortion is measured via FFT analysis at the input to the relevant bus (for the UK network shown in Figure 5.64 and for the TH network shown in Figure 5.65). The harmonic distortion scenario 1 from Table 3.7 was used to investigate the impacts of SSDGs and EVs/PHEVs on the harmonic profiles in the distribution network.

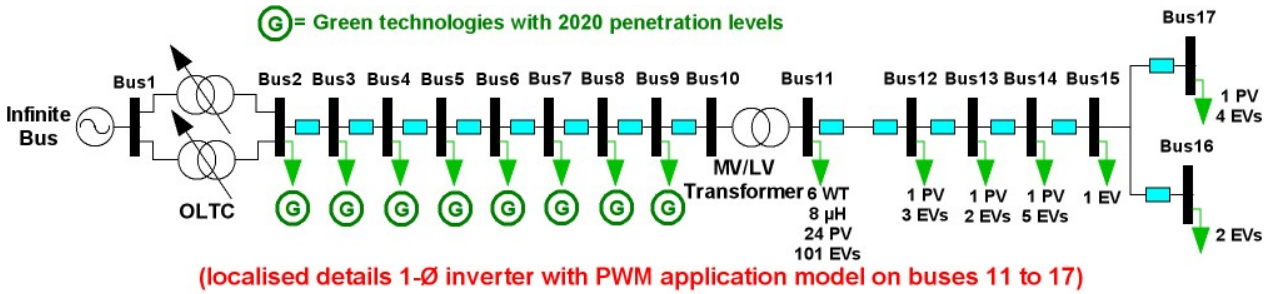

Figure 5.62 Single line diagram of the UK network for scenario 1 (from Table 3.7)

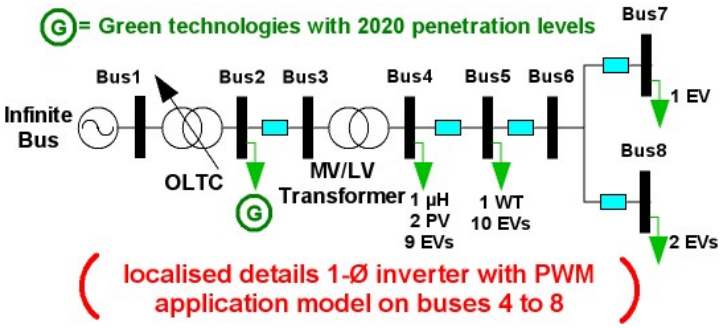

Figure 5.63 Single line diagram of the TH network for scenario 1 (from Table 3.7)

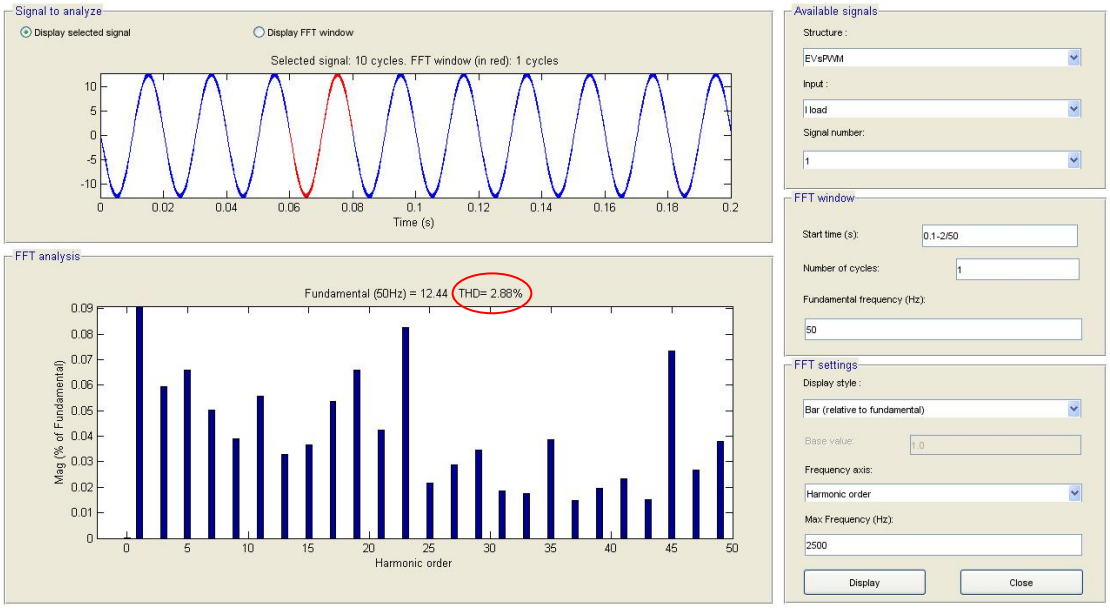

Figure 5.64 Harmonic profiles of the UK network at the far end of the LV feeder for scenario 1 (from Table 3.7)

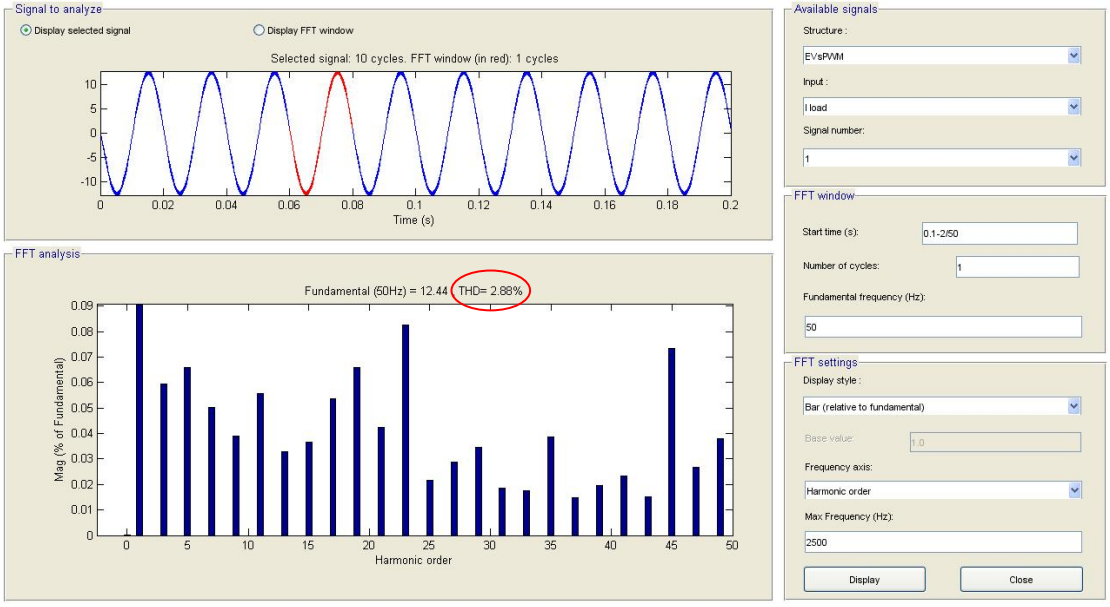

Figure 5.65 Harmonic profiles of the TH network at the far end of the LV feeder for scenario 1 (from Table 3.7)

The results of both the UK and TH networks shown in Figures 5.64 and 5.65 show that the voltage THD was found to rise as the number of SSDG inverters (especially incorporated with PV and wind turbine) and EVs/PHEVs chargers (operating in charging mode) increases. It is interesting to note that the THD at the far end of the LV feeder rises and may become significant when the PV and wind turbine inverters operate at less than 10 percent of full rating (low solar irradiation and low wind speed at the same time).

This is due to the duty cycle of SSDGs inverters (particularly PV and wind turbine) varies according to the surrounding environment (which are solar irradiance and wind speed) in order to maximise its output power. Hence, the THD that increases due to the PV and wind turbine inverter connect into the distribution network is unavoidable, especially long distribution feeder. It must be noted that, the THD are still within the standard limits, if the THD of each device are within the maximum harmonic statutory limit, with similar conclusions in references [37] and [38]. The standard practice for electrical system design specifies the major harmonic voltage, which can occur on the network is typically 5 percent of THD with no individual harmonic exceeding 3 percent of the fundamental [40].

To concluded, existing MV/LV distribution networks were originally designed for one-directional power flow. That means power flow from central generating units downward to the consumers. Hence, in order to maintain the voltage within the statutory limits, PQ has been ensured by the centralised control. However, this flow will be changed from one-directional to bi-directional because the increased connection of SSDGs and EVs/PHEVs into LV distribution networks (in residential area). Consequently, the performance of inverters is also considered an important factor to the THD as it can cause harmonic resonance in the network thus it effects on the neighbouring devices, which have the same harmonic order. Because green technologies are gradually being adopted and their penetration level is increasing, hence the power flow needs to be optimised. Then, the concept of the SDSM technique and smart control devices incorporated with the smart meter have been proposed in the thesis, which are considered the potential of available technologies, technologies investment and current standards, are presented in chapter 6.

CHAPTER 6
PROPOSED SMART GRID SOLUTIONS

Future power networks will have the ability to integrate central control with SSDGs, EVs/PHEVs and smart appliances at consumer sites. These can optimise power flow and deliver up-to-date information to all consumers via the use of smart meters. Therefore, it can be expected that some parts of the existing (passive) network will become active zones, which accommodate one or more SSDGs where it is also agreed in reference [249]. Joode, [250] reported that an increasing penetration of DGs is only possible with active network control and strict regulations in order to manage power flows quickly and accurately. Browning, [251] proposed solutions based on accurate forecasting of demand for operating and controlling power plants and distribution generators. They considered the use of energy storage to reduce the effects of power fluctuation to improve operation flexibility and meet regulatory targets. Jenkins, [252] studied active network management and found that existing power networks do not require major changes in the regulations and can rely on the DMS to control the network voltages. The DMS normally uses OLTC to control voltage limits, reactive power and constrain power. This management can satisfy the consumers with a moderate penetration level of DGs. For higher levels of DGs, network control becomes difficult, and there is a need for local control devices, as shown in Figure 6.1.

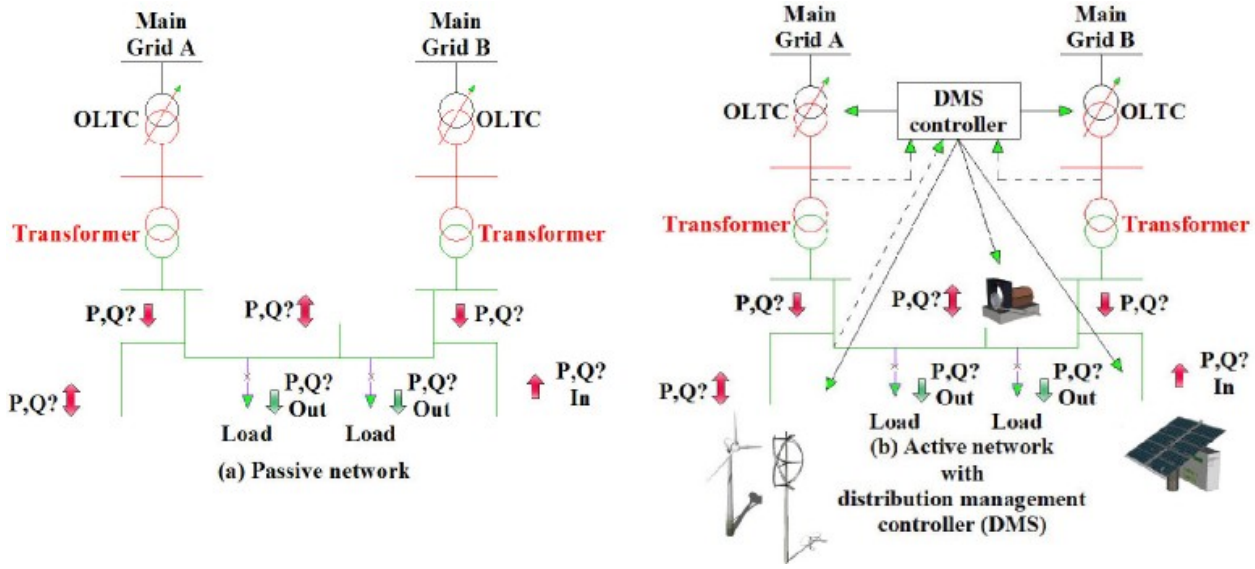

Figure 6.1 Passive network and active network

Chuang, [253] suggested that local control devices play an important role to communicate in the local area because it allows the network operator to achieve the configuration of consumer equipment in order to ensure reliability and safety. The control devices can receive information via direct connection (fibre optic cable) or wireless transmission (Wi-Fi). Therefore, an advanced metering system, which includes advanced sensor measurements and provides two-way communication, may remotely connect/disconnect and update information of the devices in real-time. References [254] and [255] proposed an adaptive smart control for active distribution networks by using advanced sensors measurement incorporating compensation devices in order to optimise reactive power in the network, where it can decrease losses due to the transmission system.

Therefore, the boundary of the solutions proposed in this thesis is to optimise the power flow in the MV/LV distribution networks with high penetration levels of SSDGs (PV, wind and hydro turbines) and EVs/PHEVs. The feasibility functions of the proposed smart controllers are achieved by using the Boolean logical operator. Accordingly, it can support an interpretation model for the properties of neural networks, as well as give a precise description of their performance without having a learning algorithm. Hence, it can be used to specify a system directly and even produce a simple set of control rules for a dynamic system. Fuzzy logic is not considered in the development of the smart controllers because it is usually developed for a user friendly interfaces in practical work where this is beyond the scope of the thesis. Moreover the Fuzzy theory is the formal method to deal with either expression or rules (based on text command to setting their expressions/rules), and hence a computer is still using rigid Boolean logic to control these expressions [144].

Before presenting the proposed smart controllers, the theorems of Boolean logical operator is first considered. In practice, a drawing of the control system includes mechanical switches or relay contacts, and therefore logic true contact is shown on the circuit as a closed contact and logic false contact is shown as an open contact because all switches should be shown in un-energised positions. That means when the logic true contact is operated it becomes a closed contact where the logic false contact is operated it becomes an open contact.

Figure 6.2 shows the symbols, the equivalent circuit and the truth tables of basic gate circuits that found in digital circuits and current market.

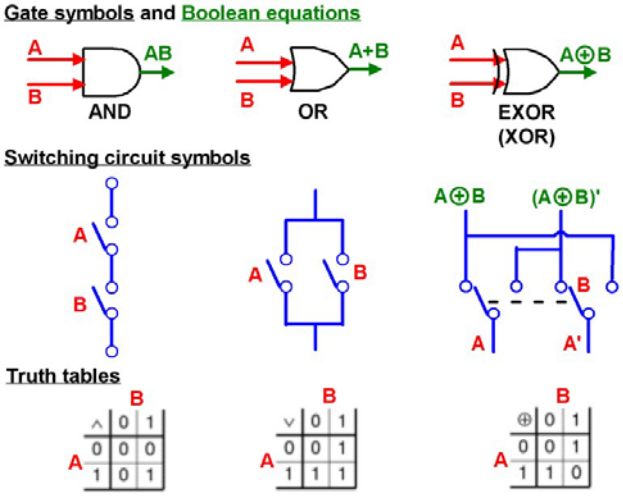

Figure 6.2 Basic Boolean algebra with gate, switching symbols and truth tables

The Boolean algebra is normally based on these three binary operators. The truth tables in Figure 6.2 show the conditions of the operators under logic true and false values. All possible variations of the input variables are shown on the left of the truth table (in binary numerical order) and the results of the operators are shown on the right of the truth table. It can be seen that the output AND gate is high (equal to 1 or closed circuit) only when both inputs of the gate are high (input switches in the circuit are closed). Secondly, the output OR gate is high (equal to 1 or closed circuit) when either or both inputs of the gate are high (either or both input switches in the circuit are closed). Lastly, the output EXOR (XOR) gate is high (equal to 1 or closed circuit) if either but not both inputs are high together, and therefore the input switches can be cascaded. That means both logic true and logic false signals of the EXOR gate are carried through a chain of these circuit. However, actual gate circuits can have as many inputs as are required within the limitations of the circuits.

6.1 Smart Demand Side Management (SDSM) Technique and Central Data Bank

In practice, the network operator cannot control devices in residence properties (such as refrigerator, washing machine, PC etc) due to ownership and private rights. That means future distribution networks, need local controllers, which support power consumption/supply such as, manage charging time of EVs/PHEVs and the use of energy storage systems. Therefore, this thesis

proposes a “Smart Demand Side Management (SDSM) Technique” based on the “Smart Grids” concept, which is an entirely new solution to distribute power at LV level. This solution can manage power flow by providing local data via a central data bank to smart controllers at public areas (SOLTC, SCP, SEVGC, SES and SLC) on power networks in order to ensure the power is sufficient at all times, as shown in Figure 6.3.

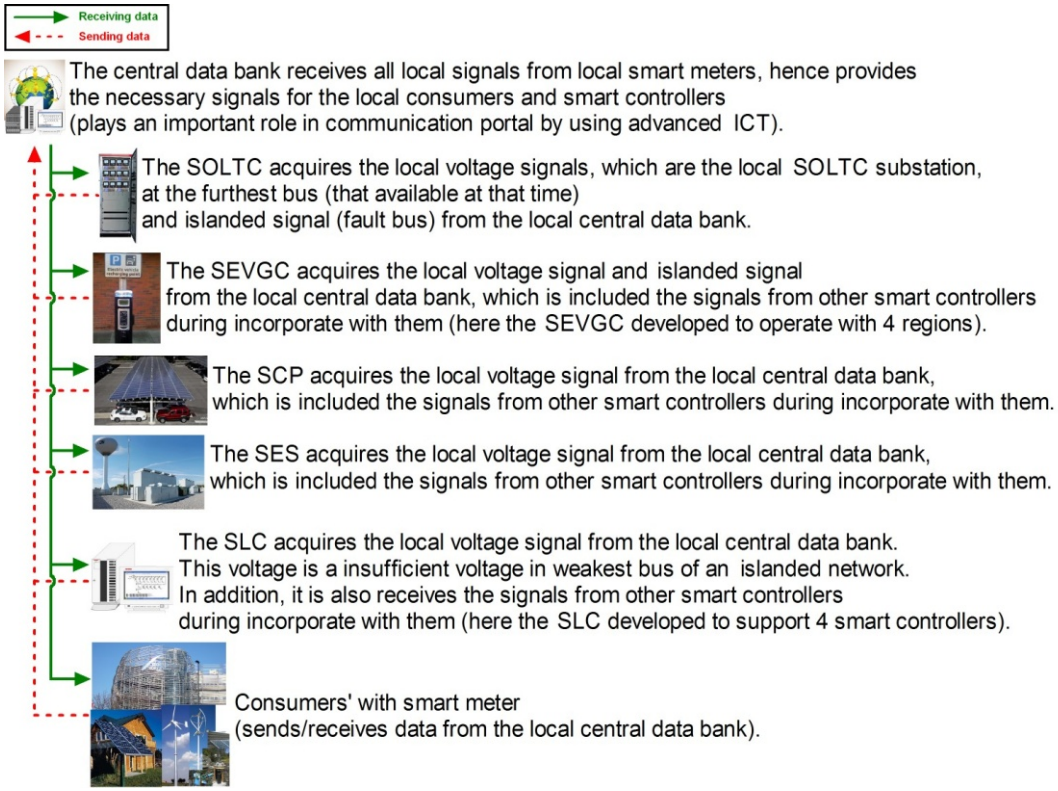

Figure 6.3 Schematic of the central data bank

This technique can facilitate integration of SSDGs and EVs/PHEVs where smart meters are used in conjunction with other smart controllers. Accordingly, these data can be updated by using existing fibre optic cable, Wi-Fi or satellite to retrieve/update data from smart meters, as shown in Figure 6.4.

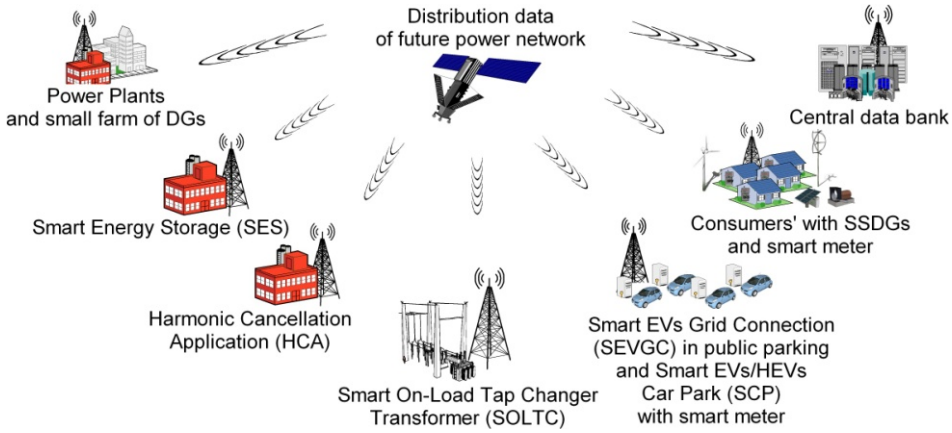

Figure 6.4 The SDSM technique and the central data bank on future power networks

Figure 6.5 shows the control diagram of the SDSM technique in future power networks by using a central data bank to receive/send data between local devices (smart controllers and consumers) via smart meters. The main signals received from local consumers/devices are bus location, voltage profiles, power factor, energy consumption, harmonic distortion, generated power of DGs, connection time of EVs/PHEVs, fault status, prices and operating status. The local smart controllers (SOLTC, SEVGC, SCP, SES, SLC and harmonic cancellation applications, more details in section 6.2 to 6.6) acquire the necessary local data from the central data bank to operate, whereas the local consumers (residences) receive the electricity tariff and signals from the central data bank.

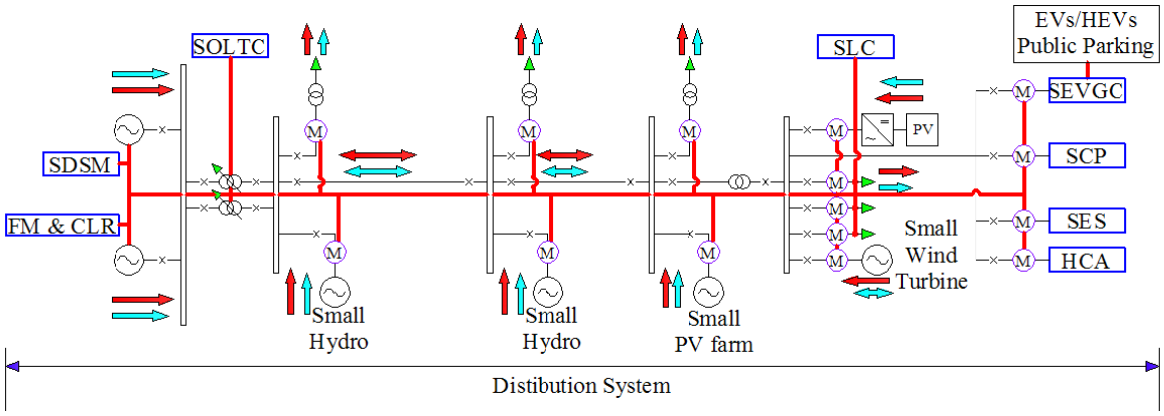

Legend	Details	Legend	Details
×	Breaker	SDSM	Smart Demand Side Management Control
	Loads	SOLTC	Smart On-Load Tap Changer Transformer
	Transformer	FM & CLR	Fault Level Monitor and Fault Current Limiter
	On-Load Tap Changer Transformer	SEVGC	Smart EVs Grid Connection
	Generation Unit	SCP	Smart EVs/HEVs Car Park
	Active Power	SES	Smart Energy Storage Systems
	Reactive Power	SLC	Smart Load Controller
	Inverter DC-AC	HCA	Harmonic Cancellation Application
M	Smart Meter		Fibre Optic Cable or Communication Signal

Figure 6.5 Control diagram of the SDSM technique in future power networks

Therefore, in order to ensure the local smart controllers operate within the standards and personnel safety, the local measured data needs to be checked against the standards, regulations and connection agreement of network providers, as shown in the schematic of data acquisition of the SDSM technique (shown in Figure 6.6).

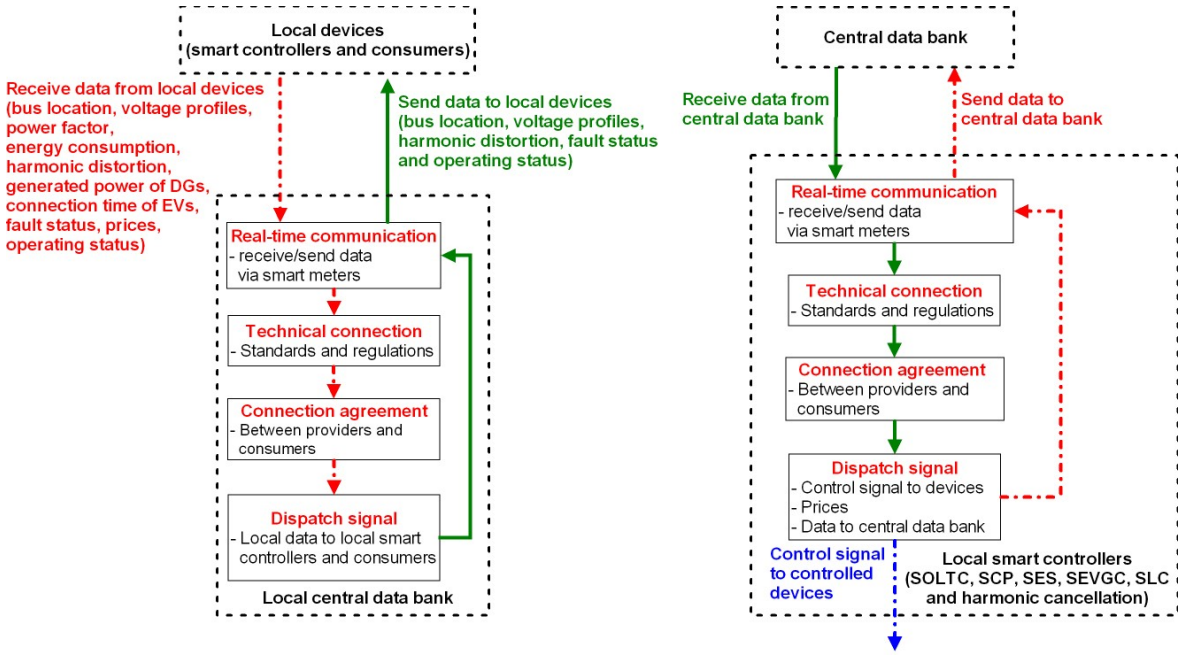

Figure 6.6 Schematic of data acquisition of the SDSM technique

It can be seen that the devices in this concept require intelligent and secure functions in order to respond to unpredictable conditions, and hence the SDSM technique can support real-time monitoring and provide fast response control. In addition, the central data bank can be installed within either the existing centralised control or elsewhere in the network. Therefore, the central data bank has low investment similar to a service station of a mobile phone network. The following requirements were used to develop the SDSM technique in this thesis:

1) All the residences must have smart meters, which allow updating data (such as energy consumption, voltage/current/harmonic profiles, power factor and location) to the local central data bank or smart controllers. These data can be directly accessed by the local smart controllers and the central control.

2) All the proposed smart controllers (SCP, SEVGC, SES and SLC) integrate with PLLs in order to ensure the voltage, phase and frequency of the devices synchronise with the main network.

3) Data from all RCBs used in MV/LV buses must be provided to the local central data bank regarding personnel safety in power networks (e.g. loss of main or cable fault at any load feeder). The RCB can use active detection (e.g. pulse/echo), passive detection (e.g. impedance measuring, vector surge, frequency gradient) or the coordination of a series of measures to identify

transmission status. These also allow the smart network to specify where and when the islanded network has happened, which depends on the tripping signal from the RCB or the measurement from passive/active detection.

4) In order to allow EVs/PHEVs to support supply/demand matching in future power networks, their battery charger must include V2G function, which usually employs PWM techniques. Accordingly, appropriate PWM control can allow EVs/PHEVs to feedback power to the grid at low harmonic level. In addition, EVs/PHEVs are considered as active mobile loads because they are not available for either absorbing or supplying electrical energy when they are used for transport. This situation normally occurs in the rush hours in the morning and evening (during the working day). Furthermore, EVs/PHEVs can be possibly parked at different locations at different times of the day. This will affect the daily variations in energy supply and demand. For instance, during the working day, cars will likely be parked close to the owner's place of work, whereas during the night, vehicles will be parked at home.

5) The location of SSDGs, SCPs and EVs/PHEVs public parking is considered because installation at an appropriate location can optimise the power flow and investment. Accordingly, the capacity of these devices has a significant effect on the voltage at the local bus.

6) It is known that the generated power due to SSDGs (e.g. PV, wind and hydro turbines) and EVs/PHEVs operating in V2G mode can exceed the consumer demand, and hence the maximum voltage statutory limit at that time may be exceeded. Therefore, energy storage systems should be used to store electrical energy when there is an energy surplus, and return this energy back to the network during high demand. That means the proposed SES can be used to supply/consume energy, and hence its location is an important factor to determine the capacity of the distribution network as well.

7) All bus faults must be reported to the local central data bank, and hence the smart controllers should have the right to access the fault data (such as location, fault and bus status) in order to ensure that the smart controllers are functioning correctly.

8) In order to allow islanding of a network, all secondary off-load tap changer transformers of the LV network must provide an isolated (local) grounding system to support the islanded network. Furthermore, all SSDGs must include controllers in order to maintain voltage and frequency in an islanded network within the statutory limits.

9) Allow load shedding management in the islanded network in order to match supply/demand in the islanded network. Hence, high speed detection and fast response of load shedding management that handles the frequency and voltage variation due to the isolated SSDGs and loads are required. That means in emergency, network operators should have the rights to access and control the smart controllers without notice to the providers. Furthermore, appropriate standards and regulations will be required in case of parallel operation of the isolated DGs/SSDGs.

The function of the SDSM technique in this thesis is divided into two main parts. Firstly, independent mode; allow smart controllers to operate independently in the network by acquiring the local data directly from either the local central data bank or the local buses. Figure 6.7a shows that the local smart controller can easily access the local data via the local central data bank, which provides data in the same way that a student borrow a book from the library. That means more signals are available for the controllers. For instance, the controllers can use the signal from the weakest bus instead of the local bus. Hence, this can increase the performance of the SDSM technique. This also allows these controllers to acquire the necessary data instead of receiving multiple data from the local buses, preventing over flow of data and malfunction at the controllers, (like the student requiring the specific book in the library). Hence, the size of the central database depends on the number of the consumers in the network. In order to ensure the provided data are correct, the local network operator that monitors the local central data bank works as librarians in the library. Accordingly, the local network operator also has the right to access and control the smart controllers in emergency cases, which is similar to the librarian charging for the overdue book from the student. Furthermore, the use of the local central data bank as a gateway for the smart network supports the network in both the short and long term.

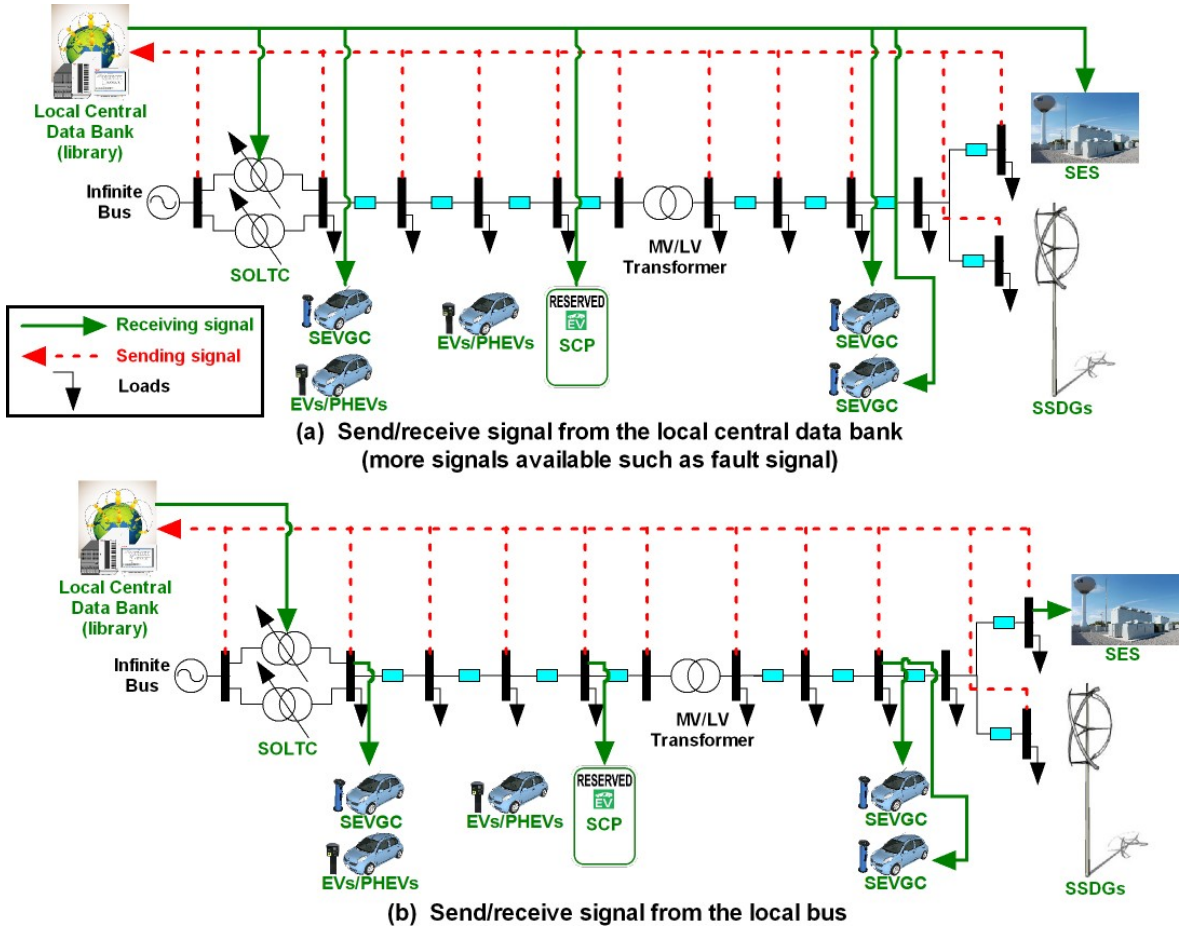

Figure 6.7 The SDSM technique with smart controllers operate independently (independent mode)

Figure 6.7b shows the controllers that directly acquire the data from the local bus only support the network in the short term because the number of consumer and providers are continually increasing and therefore complexity of infrastructure of distribution networks is unavoidable. As a result, the higher the complexity of distribution networks, the larger the local database can be expected where the change of the network infrastructure can increase the difficulty of update local data. For instance, a SEVGC may require an extra communication link to a SCP (such as hard wire of fibre optic, Wi-Fi setting), and hence the SEVGC provider may need agreement from the SCP provider in order to access the SCP data. Therefore, this type of setting is suitable in the short term and support the local bus only. The setting of the SDSM technique with independent mode is shown in Figure 6.8.

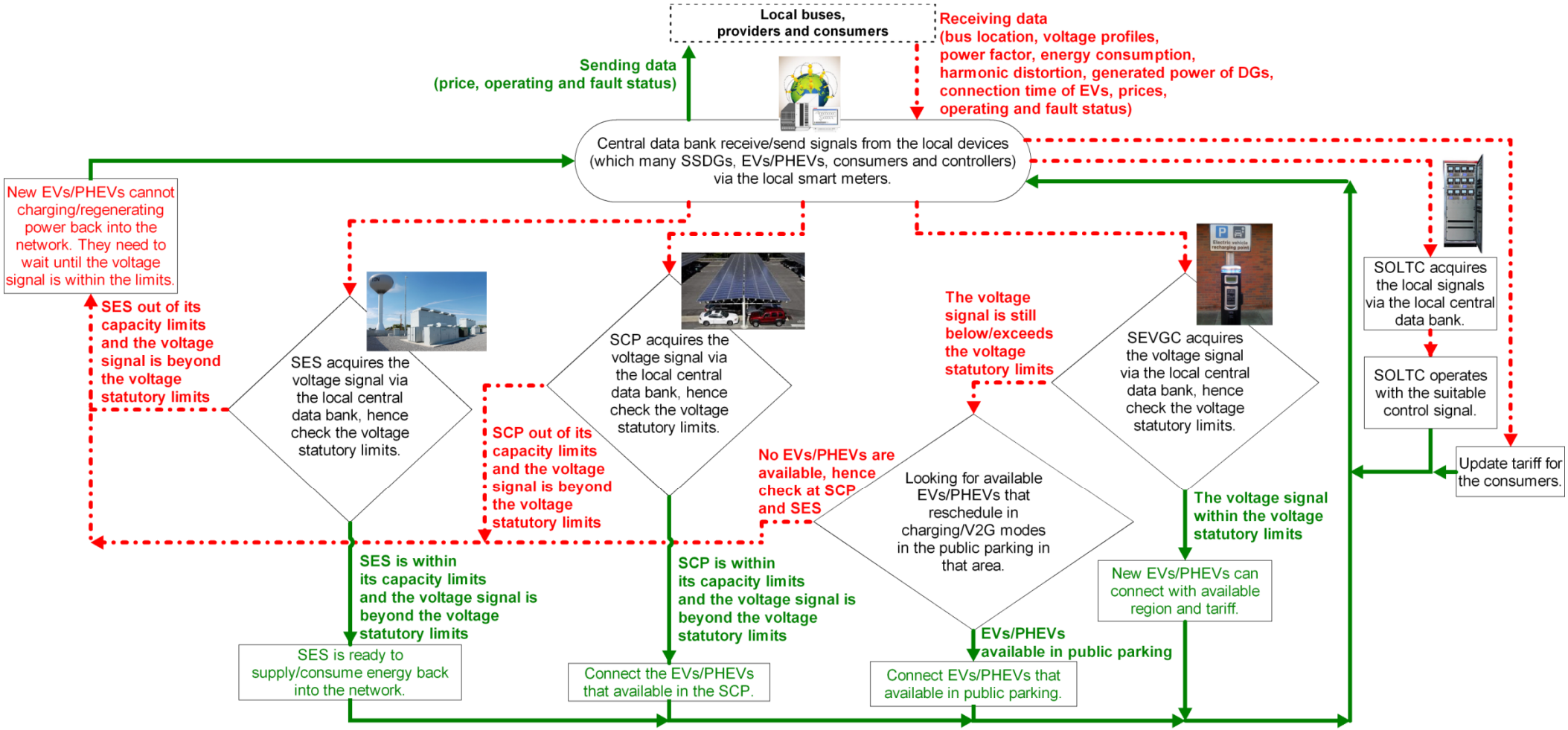

Figure 6.8 Flow chart of the SDSM technique with smart controllers operate in independent mode

Secondly, incorporated mode; the smart controllers are incorporated together by using priority configuration (addressed as master and slave devices by considering their impacts on power networks and/or agreement between providers), as shown in Figure 6.9. It can be seen that the data acquisition of controllers in incorporated mode is similar to those conditions for the independent mode as all smart controllers are still acquire the data directly from either the local central data bank or the local buses. However, the slave devices also need the signal from the master devices in order to operate. This concept is proposed for providers who own more than one smart controller in the network or providers who work as a joint venture.

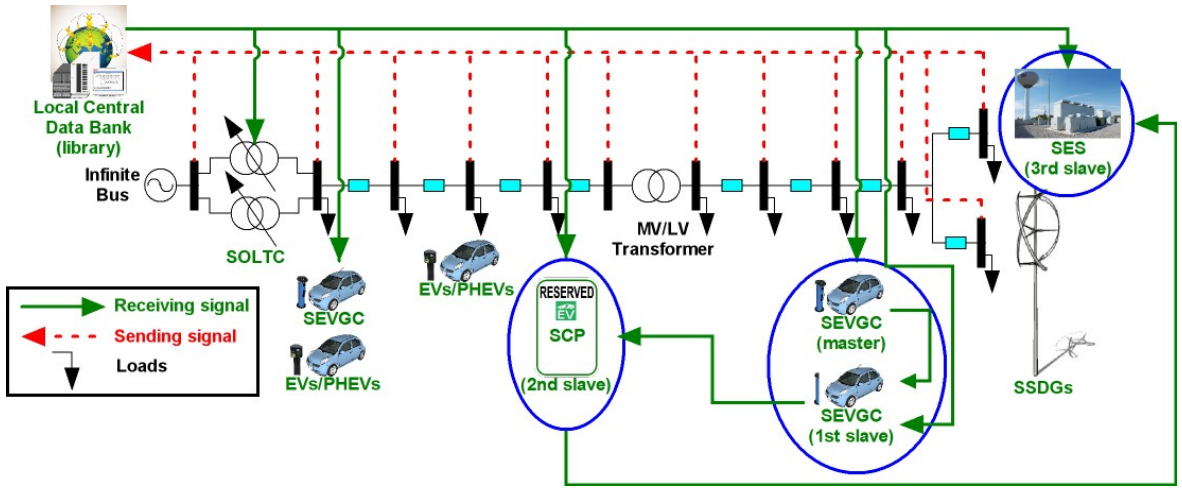

Figure 6.9 The SDSM technique with smart controllers operate as master and slave (incorporated mode)

The setting of the SDSM technique with incorporated mode is shown in Figure 6.10.

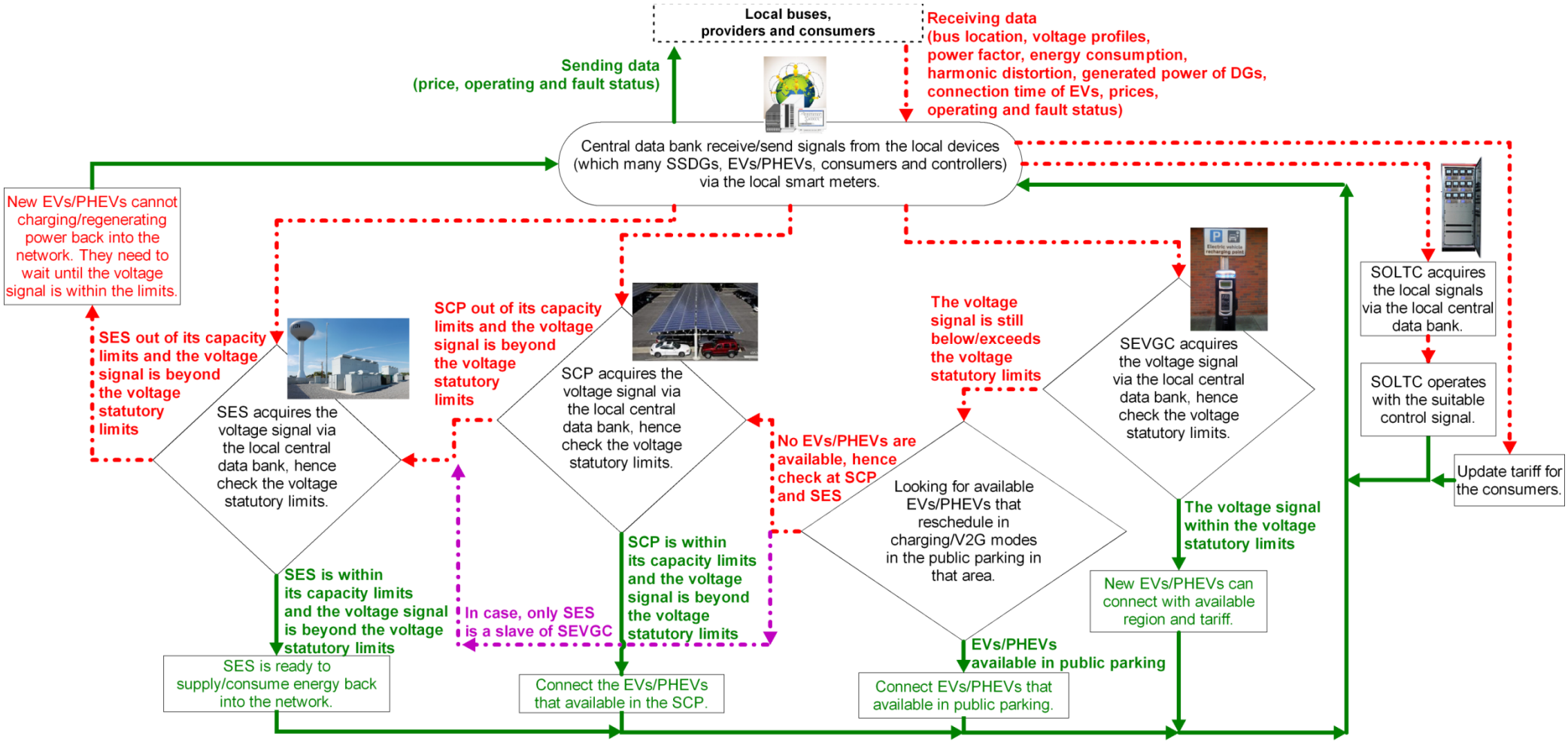

Figure 6.10 Flow chart of the SDSM technique with smart controllers operate in incorporated mode

Hence, the smart controllers can be operated independently or incorporated together, which depends on the characteristic of the network. The crucial key of this setting is the network operator in that network. Indeed, the function of the SDSM technique is suitable for the MV/LV network. Moreover, this technique can be incorporated with the SCADA system, which is currently used on the HV/MV network as well. This can be done by allowing the network operator at the SCADA system to monitor the MV/LV network. Hence, it can decrease the data over flow at the SCADA level, increase fast management and optimise power flow in the network. It must be noted that the main system can override the monitored system in emergency cases, much as the local network operator overrides the smart controllers, the regional network operator overrides the local network operator. Figure 6.11 shows the concept of the SDSM technique incorporated with the SCADA system.

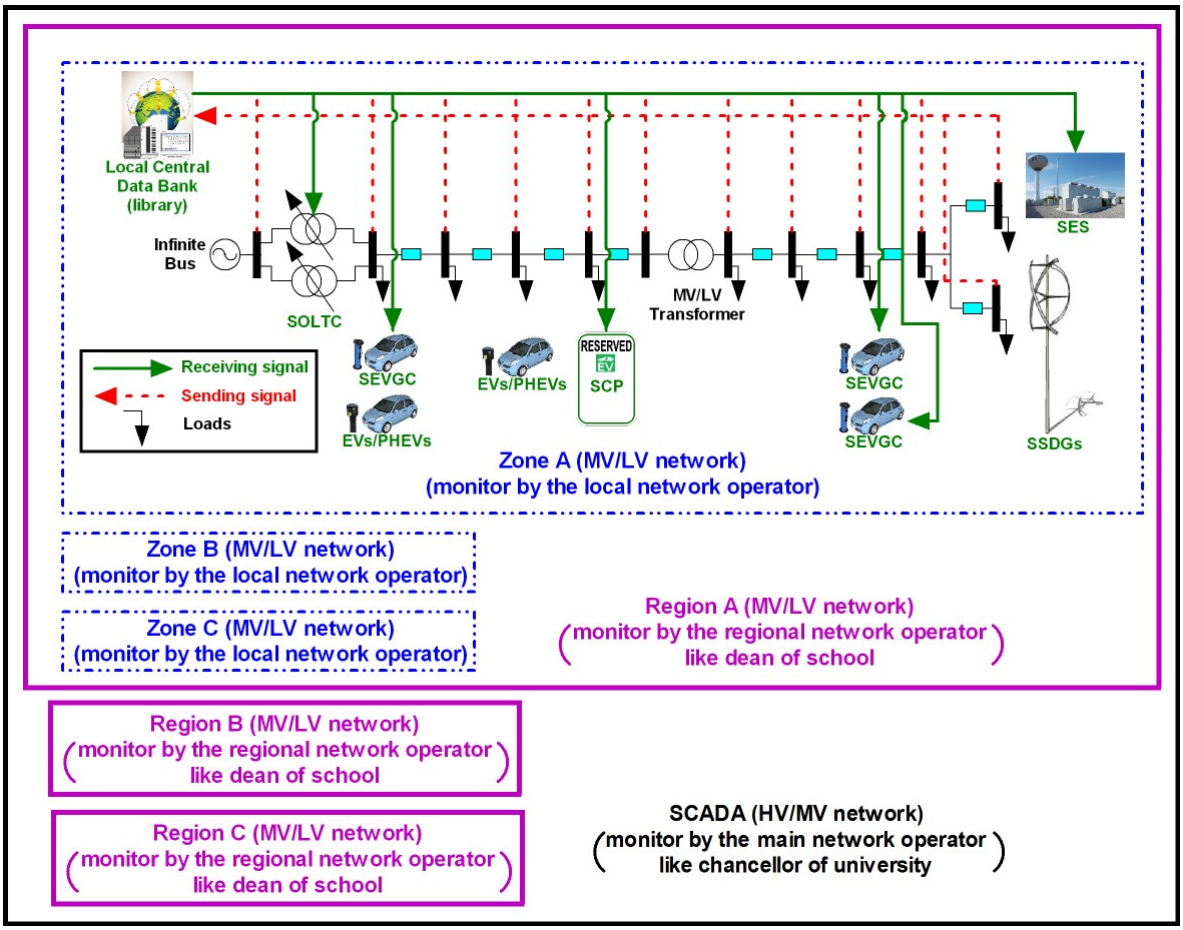

Figure 6.11 The SDSM technique incorporate with SCADA system

6.2 Smart On-Load Tap Changer Transformer (SOLTC)

A typical OLTC that is currently available in the market usually uses a single local voltage signal at its bus to maintain voltage at its bus within the acceptable limits (i.e. it does not consider the voltages at other buses). Nevertheless, the voltages at the other buses that are located after the OLTC substation are still affected because the infrastructure of an existing distribution network is normally a radial network. However, in future power networks with many SSDGs and EVs/PHEVs connected into the MV/LV distribution network, the voltage at the far end of the LV feeder may exceed the statutory limits because it experiences large supply/demand (as described in section 5.1). Conversely, a similar phenomenon may also happen, if the voltage at the furthest bus (at the far end of the LV feeder) is used to control the OLTC (active network control). In this case, the voltage at the furthest bus will be maintained within voltage statutory limits, and this may lead to the voltage violation at the local OLTC substation.

To improve the ability of existing OLTC, this thesis proposes the SOLTC, which allows a suitable signal to control the tap changer by using two significant signals in the distribution network. The SOLTC updates the two voltage signals, which are at the SOLTC substation and the furthest bus (that available at that time) via the local central data bank. Therefore, Analogue to Digital devices (A/D) are used to convert the analogue data (here transforms voltage profiles in the network) into digital data, and then the Boolean equation is used to define the control algorithm of the SOLTC. Thus, the voltage deviation equations $f(\Delta V_m)$ at the SOLTC substation (ΔV_{mSOLTC}) and the furthest bus (ΔV_{mCCP}) are:

$$f(\Delta V_m) = \begin{pmatrix} \Delta V_{mSOLTC} = V_{mSOLTC} - V_{ref} \\ \Delta V_{mCCP} = V_{mCCP} - V_{ref} \end{pmatrix} \quad (6.1)$$

Both voltages at the SOLTC substation (V_{mSOLTC}) and the furthest bus (V_{mCCP}) are compared to the reference voltage of the SOLTC (V_{ref}) in per unit system (here 1 per unit).

The main key to the successful set up of the SOLTC is the following operation condition $f(\mathrm{Cond}\Delta V_m)$; which results in the percent voltage deviation at the SOLTC substation and at the furthest bus to be kept within the voltage statutory limits. Hence, the highest voltage deviation signal $f(V_{mMax})$ will be used to control the tap changer. However, if signals from both the SOLTC substation and the furthest bus do not meet the above conditions, then the signal at the SOLTC substation is used to control the SOLTC. Then, $f(\mathrm{Cond}\Delta V_m)$ is:

$$f(\mathrm{Cond}\Delta V_m) = \begin{cases} \mathrm{Ex}V_{mSOLTC} = 1,\ \Delta V_{mSOLTC} > \mathrm{MaxLimit} \\ \mathrm{Be}V_{mSOLTC} = 1,\ \Delta V_{mSOLTC} < \mathrm{MinLimit} \\ \mathrm{Pos}V_{mSOLTC} = 1,\ 0 < \Delta V_{mSOLTC} \leq \mathrm{MaxLimit} \\ \mathrm{Neg}V_{mSOLTC} = 1,\ 0 > \Delta V_{mSOLTC} \geq \mathrm{MinLimit} \\ \mathrm{Pos}V_{mCCP} = 1,\ 0 < \Delta V_{mCCP} \leq \mathrm{MaxLimit} \\ \mathrm{Neg}V_{mCCP} = 1,\ 0 > \Delta V_{mCCP} \geq \mathrm{MinLimit} \end{cases} \quad (6.2)$$

$\mathrm{Ex}V_{mSOLTC}$ is equal to 1 when the voltage deviation at the SOLTC substation exceeds the maximum voltage statutory limit and $\mathrm{Be}V_{mSOLTC}$ is equal to 1 when the voltage deviation at the SOLTC substation is below the minimum voltage statutory limit. Furthermore, $\mathrm{Pos}V_{mSOLTC}$ is equal to 1 when the voltage deviation at the SOLTC substation is within the positive limit of voltage statutory limit and $\mathrm{Neg}V_{mSOLTC}$ is equal to 1 when the voltage deviation at the SOLTC substation is within the negative limit of voltage statutory limit. In addition, $\mathrm{Pos}V_{mCCP}$ is equal to 1 when the voltage deviation at the furthest bus is within the positive limit of voltage statutory limit and $\mathrm{Neg}V_{mCCP}$ is equal to 1 when the voltage deviation at the furthest bus is within the negative limit of voltage statutory limit. That means the percent voltage deviation of each signal is determined under the existing regulations.

Hence, the equations for $f(V_{mMax})$ and $f(V_{mUse})$ can be expressed by:

$$f(V_{mMax}) = \begin{cases} V_{mSOLTCMax} = 1,\ |\Delta V_{mSOLTC}| > |\Delta V_{mCCP}| \\ V_{mCCPMax} = 1,\ |\Delta V_{mSOLTC}| < |\Delta V_{mCCP}| \end{cases} \quad (6.3)$$

$$f(V_{mUse}) = \begin{cases} \mathrm{Use}V_{mSOLTC} = 1,\ V_{mMax} = V_{mSOLTCMax} \\ \mathrm{Use}V_{mCCP} = 1,\ V_{mMax} = V_{mCCPMax} \end{cases} \quad (6.4)$$

$V_{mSOLTCMax}$ is equal to 1 when the voltage deviation at the SOLTC substation that is higher than at the furthest bus, $V_{mCCPMax}$ is equal to 1 when the voltage deviation at the furthest bus that is higher than at the SOLTC substation, $\mathrm{Use}V_{mSOLTC}$ is equal to 1 when the voltage at the SOLTC substation prompts to control the SOLTC and $\mathrm{Use}V_{mCCP}$ is equal to 1 when the voltage at the furthest bus is ready to control the SOLTC.

Therefore, the control algorithm of the SOLTC $f(\mathrm{SOLTC})$ can be given by:

$$f(\mathrm{SOLTC}) = \begin{cases} \mathrm{Sub}_{\mathrm{SOLTC}}=1,\ \mathrm{Use}V_{mSOLTC}\mathrm{Ex}V_{mSOLTC}\mathrm{Be}V_{mSOLTC} \\ \mathrm{Sub}_{\mathrm{CCP}}=1,\ \mathrm{Use}V_{mCCP}\mathrm{Pos}V_{mSOLTC}\mathrm{Pos}V_{mCCP} \\ \mathrm{Sub}_{\mathrm{CCP}}=1,\ \mathrm{Use}V_{mCCP}\mathrm{Neg}V_{mSOLTC}\mathrm{Neg}V_{mCCP} \end{cases} \quad (6.5)$$

$\mathrm{Sub}_{\mathrm{SOLTC}}$ is equal to 1 (use voltage at the SOLTC substation) when $\mathrm{Use}V_{mSOLTC}$ and either $\mathrm{Ex}V_{mSOLTC}$ or $\mathrm{Be}V_{mSOLTC}$ are equal to 1. In addition, $\mathrm{Sub}_{\mathrm{CCP}}$ is equal to 1 (use voltage at the furthest bus which is available at that time) when $\mathrm{Use}V_{mCCP}$, $\mathrm{Pos}V_{mSOLTC}$ and $\mathrm{Pos}V_{mCCP}$ are equal to 1 or $\mathrm{Use}V_{mCCP}$, $\mathrm{Neg}V_{mSOLTC}$ and $\mathrm{Neg}V_{mCCP}$ are equal to 1.

In order to prevent sensitive voltage deviation of the SOTLC, the dead zone of the SOLTC (DZ_{SOLTC}) is considered. The DZ_{SOLTC} is given as:

$$DZ_{SOLTC} = k(\mathrm{StepVoltage}) \quad (6.6)$$

Where, k is the correction factor of the dead zone for the smart controller

The correction factor (k) can be defined as:

$$k = \left[\frac{(2)(\text{peak amplitude of voltage deviation during switching tap changer of the smart controller})}{\text{existing step voltage of the smart controller}}\right](1.10) \quad (6.7)$$

Therefore, the voltage deviation at the SOLTC substation within a specified region that is compared to the dead zone region $(DZ\Delta V_{mSOLTC})$ and the voltage deviation at the furthest bus within a specified region that is compared to the dead zone region $(DZ\Delta V_{mCCP})$ are given as:

$$f(DZ\Delta V_{mSOLTC}) = \begin{cases} (V_{mSOLTC} - V_{ref}) - \left[-\left(\frac{DZ_{SOLTC}}{2}\right)\right],\ V_{mSOLTC} - V_{ref} < -\left(\frac{DZ_{SOLTC}}{2}\right) \\ (V_{mSOLTC} - V_{ref}) - \left(\frac{DZ_{SOLTC}}{2}\right),\ V_{mSOLTC} - V_{ref} > \left(\frac{DZ_{SOLTC}}{2}\right) \end{cases} \quad (6.8)$$

$$f(DZ\Delta V_{mCCP}) = \begin{cases} (V_{mCCP} - V_{ref}) - \left[-\left(\frac{DZ_{SOLTC}}{2}\right)\right],\ V_{mCCP} - V_{ref} < -\left(\frac{DZ_{SOLTC}}{2}\right) \\ (V_{mCCP} - V_{ref}) - \left(\frac{DZ_{SOLTC}}{2}\right),\ V_{mCCP} - V_{ref} > \left(\frac{DZ_{SOLTC}}{2}\right) \end{cases} \quad (6.9)$$

Equations (6.8) or (6.9) are used to define a tap position of the SOLTC, if $V_{mSOLTC} - V_{ref}$ or $V_{mCCP} - V_{ref}$ (considered as input term) is less than or equal to the lower limit and therefore the input term minus the lower limit, whereas the input term minus the upper limit, if the input term is greater than or equal to the upper limit. However, if the input term is within the dead zone (greater than the lower limit and less than the upper limit), the voltage deviation is equal to zero. The DZ_{SOLTC} of the SOLTC in the UK network is set at 0.044 per unit whilst the DZ_{SOLTC} of the SOLTC in the TH network is set at 0.0708 per unit. These setting are due to the percent voltage deviation, the number of steps of the OLTC and the infrastructure of the distribution network. The voltage reference at the voltage regulator of the SOLTC still set at 1 per unit.

It can be concluded that the voltage control signal of the SOTLC can use either a signal from the local SOLTC or the furthest bus (that is available at that time), as shown in equation (6.5). This proposed model can improve the voltage profiles of the network without any voltage violation at the SOLTC substation and the furthest bus, as shown in Figure 6.12a.

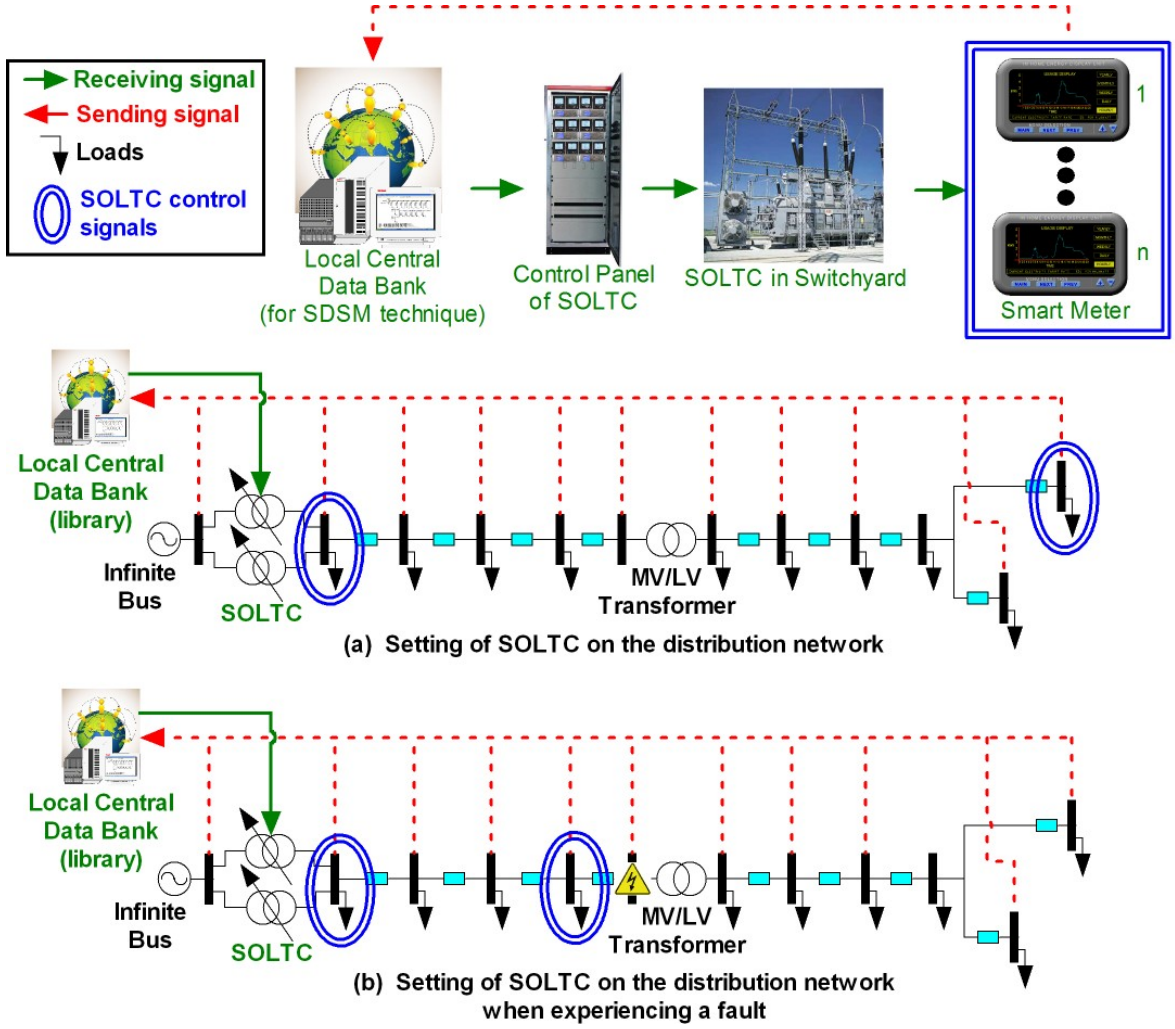

Figure 6.12 Control diagram of the SOLTC

Figure 6.12b shows that if a fault is detected in the network, then the local central data bank will provide the voltage signal at the furthest bus of the main network, which is available at that time (here at bus before the fault area instead of at the far end of the LV feeder). This increases the potential of the SOLTC to operate while the power network is experiencing a fault. It can be seen that the function of the SOLTC can increase the reliability of the network without the need for multiple control signals (just only two signals from the local central data bank). To understand the operation of the SOLTC, the flow chart of the SOLTC is shown in Figure 6.13 and the schematic of the MATLAB/Simulink is shown in appendix B.

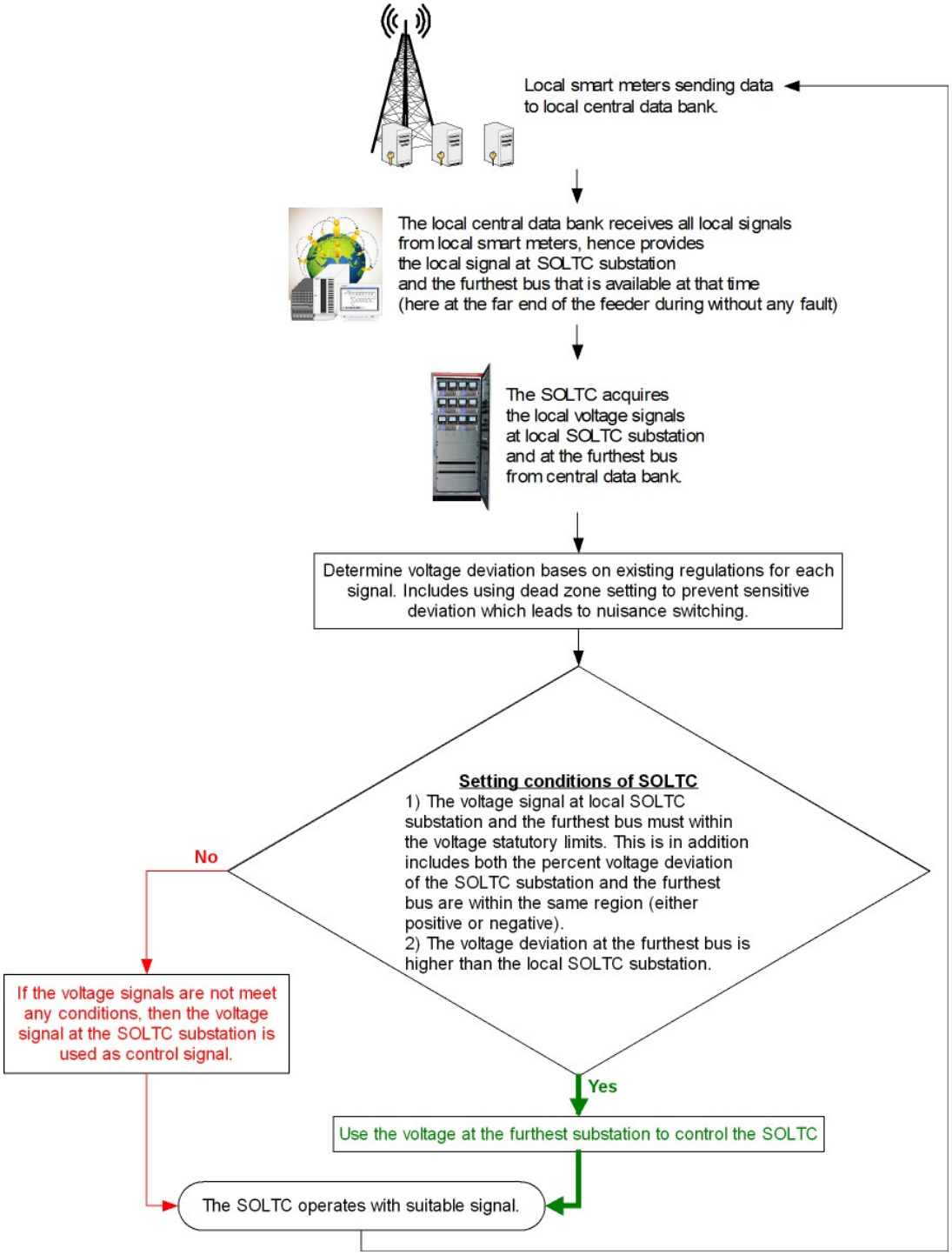

Figure 6.13 Flow chart of the SOLTC

6.3 Smart Electric Vehicles Grid Connection (SEVGC)

As described in chapter 5, high penetration levels of SSDGs and EVs/PHEVs can affect the voltage profiles of the network (particularly a weak network) because the output power of SSDGs is a function of the surrounding environment, and EVs/PHEVs demand depends on consumers' behaviour. Therefore, this section proposes a Smart Electric Vehicles Grid Connection (SEVGC) with four regions for public parking on the street, which allow EVs/PHEVs operating in charging/V2G modes with the dynamic electricity tariff (which depends on the connection region). The concept considers incorporation of EVs/PHEVs charging station and grid interface devices of EVs/PHEVs, which are based on PWM and PLL control. Hence, the EVs/PHEVs can be allowed to provide ancillary services and support the supply network, such as supply/demand matching and reactive power support, which is part of the SDSM technique (explained in section 6.1). This thesis considers EVs/PHEVs as mobile active loads because they can operate in charging (create extra loading at the local bus) and V2G (feeding power back into the network) modes where they can plug in the network anytime and anywhere. Therefore, the voltage control signal of the SEVGC is acquired from the local bus (directly or via central data bank). The voltage deviation equation of the SEVGC bus (ΔV_{mCCP}) is:

$$\Delta V_{mCCP} = V_{mCCP} - V_{ref} \tag{6.10}$$

The voltage at the SEVGC bus (V_{mCCP}) is compared with the reference voltage of the SEVGC (V_{ref}) in per unit (here 1 per unit).

A similar explanation to that for equation (6.9) for the SOLTC in section 6.2 is used to describe equation (6.11) for the voltage deviation at the SEVGC bus within a specified region that is compared to the dead zone region ($DZ\Delta V_{mCCP}$). Therefore, function of $DZ\Delta V_{mCCP}$ is given as:

$$f(DZ\Delta V_{mCCP}) = \begin{cases} (V_{mCCP} - V_{ref}) - \left[-\left(\frac{DZ_{SEVGC}}{2}\right)\right], & V_{mCCP} - V_{ref} < -\left(\frac{DZ_{SEVGC}}{2}\right) \\ (V_{mCCP} - V_{ref}) - \left(\frac{DZ_{SEVGC}}{2}\right), & V_{mCCP} - V_{ref} > \left(\frac{DZ_{SEVGC}}{2}\right) \end{cases} \tag{6.11}$$

This allows the percentage voltage deviation of each signal to be determined under the existing regulations. The dead zone settings in equation (6.12) are set to prevent the sensitive deviation, which causes nuisance connecting EVs/PHEVs in charging/V2G modes as follows.

In order to define the appropriate dead zone to control SEVGC (DZ_{SEVGC}), the impacts of EVs/PHEVs on the distribution network were studied (voltage variation scenario 1, Table 3.5). It is interesting to note that DZ_{SEVGC} is a function of the maximum penetration level of EVs/PHEVs that can be connected on the distribution network with low voltage variation problem, which is 25 percent of network capacity. Then, DZ_{SEVGC} is:

$$DZ_{SEVGC} = k\left(\frac{1}{4}\right)\left[\frac{(\text{No. of EVs/PHEVs per SEVGC})(\text{Max. charging current of EV/PHEV})}{\text{Base current at network capacity}}\right] \quad (6.12)$$

Therefore, the controller orders further voltage boosting and stabilises the voltage within a maximum voltage error (which is equal to $\frac{DZ_{SEVGC}}{2}$), and hence the maximum and minimum permitted voltage of the SEVGC is:

$$V_{ref} - \left(\frac{DZ_{SEVGC}}{2}\right) < V < V_{initialtapposition} + \left(\frac{DZ_{SEVGC}}{2}\right) \quad (6.13)$$

Where, V_{ref} is the reference voltage in per unit and $V_{initialtapposition}$ is the voltage at the tap position in per unit (used to operate in region 4).

Based on equations (6.12) and (6.13), DZ_{SEVGC} in the UK and TH networks was set at 0.0298 per unit. This value was determined from the input parameters of the SEVGC as given in Figure 6.14.

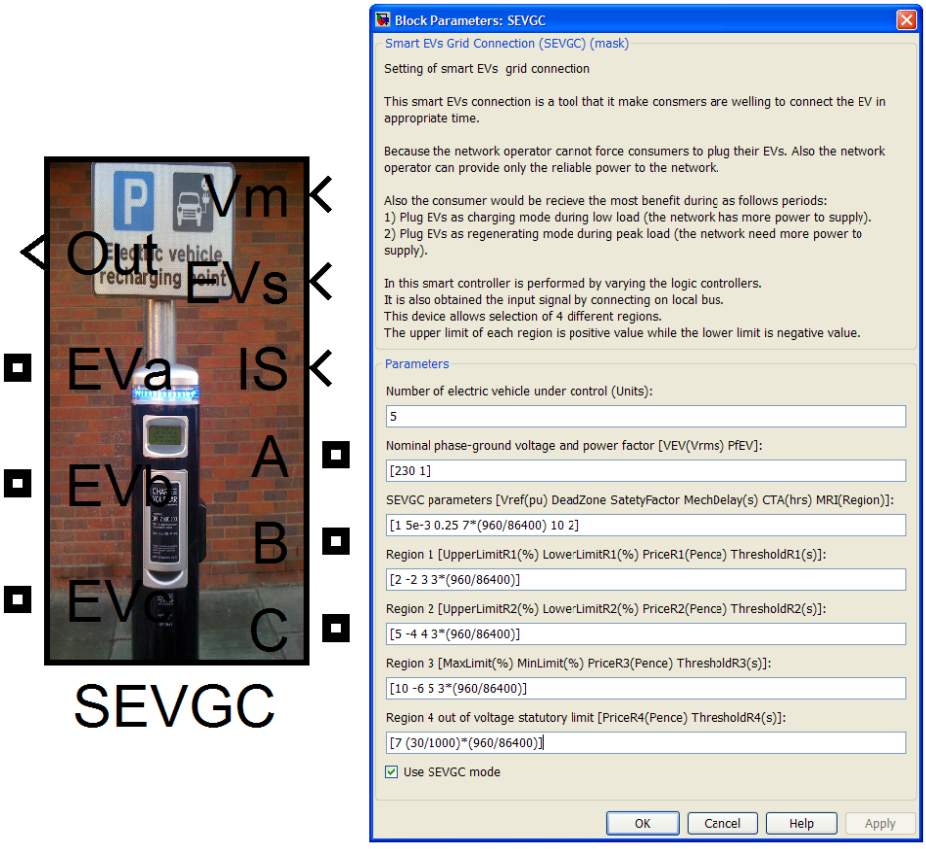

Figure 6.14 Input parameters of the SEVGC for the UK and TH networks

The SEVGC connection region equation $f(\text{Region})$ can be explained by:

$$f(\text{Region}) = \begin{cases} \text{Region1} = 1, \ \text{-R}_1 \leq \Delta V_{mCCP} \leq \text{R}_1 \\ \text{Region2} = 1, \ \text{-R}_1 > \Delta V_{mCCP} \geq \text{-R}_2 \\ \qquad\qquad \wedge \text{R}_1 < \Delta V_{mCCP} \leq \text{R}_2 \\ \text{Region3} = 1, \ \text{-R}_2 > \Delta V_{mCCP} \geq -0.06\text{p.u.} \\ \qquad\qquad \wedge \text{R}_2 < \Delta V_{mCCP} \leq 0.1\text{p.u.} \\ \text{Region4} = 1, \ \Delta V_{mCCP} < -0.06\text{p.u.}(\text{SafetyFactor}) \\ \qquad\qquad \wedge \Delta V_{mCCP} > 0.1\text{p.u.}(\text{SafetyFactor}) \end{cases} \tag{6.14}$$

Let R_1 be the voltage within the positive limit of region 1 in per unit, -R_1 be the voltage within the negative limit of region 1 in per unit, R_2 be the voltage within the positive limit of region 2 in per unit, -R_2 be the voltage within the negative limit of region 2 in per unit and the voltage statutory limits of 400 V be the limits at regions 3 and 4. Therefore, Region1 is equal to 1 when ΔV_{mCCP} is within -R_1 and R_1, Region2 is equal to 1 when ΔV_{mCCP} is within negative and positive regions of R_2, Region3 is equal to 1 when ΔV_{mCCP} is within negative and positive regions of R_3 and Region4 is equal to 1 when ΔV_{mCCP} is greater than the maximum voltage statutory limit multiply safety factor and less than the minimum voltage statutory limit multiply safety factor.

It can be noted that the number of SEVGC regions is defined by the network capacity with uniformly distributed EVs/PHEVs (which is presented in voltage variation scenario 1, Table 3.5). Regions 1 to 3 are usually set within the voltage statutory limits whilst region 4 is set below/exceeds the voltage statutory limits. Furthermore, region 4 also provides the safety factor of the voltage limits in order to ensure that the other smart controllers have sufficient time to operate before the local voltage reaches the limits, and also ensures that the voltage in the network will be sufficient at all times. Therefore, region 4 of the SEVGC is incorporated with other smart controllers in order to ensure the local voltage does not violate the voltage statutory limits.

The SEVGC is developed with ±8 steps in order to prevent long simulation time and insufficient computer memory. The positive tap number of the SEVGC is used to increase the number of EVs/PHEVs in charging mode, whereas the negative tap number allows the EVs/PHEVs to regenerate power back into the network (V2G mode). The higher the step number, the more EVs/PHEVs can be connected without causing power flow problems.

If the EVs/PHEVs connect to the network via the SEVGC while the local voltage is below/exceeds the voltage statutory limits (region 4), the SEVGC also offers the function to determine the number of EVs/PHEVs (ready to charge/regenerate in other public parking or SCP) or energy storage (on standby to consume/supply at the SES). The control diagrams of the SEVGC are shown in Figures 6.15 and 6.16.

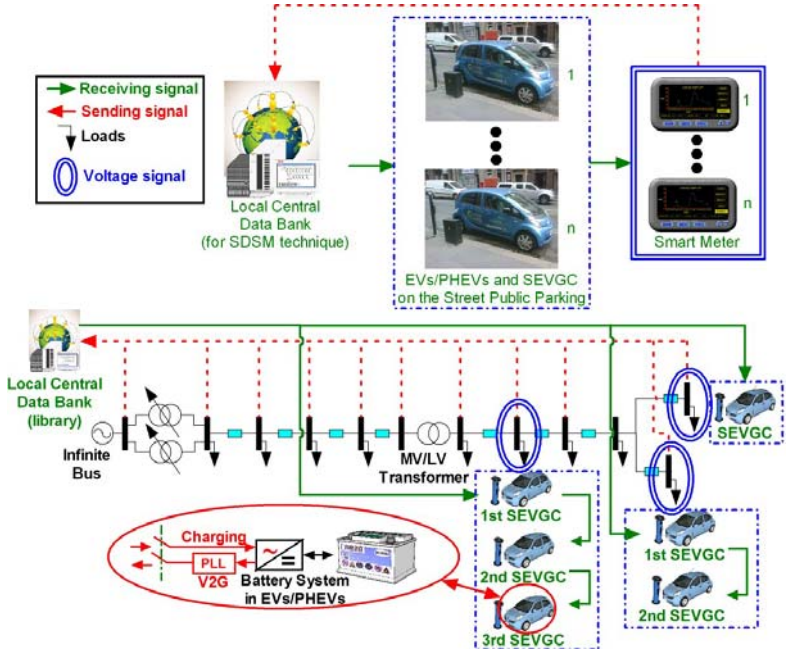

Figure 6.15 Control diagram of the SEVGC (independent mode)

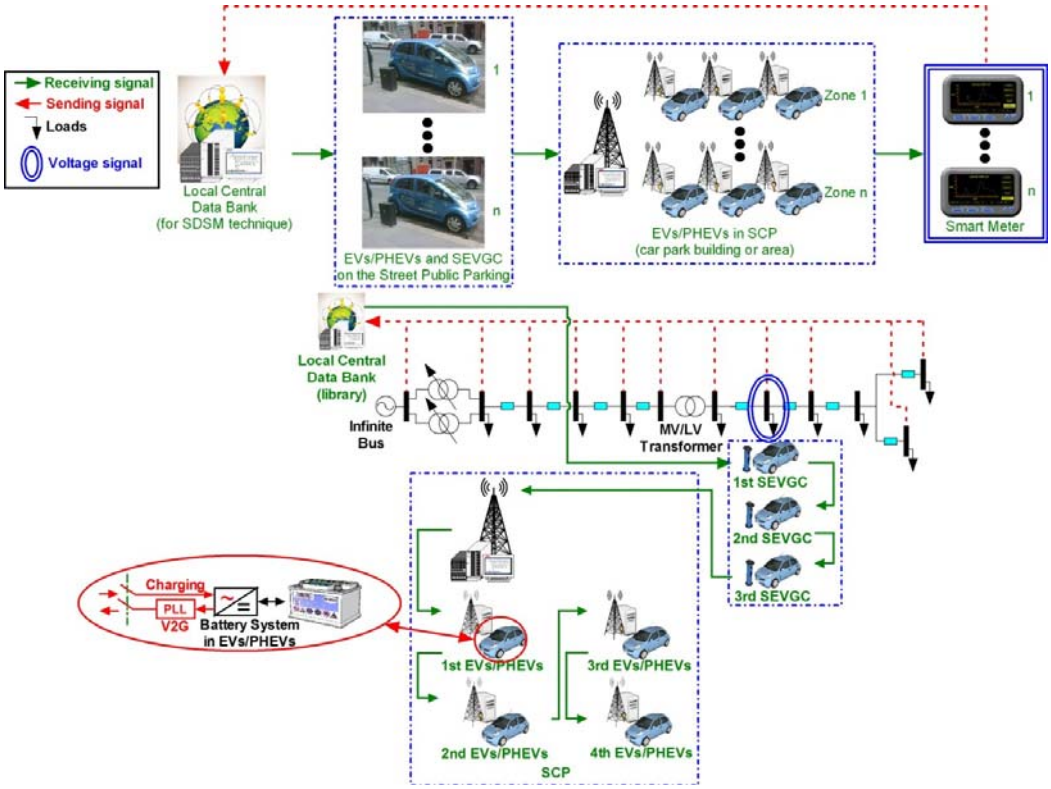

Figure 6.16 Control diagram of the SEVGC with other the SCP/SES units (incorporated mode)

The equations of the SEVGC operating in independent mode $(\mathrm{UseIndependent})$ or together with other SEVGC for region 4 $(\mathrm{UseSEVGC})$ or incorporated mode with other SCP (UseSCP) and SES (UseSES) units can be described as $f(\mathrm{Cond})$:

$$f(\mathrm{Cond}) = \begin{cases} \mathrm{Solely} = 1, \ \mathrm{UseIndependent} \\ \mathrm{WithSEVGC} = 1, \ \mathrm{UseSEVGC} \\ \mathrm{WithSCP} = 1, \ \mathrm{UseSCP} \\ \mathrm{WithSES} = 1, \ \mathrm{UseSES} \end{cases} \tag{6.15}$$

Solely is equal to 1 when the SEVGC operates in independent mode, $\mathrm{WithSEVGC}$ is equal to 1 when the SEVGC operates with other SEVGC in incorporated mode, $\mathrm{WithSCP}$ is equal to 1 when the SEVGC operates with other SCP in incorporated mode, $\mathrm{WithSES}$ is equal to 1 when the SEVGC operates with other SES in incorporated mode.

Therefore, the control algorithm of the SEVGC $f(\mathrm{SEVGC})$ can be defined as:

$$f(\mathrm{SEVGC}) = \begin{cases} \mathrm{ConnectEV} = 1, \ \mathrm{Region1Solely} \\ \mathrm{ConnectEV} = 1, \ \mathrm{Region2Solely} \\ \mathrm{ConnectEV} = 1, \ \mathrm{Region3Solely} \\ \mathrm{ConnectEV} = 1, \ \mathrm{Region4WithSEVGC} \\ \mathrm{ConnectEV} = 1, \ \mathrm{Region4WithSCPLimitSCP} \\ \mathrm{ConnectEV} = 1, \ \mathrm{Region4WithSESLimitSES} \end{cases} \tag{6.16}$$

$\mathrm{LimitSCP}$ is equal to 1 when the SCP operate within its limit (capacity) and $\mathrm{LimitSES}$ is equal to 1 when the SES operate within its limit (capacity). Therefore, $\mathrm{ConnectEV}$ is equal to 1 (allows EVs connect to the grid) when $\mathrm{Region1}$ and Solely are equal to 1 or $\mathrm{Region2}$ and Solely are equal to 1 or $\mathrm{Region3}$ and Solely are equal to 1 or $\mathrm{Region4}$ and $\mathrm{WithSEVGC}$ are equal to 1 or $\mathrm{Region4}$, $\mathrm{WithSCP}$ and $\mathrm{LimitSCP}$ are equal to 1 or $\mathrm{Region4}$, $\mathrm{WithSES}$ and $\mathrm{LimitSES}$ are equal to 1.

The SEVGC also includes the connection time allowance function in order to ensure the available charging/regenerating time (shown in Figure 6.17). This function was considered regarding the public car park policy (which allows the maximum parking with 4 hours in the daytime) and the lifetime of the battery (here considering maximum with 2 hours in V2G mode). This is very useful to define the available EVs/PHEVs on the street public parking (based on priority and availability) connected into the network. The flow chart of the SEVGC is shown in Figure 6.18 and the schematic of the MATLAB/Simulink is given in appendix B.

Figure 6.17 Schematic of connect time allowance of EVs/PHEVs in the SEVGC

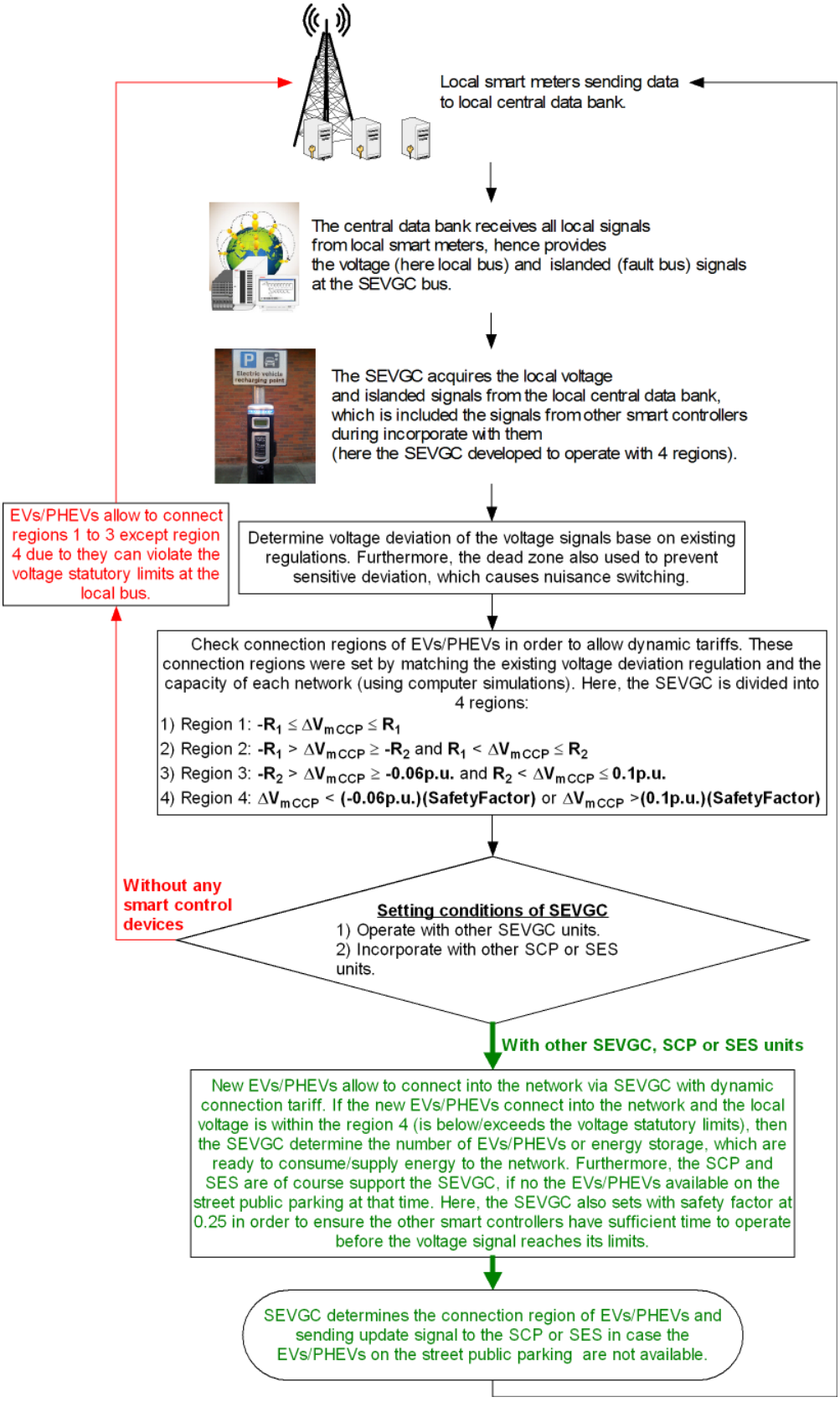

Figure 6.18 Flow chart of the SEVGC

The SEVGC also allows the EVs/PHEVs operation when connected in an islanded network. In the event of loss of main supply (main network), the islanded network may experience a sudden voltage change because the consumers' demand does not match generation (described in chapter 2). Therefore, the SEVGC is also designed to receive the islanded signal from the local central data bank and decrease the number of connection regions (from region 4 that is used for below/exceed the voltage statutory limits) to a suitable region where the regions settings are determined by the network operator in that area.

6.4 Smart EVs/PHEVs Car Park (SCP) and Smart Energy Storage (SES)

The continuous increase of EVs/PHEVs can increase the demand on the power network. That means EVs/PHEVs car park buildings and areas without appropriate management of charging/regenerating can cause significant effects on the voltage profiles on the distribution network as well as SSDGs. Accordingly, the generated power of SSDGs may cause violation of the voltage statutory limits during high generation and low demands (described in chapter 5). For this reason, the power generation in this period will not be utilised and it will be wasted energy. Therefore, in order to optimise the power flow in the power network, especially at MV/LV levels, smart control devices that support SSDGs and EVs/PHEVs are necessary.

Another future technology is to make the use of EVs/PHEVs car park as an energy storage system to increase the reliability of the network. This is similar to the grid interfaces of EVs/PHEVs that mostly use PWM applications for charging/regenerating power (explained in section 2.5 and 4.5). That means EVs/PHEVs can provide ancillary services and support the supply network, such as supply/demand matching and reactive power support, if these PWM inverters integrated together with a PLL, are properly designed and controlled. This type of operation leads to the concept of Smart EVs/PHEVs Car Park (SCP) and Smart Energy Storage (SES), which support the SDSM technique and balance supply/demand.

The SCP and the SES were designed such that they operate independently (independent mode) or can be operated with other smart controllers (incorporated mode). Their functions include acquiring the voltage signal (here local voltage) from either the local central data bank or the local bus. That means if the local bus has more than one SCP or SES, these devices can still determine their control signal independently (operate in independent mode), as shown in Figures 6.19 and 6.20. However, the priority devices are set during incorporated mode, as shown in Figure 6.21. That means the slave devices require the limit signal from the master devices (located in the neighbour area) in order to ensure the master device operates at its limits. MATLAB/Simulink schematics for the SCP and the SES are shown in appendix B.

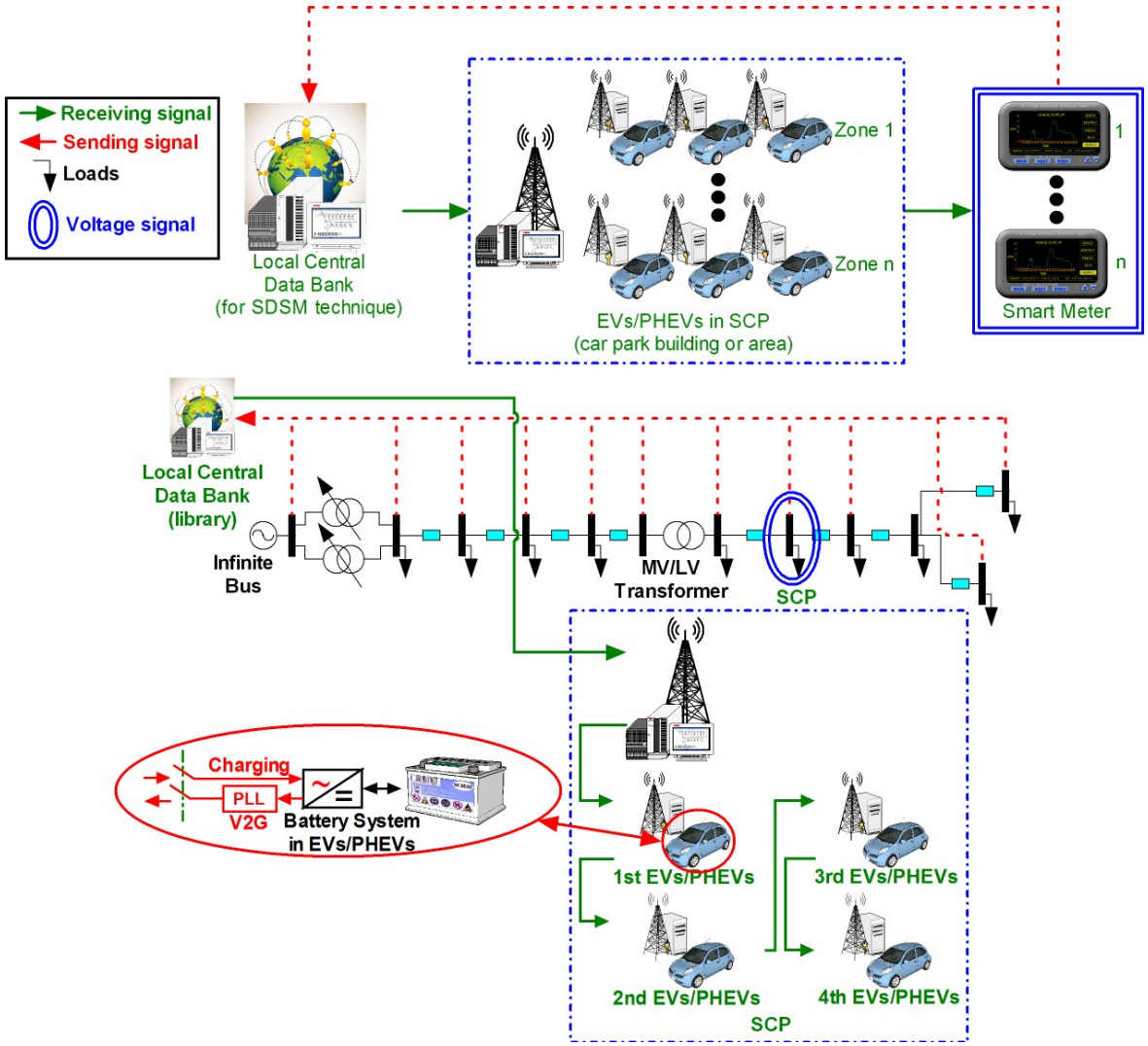

Figure 6.19 Control diagram of the SCP (independent mode)

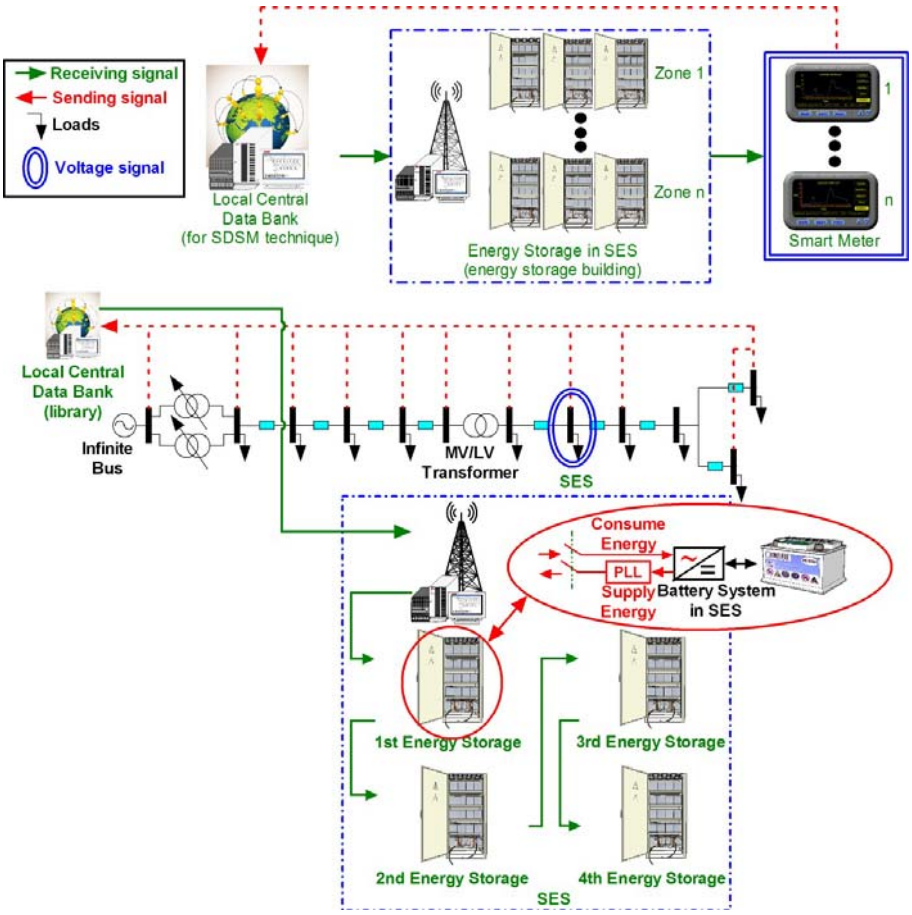

Figure 6.20 Control diagram of the SES (independent mode)

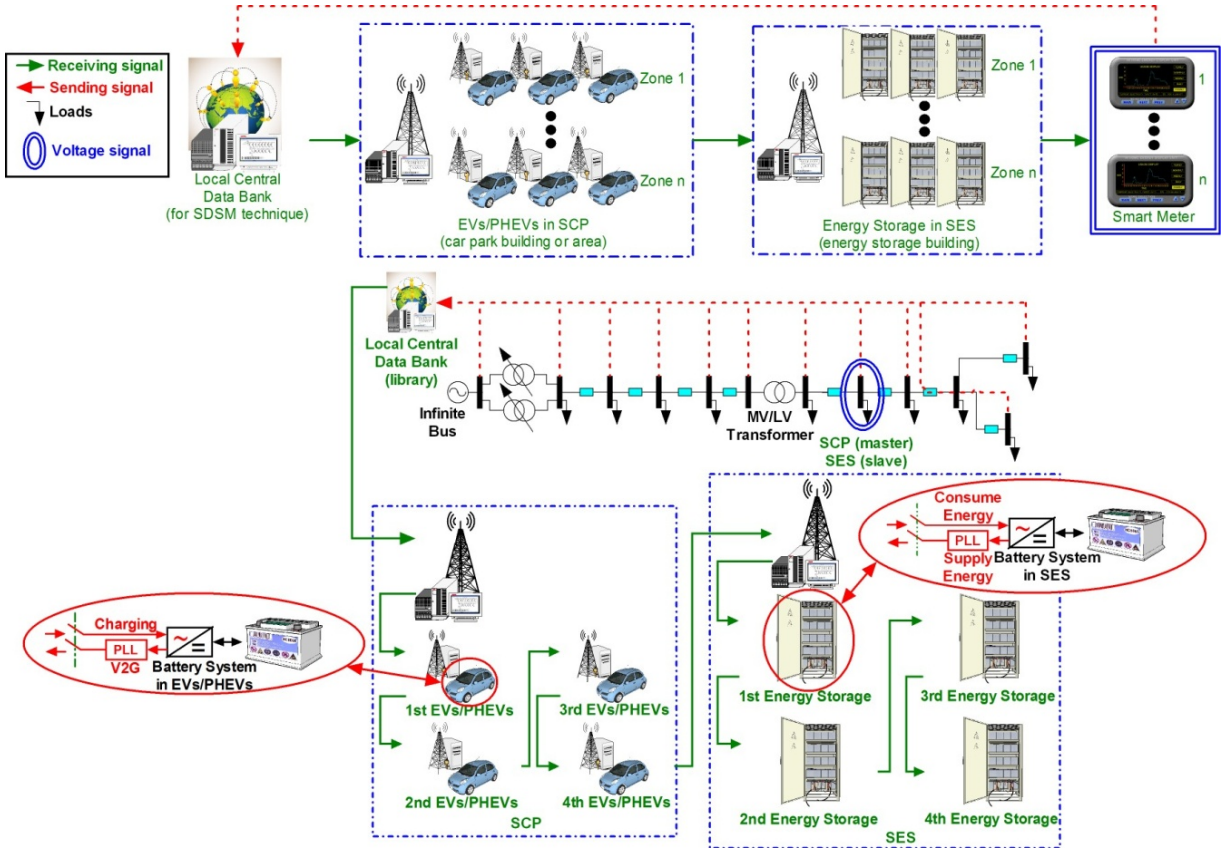

Figure 6.21 Control diagram of the SCP with other SES units (incorporated mode)

It can be noted that while the SCP and the SES are operating solely, they use the acquired voltage signal to determine their step control signal (here developed at ±8 steps) where the positive step is consuming energy from the network and negative step is supplying energy back into the network. Furthermore, the SCP also includes the connection time allowance function in order to ensure the available charging/regenerating time, similar to the SEVGC shown in Figure 6.17.

In order to allow the SCP and the SES to operate in independent or incorporated modes, the voltage signal (V_m) is required, here considered at the local bus. V_m may be received via the local central data bank or the local bus via the smart meter. Hence, the voltage deviation equation of the local bus with either SCP or SES (ΔV_{mCCP}) is:

$$\Delta V_{mCCP} = V_{mCCP} - V_{ref} \tag{6.17}$$

The voltage at the SCP or the SES bus (V_{mCCP}) is compared to the reference voltage of the SCP or the SES (V_{ref}) in per unit (here 1 per unit). Therefore, the function of the voltage deviation at the SCP or the SES bus within a specified region that is compared to the dead zone region ($DZ\Delta V_{mCCP}$) can be described as:

$$f(DZ\Delta V_{mCCP}) = \begin{cases} (V_{mCCP} - V_{ref}) - \left[-\left(\frac{DZ_{SCP}, DZ_{SES}}{2}\right)\right], & V_{mCCP} - V_{ref} < -\left(\frac{DZ_{SCP}, DZ_{SES}}{2}\right) \\ (V_{mCCP} - V_{ref}) - \left(\frac{DZ_{SCP}, DZ_{SES}}{2}\right), & V_{mCCP} - V_{ref} > \left(\frac{DZ_{SCP}, DZ_{SES}}{2}\right) \end{cases} \tag{6.18}$$

A similar explanation to that for equation (6.9) of the SOLTC in section 6.2 is used to describe equation (6.18). Furthermore, a similar explanation to that for equation (6.12) for the SEVGC in section 6.3 is used to describe equation (6.19). It is interesting that the dead zone to control SCP (DZ_{SCP}) is similar to DZ_{SEVGC}, which is a function of the maximum penetration level of EVs/PHEVs on the distribution network and it is 25 percent of network capacity. Furthermore, DZ_{SCP} is also a function of the number of EVs/PHEVs per step in the SCP and network capacity. Hence, the appropriate value for DZ_{SCP} can be defined as:

$$DZ_{SCP} = k\left(\frac{1}{4}\right)\left[\frac{(\text{No. of EVs/PHEVs per step in the SCP})(\text{Max. charging current of EV/HEV})}{\text{Base current at network capacity}}\right] \tag{6.19}$$

On the other hand, the dead zone of SES (DZ_{SES}) is proportional to the capacity of the transformer that is installed with the SES (determined from the impacts of energy storage at the far end of the LV feeder). Then, DZ_{SES} can be expressed by:

$$DZ_{SES} = k\left(\frac{Max.current\ of\ energy\ storage\ per\ step\ in\ the\ SES}{Base\ current\ at\ the\ transformer\ that\ installs\ the\ SES}\right) \tag{6.20}$$

The consumption/supply conditions of the SCP and the SES can be expressed by the voltage deviation within positive and negative limits of voltage statutory limits. A condition of ΔV_{mCCP}, $f(\mathrm{Cond}\Delta V_{mCCP})$ is:

$$f(\mathrm{Cond}\Delta V_{mCCP}) = \begin{cases} \Delta V_{mExceedVref} = 1,\ \Delta V_{mCCP} > 0 \\ \Delta V_{mBelowVref} = 1,\ \Delta V_{mCCP} < 0 \end{cases} \quad (6.21)$$

$\Delta V_{mExceedVref}$ is equal to 1 when the voltage deviation exceeds the reference voltage in per unit and $\Delta V_{mBelowVref}$ is equal to 1 when the voltage deviation is below the reference voltage in per unit.

It can be seen that either the SCP or the SES consume energy from the network when the voltage deviation at its bus exceeds the reference voltage, whereas they supply power back into the network, if the voltage deviation at its bus is below the reference voltage. The condition of the SCP and the SES when operating in either independent mode $(\mathrm{UseIndependent})$ or incorporated mode with other SCP/SES units $(\mathrm{UseOther})$ or SEVGC $(\mathrm{UseSEVGC})$ can be described as $f(\mathrm{Cond})$:

$$f(\mathrm{Cond}) = \begin{cases} \mathrm{Solely} = 1,\ \mathrm{UseIndependent} \\ \mathrm{WithSCP/SES} = 1,\ \mathrm{UseOther} \\ \mathrm{WithSEVGCPos} = 1,\ \mathrm{UseSEVGC\ with\ consume\ signal} \\ \mathrm{WithSEVGCNeg} = 1,\ \mathrm{UseSEVGC\ with\ supply\ signal} \end{cases} \quad (6.22)$$

Solely is equal to 1 when the SCP or the SES operates in independent mode, $\mathrm{WithSCP/SES}$ is equal to 1 when the SCP or the SES incorporates with other SCP or SES in incorporated mode, $\mathrm{WithSEVGCPos}$ is equal to 1 when the SCP or the SES incorporates with other SEVGC while consuming power in incorporated mode, $\mathrm{WithSEVGCNeg}$ is equal to 1 when the SCP or the SES incorporates with other SEVGC during supply power in incorporated mode.

Therefore, the controllers order further voltage boosting and stabilises the voltage within a maximum voltage error (which is equal to $\frac{DZ_{SCP},DZ_{SES}}{2}$), and hence the maximum and minimum permitted voltage of the SCP or the SES are described as:

$$V_{ref} - \left(\frac{DZ_{SCP},DZ_{SES}}{2}\right) < V < V_{initialtapposition} + \left(\frac{DZ_{SCP},DZ_{SES}}{2}\right) \quad (6.23)$$

Where, V_{ref} is the reference voltage of the SCP or the SES in per unit and $V_{initialtapposition}$ is the voltage at tap position in per unit.

The reference voltage for both the UK and TH networks is 1 per unit. Therefore, DZ_{SCP} in the UK network is set at 0.0298 per unit and the response of the SCP is 5 sec where DZ_{SES} is set at 0.088 per unit and the response of the SES is 22 sec. In the TH network, DZ_{SCP} is set at 0.0298 per unit and the response of the SCP is 5 sec where DZ_{SES} is set at 0.0251 per unit and the response of the SES is 4 sec. These setting are determined by the summation of control, safety and mechanical delays. The step response of a smart control device must consider the response of the tap changer transformer (here set at ~8 sec) in order to ensure that the smart devices operate in an appropriate situation (preventing frequent switching and high transient voltages). Moreover, both SCP and SES could support an islanding network as well. The input parameters of the SCP and the SES are shown in Figures 6.22 and 6.23, respectively.

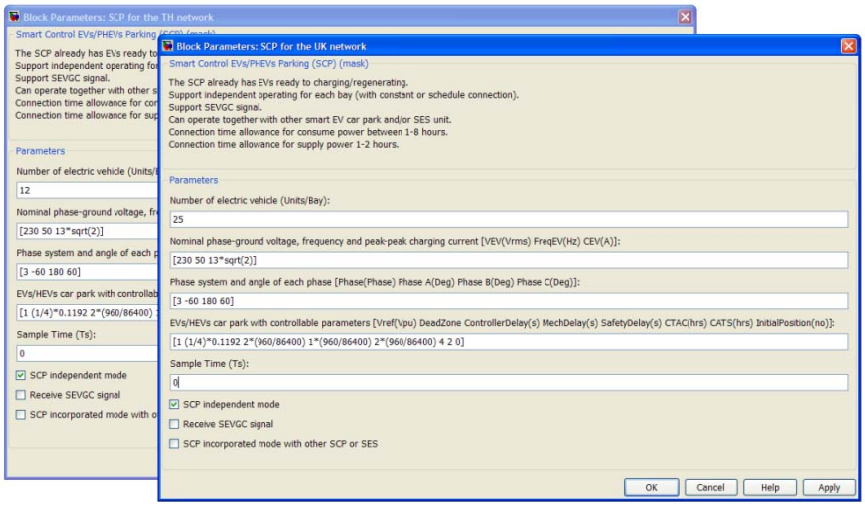

Figure 6.22 Input parameters of the SCP (incorporated mode, as slave controller) for the UK and TH networks

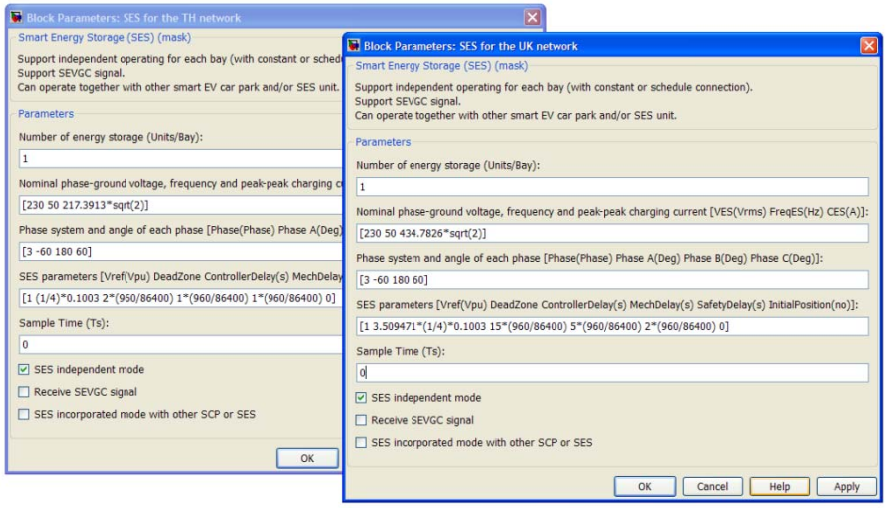

Figure 6.23 Input parameters of the SES (incorporated mode, as master controller) for the UK and TH networks

The flow chart of the SCP is shown in Figures 6.24 and the control algorithm of the SCP $f(\mathrm{SCP})$ can be identified by:

$$f(\mathrm{SCP}) = \begin{cases} \mathrm{EVs/PHEVs\ charging} = 1,\ \mathrm{Solely}\Delta V_{mExceedVref} \\ \mathrm{EVs/PHEVs\ regenerating} = 1,\ \mathrm{Solely}\Delta V_{mBelowVref} \\ \mathrm{EVs/PHEVs\ charging} = 1,\ \mathrm{WithSCP/SES}\Delta V_{mExceedVref} \\ \mathrm{EVs/PHEVs\ regenerating} = 1,\ \mathrm{WithSCP/SES}\Delta V_{mBelowVref} \\ \mathrm{EVs/PHEVs\ charging} = 1,\ \mathrm{WithSEVGCPos} \\ \mathrm{EVs/PHEVs\ regenerating} = 1,\ \mathrm{WithSEVGCNeg} \end{cases} \quad (6.24)$$

$\mathrm{EVs/PHEVs\ charging}$ is equal to 1 (allows EVs in the SCP operating in charging mode) when Solely and $\Delta V_{mExceedVref}$ are equal to 1 or $\mathrm{WithSCP/SES}$ and $\Delta V_{mExceedVref}$ are equal to 1 or $\mathrm{WithSEVGCPos}$ is equal to 1. On the other hand, $\mathrm{EVs/PHEVs\ regenerating}$ is equal to 1 (allows EVs in the SCP operating in V2G mode) when Solely and $\Delta V_{mBelowVref}$ are equal to 1 or $\mathrm{WithSCP/SES}$ and $\Delta V_{mBelowVref}$ are equal to 1 or $\mathrm{WithSEVGCNeg}$ is equal to 1.

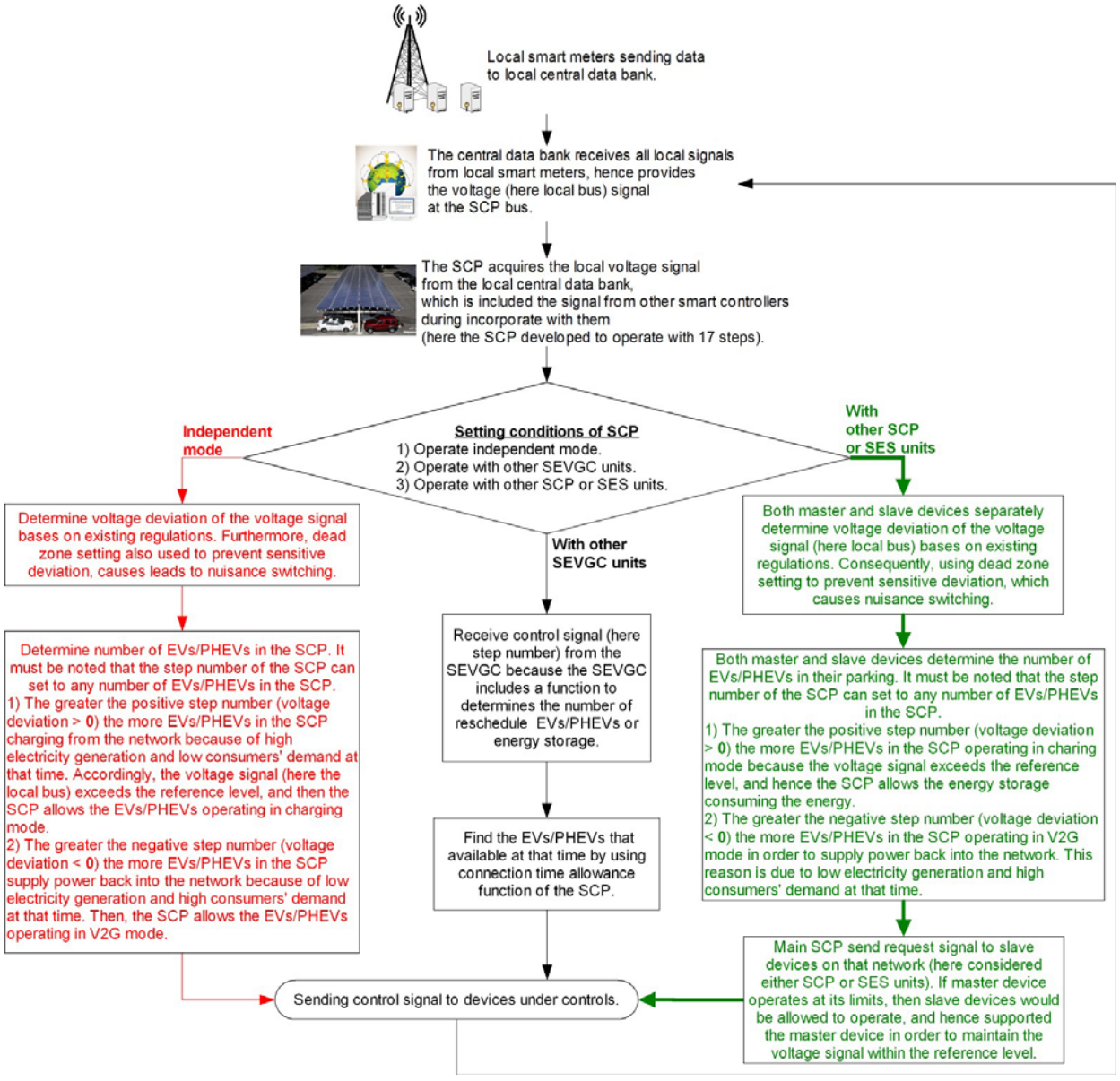

Figure 6.24 Flow chart of the SCP

On the other hand, the flow chart of the SES is shown in Figures 6.25 and the control algorithm of the SES $f(\mathrm{SES})$ can be given as.

$$f(\mathrm{SES}) = \begin{cases} \text{Energy storage consuming} = 1,\ \mathrm{Solely}\Delta V_{mExceedVref} \\ \text{Energy storage supplying} = 1,\ \mathrm{Solely}\Delta V_{mBelowVref} \\ \text{Energy storage consuming} = 1,\ \mathrm{WithSCP/SES}\Delta V_{mExceedVref} \\ \text{Energy storage supplying} = 1,\ \mathrm{WithSCP/SES}\Delta V_{mBelowVref} \\ \text{Energy storage consuming} = 1,\ \mathrm{WithSEVGCPos} \\ \text{Energy storage supplying} = 1,\ \mathrm{WithSEVGCNeg} \end{cases} \quad (6.25)$$

$\text{Energy storage consuming}$ is equal to 1 (allows SES operating in consumption mode) when Solely and $\Delta V_{mExceedVref}$ are equal to 1 or $\mathrm{WithSCP/SES}$ and $\Delta V_{mExceedVref}$ are equal to 1 or $\mathrm{WithSEVGCPos}$ is equal to 1. On the other hand, $\text{Energy storage supplying}$ is equal to 1 (allows SES operating in supply mode) when Solely and $\Delta V_{mBelowVref}$ are equal to 1 or $\mathrm{WithSCP/SES}$ and $\Delta V_{mBelowVref}$ are equal to 1 or $\mathrm{WithSEVGCNeg}$ is equal to 1.

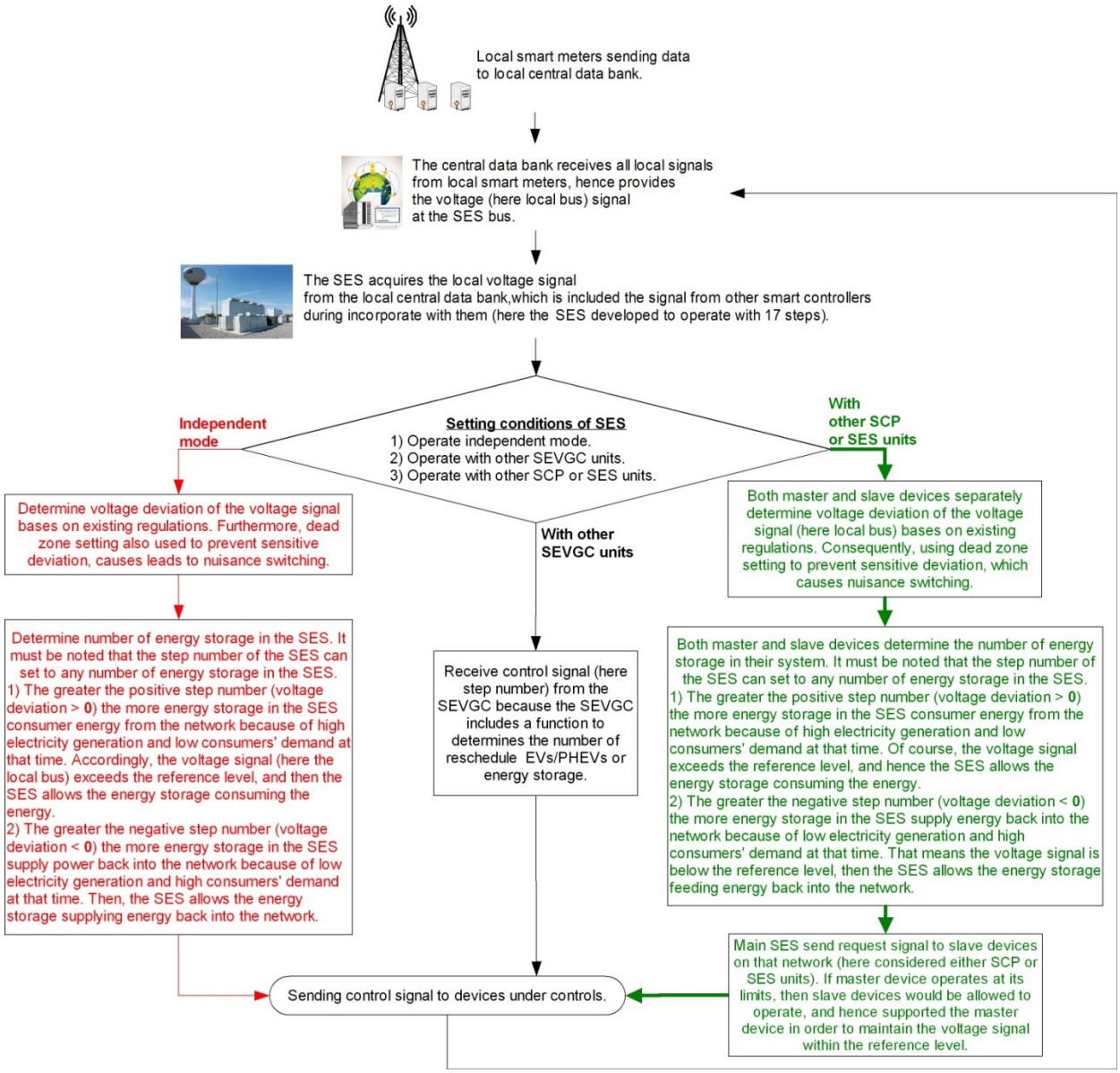

Figure 6.25 Flow chart of the SES

6.5 Smart Load Controller (SLC)

This section presents the requirements and conditions of the SLC in future power networks. The SLC device is designed to be part of future power networks, to prevent a sudden voltage change in islanded networks. The islanding operation in distribution networks is normally described as an operation of a distribution network section with one or more DGs isolated from the main network and still supplying power to local consumers at voltage and frequency within acceptable limits whilst ensuring personnel safety. This operation can be used to prevent power interruption in the islanded network, and therefore it can increase the reliability of power networks, if it would be allowed in the future as appropriate technologies are developed. According to the requirement of the SDSM technique in section 6.1, the SDSM technique can detect the faulty bus by using RCBs, hence this data is sent to the local central data bank. This thesis proposes the SLC to integrate the smart meter of the consumers in order to allow load shedding during the islanded network, as shown in Figures 6.26.

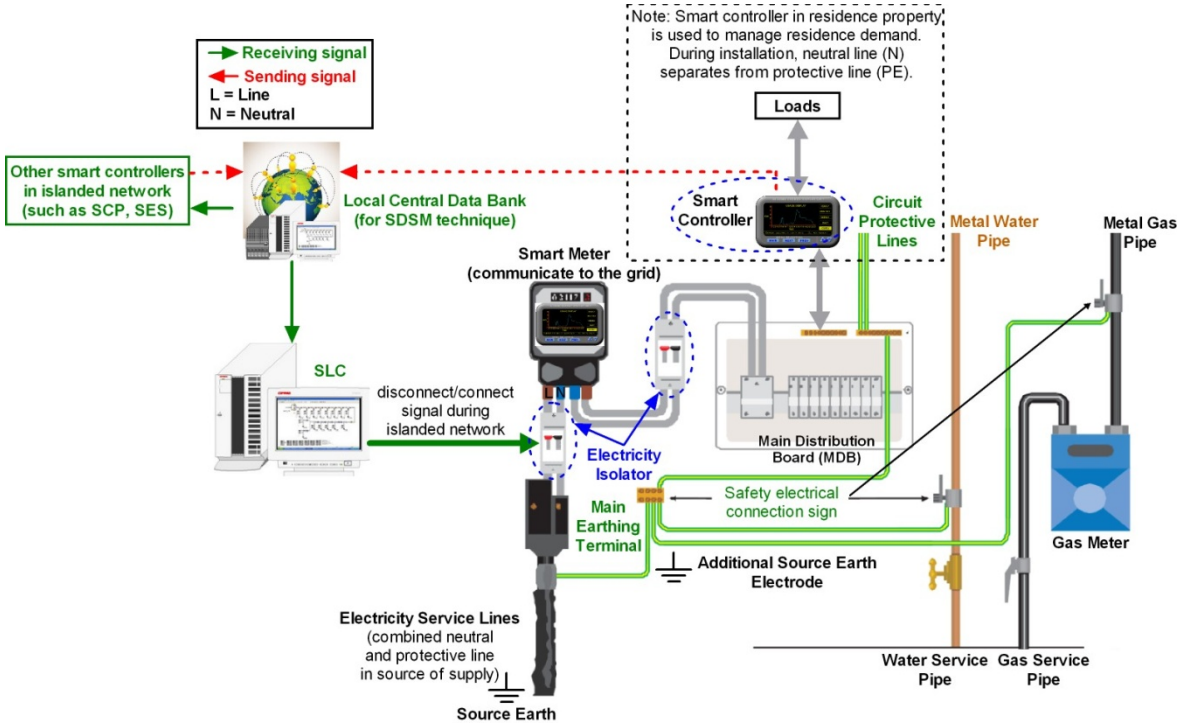

Figure 6.26 Smart meter integrates with the SLC in TN-C-S system

The islanded signal is the signal of the faulty bus, which includes its status (such as fault location and status). This allows the SLC and other smart controllers, which are located in the islanded network, to operate in islanded mode. Therefore, the smart controllers (which are SEVGC, SCP and SES) in the islanded network acquire at least two signals; the voltage control signal and islanded signal.

The controllers that operate as slave devices (incorporated mode) in the islanded network still need the required signal from the master device. This is in addition to the SLCs acquiring the update signals from the other smart controllers in the islanded network when they exceed their limits (capacity). This allows the SLCs to perform load shedding in the islanded network by connecting/disconnecting the consumers' base on the basis of community priority and electricity tariff. Here, the SLC can receive up to four-update signals from the other controllers in the islanded network. Therefore, the condition of the SLC, $f(\mathrm{Cond})$ can be explained as:

$$f(\mathrm{Cond}) = \{\mathrm{OtherSmartDevices} = 1,\ \forall \mathrm{Smart\ controls\ operate\ at\ limits} \quad (6.26)$$

$\mathrm{OtherSmartDevices}$ is equal to 1 when all other smart controllers in the islanded network operate at their limits.

The reference voltage signal of the SLC is assigned by the bus with highest insufficient voltage deviation in the islanded network from the local central data bank or the local bus (V_{mCCP}). This signal is used to determine connection/disconnection of the loads based on priority in the islanded network and it is used until the islanded network reconnects to the main network. Hence, the greater number of the control signals, the higher the priority of the load would be (shown in Figure 6. 27). The schematic of the MATLAB/Simulink is shown in appendix B.

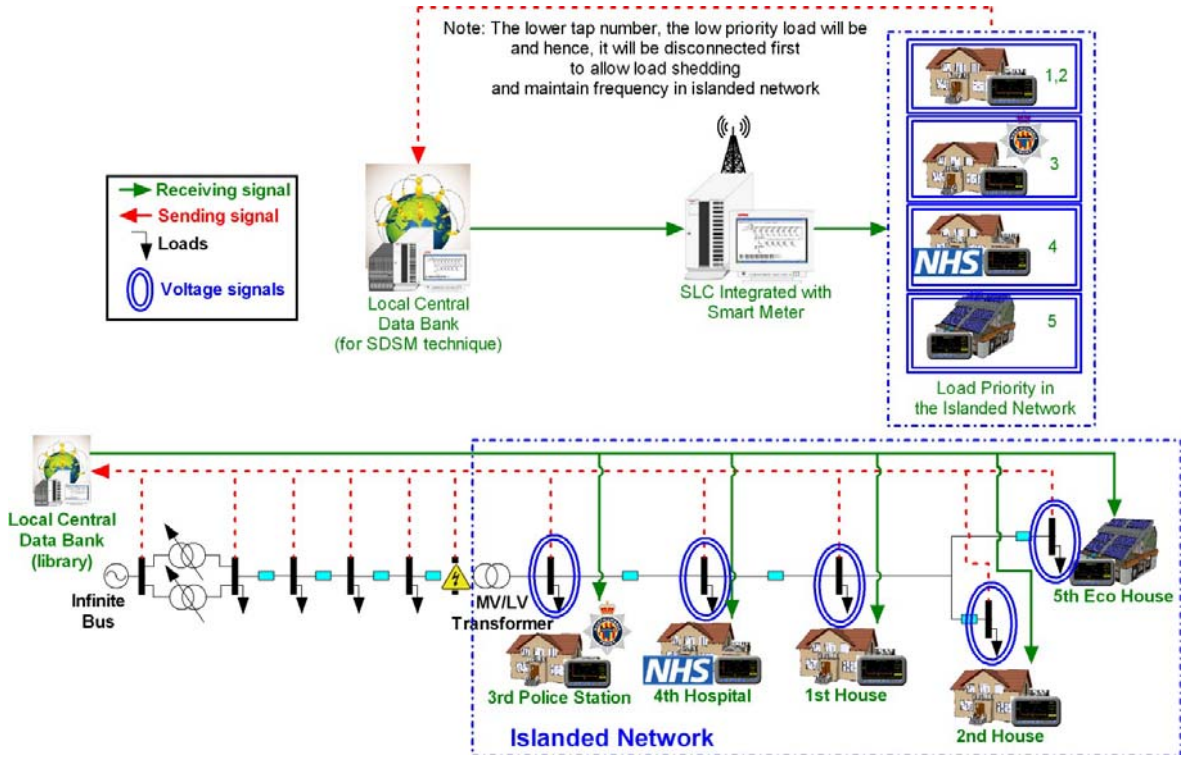

Figure 6.27 Control diagram of the SLC

Similar to equation (6.1), the voltage deviation at the SLC bus (ΔV_{mCCP}) is given as:

$$\Delta V_{mCCP} = V_{mCCP} - V_{ref} \tag{6.27}$$

Where, the voltage at the weakest bus in islanded network (V_{mCCP}) is compared to the reference voltage of the SLC (V_{ref}) in per unit (here 1 per unit).

Hence, the conditions of ΔV_{mCCP}, $f(\mathrm{Cond}\Delta V_{mCCP})$ is given as:

$$f(\mathrm{Cond}\Delta V_{mCCP}) = \begin{cases} \Delta V_{mExceedVref} = 1, & \Delta V_{mCCP} > 0 \\ \Delta V_{mBelowVref} = 1, & \Delta V_{mCCP} < 0 \\ \Delta V_{moptSLC} = 1, & \Delta V_{mCCP} < 0.94\text{p.u.} \\ & \wedge\, \Delta V_{mCCP} > 1.1\text{p.u.} \end{cases} \tag{6.28}$$

$\Delta V_{mExceedVref}$ is equal to 1 when the voltage deviation exceeds the reference voltage in per unit, $\Delta V_{mBelowVref}$ is equal to 1 when the voltage deviation is below the reference voltage in per unit and $\Delta V_{moptSLC}$ is equal to 1 when the voltage deviation outside the voltage statutory limits.

Similar to equation (6.1), the frequency deviation at the SLC bus (ΔF_{mCCP}) is given as:

$$\Delta F_{mCCP} = F_{mCCP} - F_{ref} \tag{6.29}$$

Where, the frequency at the weakest bus in islanded network (F_{mCCP}) is compared to the reference frequency of the SLC (F_{ref}) in Hz (here 50 Hz).

Hence, the conditions of ΔF_{mCCP}, $f(\mathrm{Cond}\Delta F_{mCCP})$ is given as:

$$f(\mathrm{Cond}\Delta F_{mCCP}) = \begin{cases} \Delta F_{mExceedFref} = 1, & \Delta F_{mCCP} > 0 \\ \Delta F_{mBelowFref} = 1, & \Delta F_{mCCP} < 0 \\ \Delta F_{moptSLC} = 1, & \Delta F_{mCCP} < 49.5\text{Hz} \\ & \wedge\, \Delta F_{mCCP} > 50.5\text{Hz} \end{cases} \tag{6.30}$$

$\Delta F_{mExceedFref}$ is equal to 1 when the frequency deviation exceeds the reference frequency in Hz, $\Delta F_{mBelowFref}$ is equal to 1 when the frequency deviation is below the reference frequency in Hz and $\Delta F_{moptSLC}$ is equal to 1 when the frequency deviation outside the frequency statutory limits.

The flow chart of the SLC is shown in Figure 6.28 and the control algorithm of the SLC $f(\mathrm{SLC})$ can be expressed by:

$$f(\mathrm{SLC}) = \begin{cases} \text{Decrease load}=1,\ \text{OtherSmartDevices}\Delta V_{moptSLC}\Delta V_{mExceedVref}\Delta F_{moptSLC}\Delta F_{mBelowFref} \\ \text{Increase load}=1,\ \text{OtherSmartDevices}\Delta V_{moptSLC}\Delta V_{mBelowVref}\Delta F_{moptSLC}\Delta F_{mExceedFref} \end{cases} \quad (6.31)$$

Decrease load is equal to 1 (allows the SLC disconnecting the consumer bases priority) when OtherSmartDevices, $\Delta V_{moptSLC}$, $\Delta V_{mExceedVref}$, $\Delta F_{moptSLC}$ and $\Delta F_{mExceedFref}$ are equal to 1. On the other hand, Increase load is equal to 1 (allows the SLC connecting the consumer bases priority) when OtherSmartDevices, $\Delta V_{moptSLC}$, $\Delta V_{mBelowVref}$, $\Delta F_{moptSLC}$, and $\Delta F_{mBelowFref}$ are equal to 1.

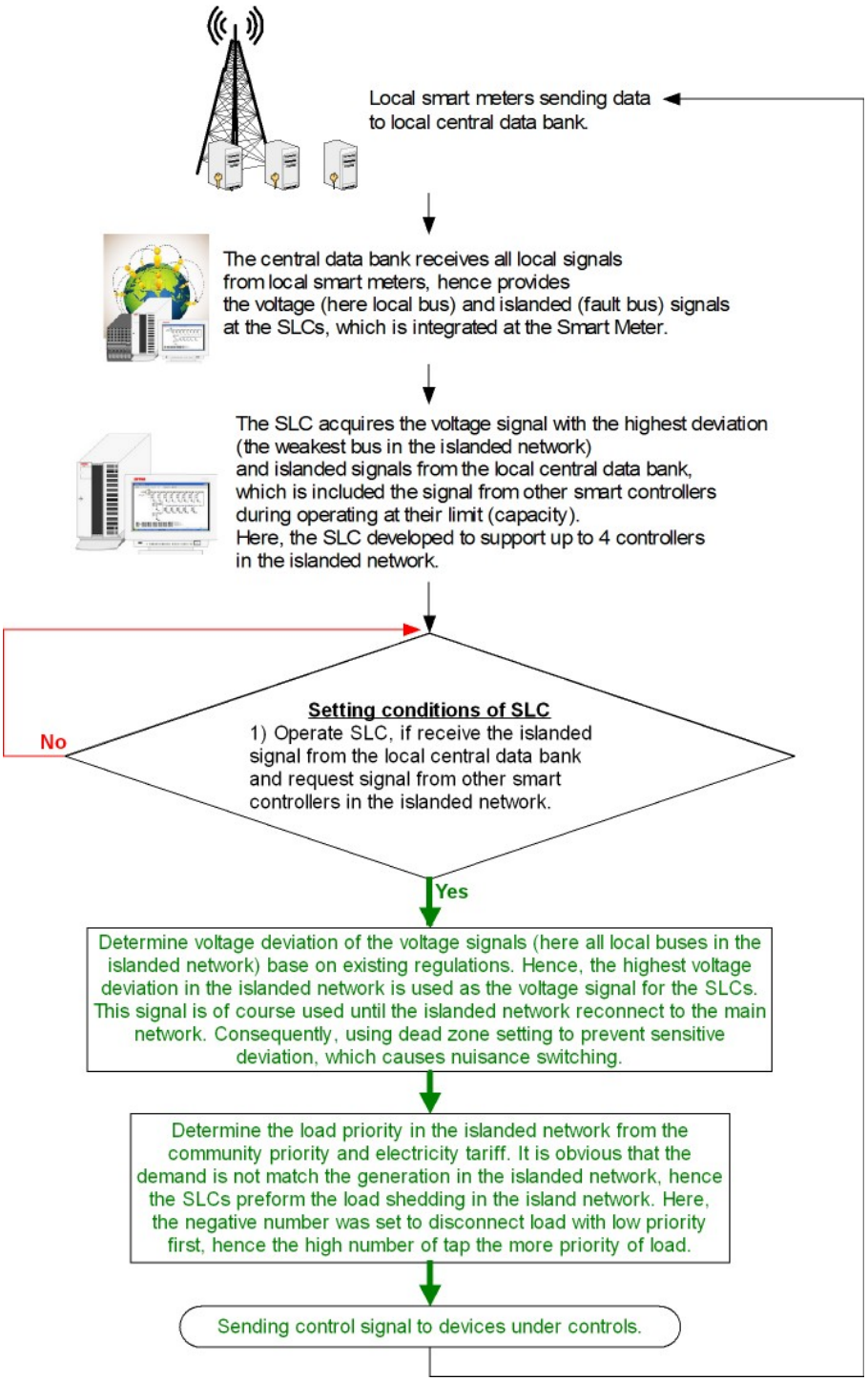

Figure 6.28 Flow chart of the SLC

6.6 Harmonic Solutions

It is known that any harmonic current that flows through the impedance in the power network can cause a harmonic voltage, and hence the harmonic current is a function of the harmonic voltage in the network. If the current and voltage waveforms are not aligned together, the efficiency of the electrical system is diminished and the ratio between the active power and apparent power (called "power factor") is affected. Two non-linear loads that combine to affect the power factor are inductive and capacitive loads. Therefore, adding capacitors can correct the power factor of an inductive source. However, the capacitive impedance of the compensator nears the inductive impedance of load at a certain harmonic order this can create resonance in the network instead of reducing the harmonics. This leads to transient voltages and voltage distortions thus the network operator with experience is required. In addition, the harmonic current of non-linear loads also affects the ratio between fundamental current and RMS current (called "the distortion factor"). It can be mentioned that harmonic distortion can cause significant effects in an islanded network since the islanded network is normally considered as a small and weak network, and hence the change in the current waveform affects the harmonic profile of the network voltage as well. Therefore, in order to reduce harmonic current in the network, phase shifting is used to correct the distortion factor at the harmonic source. By reducing the level of harmonic current in the power network, the power factor of network is also improved.

In this thesis, the impacts of single-phase EVs/PHEVs charger and the integration of SSDGs and EVs/PHEVs on the distribution networks were studied in section 5.3. Results in section 5.3 show that the EVs chargers produced harmonic currents and the integration of SSDGs and EVs/PHEVs may affect the harmonic profiles in the network, if the grid interfaces of SSDGs are operating at less than 10 percent of full rating and/or the EVs are fully charging with significant penetration levels. However, it is still possible to eliminate the 3rd harmonic current in a controlled charger [121-122]. Bentley, Suwanapingkarl, Weerasinghe, et al., [121] suggested that this cancelling could be increased by the use of PWM controllers, as the phase (firing) angle can be adjusted. References [121-122, 124] also mentioned that the reduction in the magnitude of harmonic current appeared in the summation of the same type of chargers at that connection point, and hence the THD at that connection points will be minimised. If those chargers of

EVs/PHEVs are based on the phase shift types, then harmonics cancellation at the local bus can become more efficient. However, it must be noted that the net harmonic current produced by EVs chargers are not proportional to the number of charger because the harmonic vectors of chargers tend to counteract each charger. Under this condition, the summation of magnitude of harmonic current is obviously smaller than the total value of harmonic current by each charger; similar results were also observed in references [121-124, 125-126]. Harmonic distortion due to the same type of EVs/PHEVs can be reduced when connect at the same point whilst the different types of charger (independently operated) cannot reduce the harmonic yield in this way.

Lo, Sustanto, and Fok, [123] also investigated the single-phase EV charger and harmonic profiles. Their charger is based on the constant current and voltage. Their results still show that the harmonic profile is mainly affected at the local connection points. However, the charger connected close to the capacitor compensators (e.g. capacitor bank) are slightly affected when compared with the furthest connection points. References [130] and [131] studied the de-rating of a substation transformer in the presence of a number of EVs connected to the distribution network by using the adaption of statistical methods to predict the net current harmonic due to the concentration of EVs. They found that the transformer de-rating is highly dependent on the EVs charging time, initial SOC of the battery and load demands.

So far, it can be seen that the growth in the harmonic distortion of power systems is inevitable due to the increasing use of power electronics. Standards and regulations (e.g. IEEE-519, IEEE-929, and EN50160) are used to control the PQ of devices and network within acceptable limits, as presented in appendix A. As a result, standard practice for electrical system design specify the THD, which can occur on the network to be typically 5 percent with no individual harmonic exceeding 3 percent of the fundamental [40]. The average THD of grid interface devices (e.g. grid inverter, EVs/PHEVs grid connection, etc.) is 3 percent and the maximum THD is 8 percent [47].

For the above reasons, this section suggests the use of PWM applications (optimise the output power of SSDGs and input power of EVs/PHEVs) and Phase-Shifting Transformer (PST) as they are available in the current market. The PWM

applications will be an application of choice for SSDGs and EVs/PHEVs grid interface in view of flexibility and operation. PWM applications with appropriate design can be used to either reduce or remove unwanted harmonics from a system because a PWM operating regime has a function to produce any given harmonic at pre-determined amplitude and phase angle. Hence, PWM can cancel certain harmonics produced by other devices, which may magnify the levels of particular harmonics. If PWM appropriately controlled, harmonic cancellation due to the effects of diversity can be achieved.

Moreover, PWM converters can combine with harmonic filters for grid interface devices in order to ensure that the devices will produce low harmonics. The harmonic filters (usually are passive and active filters) will be the first choice that is integrated into the grid interface devices. Passive filters are normally based on resonant filters or high pass filters and their effectiveness depends on the filter characteristic. On the other hand, active filters can suppress the harmonic currents by feeding a compensating current and shifting the phase angle of the harmonic currents into the load, hence the sine wave is restored, and distortion is reduced. It is important to note that an inappropriate design of passive and active filters can cause variation in voltage and current, and also frequency resonance (between the line impedance and the resonant circuit) [106]. It must be noted that closed loop control is required to automatically change the compensating current. If the network harmonic is greater than the performance of the filter, then the filter must supply maximum compensating current. If further reduction is still required, multiple units must be connected in parallel to increase compensation. Then, the performance of the grid interface of SSDGs and EVs/PHEVs is definitely improved.

Another method that is used to mitigate the harmonics problems in power networks is the Phase-Shifting Transformer (PST), which is designed for non-linear loads to reduce odd harmonic (assuming balanced loads). Accordingly, this type of transformer is designed with low impedance to reduce the voltage distortion and withstand the additional overheating caused by harmonic currents, (similar to multi-pulse transformer) and it can displace the harmonic currents and bring them to cancel each other for instance, Harmonic Mitigating Transformer (HMT) with zigzag connected on the secondary side. The HMT is also used to reduce zero sequence harmonic current, usually known as “Triplens” by operating

similarly to multi-pulse transformers. The Triplens are the 3rd harmonics multiple with their odd harmonic (for instances, 3rd, 9th, 15th, etc.), and then they add together in the neutral wire instead of cancelling each other. Therefore, the PST can reduce the harmonic profiles in the network, and hence the grid interface devices of green technologies (such as DGs and EVs) must produce harmonics within the statutory limits.

6.7 Summary of Proposed Solutions

In summary, this chapter has proposed the SDSM technique; a management technique that is designed to support multiple smart controllers and offer flexible functions, suitable for any architecture of future distribution networks (including SSDGs and EVs/PHEVs). This technique has the ability to integrate with other, possibly multiple data history from both generation and consumer sides' via smart meters, which acts as a communication portal to acquire data from local areas.

Moreover, the SOLTC receives signals in distribution networks from the local central data bank and determines suitable control signals for the tap changer instead of using a single local signal. The SEVGC analyses voltage profiles and allows connection/disconnection of EVs/PHEVs with dynamic connection tariff. Its function can be incorporated with other smart control devices that support consumption/supply of power networks (here considers the SCP and SES). In addition, SCP and SES were developed to operate in the two modes. Firstly, in the independent mode, SEVGC, SCP and SES are allowed to operate without any signals from other smart controllers such as SEVGC signal. Hence, they can use the signal from either the local central data bank or the local bus. In the second, incorporated mode, either SEVGC, SCP or SES receives a request signal from other smart controller such as the SEVGC, SCP and SES via the central data bank in order to manipulate the devices under their control. Lastly, this chapter also presents the SLC that is used in an islanded network in order to maintain voltage profiles in the islanded network within acceptable limits. The SLC connects/disconnects the necessary consumers' (which is based on the consumer priority and electricity tariff) in the islanded area, and hence keep the voltage and frequency within acceptable limits. It must be noted that the cancellation harmonic and its applications is beyond the scope of this thesis, and hence it will be considered as the future work.

CHAPTER 7
EVALUATION OF PROPOSED SOLUTIONS

7.1 Analysis of Voltage Profiles for the UK and TH Distribution Networks with smart controllers

Scenario 6 from Table 3.5 was chosen to demonstrate the effectiveness of the proposed smart controllers (SOLTC, SEVGC, SCP and SES) because it is an extreme scenario, which involves community and/or attraction areas. The smart devices are placed at the weakest and appropriate buses. In addition, it must be noted that the unrealistic transient voltages in the simulation results can be explained by the sudden connection/disconnection of large numbers of EVs/PHEVs in the simulation network at the same time and a large size of step voltage of the SES model (described in chapter 5).

7.1.1 Evaluation of the smart controllers for the UK distribution network

The single line diagram of the UK network with smart controllers is shown in Figure 7.1. Two existing OLTCs are replaced by two SOLTCs, the EVs/PHEVs car parks at the 11 kV feeder (buses 7, 8 and 9) are replaced by the SCP with 200 parking (±8 steps and each step controls 25 EVs/PHEVs units). A single EVs car park with 30 parking, an SES of 800 kW (±8 steps and each step supports 100 kW) and a 50 kW wind turbine farm (10 paralleled small-scale wind turbines, each with a rating of 5 kW) are also included at the far end of the LV feeder in order to optimise the power flow in the network. All buses communicated via the smart meter in order to send/receive data from the local central data bank.

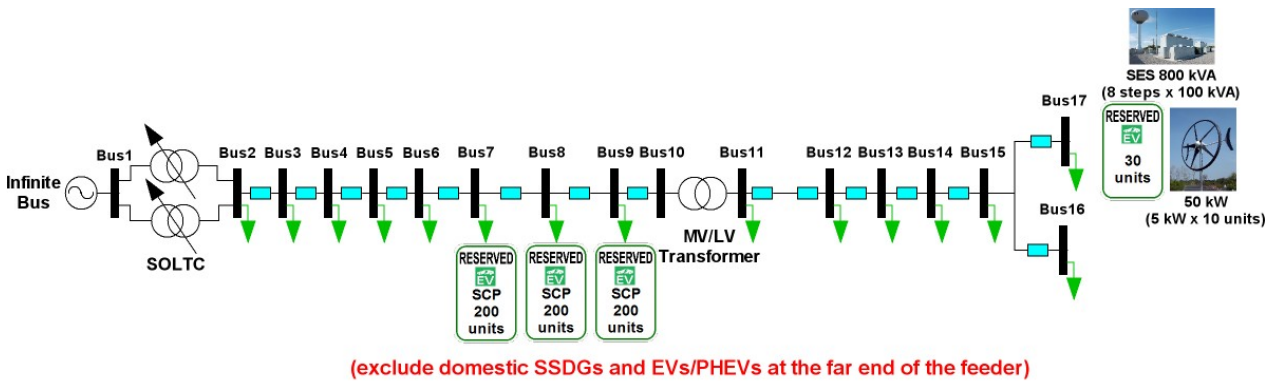

Figure 7.1 Single line diagram of the UK network with smart controllers for scenario 6 (from Table 3.5)

7.1.1a) The UK network with SOLTC only

Figure 7.2 shows the voltage profiles in the UK network in the winter with only SOLTCs. It can be seen that the voltage at the far end of the LV feeder still exceeded the maximum voltage statutory limit of 400 V (about 6.25 percent) during 13.30-15.30 due to the low consumers' demand in the winter and EVs operating in V2G mode. It is interesting to note that the voltage at bus 11 is close to the maximum statutory limit due to the transformer ratio at the furthest off-load tap changer transformer substation. Furthermore, the voltage profile at the far end of the LV feeder is below the minimum statutory limit of -6 percent for 400 V during 19.00-19.45 because high consumers' demand. However, the voltages at the other buses were kept within the voltage statutory limits by the operation of the SOLTCs. The tap changer profile of the SOLTCs was different from the existing OLTCs (and voltage profiles has improved) because for some period the voltage at the far end of the LV feeder is used to control the SOLTCs instead of the local bus (at bus 2).

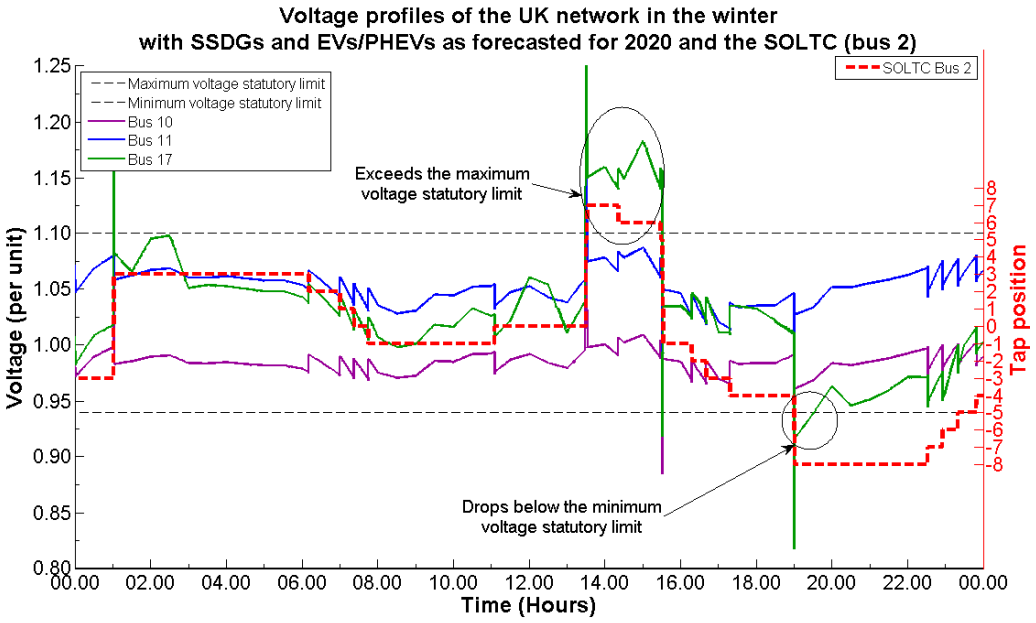

Figure 7.2 Voltage profiles of the UK network in the winter with only two SOLTCs for scenario 6 (from Table 3.5)

Figure 7.3 shows that the voltages at the LV side of the furthest off-load tap changer transformer and the far end of the LV feeder in the summer are higher than in winter due to the consumers' demand, whereas the voltage drops below the minimum voltage statutory limit in the summer is slightly less than in winter. This is due to low consumers' demand.

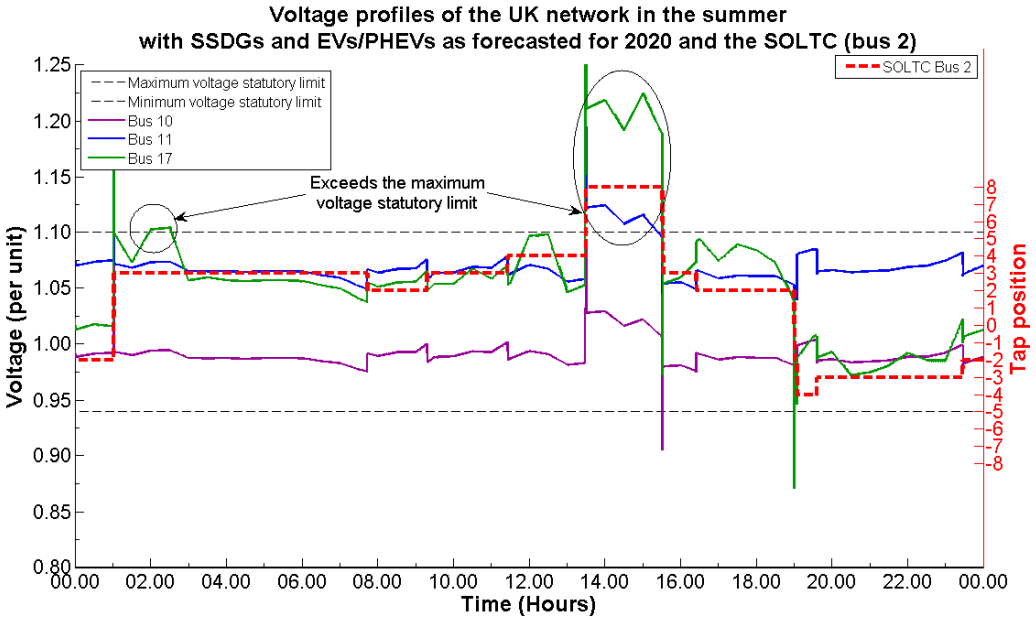

Figure 7.3 Voltage profiles of the UK network in the summer with only two SOLTC for scenario 6 (from Table 3.5)

It can be noted that the voltage violation in Figures 7.2 and 7.3 can be reduced by increasing tap number of the SOLTC as the computer model is designed with ±8 steps.

7.1.1b) The UK network with SCP and/or SEVGC only

Figure 7.4 shows the voltage profiles in the UK network in the winter with the OLTCs and three SCPs at buses 7, 8 and 9. Each SCP use control signal from its local bus and operate in independent mode. Therefore, the third SCP (at bus 9) allows 200 EVs/PHEVs to operate in V2G mode and attempt to feed power back into the network during 06.30-13.30 and again at 16.00-01.00 because the voltage signal (here its local voltage, the SCP bus) drops below the reference voltage (set at 1 per unit). Consequently, during 01.00-06.30, 50 EVs/PHEVs parked at the third SCP also operate in V2G mode as well. However, the voltage at the far end of the LV is still outside the voltage statutory limits during 02.00-03.00, 13.30-15.30 and 19.00-19.30 because three SCPs are maintained the voltage at their local buses.

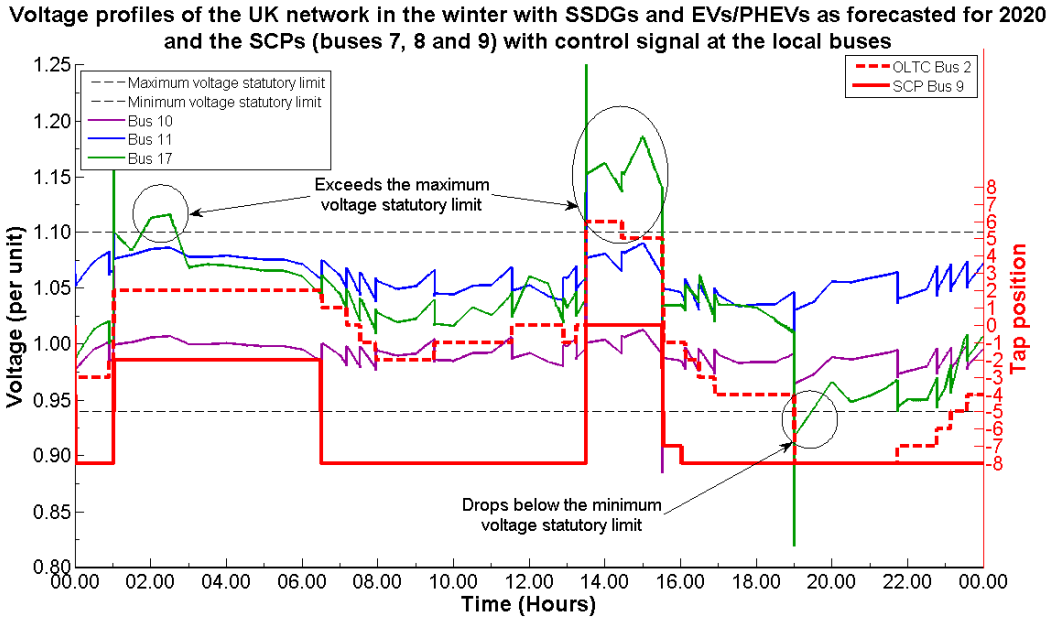

Figure 7.4 Voltage profiles of the UK network in the winter with only three SCPs that use local signal for scenario 6 (from Table 3.5)

Figure 7.5 show the voltage at the far end of the LV feeder exceeds only the maximum voltage statutory limit of 400 V in the summer. Moreover, the voltage at the SCP buses that drop below/exceed the reference voltage allows EVs/PHEVs parked in that SCP to operate in either charging or V2G modes.

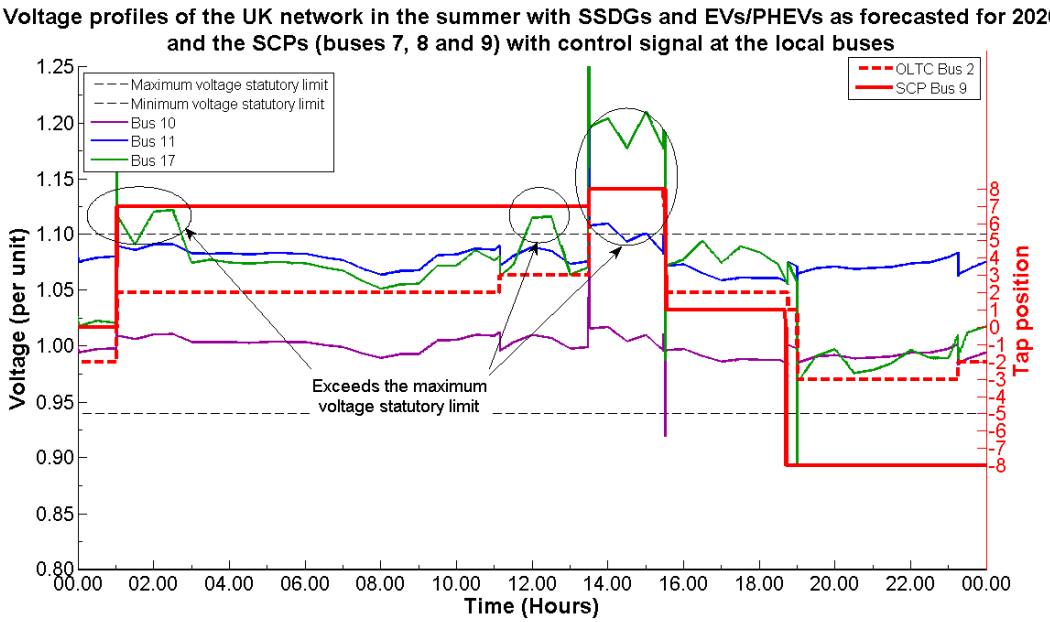

Figure 7.5 Voltage profiles of the UK network in the summer with only three SCPs that use local signal for scenario 6 (from Table 3.5)

This section also investigates the use of the far end of the LV feeder to control the SCP in incorporated mode. Hence, in order to analyse the effectiveness of the control signal, the SCP at bus 7 is set as master and therefore two SCPs at buses 8 and 9 are set as slave devices, respectively. Figures 7.6 and 7.7 show that the voltage at far end of the LV feeder in the UK network is improved as compared to Figures 7.4 and 7.5. However, the voltage at the far end of the LV feeder still drops below/exceeds the voltage statutory limits because each SCP is support EVs/PHEVs only 200 units. Therefore, the high number of EVs/PHEVs parking in the SCP, the high performance of the SCP can be expected. The SCP is mainly proposed for car park areas whilst the SEVGC is proposed for public parking on street, and hence the SEVGC considers the connection time allowance in a public area.

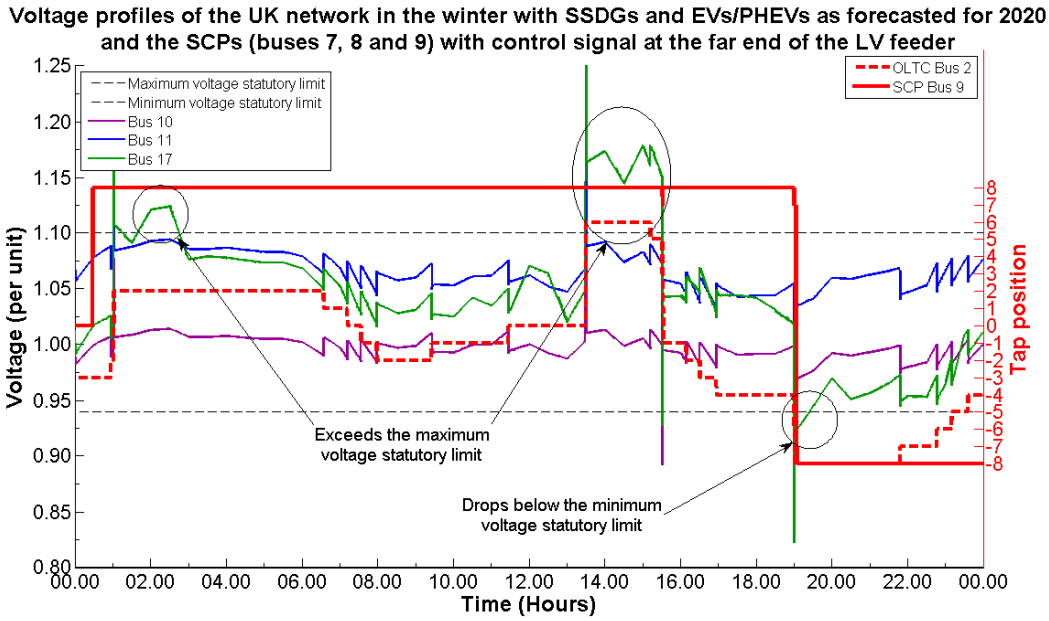

Figure 7.6 Voltage profiles of the UK network in the winter with only three SCPs that use the far end of the LV feeder signal for scenario 6 (from Table 3.5)

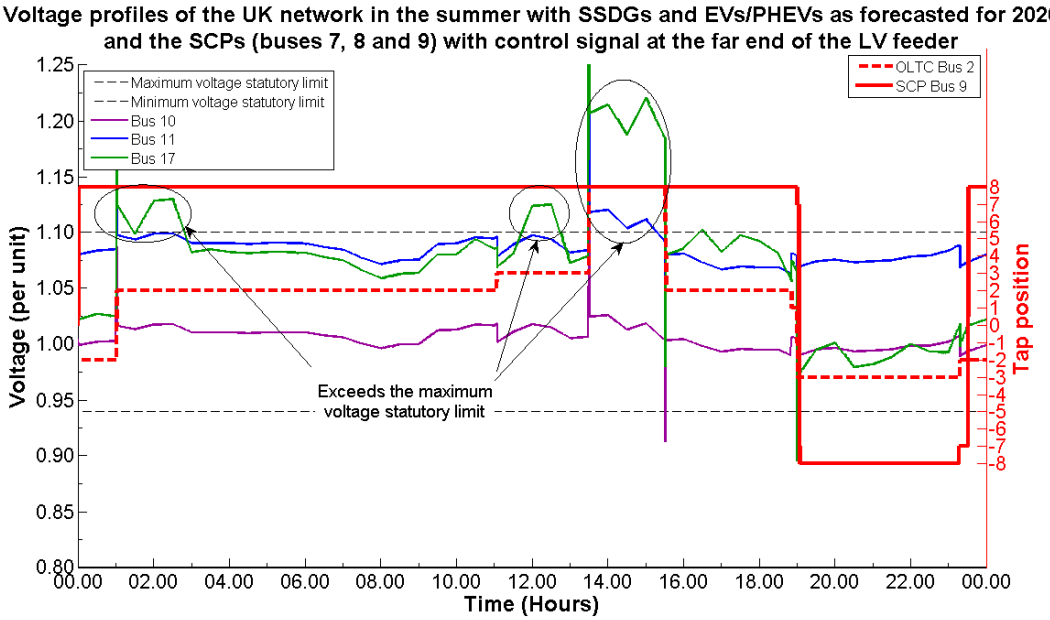

Figure 7.7 Voltage profiles of the UK network in the summer with only three SCPs that use the far end of the LV feeder signal for scenario 6 (from Table 3.5)

7.1.1c) The UK network with SES only

The impacts of the SES in the UK network are also investigated. In the winter, the SES at the far end of the LV feeder (at bus 17) was set with ±8 steps and each step controls 100 kW. The voltages at all buses were kept within the voltage statutory limits by the OLTCs (operate at its limits) and SES, as shown in Figure 7.8. As can be seen, the SES operates in consumption mode (tap position 1 at 100 kW) during 01.00-07.00 when the SES consumes 700 kWh and it consumes 400 kWh again in the afternoon (which increases to tap position 2 at 200 kW during 13.30-15.30). Conversely, in the evening with high consumers' demand and low generation from the SSDGs, especially during 19.00-23.00, the tap changer of the SES decreases to tap position -1 (supplies power at 100 kW), hence 400 kWh is supplied back into the network. Indeed, the SES consumes/supplies the power at its bus, if the voltage at signal bus (here the SES bus) exceeds/drops below the voltage reference (set at 1 per unit).

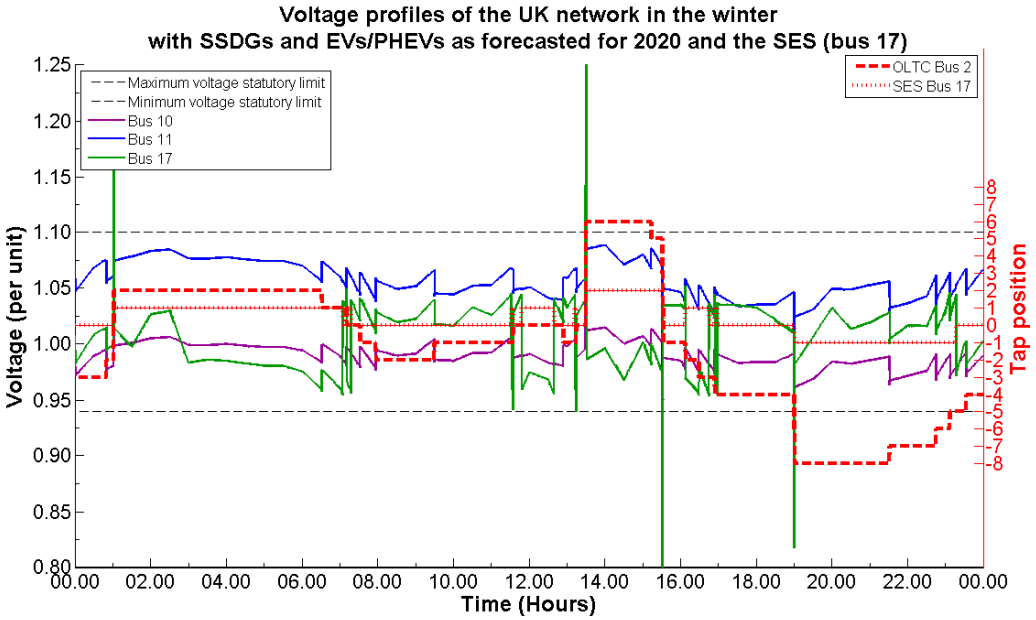

Figure 7.8 Voltage profiles of the UK network in the winter with only SES for scenario 6 (from Table 3.5)

Figure 7.9 shows that the SES is increased to tap 1 (supplied power at 100 kW) and consumed 1250 kWh during 01.00-13.30 where the tap position is raised up to 2 (supplies power at 200 kW) and consumed 400 kWh during 13.30-15.30. The voltage at the furthest off-load tap change transformer (at bus 11) slightly exceeds the maximum voltage statutory limit about 2 percent in the afternoon during 13.30-15.30. However, an adjustment of the SES setting can improve this violation because the SES was still not operating at its limits yet.

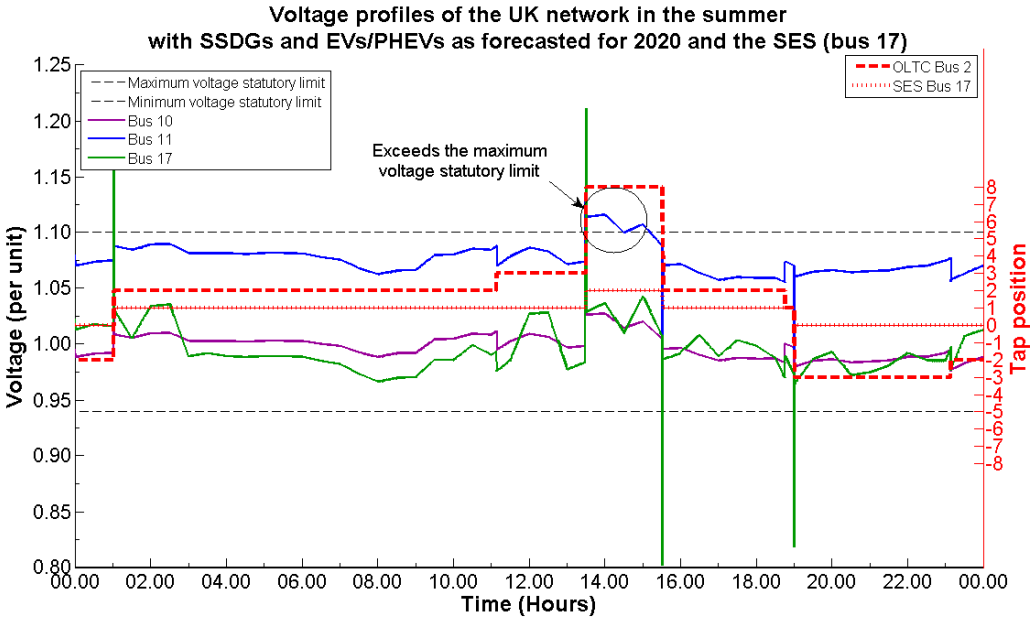

Figure 7.9 Voltage profiles of the UK network in the summer with only SES for scenario 6 (from Table 3.5)

7.1.1d) The UK network with SOLTC, SCP/SEVGC and SES operating in independent mode

In the winter and the summer, the SOLTC, three SCPs (at buses 7, 8 and 9) and SES (at bus 17) that operate in independent mode keep the voltage at all buses within the statutory limits, as shown in Figures 7.10 and 7.11.

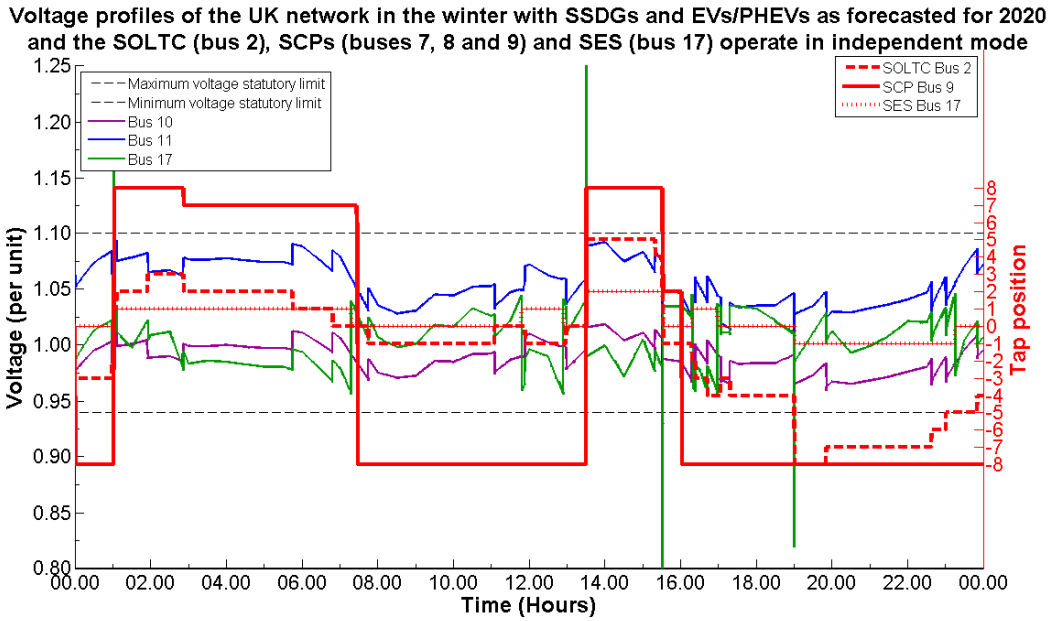

Figure 7.10 Voltage profiles of the UK network in the winter with smart controllers operating in independent mode for scenario 6 (from Table 3.5)

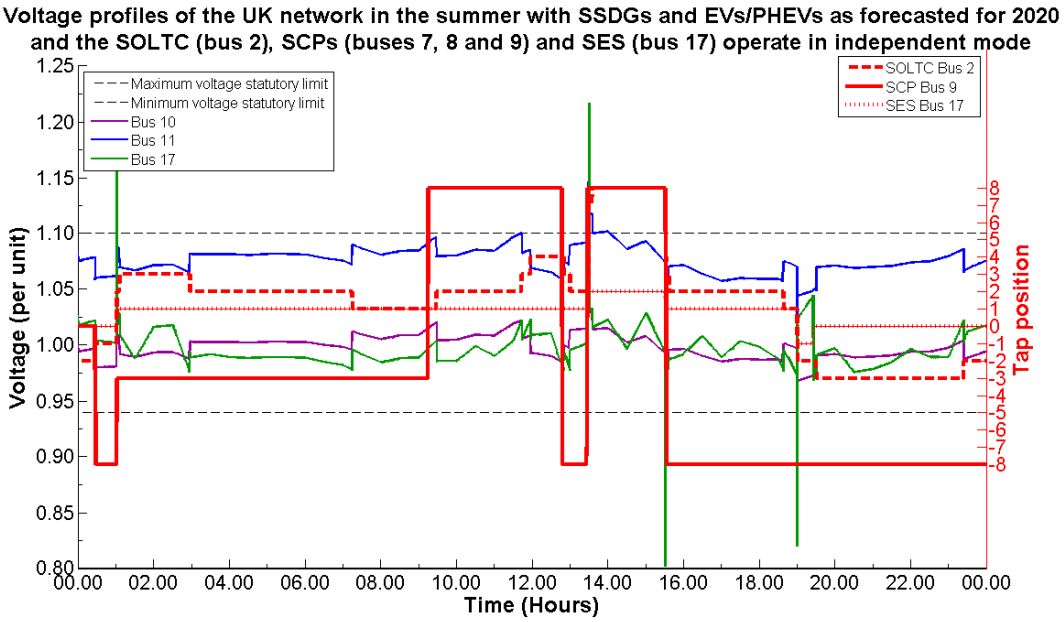

Figure 7.11 Voltage profiles of the UK network in the summer with smart controllers operating in independent mode for scenario 6 (from Table 3.5)

7.1.1e) The UK network with SOLTC, SCP/SEVGC and SES operating in incorporated mode

In order to investigate the relationship between the combinations of smart controllers, the capacity of the SES is considered. The SES is set as master controller and three SCPs (at buses 7, 8 and 9) are set as slave controllers, respectively. These controllers were operated in incorporated mode and the control signal of each controllers depended on the far end of the LV feeder and master controller. It can be noted that the capacity of the SES was reduced to 15 percent of the LV transformer rated of 500 kVA, and hence each step controls 9.375 kW. Figure 7.12 demonstrates that the combination described above of can improve the reliability of the UK network and keep the voltages at all buses within the statutory limits, except the voltage at the far end of the LV feeder during 14.30-15.30. This voltage rise (about 1.5 percent higher than the limit) is due to the dead zone setting of the smart controllers. As can be seen, the SOLTC still not reach its limits yet and therefore an adjustment of the SOLTC setting can remove this voltage violation.

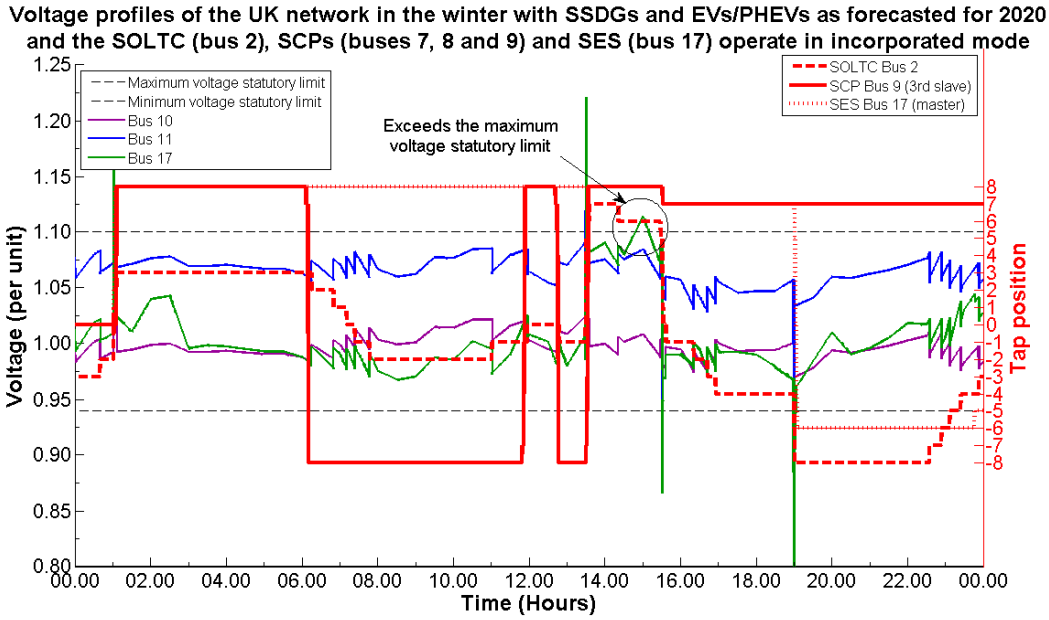

Figure 7.12 Voltage profiles of the UK network in the winter with smart controllers operating in incorporated mode for scenario 6 (from Table 3.5)

In the summer, each step control of the SES was reduced to 25 kW. The voltage at bus 11 in the UK network slightly exceeds the maximum voltage statutory limit in the daytime (about 0.75 to 1 percent higher than the limit) because of high generation of SSDGs, as can be seen from Figure 7.13. However, the voltages at the other buses were kept within the voltage statutory limits.

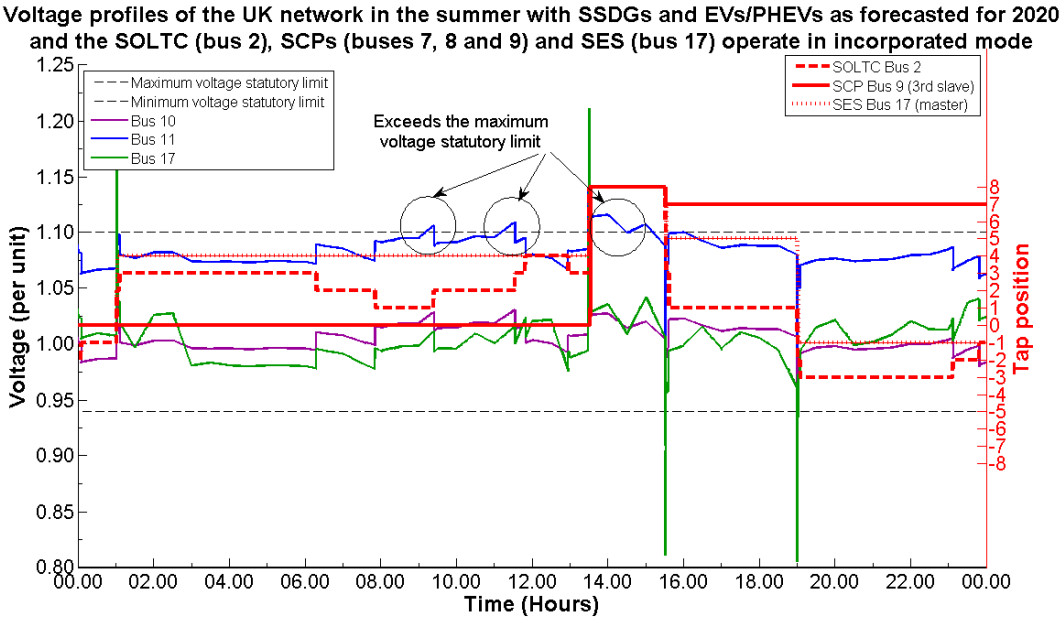

Figure 7.13 Voltage profiles of the UK network in the summer with smart controllers operating in incorporated mode for scenario 6 (from Table 3.5)

7.1.2 Evaluation of the smart controllers for the TH distribution network

The single line diagram of the TH network with smart controllers is shown in Figure 7.14. It can be seen that the existing OLTC is replaced by the SOLTC with the same rating and the EVs/PHEVs car park at bus 2 is replaced by the SCP for 96 EVs/PHEVs units. The SCP is divided into ±8 steps and each step controls 12 EVs/PHEVs units. The normal EVs/PHEVs car park that supports 30 units is also included at the far end of the LV feeder where the SES is also installed to optimise the power flow in the network together with a small PV farm of 48 kW (12 paralleled small-scale PV, each with a rating of 4 kW). Accordingly, the SES is set with ±8 steps and each step supports 50 kW (10 percent of the LV transformer rated). All buses communicated with the smart meter in order to send/receive data from the central data bank.

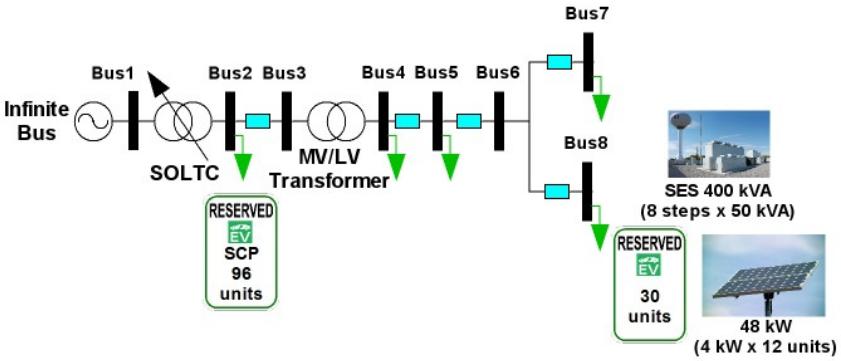

(exclude domestic SSDGs and EVs/PHEVs at the far end of the feeder)

Figure 7.14 Single line diagram of the TH network
with smart controllers for scenario 6 (from Table 3.5)

7.1.2a) The TH network with SOLTC only

Figures 7.15 and 7.16 show the impacts of the SOLTC in the TH network in the winter and the summer. The voltage at all buses was improved (when compare to Figures 5.49 and 5.50) and was kept within the voltage statutory limits due to the operation of the SOLTC. As can be seen, the changes of the tap changer were due to the use of the voltage at the far end of the LV feeder to control the SOLTC instead of the local bus.

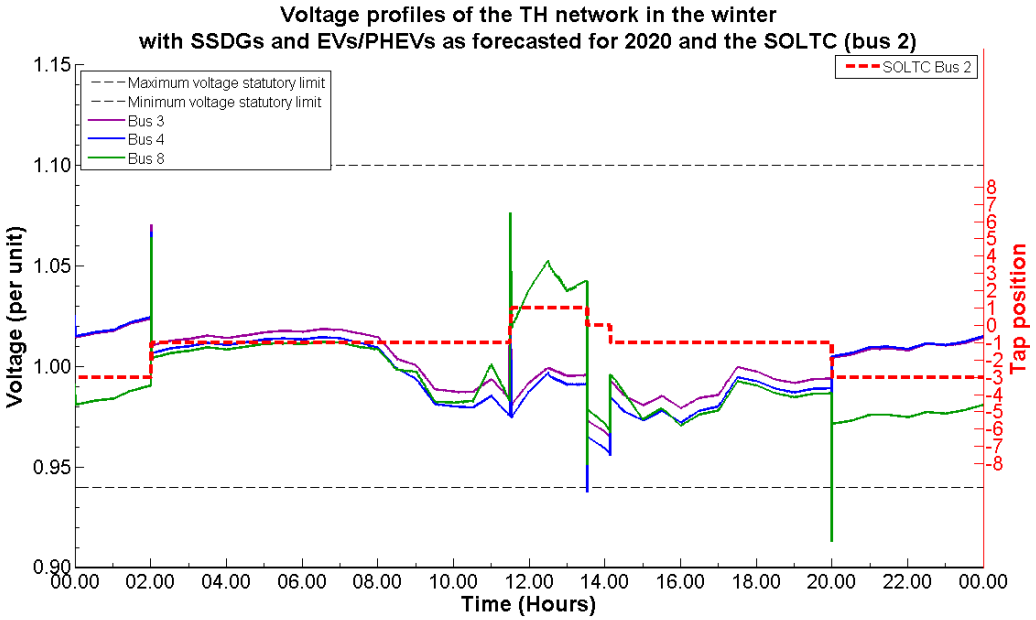

Figure 7.15 Voltage profiles of the TH network in the winter
with only SOLTC for scenario 6 (from Table 3.5)

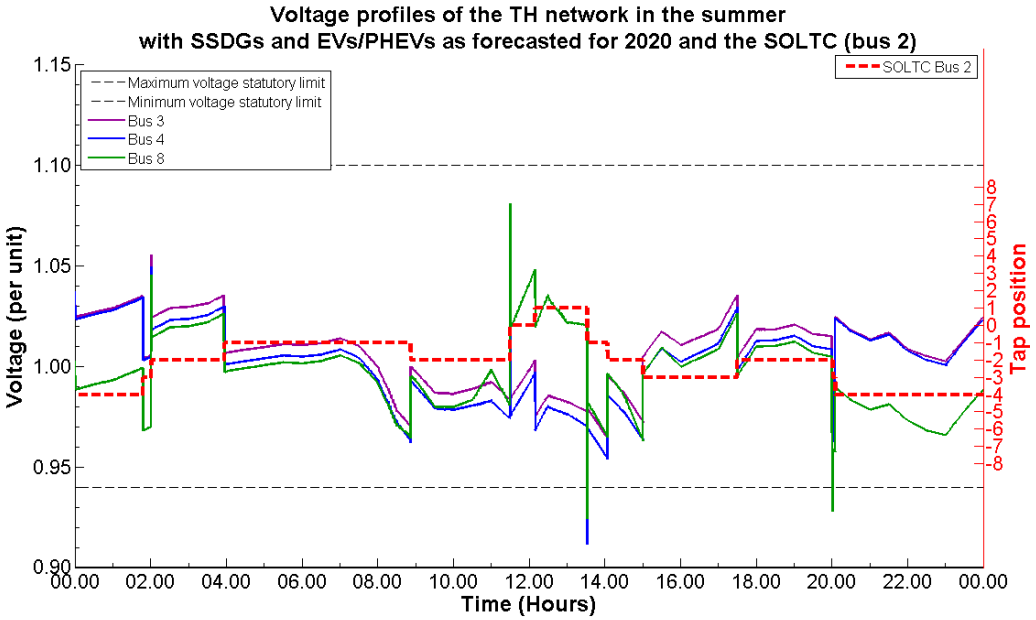

Figure 7.16 Voltage profiles of the TH network in the summer with only SOLTC for scenario 6 (from Table 3.5)

7.1.2b) The TH network with SCP only

In this section, the control signal is taken either from the local SCP bus (shown in Figures 7.17 and 7.18) or from the far end of the LV feeder (shown in Figures 7.19 and 7.20). Figure 7.17 shows the voltage profiles in the TH network in the winter with only SCP (at bus 2). The SCP that uses a local voltage control signal allows 96 EVs/PHEVs to operate in charging mode during 00.00-11.30 and 11.45-14.15 because the local voltage (at bus 2) exceeds the reference voltage (set at 1 per unit). However, the 96 EVs/PHEVs in the SCP operate in V2G mode and attempt to supply power to the network during 14.15-00.00. It should be noted that the voltages at the other buses were kept within the voltage statutory limits by the operation of the OLTC and the SCP. The control signal of the SCP is defined by the voltage deviation between the voltage signal (here SCP bus) and the reference voltage, hence any change either positive or negative deviation directly affects the connection of EVs/PHEVs in that SCP.

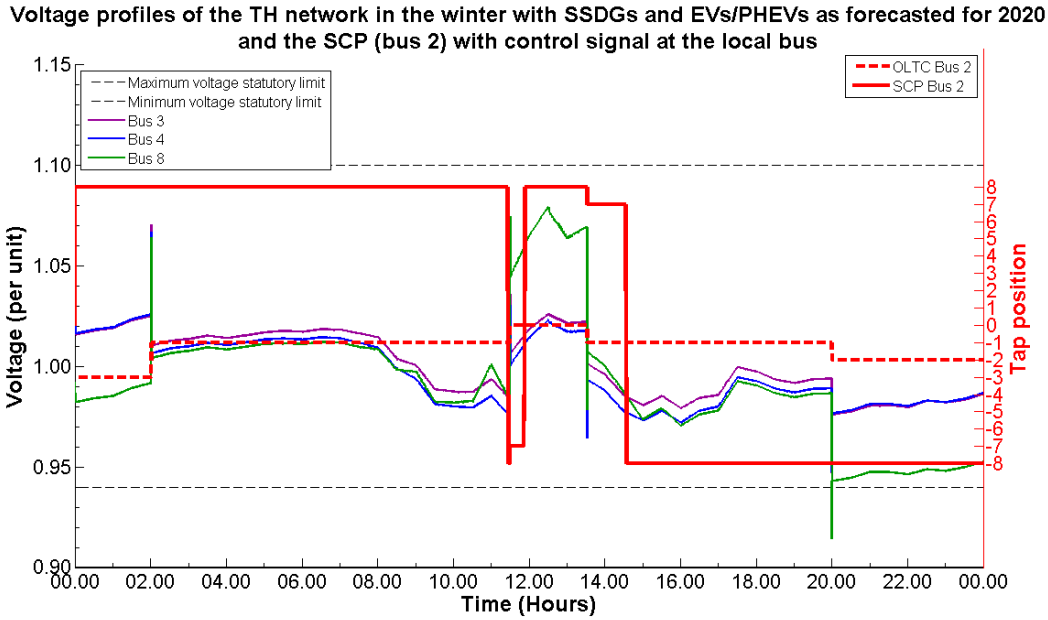

Figure 7.17 Voltage profiles of the TH network in the winter with only SCP that use local signal for scenario 6 (from Table 3.5)

In the summer, all EVs/PHEVs parking in the SCP in the TH network are operated in charging mode during 02.00-08.00 and 11.30-13.30 because of high generation of SSDGs in the daytime and energy saving policies, as shown in Figure 7.18. Conversely, during 08.00-11.30, 13.30-15.30 and 21.00-23.30, all EVs/PHEVs parking in the SCP are operated in V2G mode due to high consumers' demand. It can be noted that the impacts of the SEVGCs for public parking on the street in the TH network are also similar to the SCP.

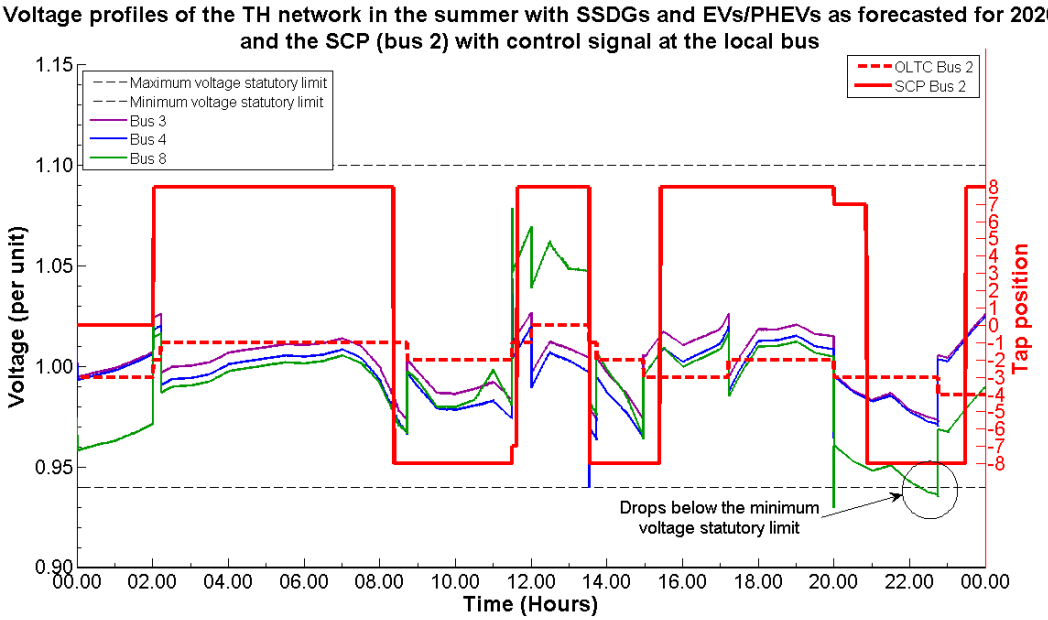

Figure 7.18 Voltage profiles of the TH network in the summer with only SCP that use local signal for scenario 6 (from Table 3.5)

On the other hand, the SCP that uses the voltage at far end of the LV feeder as control signal are shown in Figures 7.19 and 7.20. In the winter and the summer, the voltage at all buses was kept within the voltage statutory limits by the operation of the OLTC and the SCP except at the far end of the LV feeder in the summer. Moreover, the results shown in Figures 7.19 and 7.20 show that the number of EVs/PHEVs that use to support in the SCP is higher than Figures 7.17 and 7.18.

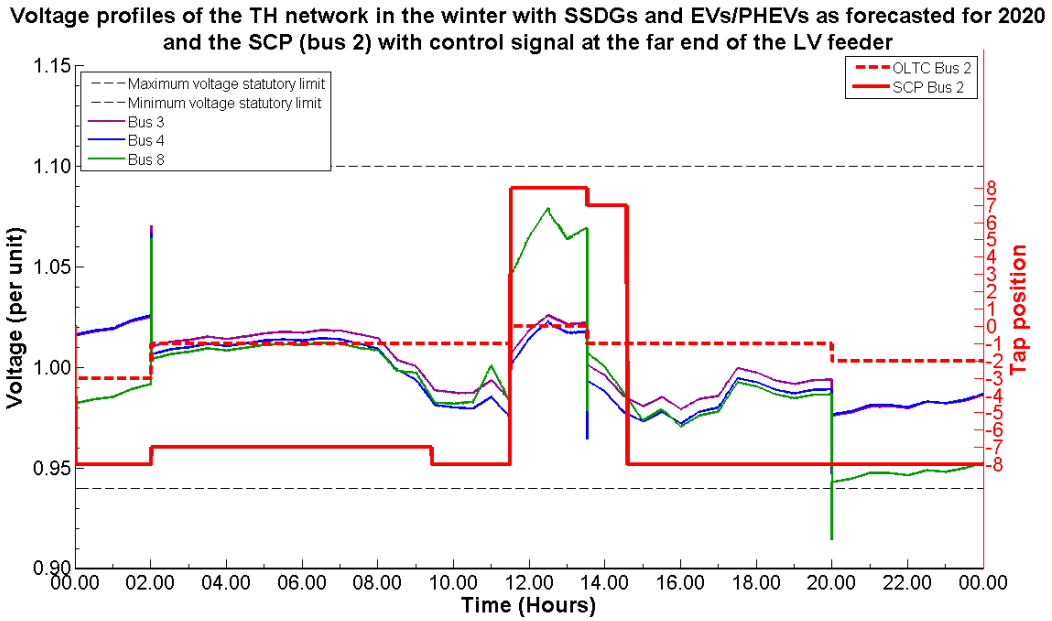

Figure 7.19 Voltage profiles of the TH network in the winter with only SCP that use the far end of the LV feeder signal for scenario 6 (from Table 3.5)

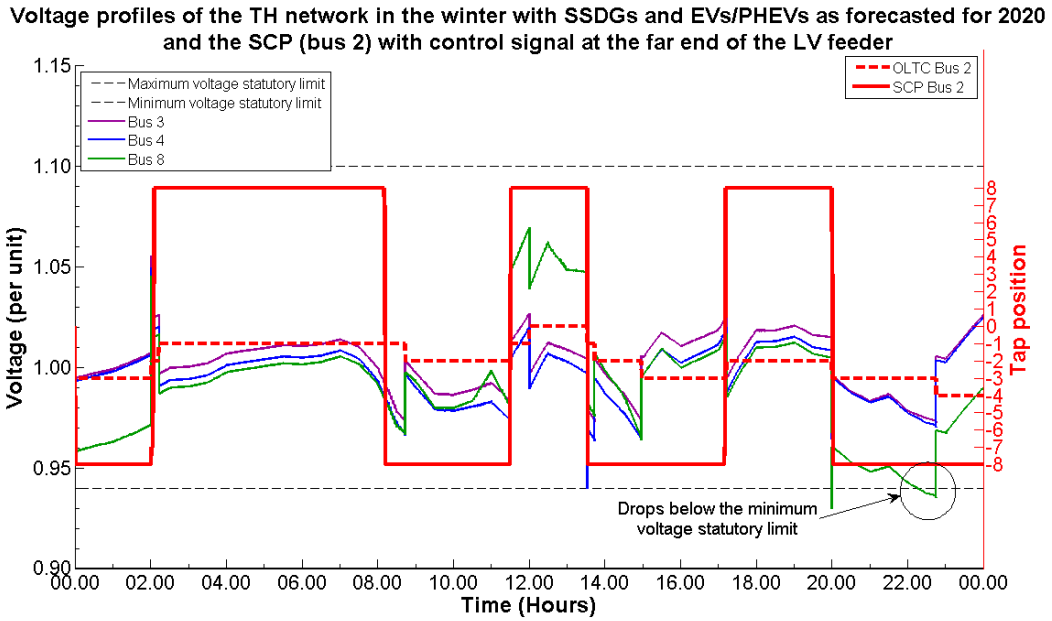

Figure 7.20 Voltage profiles of the TH network in the summer with only SCP that use the far end of the LV feeder signal for scenario 6 (from Table 3.5)

7.1.2c) The TH network with SES only

The impacts of the SES at the far end of the LV feeder (at bus 8) in the TH network in the winter are shown in Figure 7.21. The SES was set with ±8 steps and each step controls 50 kW. This is in addition to the SES consuming/supplying the power at its bus, which depends on the voltage deviation of the control signal (here SES bus) from the reference voltage. The voltages at all buses were kept within the voltage statutory limits by the operation of the OLTC and the SES. The SES has the highest supply 800 kWh during 20.00-00.00 (tap position -4 at 200 kW) and the highest consumption 150 kWh during 11.30-12.30 (tap position 3 at 150 kW).

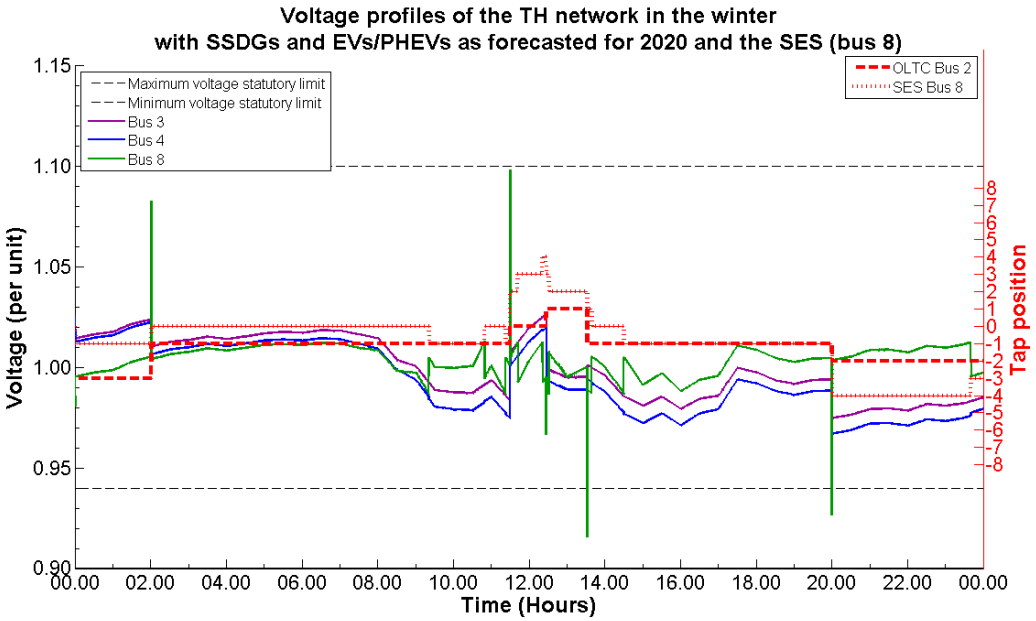

Figure 7.21 Voltage profiles of the TH network in the winter with only SES for scenario 6 (from Table 3.5)

In the summer, the voltage profiles (shown in Figure 7.22) slightly fluctuates, especially in the daytime with high consumers' demand due to the effects of the OLTC and the SES. The voltage at all buses was keep within the statutory limits because the operation of the OLTC and the SES. The highest consumption of the SES is 262.5 kWh in the afternoon (tap position 3 at 150 kW).

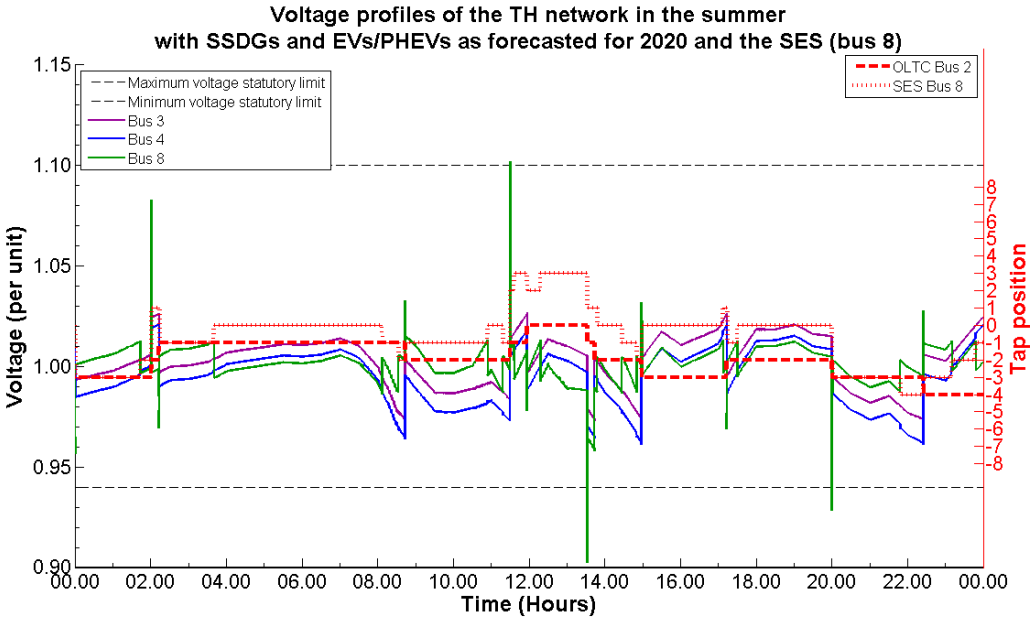

Figure 7.22 Voltage profiles of the TH network in the summer with only SES for scenario 6 (from Table 3.5)

7.1.2d) The TH network with SOLTC, SCP/SEVGC and SES operating in independent mode

Figures 7.23 and 7.24 show that the combination of SOLTC, SCP (at bus 2) and SES (at bus 8), which operate in independent mode. In the winter and the summer, the SOLTC, SCP and SES kept the voltages within the limits.

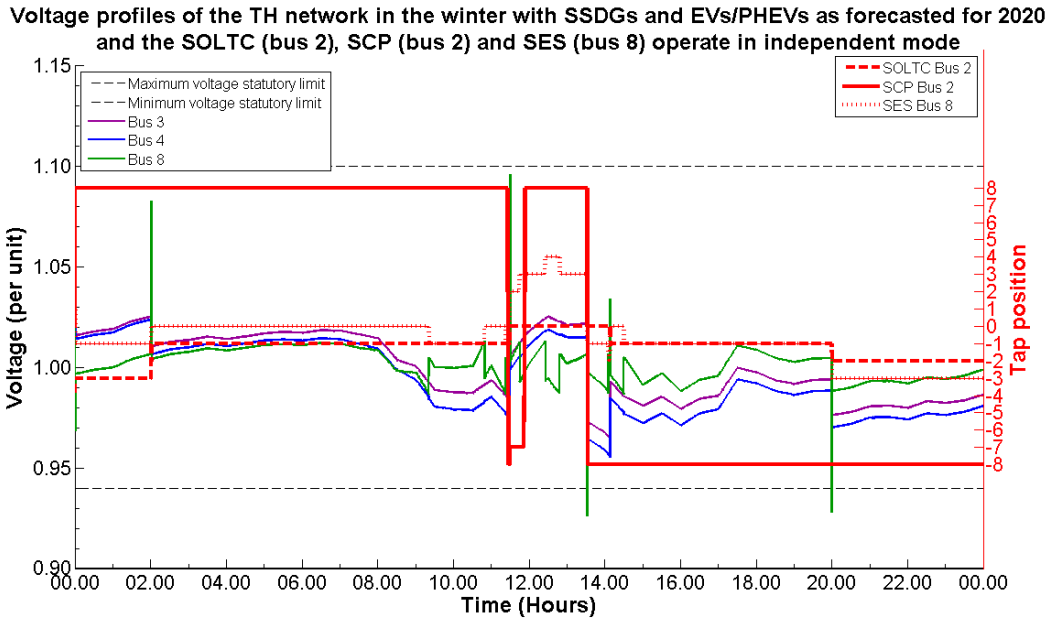

Figure 7.23 Voltage profiles of the TH network in the winter with smart controllers operating in independent mode for scenario 6 (from Table 3.5)

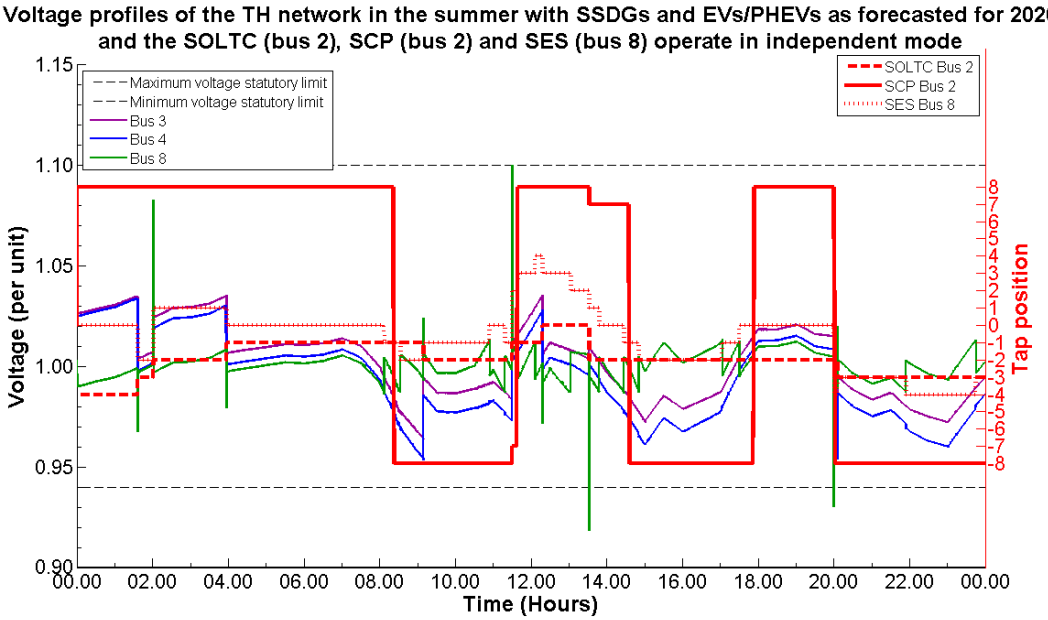

Figure 7.24 Voltage profiles of the TH network in the summer with smart controllers operating in independent mode for scenario 6 (from Table 3.5)

7.1.2e) The TH network with SOLTC, SCP and SES operating in incorporated mode

In order to investigate the relationship between the combinations of smart controllers, the controllers were set to operate in incorporated mode. The SES is set as master controller, and therefore the SCP at bus 2 is used as slave controller. The control signal for each controllers is acquired from the far end of the LV feeder. In the winter and the summer, the capacity of the SES was reduced to 40 percent of the LV transformer (rated at 500 kVA), and hence each step controls 25 kW. Figure 7.25 demonstrates that the combination of SOLTC, SCP (at bus 2) and SES (at bus 8) can keep the voltages at all buses in the TH network in the winter within the voltage statutory limits. The SOLTC operates to control the voltage either bus 2 or bus 8 whilst the SES and the SCP control the voltage at far the end of the LV feeder. Moreover, result shown in Figure 7.25 show that the operation of the SES still does not reaches its limit in the early morning and in the evening and therefore the SCP is available to support the network, if high penetration levels of SSDGs and EVs/PHEVs are connected into the network at that time. The TH network performance in the summer is shown in Figure 7.26. The voltages at all buses are keep within the voltage statutory limits by the operation of the SOLTC and the SES.

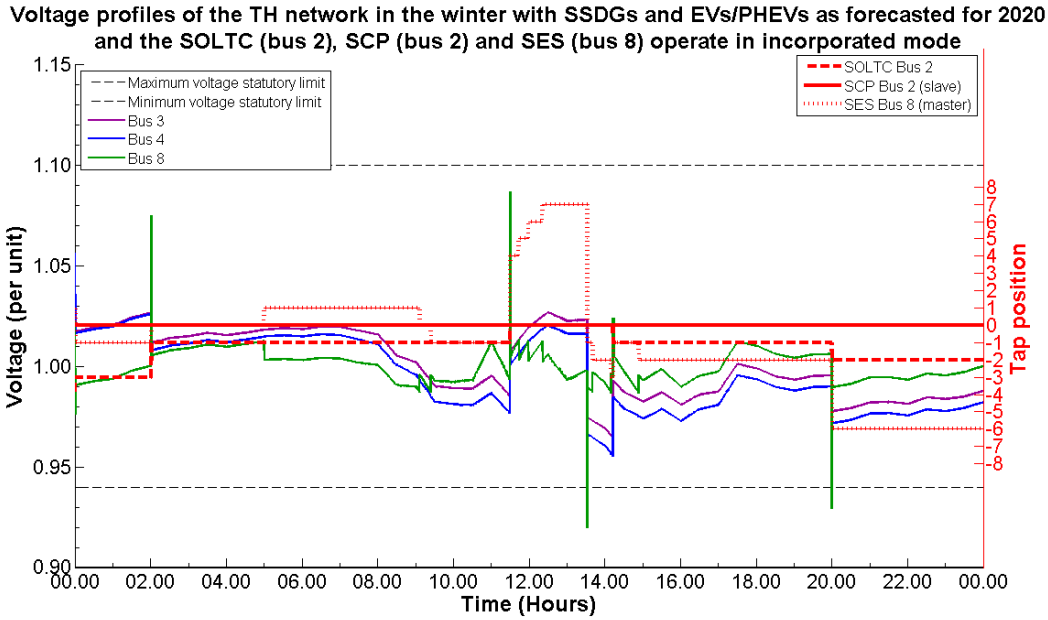

Figure 7.25 Voltage profiles of the TH network in the winter with smart controllers operating in incorporated mode for scenario 6 (from Table 3.5)

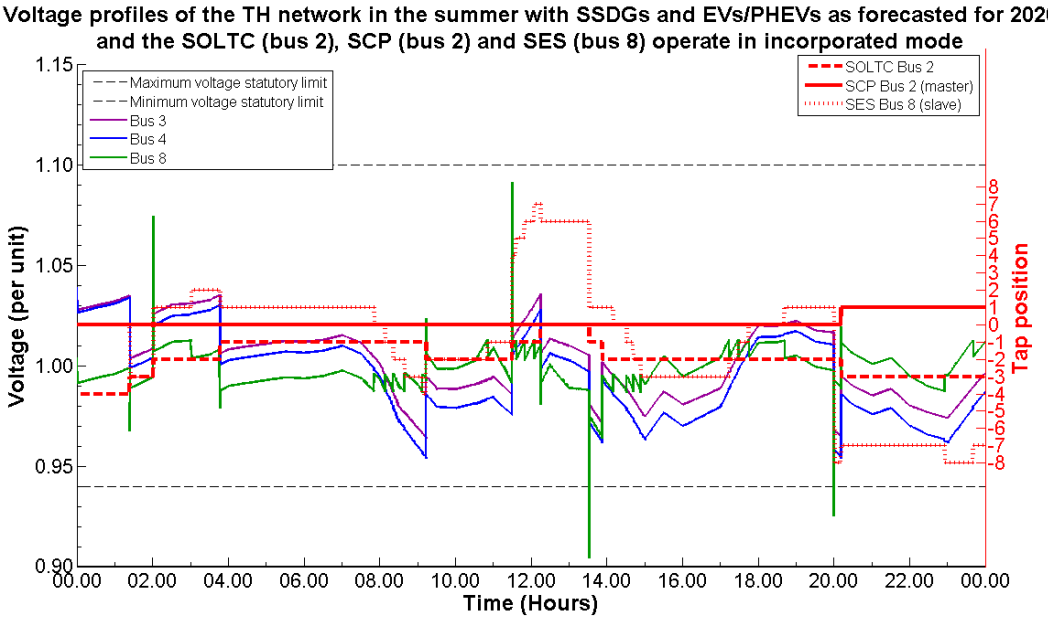

Figure 7.26 Voltage profiles of the TH network in the summer with smart controllers operating in incorporated mode for scenario 6 (from Table 3.5)

It can be concluded from the analysis in section 7.1 that the use of proposed smart controllers (SOLTC, SEVGC, SCP and SES) improves the network performance and maintain voltage deviations in the network within acceptable limits. Therefore, allowing high penetration levels of SSDGs and EVs/PHEVs into the distribution network without compromising the reliability of the network. The capacity of the SCP and SES can be determined based on the maximum and

minimum demand in the network. Furthermore, the dead zone of the SCP and the SES those operate in incorporated mode need to multiply with the correction factor (k, showed in section 6.4). Therefore, these smart controllers require a network operator with experience to set their step voltage and dead zone in order to ensure the performance and prevent the unnecessary cost.

7.2 Islanding Operation with Smart Controllers

7.2.1 Evaluation of the smart controllers for the UK islanded network

In order to investigate the impacts of smart control devices in future power networks, scenario 2 from Table 3.6 was chosen, as it is an extreme scenario, with community, and/or attraction areas including a small farm of SSDGs. The single line diagram of the UK network with smart devices for islanded networks is shown in Figure 7.27. The smart controllers are installed at appropriate (the weakest) buses. Hence, two existing OLTCs are replaced by two SOLTCs with the same rating and the EVs/PHEVs car parks at buses 7, 8 and 9 are replaced by the SCP with EVs/PHEVs of 200 units each. The SCP is divided into ±8 steps and each step controls 25 EVs/PHEVs units. Furthermore, for the normal EVs/PHEVs car park with 30 units, the SES has ±8 steps (each step supports 100 kW) and a small wind turbine farm of 50 kW (10 paralleled small-scale wind turbine, each with a rating of 5 kW) is installed at the far end of the LV feeder. All smart controllers operated in independent mode and all buses communicated with the smart meter in order to send/receive data from the local central data bank and load priority is also presented.

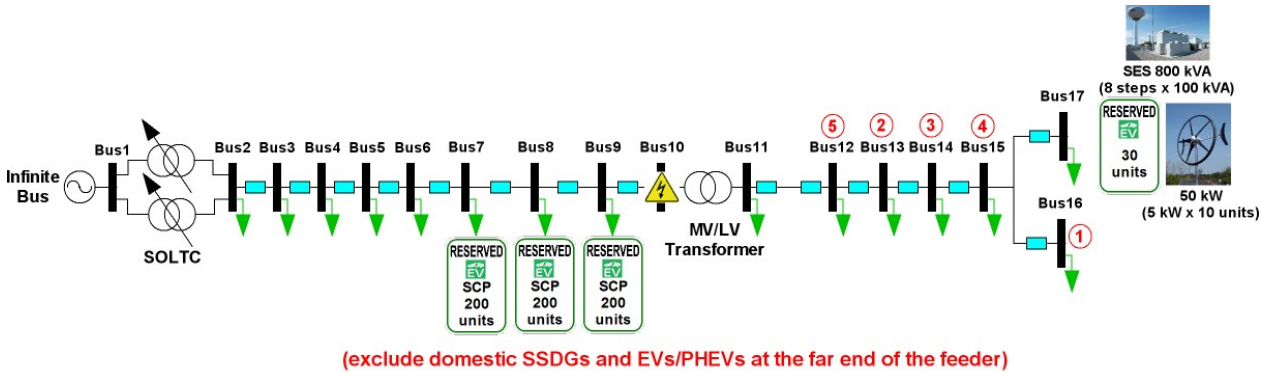

Figure 7.27 Single line diagram of the UK network for scenario 2 (from Table 3.6)

The voltage profiles of the UK network with highest demand and generation were chosen to present the impacts of smart controllers on the distribution network when experiencing a fault, as shown in Figure 7.28. A three-phase fault was detected at bus 10, and therefore the breaker isolated buses 11 to 17 from the main network until the fault had been cleared. During the network operation in islanding mode, 384 consumers', 52 SSDGs (28 PV rated at 4 kW, 16 wind turbine rated at 5 kW and 8 hydro turbine rated at 4 kW) and the SES (rated 800 kW) are available during this time. The lowest load priority was set at buses 16, 13, 14, 15 and 12 respectively. It can be seen that the voltage profiles in the islanded network were kept within the voltage statutory limits by the smart controllers. Consequently, the SLCs were set at 50 ms in order to maintain supply/demand and frequency voltage in the islanded network by disconnecting/connecting unnecessary loads, based on the community priority and electricity tariff. The SLCs also included the function to ensure that the isolated SSDGs in the islanded network cannot supply power, if there is no consumer in the islanded network at that time. The SES in the islanded network also operates in supply mode (tap position -6 at 600 kW), and hence the SES consumes 150 kWh.

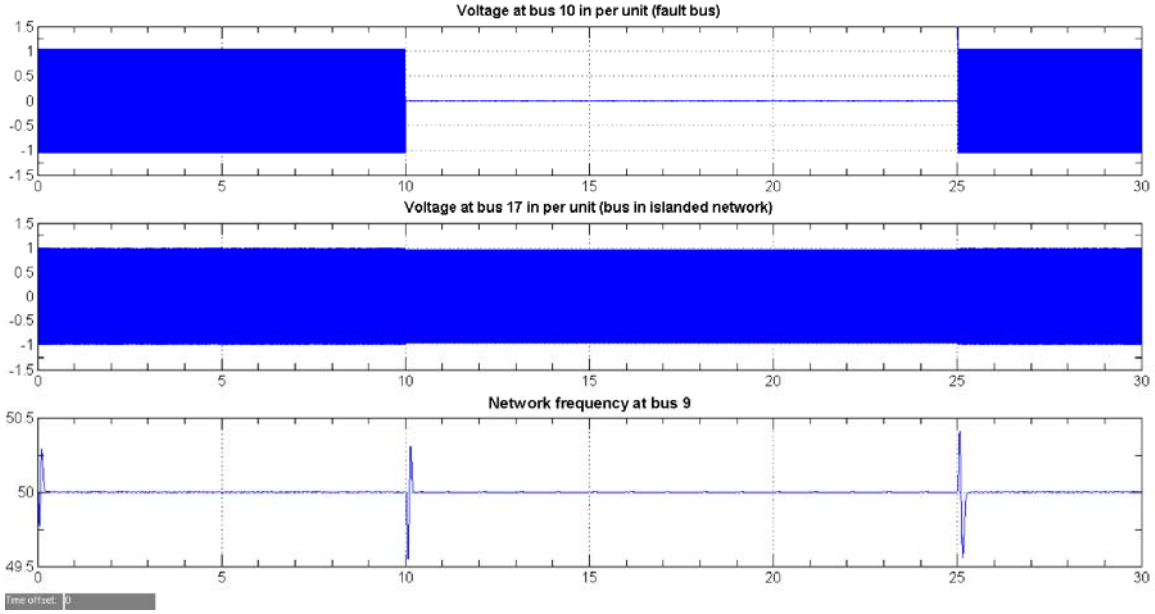

Figure 7.28 Voltage profiles of the UK network with highest demand and generation profiles with smart controllers for scenario 2 (from Table 3.6)

7.2.2 Evaluation of the smart controllers for the TH islanded network

The single line diagram of the TH network with smart controllers for the islanded network is shown in Figure 7.29. The existing OLTC is replaced by a SOLTC with the same rating and the EVs/PHEVs car park at bus 2 is replaced by a single SCP, which is divided into ±8 steps and each step controls 12 EVs/PHEVs units. Hence, the SCP supports a total of 96 EVs/PHEVs in both charging and V2G modes. Moreover, a normal EVs/PHEVs car park (supporting 30 units), the SES (with ±8 steps; each step supports 50 kW) and a small PV farm with a total generation 48 kW (12 paralleled small-scale PV, each with a rating of 4 kW) were installed at the far end of the LV feeder. All smart controllers operated in independent mode and all buses communicated with the smart meter in order to send/receive data from the local central data bank and load priority is also presented.

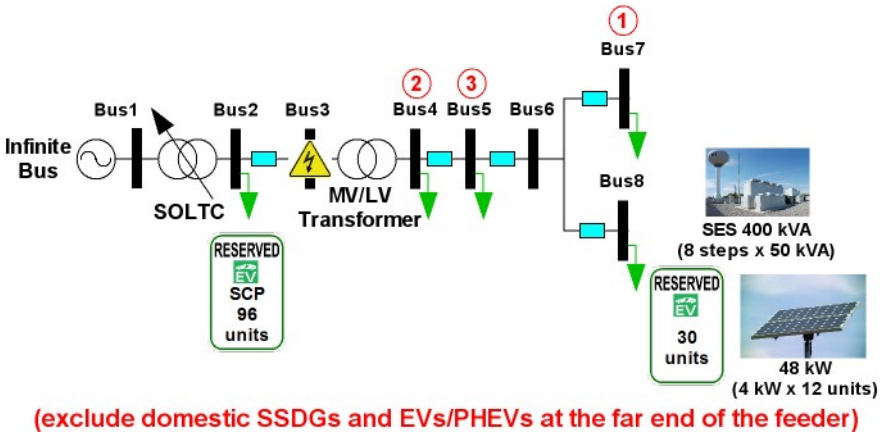

Figure 7.29 Single line diagram of the TH network for scenario 2 (from Table 3.6)

The voltage profiles in the TH distribution network while experiencing a fault in the summer (extreme demand) are shown in Figure 7.30. A three-phase fault was detected at bus 3, and hence the breaker at bus 3 was operated to clear the fault in the system. The SLCs were used to manage load shedding in the islanded network (between buses 4 to 8 with response at 50 ms), as shown in Figure 7.30. In the islanded network, 37 consumers', 1 university, 16 SSDGs (14 PV rated at 4 kW, 1 wind turbine rated at 5 kW and 1 hydro turbine rated at 5 kW) and the SES (rated 400 kW) were presented at that time without supply from a small PV farm (loss of solar irradiation in the evening). The lowest load priority was set at buses 7, 4, and 5 respectively. The voltages in the islanded network (buses 4 to 8) were kept within the voltage statutory limits by the smart controllers' even with the loss

of PV generation. The SES in the islanded network also operates in supply mode (tap position -4 at 200 kW), and hence the SES consumes 50 kWh.

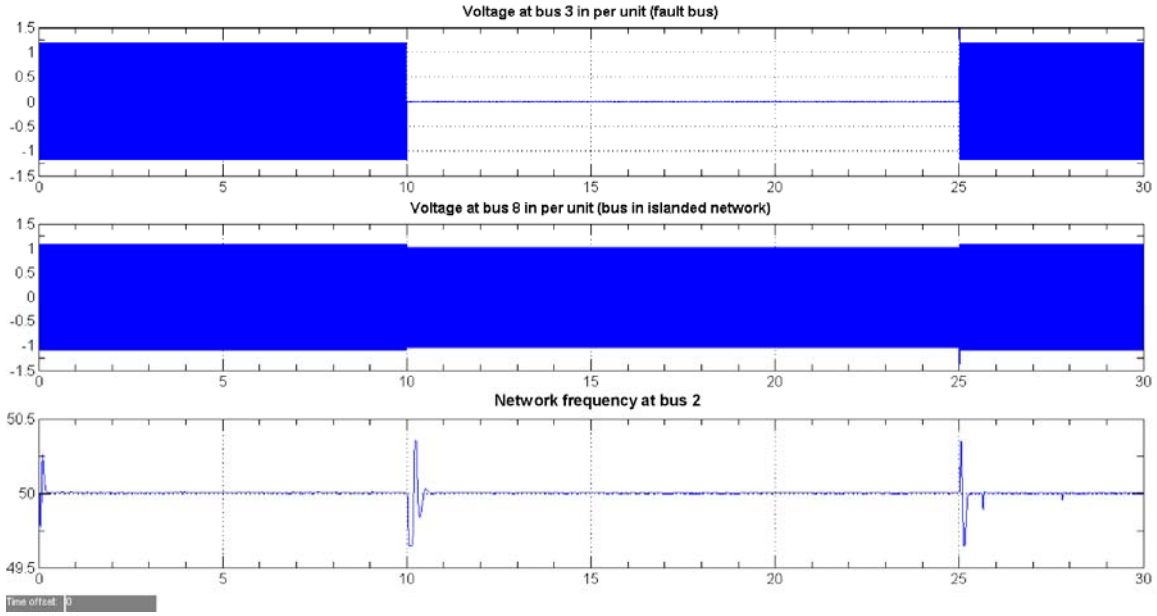

Figure 7.30 Voltage profiles of the TH network with highest demand and generation profiles with smart controllers for scenario 2 (from Table 3.6)

From the results in section 7.2, it can be seen that the smart controllers can match supply/demand in the islanded network. Accordingly, the large numbers of consumers' in the islanded network were lumped into sets, and hence the load priority in here was identified by bus instead of individual loads. Therefore, the SLC cannot perform at its fullest performance. Hence, the load priority should be persevered by the community priority and electricity tariff, hence assigned into the micro level (individual consumer) via the smart meter (restructure).

Then, these proposed solutions could coexist with the existing and future power networks and increase the reliability/flexibility in the network. In order to utilise the SLCs in the islanded network, the high speed detection and fast response of load shedding management that handles the over frequency and low voltage of SSDGs and loads during transient response are required (here 50 ms to 5 sec are considered). The SLC also updates signals to the local central data bank, hence allowing the isolated SSDGs to update this data because all SSDGs in the islanded network are needed to disconnect, if there are no consumers' at that time. Moreover, in order to operate SSDGs in an islanded network, it must include a synchronisation (incorporated with PLL controller) and isolated (local) grounding systems to ensure the personnel safety during islanding and reconnection to the main network.

CHAPTER 8
DEVELOPMENT OF A COMPUTER MODELLING TOOL FOR PQ ANALYSIS

8.1 Concept of the PSmartDN Tool

This chapter presents a computer modelling tool, which is proposed for investigation of the impacts of SSDGs and EVs/PHEVs in a typical MV/LV distribution power network. The tool is called the “Power Self-Monitoring, Analysis and Reporting Tool for Distribution Network (PSmartDN)”. This tool uses a combination of MS Excel and MATLAB/Simulink in order to analyse the performance of a distribution network with dynamic input data. The tool is used to demonstrate the response of the control devices in the network (such as SOLTC, SCP and SES). This tool can simulate 1 section of the MV level and up to 10 sections of the LV network. The user input data section (MS Excel) includes transformer parameters, feeder impedances in addition to the daily load profile at each bus, on site generation, type of EVs/PHEVs charging and charging/regenerating profiles of EVs/PHEVs. The tool has a user friendly front page in MS Excel, whilst the simulation is actually executed in MATLAB/Simulink.

The flow chart of PSmartDN Tool is shown in Figure 8.1. The PSmartDN Tool files contain the distribution network data and resources availability required to analyse power flow. In order to start PSmartDN Tool, the user needs to input data in MS Excel (open PSmartDNToolData.xls) and save it before recalling the PSmartDN Tool via the MATLAB/Simulink (run PSmartDNTool.m), more details in appendix C. It can be noted that MS Excel is used as an input interface due to its simple functionality, availability in the current market, widespread use in academic research, and so most of end-users are familiar with it. After the PSmartDN Tool runs in the MATLAB/Simulink, it will check the input data in the MS Excel and build the simulation with components according to the data in the MS Excel. The user must be running the computer model and waiting for the results until the simulation is finished and closed. When simulation is completed, PSmartDN Tool displays a report window, which shows the results of each measurement with an option to plot the results (done by PSmartDNToolReport.m).

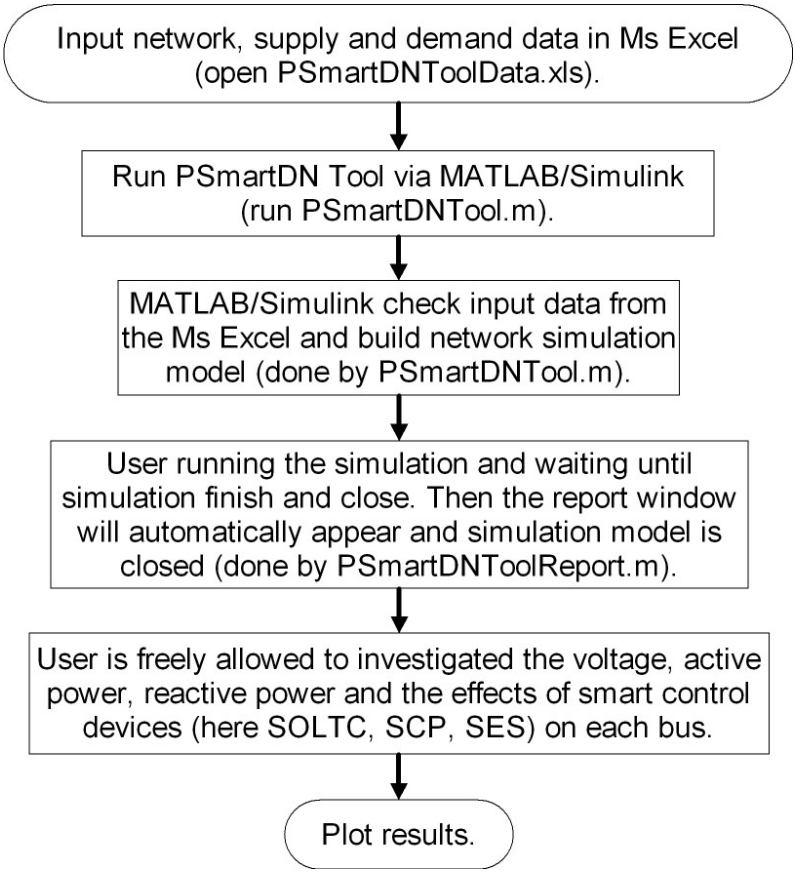

Figure 8.1 Flow chart of PSmartDN Tool

8.2 Demonstration of the Effectiveness of the PSmartDN Tool

The PSmartDN Tool can be used to study a wide range of network scenarios and analyse the variation of voltage, active power and reactive power due to deployment of SSDGs and EVs/PHEVs. The tool can give the user a clear idea where is the weakest bus in the distribution network as well as allowing the user to investigate the impacts of smart control devices (SOLTC, SCP and SES). PSmartDN Tool and results have been validated against references [24] for the UK network and [17] for the TH network to ensure accuracy. In order to demonstrate the effectiveness of PSmartDN Tool, the scenario with extreme maximum demand in section 7.1.1d (and 7.1.2d) was chosen.

Figure 8.2 demonstrates that the combination of the SOLTC, SCP and SES can improve the reliability of the UK network in the winter, as the voltage at all buses was kept within the voltage statutory limits by the operation of the smart controllers (similar results to Figure 7.10). It should be noted that two conventional OLTCs are replaced by a single SOLTC with the same rating and the EVs/PHEVs car parks at buses 7, 8 and 9 are replaced by a single SCP with 600 units at bus MV1. A typical EVs/PHEVs car park with 30 units is also connected at the far end of the LV feeder (at bus LV.7 in PSmartDN). An 800 kW SES (set with ±8 steps) and a small wind turbine farm with a total generation of 50 kW are also installed at the far end of the LV feeder to optimise the power flow in the network. All buses communicate with the smart meter in order to send/receive data to/from the central data bank.

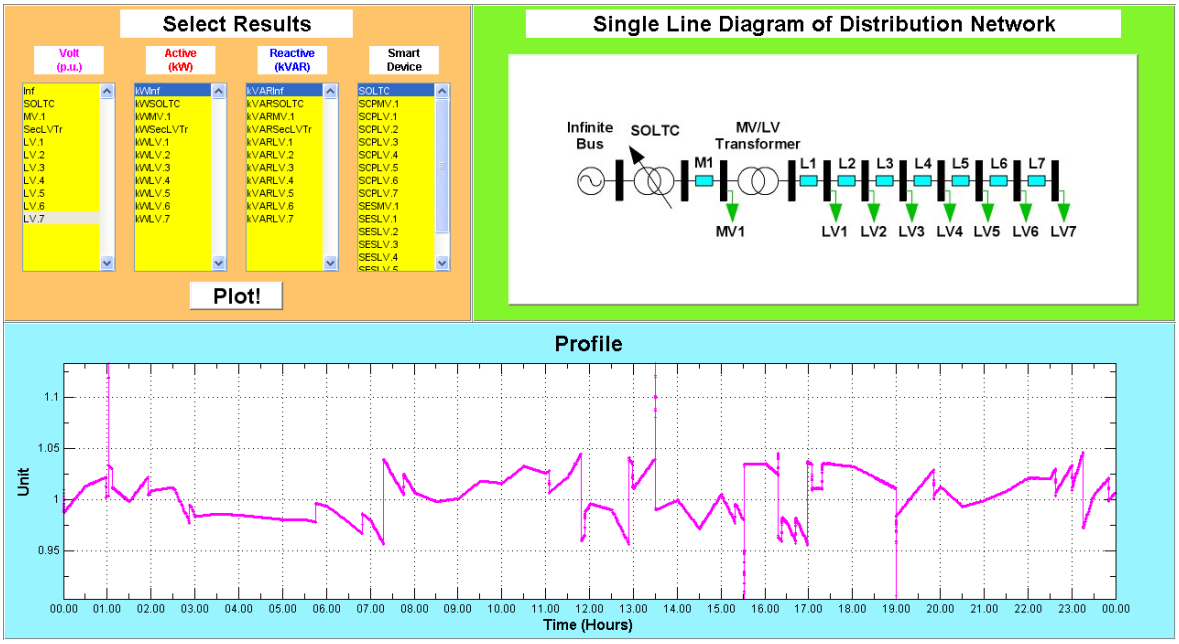

Figure 8.2 Voltage at the far end of the LV feeder in the UK network in the winter for section 7.1.1d by PSmartDN Tool

Figure 8.3 shows the voltage at the far end of the LV feeder in the TH network in the summer for scenario 7.1.2d. As can be seen, the conventional OLTC is replaced by a SOLTC with the same rating. A single SCP with 96 units at bus MV1 replaces the EVs/PHEVs car park at bus 2, and a normal EVs/PHEVs car park that supports 30 units is included at the far end of the LV feeder as well as the SES with ±8 steps and each step supports 50 kW. A small PV farm with a total generation of 48 kW is connected at the far end of the LV feeder and all buses communicate with the smart meter in order to send/receive data to/from the central data bank. Results shown in Figure 8.3 is similar to Figure 7.24, the voltages at all buses were kept within the voltage statutory limits by the smart controllers.

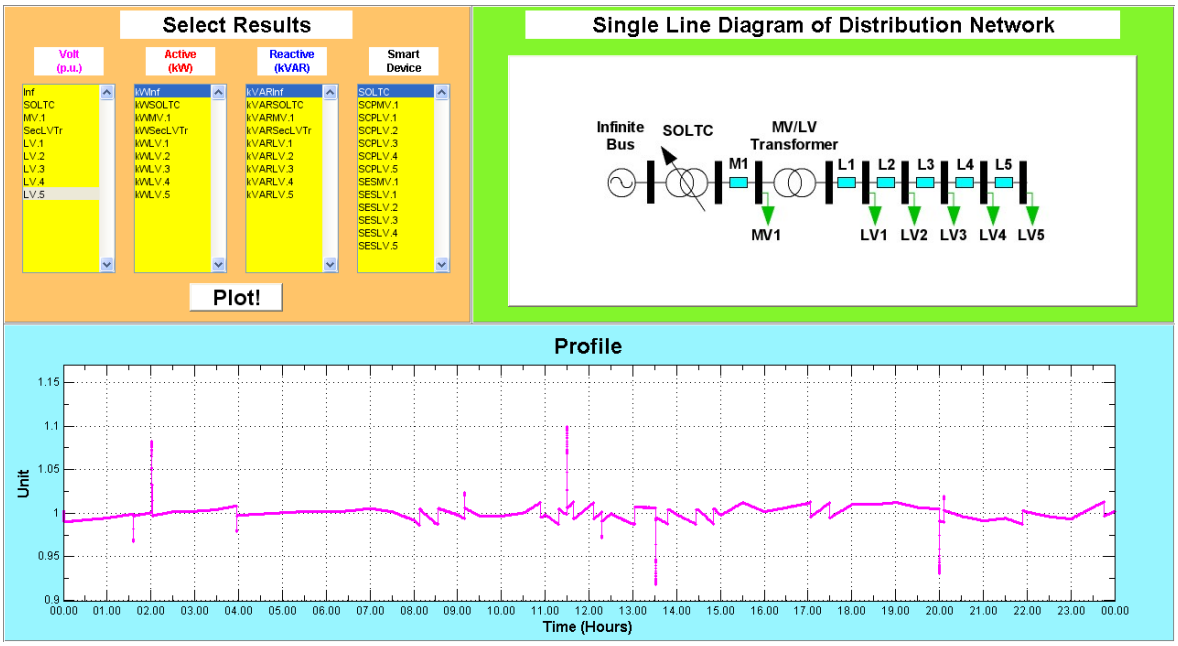

Figure 8.3 Voltage at the far end of the LV feeder in the TH network in the summer for section 7.1.2d by PSmartDN Tool

CHAPTER 9
CONCLUSIONS AND FUTURE WORK

9.1 Conclusions

Green technologies are continually being deployed in existing distribution networks, at the MV and LV levels. These technologies include DGs (from renewable energy sources) and EVs/PHEVs. The output power of DGs depends on the surrounding environment and EVs/PHEVs may be considered as mobile active loads. It can be noted that EVs can operate as generators when operating in V2G mode to supply power to the grid. Therefore, power flow in existing distribution power networks is changed to a bi-directional flow instead of a one directional flow (where power is supplied by centralised units). That means the existing SCADA systems are not suitable for future power networks, especially at MV and LV levels with high penetration levels of DGs and EVs. Therefore, it is necessary to change existing distribution networks to become more active and smart in order to balance supply and demand.

This thesis investigated the impacts of SSDGs and EVs/PHEVs (especially voltage profiles) on existing urban distribution network in the UK and rural distribution network in TH. It can be noted that an existing urban network normally supports demand close to the network capacity because the short length feeders have small impedance and hence a low voltage drop. This allows more consumers to connect to the network, whereas the opposite is the case for the distribution network in rural areas. Typical networks from the UK and TH were used and scenarios considered were based on a realistic worse case potential network operation. Extreme conditions considered include, consumers' demand in the winter and the summer along with possible DGs connection and connection time allowance of EVs/PHEVs. EVs/PHEVs in all scenarios were assumed to be privately owned cars and their connection is based on the extreme scenarios from Tables 3.1 and 3.2. It is assumed that commercial and public transport electric vehicles (e.g. buses, trucks, etc) would be unavailable for network support for most of the time, and during the time that they are connected, their priority would be recharging for the next day. This would allow little flexibility for supply/demand matching except for re-scheduling to off-peak hours.

The thesis identified the requirements that would allow an existing distribution network to change to a smart grid. It proposed and demonstrated the effectiveness of possible solutions (such as the SOLTC, SEVGC, SCP, SES and SLC). A computer modelling tool (PSmartDN Tool) to analyse the PQ of future power networks is also suggested. The proposed solutions that have been analysed in this thesis to manage power flow in future power networks can be summarised as follows:

1) Two simplified generic models of inverter/converter based DGs and EVs have been developed to investigate voltage and harmonic profiles in distribution networks. The models employ a user friendly interface and allow investigation of inverters/converters by using an Interpolation-Extrapolation technique to study voltage profiles and a typical PWM controller to study harmonic profiles.

2) The PV and PMG wind turbine models provided in MATLAB/Simulink library are not suitable for use with the OLTC model in the distribution network because the OLTC model is in phasor mode, whereas the PV and PMG wind turbine models are not. For instances, the PV model in MATLAB/Simulink library is also not supported for various types of dynamic input (e.g. solar irradiation, wind speed) and the PMG wind turbine model has an ideal switch, which does not respond in the phasor mode. In order to investigate the voltage profiles of the distribution network with the operation of the OLTC, simplified models of SSDGs were required and a user friendly interface that supported commercial datasheets was developed. The thesis proposes a simplified model of a PV system that includes the MPP of output power as explained in section 4.3. The model was developed based on a typical crystalline Silicon (c-Si) cell, as its characteristics are close those of an ideal cell and this cell is commonly used in the current market. The proposed model is a generic and may be modified to represent various types of PV.

3) A generic model for small-scale PMG wind and hydro turbines (rating less than 50 kW) is also proposed. The proposed model includes two parts; the turbines and the PMG. The proposed small-scale wind turbine model allows the user to study either HAWT or VAWT. This model employs a non-linear blade dynamic equation to simulate the performance, as demonstrated in section 4.4.1a. The proposed computer model for the hydro turbine is suitable for the closed pipe

and open channel systems as well as support the impulse and reaction hydro turbines. In the closed pipe system, the main loss due to pipe friction was considered. The characteristics of open channel systems (e.g. natural, artificial) were considered as either rectangular or trapezoidal channels, as described in section 4.4.1b. The Bernoulli's equation for steady frictionless incompressible flow along a streamline and mass-conservation equation were used to define the mechanical output power. Section 4.4.2 presented the simplified PMG model, based on the Two-axis theory and phasor diagram of the synchronous machine.

4) Analysis of typical distribution networks in the UK and TH showed that these networks can accommodate each type of SSDG and EVs/PHEVs uniformly distributed in the network up to 10 percent in the UK network (urban network) and 45 percent in the TH network (rural network). It can be noted that the UK network can support the penetration levels of a combination of SSDGs at 10 and 5 percent in the winter and the summer, respectively. However, the TH network can support up to 35 percent in both the winter and the summer before violation of the voltage statutory limits. The penetration levels of SSDGs and EVs/PHEVs in 2020 were also investigated and showed that the voltage in the UK network exceeds the maximum voltage statutory limit in the summer, whereas the TH network is slightly below the limits in the summer. The impacts depend on the network structure, capacity, types and concentration of SSDGs and EVs/PHEVs. The voltage profiles are affected by the impedance in the network and transformer ratio of the off-load tap changer transformer at the far end of the LV feeder, as discussed in section 5.1. The percentage penetration levels considered in this research are based on consumer's maximum or minimum demand at each bus. Furthermore, the potentially weak buses in the typical existing distribution network were discovered. They are at the OLTC bus and the two buses, at the far end of the MV and LV feeders.

5) In practice, inverters/converters used with DGs and EVs/PHEVs must comply with relevant standards and regulations (e.g. IEEE-519, IEEE-929 and EN50160) in order to ensure that harmonics produced are within acceptable limits. Therefore, typical filter (passive or active) devices are usually integrated into the inverter/converter in order to reduce the harmonics generated. Due to this, manufactures claim that harmonics generated will not cause problems for the distribution network. However, analysis conducted in this research showed that the

combination of DG inverters (operating at less than 10 percent of rating) and EVs/PHEVs (operating in charging mode with low charge batteries) can produce noticeable harmonic distortion in the network. This is due to variation of the duty cycle (or modulation) of MPPT of the inverter as it is necessary to optimise the output power of the inverter.

6) New controllers for active control distribution networks, namely SOLTC, SEVGC, SCP, SES and SLC are proposed. Mathematical and computer models of these controllers that are suitable for investigation of voltage/harmonic profiles were developed, as described in chapter 6. The Boolean logical operator was used because it can specify networks directly and produce a simple set of control rules for a dynamic system. Therefore, the proposed controllers could be operated with a more precise description of their performance without having learning algorithms, as well as the logical operators being available in the current market. The effectiveness of the proposed solutions was examined showing that the SDSM technique and smart control devices would assist and preserve the voltage profiles in future power networks within acceptable limits. The analysis conducted showed that the penetration levels of SSDGs and EVs/PHEVs can be increased by at least 10 and 15 percent in the UK and TH networks, respectively. The increase depends on the capacity of the SCP and the SES available in the network in addition to the response time, location and capacity of the smart controllers/devices. It can be noted that historical data of demand and generation profiles allow the maximum/minimum of supply/demand to be predicted and suitable size and location of smart controllers determined.

7) The study of islanding operation showed that smart controllers are essential if the power network is to operate in islanded mode and maintain an acceptable quality of supply. The network operator needs to assign the load priority in the network, where the SLC is automatically controlled for connection/disconnection of the load in the islanded network. The results obtained show that by using the SDSM technique and smart control devices (explained in section 7.3), the voltage profiles in the islanded network remain within the statutory limits (assuming that enough generation is available in the islanded network).

8) The computer modelling tool (PSmartDN Tool) developed, (based on MS Excel and MATLAB/Simulink programs) allows investigation of the daily profiles of voltage, active power and reactive power of MV/LV distribution networks. This tool also supports SSDGs, EVs/PHEVs and smart controllers, allowing investigation of their impacts on future power networks. Dynamic input/output data for each bus were considered, as described in chapter 8.

In summary, large deployment of green technologies in power networks without appropriate control and demand side management lead to potential problems with regard to voltage levels and harmonic distortion. In order to match supply and demand in future power networks, smart controllers are required. Therefore, this thesis proposes the SDSM technique incorporating smart controllers (namely SOLTC, SCP, SES, SEVGC and SLC) to effectively control the power flow and improves the quality of supply. These controllers can provide support for distribution networks in the short and long term and therefore support high penetration levels of green technologies such as SSDGs and EVs, as shown in chapter 7.

The proposed controllers can operate either in independent mode or in incorporated mode with other smart controllers in that local area. Therefore, a central controller could be used to monitor the system or coordinate the operation of the smart controllers. The two main keys for successful implementation are advanced ICT systems and smart control devices, which use smart meters to communicate in the local area of the distribution network. Accordingly, the smart meter must have a two-way communication link, and hence allow updating of the local signal to the local central data bank or the local devices. This allows the smart controllers to support the local area (self-healing) with fast response. These proposed controllers also allow both electricity providers and consumers to use dynamic electricity tariff to import/export their power. Other advantages of the proposed controllers is that they use a well established technologies (e.g. power electronics, microcontrollers, ICT) and can be easily implemented to manage power flow in existing and future power networks. The proposed solutions could be used as an alternative to network reinforcement, which can be very expensive. Figure 9.1 shows the hierarchy of the proposed controllers in future power networks and Table 9.1 summarises the function and benefits of each smart controllers.

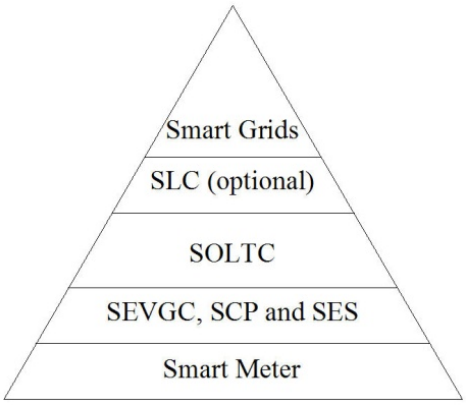

Figure 9.1 Smart controllers in future power networks

Table 9.1: Summary of smart control devices

Devices	Description	Remark
Smart meters	Acquire local data at consumer level in real-time (such as voltage, power factor, active/reactive power, harmonics, kWh, location, etc.) and directly communicate to either the central control or other local devices. They implement two-way communication link, which is essential for the control of future power networks.	Supports all consumer and network operator levels.
Smart EVs Grid Connection (SEVGC)	Encourage the vehicle owner to plug in their vehicle to support the network by using a suitable charging/regenerating tariff. The SEVGC automatically requests the support from other smart devices (here e.g. SCP and SES), if the consumer needs to plug in the vehicle when the voltage is outside the limits.	Supports all consumers and network operators, especially at the commercial level.
Smart EVs/PHEVs Car Park (SCP) and Smart Energy Storage system (SES)	The SCP aims to optimise the voltage profiles in the network by managing the charging/regenerating time of EVs/PHEVs in the car park. The SES helps the network provider to improve the network reliability by supply/demand balancing. Both devices can communicate and support other smart devices.	Supports all consumers using three-phase system and network operators, especially at the commercial level.
Smart On-Load Tap Changer transformer (SOLTC)	The SOLTC maintains the voltage profiles within the acceptable limits by implementing active network control where two voltage control signals (local bus and at the furthest bus that available at that time) are used to control the SOLTC. This control is necessary for the future power network where this device is used together with the other smart controllers to allow high penetration of SSDGs and EVs/PHEVs accommodated in the network.	Suitable for network operators.
Smart Load Controller (SLC)	This device is used to connect/disconnect unessential loads (bases on load priority) to assist in system voltage and frequency control. In order to provide effective support, this controller must communicate with other smart controllers, particularly when operating in islanded network.	Suitable for network operators.
Smart Grids or Smart Network	The power network has the Self-Monitoring, Analysis and Reporting Technology (SMART) in order to automate management of power flow within acceptable levels, consider safety and satisfy the demands of consumers and suppliers. Here, the uses of SOLTC, SEVGC, SCP, SES and SLC (in case islanded network) are considered.	Support future power network, especially MV/LV level.

9.2 Future Work

Develop practical modules (hardware) for each smart controller and evaluate their performance in a small distribution network under realistic scenarios for both the UK and TH. In addition, the PSmartDN Tool could be further developed to enable more detailed investigation of distribution network, including islanded networks. The investigation could include unbalanced operation, protection coordination, harmonic profiles, etc.

Another work that would be useful for investigation of future power networks is development of computer models for smart synchronisation and various green technologies that were out of the scope of this thesis such as geothermal, wave, tidal, etc.

REFERENCES

1. Seitz, J. L. (2002) *Global issues*. 2 edn. Massachusetts: Blackwell Publishing.
2. Schellnhuber, H. J., Cramer, W., Nakicenovic, N., Wigley, T. and Yohe, G. (2006) *Avoiding dangerous climate change*. Cambridge: Cambridge University Press.
3. International Energy Agency. (2009) *CO_2 emissions from fuel combustion Highlights 2009*. [Online]. Available at: http://www.iea.org/co2highlights/co2highlights.pdf (Accessed: 1 August 2010).
4. Hassmann, K. (1993) 'Electric power generation', *IEEE Journals & Magazines,* 81 (3), pp. 346-354.
5. Boyle, G. (1996) *Renewable energy: Power for a sustainable Future*. United Kingdom: Oxford University Press.
6. International Energy Agency (2010) *Key world energy statistics.* France: International Energy Agency.
7. Department of Energy and Climate Change. (2009) *Adapting to climate change UK climate projections June 2009.* [Online]. Available at: http://www.decc.gov.uk/assets/decc/what%20we%20do/global%20climate%20change%20and%20energy/tackling%20climate%20change/five_point_plan/uk-climate-projections.pdf. (Accessed: 1 August 2010).
8. Renewable Energy Policy Network for the 21st Century. (2010) *Renewables global status report 2010.* [Online]. Available at: http://ren21.net/globalstatusreport/REN21_GSR_2010_full_revised%20Sept2010.pdf. (Accessed: 1 October 2010)
9. Renewable Energy Policy Network for the 21st Century. (2009) *Renewables global status report 2009 updated.* [Online]. Available at: http://www.ren21.net/pdf/RE_GSR_2009_update.pdf. (Accessed: 1 August 2010).
10. Department of Energy and Climate Change. (2009) *National renewable energy action plan for the United Kingdom article 4 of the renewable energy directive 2009/28/EC.* [Online]. Available at: http://www.decc.gov.uk/assets/decc/what%20we%20do/uk%20energy%20supply/energy%20mix/renewable%20energy/ored/25-nat-ren-energy-action-plan.pdf. (Accessed: 1 August 2010).

11. Department of Energy and Climate Change. (2006) *Our energy challenge power from the people.* [Online]. Available at: http://www.decc.gov.uk/assets/decc/what%20we%20do/global%20climate%20change%20and%20energy/tackling%20climate%20change/five_point_plan/uk-climate-projections.pdf. (Accessed: 1 August 2010)
12. Department of Energy and Climate Change. (2010) *2050 pathways analysis July 2010.* [Online]. Available at: http://www.decc.gov.uk/assets/decc/What%20we%20do/A%20low%20carbon%20UK/2050/216-2050-pathways-analysis-report.pdf. (Accessed: 1 August 2010).
13. Mott MacDonald. (2004) *System integration of additional micro-generation (SIAM) (DG/CG/00028/REP)*. UK: Department of Trade and Industry (DTI) & OFGEM.
14. Department of Energy and Climate Change. (2010) *Small scale onsite energy generation.* [Online]. Available at: http://www.decc.gov.uk/en/content/cms/what_we_do/uk_supply/energy_mix/renewable/explained/microgen/microgen.aspx. (Accessed: 1 August 2010).
15. Energy Networks Association (ENA). (2010) *Recommendations for the connection of generating plant to the distribution systems of licensed distribution network operators (G59/2).* UK: ENA.
16. Energy Networks Association (ENA). (2008) *Recommendations for the connection of small-scale embedded generators (up to 16A per phase) in parallel with public low-voltage distribution networks (G83/1-1).* UK: ENA.
17. Metropolitan Electricity Authority of Thailand. (2010) *Very small power producer (VSPP) standard for MEA, Thailand.* Bangkok: MEA Press.
18. Chan, E. H. P., Delson, M. G., Green, J. L. and Nash, C. L. (1983) 'A coordinated state wide load management and scada System', *Power Apparatus and Systems, IEEE Transactions on Power Apparatus and Systems,* PAS-102 (11), pp. 3496-3501.
19. Hauser, C. H., Bakken, D. E. and Bose, A. (2005) 'A failure to communicate: next generation communication requirements, technologies, and architecture for the electric power grid', *Power and Energy Magazine,* 3 (2), pp. 47-55.
20. Ackerman, W. J. and Block, W. R. (1992) 'Understanding supervisory systems', *Computer Applications in Power,* 5 (4), pp. 37-40.

21. Robert, D. A. (2004) *Network management systems for active distribution networks a feasibility study.* [Online]. Available at: http://www.ensg.gov.uk/assets/kel00310rep.pdf (Accessed: 08 October 2008).
22. Sciacca, S. C. and Block, W. R. (1995) 'Advanced SCADA concepts', *Computer Applications in Power, IEEE,* 8 (1), pp. 23-28.
23. Energy Technology Support Unit (ETSU) (2001) *Embedded generation on actively managed distribution networks (ETSU K/EL/00233/REP)* [Online]. Available at: http://webarchive.nationalarchives.gov.uk/tna/+/http://www.dti.gov.uk/renewables/publications/pdfs/KEL00233.pdf/ (Accessed: 08 October 2008).
24. Barbier, C., Maloyd, A. and Putrus, G. (2007) *Embedded controller for LV network with distributed generation (K/EL/00334/00/REP)*. UK: Department of Trade and Industry (DTI).
25. Liserre, M., Sauter, T. and Hung, J. Y. (2010) 'Future energy systems: integrating renewable energy sources into the smart power grid through industrial electronics', *Industrial Electronics Magazine,* 4 (1), pp. 18-37.
26. Chicco, G. and Mancarella, P. (2009) 'Distributed multi-generation: A comprehensive view', *Renewable and Sustainable Energy Reviews,* 13 (3), pp. 535-551.
27. Ipakchi, A. and Albuyeh, F. (2009) 'Grid of the future', *Power and Energy Magazine,* 7 (2), pp. 52-62.
28. Bumiller, G., Sauter, T., Pratl, G. and Treytl, A. (2005) 'Secure and reliable wide-area power-line communication for soft-real-time applications within REMPLI'*, Power Line Communications and Its Application, 2005 International Symposium on*, Germany 6-8 April. pp. 57-60.
29. Calderaro, V., J.V.Milanovic, M.Kayikci and A.Piccolo (2008) 'The impact of distributed synchronous generators on quality of electricity supply and transient stability of real distribution network', *Electric Power Systems Research*, pp. 1-10.
30. Gu, Y. H. and Bollen, M. H. J. (2000) 'Time-frequency and time-scale domain analysis of voltage disturbances', *IEEE Transactions on Power Delivery,* 15 (4), pp. 1279-1284.
31. Van Casteren, J. F. L., Bollen, M. H. J. and Schmieg, M. E. (2000) 'Reliability assesment in electrical power systems: the Weibull-Markov stochastic model', *IEEE Transactions on Industry Applications,* 36 (3), pp. 911-915.

32. Zhang, L. D., Bollen, M. H. J., Aller, J. M., Restrepo, J. A., Bueno, A. A., Gimenez, M. I., Guzman, V. M., Jota, P. R. S. and Islam, S. M. (1998) 'Power engineering letters', *Power Engineering Review, IEEE,* 18 (7), pp. 50-56.
33. Vale, Z., Morais, H., Faria, P., Khodr, H., Ferreira, J. and Kadar, P. (2010) 'Distributed energy resources management with cyber-physical SCADA in the context of future smart grids', *MELECON 2010 - 2010 15th IEEE Mediterranean Electrotechnical Conference.* Valletta 26-28 April 2010, pp. 431-436.
34. Lopez, R., Moore, A. and Gillerman, J. (2010) 'A model-driven approach to smart substation automation and integration for commission federal de electricidad', *2010 IEEE PES Transmission and Distribution Conference and Exposition,* New Orleans, LA, USA 19-22 April, pp. 1-8.
35. Bollen, M. H. J. and Häger, M. (2005) 'Impact of increasing penetration of distributed generation on the number of voltage dips experienced by end-customers', *18th International Conference and Exhibition on Electricity Distribution, 2005. CIRED 2005*, Turin, 6-9 June. Sweden: CIRED, pp. 1-5.
36. The Institute of Electrical and Electronics Engineers (IEEE). (2008) 'IEEE application guide for IEEE Std 1547, IEEE Standard for Interconnecting Distributed Resources with Electric Power Systems', *IEEE Std 1547.2-2008*.
37. Jensen, M.M. (2011) *Power quality in 0.4 KV grid*. Denmark: EDISON.
38. Heskes, P.J.M. and Enslin, J.H.R. (2003) 'Power quality behaviour of different photovoltaic inverter topologies', *PCIM-2003, 24th International Conference*. Nurnberg, Germany 20-23 May, pp. 1-10.
39. Bollen, M. H. J. (2000) *Understanding power quality problems: Voltage sags and interruptions*. New York: The Institute of Electrical and Electronics Engineers, IEEE Press series on power engineering.
40. The Institute of Electrical and Electronics Engineers (IEEE). (1993) 'IEEE recommended practices and requirements for harmonic control in electrical power systems', *IEEE Std 519-1992 (Revision of IEEE Std 519-1981)*.
41. European Committee for Electrotechnical Standardization (CENELEC). (2004) *Standard EN 50160: Voltage characteristics in public distribution systems (EN Std 50160)*.
42. McDermott, T. E. and Dugan, R. C. (2003) 'PQ, reliability and DG', *Industry Applications Magazine,* 9 (5), pp. 17-23.
43. Arrillaga, J., Bollen, M. H. J. & Watson, N. R. (2000) 'Power quality following deregulation', *Proceedings of the IEEE,* 88 (2), pp. 246-261.

44. Bollen, M. H. J. and Gu, I. Y. H. (2005) 'Characterization of voltage variation in the very-short time-scale', *IEEE Transactions on Power Delivery,* 20 (2), pp. 1198-1199.
45. The Institute of Electrical and Electronics Engineers (IEEE). (2009) *IEEE recommended practice for monitoring electric power quality (IEEE Std 1159-2009) (Revision of IEEE Std 1159-1995)*.
46. The Institute of Electrical and Electronics Engineers (IEEE). (2000) *IEEE recommended practice for utility interface of photovoltaic (PV) systems (IEEE Std 929-2000) (Revision of IEEE Std 929-1988)*.
47. European Committee for Electrotechnical Standardization (CENELEC). (2010) *Voltage characteristics of electricity supplied by public distortion system (EN50160)*.
48. Sontidpanya, C., Radman, G. and Craven, R. (2011) 'An island detection demonstration on a laboratory sized power Grid (LabGrid)', *2011 Proceedings of IEEE Southeastcon*, Nashville, TN 17-20 March. USA: Tennessee Tech University, pp. 158-163.
49. Friedl, W., Fickert, L., Schmautzer, E. and Obkircher, C. (2009) 'Safety and reliability for smart, micro-and islanded grids', *20th International Conference on Electricity Distribution*, Prague 8-11 June. Austria: Graz University of Technology, pp. 1-4.
50. Conti, S., Raiti, S. and Tina, G. (2003) 'Small-scale embedded generation effect on voltage profile: an analytical method', *Generation, Transmission and Distribution,* 150 (1), pp. 78-86.
51. Dugan, R. C., Beaty, H. W. and McGranaghan, M. F. (1996) *Electrical power systems quality*. New York: McGraw-Hill.
52. Hadjsaid, N., Canard, J. F. and Dumas, F. (1999) 'Dispersed generation impact on distribution networks', *Computer Applications in Power,* 12 (2), pp. 23-28.
53. Jerkins, N. (2000) *Embedded generation*. London: Institution of Electrical Engineers, IEE power and energy series; 31.
54. Barker, P. P. and De Mello, R. W. (2000) 'Determining the impact of distributed generation on power systems: Part 1-Radial distribution systems', *Power Engineering Society The summer Meeting, 2000,* Seattle, WA, USA 16-20 July, pp. 1645-1656.

55. Girgis, A. and Brahma, S. (2001) ‘Effect of distributed generation on protective device coordination in distribution system’ *2001 Large Engineering Systems Conference on Power Engineering, 2001. LESCOPE '01*, Halifax, NS 2001. SC: Clemson University, pp. 115-119.
56. Masters, C. L. (2002) ‘Voltage rise: the big issue when connecting embedded generation to long 11 kV overhead lines’, *Power Engineering Journal,* 16 (1), pp. 5-12.
57. Walling, R. A., Saint, R., Dugan, R. C., Burke, J. and Kojovic, L. A. (2008) ‘Summary of distributed resources impact on power delivery systems’, *IEEE Transactions on Power Delivery,* 23 (3), pp. 1636-1644.
58. Persaud, S., Fox, B. and Flynn, D. (2003) 'Effects of large scale wind power on total system variability and operation: Case study of Northern Ireland', *Wind Engineering*, 27(1), pp. 3-20.
59. Pandiaraj, K., Fox, B., Morrow, D.J., Persaud, S. and Martin, J.P. (2002) 'Centralised control of diesel gen-sets for peak shaving and system support', *Transmission and Distribution*, 149 (2), pp. 126-132.
60. Persaud, S., Fox, B. and Flynn, D. (2000) 'Impact of remotely connected wind turbines on steady state operation of radial distribution networks', *Transmission and Distribution*, 147 (3), pp. 157-163.
61. Jayaweera, D., Burt, G. and McDonald, J. (2007) ‘Customer security assessment in distribution networks with high penetration of wind power’, *IEEE Transactions on Power Systems,* 22 (3), pp. 1360-1368.
62. Quezada, V. H. M., Abbad, J. R. and Roman, T. G. S. (2006) ‘Assessment of energy distribution losses for increasing penetration of distributed generation, *IEEE Transactions on Power Systems,* 21 (2), pp. 533-540.
63. Dent, C. J., Ochoa, L. F. and Harrison, G. P. (2010) ‘Network distributed generation capacity analysis using OPF with voltage step constraints’, *IEEE Transactions on Power Systems,* 25 (1), pp. 296-304.
64. Harrison, G. P. and Wallace, A. R. (2005) ‘Optimal power flow evaluation of distribution network capacity for the connection of distributed generation’, *IEEE Proceedings-Generation, Transmission and Distribution,* 152 (1), pp. 115-122.
65. Electricity Networks Association (ENA). (1989) *Planning limits for voltage fluctuations caused by industrial, engineering recommendation P28.*

66. Durairaj, S. and Fox, B. (2008) 'Optimal power flow under variable wind generation', *International Journal of Energy and Policy*, 6(5/6), pp. 608-620.
67. Meegahapola, L., Durairaj, S., Flynn, D. and Fox, B. (2010) 'Coordinated utilisation of wind farm reactive power capability for system loss optimisation', *European Transactions on Electrical Power*, 21, pp. 40-51.
68. Jovanovic, S., Hogg, B.W. and Fox, B. (1995) 'Intelligent adaptive turbine controller', *IEEE Transactions on Energy Conversion*, 10(1), pp. 195-198.
69. Brooks, D. L., Dugan, R. C., Waclawiak, M. and Sundaram, A. (1998) 'Indices for assessing utility distribution system RMS variation performance', *Power Delivery, IEEE Transactions on,* 13 (1), pp. 254-259.
70. Kiprakis, A. E. and Wallace, A. R. (2004) 'Maximising energy capture from distributed generators in weak networks', *IEE Proceedings-Generation, Transmission and Distribution,* 151 (5), pp. 611-618.
71. Cong, L. and Wang, Y. (2002) 'Co-ordinated control of generator excitation and STATCOM for rotor angle stability and voltage regulation enhancement of power systems', *IEE Proceedings-Generation, Transmission and Distribution,* 149 (6), pp. 659-666.
72. Khargonekar, P. P., Petersen, I. R. and Zhou, K. (1990) 'Robust stabilization of uncertain linear systems: quadratic stabilizability and H^{∞} control theory', *IEEE Transactions on Automatic Control,* 35 (3), pp. 356-361.
73. Wang, Y., Zhou, R. and Wen, C. (1993) 'Robust load-frequency controller design for power systems', *IEE Proceedings C,* 140 (1), pp. 11-16.
74. Kong, W., Dong, X. and Chen, Z. (2008) 'Voltage sag source location based on instantaneous energy detection', *Electric Power Systems Research,* 78 (11), pp. 1889-1898.
75. Qader, M. R., Bollen, M. H. J. and Allan, R. N. (1999) 'Stochastic prediction of voltage sags in a large transmission system', *IEEE Transactions on Industry Applications,* 35 (1), pp. 152-162.
76. Bollen, M. H. J. (1996) 'Fast assessment methods for voltage sags in distribution systems', *IEEE Transactions on Industry Applications,* 32 (6), pp. 1414-1423.
77. Gu, I. Y. H. and Bollen, M. H. J. (2008) 'Estimating interharmonics by using sliding-window ESPRIT', *IEEE Transactions on Power Delivery,* 23 (1), pp. 13-23.

78. Filho, J. M. C., Leborgne, R. C., de Abreu, J. P. G., Novaes, E. G. C. and Bollen, M. H. J. (2008) 'Validation of voltage sag simulation tools: ATP and short-circuit calculation versus field measurements', *IEEE Transactions on Power Delivery,* 23 (3), pp. 1472-1480.
79. De Brabandere, K., Bolsens, B., Van den Keybus, J., Woyte, A., Driesen, J. and Belmans, R. (2007) 'A voltage and frequency droop control method for parallel inverters', *IEEE Transactions on Power Electronics,* 22 (4), pp. 1107-1115.
80. Il-Yop, C., Sung-Woo, P., Hee-Jung, K., Seung-Il, M., Byung-Moon, H., Jae-Eon, K. and Joon-Ho, C. (2005) 'Operating strategy and control scheme of premium power supply interconnected with electric power systems', *IEEE Transactions on Power Delivery,* 20 (3), pp. 2281-2288.
81. Demoulias, C. S. and Dokopoulos, P. (1996) 'Electrical transients of wind turbines in a small power grid', *IEEE transactions on Energy conversion,* 11 (3), pp. 636-642.
82. Wang, P., Jenkins, N. and Bollen, M. H. J. (1998) 'Experimental investigation of voltage sag mitigation by an advanced static VAr compensator', *IEEE Transactions on Power Delivery,* 13 (4), pp. 1461-1467.
83. Riezenman, M. J. (1998) 'Engineering the EV future', *IEEE Spectrum*, 35(11), pp. 18-20.
84. Reizenman, M. J. and Wouk, V. (1998) 'EVs: The road ahead', *IEEE Spectrum,* 35 (12), pp. 42-51.
85. Salihi, J. T. (1972) 'Two for the road', *IEEE Spectrum,* 9 (7), pp. 43-47.
86. Salihi, J. T. (1972) 'The electric car-fact and fancy', *IEEE Spectrum,* 9 (6), pp. 44-48.
87. Cook, E. (1971) 'The flow of energy in industrial society', *Scientific American*, pp. 135-143 [Online]. Available at: http://www.greentechhistory.com/wp-content/uploads/2009/11/reading-1a-flow-of-energy-ind-soc_sciam1971.pdf (Accessed: 08 October 2008).
88. Putrus, G. A., Suwanapingkarl, P., Johnston, D., Bentley, E. C. and Narayana, M. (2009) 'Impact of electric vehicles on power distribution networks*', IEEE Vehicle Power and Propulsion Conference, 2009. VPPC '09.* Dearborn, MI 7-10 September, pp. 827-831.

89. Koyanagi, F., Inuzuka, T., Uriu, Y. and Yokoyama, R. (1999) ‘Monte Carlo simulation on the demand impact by quick chargers for electric vehicles’, *IEEE Power Engineering Society The summer Meeting,* Edmonton, Alta., Canada 18-22 July, pp. 1031-1036.
90. Salihi, J. T. (1973) ‘Energy requirements for electric cars and their impact on electric power generation and distribution systems’, *IEEE Transactions on Industry Applications,* IA-9 (5), pp. 516-532.
91. Johnston, D., Bentley, E., Narayana, M., Jiang, T., Suwanapingkarl, P. and Putrus, G. (2010) ‘Electric vehicles as storage devices for supply-demand management’, *IEEE Vehicle power and propulsion conference: clean tech for transportation*. Lille, France 1-3 September.
92. Caldon, R., Stocco, A. and Turri, R. (2008) 'Feasibility of adaptive intentional islanding operation of electric utility systems with distributed generation', *Electric Power Systems Research,* 78 (12), pp. 2017-2023.
93. Stephen, D. (1994) *Independent generation of electric power*. Oxford: Butterworth-Heinemann.
94. Wildi, T. o. (2006) *Electrical machines, drives, and power systems*. 6 edn. Upper Saddle River, N.J.: Prentice Hall.
95. Econnect Ltd. (2005) *Island operation of distribution networks.* International Energy Agency [Online]. Available at: http://www.ensg.gov.uk/assets/dgcg00026.pdf (Accessed: 1 August 2010).
96. Northern Ireland Environment Link (2008) *Climate Change: The energy issue*. Belfast: Northern Ireland Environment Link.
97. Shang, W.T. and Redfern, M.A. (2010) ‘Enhancing the contribution from distributed generation using smart grids’, *2010 China International Conference on Electricity Distribution (CICED)*, Nanjing 13-16 September. Bath: University of Bath, pp. 1-6.
98. Mahat, P., Chen, Z., and Bak-Jensen, B. (2008), ‘Review of islanding detection methods for distributed generation’, *in Proceeding 3rd International Conference on Electric Utility Deregulation and Restructuring and Power Technologies*, 6-9 April, pp. 2743-2748.
99. Kunte, R.S., and Gao, W. (2008), ‘Comparison and review of islanding detection techniques for distributed energy resources’, *Power Symposium, NAPS '08. 40th North American*, pp.1-8, 28-30 September.

100. Costabeber, A., Tenti, P. and Mattavelli, P. (2010) ‘Surround control of distributed energy resources in micro-grids’, *2010 IEEE International Conference on Sustainable Energy Technologies (ICSET)*, Kandy 6-9 December. Padova: University of Padova, pp. 1-6.
101. Tenti, P., Costabeber, A., Trombetti, D. and Mattavelli, P. (2010) ‘Plug & play operation of distributed energy resources in micro-grids’, *32nd International Telecommunications Energy Conference (INTELEC)*, Orlando, FL, USA 6-10 June. Italy: University of Padova, pp. 1-6.
102. Vandoorn, T.L., Renders, B., Degroote, L., Meersman, B. and Vandevelde, L. (2011) ‘Active Load Control in Islanded Microgrids Based on the Grid Voltage’, *IEEE Transactions on Smart Grid*, 2 (1), pp. 139-151.
103. Best, R., Morrow, D. J., Laverty, D., and Crossley, P. (2008) ‘Universal application of synchronous islanded operation’, in *Proceeding CIRED Seminar SmartGrids Distrib.*, June, pp. 1–4.
104. Mehrizi-Sani, A. and Iravani, R. (2010) ‘Potential-function based control of a microgrid in islanded and grid-connected Modes’, *IEEE Transactions on Power Systems*, 25 (4), pp. 1883-1891.
105. Saha, A.K., Chowdhury, S., Chowdhury, S.P. and Crossley, P.A. (2008) ‘Microturbine based distributed generator in smart grid application’, *CIRED Seminar 2008: SmartGrids for Distribution*, Frankfurt 23-24 June. India: Jadavpur University, pp. 1-4.
106. Invernizzi, A. (2004) 'Transition from passive to active distribution networks: CIGRE Actions', *IEA Workshop,* [Online]. Available at: http://www.iea.org/dbtw-wpd/Textbase/work/2004/distgen/Invernizzi.pdf (Accessed: 30/09/2008).
107. Paredes, H.K.M., Costabeber, A. and Tenti, P. (2010) ‘Application of conservative power theory to cooperative control of distributed compensators in smart grids’, *2010 International School on Nonsinusoidal Currents and Compensation (ISNCC)*, Lagow 15-18 June. Campinas: University of Campinas, pp. 190-196.
108. Mitra, J. and Suryanarayanan, S. (2010) ‘System analytics for smart microgrids’, *2010 IEEE Power and Energy Society General Meeting*, Minneapolis, MN 25-29 July. USA: Michigan State University, pp. 1-4.
109. Best, R.J., Morrow, D.J., Laverty, D.M. and Crossley, P.A. (2011) ‘Techniques for multiple-set synchronous islanding control’, *IEEE Transactions on Smart Grid*, 2 (1), pp. 60-67.

110. Laverty, D. M., Morrow, D. J., Best, R. J., and Crossley, P. A. (2009) 'Differential ROCOF relay for loss-of-mains protection of renewable generation using phasor measurement over internet protocol', in *Proceeding CIGRE/IEEE Joint Symp.*, Calgary, AB, Canada, July, pp. 1–7.
111. Mohamad, H., Bakar, A.H.A., Ping, H.W. and Mokhlis, H. (2010) 'An adaptive controller of hydro generators for smart grid application in Malaysia', *2010 International Conference on Power System Technology (POWERCON)*, Hangzhou 24-28 October, pp. 1-6.
112. Bollen, M. H. J. and Häger, M. (2005) 'Power quality: integrations between distributed energy resources, the grid, and the other customers', *Electrical power quality and utilization magazine,* 1 (1), pp. 51-61.
113. Bollen, M. (2007) 'Power quality and reliability impacts of distributed generation', *2007 Institution of Engineering and Technology Seminar on Reducing the Carbon Footprint in the Built Environment,* London, UK 12-12 December. pp. 1-96.
114. Schlabbach, J., Stephanblome, T. and Blume, D. (2001) *Voltage quality in electrical power system*. london: Institution of Electrical Engineers, IEE power and energy series.
115. Masters, G.M. (2004). *Renewable and efficient electric power system*. John Wiley & Sons, Inc.: United States of America.
116. Spagnuolo, G., Petrone, G., Araujo, S. V., Cecati, C., Friis-Madsen, E., Gubia, E., Hissel, D., Jasinski, M., Knapp, W., Liserre, M., Rodriguez, P., Teodorescu, R. and Zacharias, P. (2010) 'Renewable energy operation and conversion schemes: A summary of discussions during the seminar on renewable energy systems', *IEEE Industrial Electronics Magazine,* 4 (1), pp. 38-51.
117. Fauvette, X., Rombaut, C., Le Moigne, P. and Castelain, A. (1994) 'Battery charger with unity power factor for electric car', *Power Electronics and Variable-Speed Drives, London, UK* 26-28 October 1994*, pp. 568-573.*
118. Berisha, S. H., Karady, G. G., Ahmad, R., Hobbs, R. and Karner, D. (1996) 'Current harmonics generated by electric vehicle battery chargers' *Proceedings of the 1996 International Conference on Power Electronics, Drives and Energy Systems for Industrial Growth,* New Delhi 8-11 January. Phoenix: GateWay Community College, pp. 584-589.

119. Buckle, K. A. ad Luce, J. W. (1996) 'Battery vehicle charger design eliminates harmonic current generation', *Proceedings of the IEEE Southeast on '96. 'Bringing Together Education, Science and Technology,* Tampa, FL, USA 11-14 April, pp. 561–564.
120. Wang, Y. J., O'Connell, R. M. and Brownfield, G. (2001) 'Modeling and prediction of distribution system voltage distortion caused by nonlinear residential loads', *IEEE Transactions on Power Delivery,* 16 (4), pp. 744-751.
121. Bentley, E.C., Suwanapingkarl, P., Weerasinghe, S., Jiang, T., Putrus, G. A. and Johnston, D. (2010) 'The interactive effects of multiple EV chargers within a distribution network', *IEEE Vehicle power and propulsion conference: clean tech for transportation*. Lille, France 1-3 September.
122. Orr, J. A., Emanuel, A. E. and Pileggi, D. G. (1982) 'Current harmonics, voltage distortion, and powers associated with battery chargers part I: comparisons among different types of chargers', *IEEE Transactions on Power Apparatus and Systems,* PAS-101 (8), pp. 2703-2710.
123. Lo, E. W. C., Sustanto, D. and Fok, C. C. (1999) 'Harmonic load flow study for electric vehicle chargers'*, IEEE 1999 International Conference on Power Electronics and Drive Systems, PEDS '99*, July, pp. 495-500.
124. Chan, M. S. W., Chau, K. T. and Chan, C. C. (1998) 'Modeling of electric vehicle chargers', *Proceedings of the 24th Annual Conference of the IEEE Industrial Electronics Society, IECON '98,* Aachen, Germany 31 August-4 September, pp. 433-438.
125. Lu, Y. and Jiang, J. (2005) 'Harmonic-study of electric vehicle chargers', *Proceedings of the Eighth International Conference on Electrical Machines and Systems, ICEMS 2005,* 27-29 September, pp. 2404-2407.
126. Orr, J. A., Emanuel, A. E. and Pileggi, D. J. (1984) 'Current harmonics, voltage distortion, and powers associated with electric vehicle battery chargers distributed on the residential power system', *IEEE Transactions on Industry Applications,* IA-20 (4), pp. 727-734.
127. Staats, P. T., Grady, W. M., Arapostathis, A. and Thallam, R. S. (1997) 'A statistical method for predicting the net harmonic currents generated by a concentration of electric vehicle battery chargers', *IEEE Transactions on Power Delivery,* 13 (2), pp. 1258-1266.
128. Orr, J. A., Emanuel, A. E. and Oberg, K. W. (1982) 'Current harmonics generated by a cluster of electric vehicle battery chargers', *IEEE Transactions on Power Apparatus and Systems,* PAS-101 (3), pp. 691-700.

129. Bass, R., Harley, R., Lambert, F., Rajasekaran, V. and Pierce, J. (2001) 'Residential harmonic loads and EV charging', *IEEE Power Engineering Society The winter Meeting,* Columbus, OH, USA 28 January-01 February, pp. 803-808.
130. Staats, P. T., Grady, W. M., Arapostathis, A. and Thallam, R. S. (1997) 'A procedure for derating a substation transformer in the presence of widespread electric vehicle battery charging', *IEEE Transactions on Power Delivery,* 12 (4), pp. 1562-1568.
131. Staats, P. T., Grady, W. M., Arapostathis, A. and Thallam, R. S. (1997) 'A statistical method for predicting the net harmonic currents generated by a concentration of electric vehicle battery chargers', *IEEE Transactions on Power Delivery,* 12 (3), pp. 1258-1266.
132. Department for Transport (DFT) (2011) *National travel survey: 2010 Trips in progress by time of day of week - index: Great Britain, 2010*. UK.
133. United Kingdom Generic Distribution System (UKGDS). (2010) *Generation profiles of UK GDS at 24h x 0.5h mix*.
134. Narec Company. (2011) *Wind profiles of Northeast UK*.
135. The Royal Borough of Kensington and Chelsea (2011) *Electric vehicles parking and charging*. Available at: http://www.rbkc.gov.uk/environmentandtransport/parking/electricvehicleparking.aspx (Accessed: 24 June 2011).
136. Ministry of Transport (MOT) (2010) *National travel survey: 2010 Trips in progress by time of day of week - index: Bangkok, 2010*. Thailand: Ministry of Transport.
137. Thai Meteorological Department (2011) *Environmental profiles in Thailand*, Thailand: Thai Meteorological Department
138. Slootweg. J.G., de Haan, S.W.H, Polinder, H. And Kling, W.L. (2001) 'Modeling wind turbines in power system dynamics simulations', Power Engineering Society The summer Meeeting, 1, pp. 22-26.
139. Häberlin, H., Borgna, L., Kaempfer, M. and Zwahlen, U. (2005) 'Total Efficiency η_{tot}–A new quantity for better characteristic of grid connected PV inverters', *Proceedings of 20th European Photovoltaic Solar Energy Conference*, Barcelona, Spain, June.

140. Häberlin, H. and Borgna, L. (2004) 'A new approach for semi-automated measurement of PV inverters especially MPP tracking efficiency, using a linear PV array simulator with high stability', *Proceedings 19th EU PV Conference*, Paris.
141. Islam, S., Woyte, A., Belmans, R. and Nijs, J. (2002) 'Undersizing inverters for grid connection – What is the optimum?', *PV in Europe*, Rome, Italy, 7-11 October, pp. 780-783.
142. Biczel, P. and Michalski, L. (2009) 'Simulink models of power electronic converters for DC microgrid simulation', *Compatibility and Power Electronics (CPE'09)*, Badajoz, Spain, 20-22 May, pp. 161-165.
143. Biczel, P. and Koniak, M. (2009) 'Design of power plant capacity in DC hybrid system and microgrid', *Ecologic vehicles renewable energies*, Monaco 26-29 March. Poland: Institute of Electrical Power Engineering.
144. Hydro-Québec and TransÉnergie Technologies. (2010) *SimPowerSystems User's Guide For Use with Simulink R2010a*.
145. Go Solar California. (2011) *Inverter performance test summaries*. Available at: http://www.gosolarcalifornia.org/equipment/inverter_tests/summaries/ (Accessed: 24 May 2011).
146. SMA Solar Technology (2011) Datasheet WINDYBOY 5000-US/6000-US/7000-US/8000-US the customized solution for wind turbine systems. Available at: http://files.sma.de/dl/10148/WB5678000US-DUS103816W.pdf (Accessed: 13 June 2011).
147. Fluke Corporation Users manual Fluke 114, 115 and 117 True-rms multimeters. USA: Fluke Corporation.
148. TT electronics (2011) Ultra low profile power resistors. Available at: http://www.welwyn-tt.com/pdf/datasheet/WDBR.PDF (Accessed: 13 June 2011).
149. Dumitru, C.D. and Gligor, A. (2008) 'Software development for analysis of soalr-wind hybrid systems supplying local distribution networks', *2nd International Conference on Modern Power systems (MPS 2008)*, Cluj-Napoca, Romania, 12-14 November, pp. 220-223.
150. Bică, D., Dumitru, C.D., Gligor, A. and Duka, A.V. (2011) Isolated hybrid solar-wind-hydro renewable energy systems. *Intech* [Online]. Available at: http://www.intechopen.com/books/renewable-energy (Accessed: 12 August 2011).

151. Altas, I.H. and Sharaf, A.M. (2007) 'A photovoltaic array simulation model for Matlab-Simulink GUI environment', International Conference on Clean Electrical Power (ICCEP'07), Capri 21-23 May.
152. Nema, R.K., Nema, S. and Agnihotri, G. (2009) 'Computer simulation based study of photovoltaic cells/modules and their experimental verification', International Journal of Recent Trends in Engineering, 1(3), pp. 152-156.
153. Walker, G. (2001) 'Evaluating MPPT converter topologies using a Matlab PV model', Dept of Computer Science and Electrical Engineering, 21(1), pp. 49-55.
154. Longatt, F.M.G. (2005) 'Model of photovoltaic module in MATLAB', 2Do congreso iberoamericano de estudiantes de ingenieria electrica, electrica y computacion (II CIBELEC 2005), Puerto La Cruz, Venezuela 3-7 April.
155. Adamo, F., Attivissimo, F., Nisio, A.D., Lanzolla, A.M.L. and Spadavecchia, M. (2009) 'Parameters estimation for a model of photovoltaic panels', XIX IMEKO World Congress Fundamental and Applied Metrology, Lisbon, Portugal, 6-11 September.
156. Salazar, J., Tadeo, F., Prada, C. and Palacin, L. (2010) 'Simulation and control of a PV system connected to a low voltage network', XXXI Jornadas de automatica, Jaen, Spain, 8-10 September.
157. Petreus, D., Farcas, C. and Ciocan, I. (2008) 'Modelling and simulation of photovoltaic cells', Electronics and Telecommunications, 49(1), pp. 42-47.
158. Skočil, T. and Donsión, M.P. (2008) 'Mathematical modeling and simulation of photovoltaic array', International Conference on Renewable Energy and Power Quality (ICREPQ'08), Santander, Spain 12-14 March.
159. Lorenzo, E. (1994) *Solar electricity engineering of photovoltaic systems*. Spain: PROGENSA.
160. Luque, A. and Hegedus, S. (ed.) (2010) *Handbook of photovoltaic science and engineering*. 2nd edn. Great Britain: John Wiley & Sons Ltd.
161. Hall, R.N. (1981) 'Silicon photovoltaic cells', Solid-State Electronics, 24, pp. 595-616.
162. Xiao, W., Dunford, W.G. and Capel, A. (2004) 'A novel modeling method for photovoltaic cells', 35th Annual IEEE Power Electronics Specialists Conference, Aachen, Germany 2004.
163. Rosell, J.I. and Ibanez, M. (2006) 'Modelling power output in photovoltaic modules for outdoor operating conditions', Energy Conversion and Management, 47, pp. 2424-2430.

164. Villalva, M. G., Gazoli, J.R. and Filho, E.R. (2009) 'Modeling and circuit-based simulation of photovoltaic arrays', 10th Brazilian Power Electronics Conference (COBEP), Brazil.
165. Shockley, W. and Queisser, H.J. (1961) 'Detailed balance limit of efficiency of p-n junction solar cells', Journal of Applied Physics, 32(3), pp. 510-519.
166. Ramos, H.JA., Campayo, M.J.J., Zamora, B.I., Larranaga, L.J., Zulueta, G.E. and Puelles, P.E. (2010) 'Modelling of photovoltaic module', International Conference on Renewable Energies and Power Quality (ICREPQ'10), Granada, Spain 23-25 March.
167. Houabes, M. (2010) 'PV cell 5p modeling with shunt resistance correction', EFEEA'10 International Symposium on Environment Friendly Energies in Electrical Applications, Algeria 2-4 November.
168. Mitroi, M.R., Iancu, V., Fara, L. and Ciurea, M.L. (2010) 'Numerical analysis of J-V characteristics of a polymer solar cell', Prog. Photovolt: Res. Appl., Wiley InterScience.
169. Green, M.A. (1977) 'General solar cell curve factors including the effects of ideality factor, temperature and series resistance', Solid-State Electronics, 20, pp. 265-266.
170. Pulfrey, D.L. (1978) 'On the fill factor of solar cells', Solid-State Electronics, 21, pp. 519-520.
171. Singal, C.M. (1981) 'Analytical expressions for the series-resistance-dependent maximum power point and curve factor for solar cells', Solar Cells, 3, pp. 163-177.
172. Green, M.A. (1981) 'Solar cell fill factors: general graph and empirical expressions', Solid-State Electronics, 24(8), pp. 788-789.
173. Araujo,G.L. and Sanchez, E. (2003) 'Analytical expressions for the determination of the maximum power point and the fill factor of a solar cell', Solar Cells, 5, pp. 377-386.
174. Vos, A.D. (1983) 'The fill factor of a solar cell from a mathematical point of view', Solar Cells, 8, pp. 283-296.
175. Quanxi, J. and Enke, L. (1987) 'A method for the direct measurement of the solar cell junction ideality factor', Solar Cells, 22, pp. 15-21.
176. Green, M.A. (1982) Solar cells: operating principles, technology, and system applications. Englewood Cliffs: Prentice-Hall.
177. Wenham, S.R., Green, M.A., Watt, M.E. and Corkish, R. (2007) Applied photovoltaics. UK: TJ International Ltd.

178. Messenger, R.A. and Ventre, J. (2005) Photovoltaic systems engineering. 2nd edn. CRC press: Florida.
179. Shahat, A.E. (2010) 'PV cell module modeling & ANN simulation for smart grid applications', Journal of Theoretical and Applied Information Technology, pp. 9-20.
180. PVeducation (2010) Ideality factor. Available at: http://pvcdrom.pveducation.org/index.html (Accessed: 24 June 2010).
181. Tsai, H.L., Tu, C.S. and Su, Y.J. (2008) 'Development of generalized photovoltaic model using Matlab/Simulink', Proceeding of the world congress on engineering and computer science. San Francisco, USA 22-24 October.
182. Tsai, H.L. (2010) 'Insolation-oriented model of photovoltaic module using Matlab/Simulink', Solar Energy, 84, pp. 1318-1326.
183. Swaleh, M.S. and Green, M.A. (2003) 'Effect of shunt resistance and bypass diodes on the shadow tolerance of solar cell modules', Solar Cells, 5, pp. 183-198.
184. Jr. Ross, R.G. and Smokler, M.I. (1986) Flat-plate solar array project final report. California: Jet Propulsion Laboratory.
185. Ishengoma, F.M. and Norum, L.E. (2002) 'Design and implementation of a digitally controlled stand-alone photovoltaic power supply', Nordic Workshop on Power and Industrial Electronics. Norwegian University of Science and Technology, Norway 12-14 August 2002. Norwegian University of Science and Technology. Available at: http://www.elkraft.ntnu.no/eno/Papers2002/Design-and-impl-norpie02.pdf (Accessed: 10 June 2010).
186. Malik, A.Q. and Damit, S.J.B.H. (2003) 'Outdoor testing of single crystal silicon solar cells', Renewable Energy, 28, pp. 1433-1445.
187. Odeh, N., Grassie, T., Henderson, D. and Muneer, T. (2006) 'Modelling of flow rate in a photovoltaic-driven roof slate-based solar ventilation air preheating system', Energy Conversion and Management, 47, pp. 909-925.
188. Perpinan, O., Lorenzo, E. and Castro, M.A. (2007). 'On the calculation of energy produced by a PV grid-connected system', 15, pp. 265-274.
189. Mattei, M., Notton, G., Cristofari, C., Muselli, M. and Poggi, P. (2006) 'Calculation of the polycrystalline PV module temperature using a simple method of energy balance', Renewable Energy, 31, pp. 553-567.
190. Fuentes, M.K. (1987) A simplified thermal model for flat-plate photovoltaic arrays. United States of America: Sandia National Laboratories.

191. Skoplaki, E. and Palyvos, J.A. (2009) 'Operating temperature of photovoltaic modules: A survey of pertinent correlations', Renewable Energy, 34, pp. 23-29.
192. Nordmann, T. and Clavadetscher, L. (2003) 'Understanding temperature effects on PV system performance', 3rd World Conference on Photovoltaic Energy Conversion, Osaka, Japan May 11-18, 2003. TNC Consulting AG. Available at: http://www.iea-pvps-task2.org/public/download/OSAKA7PB314.pdf (Accessed: 10 June 2010).
193. King, D. L. (1997) Photovoltaic module and array performance characterization methods for all system operating conditions. [Online]. Available at: http://photovoltaics.sandia.gov/docs/PDF/KINGREL.PDF (Accessed: 10 June 2010).
194. King, D. L., Kratochvil, J.A., Boyson, W.E. (1998) 'Field experience with a new performance characterization procedure for photovoltaic arrays', 2nd world conference and exhibition on PV solar energy conversion, Vienna, Austria July 1998. Sandia National Laboratories. Available at: http://www.mauisolarsoftware.com/MSESC/Sandia_Model/Sandia_Model.htm (Accessed: 10 June 2010).
195. King, D. L., Boyson, W.E. and Kratochvil, J.A. (2004) Photovoltaic array performance model. New Mexico: Sandia National Laboratories.
196. Solar electric supply (2003) Bp solar. Available at: http://www.solarelectricsupply.com/pdf/BP/BP_SX5-SX10.pdf (Accessed: 2 July 2010).
197. Osram Powerstar HQI/HCI powerball HCI technical information. Available at: https://www.darlas.gr/comersus/store/catalog/pf/datasheets/46567.pdf (Accessed: 2 July 2010).
198. Solar light (2009) Single input radiometer-PMA2200. Available at: http://www.solarlight.com/products/pma2200.html (Accessed: 24 June 2010).
199. Testo (2011) Mini thermometer. Available at: http://www.testo.co.uk/online/abaxx-?$part=PORTAL.GBR.SimpleContentDesk&$event=show-from-menu&categoryid=1690468 (Accessed: 10 March 2011).
200. Voltech instruments ltd. PM1000 AC Power analysis manual. England: Voltech instruments ltd.

201. Fronius (2011) Solar electronics: Grid-connected inverters. Available at: http://www.fronius.com/cps/rde/xchg/SID-E52ADC1D-EAB15F2C/fronius_international/hs.xsl/83_318_ENG_HTML.htm (Accessed: 12 June 2011).
202. Cutululis, N., Larsen, T.J., Sorensen, P., Iov, F. and Hansen, A.D. (2007) *Electrical components library for HAWC2 (ENS 1363/04-0008)*. Roskilde: Technical University of Denmark.
203. Ackermann, T. (.ed) (2005) *Wind power in power systems*. England: John Wiley & Sons Ltd.
204. Eid, A.M., Abdel-Salam, M. And Abdel-Rahman, M.T. (2006) 'Vertical-Axis Wind Turbine modeling and performance with axial-flux permanent magnet synchronous generator for battery charger applications', *the 11th International Middle East Power Systems Conference (MEPCON'06)*, Egypt, 19-21 December, pp. 162-166.
205. Bergey, K.H. (1979) 'The Lanchester-Betz limit', Journal of Energy, 5, pp. 382-384.
206. Wasynczuk, O., Man, D.T. and Sullivan, J.P. (1981) 'Dynamic behaviour of a class of wind turbine generators during random wind fluctuations', *IEEE Transactions on Power Apparatus and Systems,* PAS-100 (6), pp. 2837-2845.
207. Anderson, P.M. and Bose, A. (1983) 'Stability simulation of wind turbine systems', *IEEE Transactions on Power Apparatus and Systems*, PAS-102 (12), pp. 3791-3795.
208. Wilson, R.E. and Lissaman, P.B.S. (1974) *Applied aerodynamics of wind power machines*. Oregon: Oregon State University.
209. Lysen, E.H. (1983) *Introduction to wind energy: Basic and advanced introduction to wind energy with emphasis on water pumping windmills*. 2nd edn. The Netherlands: Consultancy Services Wind Energy Developing Countries.
210. Durand, W.F. (.ed) (1935) *Aerodynamic theory: A general review of progress under a grant of the Guggenheim fund for the promotion of aeronautics*. Berlin: Julius Springer.
211. Heier, S., (2006) *Grid integration of wind energy conversion systems*. 2nd edn. England: John Wiley & Sons Ltd.

212. Manwell, J.F., Mcgowan, J.G. and Rogers, A.L. (2009) *Wind energy explained theory, design and application*. 2nd edn. England: John Wiley & Sons Ltd.
213. Burton, T., Sharpe, D., Jenkins, N. and Bossanyi, E. (2001) *Wind energy handbook*. England: John Wiley & Sons Ltd.
214. Sorensen, J.N. (2011) 'Aerodynamic aspects of wind energy conversion', *Annual Review of Fluid Mechanics*, pp. 427-448.
215. Paraschivoiu, I. *(2009) Wind turbine design-with emphasis on darrieus concept*. Canada: Presses internationals Polytechnique.
216. Vaahedi, E. and Barnes, R. (1982) 'Dynamic behaviour of a 25m variable-geometry vertical-axis wind-turbine generator', *IEE Proceedings C Generation, Transmission and Distribution*, 129 (6), pp. 249-259.
217. Muljadi, E. and Jr. Buhl, M. (1997) 'Effects of turbulence on power generation for variable-speed wind turbine, *1997 ASME Wind Energy Symposium*, Reno, Nevada, 6-9 January.
218. Rudion, K. and Orths, A. and Styczynski, Z. (2004) 'Modelling of variable speed wind turbines with pitch control', *Securing Critical Infrastructures*, Grenoble, October.
219. Mayurappriyan, P.S., Jerome, J., Ramkumar, M. and Rajambal, K. (2009) 'Dynamic modeling and analysis of wind turbine driven doubly fed induction generator', International Journal of Recent Trends in Engineering, 2(5), pp. 367-372.
220. Oliveira, R.G., Parma, G.G. and Silva, S.R. (2007) 'Development of a wind turbine simulator for wind energy conversion systems-experimental Results', *9th Brazilian Power Electronics Conference*, Blumenau, Brazil, pp. 313-318.
221. Bhattacharya, P. and Bhattacharjee, R. (2010) 'A study on Weibull Distribution for estimating the parameters', Journal of Applied Quantitative Methods (JAQM), 5(2), pp. 234-241.
222. National Aeronautics and Space Administration (1976) *U.S. Standard atmosphere*. Washington D.C.: U.S. Government Printing Office.
223. Evance wind (2008) Product certification: Evance R9000 MCS certification summary. Available at: http://www.evancewind.com/images/uploads/products/TR098_v3_Product_Certification_-_Evance_R9000_UK_MCS_Certification_Summary.pdf (Accessed: 12 June 2011).

224. Quiet revolution (2011) *qr5*. Available at: http://www.quietrevolution.com/qr5-turbine.htm (Accessed: 12 June 2011).
225. Wind Power (2011) *WindPower Program*. Available at: http://www.wind-power-program.com/ (Accessed: 12 June 2011).
226. Penche, C. and Minas, I.D. (1998) *Layman's handbook on how to develop a small hydro site*. 2nd edn. Belgica: DG XVII.
227. White, H.M. (2003) *Fluid mechanics*. 5th edn. New York: McGraw-Hill.
228. Holland, R. (1983) *Micro hydro electric power*. England: Intermediate Technology Development Group.
229. Kostenko, M. and Piotrovsky, L. (1974) *Electrical machines: Vol. 2 Alternating current machines*. Translated by Chernukhin, A., 3rd edn. Moscow: MIR Publishers.
230. Adkins, B. and Harley, R.G. (1975) *The general theory of alternating current machines*: *application to practical problems*. London: Chapman and Hall.
231. Toliyat, H.A. and Kliman, G.B. (.ed) (2004) *Handbook of electric motors*. 2nd edn. Boca Raton: Taylor & Francis Group.
232. Bakshi, U.A. and Bakshi, M.V. (2009) *Electrical and electronics engineering*. India: Technical Publication Pune.
233. Hansen, A.D., Iov, F., Sorensen, P., Cutululis, N., Jauch, C. and Blaabjerg, F. (2007) *Dynamic wind turbine models in power system simulation tool DIgSILENT (ENS 1363/04-0008)*. Roskilde: Technical University of Denmark.
234. Eltamaly, A.M. (2007) 'Modeling of wind turbine driving permanent magnet generator with maximum power point tracking system', *Journal of King Saud University, Engineering Science*, 19 (2), pp. 223-237.
235. Bumby, J.R. and Martin, R. (2005) 'Axial-Flux permanent magnet air-cored generator for small-scale wind turbines', *Journal of Electric Power Applications*, 152(5), pp. 1065-1075.
236. Slootweg, J.G., Polinder, H. and Kling, W.L. (2001) 'Initialization of wind turbine models in power system dynamics simulations', *PPT2001 IEEE Porto Power Tech Conference*, Porto, Portugal, 10-13 September.
237. Bewley, L.V. (1930) 'Induced voltage of electrical machines', *Transaction of American Institute of Electrical Engineers*, 49(2), pp. 456-466.
238. Hanrahan, D.J. and Toffolo, D.S. (1957) 'Permanent magnet generators Part I-Theory', Transactions of the American Institute of Electrical Engineers in Power Apparatus and Systems, 76(3), pp. 1098-1103.

239. Hanrahan, D.J. and Toffolo, D.S. (1963) ‘Permanent magnet generators’, IEEE Transactions on Power Apparatus and Systems, 68(65), pp. 68-74.
240. Global Water FP111-FP211-FP311 Water flow probe User’s Manual. USA: Global Water.
241. Fluke Corporation Users manual SW43W Fluke Power quality analyzer software version 3.20 onwards. USA: Fluke Corporation.
242. MAGNA Co., Ltd. Gauss (Tesla) meter MG-701 users manual. Japan: MAGNA Co., Ltd.
243. Tektronix TDS1000B & TDS2000B Series digital storage oscilloscope operator training kit manual. USA: Tektronix.
244. The Institute of Electrical and Electronics Engineers (IEEE). (1991) *IEEE Application Guide for Distributed Digital Control and Monitoring for Power Plants (IEEE Std 1046-1991)*.
245. Van der Hoven, I. (1957) ‘Power spectrum of horizontal wind speed in the frequency range from 0.0007 to 900 cycles per hour’, *American Meteorological Society*, 14(2), pp. 160-164.
246. Liu, X., Aichhorn, A., Liu, L. and Li, H. (2012) ‘Coordinated control of distributed energy storage system with tap changer transformers for voltage rise mitigation under high photovoltaic penetration’, *IEEE Transactions on Smart Grid,* 3(2), pp. 897-906.
247. Cowan, J.M., Edmondson, K.L. and Preston, L.L. (1964) ‘Parallel operation of transformers with on-load tap changers and negative-reactance-compounding control’, *Proceedings of the Institution of Electrical Engineers,* 111 (12), pp. 2026-2040.
248. The Institute of Electrical and Electronics Engineers (IEEE). (2012) ‘IEEE Standard Requirements for Tap Changers’, IEEE Std C57.131™-2012 (Revision of IEEE Std C57.131-1995).
249. Hawkins, D. And Guha, C. (2008) Business drivers for distribution network operators and active distribution management system development: how should India embrace best developed practice' [Online]. Available at:http://www.gepower.com/prod_serv/plants_td/en/downloads/gridtech_advanceddms.pdf (Accessed: 30/09/2008).

250. Joode, J. d. (2008) 'Increasing penetration of DG and the need for different network regulation', *ECN*, 22/05/2008*11th Economics of Infrastructures conference, Delft, the Netherlands* [Online]. Available at: http://www.tbm.tudelft.nl/live/pagina.jsp?id=27ed35a1-5d2b-4010-acab-46e8c85d5c22&lang=en&binary=/doc/De%20Joode.pdf (Accessed: 07/10/2008).
251. Browning, S. (2008) *Future power systems 7 - Active distribution management.* [Online]. Available at: http://www.leonardo-energy.org/drupal/node/2535 (Accessed: 30/09/2008).
252. Jenkins, N. (2008) 'Tutorial on active distribution networks for wind energy', [Online]. Available at: http://www.ee.qub.ac.uk/blowing/activity/Belfast2/jenkins.pdf (Accessed: 30/09/2008).
253. Chuang, A. and McGranaghan, M. (2008) 'Functions of a local controller to coordinate distributed resources in a smart grid'*, IEEE Power and Energy Society General Meeting - Conversion and Delivery of Electrical Energy in the 21st Century,* Pittsburgh, PA 20-24 July. Palo Alto, CA, pp. 1-6.
254. McDonald, J. (2008) 'Adaptive intelligent power systems: active distribution networks', [Online]. Available at: http://www.foresight.gov.uk/Energy/adaptive_intelligent_power_systems_active_distribution_networks.pdf (Accessed: 30/09/2008).
255. Zhang, X. P. (2008) 'A framework for operation and control of smart grids with distributed generation', *IEEE Power and Energy Society General Meeting - Conversion and Delivery of Electrical Energy in the 21st Century,* Pittsburgh, PA 20-24 July 2008, pp. 1-5.
256. British Standard. (2008) *Requirements for electrical installation 17th edn (BS7671)*.
257. Haggis, T. (2006) *Network design manual version 7.7*. UK: e-on central network.

APPENDICES

Appendix A: Typical Data and Parameters of the UK and TH Networks

Table A.1: Standard voltage levels in UK

Standard voltage in the UK	
Low Voltage (LV)	216 V<LV<253 V
Medium Voltage (MV)	6.6k V<MV<33 kV

Source: [256], [257]

Table A.2: Standard voltage levels in TH

Standard voltage in TH		Typical TH voltages		
		MEA	PEA	EGAT
Low Voltage (LV)	120 V<LV<600 V	220 V-300 V	230 V-400 V	240 V-416 V
Medium Voltage (MV)	2.40 kV<MV<69 kV	12 kV	22 kV	69 kV
High Voltage (HV)	345 kV<HV<765 kV	345 kV<HV<765 kV		
Ultra High Voltage (UHV)	1 MV<UHV<1.2 MV	1 MV<UHV<1.2 MV		

Source: [17]

Note: Metropolitan Electricity Authority (MEA) is the electricity distribution organisation, which supplies the electricity in the central area of TH. On the other hand, the other areas in TH receive power from the Provincial Electricity Authority (PEA), the electricity distribution and generation organisation for province levels. In addition, the main supplier of electricity in TH is the Electricity Generating Authority of Thailand (EGAT) who generates and provided the power directly to the consumers' or via two main distributors such MEA and PEA.

Table A.3: Typical levels of DG connects in urban area in TH network

Network location	Maximum capacity of DG
Out on 400 V at network	50 kVA
At 400 V busbars	200 kVA-250 kVA
Out on 11 kV or 11.5 kV network	2 MVA-3 MVA
At 11 kV or11.5 kV at busbars	8 MVA
On 15 kV or 20 kV network and at busbars	6.5 MVA-10 MVA
On 63 kV to 90 kV network	10 MVA-40 MVA

Source: [17]

Table A.4: Typical levels of DG connects in rural area in TH network

Network location	Maximum capacity of DG
On 22 kV or 33 kV network and at busbars	66 kVA
Depend on PEA decision	<66 kVA

Source: [17]

Table A.5: Standard voltage tolerance when DG connects to TH network

Voltage level	Normal circumstances		Exceptional circumstances	
	Minimum	Maximum	Minimum	Maximum
115 kV	109.2 kV	120.7 kV	103.5 kV	126.5 kV
69 kV	65.5 kV	72.4 kV	62.1 kV	75.9 kV
33 kV	31.3 kV	34.7 kV	29.7 kV	36.3 kV
22 kV	20.9 kV	23.1 kV	19.8 kV	24.2 kV
220 V	200 V	240 V	200 V	240 V
380 V	342 V	418 V	342 V	418 V

Source: [17]

Table A.6: Standard of harmonic order of DG connects to the network

Categories	Typical spectral content	Typical duration	Typical voltage magnitude
1.0 Transient			
1.1 Impulsive			
1.1.1 Nanosecond	5 ns rise	< 50 ns	
1.1.2 Microsecond	1 µs rise	50 µs-1 ms	
1.1.3 Millisecond	0.1 ms rise	>1 ms	
1.2 Oscillatory			
1.2.1 Low frequency	<5 kHz	0.3-50 ms	0-4 per unit
1.2.2 Medium frequency	5-500 kHz	20 µs	0-8 per unit
1.2.3 High frequency	0.5-5 MHz	5 µs	0-4 per unit
2.0 Short duration variations			
2.1 Instantaneous			
2.1.1 Sag		0.5-30 cycles	0.1-0.9 per unit
2.1.2 Swell		0.5-30 cycles	1.1-1.8 per unit
2.2 Momentary			
2.2.1 Interruption		0.5 cycles-3 s	<0.1 per unit
2.2.2 Sag		30 cycles-3 s	0.1-0.9 per unit
2.2.3 Swell		30 cycles-3 s	1.1-1.4 per unit
2.3 Temporary			
2.3.1 Interruption		3s-1 min	<0.1 per unit
2.3.2 Sag		3s-1 min	0.1-0.9 per unit
2.3.3 Swell		3s-1 min	1.1-1.4 per unit
3.0 Long duration variations			
3.1 Interruption, sustained		>1 min	0.0 per unit
3.2 Undervoltages		>1 min	0.8-0.9 per unit
3.3 Overvoltages		>1 min	1.1-1.2 per unit
4.0 Voltage imbalance		Steady-state	0.5-2 percent
5.0 Waveform distortion			
5.1 DC offset		Steady-state	0-0.1 percent
5.2 Harmonics	0-100 THz	Steady-state	0-20 percent
5.3 Interharmonics	0-6 kHz	Steady-state	0-2 percent
5.4 Notching		Steady-state	
5.5 Noise	Broad-band	Steady-state	0-1 percent
6.0 Voltage fluctuations	<25 Hz	Intermittent	0.1-7 percent
7.0 Power frequency variations		<10 s	

Source: [45]

Table A.7: Standard of harmonic order of DG connects to the network

	Nominal	Minimum	Maximum
Frequency	50 Hz (±1%)	49.5	50.5

Source: [40]

Table A.8: Current distortion of DG connects to UK network at 120V to 69kV

I_{SC}/I_l	Individual harmonic order (Odd harmonic)					
	<11	**11≤*h*<17**	**17≤*h*<23**	**23≤*h*<35**	**35≤*h***	**TDD**
<20*	4	2	1.5	0.6	0.3	5
20<50	7	3.5	2.5	1	0.5	8
50<100	10	4.5	4	1.5	0.7	12
100<1000	12	5.5	5	2	1	15
>1000	15	7	6	2.5	1.4	20

Source: [40]

Note: Even harmonics are limited to 25 percent of the odd harmonic limits from Table A.7 and current distortions that result in a DC offset, e.g. half wave converters, are not allowed. *All the power generation equipment is limited t o these values of current distortion regardless of actual $\frac{I_{SC}}{I_l}$ where,

I_{SC} = Maximum short-circuit current at common connection point

I_l = Maximum demand load current (with fundamental frequency component) at common connection point

TDD = Total Demand Distortion, harmonic current distortion in percent of maximum load current (in 15 or 30 minute demand)

Table A.9: Current distortion of DG connects to TH network

Network location	**Harmonic order and harmonics current (A_{RMS}) in the network**																			
	$MVA_{SC(Base)}$	**2**	**3**	**4**	**5**	**6**	**7**	**8**	**9**	**10**	**11**	**12**	**13**	**14**	**15**	**16**	**17**	**18**	**19**
400 V	10	48	34	22	56	11	40	9	8	7	19	6	16	5	5	5	6	4	6
11 kV and 12 KV	100	13	8	6	10	4	8	3	3	3	7	2	6	2	2	2	2	1	1
22, 24 and 33 kV	500	11	7	5	9	4	6	3	2	2	6	2	5	2	1	1	2	1	1
69 kV	500	8.8	5.9	4.3	7.3	3.3	4.9	2.3	1.6	1.6	4.9	1.6	4.3	1.6	1	1	1.6	1	1
115 kV>	1000	5	4	3	4	2	3	1	1	1	3	1	3	1	1	1	1	1	1

Source: [17]

Table A.10: Standard of percent harmonic distortion of DG in TH network

Network location	**THD (%)**	**Harmonic distortion (HD)**	
		Even order	**Odd order**
400 V	5	4	2
11, 12, 22 and 24 kV	4	3	1.75
33 kV	3	2	1
69 kV	2.45	1.63	0.82
115 kV	1.5	1	0.5

Source: [17]

Note: Tables A9. and A.10, the exceptional network current harmonic is ±10 percentage of current harmonic from Table A.10 or ±0.5A for 2nd orders. The current harmonic can be expressed equation as:

$$I_h = I_{hp} \times \frac{\mathrm{MVA_{sc1}}}{\mathrm{MVA_{SC(Base)}}} \quad \text{(A.1)}$$

Where,

I_h = Current harmonic order h flow to the network when $\mathrm{MVA_{sc}}$ is $\mathrm{MVA_{sc1}}$

I_{hp} = Current harmonic order h from Table A.10

$\mathrm{MVA_{sc1}}$ = Minimum of $\mathrm{MVA_{sc}}$ at network connection

$\mathrm{MVA_{SC(Base)}}$ = $\mathrm{MVA_{SC(Base)}}$ from Table A.10

In practice, the large size of distributed generation always has more inductance than resistance $(X \gg R)$ due to this manner the quality factor of the internal source impedance $\left(\frac{X}{R}\right)$ in both UK and TH case studies are chosen to 999. This setting is shown that the resistance (R) is not mainly affected in the medium voltage networks. The source impedance in Simulink models can be expressed by the equation of three-phase inductive short-circuits level:

$$L = \left[\frac{(V_{base})^2}{P_{SC}}\right]\left(\frac{1}{2\pi f}\right) \quad (4.1)$$

And also,

$$R = \frac{2\pi f L}{\left(\frac{X}{R}\right)} \quad (4.2)$$

Where,

L = The internal inductance (H)

P_{SC} = The inductive 3-phase short-circuit power (VA)

V_{base} = Base voltage used to specify the three-phase short-circuit level (ph-ph V_{RMS})

f = Source frequency (Hz)

R = The internal resistance (Ω)

$\frac{X}{R}$ = The ratio at nominal source frequency or quality factor of the internal source Impedance

Appendix B: MATLAB/Simulink Schematic Diagram of Computer Models

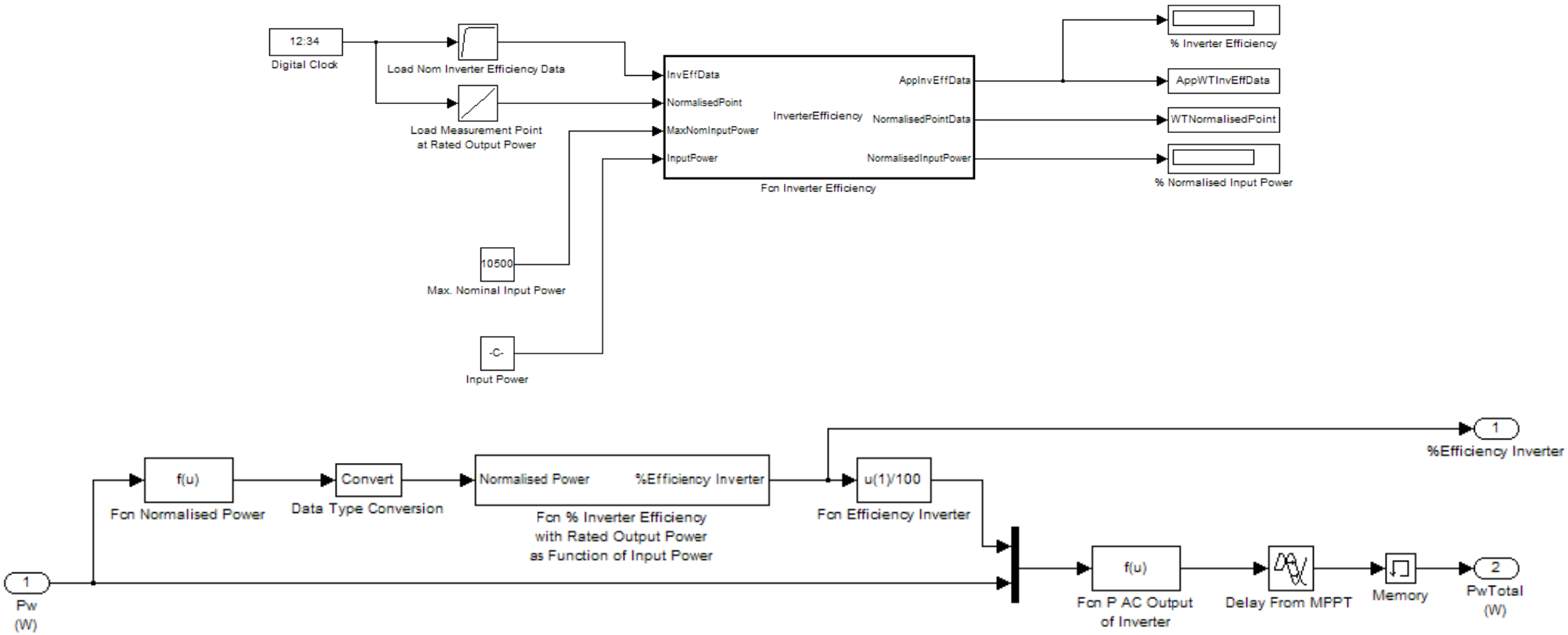

Figure B.1 MATLAB schematic of converter/inverter model (for voltage analysis)

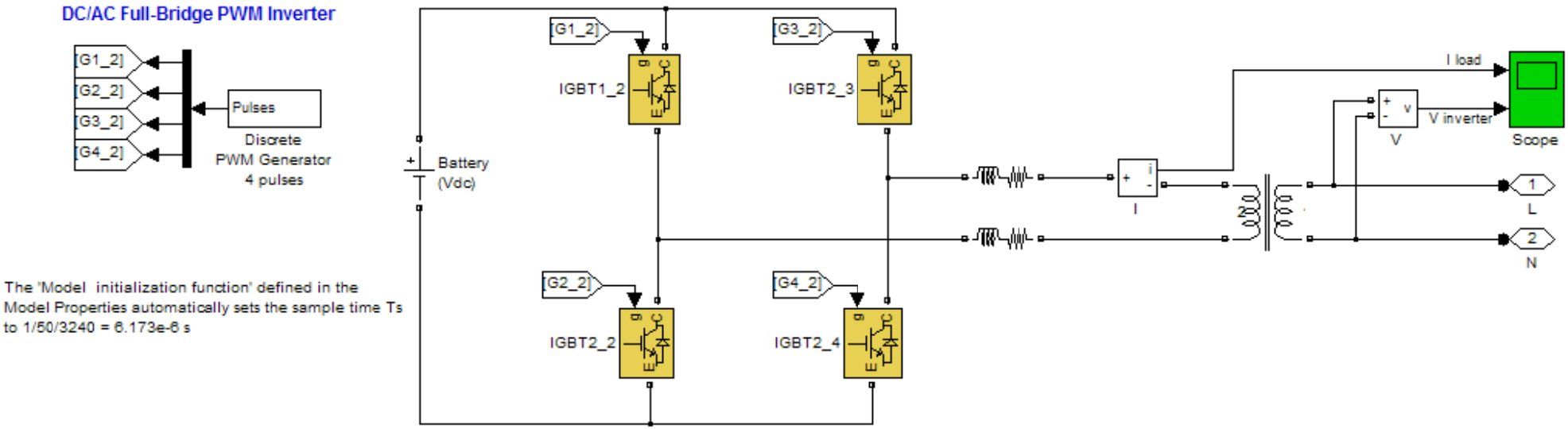

Figure B.2 MATLAB schematic of converter/inverter model (for harmonic analysis)

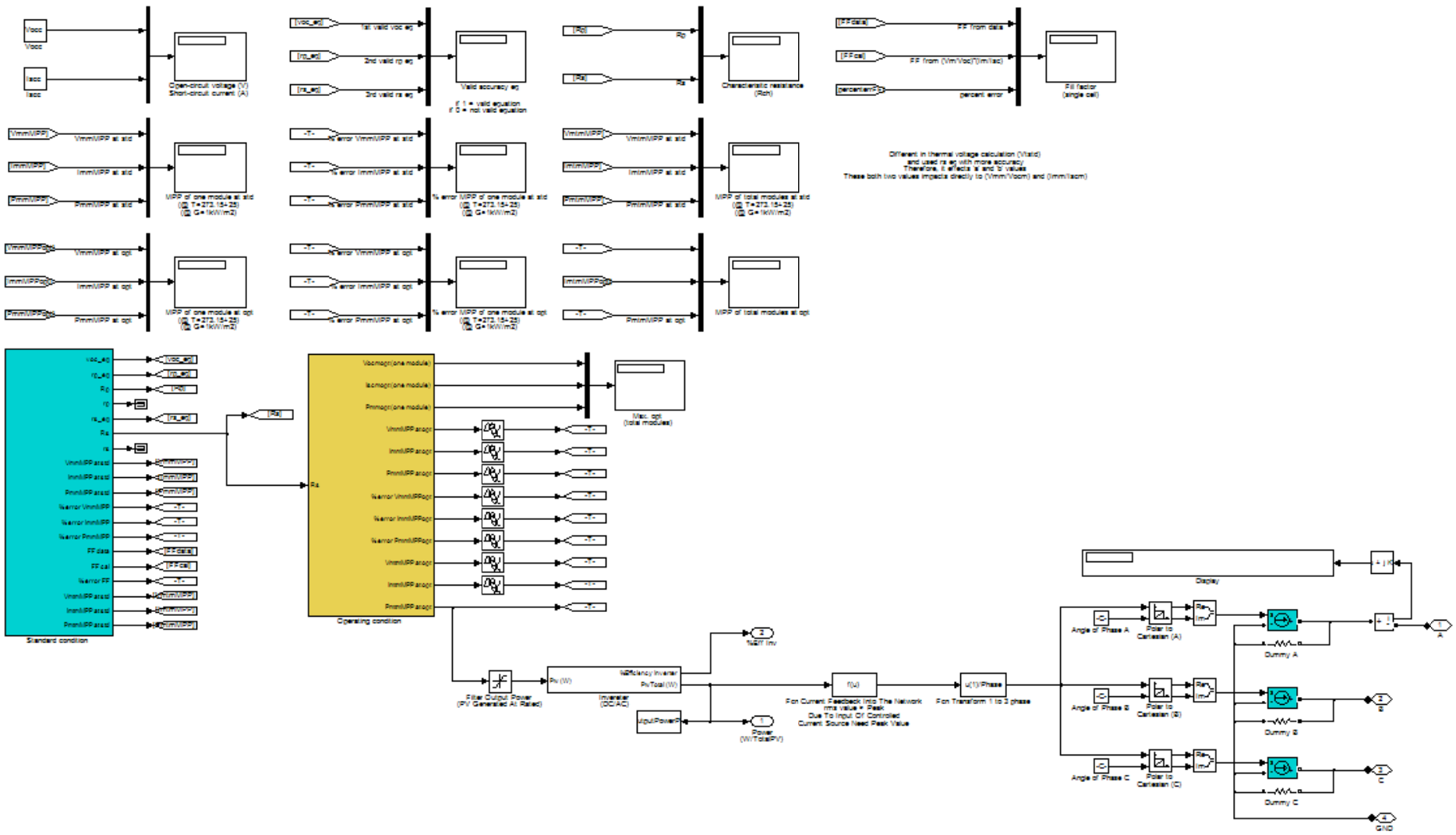

Figure B.3 MATLAB schematic of PV model

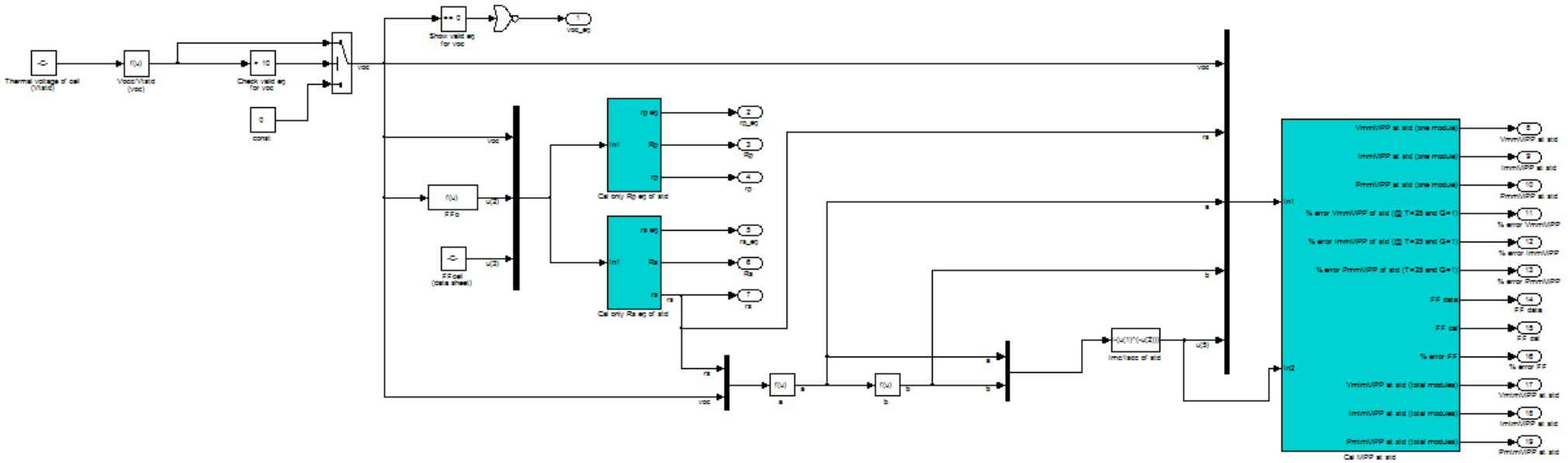

Figure B.4 MATLAB schematic under standard condition for PV model

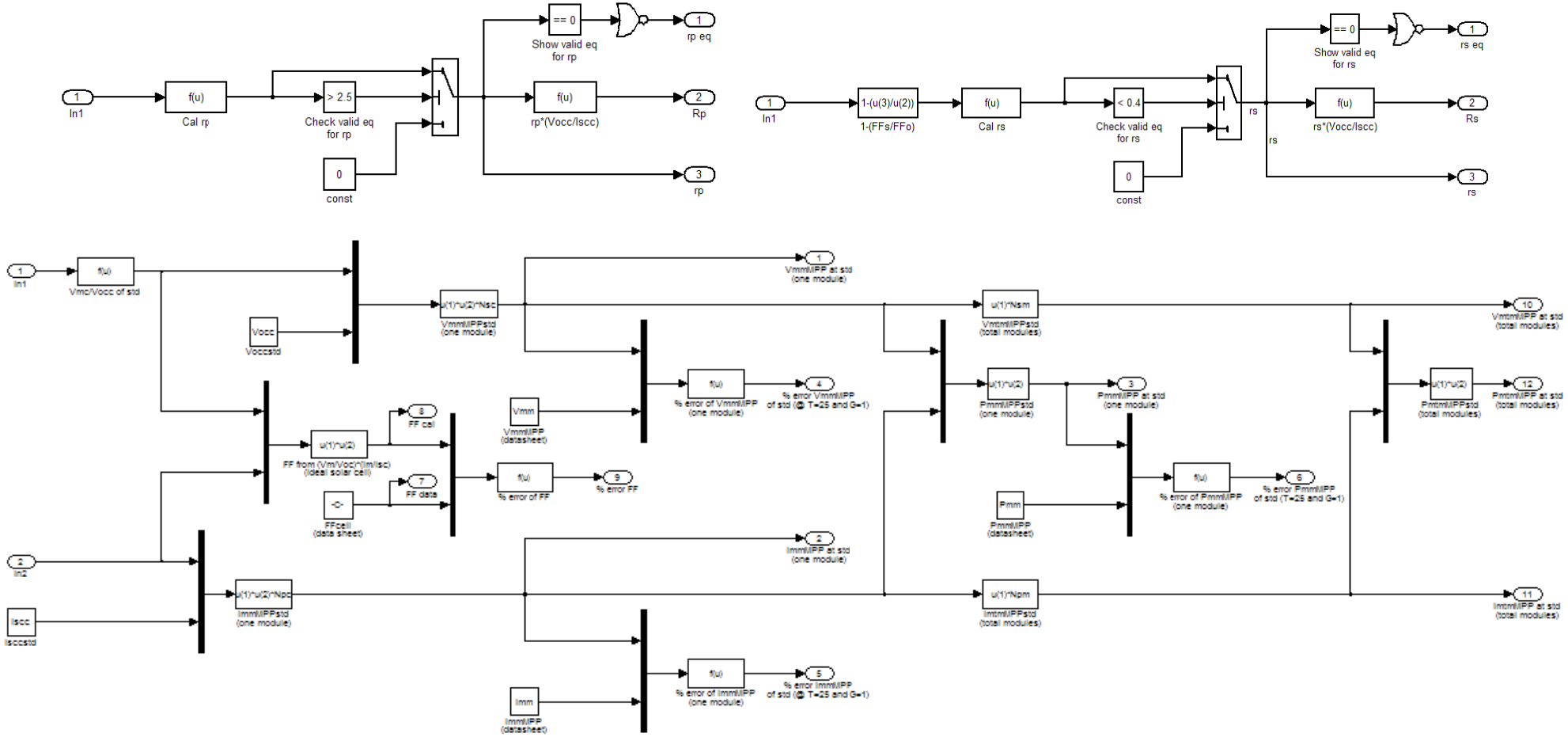

Figure B.5 MATLAB schematic of parasitic resistance for PV model

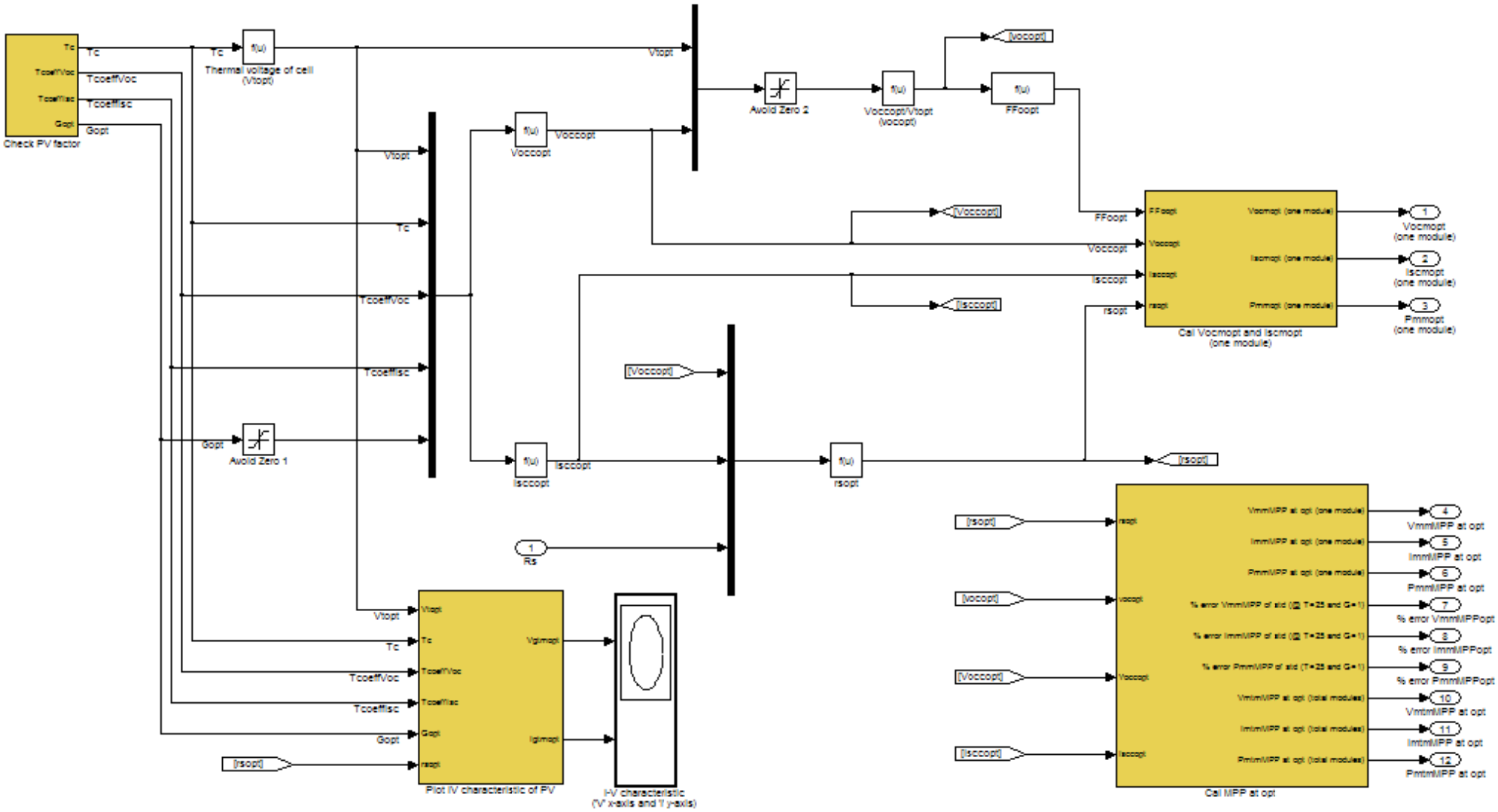

Figure B.6 MATLAB schematic under variable condition for PV model

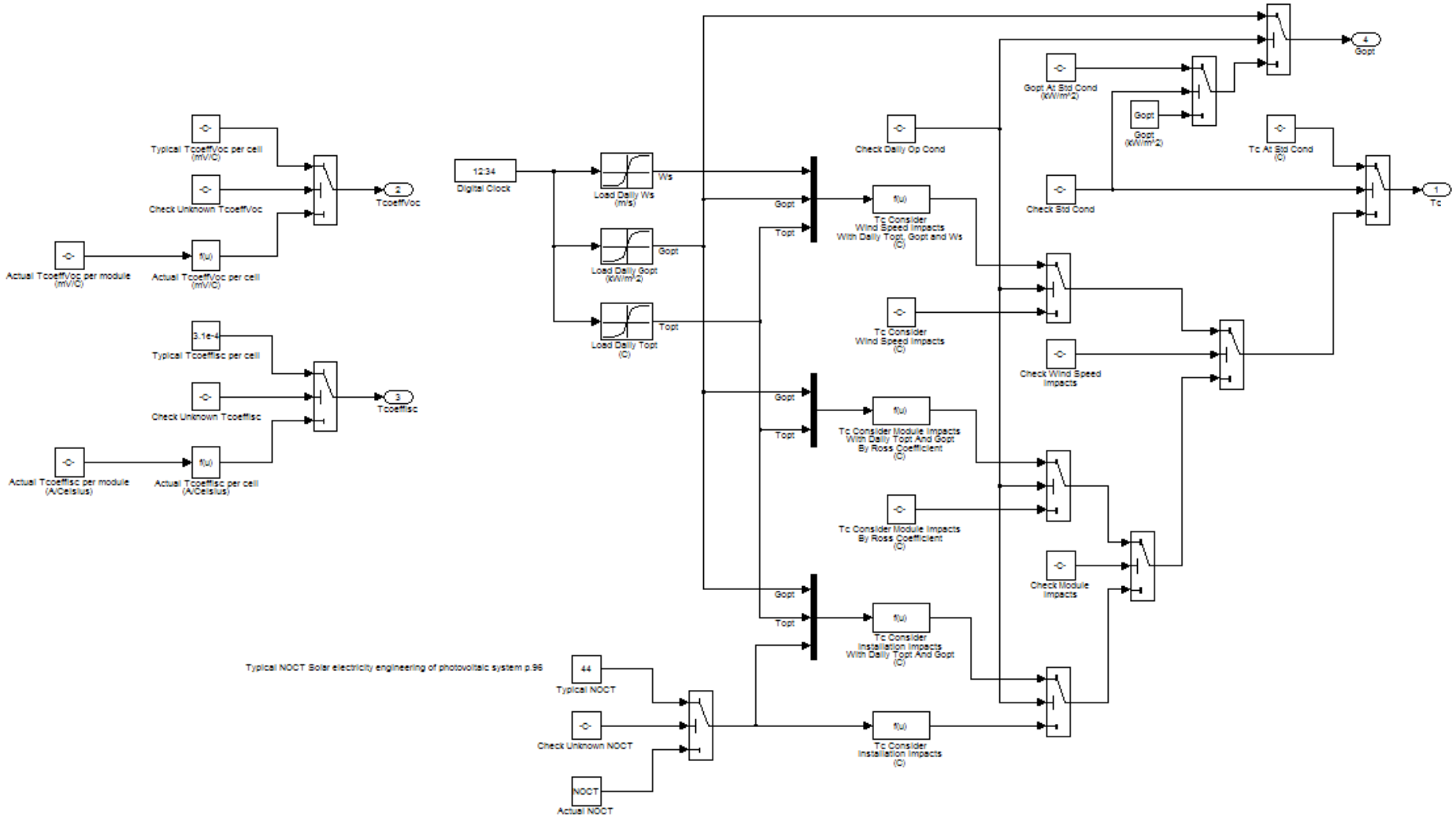

Figure B.7 MATLAB schematic of the variable environment and installation for PV model

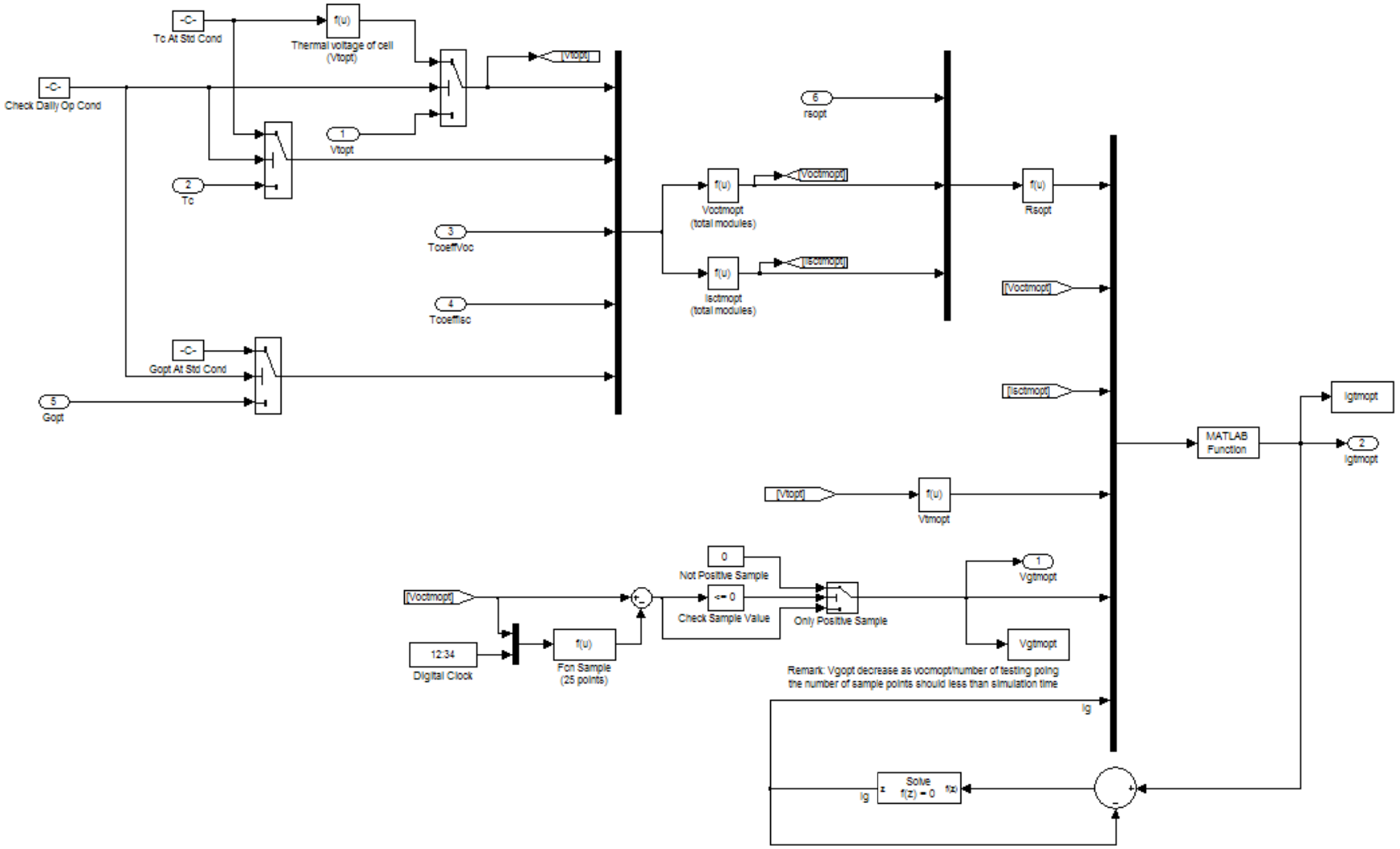

Figure B.8 MATLAB schematic of I-V characteristic for PV model

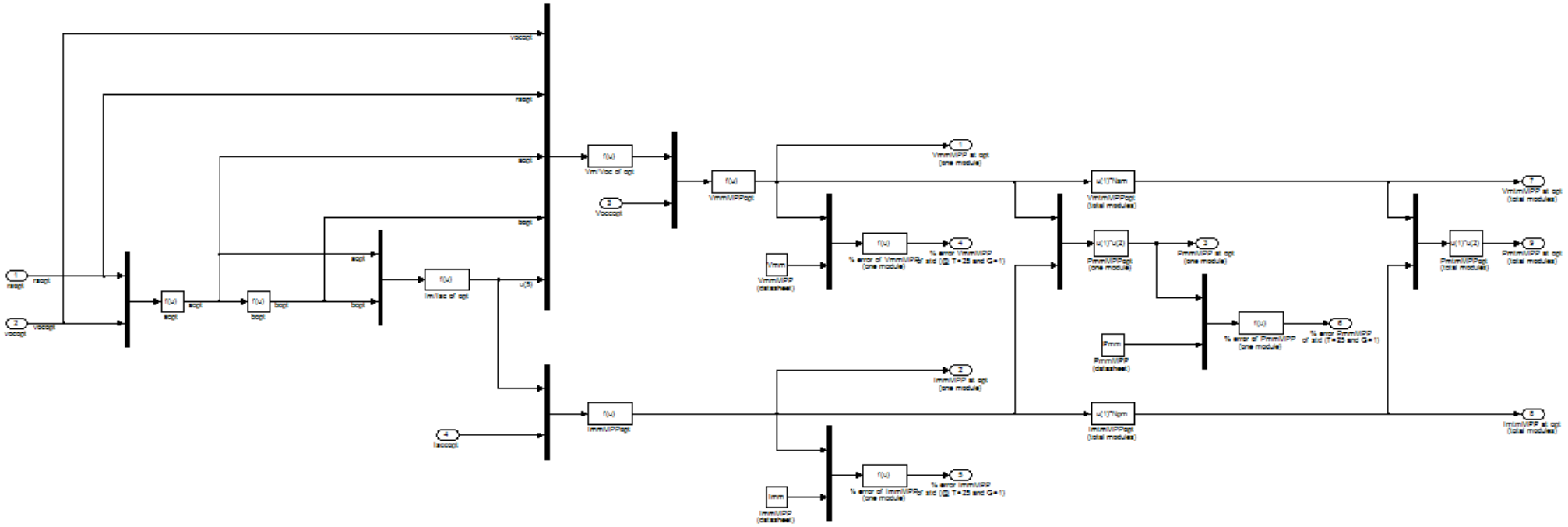

Figure B.9 MATLAB schematic of MMP for PV model

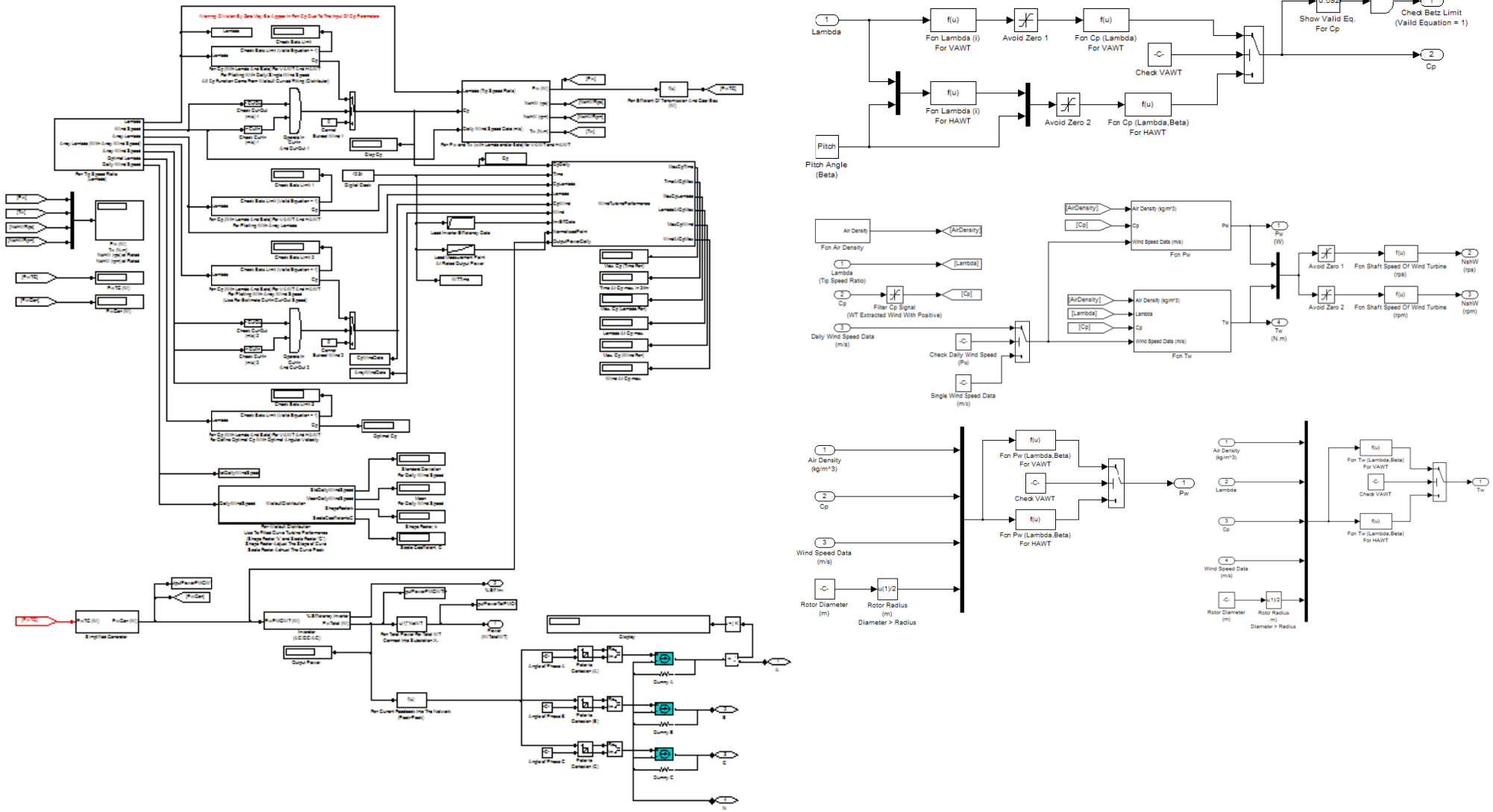

Figure B.10 MATLAB schematic of small wind turbine model

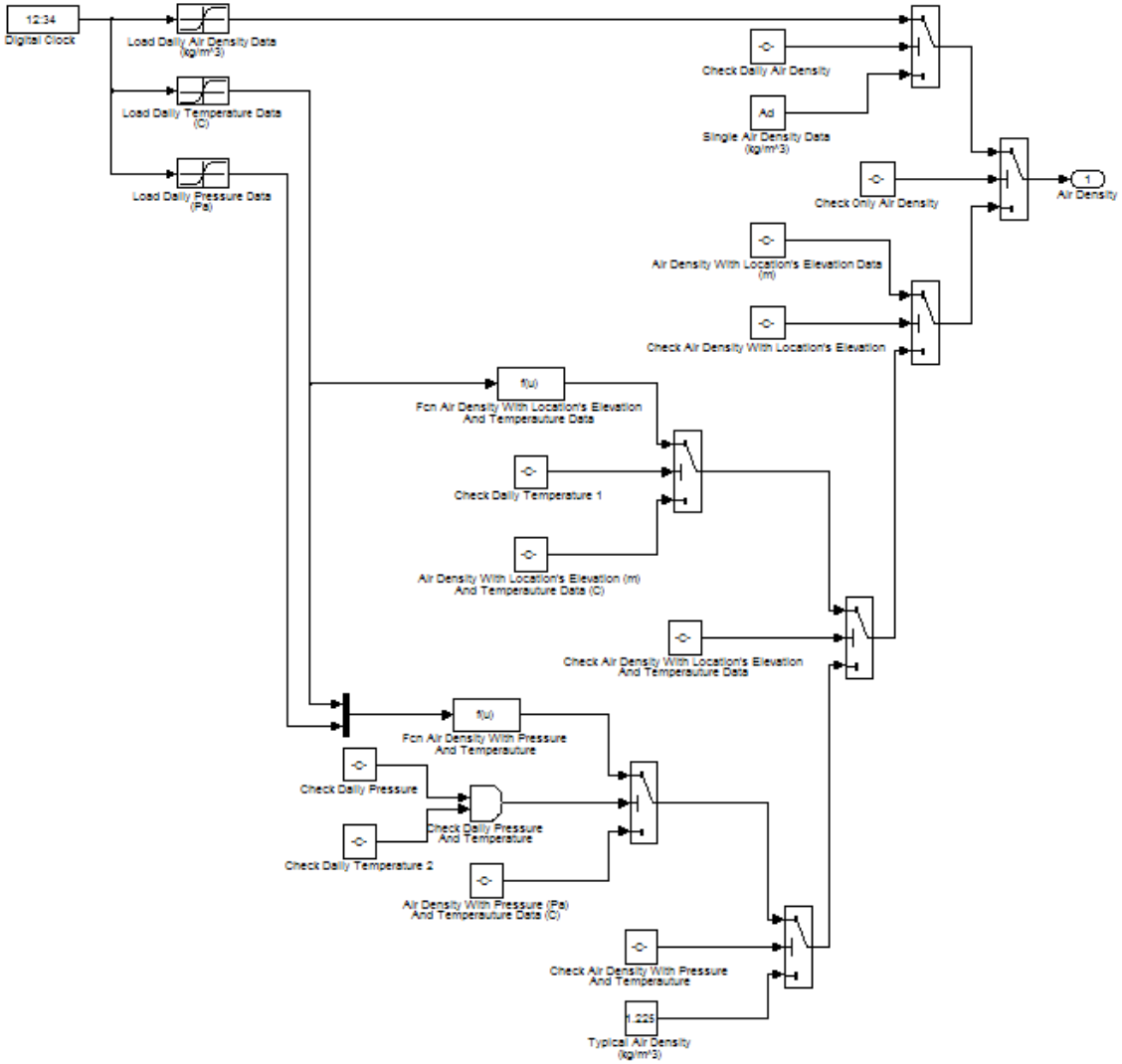

Figure B.11 MATLAB schematic of the variable environment for small wind turbine model

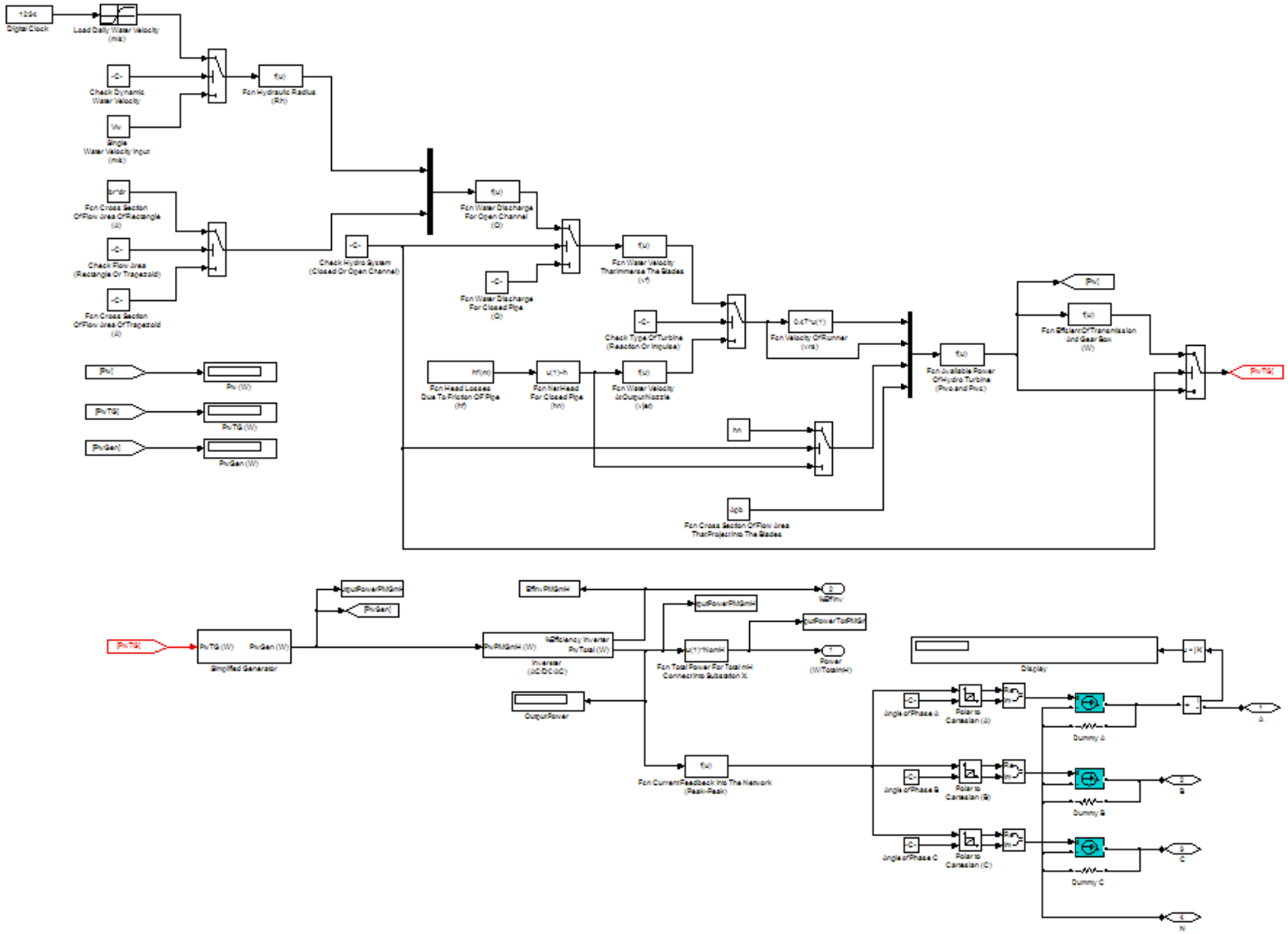

Figure B.12 MATLAB schematic of small hydro turbine model

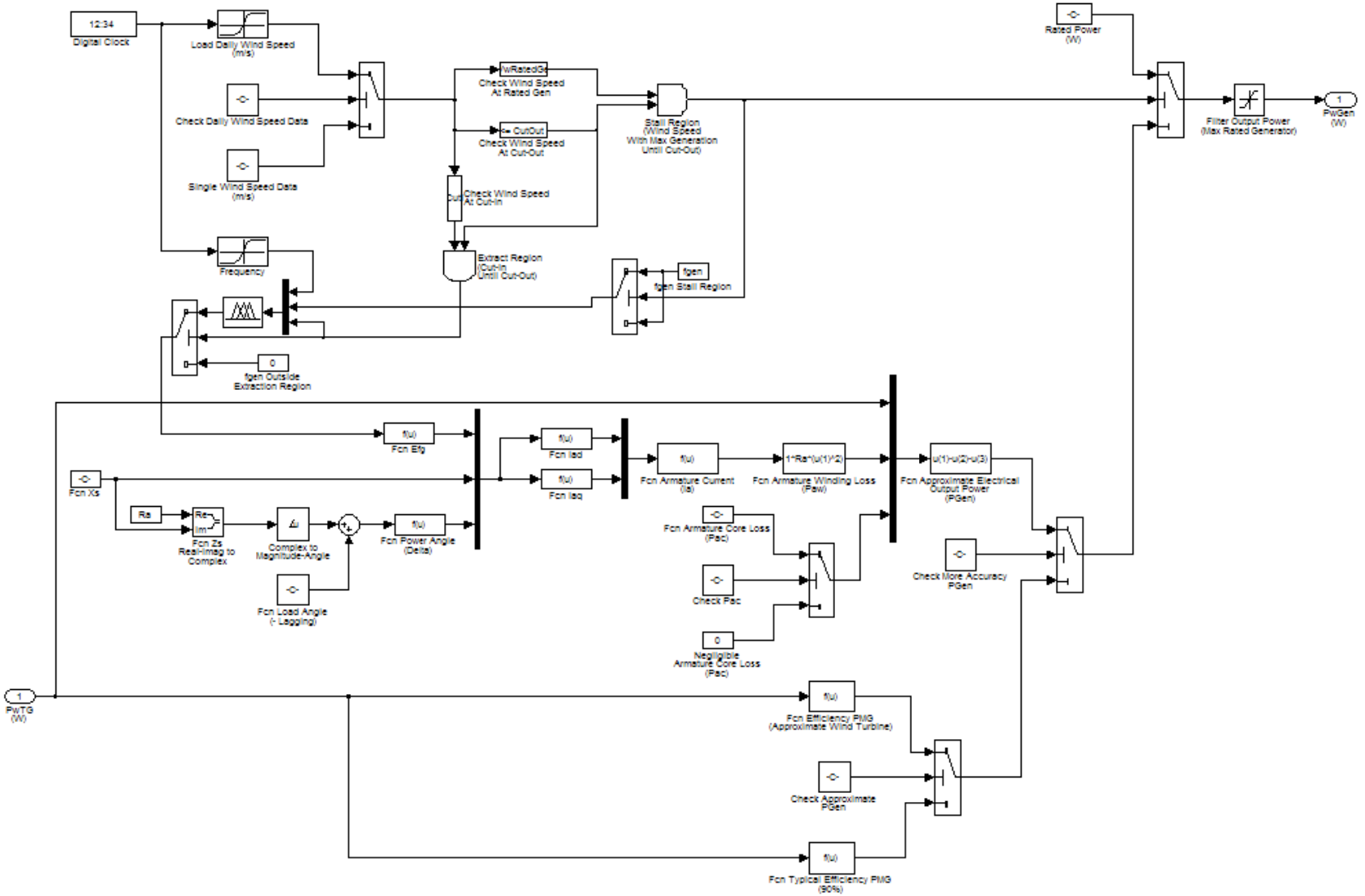

Figure B.13 MATLAB schematic of PMG model

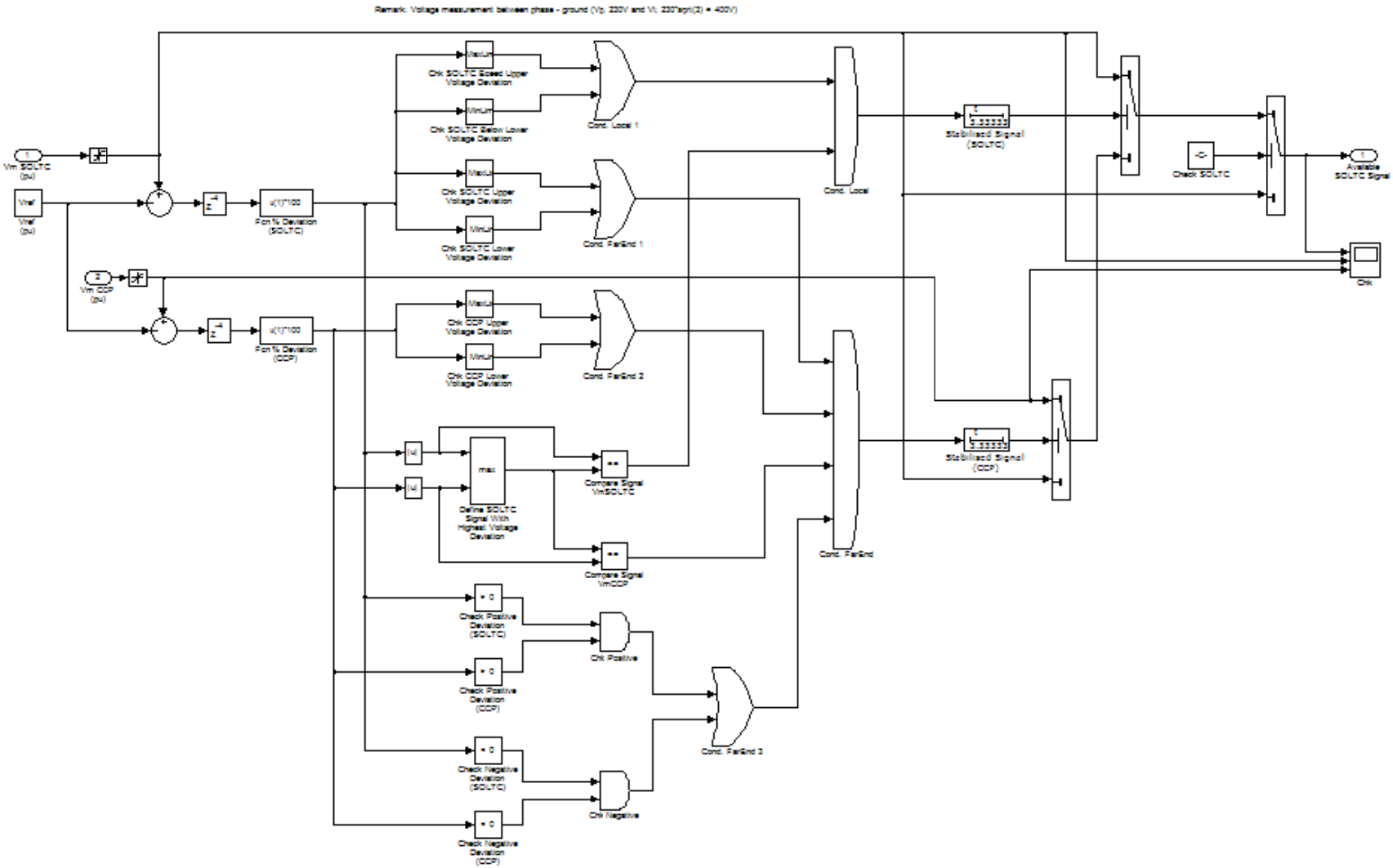

Figure B.14 MATLAB schematic of control signal for the SOLTC

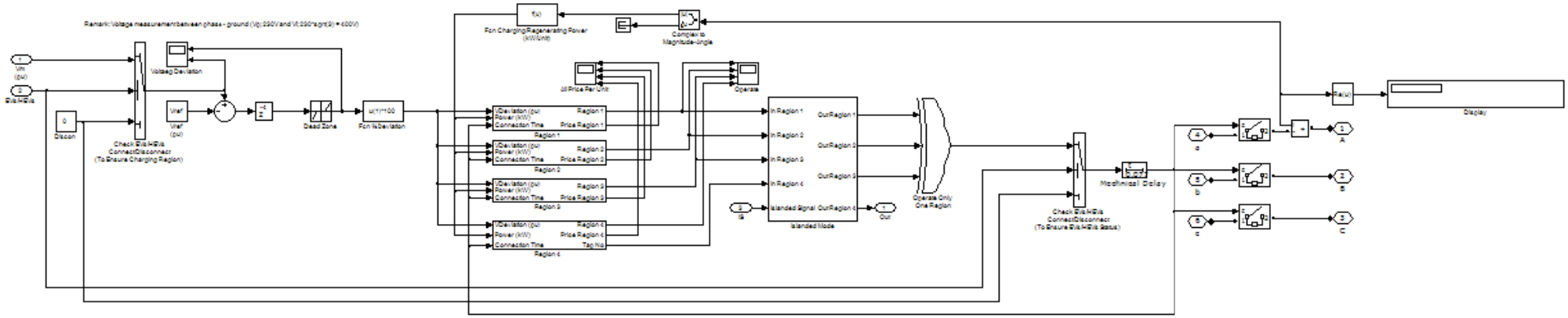

Figure B.15 MATLAB schematic of the SEVGC

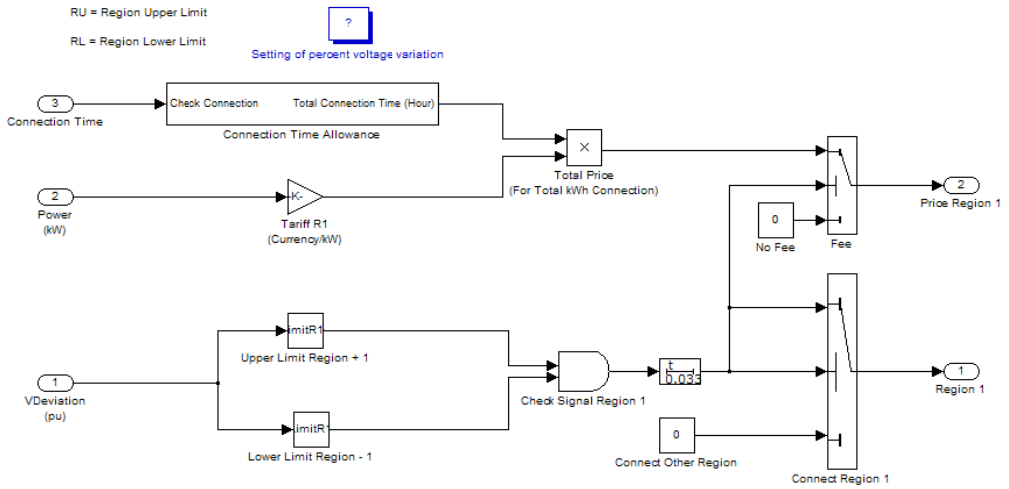

Figure B.16 MATLAB schematic of connection region 1,2 and 3 for the SEVGC

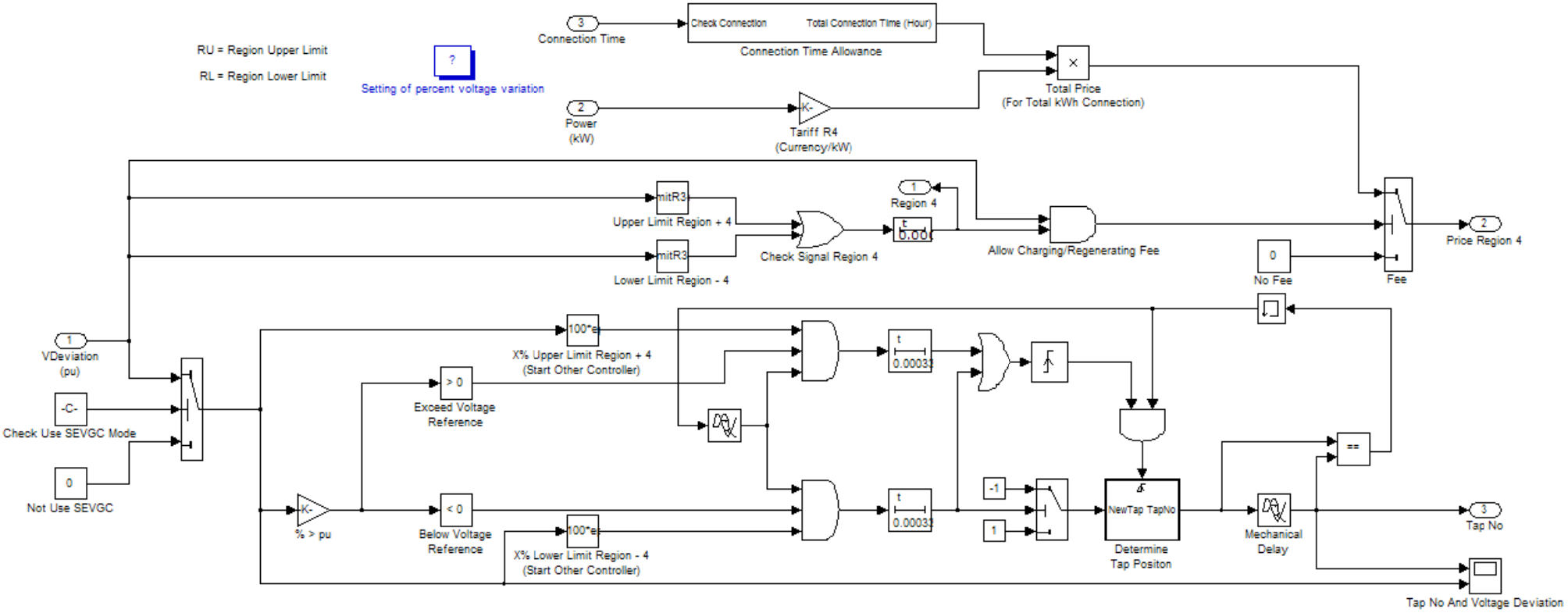

Figure B.17 MATLAB schematic of connection region 4 for the SEVGC

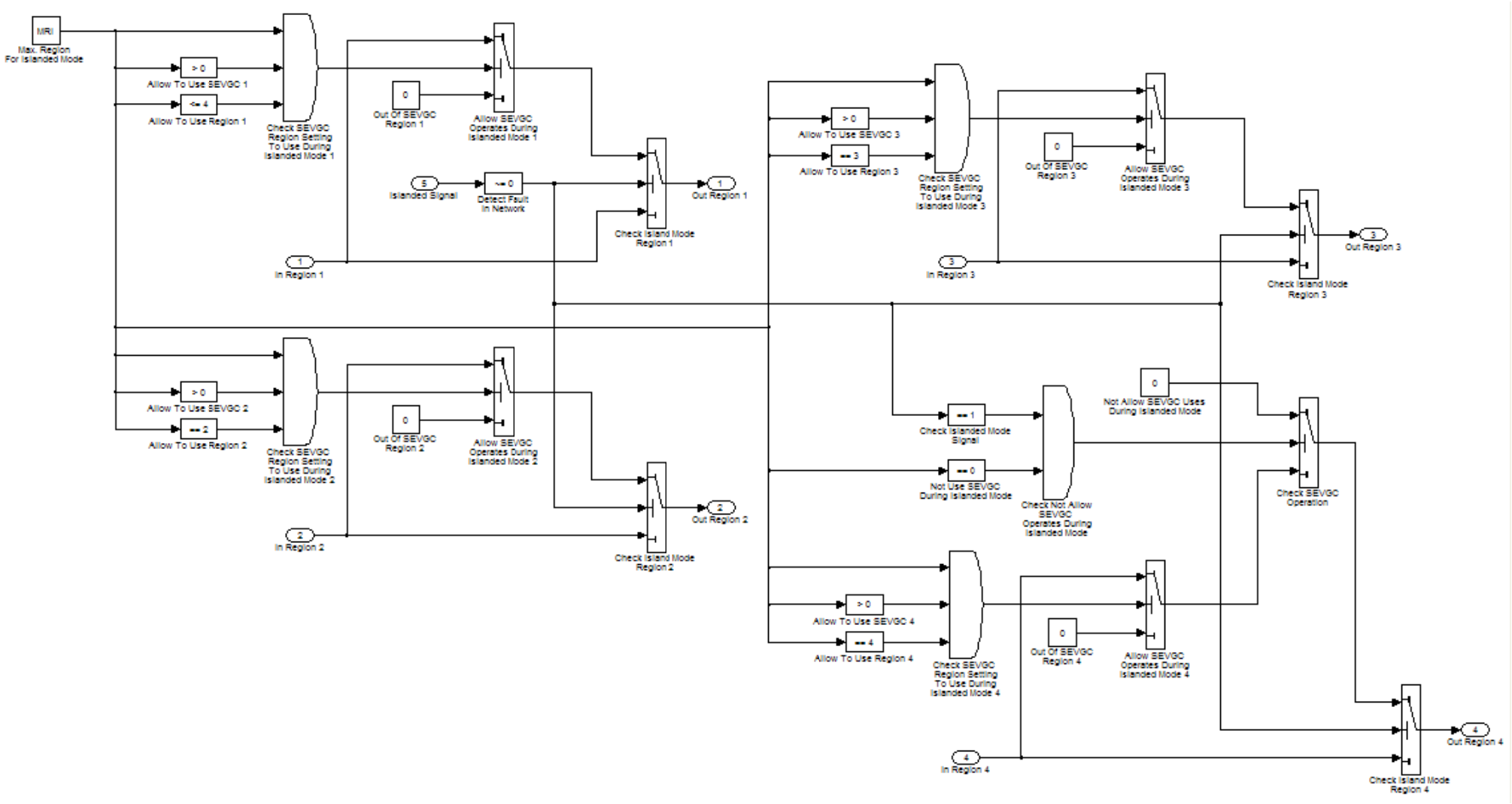

Figure B.18 MATLAB schematic of connection region during islanding operation for the SEVGC

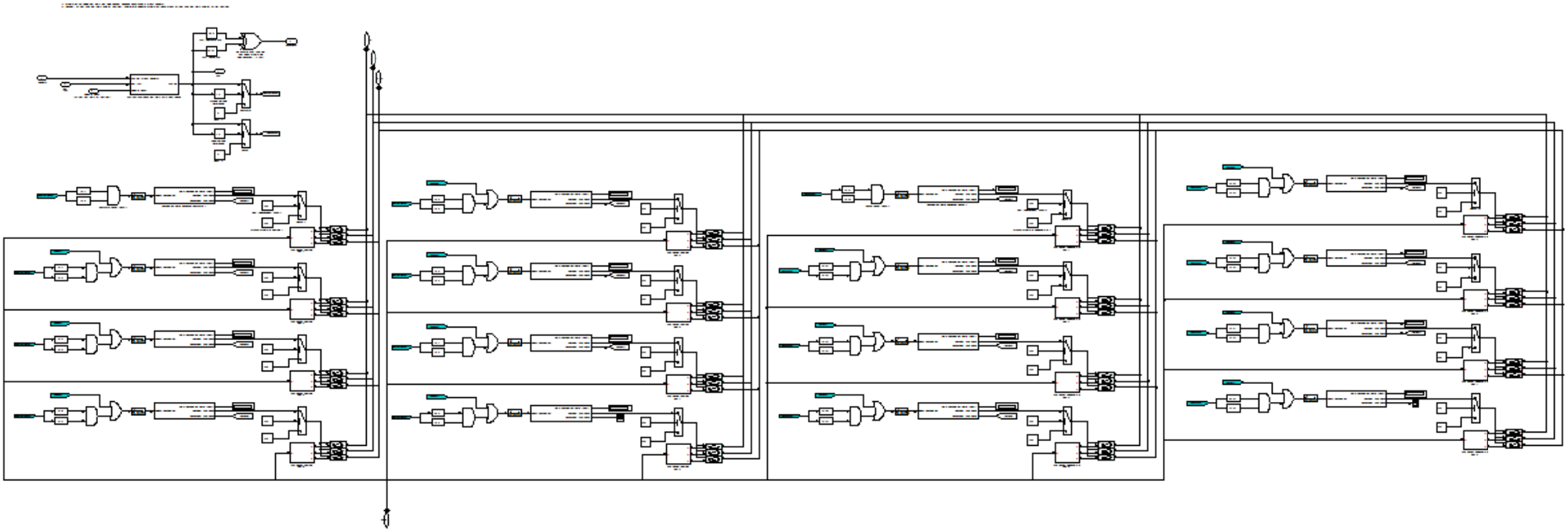

Figure B.19 MATLAB schematic of the SCP and/or the SES

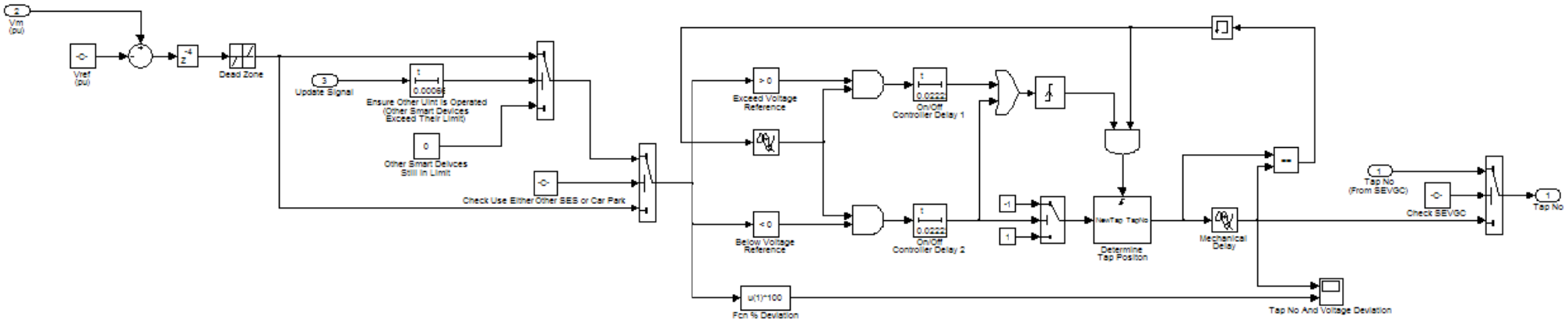

Figure B.20 MATLAB schematic of control signal for the SEVGC, SCP and/or the SES

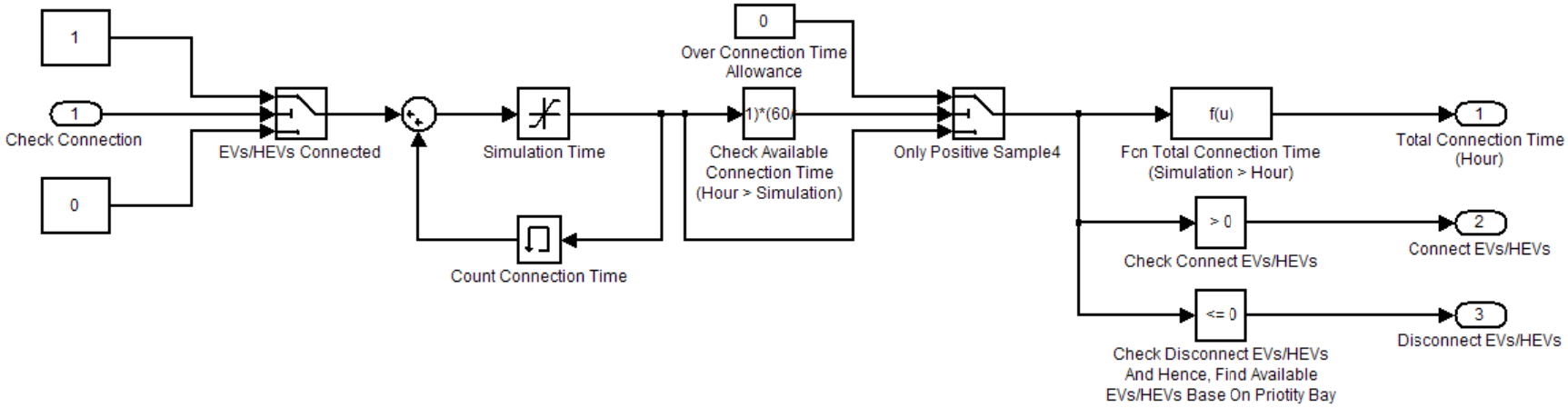

Figure B.21 MATLAB schematic of connection time for the SEVGC and/or SCP

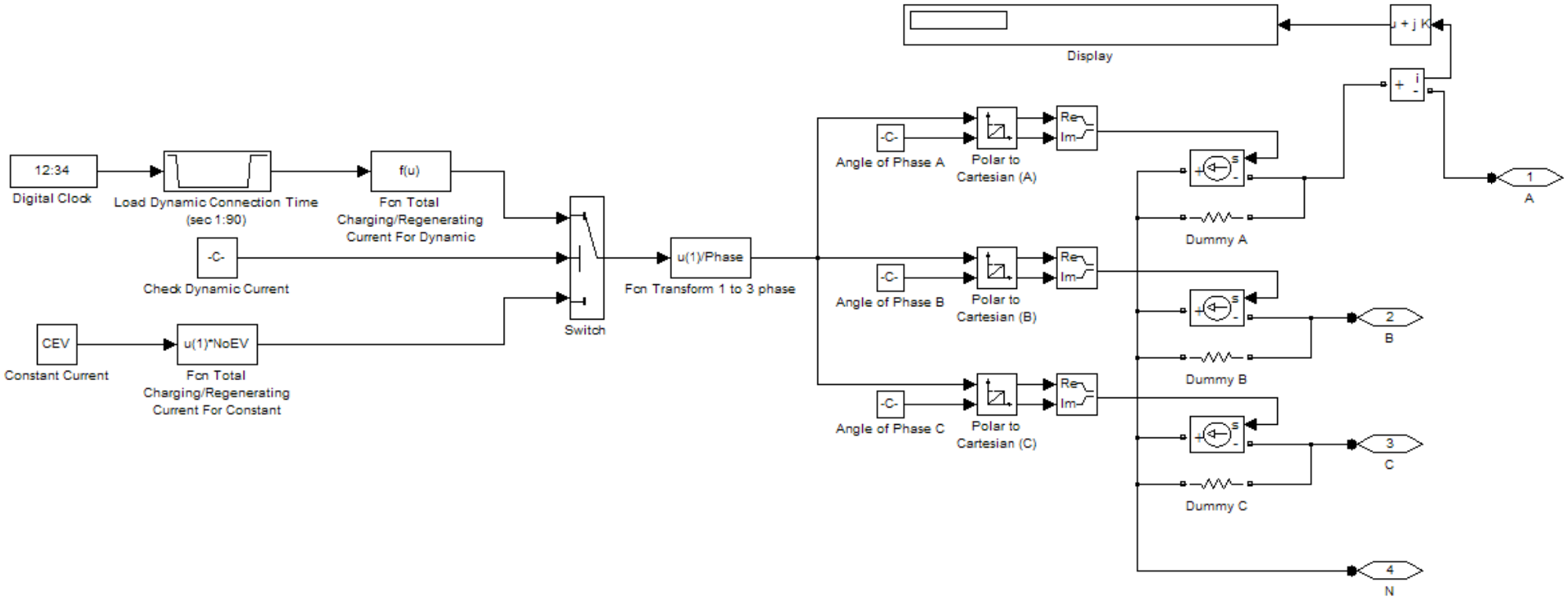

Figure B.22 MATLAB schematic of connection time for the SEVGC, SCP and/or SES (operating in charging or consumption mode)

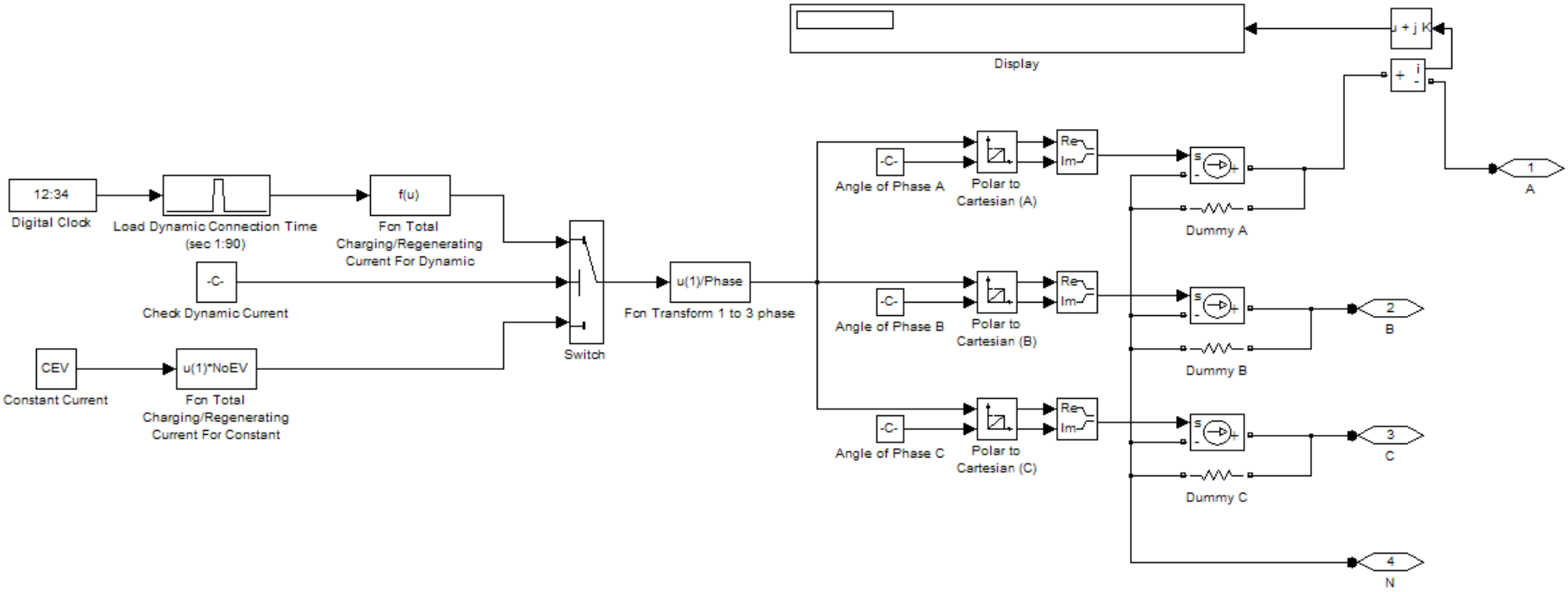

Figure B.23 MATLAB schematic for the SEVGC, SCP and/or SES (operating in mode V2G or supply mode)

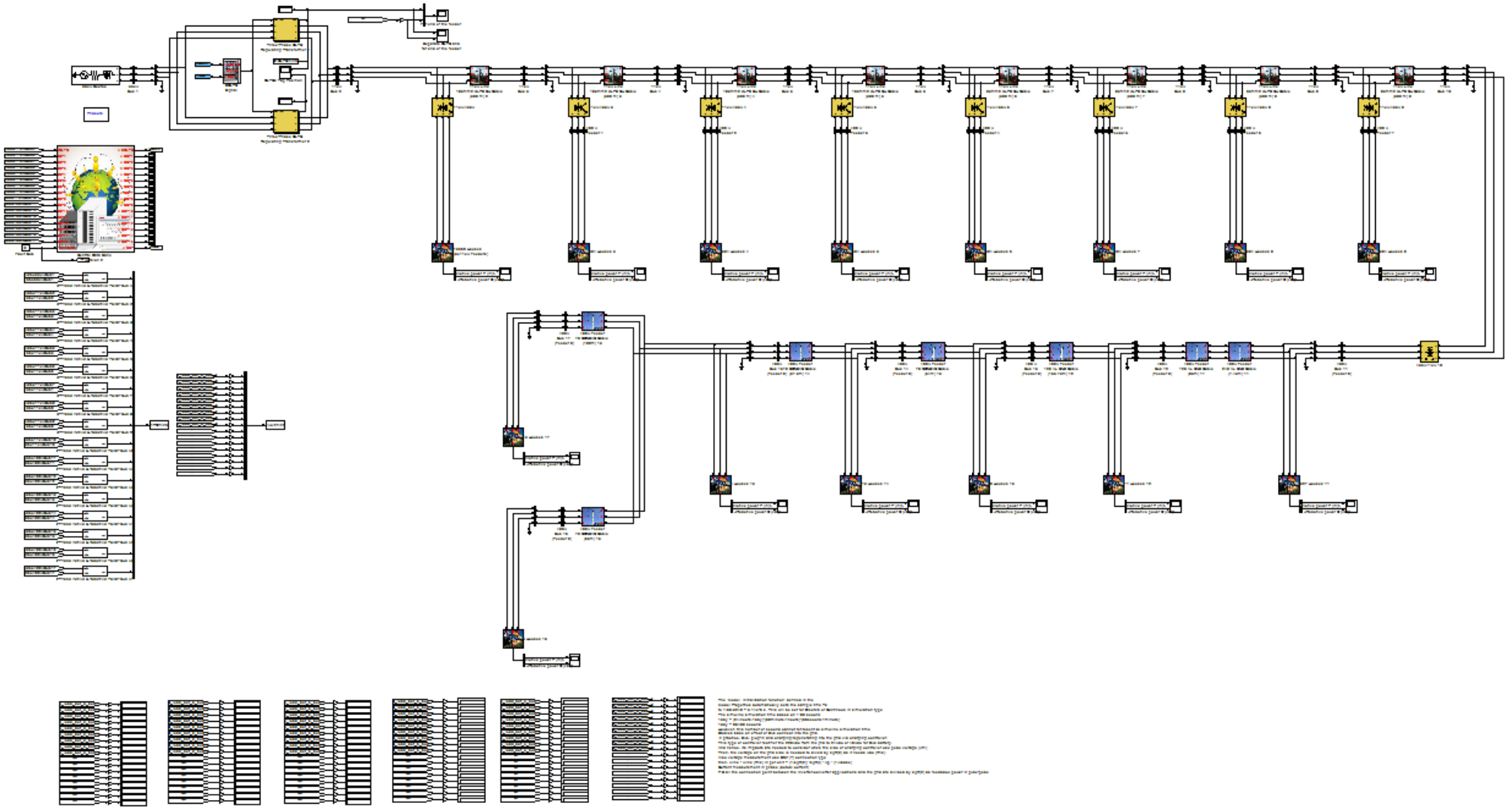

Figure B.24 Simulation network for the UK without SSDGs, EVs and smart controllers

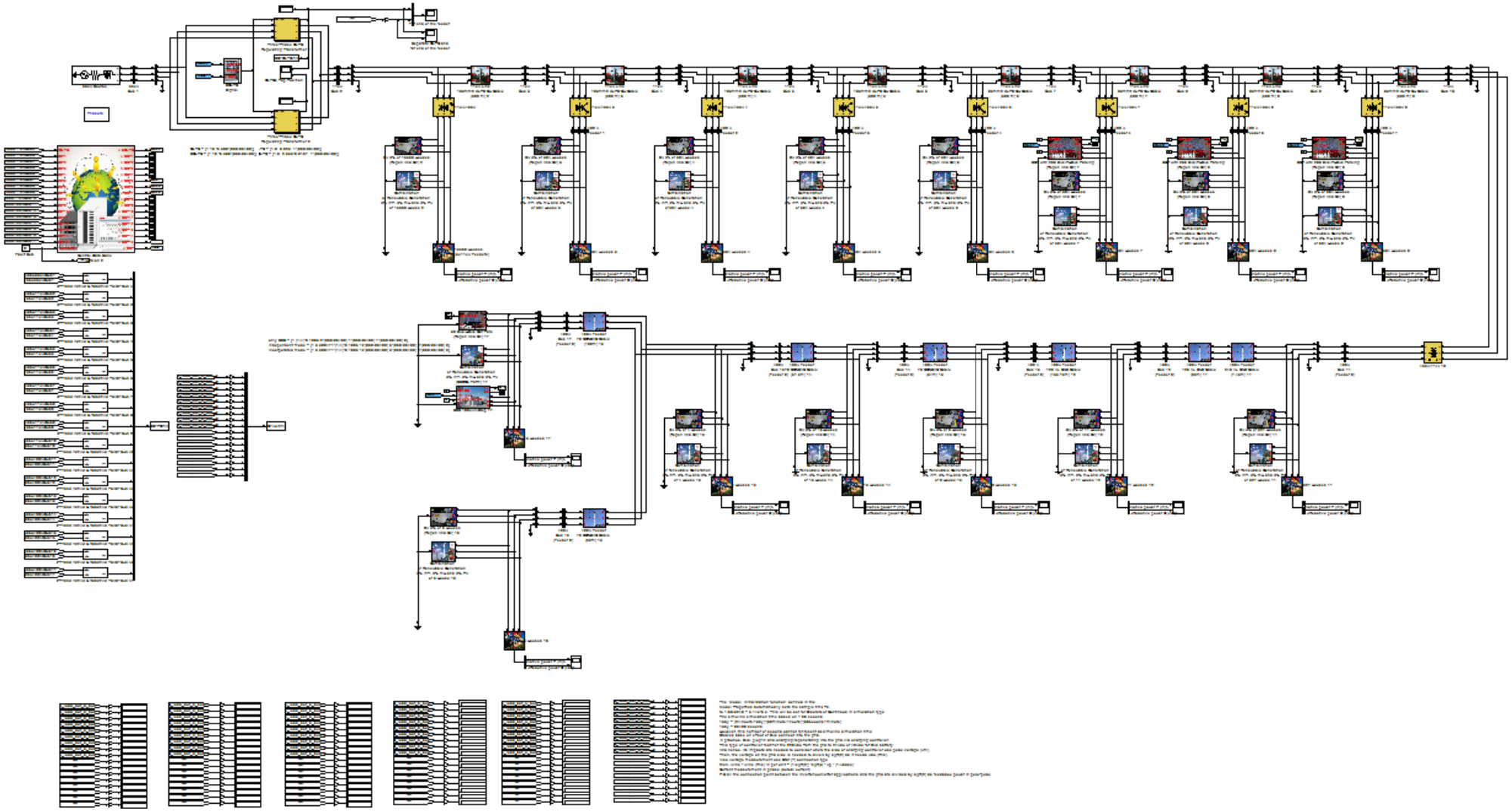

Figure B.25 Simulation network for the UK with SSDGs, EVs and smart controllers (scenario 6 from Table 3.5)

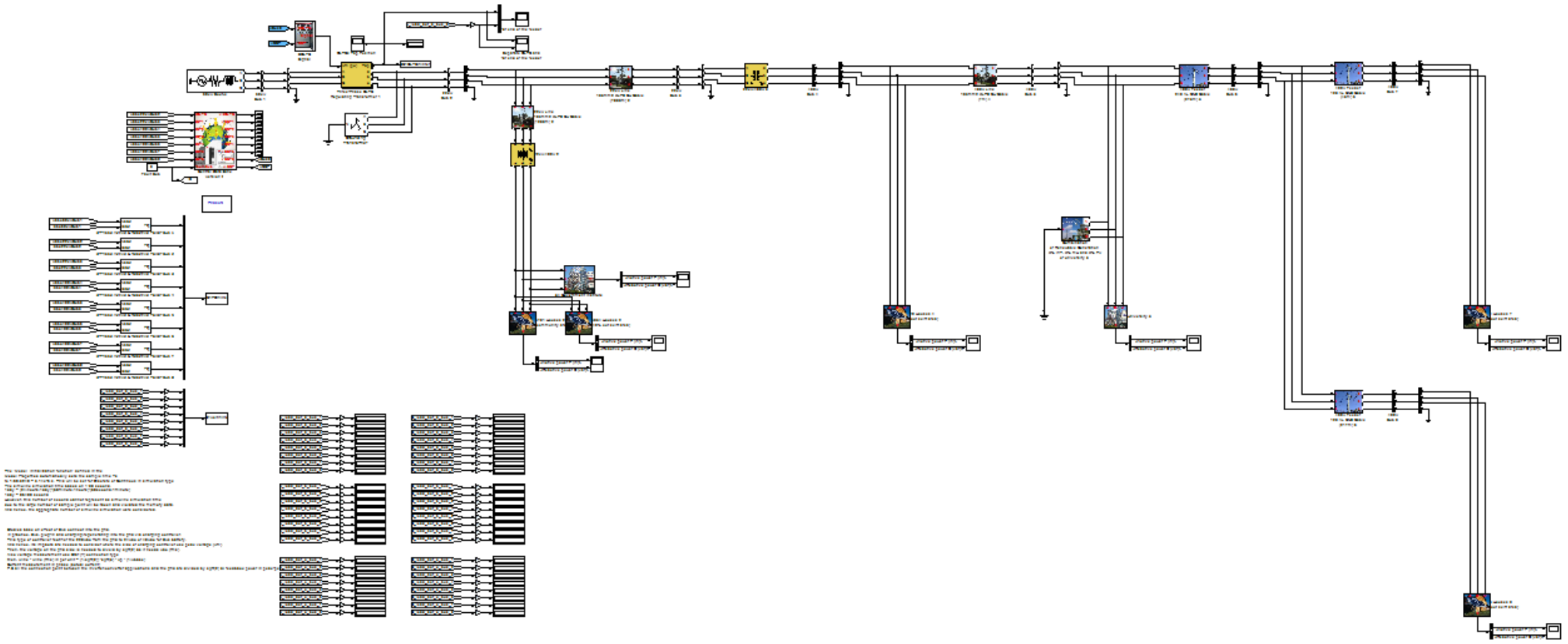

Figure B.26 Simulation network for TH without SSDGs, EVs and smart controllers

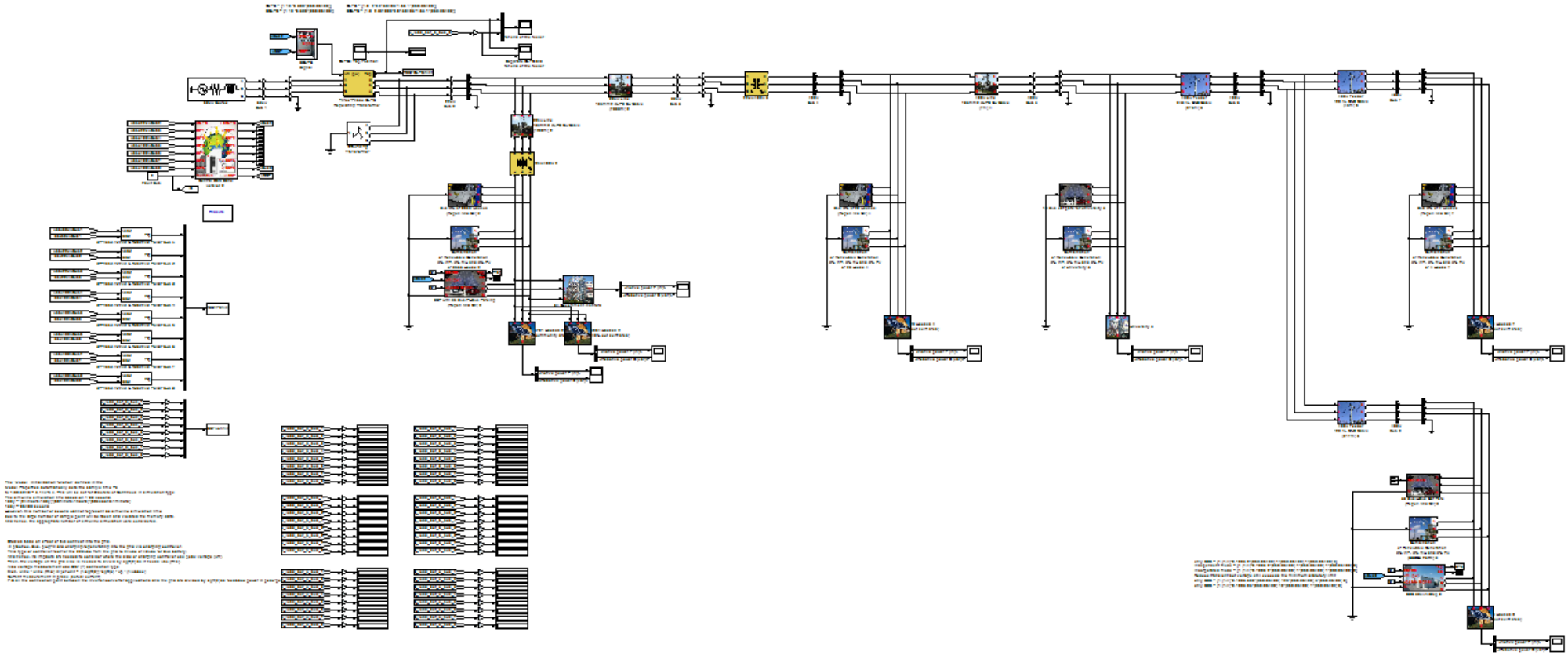

Figure B.27 Simulation network for TH with SSDGs, EVs and smart controllers (scenario 6 from Table 3.5)

Appendix C: Typical m-files Command of PSmartDN Tool

PSmartDNTool.m

```
function PSmartDNToolPasist
clc;
display = 1;
if display == 1;
  fprintf('[Completed setting workspace!]\n');
end
ChkSLG = xlsread('PSmartDNToolData','MVSec1');
VoltMVLV = load('MSmartVolt.mat');
PSmartDNMain = figure('Units','normalized',...
      'Position',[0.05 0.05 0.85 0.85],...
      'HandleVisibility','callback',...
      'Renderer','painters',...
      'Toolbar','figure',...
      'Numbertitle','off',...
      'Name','Power Self-Monitoring, Analysis and Reporting Technology of Distribution Network
(PSmartDN) Tool By Pasist Suwanapingkarl UNN');
if PSmartDNMain ~= 1;
  fprintf('The old display of PSmartDN Tool still openning !!!\n');
  helpdlg(('The old display of PSmartDNMain Tool still openning !!!'),'Window Error!');
end
if isempty(PSmartDNMain);
  helpdlg(('Please contact programmer!'),'Program Error!');
end
PSmartDNResultsPanel = uipanel(PSmartDNMain,'BorderType','etchedin','BackgroundColor',[255
196 105]/255,...
      'Units','normalized',...
      'Position',[0 0.5 0.4 0.5]);
uicontrol(PSmartDNResultsPanel,'Style','text','BackgroundColor',[1 1 1],...
      'Units','normalized',...
      'Position',[0.25 0.9025 0.5 0.09],...
      'String','Select Results',...
      'FontName','Ariel',...
      'FontSize',18,...
      'FontWeight','bold',...
      'ForegroundColor',[0  0  0]/255);
uicontrol(PSmartDNResultsPanel,'Style','text','BackgroundColor',[1 1 1],...
      'Units','normalized',...
      'Position',[0.065 0.785 0.15 0.09],...
      'String',{'Volt','(p.u.)'},...
      'FontName','Ariel',...
      'FontSize',9,...
      'FontWeight','bold',...
      'ForegroundColor',[1  0  1]);
uicontrol(PSmartDNResultsPanel,'Style','listbox','BackgroundColor','yellow',...
      'Units','normalized',...
      'Position',[0.04 0.1575 0.2 0.6],...
      'Enable','on',...
      'String',{'Inf','SOLTC','MV.1','SecLVTr','LV.1','LV.2','LV.3','LV.4','LV.5','LV.6','LV.7'},...
      'Tag','PlotVolt');
uicontrol(PSmartDNResultsPanel,'Style','text','BackgroundColor',[1 1 1],...
      'Units','normalized',...
      'Position',[0.305 0.785 0.15 0.09],...
      'String',{'Active','(kW)'},...
      'FontName','Ariel',...
      'FontSize',9,...
      'FontWeight','bold',...
      'ForegroundColor',[1  0  0]);
uicontrol(PSmartDNResultsPanel,'Style','listbox','BackgroundColor','yellow',...
      'Units','normalized',...
```

```
        'Position',[0.28 0.1575 0.2 0.6],...
        'Enable','on',...

'String',{'kWInf','kWSOLTC','kWMV.1','kWSecLVTr','kWLV.1','kWLV.2','kWLV.3','kWLV.4','kWLV.5','
kWLV.6','kWLV.7'},...
        'Tag','PlotkW');
uicontrol(PSmartDNResultsPanel,'Style','text','BackgroundColor',[1 1 1],...
        'Units','normalized',...
        'Position',[0.545 0.785 0.15 0.09],...
        'String',{'Reactive','(kVAR)'},...
        'FontName','Ariel',...
        'FontSize',9,...
        'FontWeight','bold',...
        'ForegroundColor',[0  0  1]);
uicontrol(PSmartDNResultsPanel,'Style','listbox','BackgroundColor','yellow',...
        'Units','normalized',...
        'Position',[0.52 0.1575 0.2 0.6],...
        'Enable','on',...

'String',{'kVARInf','kVARSOLTC','kVARMV.1','kVARSecLVTr','kVARLV.1','kVARLV.2','kVARLV.3','k
VARLV.4','kVARLV.5','kVARLV.6','kVARLV.7'},...
        'Tag','PlotkVAR');
uicontrol(PSmartDNResultsPanel,'Style','text','BackgroundColor',[1 1 1],...
        'Units','normalized',...
        'Position',[0.785 0.785 0.15 0.09],...
        'String',{'Smart','Device'},...
        'FontName','Ariel',...
        'FontSize',9,...
        'FontWeight','bold',...
        'ForegroundColor',[0  0  0]/255);
uicontrol(PSmartDNResultsPanel,'Style','listbox','BackgroundColor','yellow',...
        'Units','normalized',...
        'Position',[0.76 0.1575 0.2 0.6],...
        'Enable','on',...

'String',{'SOLTC','SCPMV.1','SCPLV.1','SCPLV.2','SCPLV.3','SCPLV.4','SCPLV.5','SCPLV.6','SCP
LV.7',...
        'SESMV.1','SESLV.1','SESLV.2','SESLV.3','SESLV.4','SESLV.5','SESLV.6','SESLV.7'},...
        'Tag','PlotStep');
uicontrol(PSmartDNResultsPanel,'Style','pushbutton','BackgroundColor',[1 1 1],...
        'Units','normalized',...
        'Position',[0.4 0.03375 0.2 0.09],...
        'String','Plot!',...
        'FontName','Ariel',...
        'FontSize',18,...
        'FontWeight','bold',...
        'ForegroundColor',[0  0  0]/255,...
        'value',0,...
        'Enable','on',...
        'Callback',@SelectedResultsFcn);
function SelectedResultsFcn (~, ~)
IndexPlotVolt = get(findobj('Tag','PlotVolt'),'Value');
TimeSeriesVoltP = VoltMVLV.MatMSmartVolt(1,1:end);
if IndexPlotVolt == 1
Inf = VoltMVLV.MatMSmartVolt(2,1:end);
PlotInf = plot(TimeSeriesVoltP,Inf,'Parent',PSmartDNAxes);
set(PlotInf,'MarkerSize',2,'Marker','+','Color',[1  0  1],'DisplayName','Inf');
elseif IndexPlotVolt == 2
SOLTC = VoltMVLV.MatMSmartVolt(3,1:end);
PlotSOLTC = plot(TimeSeriesVoltP,SOLTC,'Parent',PSmartDNAxes);
set(PlotSOLTC,'MarkerSize',2,'Marker','+','Color',[1  0  1],'DisplayName','SOLTC');
elseif IndexPlotVolt == 3
MV1 = VoltMVLV.MatMSmartVolt(4,1:end);
PlotMV1 = plot(TimeSeriesVoltP,MV1,'Parent',PSmartDNAxes);
set(PlotMV1,'MarkerSize',2,'Marker','+','Color',[1  0  1],'DisplayName','MV.1');
```

```
elseif IndexPlotVolt == 4
SecLVTr = VoltMVLV.MatMSmartVolt(5,1:end)';
PlotSecLVTr = plot(TimeSeriesVoltP,SecLVTr,'Parent',PSmartDNAxes);
set(PlotSecLVTr,'MarkerSize',2,'Marker','+','Color',[1  0  1],'DisplayName','SecLVTr');
elseif IndexPlotVolt == 5
LV1 = VoltMVLV.MatMSmartVolt(6,1:end);
PlotLV1 = plot(TimeSeriesVoltP,LV1,'Parent',PSmartDNAxes);
set(PlotLV1,'MarkerSize',2,'Marker','+','Color',[1  0  1],'DisplayName','LV.1');
elseif IndexPlotVolt == 6
LV2 = VoltMVLV.MatMSmartVolt(7,1:end);
PlotLV2 = plot(TimeSeriesVoltP,LV2,'Parent',PSmartDNAxes);
set(PlotLV2,'MarkerSize',2,'Marker','+','Color',[1  0  1],'DisplayName','LV.2');
elseif IndexPlotVolt == 7
LV3 = VoltMVLV.MatMSmartVolt(8,1:end);
PlotLV3 = plot(TimeSeriesVoltP,LV3,'Parent',PSmartDNAxes);
set(PlotLV3,'MarkerSize',2,'Marker','+','Color',[1  0  1],'DisplayName','LV.3');
elseif IndexPlotVolt == 8
LV4 = VoltMVLV.MatMSmartVolt(9,1:end);
PlotLV4 = plot(TimeSeriesVoltP,LV4,'Parent',PSmartDNAxes);
set(PlotLV4,'MarkerSize',2,'Marker','+','Color',[1  0  1],'DisplayName','LV.4');
elseif IndexPlotVolt == 9
LV5 = VoltMVLV.MatMSmartVolt(10,1:end);
PlotLV5 = plot(TimeSeriesVoltP,LV5,'Parent',PSmartDNAxes);
set(PlotLV5,'MarkerSize',2,'Marker','+','Color',[1  0  1],'DisplayName','LV.5');
elseif IndexPlotVolt == 10
LV6 = VoltMVLV.MatMSmartVolt(11,1:end);
PlotLV6 = plot(TimeSeriesVoltP,LV6,'Parent',PSmartDNAxes);
set(PlotLV6,'MarkerSize',2,'Marker','+','Color',[1  0  1],'DisplayName','LV.6');
elseif IndexPlotVolt == 11
LV7 = VoltMVLV.MatMSmartVolt(12,1:end);
PlotLV7 = plot(TimeSeriesVoltP,LV7,'Parent',PSmartDNAxes);
set(PlotLV7,'MarkerSize',2,'Marker','+','Color',[1  0  1],'DisplayName','LV.7');
elseif IndexPlotVolt == 12
LV8 = VoltMVLV.MatMSmartVolt(13,1:end);
PlotLV7 = plot(TimeSeriesVoltP,LV7,'Parent',PSmartDNAxes);
set(PlotLV7,'MarkerSize',2,'Marker','+','Color',[1  0  1],'DisplayName','LV.8');
elseif IndexPlotVolt == 13
LV9 = VoltMVLV.MatMSmartVolt(14,1:end);
PlotLV7 = plot(TimeSeriesVoltP,LV7,'Parent',PSmartDNAxes);
set(PlotLV7,'MarkerSize',2,'Marker','+','Color',[1  0  1],'DisplayName','LV.9');
elseif IndexPlotVolt == 14
LV10 = VoltMVLV.MatMSmartVolt(15,1:end);
PlotLV7 = plot(TimeSeriesVoltP,LV7,'Parent',PSmartDNAxes);
set(PlotLV7,'MarkerSize',2,'Marker','+','Color',[1  0  1],'DisplayName','LV.10');
else
   errordlg('Plot error!','Plot error','modal')
end
end
PSmartDNSingleLinePanel =
uipanel(PSmartDNMain,'BorderType','etchedin','BackgroundColor',[131  245  44]/255,...
       'Units','normalized',...
       'Position',[0.4 0.5 0.6 0.5]);
uicontrol(PSmartDNSingleLinePanel,'Style','text','BackgroundColor',[1 1 1],...
       'Units','normalized',...
       'Position',[0.075 0.9025 0.85 0.09],...
       'String','Single Line Diagram of Distribution Network',...
       'FontName','Ariel',...
       'FontSize',18,...
       'FontWeight','bold',...
       'ForegroundColor',[0  0  0]/255);
MVSec = ChkSLG(4,3);
LVSec = ChkSLG(5,3);
FqN = ChkSLG(6,3);
if (MVSec == 1) && (LVSec == 1) && (FqN == 50) && display == 1 || (MVSec == 1) && (LVSec ==
1) && (FqN == 60) && display == 1 ;
```

```
SLGDisp = imread('PSmartDNToolMV1LV1.jpg');
uicontrol(PSmartDNSingleLinePanel,'Style','pushbutton','BackgroundColor',[1 1 1],...
        'Units','normalized',...
        'Position',[0.05 0.05 0.9 0.8],...
        'value',0,...
        'Enable','on',...
        'CData',SLGDisp);
  fprintf('[Completed input data of distribution network with 1 MV section and 1 LV section!]\n');
elseif  (MVSec == 1) && (LVSec == 2) && (FqN == 50) && display == 1 || (MVSec == 1) && (LVSec
== 2) && (FqN == 60) && display == 1 ;
SLGDisp = imread('PSmartDNToolMV1LV2.jpg');
uicontrol(PSmartDNSingleLinePanel,'Style','pushbutton','BackgroundColor',[1 1 1],...
        'Units','normalized',...
        'Position',[0.05 0.05 0.9 0.8],...
        'value',0,...
        'Enable','on',...
        'CData',SLGDisp);
  fprintf('[Completed input data of distribution network with 1 MV section and 2 LV section!]\n');
elseif  (MVSec == 1) && (LVSec == 3) && (FqN == 50) && display == 1 || (MVSec == 1) && (LVSec
== 3) && (FqN == 60) && display == 1 ;
SLGDisp = imread('PSmartDNToolMV1LV3.jpg');
uicontrol(PSmartDNSingleLinePanel,'Style','pushbutton','BackgroundColor',[1 1 1],...
        'Units','normalized',...
        'Position',[0.05 0.05 0.9 0.8],...
        'value',0,...
        'Enable','on',...
        'CData',SLGDisp);
  fprintf('[Completed input data of distribution network with 1 MV section and 3 LV section!]\n');
elseif  (MVSec == 1) && (LVSec == 4) && (FqN == 50) && display == 1 || (MVSec == 1) && (LVSec
== 4) && (FqN == 60) && display == 1 ;
SLGDisp = imread('PSmartDNToolMV1LV4.jpg');
uicontrol(PSmartDNSingleLinePanel,'Style','pushbutton','BackgroundColor',[1 1 1],...
        'Units','normalized',...
        'Position',[0.05 0.05 0.9 0.8],...
        'value',0,...
        'Enable','on',...
        'CData',SLGDisp);
  fprintf('[Completed input data of distribution network with 1 MV section and 4 LV section!]\n');
elseif  (MVSec == 1) && (LVSec == 5) && (FqN == 50) && display == 1 || (MVSec == 1) && (LVSec
== 5) && (FqN == 60) && display == 1 ;
SLGDisp = imread('PSmartDNToolMV1LV5.jpg');
uicontrol(PSmartDNSingleLinePanel,'Style','pushbutton','BackgroundColor',[1 1 1],...
        'Units','normalized',...
        'Position',[0.05 0.05 0.9 0.8],...
        'value',0,...
        'Enable','on',...
        'CData',SLGDisp);
  fprintf('[Completed input data of distribution network with 1 MV section and 5 LV section!]\n');
elseif  (MVSec == 1) && (LVSec == 6) && (FqN == 50) && display == 1 || (MVSec == 1) && (LVSec
== 6) && (FqN == 60) && display == 1 ;
SLGDisp = imread('PSmartDNToolMV1LV6.jpg');
uicontrol(PSmartDNSingleLinePanel,'Style','pushbutton','BackgroundColor',[1 1 1],...
        'Units','normalized',...
        'Position',[0.05 0.05 0.9 0.8],...
        'value',0,...
        'Enable','on',...
        'CData',SLGDisp);
  fprintf('[Completed input data of distribution network with 1 MV section and 6 LV section!]\n');
elseif  (MVSec == 1) && (LVSec == 7) && (FqN == 50) && display == 1 || (MVSec == 1) && (LVSec
== 7) && (FqN == 60) && display == 1 ;
SLGDisp = imread('PSmartDNToolMV1LV7.jpg');
uicontrol(PSmartDNSingleLinePanel,'Style','pushbutton','BackgroundColor',[1 1 1],...
        'Units','normalized',...
        'Position',[0.05 0.05 0.9 0.8],...
        'value',0,...
```

```
        'Enable','on',...
        'CData',SLGDisp);
  fprintf('[Completed input data of distribution network with 1 MV section and 7 LV section!]\n');
elseif  (MVSec == 1) && (LVSec == 8) && (FqN == 50) && display == 1 || (MVSec == 1) && (LVSec
== 8) && (FqN == 60) && display == 1 ;
SLGDisp = imread('PSmartDNToolMV1LV8.jpg');
uicontrol(PSmartDNSingleLinePanel,'Style','pushbutton','BackgroundColor',[1 1 1],...
        'Units','normalized',...
        'Position',[0.05 0.05 0.9 0.8],...
        'value',0,...
        'Enable','on',...
        'CData',SLGDisp);
  fprintf('[Completed input data of distribution network with 1 MV section and 8 LV section!]\n');
elseif  (MVSec == 1) && (LVSec == 9) && (FqN == 50) && display == 1 || (MVSec == 1) && (LVSec
== 9) && (FqN == 60) && display == 1 ;
SLGDisp = imread('PSmartDNToolMV1LV9.jpg');
uicontrol(PSmartDNSingleLinePanel,'Style','pushbutton','BackgroundColor',[1 1 1],...
        'Units','normalized',...
        'Position',[0.05 0.05 0.9 0.8],...
        'value',0,...
        'Enable','on',...
        'CData',SLGDisp);
  fprintf('[Completed input data of distribution network with 1 MV section and 9 LV section!]\n');
elseif  (MVSec == 1) && (LVSec == 10) && (FqN == 50) && display == 1 || (MVSec == 1) &&
(LVSec == 10) && (FqN == 60) && display == 1 ;
SLGDisp = imread('PSmartDNToolMV1LV10.jpg');
uicontrol(PSmartDNSingleLinePanel,'Style','pushbutton','BackgroundColor',[1 1 1],...
        'Units','normalized',...
        'Position',[0.05 0.05 0.9 0.8],...
        'value',0,...
        'Enable','on',...
        'CData',SLGDisp);
  fprintf('[Completed input data of distribution network with 1 MV section and 10 LV section!]\n');
elseif isempty(MVSec) && isempty(LVSec) && isempty(FqN) && display == 1;
  helpdlg(({'Require numerical input!','This tool supports maximum 1 sections of MV level','and
maximum 10 sections of LV level!'}),'Input Error!');
else
  helpdlg(({'Please check your input!','This tool supports maximum 1 sections of MV level','and
maximum 10 sections of LV level','and network frequency at 50Hz and 60 Hz!'}),'Input Error!');
  fprintf('[Error input data of distribution network]\n');
end
PSmartDNGraphPanel = uipanel(PSmartDNMain,'BorderType','etchedin','BackgroundColor',[152
245  255]/255,...
        'Units','normalized',...
        'Position',[0 0 1 0.5]);
PSmartDNAxes = axes('parent',PSmartDNGraphPanel,'YAxisLocation','left',...
        'Position',[0.05 0.125 0.9 0.75],...
        'xlim',[0 960],...
        'ylim',[0 1.8],...
        'YMinorTick','on',...

'XTickLabel',{'00.00','01.00','02.00','03.00','04.00','05.00','06.00','07.00','08.00','09.00','10.00','11.00',
'12.00','13.00','14.00','15.00','16.00','17.00','18.00','19.00','20.00','21.00','22.00','23.00','00.00'},...
        'XTick',0:960/24:960,...
        'XMinorTick','on',...
        'Box','on',...
        'FontName','Arial',...
        'FontSize',9,...
        'Color',[1 1 1],...
        'XColor',[0 0 0],...
        'YColor',[0 0 0],...
        'XGrid','on',...
        'YGrid','on');
axis(PSmartDNAxes,'on');
```

```
xlabel(PSmartDNAxes,'Time (Hours)','Color',[0 0
0],'FontName','Arial','FontSize',12,'FontWeight','bold');
ylabel(PSmartDNAxes,'Unit','Color',[0 0 0],'FontName','Arial','FontSize',12,'FontWeight','bold');
title(PSmartDNAxes,'Profile','Color',[0 0 0],'FontName','Arial','FontSize',18,'FontWeight','bold');
hold(PSmartDNAxes,'all');
zoom(PSmartDNAxes,'on');
pan(PSmartDNAxes,'off');
end
```

Appendix D: List of publications

1) Suwanapingkarl, P., Putrus, G. A. and Pearsall, N. (2012) 'Feasibility functions and impacts of Smart Demand Side Management (SDSM) and Smart On-Load Tap Changer transformer (SOLTC) on MV/LV distribution network'. Prepared for publication in IEEE Transactions on Power Systems.

2) Suwanapingkarl, P., Putrus, G. A. and Pearsall, N. (2012) 'Feasibility functions and impacts of Smart EVs/PHEVs Car Parks (SCPs) and Smart Energy Storages (SESs) on MV/LV distribution network'. Prepared for publication in IEEE Transactions on Power Systems.

3) Suwanapingkarl, P., Putrus, G. A. and Pearsall, N. (2012) 'Modelling and investigating photovoltaic (PV) incorporate with DC/AC inverter under variable environment by using MATLAB/Simulink'. Prepared for publication in IEEE Transactions on Energy Conversion.

4) Suwanapingkarl, P., Putrus, G. A., Pearsall, N. and Suwanapingkarl, M. (2012) 'Modelling and investigating Small-Scale wind and hydro turbines incorporate with Permanent Magnet Generator (PMG) and inverter by using MATLAB/Simulink'. Prepared for publication in IEEE Transactions on Energy Conversion.

5) Bentley, E.C., Suwanapingkarl, P., Weerasinghe, S., Jiang, T., Putrus, G. A. and Johnston, D. (2010) 'The interactive effects of multiple EV chargers within a distribution network', *IEEE Vehicle power and propulsion conference: clean tech for transportation*. Lille, France 1-3 September, pp. 1-6.

6) Johnston, D., Bentley, E., Narayana, M., Jiang, T., Suwanapingkarl, P. and Putrus, G. (2010) 'Electric vehicles as storage devices for supply-demand management', *IEEE Vehicle power and propulsion conference: clean tech for transportation*. Lille, France 1-3 September, pp. 1-6.

7) Putrus, G. A., Suwanapingkarl, P., Johnston, D., Bentley, E. C. and Narayana, M. (2009) 'Impact of electric vehicles on power distribution networks', *IEEE Vehicle Power and Propulsion Conference, 2009. VPPC '09.* Dearborn, MI 7-10 September, pp. 827-831.